



DEUTSCHE
GESELLSCHAFT FÜR
PATHOLOGIE E.V.
Seit 1897 – dem Leben verpflichtet

125 Jahre



105. Jahrestagung der Deutschen Gesellschaft für Pathologie

Münster · 9. - 11. Juni 2022

Connective (tissue) pathology: Was uns verbindet!

ABSTRACTBAND



www.pathologie-jahrestagung.de

Abstractband



105. Jahrestagung der Deutschen Gesellschaft für Pathologie e.V. 9. – 11. Juni 2022, Münster

„Connective (tissue) pathology: Was uns verbindet!“

Schwerpunkte der Jahrestagung

- Knochen- und Weichgewebspathologie
- Referenzpathologie
- Neue Klassifikationen
- Big Data und Künstliche Intelligenz
- Automation in der Pathologie
- Responseevaluation
- COVID-19

Vorsitzender der Gesellschaft

Prof. Dr. med. Gustavo Baretton, Dresden

Tagungspräsidentin

Prof. Dr. med. Eva Wardelmann, Münster

Herausgeberin, Lektorat und Copyright

Deutsche Gesellschaft für Pathologie e.V.
Geschäftsstelle
Robert-Koch-Platz 9
10115 Berlin
geschaeftsstelle@pathologie-dgp.de

Tagungsorganisation

Kongress- und Kulturmanagement GmbH (KUKM)
dgp2022@kukm.de

Inhaltsverzeichnis

(Klicken Sie auf den Beitragstitel, um direkt zum ausgewählten Abstract zu gelangen.)

DGP02.01 Mikroskop adé?

Goodbye, microscope!

H03 Pressekonferenz - Preisverleihungen

Imaging intact human organs with local resolution of cellular structures using hierarchical phase-contrast tomography

Super-enhancer-based identification of a BATF3/IL-2R-module reveals vulnerabilities in anaplastic large cell lymphoma

Alarm in the bone marrow - how to untangle fibrosis in the bone marrow

DGP01 Weichgewebe- und Knochentumoren - State of the art

Abdominal soft tissue tumors

Soft tissue and bone tumors of head and neck

Giant cell-containing tumors of bone and differential diagnoses

Small round cell sarcomas

Vascular and perivascular Tumors

DGP02 Automation

Automation and Application of Robotics in the Pathology Laboratory

Workflow efficiency and change management in a pathology laboratory

Automated image acquisition as an integrative key of a seamless digital pathology workflow

Process optimization in preparation of a digital pathology workflow and the use of machine intelligence

DGP03 Referenzpathologie, Register

Reference Pathology Breast

Consultation pathology - Lung

Consultation pathology of testis tumors

Development and current challenges of central pathology for malignant lymphomas

DGP04 Rising Stars (Vorträge der Preisträger*innen des Gerhard-Domagk-, Rudolf-Virchow- und Novartis-Preises)

Characterization of the Tumor Microenvironment by Highly Multiplexed Microscopy

Imaging intact human organs with local resolution of cellular structures using hierarchical phase-contrast tomography

Alarm in the bone marrow - how to untangle fibrosis in the bone marrow

Super-enhancer-based identification of a BATF3/IL-2R-module reveals vulnerabilities in anaplastic large cell lymphoma

DGP05 DGP-Promotionspreis 2022 - Auswahlrunde Bewerber*innen

Analysis of the super-enhancer self-maintenance feedback loop of TBXT gene expression in chordomas

Novel Criteria for Intratumoral Budding with Prognostic Relevance for Colon Cancer and Its Histological Subtypes

scRNA-seq uncovers metabolism and CD52 as new targets in ibrutinib surviving mantle cell lymphoma cells

Impact of P-selectin-PSGL-1 axis on platelet-endothelium-leucocyte interactions in COVID-19

Machine Learning Models Predict the Primary Sites of Head and Neck Squamous Cell Carcinoma Metastases Based on DNA Methylation

Small particles of *E. granulosus* (SPEGS) and *E. multilocularis* (SPEMS) induce selective activation of NK-cells in human blood and in the lymph nodes

The Wnt- β -catenin signalling pathway influences TBXT expression in chordoma.

Regulation of HOXB7-expression and the impact on the Ras-Raf-MAPK-pathway regarding the viability of chordoma cell lines

DGP06 Junges Forum I - Social Media

How Twitter & Facebook Changed My Life: The Role of Social Media in Pathology & Medicine

The pros and cons of the use of Social Media in Pathology

Pathology findings made audible-Prof. Dr. Sven Perner and Dr. Christiane Kümper of the University of Lübeck launch podcasts "Patho aufs Ohr" and "Patho?Logisch!"

DGP07 Odontogenic and head and neck tumors

Clinical and Pathomorphological Aspects of Odontogenic Tumors

Differential Diagnostics and Molecular Profiles of Odontogenic Tumors

Reappraisal of Grading in Intestinal-Type Sinonasal Adenocarcinoma: Tumor Budding as an Independent Prognostic Parameter

Elevated LSD1 and SNAIL expression indicate poor prognosis in hypopharynx carcinoma
DNA methylation-based classification of salivary gland tumors

DGP08 Aktuelle Habilitationen

The tumor microenvironment - relay station for prognosis and therapy response

Prognostic and predictive biomarkers in invasive breast cancer

Tumor-microenvironment in colorectal cancer: the role of budding and tumor-infiltrating lymphocytes as tumor-host antagonists.

DGP09 Big Data and AI

Artificial Intelligence helps pathologists improve diagnostic efficiency and accuracy in prostatic biopsy diagnosis.

AI-Assisted Cancer Detection

Fast and Robust Deep Tissue Cartography for Colon Sections

DGP10 Junges Forum II: Pathologie Quo vadis?

Board certification in Europe - differences in duration, examination and acknowledgement

DGP11 Neues aus der WHO

Uterine Leiomyosarcome – was sagt die WHO-Klassifikation 2020?

The 5.th Edition of the WHO (URO5): Prostate Cancer

What is new in the 5th edition of the WHO classification of lymphoid tissue tumours?

DGP12 Strukturierte Befundung - sinnvoll?

Strukturierte Befundung am Beispiel Prostata

Structured Reporting in Gastrointestinal Pathology

DGP13 Therapieansprechen: Synergien von Radiologie und Pathologie?

Response evaluation in breast pathology after neoadjuvant treatment

Morphological and Molecular Aspects of Therapy Response - the View of the Pathologist

Grading and Response Assessment of Sarcoma: Potential and Limitations of Radiological Data

Histopathological parameters of lymph node involvement after chemoradiation reveal viable tumor cells but no keratin debris as a prognostic factor in head and neck squamous cell carcinoma

DGP14 Update COVID-19 I (inkl. Ungarischer Workshop)

The German Registry of COVID-19 Autopsies (DeRegCOVID) & the National Autopsy Network (NATON)

New insights into COVID-19

Rapid Identification of Serological Reagents for the Immunohistochemical Detection of Coronavirus-associated Proteins in Formalin-fixed Paraffin-embedded Tissue

COVID-19 associated pathology and categorization of death causes in 100 autopsy cases
Placenta and COVID-19

DGP14 Update COVID-19 II

Minimally invasive autopsies for the investigation of pulmonary pathology of COVID19 - experiences of a longitudinal series of 92 patients.

Update of a German Autopsy Study of Fatal Cases with SARS-CoV-2 Infection after Vaccination

Clinical, serological and postmortem findings in SARS-CoV2-vaccine-induced thrombotic thrombocytopenia

Stage Dependend Mast Cell densities in Lung Damage of COVID-19 Autopsies

Impact of P-selectin-PSGL-1 axis on platelet-endothelium-leucocyte interactions in COVID-19
Inflammation and vascular remodelling in COVID-19 hearts

AG01 AG Gastroenteropathologie I

Stroma Areactive Invasion Front Areas (SARIFA) in gastric carcinoma as a new biomarker implicating an interaction between adipocytes and tumor cells – a validation study

The expression and biological effect of RNF43 and LRP1B in gastric cancer is context-dependent.

Morphology Matters: A Critical Reappraisal of the Clinical Relevance of Morphologic Criteria From the 2019 WHO Classification in a Large Colorectal Cancer Cohort Comprising 1004 Cases

Delineating the evolutionary trajectories of colorectal cancer development in inflammatory bowel disease

TROP2 as a novel marker for cell stiffness in colon cancer cells

Identification of novel candidate biomarkers in early adenoma transition

Neuroendocrine Differentiation in Conventional Colorectal Adenocarcinomas.

AG01 AG Gastroenteropathologie II

SARIFA (Stroma AReactive Invasion Front Areas) proofs to be prognostic biomarker also in pancreatic adenocarcinoma.

Immunological microenvironment of precursor lesions of pancreatic ductal adenocarcinoma (PDAC) in a transgenic mouse model

Clinicopathologic evaluation of intrahepatic cholangiocarcinoma subtypes

PD-1+ T-cells correlate with Nerve Fiber Density as a prognostic biomarker in patients with resected perihilar cholangiocarcinoma.

The Hippo pathway effector TAZ induces intrahepatic cholangiocarcinoma in mice and is ubiquitously activated in the human disease

Mesoscopic optical imaging reveals the microarchitecture of hepatic lymphatic vessels

Hepatocellular ballooning in human cirrhotic livers is based on distinct glycogenosis associated with further metabolic and proto-oncogenic aberrations

Identification of DUSP4/6 overexpression as a rheostat to N-Ras induced hepatocarcinogenesis

Direct interaction of the oncogenes YAP and TAZ with the transcription factor HNF1B in hepatocellular carcinoma

AG01 AG Gastroenteropathologie III

Increase of Ki67 during progression of NET G3

The role of ATF2 in 5-Fluorouracil resistance of colorectal cancer cells

Cytoskeleton associated DAPK links autophagy with EMT

Molecular subtyping of gastric cancer according to ACRG using immunohistochemistry – correlation with clinical parameters

AG02 AG Uropathologie I

Anti-Angiogenic Properties of A Novel Secreted Neuropilin-2 Isoform In Bladder Cancer

A simplified method for molecular subtype classification of urinary bladder cancer based on RT-qPCR

Identifying proteins interacting with KDM5C in prostate cancer

Frequency of TERT gene promoter mutations in upper tract urothelial carcinoma

The new WHO classification of testicular tumors - The main changes

AG02 AG Uropathologie II

Update WHO-classification (5.edition, 2022): Tumors of the urinary system.

Primary pseudomyogenic hemangioendothelioma of the testis with a novel POTEI-FOSB gene fusion

GRHL3 in bladder cancer: a dual role depending on molecular and histological background?

NeuroSAFE frozen section examination in potentially nerve-sparing radical prostatectomy: Comparison of conventional frozen sections and fluorescence-based confocal microscopy (FCM) - Initial results

Spatial immune phenotypes of distant metastases but not matched primary urothelial carcinomas predicts response to immune checkpoint blockade.

Epigenetically regulated transcription factor BNC1 shows oncogenic effects in squamous

bladder cancer cells

AG03 AG Knochen-, Gelenk- und Weichgewebspathologie I

Chordoma- Overview

Morphological characteristics of chondrocyte spheroids used for spheroid-based ACI

CD47 prevents the elimination of diseased fibroblasts in scleroderma

Intercellular effects of EVs from pathologically altered osteoblasts on mesenchymal stem cells

Murine osteoporotic fracture healing and hyperalgesia are modulated by the peripheral nervous system

Regulation of HOXB7-expression and the impact on the Ras-Raf-MAPK-pathway regarding the viability of chordoma cell lines

Ultrastructural Analysis of Mitochondria from Osteoblasts and Osteocytes from Patients with Osteomyelitis

AG03 AG Knochen-, Gelenk- und Weichgewebspathologie II

Histomorphometric analysis of 35 giant cell tumors of bone after recurrence as compared to changes following denosumab treatment

Superficial fibromas with CTNNB1-mutation: subtype of fibromatosis or new entity?

Identification of Wee1 kinase activity as functional liability in myxoid liposarcoma

IGF-IR-dependent cooperation of FUS-DDIT3 and YAP1 in myxoid liposarcoma

Integrated Proteogenomics of Non-Uterine Leiomyosarcomas for Outcome Risk Prediction

Interdependency between YAP1 and β -catenin activation in synovial sarcoma

VISTA in Soft Tissue Sarcomas: A Perspective for Immunotherapy?

NTRK-rearranged uterine sarcomas: A rare tumor entity with the option of targeted therapy in advanced stages.

AG04 AG Hämatopathologie I

Histiocytic and Dendritic Cell Neoplasms (HDCNs)

Landscape of 4D cell interaction in malignant lymphomas

Genetic characterization of localized follicular lymphomas reveals novel somatic copy number alterations and somatic mutations using OncoScan and whole-exome sequencing

Routine application of the Lymph2Cx Assay for the subclassification of diffuse large B-cell lymphoma: report of a prospective real-world series with immunohistochemistry and FISH correlation.

Genome wide methylation profiling allows the separation of blastic variant of nodal marginal zone Lymphoma and primary nodal DLBCL. Work in progress.

High prevalence of CHIP mutations in the blood of patients with peripheral bypass graft occlusion

AG04 AG Hämatopathologie II

What is new in the 5th edition of the WHO classification of lymphoid tissue tumours?

Molecular genetic profiling of hematopoietic malignancies by gene panel sequencing in bone marrow core biopsies and its corresponding aspirates

Efficacy of avapritinib in patients with advanced systemic mastocytosis (AdvSM): hematologic and bone marrow (BM) responses from the phase 2 open-label, single-arm, Pathfinder study

Mutations in distinct molecules of the extracellular matrix are associated with tumor mutational burden and overall survival in multiple myeloma

CD70⁺ subclones drive disease progression in Multiple Myeloma

Functional investigation of the IGF1R-PYK2 signaling network in Multiple Myeloma

AG05 AG Herz-, Gefäß-, Nieren- und Transplantationspathologie

Sudden Cardiac Death UK National Programme Implementation

10 years transplant on-call duty. Lessons learned

Actual aspects on diagnosis of renal transplants – Banff and beyond

Mass spectrometry-based proteomics (LC-MS/MS) without Laser Microdissection (LMD) - a reliable approach to classify cardiac amyloidosis?

iNOS expression in postmortem human myocardial infarction hearts for validation of oxidative stress

Histopathology of 61 human explanted atrial septal defect occlusion devices without removal of metal/polymer parts

α -Parvin defines a specific integrin adhesome to maintain podocyte adhesion and the kidney filtration barrier

AG06 AG Gynäko- und Mammopathologie I

Loss of tumor suppressor TGF- β pathway proteins phosphoSmad2 and Smad4 indicate poor survival in high grade serous ovarian carcinoma

Prognostic value of Regulatory T cells and T helper 17 cells in high grade serous ovarian carcinoma

Desmoplastic stroma reaction and CAF activity contribute to poor therapy response in HGSOC.

Histomorphologic and molecular biomarkers in copy number low and microsatellite instable endometrioid adenocarcinoma – mutual correlations and prognostic impact

“Recent developments in guidelines in endometrial carcinomas (WHO, ESGO-ESTRO-ESP guidelines, ICCR)”

Transcription Factor AP-2beta (TFAP2B) - a differentiation marker in breast cancer and human breast epithelial cells

Differential impact of prognostic parameters in hormone receptor-positive lobular breast cancer

AG06 AG Gynäko- und Mammopathologie II

Highly multiplexed imaging of in situ tumor ecosystems towards precision medicine

Implementation of an external quality assessment for PIK3CA mutation testing on tumor tissue samples (2021) - lessons learned.

The age-specific differences in histopathological tumor characteristics and TNM classification of breast carcinomas in Quality assured Mamma Diagnostic (QuaMaDi) Program in the State of Schleswig-Holstein in Germany

Class II tumor suppressor genes in breast cancer can be classified according to intrinsic molecular subtypes and may be suitable for risk classification of ductal carcinoma in situ (DCIS)

Impact of TROP-2 and its cellular localization on prognosis of breast cancer – an analysis of 1164 tumors from a prospective clinical trial

E-cadherin to P-cadherin switching in lobular breast cancer with tubular elements

Inter-observer agreement for the histological diagnosis of invasive lobular breast cancer – An international concordance study

AG07 AG Dermatopathologie

Dermatopathology of COVID-19 infection and vaccine-related cutaneous manifestations.

Histopathological and immunohistochemical study of PRAME expression in different benign, dysplastic and malignant primary and metastatic melanocytic lesions

Mutational Profiling in Spindle Cell and Desmoplastic Melanoma

AG08 AG Thoraxpathologie I

Does alveolar fibroelastosis recur after lung transplantation

The challenge of long-term cultivation of human precision-cut lung slices
Lung Pathology of postCOVID

Comparative analysis of fibroblastic foci in patients with idiopathic pulmonary fibrosis and pulmonary sarcoidosis

AG08 AG Thoraxpathologie II

Fluorescence in situ hybridization and functional analysis of the KMT2A-MAML2 gene fusion in thymic epithelial tumors and in the thymic carcinoma cell lines 18889c and MP57

CDK7 is a prognostic biomarker for non small cell lung cancer

Activation of AKT signaling promotes resistance to FGFR1 inhibition in squamous-cell lung cancer

Proteomics to connect lung cancer molecular phenotype to tumor genotype and histopathology

AG09 AG Kopf-Hals-Pathologie

CDK7 Expression implies a poor prognosis in HNSCC

Revealing differences of local PD-L1 mRNA expression and corresponding protein occurrence in head and neck tumour

Who's Driving? Switch of Drivers in Immunotherapy-Treated Progressing Sinonasal Melanoma

Molecular alterations underlying tumor cell budding in head and neck cancer

Current Advances in the Morphological and Molecular Classification of Salivary Gland Tumors

AG10 AG Zytopathologie

Molekulare Zytologie: Chancen und Herausforderungen

Non-cellular findings in cytological preparations

Add-on Opportunistic Screening for Oral Cancer and Precursors in Patients with Fanconi Anemia using Brush Biopsy-Based Cytology

AG11 AG Molekularpathologie I

EGFR exon 20 insertion mutations in NSCLC: spectrum, frequency and results of the first German proficiency test

Immuno-histomorphological comparison regarding heterogeneity between primary lung carcinomas and corresponding lymph node metastases

Spatial patterns of specific immune cells populations in the tumor microenvironment as biomarkers in lung adenocarcinoma

Biomarker testing in lung cancer patients- upscaling the fast track analysis

The immune microenvironment in EGFR- and ERBB2-mutated lung cancer

AG11 AG Molekularpathologie II

Genomic Large Rearrangements (LRs) in HRR genes in high-grade ovarian carcinomas

TP53 mutations are associated with primary endocrine resistance in luminal early breast cancer

Implementation of HRD analysis in daily routine diagnostics-overall performance and pitfalls

Assessing and evaluating the scope and constraints of Idylla molecular assays by using different source materials in routine diagnostic settings.

Results of studies to validate HRD analysis using the Qiaseq HRD assay from Qiagen

AG11 AG Molekularpathologie III

Targeted and explorative mass spectrometry show kallikrein 6 and 10 overexpression in PDAC and suggest a collective cell migration for pancreatic cancer

The role of TROP2 methylation in colon cancer cells

A helpful tool to estimate the disease-causing value of unknown gene fusion.

Implications for molecular testing of FGFR2 fusions in cholangiocarcinoma

Two years of targeted therapy- a single center molecular tumor board observational study

AG12 AG Kinder- und Fetalpathologie I

Placental pathology in sudden intrauterine death (SIUD) in SARS-CoV-2 positive oligosymptomatic women

Placental pathology associated with SARS-CoV-2 infection - case series conducted at the Institute for Surgical Pathology, Medical Centre, University Freiburg

Review of placentas submitted for histological examination with regard to their clinical indication and correlation with the histological findings

Meta-analysis on COVID-19-pregnancy-related placental pathologies shows no specific pattern

Prognosis of postoperative clinical course of neonates after surgical intervention for necrotizing enterocolitis - is the histological examination of the surgical specimen helpful?

Case Report: Autopsy of a 4-month-old infant with Waterhouse-Friderichsen syndrome and lymphocytic interstitial pneumonia due to co-infection with SARS-CoV-2 and Neisseria meningitidis

AG12 AG Kinder- und Fetalpathologie II

Development of 3D spheroid models highlights the therapeutic potential of combining BH3 mimetics with Natural Killer (NK) cells as a novel therapeutic strategy in pediatric rhabdomyosarcoma

Non-Hodgkin lymphoma in children and adolescents: Important aspects of diagnosis and new insights into the biology of mature B-cell neoplasia.

AG13 AG Geschichte und Ethik der Pathologie - Special topic: Aufbau und Erhalt pathologischer Sammlungen

Rudolf Virchow and His Pathological Specimens

The Military Pathological Collection of the Bundeswehr Medical Service

How to handle unknown fluids in fluid-preserved collections

Integration of historical macro-pathological specimens in current medical digital teaching

Soft tissue tumors and its aid technologies for diagnosis over time: immunohistochemistry and fluorescence-in-situ-hybridization.

AG14 AG Informatik, digitale Pathologie und Biobanking I

Deep learning-based prediction of upper tract urothelial cancer molecular subtypes from histopathological slides

Deep Learning outperforms conventional laboratory staining methods in predicting molecular subtypes of gastric adenocarcinoma.

Vendor Agnostic vs. Proprietary User Interfaces for AI Solutions in Digital Pathology

Going digital in Pathology – Where to store the big data?

High resolution multiclass semantic segmentation in prostate

Quality aspects for benchmark datasets for AI solutions in pathology

Unsupervised image analysis and linear expression of focal adhesion kinase (FAK) as a prognostic digital biomarker in colon cancer and precursor lesions

AG14 AG Informatik, digitale Pathologie und Biobanking II

Evaluation of an artificial intelligence approach to assist the detection of melanoma metastasis in lymph nodes

Fast-track AI-assisted immunohistochemical stain evaluation and statistical analysis of TMAs

Pre-Scan QC – Preliminary Results for Artefact Detection in Slide Overview Images

Syntax and Semantics for interoperable, standard-based, Anatomic Pathology Structured Reports (APSR)

Deep learning-assisted differential detection of pancreatic intraepithelial neoplasia and characterization of inflammatory structures in proximity

Extracting HCC-related Data from histological reports by using a Dependency Grammar

P01 Postersitzung Gastroenteropathologie I

Differentiation of inflammatory alterations in esophageal biopsies using FFPE proteomics (LC-MS/MS).

Putative tumor biological significance of PCLO in gastric cancer – Results from a large Central European cohort

Elevated microsatellite instability at selected tetranucleotide repeats (EMAST) in gastric cancer: a distinct microsatellite instability type with potential clinical impact?

Paradox inflammatory manifestation of acute appendicitis in anti-inflammatory Januskinase inhibitor-based therapy with Tofacitinib (XeljanzTM) for ulcerative colitis

Proteome-based (LC-MS/MS) characterization of microsatellite stable (MSS) and unstable (MSI) colorectal cancer

Murine Organoids as a Model System for Quantitative Evaluation of Tumor Antigen Presentation

Expression patterns of HSP90, HSP70 and MLKL in human colon cancer

The impact of cancer-associated fibroblasts on the biology and progression of colorectal carcinomas

Peritoneal tumor lesions - representative case series on rare diagnoses at a tertiary center

Rare case of diverticulitis of the ascending colon in Western countries

Representative spectrum of various appendix vermiformis-associated lesions (case series)

Acute Epiploic Appendagitis - a rare differential diagnosis of acute abdomen

Uncomplicated diverticulitis of the sigmoid colon in ongoing immunosuppressive and anti-inflammatory treatment of a female patient with rheumatoid arthritis (RA)

P01 Postersitzung Gastroenteropathologie II

Lipid droplets and associated proteins in viral hepatitis

Impact of ALDH1A1 on patient overall survival in intrahepatic cholangiocellular carcinoma and the tumor stroma

Epigenetic differences between HCC and iCCA reveal clinically relevant targets as potential biomarkers for individualized therapy

A clinicopathologic and immunohistochemical analysis of precursor lesions of pancreatic ductal adenocarcinoma.

Resistin activating key signaling pathways in pancreatic ductal adenocarcinoma

Leptin and tumor plasticity in pancreatic ductal adenocarcinoma

Proteomic Analysis of Primary PDAC and Metastasis

CPA1 and CELA3B are highly specific markers for the diagnosis of pancreatic acinar cell carcinoma

The impact of adjuvant therapy on outcome in UICC stage I pancreatic cancer

Left hepatic lobe within an epigastric hernia

Unusual inflammation as appendicitis epiploicae in immunosuppressants after liver transplantation

P02 Postersitzung Uropathologie

Response to adjuvant chemotherapy of luminal and basal phenotypes and molecular subtyping of “double-negative” muscle-invasive bladder cancer

Proteomic analysis of non-muscle invasive and muscle invasive bladder cancer highlights distinct subgroups

Molecular subtypes associate with the immunological microenvironment in upper tract urothelial carcinomas

High NECTIN4 protein levels in urothelial high-risk non-muscle-invasive bladder cancer

Nectin4 expression in muscle-invasive bladder cancer

Expression of the enfortumab vedotin target Nectin-4 strongly decreases during metastatic progression of urothelial carcinoma.

Somatostatin receptor (SSTR) mRNA expression reveals distinct subtypes of neuroendocrine-like bladder cancer and bears potential for radioligand therapies

Tumor budding in pT1 high grade urothelial carcinoma of the urinary bladder: an independent

parameter to estimate the risk of progression

MALDI mass spectrometry imaging - Prognostic pathways and metabolites for renal cell carcinomas

The role of CD103+ tissue resident T-lymphocytes in ccRCC and distant metastases

Targeting CDK7 - Characterization of the CDK7-MED1 Signaling Axis in Prostate Cancer Tissue

PSMA as prognostic biomarker – results of internal prostate needle biopsies

Analysis of histological inflammation and atrophy in correlation with mpMRI changes in men without prostate cancer

The SDF-1/CXCL12 polymorphism rs1801157 does not influence the risk for penile cancer development in Caucasians

P03 Postersitzung Knochen-, Gelenk- und Weichgewebspathologie

Case report: IgG4-related pseudotumor with multinucleated giant cells in the axilla

Effects of sensory and sympathetic neurotransmitter on histological callus maturation during osteoporotic fracture healing

Whole-Exome Sequencing of Chordoma including a Case with 4 Recurrences over 15 Years
Pitfall of Differential Diagnostic Challenge: Keratin-positive Abdominal Gastrointestinal Stromal Tumors (GIST).

Soft tissue tumors and its aid technologies for diagnosis over time: immunohistochemistry and fluorescence-in-situ-hybridization.

P04 Postersitzung Hämatopathologie

Molecular analysis of blastic plasmacytoid dendritic cell neoplasm reveals two distinct age-dependent subgroups and a role for clonal hematopoiesis in elderly patients

PTP1B Δ 6 und PTP1B Δ 2-4 – Functional analyses of the oncogenic variants of PTP1B

SOCS1 (Silencer of Cytokine Signaling 1) expression in B-cell derived cell lines and tissue.

Progressive cauda syndrome with paraparesis and sensory symptoms due to extranodular high grade large B-cell lymphoma with extensive intravascular component (autopsy case report)

Molecular analysis of myeloid sarcoma reveals a mutational profile similar to AML, but with some differences and enables separation from BPDCN

Time-dependent altered changes of neoplastic features in JAK2-mutated cells upon JAK1/JAK2 inhibition

P05 Postersitzung Herz-, Gefäß-, Nieren- und Transplantationspathologie

Monstrous pseudoaneurysm of the subclavian artery secondary to clavicle fracture

Impact of various factors and parameters onto the early postoperative and long-term outcome of vascular surgical and image-guided treatment of suture aneurysms

NUP133 controls nuclear pore assembly, transcriptome composition and cytoskeleton regulation in podocytes

Alteration of glycocalyx on endothelium of peritubular capillaries in chronic kidney disease

Large-scale segmentation and feature extraction for digital nephropathology

All-Body-Cavity (ABC)-Scopy: A Feasibility Study for an Endoscopic Method of Minimal Invasive Autopsies

Adrenal tropism of SARS-CoV-2 and adrenal findings in patients with severe fatal COVID-19: a post-mortem case series

P06 Postersitzung Gynäko- und Mammopathologie

Struma ovarii – associated with hyperthyreoidism

Squamous cell carcinoma arising from a mature cystic ovarian teratoma – histomorphologic and molecular findings

Epithelial-mesenchymal transition (EMT) in vulvar cancer

Carbonic anhydrase XII as biomarker and therapeutic target in ovarian carcinomas

Differentiated High-Grade Squamous Intraepithelial Lesion of the Uterine Cervix (d-HSLI, d-CIN 3) as a Distinct Precursor Lesion in Keratinising HPV-negative Squamous Cell Carcinoma of the Uterine Cervix

Evaluation of P16/Ki67 (CINtecplus) and L1-Capsid compared with HPV-Genotyping in cervical cytology in women above 35 years old with focussing in patients with Group IIp (ASC-US, Atypical squamous cell of undetermined significance)

Molecular classification of endometrioid endometrial carcinoma with minimal deviation-like pattern (MDA-like ECX)

Breast Cancer: Characterization of Hormone Receptor Status Using Mass Spectrometry Imaging

Co-expression of Transcription Factor AP-2beta (TFAP2B) and GATA3 in human mammary epithelial cells with intense, apicobasal immunoreactivity for CK8/18

Breast cancer tumor microenvironment in sub-Saharan Africa reveals features associated with worse survival among West African Patients

P08 Postersitzung Thoraxpathologie

Cancer or Systemic Vasculitis: a solitary pulmonary nodule in a patient with Granulomatosis with Polyangiitis mimicking malignancy

Severe adverse events of immune checkpoints inhibitors: 3 autopsy cases

Tumor spread through airspaces (STAS): a comprehensive analysis of clinicopathological features in a real-world lung adenocarcinoma cohort

Whole-exome sequencing confirms proteasomal processing alterations as a novel mechanism of immune escape, stratifying patients for immune checkpoint blockade

P11 Postersitzung Molekularpathologie

Laser microdissection (LMD) as a valuable tool for analyzing intratumoral molecular heterogeneity in colorectal cancer

Identification of a tumor-based protein biomarker panel to predict the time to recurrence for intrahepatic cholangiocarcinoma

Isotachopheresis in comparison to bead based extraction of nucleic acids from FFPE tissue and its use for routine diagnostics.

Tryptic peptide mass spectrometry imaging of solid tumors via reproducible data analysis workflows

Pan-cancer in silico analysis of the Tripartite family members (TRIM)

Peptide Mass Spectrometry Imaging (MSI) of Pancreatic Cancers and the Application of a Powerful and User-friendly Analysis Pipeline

Imipramine induces GSDME-mediated pyroptosis through upregulating NRP1

Carcinoembryonic antigen-related cell adhesion molecule 6 (CEACAM6) promotes metastatic spread to the lung in advanced prostate cancer

TMB in limited FFPE tissue specimens, pleural effusions and bronchoalveolar lavages of NSCLC cases

A comprehensive validation of targeted next-generations sequencing panels to detect gene fusions and variants, including MSI, in pan-tumor samples

Comparison of two distinct methods for the detection of PIK3CA somatic mutations in formalin-fixed and paraffin-embedded tissue of patients with breast cancer: Real-Time PCR versus Next-Generation Sequencing (NGS)

Towards Cohort-Wide Translational Proteome Studies: Reproducible Proteomic Workflows and Their Application to Skin and Cancer Diseases

Subcellular mitochondrial alterations in hepatocytes and brown adipose tissues from ChREBP knock out mice during long term choline deficient diet

P12 Postersitzung Kinder- und Fetalpathologie

Intrauterine fetal demise in extensive SARS-CoV-2-associated placental maternal vascular malperfusion in the setting of SARS-CoV-2 placentitis

Adrenocortical carcinoma (ACC) in an infant with Cushing's syndrome and virilization

Lipoblastoma as a representative example of rare soft tissue tumor lesions in infants with its challenging diagnostic and surgical management

P14 Postersitzung Informatik, digitale Pathologie und Biobanking

Snomed CT – a promise for structured reporting and interoperability

Deep learning quantified stroma and lymphocyte are independent predictors for overall survival in pancreas cancer

Comparison of manual and automated digital image analysis systems for quantification of cellular protein expression

A machine learning approach to classify whole slide images by formalin-fixed paraffin-embedded or frozen section origin

Vascular remodeling is a crucial event in the early phase of hepatocarcinogenesis in rodent models for liver tumorigenesis.

Ex vivo fluorescence confocal microscopy on diagnostic ultrasound-guided core needle biopsies of the liver: A feasibility study from a tertiary hospital

The Explainability Paradox: Challenges for xAI in Digital Pathology

Deep Learning in Pancreatic Tissue: Automatic identification of anatomical structures and diseases.

Federated Learning for Breast Cancer Classification

Diagnosis of signet ring cell carcinoma of the upper gastrointestinal tract using deep learning

Enabling stain independence for deep learning-based segmentation and quantification in kidney histopathology

Nuclei Detection and Segmentation using Instance-Segmentation Networks

Paving the way for cross-border biobank cooperation: The Bavarian-Czech Biobank Landscape Project

3D Visualization of Blood Vessels

Multimodal deep learning model for prognosis prediction in clear cell renal cancer

Patient-level proteomic network prediction by explainable artificial intelligence

Connecting a customized data management system to the GBA Sample Locator using an ETL process

Autorenindex

Keynote

DGP02.01 Mikroskop adé?

DGP02.01

Goodbye, microscope!

P. Ströbel

Universitätsmedizin Göttingen, Institut für Pathologie, Göttingen, Germany

Digitale Scans histologischer Präparate (whole slide images, WSI) werden in der Pathologie schon seit geraumer Zeit verwendet, initial allerdings vor allem in Forschung und Lehre. Durch die Entwicklung von Hochdurchsatz-Scannern eröffnet sich jetzt auch die Möglichkeit, digitale Slides in die Routinediagnostik zu integrieren. An zahlreichen Standorten ist die digitale Diagnostik inzwischen als fester Bestandteil der täglichen Arbeit etabliert und hat das Mikroskop in Teilen oder sogar vollständig abgelöst. In diesem Beitrag soll dargestellt werden, wie die Einführung digitaler Slides in einem akademischen Institut den Arbeitsalltag verändert hat und welche potentiellen Konsequenzen und Möglichkeiten sich hieraus ergeben.

Highlights

H03 Pressekonferenz - Preisverleihungen

H03.01

Imaging intact human organs with local resolution of cellular structures using hierarchical phase-contrast tomography

M. Ackermann

Universitätsmedizin der Johannes Gutenberg-Universität, Mainz, Germany

Imaging intact human organs from the organ to the cellular scale in three dimensions is a goal of biomedical imaging. To meet this challenge, we developed hierarchical phase-contrast tomography (HiP-CT), an X-ray phase propagation technique using the European Synchrotron Radiation Facility (ESRF)'s Extremely Brilliant Source (EBS). The spatial coherence of the ESRF-EBS combined with our beamline equipment, sample preparation and scanning developments enabled us to perform non-destructive, three-dimensional (3D) scans with hierarchically increasing resolution at any location in whole human organs. We applied HiP-CT to image five intact human organ types: brain, lung, heart, kidney and spleen. HiP-CT provided a structural overview of each whole organ followed by multiple higher-resolution volumes of interest, capturing organotypic functional units and certain individual specialized cells within intact human organs. We demonstrate the potential applications of HiP-CT through quantification and morphometry of glomeruli in an intact human kidney and identification of regional changes in the tissue architecture in a lung from a deceased donor with coronavirus disease 2019 (COVID-19).

Super-enhancer-based identification of a BATF3/IL-2R-module reveals vulnerabilities in anaplastic large cell lymphoma

H.-C. J. Liang

University of Pennsylvania, Pathology and Laboratory Medicine, Philadelphia, United States of America

Anaplastic large cell lymphoma (ALCL), an aggressive CD30-positive T-cell lymphoma, comprises systemic anaplastic lymphoma kinase (ALK)-positive, systemic ALK-negative, primary cutaneous and breast implant-associated ALCL. Prognosis of some ALCL subgroups remains unsatisfactory, and effective second-line treatment options are still lacking. To identify genes defining ALCL cell state and dependencies, we here characterize super-enhancer regions by genome-wide H3K27ac ChIP-seq. In addition to known ALCL key regulators, the AP-1-member *BATF3* and *IL-2 receptor (IL2R)*-components are among the top hits. Specific and high-level IL2R expression in ALCL correlates with BATF3 expression. Confirming a regulatory link, IL-2R-expression decreases following *BATF3* knockout, and BATF3 is recruited to *IL2R* regulatory regions. Functionally, IL-2, IL-15 and Neo-2/15, a hyper-stable IL-2/IL-15 mimic, accelerate ALCL growth and activate STAT1, STAT5 and ERK1/2. In line, strong IL-2R α -expression in ALCL patients is linked to more aggressive clinical presentation. Finally, an IL-2R α -targeting antibody-drug conjugate efficiently kills ALCL cells *in vitro* and *in vivo*. Our results highlight the importance of the BATF3/IL-2R-module for ALCL biology and identify IL-2R α -targeting as a promising treatment strategy for ALCL.

H03.03

Alarm in the bone marrow - how to untangle fibrosis in the bone marrow

R. Schneider-Kramann

Universitätsklinikum RWTH Aachen, Institut für Zell- und Tumorbologie, Aachen, Germany

The functional contributions of individual cellular components of the bone-marrow microenvironment to bone marrow fibrosis in patients with myeloproliferative neoplasms (MPNs) are poorly understood. We aimed to generate a comprehensive single cell map of the non-hematopoietic stroma in MPNs on a single-cell level in our established murine models and patient samples. Our analysis revealed two distinct mesenchymal stromal cell (MSC) subsets as fibrosis-driving cells. MSCs were functionally reprogrammed in a stepwise manner with loss of their MSC characteristics and initiation of differentiation in the pre-fibrotic and acquisition of a pro-fibrotic and inflammatory phenotype in the fibrotic stage. The expression of the alarmin heterocomplex S100A8/S100A9 in MSC marked disease progression toward the fibrotic phase in murine models and in patient bone marrow biopsies and plasma samples. Tasquinimod, a small-molecule inhibiting S100A8/S100A9 signaling which was already applied in clinical phase III trials for prostate cancer, significantly ameliorated the MPN phenotype and fibrosis in JAK2V617F-mutated murine models. These data highlighted that S100A8/S100A9 is an attractive therapeutic target in MPNs and specifically an actionable biomarker. Based on these findings we will start a proof-of-concept clinical trial this year - TasquForce MPN.

DGP01 Weichgewebe- und Knochentumoren - State of the art

DGP01.01

Abdominal soft tissue tumors

E. Wardelmann

Universitätsklinikum Münster, Gerhard-Domagk-Institut für Pathologie, Münster, Germany

Das Spektrum intraabdomineller Weichgewebstumoren ist wie auch in sonstigen Körperabschnitten groß und umfasst weit mehr als gastrointestinale Stromatumoren, auch wenn diese zumindest im Gastrointestinaltrakt die häufigsten mesenchymalen Tumoren darstellen. Nach einem kurzen Überblick über die aktuelle molekulare Klassifikation von GIST gibt der Vortrag verschiedenste Differentialdiagnosen zu bedenken, von denen ein Teil bereits immunhistochemisch abgegrenzt werden kann. Hierzu zählen insbesondere gutartige Läsionen wie z. B. Leiomyome und Schwannome, während bei den malignen Tumoren zumeist zusätzlich eine molekularpathologische Methodik erforderlich ist, die je nach Entität DNA- oder RNA-basiert sein kann. Gerade bei den translokationsgetriebenen Weichgewebstumoren wurde hierdurch neue Tumorentitäten definiert, die noch nicht in der aktuellen WHO-Klassifikation auftauchen, wie z. B. die *GLI*-translozierten Tumoren.

DGP01.02

Soft tissue and bone tumors of head and neck

D. Baumhoer

Universitätsspital Basel, Pathologie, Basel, Switzerland

Im Kopf-/Halsbereich kommen eine Vielzahl verschiedener mesenchymaler Tumoren vor, einige davon besonders häufig oder sogar ausschließlich in dieser Region. Der Vortrag gibt einen Überblick über diese Läsionen entsprechend der neuen WHO-Klassifikation (5. Auflage) und weist auf klinische Besonderheiten und diagnostische Pitfalls hin.

DGP01.03

Giant cell-containing tumors of bone and differential diagnoses

W. Hartmann

Universitätsklinikum Münster, Sektion für Translationale Pathologie, Gerhard-Domagk-Institut für Pathologie, Münster, Germany

Osteoclastic giant cells represent a common cellular component of lesions arising in bone. Highlighting this morphological finding, the current WHO classification of bone tumors defines a diagnostic group comprising aneurysmal bone cyst, giant cell tumor of bone and non-ossifying fibroma, which may display morphologic similarities while being distinct with regard to molecular and biological features. Based on a survey of these tumors the talk discusses common and rare lesions that may enter differential diagnosis.

Mehrkernige Riesenzellen sind in verschiedensten ossären Läsionen häufig anzutreffen. Die aktuelle WHO-Klassifikation der Knochentumoren definiert über den morphologischen Befund mehrkerniger Riesenzellen mit der aneurysmatischen Knochenzyste, dem Riesenzelltumor des Knochens und dem nicht-ossifizierenden Fibrom eine Gruppe osteoklastärer Riesenzell-reicher Tumoren, welche hinsichtlich ihres Gewebebildes Ähnlichkeiten aufweisen können, sich jedoch molekular und biologisch deutlich unterscheiden. Beginnend mit der Darstellung dieser Gruppe gibt der Vortrag eine Übersicht über differenzialdiagnostisch relevante Läsionen.

Small round cell sarcomas

T. Grünwald^{1, 2, 3}

¹German Cancer Research Center (DKFZ), Division of Translational Pediatric Sarcoma Research, Heidelberg, Germany, ²Heidelberg University Hospital, Institute of Pathology, Heidelberg, Germany, ³Hopp-Children's Cancer Center Heidelberg (KITZ), Heidelberg, Germany

Background

Small round cell sarcomas (SRCs) are a dynamic and increasing group of highly aggressive mesenchymal cancers mainly affecting children, adolescents, and young adults. They are overall characterized by their histomorphological similarities and poor prognosis. In past years, several distinct SRCs entities emerged in reference to Ewing sarcoma as the prototype of an undifferentiated small round cell tumor, which is driven by pathognomonic *FET::ETS* fusions (in 85% *EWSR1::FLI1*).

Methods

An overview on the current state-of-the-art based on a critical literature survey and own data is presented.

Results

The advent of modern high throughput technologies had a transformative effect on the discovery and reclassification of SRCs. Accumulating genetic, epigenetic, and transcriptomic data in integration with emerging clinicopathological information and experimental models culminated in the inclusion of the new chapter 'undifferentiated SRCs of bone and soft tissue tumors' in the 2020 WHO classification of soft tissue and bone tumors. Although new technologies will continue to identify even rarer SRCs entities, this presentation focusses on the most prevalent fusion-driven morphological mimics of Ewing sarcoma, including *EWSR1/FUS::non-ETS*-fused round cell sarcoma (mainly *EWSR1/FUS::NFATC2*), *CIC*-rearranged sarcomas (mainly *CIC::DUX4*) and sarcomas with *BCOR* genetic alterations (mainly *BCOR::CCNB3*). In addition, desmoplastic small round cell tumor (DSRCT), which was first described as a separate entity in 1984 and is characterized by an *EWSR1::WT1* fusion, will be discussed. Although DSRCT is currently not listed among undifferentiated SRCs of bone and soft tissue in the WHO classification, it shares the undifferentiated small-round cell morphology as well as many other genetic and clinicopathological features with SRCs. In most cases, an accurate classification of SRCs is now achievable through a combination of immunohistochemical/histological and modern molecular pathology analyses including the detection of the characteristic gene fusions.

Conclusion

Further dissection of SRCs and the underlying molecular pathomechanisms holds the promise to identify

novel prognostic and predictive biomarkers and therapeutic targets that may help to overcome clinical challenges in these difficult-to-treat entities. In this context, SRCs represent a paradigmatic example of how the integration of modern technologies can revolutionize routine diagnostics and clinical oncology.

DGP01.05

Vascular and perivascular Tumors

U. Flucke

Radboud University Nijmegen Medical Center, Department of Pathology, Nijmegen, The Netherlands

Vascular and perivascular tumors are rare comprising different benign and malignant entities with a biological diversity.

Due to recently identified molecular characteristics the neoplasms are better defined revealing often a broader clinicopathological spectrum than primarily thought. Better defined subgroups of e.g. angiosarcomas provide new therapeutical options.

DGP02 Automation

Automation and Application of Robotics in the Pathology Laboratory

H. Herbst¹, H. Herbst², C. Hofmann³

¹Vivantes Netzwerk für Gesundheit GmbH, Fachbereich Pathologie, Berlin, Germany, ²Institut für Pathologie, Städtische Kliniken Karlsruhe, Karlsruhe, Germany, ³Karlsruher Institut für Technologie (KIT), wbk Institut für Produktionstechnik, Karlsruhe, Germany

Background

During the previous 20 years, numerous technical innovations were introduced to the histopathology laboratory, providing tools for improved standardization and occupational safety.

Methods

Digital tracking serves as a backbone accompanying the workflow from labeling of cassettes and slides to final steps of preparation of whole slide images and achieving of blocks and sections.

Results

Multifunctional devices eliminated time consuming manual work prone to mistakes and loss of materials. At present, collaborative robots take over manual work that was considered to be exclusive to humans.

Conclusion

The advent of these new technologies is expected to ameliorate the increasing staffing shortage in the laboratory and on the side of histopathologists as well.

Workflow efficiency and change management in a pathology laboratory

T. Rüdiger

Städtisches Klinikum Karlsruhe, Pathologie, Karlsruhe, Germany

A laboratory in an institute of pathology can be regarded a production system. Incoming specimens are transformed into slides to be read by pathologists.

To improve the workflow, the first step is understanding it. This can be achieved by workshops and workflow analyses that are offered by many companies as part of their marketing strategy. Best would be to acquire a so-called digital twin that models the flow of objects through the laboratory and allows to simulate the effect of measures taken.

The principles of LEAN demand to only perform necessary steps in the workflow and to reduce the storage time between steps. An effective culture to deal with defects needs to be introduced to deal with defects to prevent them from multiplying during later steps in the workflow process. Thus, the technicians need to control inbound material before working on it and must be stimulated to report and mend any defect detected even if this results in delays.

Automation is another factor to improve workflow. As the solutions provided by the industry are partial, these usually effect workflow. They open chances for higher throughput but often need a change in workflow for the technicians and doctors. Depending on the solution, change management will take between minutes and several months to learn about the strengths and weaknesses of a solution and alter the workflow.

From a process perspective, the most difficult point the processing of large batches resulting from overnight embedding. Automation nowadays allows processing in smaller batches, but this needs to change the workflow from people moving through the laboratory together with the objects to people staying at their workplace and awaiting the objects to arrive.

This results in continuous workflow and objects will remain at different stages of the process at the end of the day. On one side it proves difficult for both technicians and doctors to cope with the fact that there is no defined end of the working day when everything is done. On the other side it allows to deal with fluctuating numbers of cases very efficiently, because the processing time of a biopsy until the diagnosis-ready H&E stain is only four hours. By continuously introducing specimens into the workflow day-to-day differences in case numbers can be smoothed. This results in more predicable working hours and less overtime hours thus leading to higher job satisfaction.

Automated image acquisition as an integrative key of a seamless digital pathology workflow

R. Huss^{1,2}, C. Herbst¹, J. Raffler², T. Schaller¹, B. Märkl¹

¹*Universitätsklinikum Augsburg, Institut für Pathologie und Molekulare Diagnostik, Augsburg, Germany,*

²*Universitätsklinikum Augsburg, Institut für Digitale Medizin, Augsburg, Germany*

Background

The digitization of an existing pathology workflow is a significant challenge requiring relevant financial resources, a lasting commitment of all employees and the selection of the appropriate tools and technologies. Each laboratory has to decide on their motivation to become digital, e.g. to establish paperless processes or to implement artificial / machine intelligence to support and accelerate clinical decisions including standardized reporting or to improve quality assurance to ensure lasting compliance with standards and regulations. There are different areas within the established pathology workflow where to initiate a digital process and in which order. Like many other histopathology sides we started with internal survey of a selection of available image acquisition solutions.

Methods

A technical side-by-side comparison including hands-on long-term experience of different scanning devices and platforms was performed and continuously assessed by the laboratory staff as well as technical and medical personnel. The evaluation included machine performance, technical robustness, high throughput and research capabilities, interoperability with existing systems as well as the connectivity to the laboratory information system (LIS) or image archiving system (PACS) but also the perceived quality of the images displayed on the diagnostic screen.

Results

After the scanning of a vast number of routine and archival slides, we concluded that no image acquisition platform is currently able to support the entire diagnostic value chain in a digital diagnostic and research histopathology laboratory. Besides mostly minor technical issues with an inconsistent quality of the glass slides, one of the main obstacles are proprietary image formats that prevent the connectivity of stand-alone devices with existing or information systems. This interferes with the integration of most scanning devices into an automated workflow, and the seamless use and application of artificial and machine intelligence solutions.

Conclusion

The acquisition of histological images in research and clinical practice is at the center of most efforts to initiate the digital transformation in pathology. While most scanners show a robust performance, there are existing limitations in certain technical capabilities and a generally incomplete coverage of the entire digital workflow. Therefore, digital pathology laboratories need either to utilize different image-scanning devices or compromise on the level of digital integrity.

Process optimization in preparation of a digital pathology workflow and the use of machine intelligence

R. Huss^{1,2}, M. Braunger³, C. Bartenschlager³, J. Raffler², J. O. Brunner³, B. Märkl¹

¹Universitätsklinikum Augsburg, Institut für Pathologie und Molekulare Diagnostik, Augsburg, Germany, ²Universitätsklinikum Augsburg, Institut für Digitale Medizin, Augsburg, Germany, ³Universität Augsburg, Lehrstuhl für Health Care Operations / Health Information Management, Augsburg, Germany

Background

Digital pathology and the use of machine intelligence (MI) solutions will change the workflow in a histopathology laboratory as we know it today. Many digital activities focus on the use of applications on scanned images to assist the pathologist in identifying defined regions of interests (RoI), e.g. lymph node metastasis, counting IHC positive cells, describing spatial relationships, quantifying even subtle immune signatures and assisting in making diagnostic and increasingly more predictive decisions. However, the optimization of the entire laboratory workflow which is still depending on qualified human resources is at least as important as the seamless connectivity and interoperability of the available technical assist and hardware solutions including functional and standardized interfaces and monitoring its quality. A highly efficient deployment of the laboratory staff is an indispensable prerequisite for generating the advantages that digital pathology promises.

Methods

We used the tools of economic process analysis and management to describe and visualize the daily workflow in a routine histopathology and molecular laboratory to prepare for digitization from receiving and documenting the incoming sample until a full and comprehensive pathology report is signed off.

Results

All along this way there are currently many manual and iterative working steps. Usually it starts with the digital registration and documentation allowing sample traceability throughout the following manual steps like gross examination, cut-up, paraffin embedding, cutting and staining. Digitization usually continuous with the acquisition of digital images mostly in proprietary formats of the scanner companies. If those scanning devices are connected to electronic pathology system it is possible to report cases but also to use an MI-assisted interpretation of the high-dimensional complexity in heterogeneous tissue and its spatial and immunological communication network as well as the integration of big molecular and metadata also for research purposes.

Conclusion

Nevertheless, the workflow analysis of the existing manual process revealed many redundant steps prone for error and inconsistent quality measures still tying up qualified personnel. The imminent integration of digital solutions along the entire histopathology and molecular workflow will require an additional human and financial investments along with a disruptive processes optimization including automation robotics and MI-

assisted decision support.

DGP03 Referenzpathologie, Register

DGP03.02

Reference Pathology Breast

H. H. Kreipe

Institut für Pathologie, Medizinische Hochschule Hannover, 30625 Hannover, Germany

In unserem Institut stattfindende Zweitbefundungen von Mammagewebeproben lassen sich drei Kategorien zuordnen. Anders als bei selteneren Erkrankungen, wie z.B. Knochentumoren, wird eine Zweitmeinung durch die behandelnden Kliniker nur in Ausnahmen als notwendig angesehen und das vor allem aufgrund von Diskrepanzen. Solche Diskrepanzen betreffen z.B. einen divergierenden HER2 Status zwischen Stanzbiopsie und Resektat oder Primärtumor und Metastase. Gelegentlich kommen auch Diskrepanzen in der histologischen Klassifikation und dem Grading vor, bei denen das klinische Bild und die histologische Klassifikation nicht plausibel miteinander vereinbar erscheinen. Die zweite Kategorie der Zusendungen zur Zweitmeinung rekrutiert sich aus der Pathologie selbst, indem lokale Erstbefunder um Unterstützung bei der Klassifikation seltener Läsionen, wie z.B. Spindelzelltumoren, fibrosierten Papillomen bzw. intraduktalen Adenomen, neuroendokrinen Tumoren oder der mikroglandulären Adenose, bitten. Die umfangreichste und 3. Kategorie wird durch Fälle für die Referenzpathologie im Rahmen von prospektiven klinischen Studien in Zusammenarbeit mit der Westdeutschen Studiengruppe (ADAPT-Studien) ausgemacht, wobei bis heute mehr als 10.000 Fälle in dieses Studienregister eingegangen sind. Ein Ergebnis dieser Studientätigkeit ist z.B. das dynamische Ki67 als neuer prognostischer Marker beim luminalen Mammakarzinom, mit dem anhand einer Kurzzeit präoperativen endokrinen Therapie von 3-4 Wochen anhand des Ki67 Abfall auf $\leq 10\%$ erkennbar wird, ob die Patientin mit einer endokrinen Therapie ausreichend behandelt ist und auch bei Lymphknotenbefall (1-3) oder prämenopausalem Status auf eine zusätzliche adjuvante Chemotherapie verzichtet werden kann (Nitz U. et al. J Clin Oncol. 2022 im Druck; doi: 10.1200/JCO.21.02759). Ein anderer Befund aus der Studienreferenzpathologie sind neue Biomarker zur Prädiktion der endokrinen Resistenz (Grote I. et al. Cancer Med. 2021;10:8581-8594).

Consultation pathology - Lung

S. Berezowska

Institut Universitaire de Pathologie, Centre hospitalier universitaire vaudois (CHUV) et Université de Lausanne, Lausanne, Switzerland

Consultation pathology plays an important role in many areas of diagnosing lung diseases. Regarding neoplasms, consultations may be necessary (a) if rare entities are in the differential diagnosis, (b) if specifically defined tumors are to be verified or excluded, and the special stains or molecular markers are not available in the primary pathology lab (e.g. thoracic SMARCA4-deficient undifferentiated tumour), or (c) for comprehensive molecular characterisation of carcinomas, increasingly gaining importance due to an extended armamentarium of oncological therapeutics. In infectious diseases of the lung, consultations may be requested for morphological typification of fungi and parasites or detection and typification of viral and bacterial disease. Those may be provided by specialised pathologists, the Robert Koch Institute in Germany or also the Center for Disease Control and Prevention in the US. Interstitial lung diseases (ILDs) are rare and warrant a specialized interdisciplinary team for providing optimal diagnoses, consisting of a specialized pathologist, a specialized radiologist, and pulmonologist and in some centers also a rheumatologist. Thus, a full interdisciplinary consultation is advisable when ILDs are considered. Pneumoconioses are chronic lung diseases induced by exposure to mineral dust or metal. Specialized laboratories are consulted for detecting the causative agent in the tissue. This is usually commissioned by insurance companies investigating the possibility of an occupational illness, and requires either formalin-fixed tissue (optimal) or FFPE tissue blocks harboring non-neoplastic lung parenchyma. Pediatric lung pathology presents a challenge to pathologists outside of dedicated centers, as developmental lung pathology, pediatric ILDs and lung neoplasms are rare. Inclusion of patients into clinical studies, not only in the setting of pediatric diseases, often requires second opinion by an assigned central pathology. Likewise, surveillance biopsies after transplantation may be requested to be centrally re-evaluated. Finally, no presentation on consultation practice would be complete without mentioning the advent of digital pathology and its possibilities for slide sharing, global consultations and collaborations and more systematic telepathology solutions. In summary, consultations may be frequently necessary in different areas of lung pathology and are in some settings facilitated by digital pathology practice.

DGP03.04

Consultation pathology of testis tumors

F. Bremmer

University Medical Center, Institute of Pathology, Göttingen, Germany

Im Jahr 2018 wurden laut Robert Koch Institut 4160 Neuerkrankungen unter dem Begriff „Hodenkrebs“ registriert. Davon sind etwa 60% Seminome, 35% nicht-seminomatöse Keimzelltumoren und 5% „andere“ Entitäten/Tumoren. Bei etwa 1800 Fachärzten für Pathologie wird man, je nach Einsendegut, einen Hodentumor eher selten begutachten. Zusätzlich weisen Hodentumoren ein sehr großes morphologisches Spektrum auf. Ein dritter wichtiger Punkt ist auch die eingeschränkte Verfügbarkeit von speziellen Antikörpern in der Immunhistochemie, die vielleicht nicht in jedem Institut zur Verfügung stehen, für die exakte Diagnose aber von großer Bedeutung sind. Diese Punkte führen dazu, dass Hodentumoren eine diagnostische Herausforderung darstellen.

Die häufigsten Konsilanfragen betreffen: Die histologische Subtypisierung von Keimzelltumoren, die genaue Diagnose eines Gonadenstromatumors, Teratome mit reifen und unreifen Gewebearten, Teratome mit somatischer Malignität, die biologische Einordnung der Tumoren des Gonadenstromas und mesenchymale Tumoren der paratestikulären Region.

In diesem Vortrag sollen die diagnostischen Probleme, die Anforderungen und Herausforderungen der Referenzpathologie für Hoden aufgezeigt, Lösungsansätze vorgestellt und der weitere Ausblick diskutiert werden.

Development and current challenges of central pathology for malignant lymphomas

W. Klapper

Institut für Pathologie, Sektion Hämatopathologie, UKSH Campus Kiel, Kiel, Germany

Background

Kaum ein Gebiet der Pathologie ist so eng mit dem Begriff der „Referenzpathologie“ verknüpft wie die Diagnostik maligner Lymphome. Auf Initiative der Deutschen Gesellschaft für Pathologie führte Prof. Dr. Dr. h.c. mult. Karl Lennert im Jahr 1965 das „Lymphknotenregisters Kiel“ ein. Mit dieser für ihre Zeit innovativen Einrichtung wollte Lennert nicht nur die Kolleg*innen persönlich in der Diagnostik beraten sondern auch systematisch Gewebe und Daten für die Erforschung der Erkrankungen sammeln. Die Geschichte der Lymphompathologie im deutschsprachigen Raum ist durch Prof. Lennert und seine Schüler*innen über Jahrzehnte geprägt worden. Im 20. Jahrhundert war diese Einrichtung ein wegweisendes System, das der Deutschen Lymphomforschung weltweit Anerkennung gebracht hat. Heute ist das Prinzip der Zweitbefundung in einem spezialisierten Zentrum bei seltenen Erkrankungen ein etabliertes Mittel der Qualitätssicherung in der Pathologie.

Methods

Das Umfeld dieser „Referenzbefundung“ hat sich seit Lennert aber grundlegend geändert. Um zu verstehen, was „Referenzpathologie“ maligner Lymphome heute bedeuten kann, ist es notwendig, die Aufgaben einer solchen Tätigkeit im aktuellen Spannungsfeld von Krankenversorgung und Forschung neu zu bewerten und auszurichten.

Results

Die Erfahrungen aus den Jahrzehnten nach der Gründung des Kieler Lymphknotenregisters haben gezeigt, dass der Mehrwert von Referenzzentren vor allem durch die Verbindung von Krankenversorgung und Forschung sowie eine langfristige (unbefristete) Archivierung der Materialien entsteht. „Referenzzentren“ werden von akademischen Studiengruppen, wie z.B. dem Kompetenznetz Maligne Lymphome e.V., benannt. Der Begriff der „Referenzpathologie“ bezieht sich also letztlich nur auf die wenigen Gewebeproben von Patient*innen, die im Rahmen von Studien behandelt werden und damit zwar auf über 90 % der Kinder und Jugendlichen, aber nur 10 % der Erwachsenen mit einer Lymphomerkrankung in Deutschland. Im Rahmen dieser namensgebenden Tätigkeit steht vor allem die treuhänderische Gewebesammlungen für die Studiengruppen und Patient*innen sowie die translationale Forschung im Mittelpunkt der Arbeit von „Referenzzentren“. Diagnostische Kompetenz für maligne Lymphome ist aber nicht auf die von Studiengruppen benannten „Referenzzentren“ begrenzt und findet sich auch in vielen anderen z.T. sogar spezialisierten Pathologien.

Conclusion

Ich möchte die aktuellen Herausforderungen aus Sicht eines akademischen Referenzzentrums beschreiben.

DGP04 Rising Stars (Vorträge der Preisträger*innen des Gerhard-Domagk-, Rudolf-Virchow- und Novartis-Preises)

DGP04.01

Characterization of the Tumor Microenvironment by Highly Multiplexed Microscopy

C. Schürch

Universitätsklinikum Tübingen, Institut für Pathologie, Tübingen, Germany

Malignant neoplasms are highly complex ecosystems consisting of tumor cells and the tumor microenvironment (TME), which is composed of structural elements (vessels, fibroblasts, extracellular matrix) and a wide variety of infiltrating immune cell types of the innate and adaptive immune systems. The TME is the main site of tumor cell-immune cell interactions and plays a critical role in antitumoral immunity. Immunotherapies, such as immune checkpoint inhibitors, can affect the interactions between immune cell types and tumor cells in the TME, boost immune responses and lead to tumor elimination. Novel highly multiplexed microscopy techniques, which enable the detection of more than 50 simultaneous markers in tissues, facilitate the in-depth characterization of the TME at single-cell resolution in clinically relevant samples. Detailed knowledge about the cellular and spatial composition of the TME, the specific cell types and their functional properties, and cell-cell interactions—revealed by highly multiplexed microscopy—will improve our understanding of immunotherapies' mechanisms of action and reveal new potential therapeutic targets and predictive biomarkers.

Imaging intact human organs with local resolution of cellular structures using hierarchical phase-contrast tomography

M. Ackermann

Universitätsmedizin der Johannes Gutenberg-Universität, --, Mainz, Germany

Imaging intact human organs from the organ to the cellular scale in three dimensions is a goal of biomedical imaging. To meet this challenge, we developed hierarchical phase-contrast tomography (HiP-CT), an X-ray phase propagation technique using the European Synchrotron Radiation Facility (ESRF)'s Extremely Brilliant Source (EBS). The spatial coherence of the ESRF-EBS combined with our beamline equipment, sample preparation and scanning developments enabled us to perform non-destructive, three-dimensional (3D) scans with hierarchically increasing resolution at any location in whole human organs. We applied HiP-CT to image five intact human organ types: brain, lung, heart, kidney and spleen. HiP-CT provided a structural overview of each whole organ followed by multiple higher-resolution volumes of interest, capturing organotypic functional units and certain individual specialized cells within intact human organs. We demonstrate the potential applications of HiP-CT through quantification and morphometry of glomeruli in an intact human kidney and identification of regional changes in the tissue architecture in a lung from a deceased donor with coronavirus disease 2019 (COVID-19).

DGP04.03

Alarm in the bone marrow - how to untangle fibrosis in the bone marrow

R. Schneider-Kramann

Universitätsklinikum RWTH Aachen, Institut für Zell- und Tumorbologie, Aachen, Germany

The functional contributions of individual cellular components of the bone-marrow microenvironment to bone marrow fibrosis in patients with myeloproliferative neoplasms (MPNs) are poorly understood. We aimed to generate a comprehensive single cell map of the non-hematopoietic stroma in MPNs on a single-cell level in our established murine models and patient samples. Our analysis revealed two distinct mesenchymal stromal cell (MSC) subsets as fibrosis-driving cells. MSCs were functionally reprogrammed in a stepwise manner with loss of their MSC characteristics and initiation of differentiation in the pre-fibrotic and acquisition of a pro-fibrotic and inflammatory phenotype in the fibrotic stage. The expression of the alarmin heterocomplex S100A8/S100A9 in MSC marked disease progression toward the fibrotic phase in murine models and in patient bone marrow biopsies and plasma samples. Tasquinimod, a small-molecule inhibiting S100A8/S100A9 signaling which was already applied in clinical phase III trials for prostate cancer, significantly ameliorated the MPN phenotype and fibrosis in JAK2V617F-mutated murine models. These data highlighted that S100A8/S100A9 is an attractive therapeutic target in MPNs and specifically an actionable biomarker. Based on these findings we will start a proof-of-concept clinical trial this year - TasquForce MPN.

Super-enhancer-based identification of a BATF3/IL-2R-module reveals vulnerabilities in anaplastic large cell lymphoma

H.-C. J. Liang

University of Pennsylvania, Pathology and Laboratory Medicine, Philadelphia, United States of America

Anaplastic large cell lymphoma (ALCL), an aggressive CD30-positive T-cell lymphoma, comprises systemic anaplastic lymphoma kinase (ALK)-positive, systemic ALK-negative, primary cutaneous and breast implant-associated ALCL. Prognosis of some ALCL subgroups remains unsatisfactory, and effective second-line treatment options are still lacking. To identify genes defining ALCL cell state and dependencies, we here characterize super-enhancer regions by genome-wide H3K27ac ChIP-seq. In addition to known ALCL key regulators, the AP-1-member *BATF3* and *IL-2 receptor (IL2R)*-components are among the top hits. Specific and high-level IL2R expression in ALCL correlates with BATF3 expression. Confirming a regulatory link, IL-2R-expression decreases following *BATF3* knockout, and BATF3 is recruited to *IL2R* regulatory regions. Functionally, IL-2, IL-15 and Neo-2/15, a hyper-stable IL-2/IL-15 mimic, accelerate ALCL growth and activate STAT1, STAT5 and ERK1/2. In line, strong IL-2R α -expression in ALCL patients is linked to more aggressive clinical presentation. Finally, an IL-2R α -targeting antibody-drug conjugate efficiently kills ALCL cells *in vitro* and *in vivo*. Our results highlight the importance of the BATF3/IL-2R-module for ALCL biology and identify IL-2R α -targeting as a promising treatment strategy for ALCL.

DGP05 DGP-Promotionspreis 2022 - Auswahlrunde Bewerber*innen

DGP05.01

Analysis of the super-enhancer self-maintenance feedback loop of *TBXT* gene expression in chordomas

S. Bette, P. Möller, T. F. E. Barth, K. Mellert

Universitätsklinikum Ulm, Institut für Pathologie, Ulm, Germany

Background

Chordomas are rare malignant neoplasias of the bone that arise from notochordal remnants along the spine. Chemotherapy and targeted therapy options like TK-Inhibitors show poor success and high relapse rates. Standard of care is radical en-bloc resection. A new target for chordoma therapy is the protein Brachyury which has a high diagnostic specificity. Brachyury is encoded by the *TBXT-gene* which is essential for the growth of chordoma cells.

We intended to elucidate the mechanisms of the super-enhancer, self-maintenance loop of *TBXT* expression of the Brachyury signalling pathway.

CDK inhibitors have been shown to disrupt the autoregulatory landscape of Brachyury. We used CDK inhibitors THZ1 and Dinaciclib to impede *TBXT* transcription.

We hypothesized that Brachyury binds the p300 HAT domain and guides it to histone H3 leading to acetylation of Lysin 27 (H3K27ac). This opens the H3 chromatin complex which facilitates the transcription of the *TBXT* gene and subsequently the translation into more Brachyury protein. We interrupted this feedback loop using the p300 inhibitors CBP30 and ICBP112 to investigate the effect of p300 inhibition on *TBXT* expression.

Methods

Chordoma cell lines (U-CH1, U-CH2, U-CH17PII, U-CH17M, UM-Chor1, MUG-Chor1, MUG-CC1) were treated with THZ1, Dinaciclib, CBP30 and ICBP112 in concentrations between 0.1 and 10 µM for 24h. Changes in the amount of Brachyury were detected by Western Blot analyses.

Anti-Brachyury Magnetic Beads were used to pull down the p300/Brachyury complex for detection of p300 *via* Western Blot.

The expression of p300 was evaluated by immunochemistry in chordoma cell lines and tissues.

qPCR was performed to analyse the effect of different inhibitors on the transcription of Brachyury mRNA.

Results

Confirming published data the CDK inhibitors THZ1 and Dinaciclib reduced levels of Brachyury in chordoma cell lines. P300 was detected *via* Western Blot after IP with anti-Brachyury magnetic beads, confirming the presence of a Brachyury/p300 complex. The p300 inhibitors CBP30 and ICBP112 reduced Brachyury

mRNA, protein, and the acetylation of histone H3, in chordoma cell lines.

Conclusion

The autoregulatory landscape of Brachyury is controlled by factors like CDKs and superenhancers. Our data suggest that p300 is a keyplayer in the autoregulatory loop of *TBXT* expression. It forms a complex with the protein Brachyury and epigenetically regulates its transcription. Inhibition of this loop may be a target for development of new chordoma treatment strategies.

Literaturangaben

[Ref01] Hadley E Sheppard, Alessandra Dall'Agnese, Woojun D Park, M Hamza Shamim, Julien Dubrulle, Hannah L Johnson, Fabio Stossi, Patricia Cogswell, Josh Sommer, Joan Levy, Tanaz Sharifnia, Mathias J Wawer, Behnam Nabet, Nathanael S Gray, Paul A Clemons, Stuart L Schreiber, Paul Workman, Richard A Young, Charles Y Lin, (2021), Targeted brachyury degradation disrupts a highly specific autoregulatory program controlling chordoma cell identity, Cell reports Medicine, 26, 2022-02-23

[Ref02] Tanaz Sharifnia, Mathias J. Wawer, Ting Chen, Qing-Yuan Huang, Barbara A. Weir, Ann Sizemore, Matthew A. Lawlor, Amy Goodale, Glenn S. Cowley, Francisca Vazquez, Christopher J. Ott, Joshua M. Francis, Slim Sassi, Patricia Cogswell, Hadley E. Sheppard, Tinghu Zhang, Nathanael S. Gray, Paul A. Clarke, Julian Blagg, Paul Workman, Josh Sommer, Francis Hornicek, David E. Root, William C. Hahn, James E. Bradner, Kwok K. Wong, Paul A. Clemons, Charles Y. Lin, Joanne D. Kotz and Stuart L. Schreiber, (2019), Small-molecule targeting of brachyury transcription factor addiction in chordoma, Nature medicine, 28, 2022-02-23

Novel Criteria for Intratumoral Budding with Prognostic Relevance for Colon Cancer and Its Histological Subtypes

P. Pour Farid^{1, 2, 3}, M. Eckstein^{2, 3}, S. Merkel^{3, 4}, R. Grützmann^{3, 4}, A. Hartmann^{2, 3}, V. Bruns⁵, M. Benz⁵, R. Schneider-Stock^{1, 2, 3}, C. I. Geppert^{2, 3}

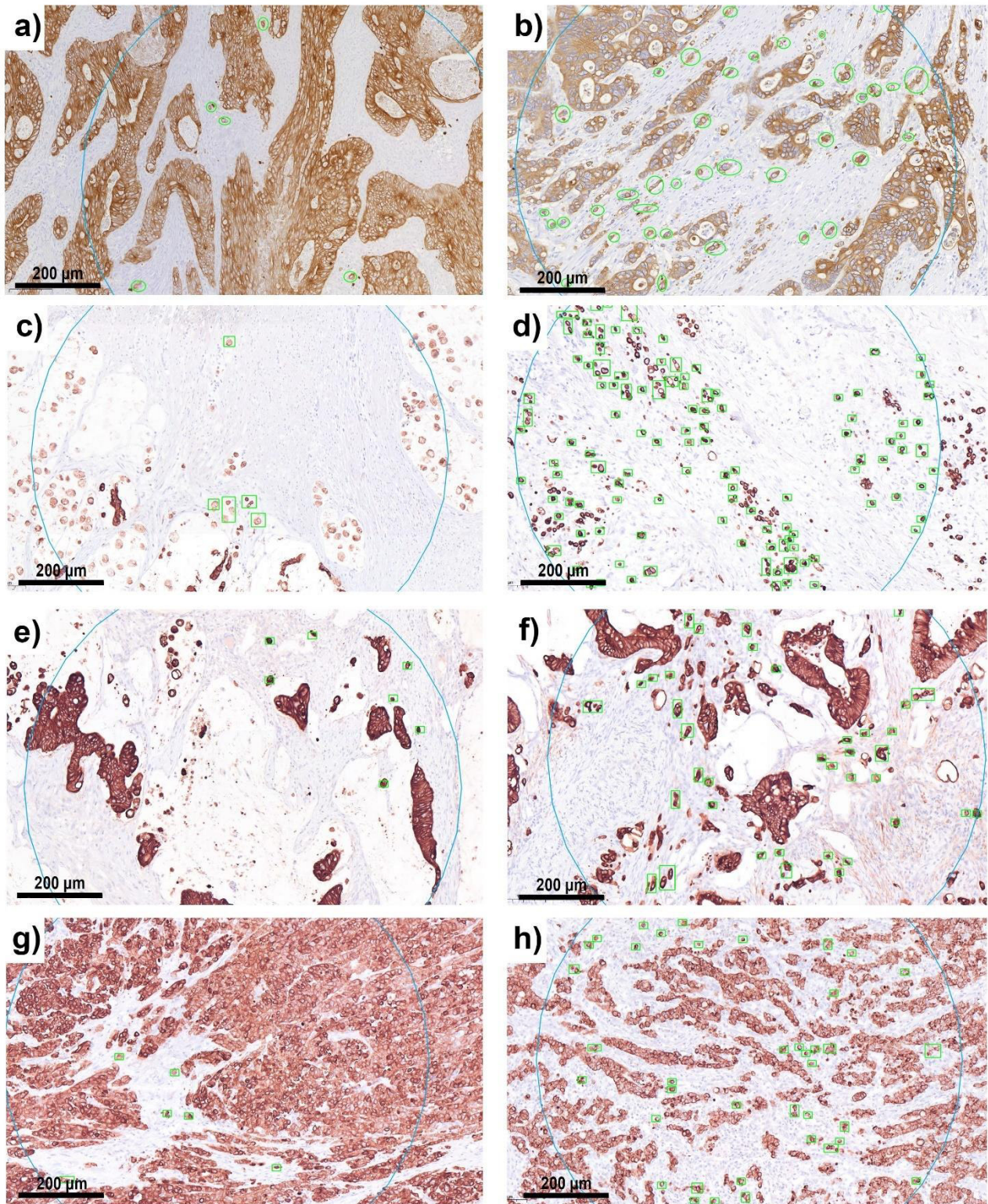
¹Institute of Pathology, University Hospital, Friedrich-Alexander-University of Erlangen-Nuremberg, Experimental Tumorpathology, Erlangen, Germany, ²Institute of Pathology, University Hospital, Friedrich-Alexander-University of Erlangen-Nuremberg, Erlangen, Germany, ³Comprehensive Cancer Center-EMN (CCC), University Hospital, Friedrich-Alexander University of Erlangen-Nuremberg, Erlangen, Germany, ⁴Department of Surgery, University Hospital, Friedrich-Alexander-University of Erlangen-Nuremberg, Erlangen, Germany, ⁵Fraunhofer Institute for Integrated Circuits IIS, Erlangen, Germany

Background

Peritumoral budding and intratumoral budding are important prognostic factors for colorectal cancer patients. Scientists worldwide have investigated the role of budding in tumor progression and its prognosis, but guidelines for reliably identifying tumor buds based on morphology are lacking.

Methods

Next-generation tissue microarray construction was used for tumor bud evaluation, and highly detailed rule-out annotation was used for tumor definition in pancytokeratin-stained tissue sections. Initially, tissues of 245 colon cancer patients were evaluated. Also, intratumoral budding in 30 cases of mucinous, medullary, and signet ring cell carcinoma was analyzed. A total of 14 530 tumor buds were manually annotated, counted and cross-checked by 2 experts.



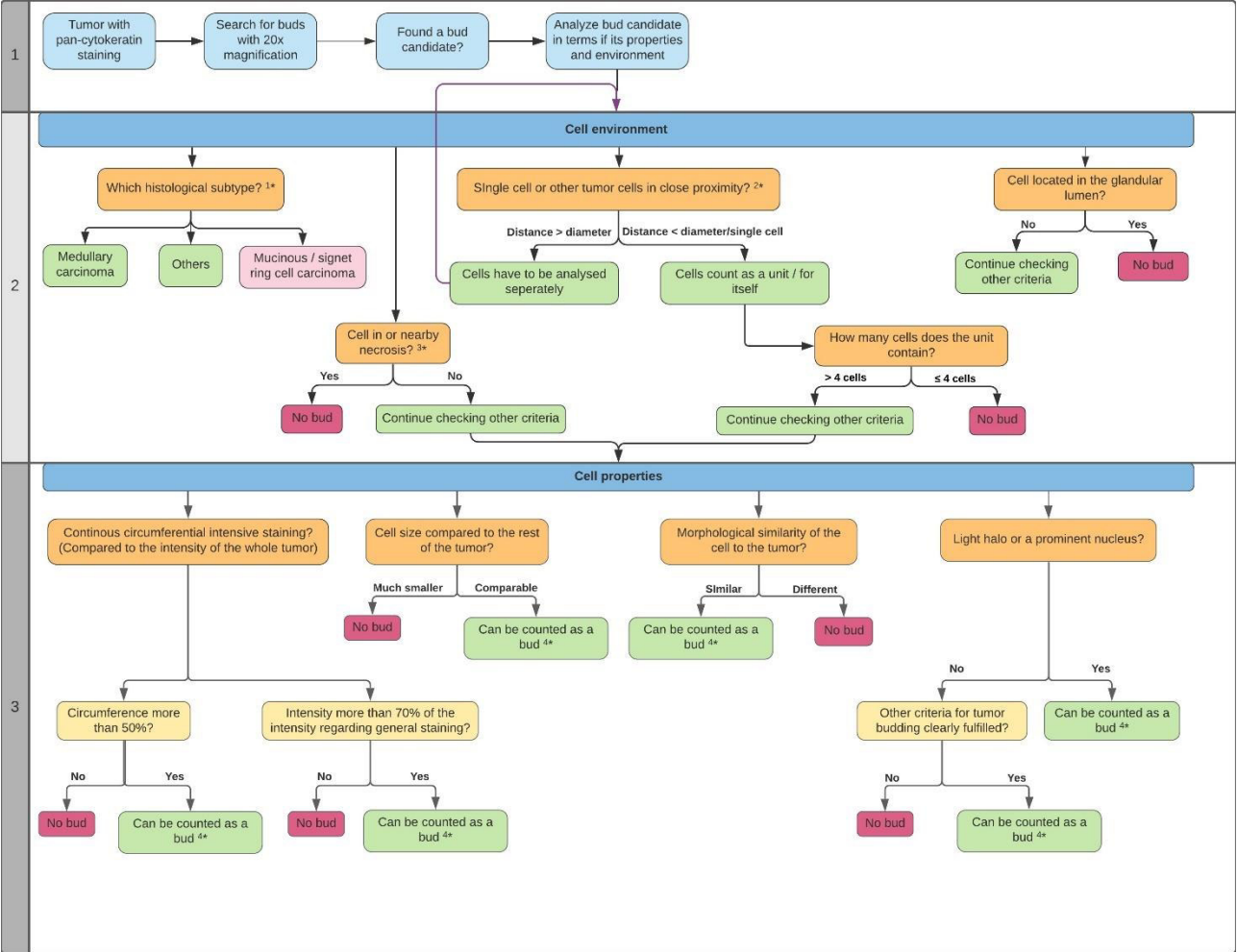
Comparison of high and low ITB areas (a-h). Pictures taken with 15x magnification. Defined tumor buds are marked in green. Each row shows the comparison between a region with low and high intratumoral budding respectively for: a,b) adenocarcinoma, c,d) signet ring cell carcinoma, e,f) mucinous carcinoma and g h) medullary carcinoma.

In addition, a tumor bud evaluation tool is already in planning in cooperation with the Fraunhofer Institute IIS, Erlangen, Germany, which will be trained as an artificial intelligence approach with our annotations to find ITB in an automated manner to facilitate diagnostics and reduce interobserver variability.

Results

High intratumoral bud scores (cut-off ≥ 10) were shown to be associated with poor distant metastasis-free survival ($p=0.006$). The cut-off was defined as the best maximum value from one of two/three cores.

Lymphatic invasion was confirmed as an independent prognostic factor ($p=0.001$). A trend for patient survival at a maximum intratumoral bud value of ≥ 20 has emerged for each of the three histological subtypes. A study in a multicenter setting seemed advisable and may be the subject of future research. The criteria were established in a not-yet-presented level of detail, which were incorporated into an easy-to-follow protocol for tumor bud annotation that is practical in clinical routine.



Flowchart to detect tumor buds. In the scheme, all relevant criteria are shown in Sections 1–3 regarding aspects for single cells and bud candidates and for their surroundings nearby. The flowchart was constructed using Lucidchart (2021 Lucid Software Inc., Amsterdam, Netherlands) and a template for UML activity diagrams.

Conclusion

The study shows that the established evaluation criteria of intratumoral budding based on morphology represent a promising approach for tumor bud evaluation. It can be assumed that this method is suitable for its adoption in clinical routines. The article was published in December 2021 in the International Journal of Molecular Science.

scRNA-seq uncovers metabolism and CD52 as new targets in ibrutinib surviving mantle cell lymphoma cells

V. Fuhr¹, E. Vafadarnejad², O. Dietrich², P. Arampatzi³, S. Heidenreich¹, A. Riedel⁴, A.-E. Saliba², A. Rosenwald¹, H. Rauert-Wunderlich¹

¹*Institute of Pathology, University of Würzburg and Comprehensive Cancer Center (CCC) Mainfranken, Würzburg, Germany,* ²*Helmholtz Institute for RNA-Based Infection Research (HIRI), Helmholtz-Center for Infection Research (HZI), Würzburg, Germany,* ³*Core Unit Systems Medicine, University of Würzburg, Würzburg, Germany,* ⁴*Mildred Scheel Early Career Center (MSNZ), University Hospital of Würzburg, Würzburg, Germany*

Background

The small molecule ibrutinib yields high response rate in relapsed/refractory patients suffering from the rare, aggressive mantle cell lymphoma. However, resistance to the Bruton tyrosine kinase inhibitor arises inevitably and the underlying mechanisms remain to be elucidated.

Methods

We performed single-cell RNA sequencing of an ibrutinib-sensitive mantle cell lymphoma cell line using the 10x Genomics platform to study the transcriptomic alterations of initially ibrutinib responding towards treatment persisting tumor cells. Flow cytometry, extracellular flux analysis, and further molecular biological methods were applied to validate the findings.

Results

Tracking the evolution of five subpopulations revealed mainly common but also individual responses to treatment. Ibrutinib led to increased expression of B cell receptor genes, shift in cell cycle, differential surface antigen expression (*CD52*), and to a metabolic switch towards reliance on oxidative phosphorylation. The combined treatment of BTK inhibition plus quenching oxidative phosphorylation with the small molecule IACS-010759 efficiently depleted the tumor cells. Targeting the upregulated *CD52* following ibrutinib pretreatment with a monoclonal antibody in combination with normal human serum caused increased complement dependent cytotoxicity. The efficacy of anti-*CD52* treatment was also demonstrated on primary mantle cell lymphoma cells.

Conclusion

Considering the risk profile, the anti-*CD52* monoclonal antibody may serve as consolidation treatment after ibrutinib regimen to minimize the risk for minimal residual disease and relapse in mantle cell lymphoma patients.

Impact of P-selectin-PSGL-1 axis on platelet-endothelium-leucocyte interactions in COVID-19

M. Granai, V. Warm, K. Greif, C. Hermann, L. Quintanilla-Martinez, U. Vogel, K. Klingel, F. Fend, H. Bösmüller
Universitätsklinikum Tübingen, Pathologie und Neuropathologie, Tübingen, Germany

Background

The lung is the central target organ in severe SARS-CoV-2 infection, and pulmonary complications the leading cause of death. In critically ill SARS-CoV-2 infected patients, early leukocyte recruitment to the respiratory system was found to be orchestrated by leukocyte trafficking molecules accompanied by secretion of pro-inflammatory cytokines and hypercoagulability[1][2]. The aim of our study is to explore the interplay between pulmonary endothelia and immune compartment in fatal COVID-19 and establish the activation status of platelets and leucocytes in relation with disease stage and in comparison to other causes of ARDS by immunohistochemistry.

Methods

Our study comprised 10 COVID-19 post-mortem lung specimens and 20 control samples (5 ARDS, 5 pneumonia, 10 normal lung) which were stained for the main adhesion molecules for each step of leucocyte migration: E-selectin, P-selectin and PSGL-1 for rolling phase, ICAM1, and VCAM1 for firm adhesion phase and CD11b for intravascular crawling. Image analysis software, QuPath, was used for quantification of positive leukocytes (PSGL-1 and CD11b) and endothelial tissue (E-selectin, P-selectin, ICAM1, VCAM1).

Results

Expression of P-selectin and PSGL-1 was strongly increased in the COVID-19 cohort compared to all control groups (ratio =17,23, $p<0,0001$; ratio=2,75, $p<0,0001$ respectively). Importantly, P-selectin was not only found in endothelial cells but also associated with aggregates of activated platelets adherent to the endothelial surface in COVID-19 cases. In addition, PSGL-1 disclosed positive perivascular leucocyte cuffs, so-called capillaritis. In contrast, VCAM1 and E-selectin were downregulated in COVID-19 compared to pneumonia (ratio=0,12, $p=0,0170$; ratio=0,43, $p=0,0112$ respectively). Moreover, CD11b showed a strongly increased positivity in COVID-19 compared to all controls (ratio=2,89; $p=0,0002$) indicating a proinflammatory immune microenvironment. Interestingly, CD11b exhibited distinct staining patterns at different disease stages.

Conclusion

The striking upregulation of PSGL-1 and P-selectin reveals an interplay of this receptor-ligand pair in COVID-19, increasing the efficiency of initial leucocyte recruitment and platelet activation, thus promoting tissue damage and immunothrombosis. Taken together, our results provide evidence that endothelial activation and unbalanced leukocyte migration play a central role in COVID-19 due to the impairment of P-selectin-PSGL-1 axis.

Literaturangaben

[1] Bösmüller H, Traxler S, Bitzer M, Häberle H, Raiser W, Nann D, Frauenfeld L, Vogelsberg A, Klingel K, Fend F, (2020), The evolution of pulmonary pathology in fatal COVID-19 disease: an autopsy study with clinical correlation, *Virchows Arch.*, 349-357, 477(3)

[2] Bösmüller H, Matter M, Fend F, Tzankov A, (2021), The pulmonary pathology of COVID-19, *Virchows Arch.*, 137-150, 478(1)

Machine Learning Models Predict the Primary Sites of Head and Neck Squamous Cell Carcinoma Metastases Based on DNA Methylation

M. Leitheiser¹, F. Klauschen^{1, 2, 3, 4}, P. Jurmeister^{1, 2, 5}, M. Bockmayr^{1, 6, 7, 8}

¹Charité - Universitätsmedizin Berlin, Institute of Pathology, Berlin, Germany, ²LMU München, Institute of Pathology, Munich, Germany, ³BIFOLD – Berlin Institute for the Foundations of Learning and Data, Berlin, Germany, ⁴Aignostics GmbH, Berlin, Germany, ⁵German Cancer Consortium (DKTK), Berlin, Germany, ⁶University Medical Center Hamburg-Eppendorf, Department of Pediatric Hematology and Oncology, Hamburg, Germany, ⁷Research Institute Children's Cancer Center Hamburg, Hamburg, Germany, ⁸Mildred Scheel Cancer Career Center HaTriCS4, Hamburg, Germany

Background

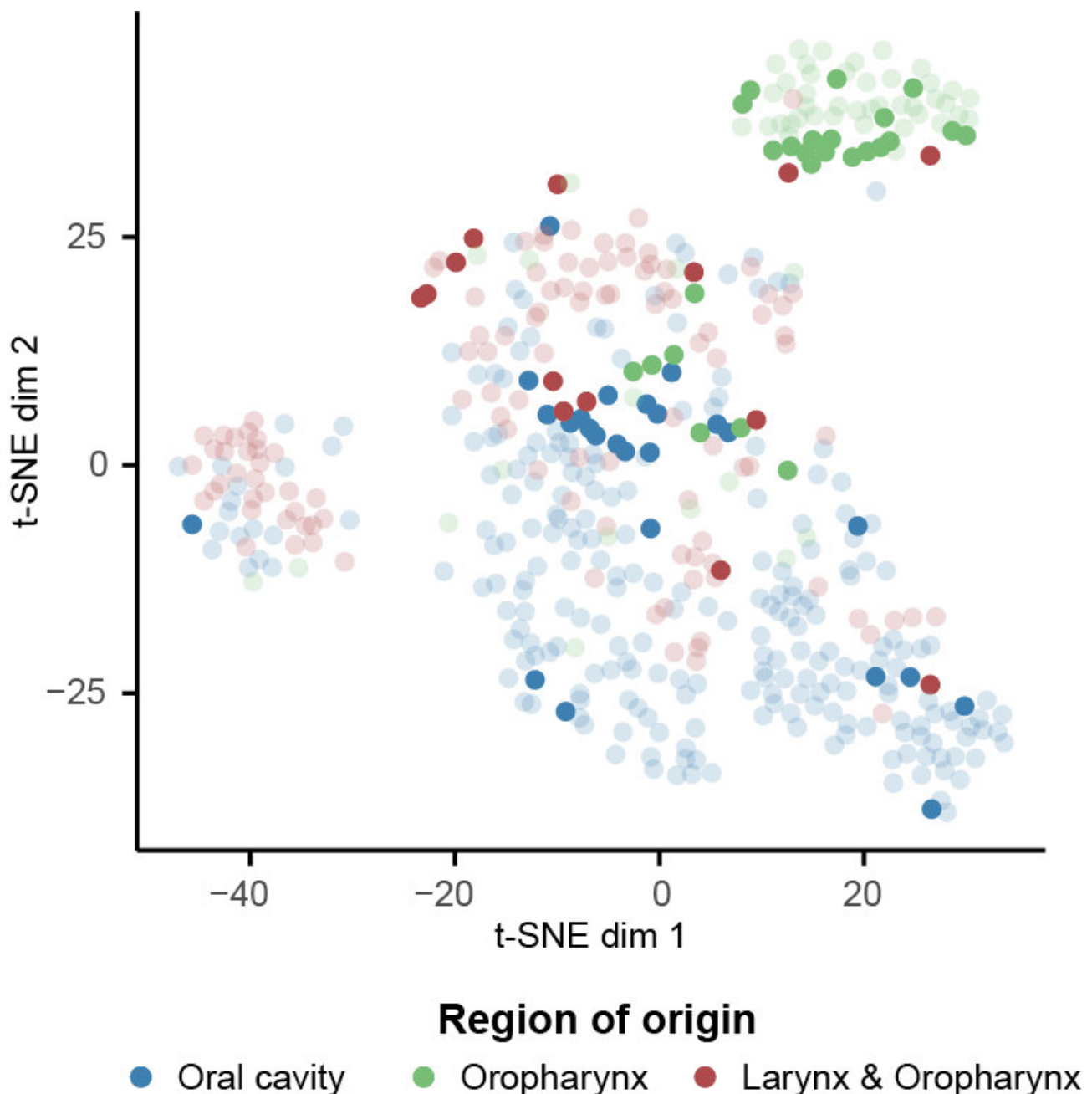
In head and neck squamous cell cancers (HNSCs) that present as metastases with an unknown primary (HNSC-CUPs), the identification of a primary tumor enables a more targeted therapy approach and increases patient survival. However, the currently available diagnostic methods are laborious and do not offer a sufficient detection rate. Recently, machine learning models have been successfully applied to DNA methylation data in various tumor classification problems. In order to improve the diagnostic workup for HNSC-CUPs, we extended this technique to HNSCs.

Methods

We compiled and annotated a reference cohort of 405 primary HNSC samples as well as an independent validation cohort of 64 pulmonary and lymph node metastasis, including 48 newly measured cases. The reference cohort was used to develop four classifiers based on different machine learning models (random forest (RF), neural network (NN), elastic net penalized logistic regression (LOGREG), support vector machine (SVM)) that predict the primary site of HNSC tumors from their DNA methylation profile. Their performance was evaluated on the validation cohort.

Results

T-SNE analysis of DNA methylation data from reference and validation cohort showed a common grouping of primary HNSC tumors and metastases by primary site, suggesting characteristic methylation profiles for the site of origin.



t-SNE plot of the reference (n=405, primary HNSC tumors) and validation (n=405, HNSC metastases) cohort based on DNA methylation data. Transparent and opaque data points correspond to samples from the reference and validation cohort, respectively.

The machine learning models achieved high classification accuracies (RF=83%, NN=88%, LOGREG=SVM=89%) on the validation cohort, supporting this claim. Further, the accuracy of all models did not show a significant difference between pulmonary and lymph node metastases and the NN, LOGREG, and SVM models significantly outperformed p16 status as a marker for oropharyngeal origin.

Conclusion

The DNA methylation profiles of HNSC metastases are characteristic for their primary sites, which can be predicted with high accuracy by the classifiers developed in this study. Thus, these classifiers can provide valuable information to guide the diagnostic workup of HNSC-CUP.

Small particles of *E. granulosus* (SPEGS) and *E. multilocularis* (SPEMS) induce selective activation of NK-cells in human blood and in the lymph nodes

L. Schreiber¹, T. Barth¹, B. Jahrsdörfer², J. Nell¹, C. Ludwig²

¹Universität Ulm, Institut für Pathologie, Ulm, Germany, ²Institut für Klinische Transfusionsmedizin und Immunogenetik Ulm (IKT) gGmbH, Immunzelltherapeutika, Ulm, Germany

Background

E. granulosus and *E. multilocularis* are cestodes and the larval stage causes one of the most life-threatening zoonosis in humans known as cystic and alveolar Echinococcosis. Humans, as a false intermediate host, ingests the eggs and after penetration of the wall of the gastrointestinal tract the larval state forms multiple hepatic lesions called metacestodes. The disease seems to deviate the immune defence by yet not well understood mechanisms. We have shown that particles shed from the outer layer of the metacestode are found in the germinal centers of the regional lymph nodes. These particles are called SPEGS and SPEMS. This finding raises question how these particles interact with the immune system.

Methods

By ultrasonic morcellation of isolated metacestodes layer we generated SPEGS and SPEMS *in vitro* as those seen in the lymph nodes. These particles were incubated with peripheral blood mononuclear cells (PBMCs) from 12 different donors for 24 hours. We stained for specific and activation markers of various populations of the peripheral blood and measured activation by flow cytometry. We analysed B cells, T cells, monocytes, dendritic cells and NK cells with differentiating antibodies using double and triple stainings with population-specific antibodies.

To verify our findings *in situ* we stained lymph node sections of infected humans with EmG3 (specific for the larval state of *E. multilocularis* and *E. granulosus*) as compared to findings of the flow cytometry.

Results

We found significant activation of NK cells as shown by increased expression of CD69 for SPEGS while incubation with SPEMS showed a positive trend after incubation for NK cells. The other tested populations showed no increase of activation markers. The monocytes stimulated with SPEGS showed a significant upregulation of TNF- α while activation with SPEMS seemed to reduce the synthesis of TNF- α .

In comparative immunohistochemical staining of lymph nodes positive for SPEGS and SPEMS, we noticed an accumulation of CD57-positive cells, also expressed by NK cells within the corresponding germinal centers

Conclusion

These findings suggest an interaction of SPEGS and SPEMS with the immune system *via* activation of NK-cells which also corresponds with the accumulation of CD57 positive cells in in germinal centers of particle enriched lymph nodes. However, both particles seem to have different effects on the synthesis of TNF- α in

monocytes pointing to distinct monocytic activation mechanisms in these 2 diseases.

The Wnt- β -catenin signalling pathway influences *TBXT* expression in chordoma.

E. Schweiger, P. Möller, T. F. E. Barth, K. Mellert

Institut für Pathologie, Universitätsklinikum Ulm, Ulm, Germany

Background

Chordomas are rare neoplasms, mainly located in the axial skeleton, generally showing a poor response to conventional therapy options. Therefore, developing new strategies for targeted therapies of these tumors is the main focus of chordoma research. [1]

One characteristic feature of chordoma is the expression of *TBXT*, a gene coding for the protein Brachyury. This protein is an important factor for growth and differentiation of chordoma cells. A knockdown of *TBXT* results in a change in cellular morphology followed by senescence and growth arrest in chordoma cell lines. Hence, *TBXT* and its gene product Brachyury are interesting targets for the development of new therapies. [2][3]

In murine embryonic stem cells, an induction of the Wnt- β -catenin signalling pathway leads to an increase in Brachyury protein levels, indicating that the expression of the corresponding gene is regulated by Wnt signalling. [4]

Our aim was to investigate whether this phenomenon also applies to chordoma cells. Moreover, we intended to test whether an inhibition of the Wnt- β -catenin signalling pathway leads to a decrease in Brachyury levels in chordoma cell lines.

Methods

To confirm *TBXT* as a target gene of the Wnt- β -catenin signalling pathway in chordoma, the chordoma cell lines U-CH1, MUG-Chor1 and UM-Chor1 were stimulated with recombinant Wnt3a. Furthermore, chordoma cells were transfected with siRNA targeting the *CTNNB1* gene, coding for β -catenin. We used Western blot analysis to assess the changes in β -catenin and Brachyury protein levels.

Results

Stimulating the chordoma cell line U-CH1 with recombinant Wnt3a resulted in a 28% (+/-4%) increase in Brachyury protein levels detected in Western blot analyses. The siRNA-mediated knockdown of *CTNNB1* led to a decrease of β -catenin protein levels to 45% (+/-12%). Subsequently the detectable amounts of Brachyury were reduced by 52% (+/-19%) in UM-Chor1. Comparable results were obtained in MUG-Chor1 with a diminution of β -catenin by 36% (+/- 10%) resulting in a 37% (+/- 3%) decrement of Brachyury levels. In contrast, Brachyury showed a reduction by only 10% (+/-6%) in U-CH1, although β -catenin was decreased by 62% (+/- 18%).

Conclusion

Our experiments show that *TBXT* is a target gene of the Wnt- β -catenin signalling pathway in chordoma.

Therefore, interfering with Wnt signalling may be a suitable option for targeted therapies in chordoma.

Literaturangaben

- [1] Walcott B P, Nahed B V, Mohyeldin A, Coumans J-V, Kahle K T, Ferreira M J, (2012), Chordoma: current concepts, management, and future directions., *The Lancet Oncology*, e69-e76, 2
- [2] Hsu W, Mohyeldin A, Shah S R, ap Rhys C M, Johnson L F, Sedora-Roman N I, Kosztowski T A, Awad O A, McCarthy E F, Loeb D M, Wolinsky J-P, Gokaslan Z L, Quiñones-Hinojosa A, (2011), Generation of chordoma cell line JHC7 and the identification of Brachyury as a novel molecular target., *Journal of Neurosurgery*, 760–769, 4
- [3] Presneau N, Shalaby A, Ye H, Pillay N, Halai D, Idowu B, Tirabosco R, Whitwell D, Jacques T S, Kindblom L-G, Brüderlein S, Möller P, Leithner A, Liegl B, Amary F M, Athanasou N N, Hogendoorn P C, Mertens F, Szuhai K, Flanagan A M, (2011), Role of the transcription factor T (brachyury) in the pathogenesis of sporadic chordoma: a genetic and functional-based study., *The Journal of Pathology*, 327–335, 3
- [4] Arnold S J, Stappert J, Bauer A, Kispert A, Bernhard G H, Kemler R, (2000), Brachyury is a target gene of the Wnt/ β -catenin signaling pathway., *Mechanisms of Development*, 249–258 , 1-2

Regulation of *HOXB7*-expression and the impact on the Ras-Raf-MAPK-pathway regarding the viability of chordoma cell lines

L. Haase, P. Möller, T. Barth, K. Mellert

Pathologie Universität Ulm, AG Chordoma, Ulm, Germany

Background

Chordomas are rare tumours of the spine thought to arise from remnants of the Chorda dorsalis. They show a strong expression of the *TBXT* gene coding for the protein Brachyury, a transcription factor of the T-box family.

Previous research revealed an increased expression of genes of the *HOX*-family in sacral tumours in comparison to clival ones, particularly *HOXA7*, *A9*, and *A10*.

In particular, the *HOX* genes of the paralogue group 7 (*HOXA7* and *HOXB7*) are of interest due to indications that *HOXB7* plays a significant role in regulation of *TBXT*.

Based on research by Martin G.R. (1998 Genes Dev), Heinonen H. (2015, Int J cancer) and Wu X. (2006, Cancer Res) we established a hypothetical pathway of *TBXT* regulation in chordoma *via* the *HOXB7*-protein by the Ras-Raf-MAPK-way.

Therefore, we tested the influence of *HOXB7* on the MAPK-kinase way and consequently on *TBXT* in chordoma cell lines.

Methods

We studied the impact of *HOXB7* on five chordoma cell lines. Cellular *HOXB7* levels were either upregulated by transfecting the cells with an *HOXB7* expression vector or downregulated using *HOXB7* specific siRNA. After an incubation time of 24-48 hours proteins were isolated. Western blot analyses were used to determine the amounts of *HOXB7* on the MAPK signalling pathway and Brachyury expression. MTS-assays were used to measure the impact of different amounts of *HOXB7* in chordoma cells on cell viability and proliferation.

Results

HOXB7 overexpression as well as *HOXB7* knockdown was convincingly detected by Western blot analysis. Interestingly, we detected no significant difference in the phosphorylation of the proteins of the MAPK-kinase way, neither in *HOXB7* upregulated nor in *HOXB7* downregulated cells. Consequently, no significant differences were detected in the amount of Brachyury expression in correlation to different amounts of *HOXB7* protein. Further, there was no significant difference regarding the cell viability of chordoma cells after *HOXB7* up- or down regulation.

Conclusion

Our study showed no indication that *HOXB7* regulates the MAPK-way and further *TBXT*. A complete siRNA mediated silencing of *HOXB7* was not achieved. This indicates that minor amounts of HOXB7 protein may suffice in activating the MAPK signalling pathway. This indicates that minor amounts of HOXB7 protein may suffice in activating the MAPK signalling pathway. Furthermore, HOXB7 and HOXA7 are described to share redundant features. Therefore, it is possible that downstream effects are not detectable unless both genes have been silenced.

DGP06 Junges Forum I - Social Media

DGP06.01

How Twitter & Facebook Changed My Life: The Role of Social Media in Pathology & Medicine

J. Gardner

Geisinger Medical Center, Danville, United States of America

This lecture will discuss various ways to use Twitter, Facebook, and Instagram to share educational content and ideas, to build your professional reputation, and to connect with colleagues and learners on a global scale. The power of sharing online educational videos via YouTube will be explained. Methods for including social media activities in one's professional curriculum vitae and leveraging them for use towards academic promotion and tenure will also be discussed.

The pros and cons of the use of Social Media in Pathology

K. Steinestel

Bundeswehrkrankenhaus Ulm, Pathologie und Molekularpathologie, Ulm, Germany

Background

Die Verbreitung sozialer Medien wie Facebook, Twitter, Instagram oder TikTok nimmt weiterhin rasant zu. Neben der privaten und Freizeitnutzung nimmt zugleich auch die Funktion der sozialen Medien als Informationsquelle für die Öffentlichkeit und damit die Relevanz der genannten Plattformen als Multiplikator von Inhalten für Politiker/politische Parteien, für staatliche und nichtstaatliche Organisationen sowie für Wissenschaftler zu. Aus Sicht der Pathologie relevant sind hier insbesondere die Aspekte Weiterbildung, Öffentlichkeitsarbeit und der Umgang mit medizinischen Falschnachrichten aus Sicht des eigenen Fachgebietes. In Bezug auf die Weiterbildung in der Pathologie ist als Beispiel die insbesondere in den USA verbreitete Möglichkeit der Diskussion von Fällen anhand geteilten Bildmaterials zu nennen, das auch in Form kompakter Weiterbildungsinhalte wie Threads/Videos oder anhand von Quizfragen stattfinden kann. In diesem Kontext ist ein besonderes Augenmerk auf nationale/internationale ethische und Datenschutzbestimmungen bei der Verwendung von Bildmaterial in sozialen Netzwerken zu legen. In Bezug auf die Öffentlichkeitsarbeit sollen Möglichkeiten vorgestellt werden, Fachinhalte in Form virtueller Diskussionen vor einem größeren Publikum zu erörtern (u.a. Clubhouse, Twitter Spaces). Eine stärkere Wahrnehmbarkeit der Pathologie könnte hier auch einen Kontrapunkt zur starken Medienpräsenz verwandter Fachgebiete setzen. Am Beispiel der sog. „Pathologiekonferenz“, bei der unbelegte Behauptungen zu COVID-19-Impfstoffen als medizinische Fakten präsentiert wurden, soll schließlich die Notwendigkeit aufgezeigt werden, medizinischen Falschinformationen aus dem Gebiet der Pathologie im öffentlichen Diskurs mit gezielter Kritik zu begegnen und somit die Einhaltung fachlich-wissenschaftlicher Standards aus Sicht des eigenen Fachgebiets zu verteidigen.

Pathology findings made audible-Prof. Dr. Sven Perner and Dr. Christiane Kümpers of the University of Lübeck launch podcasts "Patho aufs Ohr" and "Patho?Logisch!"

C. Kümpers¹, S. Perner^{1, 2}

¹Institut für Pathologie UKSH Campus Lübeck, Lübeck, Germany, ²Pathologie Forschungszentrum Borstel, Borstel, Germany

Podcasts sind beliebter denn je und in aller Ohren. Grund genug für uns, Prof. Dr. med. Sven Perner, Direktor der Pathologie des UKSH Campus Lübeck und des Forschungszentrums Borstel, und Frau Dr. med. Christiane Kümpers, Fachärztin und gleichzeitig Unterrichtsbeauftragte am Institut, dieses Medium zu nutzen, um exemplarische Befunde aus der Pathologie vorzustellen. Dabei erklären wir, wie wir von der Histologie zum Befund gelangen. Es war schon lange das Bestreben der beiden Pathologen und Podcaster, nicht nur die Themen der Pathologie, wie sie im Lehrbuch und den Vorlesungen vermittelt werden, zu unterrichten, sondern den Studierenden das Kerntätigkeitsbild eines Pathologen näher zu bringen: also das Übersetzen des histologischen Bildes in einen Befund. So wird der Podcast-Zuhörer durch die bunte Welt der Mikroskopie zum Befundtext und der Diagnose geleitet. Aus der Beschreibung einer ulzerierten Appendixschleimhaut mit granulozytären Infiltraten in der Appendixwand wird dann die Diagnose einer floriden ulzero-phlegmonösen Appendizitis nachvollziehbar - und das können sich die ZuhörerInnen während der Fahrt im Auto, beim Beladen der Waschmaschine oder beim Fensterputzen anhören. Kleine Ausflüge in die Werkzeugkiste eines Pathologen wie Sonderfärbungen, Immunhistochemie und Molekularpathologie sowie die Geschichte der Pathologie sind beim Zuhören inkludiert. Es werden zunächst Befunde, die klassische Themen der allgemeinen Pathologie wie beispielsweise Entzündungs- und Tumorpathologie besprechen vorgestellt, um in späteren Folgen in die spezielle Pathologie einzusteigen. Hier dürfen sich die ZuhörerInnen dann auch auf Interviews mit klinischen KollegInnen oder PathologInnen mit Expertenwissen freuen.


Der Podcast „Patho aufs Ohr“ richtet sich an Studierende der (Zahn-)Medizin, junge ÄrztInnen und medizinisch Interessierte. Technische Unterstützung bekommen die beiden Pathologen von Robin Brendel, Student der medizinischen Ingenieurwissenschaften der Universität zu Lübeck.


Um auch Laien für die Pathologie zu begeistern und über das Tätigkeitsbild des Pathologen aufzuklären, haben wir vor kurzem unseren neuen Podcast „Patho?Logisch!“ ins Leben gerufen.

Die Patho-Podcasts sind hier zu finden:

<https://pathoaufsohr.podbean.com>

<https://pathologisch.podbean.com>





Patho aufs Ohr

PODCAST

Patho aufs Ohr

Prof. Dr. med. Sven Perner, Dr. med. Christiane Kümpers

FOLLOWING

...

All Episodes

DGP07 Odontogenic and head and neck tumors

DGP07.01

Clinical and Pathomorphological Aspects of Odontogenic Tumors

S. E. Gültekin¹, R. Büttner²

¹Gazi University Faculty of Dentistry, Department of Oral Pathology, Ankara, Turkey, ²University of Cologne, Institute for Pathology, Cologne, Germany

Odontogenic tumors (OTs) comprise a group of heterogeneous lesions ranging from hamartomatous or non-neoplastic tissue proliferation to benign or malignant neoplasms with metastatic potential. OTs are derived from epithelial, ectomesenchymal, and/or mesenchymal elements of tooth forming ("odontogenic") tissues which show variable clinical and histopathological features.¹ Therefore, understanding tooth development is often key in diagnostic pathology.

OTs are rare tumors and the estimated incidence rate of them is less than 0.5 cases per 100.000 per year. The causes of OTs remain unclear as yet. Nonetheless, the majority of OTs seem to arise de novo, without an apparent causative factor. ² Although the etiopathogenesis of most odontogenic tumors remains unclear, there have been some recent advances in understanding the genetic basis of specific odontogenic tumors. Molecular analyses performed by different techniques, including Sanger sequencing, next-generation sequencing, and allele-specific PCR, have uncovered mutations in genes related to the oncogenic MAPK/ERK signaling pathway in odontogenic tumors. Genetic mutations in these pathway genes have been reported in epithelial and mixed odontogenic tumors, in addition to odontogenic carcinomas and sarcomas.³ Notably, B-RAF proto-oncogene serine/threonine kinase (BRAF) and KRAS proto-oncogene GTPase (KRAS) pathogenic mutations have been reported in a high proportion of ameloblastoma and ameloblastoma related tumors and adenomatoid odontogenic tumors, respectively.^{3,4}

In the tutorial, we will discuss the differential diagnosis of odontogenic tumors focusing on difficult differential diagnoses and discussing how molecular profiling aids in diagnostic classification.

References

1. Santosh ARB Ogle OE. Odontogenic Tumors. Dental Clinics of North America 64 (1): 121-138,2020.
2. Brierley JD, Speight PM, Jordan RCK. Current Concepts Of Odontogenic Tumors- An Update. Diagnostic Histopathology, 23 (6), 266-274, 2017.
3. Vered M. Wright JM. Update from the 5th Edition of the World Health Organization Classification of Head and Neck Tumors: Odontogenic and Maxillofacial Bone Tumors. Head and Neck Pathol, 2022 (published online)
4. Gültekin SE, Aziz R, Heydt C, Sengüven B, Zöller J, Safi AF, Kreppel M, Büttner R. The Landscape Of Genetic Alterations In Ameloblastomas Relates To Clinical Features. Virchows Arch. 472(5):807-814, 2018.

Differential Diagnostics and Molecular Profiles of Odontogenic Tumors

R. Büttner¹, S. E. Gültekin²

¹Uniklinik Köln, Institut für Pathologie, Köln, Germany, ²Gazi University Faculty of Dentistry, Department of Oral Pathology, Ankara, Turkey

Odontogenic tumors (OTs) comprise a group of heterogeneous lesions ranging from hamartomatous or non-neoplastic tissue proliferation to benign or malignant neoplasms with metastatic potential. OTs are derived from epithelial, ectomesenchymal and/or mesenchymal elements of tooth forming (“odontogenic”) tissues which show variable clinical and histopathological features.¹ Therefore, understanding tooth development is often key in diagnostic pathology.

OTs are rare tumors and the estimated incidence rate of them is less than 0.5 cases per 100.000 per year . The causes of OTs remain unclear as yet. Nonetheless, the majority of OTs seem to arise de novo, without an apparent causative factor. ² Although the etiopathogenesis of most odontogenic tumors remains unclear, there have been some recent advances in understanding the genetic basis of specific odontogenic tumors. Molecular analyses performed by different techniques, including Sanger sequencing, next-generation sequencing, and allele-specific PCR, have uncovered mutations in genes related to the oncogenic MAPK/ERK signaling pathway in odontogenic tumors. Genetic mutations in these pathway genes have been reported in epithelial and mixed odontogenic tumors, in addition to odontogenic carcinomas and sarcomas.³ Notably, B-RAF proto-oncogene serine/threonine kinase (BRAF) and KRAS proto-oncogene GTPase (KRAS) pathogenic mutations have been reported in a high proportion of ameloblastoma and ameloblastoma related tumors and adenomatoid odontogenic tumors, respectively .^{3,4}

In the tutorial we will discuss the differential diagnosis of odontogenic tumors focusing on difficult differential diagnoses and discuss how molecular profiling aids in diagnostic classification.

References

1. Santosh ARB Ogle OE. Odontogenic Tumors. Dental Clinics of North America 64 (1): 121-138,2020.
2. Brierley JD, Speight PM, Jordan RCK. Current Concepts Of Odontogenic Tumors- An Update. Diagnostic Histopathology, 23 (6), 266-274, 2017.
3. Vered M. Wright JM. Update from the 5th Edition of the World Health Organization Classification of Head and Neck Tumors: Odontogenic and Maxillofacial Bone Tumors. Head and Neck Pathol, 2022 (published online)
4. Gültekin SE, Aziz R, Heydt C, Sengüven B, Zöller J, Safi AF, Kreppel M, Büttner R. The Landscape Of Genetic Alterations In Ameloblastomas Relates To Clinical Features. Virchows Arch. 472(5):807-814, 2018.

Reappraisal of Grading in Intestinal-Type Sinonasal Adenocarcinoma: Tumor Budding as an Independent Prognostic Parameter

C. M. Meerwein¹, M. D. Brada², M. B. Soyka¹, D. Holzmann¹, **N. J. Rupp**^{2, 3}

¹Department of Otorhinolaryngology - Head and Neck Surgery, University Hospital Zurich, Zurich, Switzerland, ²Department of Pathology and Molecular Pathology, University Hospital Zurich, Zurich, Switzerland, ³Faculty of Medicine, University of Zurich, Zurich, Switzerland

Background

Since sinonasal intestinal-type adenocarcinomas (ITAC) show resemblance to colorectal adenocarcinomas, we aimed to investigate novel prognostic factors of outcome, with particular focus on the role of tumor budding (TB).

Methods

Retrospective clinico-pathological single-institution study on consecutive ITAC patients between 1996 and 2020. Histopathological parameters including conventional subtypes and TB features (low, intermediate, high) were evaluated with the aid of pancytokeratin (AE1/AE3) immunohistochemical staining. Parameters were correlated to clinical data and outcome.

Results

A total of 31 ITAC patients were included. Overall, 19/31 patients (61.3%) presented with stage III/IV disease. Presence of lymph node or distant metastases was rare (1/31 patient, 3.2%). Treatment protocols consisted of tumor resection in 30/31 patients (96.8%) and primary radiochemotherapy in 1/31 patient (3.2%). Adjuvant radiation therapy was conducted in 20/30 surgically treated patients (66.7%). The 3- and 5-year overall survival (OS) was 83.9% and 78.3% and the 3- and 5-years disease-specific survival (DSS) 83.7% and 78.5%, respectively. The presence of intermediate/high TB (defined as ≥ 5 buds) was associated with both, worse DSS (log rank $p = 0.03$) and OS (log rank $p = 0.006$). No patient with low TB revealed progressive disease or died of the disease. No association between TB and tumor stage or conventional tumor subtype was found.

Conclusion

Tumor budding seems to be an independent prognostic factor of worse outcome in ITAC.

This work has been published [1]

Literaturangaben

[1] Meerwein CM#, Brada MD#, Soyka MB, Holzmann D, Rupp NJ, (2022), Reappraisal of Grading in

Intestinal-Type Sinonasal Adenocarcinoma: Tumor Budding as an Independent Prognostic Parameter, Head and Neck Pathology, 2022 Jan 11. doi: 10.1007/s12105-022-01410-3. Epub ahead of print. PMID: 35015192., <https://pubmed.ncbi.nlm.nih.gov/35015192/> #contributed equally

Elevated LSD1 and SNAIL expression indicate poor prognosis in hypopharynx carcinoma

J. Bottner¹, J. Ribbat-Idel¹, L. Klapper¹, T. Jagomast¹, A.-L. Lemster¹, S. Perner^{1,2}, C. Idel³, J. Kirfel¹

¹*Institut of Pathology, University Hospital Schleswig-Holstein Campus Luebeck, Lübeck, Germany*, ²*Institute of Pathology, Reserach Center Borstel, Leibniz Lung Center, Borstel, Germany*, ³*Department of Otorhinolaryngology, University Hospital Schleswig-Holstein Campus Luebeck, Lübeck, Germany*

Background

Head and neck squamous cell carcinoma (HNSCC) is one of the most common cancers worldwide and is associated with a poor prognosis for patients. Therapy options are mostly restricted to surgery and radio- and/or chemotherapy resulting in a 5-year survival rate of around only 50 %. However, an improved knowledge of the biological mechanisms leading to tumorigenesis and tumor progression is key to develop successful targeted therapies that improve survival and reduce toxicities associated with current non-selective treatment strategies.

LSD1 is aberrantly expressed in many cancers, where it impedes differentiation and contributes to cancer cell proliferation, cell metastasis and invasiveness, and is associated with poor prognosis. Pharmacological inhibition of LSD1 has been reported to significantly attenuate tumor progression *in vitro* and *in vivo* in a range of solid tumors. The transcription factor SNAIL is overexpressed in various tumor types. SNAIL functions not only as a master regulator of epithelial–mesenchymal transition that promotes tumor metastasis, but also as an important molecule that induces immunosuppression, bestows cancer cells with stem-like traits, and mediates cancer cell survival. Expression of SNAIL was significantly correlated with that of LSD1 e.g. in breast cancer tissues.

Here, we investigated the expression of LSD1 and SNAIL, their prognostic qualities as well as their co-expression in different HNSCC sub-sites.

Methods

We used a large, representative, and clinically well-characterized cohort of 339 HNSCC patients to investigate the expression of LSD1 and SNAIL and their prognostic value. The LSD1 and SNAIL expression levels were analyzed using immunohistochemistry and were correlated with tumor characteristics and clinicopathological features of HNSCC patients.

Results

Elevated LSD1 expression correlated with advanced tumor stage and poor progression-free survival (PFS) in HNSCC originating in the hypopharynx. Overexpression of the transcription factor SNAIL independently correlates with worse overall survival (OS) and PFS in HNSCC in general and prominently in tumors of the hypopharynx. Additionally, we were able to show that the expression of LSD1 significantly correlated with that of SNAIL in HNSCC.

Conclusion

LSD1 and SNAIL might function as biomarkers especially in HNSCC of the hypopharynx. Together, our work supports the hypothesis that targeting the LSD1–SNAIL interaction in may lead to inhibition of tumor growth and tumor metastasis.

DNA methylation-based classification of salivary gland tumors

P. Jurmeister¹, D. Capper², F. Klauschen¹, S. Ihrler^{1, 3}

¹*Pathologisches Institut der LMU, München, Germany*, ²*Charité - Universitätsmedizin Berlin, Berlin, Germany*, ³*DermPath, Ihrler, Germany*

Background

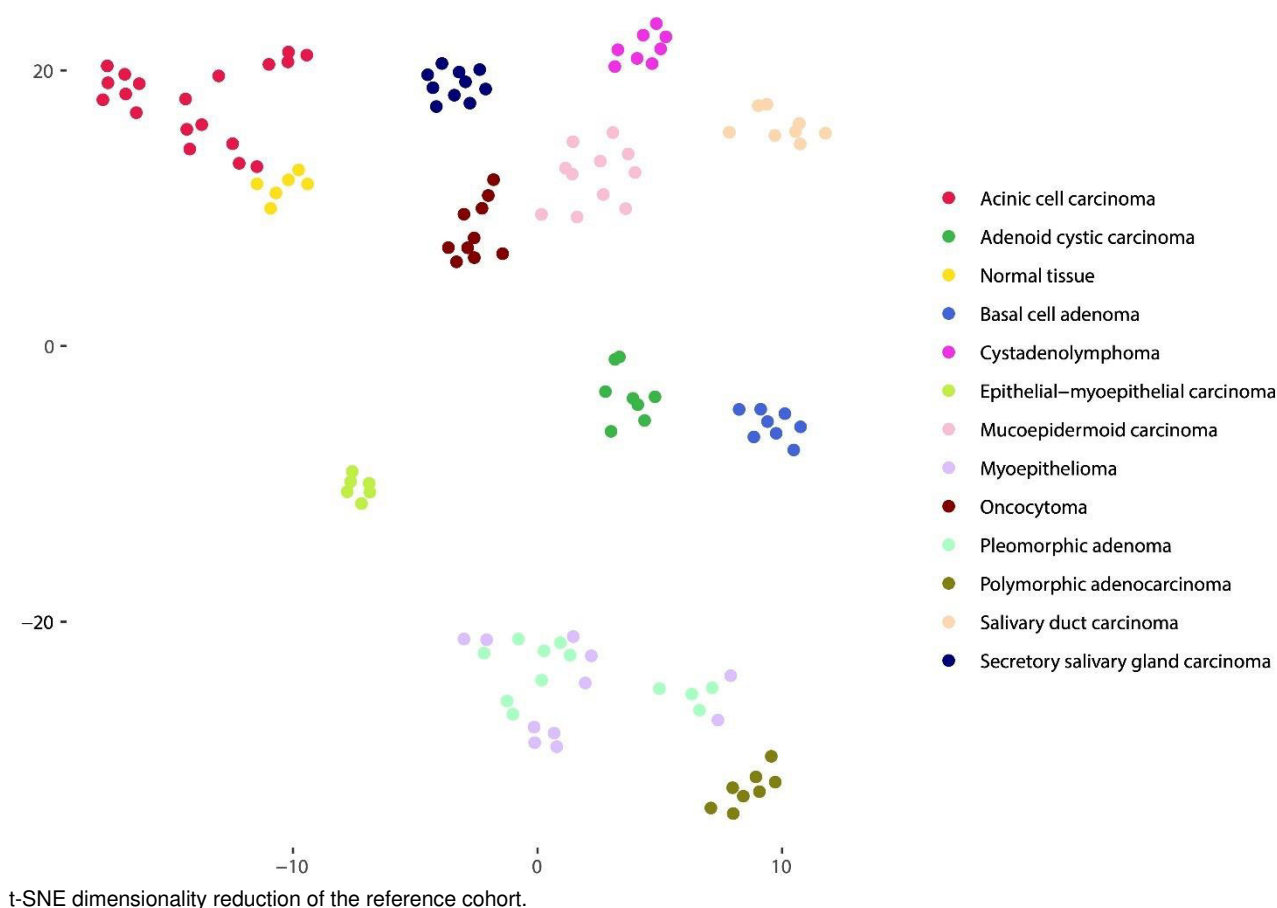
Salivary gland tumors represent a major challenge for histopathological diagnosis due to the numerous differential diagnoses and their significant histomorphological diversity. In our study, we investigated the value DNA methylation profiling for the classification of these tumors.

Methods

The genome-wide DNA methylation profile of 250 salivary gland tumors covering 13 different histopathological entities was analyzed using Infinium MethylationEPIC BeadChip. In addition, we also investigated 20 adenocarcinomas not otherwise specified (NOS) and will further expand this cohort in the following months.

Results

In a t-SNE dimensionality reduction, we showed that most groups correlated well with the established histopathological diagnosis. Only pleomorphic adenomas and myoepitheliomas showed an overlapping DNA methylation signature.



Based on this reference cohort, we trained machine learning classifier that achieved a perfect accuracy of 1.0 in a nested cross-validation and thus could be used to classify diagnostic cases.

In addition, we are currently performing a complementary analysis of adenocarcinomas NOS. The initial results indicate that in the vast majority of cases these tumors can be assigned to already established entities and thus appear to correspond primarily to poorly differentiated variants of these tumors. So far, the most frequent match with the profile of salivary duct carcinomas was found.

Conclusion

DNA methylation analysis is a promising method for the classification of salivary gland tumors and could be a valuable aid for histopathological diagnosis in the future, especially in difficult cases such as adenocarcinoma NOS as well as small or fragmented biopsy specimens.

DGP08 Aktuelle Habilitationen

DGP08.01

The tumor microenvironment - relay station for prognosis and therapy response

R. F. A. Krupar

Pathologie des Forschungszentrum Borstel, Leibniz Lungenzentrum, Borstel, Germany

Background

Head and neck squamous cell carcinoma (HNSCC) is the sixth most common cancer worldwide with a dismal prognosis. Besides tobacco and alcohol abuse, human papilloma virus (HPV) infection is an independent risk factor, particularly in oropharyngeal squamous cell carcinomas (OPSCC). One key determinant of therapy response and prognosis is the tumor immune microenvironment (TIME). A strong anti-tumor immune response represents an important mechanism of tumor cell killing. Another major determinant is the tumor metabolism. One feature of tumor cells is their reliance on glycolysis instead of oxidative phosphorylation (OXPHOS) for energy production despite of sufficient oxygen supply.

Methods

The presented studies were based on several different clinically and pathologically well annotated HNSCC cohorts. Immunohistochemical stainings were performed on tissue microarrays and whole slides against p16, different immune cell markers and metabolic markers. DNA and mRNA were extracted to detect HPV and assess immune-related and metabolic genes via RT-PCR and *Nanostring*. HNSCC cell lines and tumor spheroids were used for functional studies of metabolic modulation and anti-tumor immune response. Data of *The Cancer Genome Atlas* (TCGA) was accessed via *cBioPortal*.

Results

First, we characterized the immunological and metabolic differences of HPV+ and HPV- OPSCC showing an enhanced anti-tumor immune response together with increased levels of OXPHOS metabolism in HPV+ HNSCC. A subsequent study demonstrated that a strong anti-tumor immune response together with an OXPHOS metabolism associates with improved short-term survival in HNSCC. Based on TCGA data we furthermore discovered a correlation of *EP300* mutation frequency or *EP300* downregulation with an anti-tumor TIME in HNSCC and other solid malignancies and showed that tumor metabolism was strongly shifted towards OXPHOS in *EP300* downregulated tumors. Finally, we aimed to evaluate TIME differences of

HNSCC primary tumors (PTs) and recurrent tumors (RTs) to understand the poor therapeutic response of RTs and discovered an overall decrease of tumor infiltrating lymphocytes with significant loss of CD8⁺ T cells and B lymphocytes and a significant decrease of tertiary lymphoid structures in RTs after chemoradiation.

Conclusion

Our results delineate the interdependencies of TIME and tumor metabolism in HNSCC and stress their impact on therapy response. Additionally, they show an impairment of anti-tumor immune response in RTs after chemoradiation.

Prognostic and predictive biomarkers in invasive breast cancer

R. Erber

Institute of Pathology, University Hospital Erlangen, Friedrich-Alexander-Universität Erlangen-Nürnberg (FAU), Comprehensive Cancer Center Erlangen-EMN, Erlangen, Germany

Background

Invasive breast carcinoma (IBC) is a heterogeneous malignancy that can be subdivided into molecular subtypes with different biological behaviors and different molecular alterations. Knowledge of these subtypes and the biomarkers that identify these IBC subtypes is helpful in determining the prognosis of IBC patients and the response to specific therapies.

Methods

During post-doc phase, I investigated the value of various prognostic and predictive IBC biomarkers using classical histopathology, immunohistochemistry (IHC), in situ hybridization (ISH), and gene expression analyses in clinical IBC cohorts. Tissue microarrays (TMA) were used for some analyses. Focus was on the proliferation marker Ki-67 (IHC), the fibroblast growth factor receptor 1 (*FGFR1*; ISH; TMA), PIWI-like 1/PIWI-like 2 proteins (IHC; TMA), and tumor-infiltrating lymphocytes (TILs; histopathology).

Results

Using three expression groups (<10%, 10-19%, ≥20%), Ki-67 proved to be a significant prognostic marker in hormone receptor (HR)-positive, human epidermal growth factor receptor growth factor receptor-2 (HER2)-negative IBC (n=3140). Moreover, HR+ HER2- IBC patients at intermediate risk could be further classified into prognostic groups based on Ki-67. In an IBC cohort (n=894; all molecular subtypes), *FGFR1* amplifications were found in 6.6% of assessable IBCs (n=33/503). Most *FGFR1*-amplified IBCs (69.7%) belonged to the Luminal B-like subtype. Although no significant difference was seen in terms of overall survival (OS) and disease-free survival (DFS), *FGFR1*-amplified IBCs showed a trend toward worse prognosis in terms of distant metastasis-free survival (DMFS) compared with non-amplified IBCs [hazard ratio=2.08; 95% confidence interval (CI) 0.98; 4.39; *P*=0.05]. In the same cohort, the combination of high PIWI-like 1/low PIWI-like 2 expression was an indicator of worse prognosis [adjusted hazard ratios for OS=2.92; 95% CI 1.24; 6.90, DFS=3.27; 95% CI 1.48; 7.20, DMFS=7.64; 95% CI 2.35; 24.82] and was more likely to be found in aggressive subtypes (e.g., triple negative IBC). In a clinical IBC cohort treated with neoadjuvant chemotherapy (NACT) (n=146), TILs were a significant predictive marker of response to NACT. In IBC with a dense TIL infiltrate (>50% of stromal tumor area), a pathological complete response (pCR) was observed in 66.7%. In contrast, in IBC with lower TIL density, pCR was noted in 32.8%.

Conclusion

Pathological IBC biomarkers can be of great value in assessing prognosis and therapy response prediction.

Tumor-microenvironment in colorectal cancer: the role of budding and tumor-infiltrating lymphocytes as tumor-host antagonists.

C. Lang-Schwarz

Friedrich-Alexander-Universität Erlangen-Nürnberg, Klinikum Bayreuth GmbH, Institut für Pathologie, Erlangen, Germany

Background

Colorectal cancer (CRC) is one of the most common cancer types worldwide [1]. Staging is based on the Tumor Node Metastasis (TNM) system according to the World Health Organization (WHO) [2]. However, patients' outcomes vary, even if in the same tumor stage. Tumor budding as well as tumor-infiltrating lymphocytes (TILs) are part of the tumor-microenvironment and evolved as promising additive prognostic markers in recent years [2,3]. Therefore, we aimed to analyze tumor budding and TILs in CRC as tumor-host-antagonists and to elucidate the prognostic potential of the budding-TILs interaction as attacker-defender approach. Additionally, we wanted to analyze the role of chemotherapy and immunotherapy in this issue.

Methods

783 patients with CRC, diagnosed between 2005 and 2016 were included. Budding and TILs were assessed according to the consensus criteria of the International Tumor Budding Consensus Conference (ITBCC) and the recommendations of the International TILS Working Group (ITWG) [4, 5].

Correlation analyses as well as survival analyses were performed for different budding-TILs subgroups. The influence of chemotherapy in stage II and III colon cancer (CC) as well as PD-L1 immunohistochemistry in CC stages I-IV were additionally analyzed.

Results

We were able to categorize the tumor-budding combination into four groups with significantly different overall survival ($p=0.001$), especially in the large group of WHO low grade CRC [6,7]. The parameter TILs was superior to the parameter budding. However, budding was able to further stratify patients into prognostic subgroups. Out of these results, a new, morphology-based, simple risk score for CRC was developed [7]. The budding-TILs combination was able to identify subgroups in stage II and III CC who might not benefit, respectively do benefit from adjuvant chemotherapy to avoid under- or overtreatment [8]. Additionally, by using PD-L1-immunohistochemistry, we were able to identify cases that might benefit from immunotherapy regardless of their mismatch repair status [9].

Conclusion

The combination of budding and TILs as tumor-host antagonists is able to stratify CRC into prognostic groups. This is especially interesting in the large group of low grade CRC. The budding-TILs combination is further able to identify subgroups with or without benefit from chemotherapy as well as patient subgroups as

potential targets to immunotherapy.

Literaturangaben

- [1] Global Cancer Observatory, (2020), Cancer Today, International Agency for Research on Cancer, Lyon, <https://gco.iarc.fr/today>, 2021-04-22
- [2] Nagtegaal ID, Arends MJ, Odze RD, Lam AK, (2019), Tumours of the colon and rectum, Lokuhetty D, White VA, Watanabe R, Cree IA, WHO Classification of Tumours. Digestive system tumours., Lyon, 177-187, Digestive system tumours., International Agency for Research on Cancer
- [3] Food and Drug Administration, <https://www.accessdata.fda.gov/scripts/cder/daf/index.cfm?event=overview.process&ApplNo=125514>, 2022-02-25
- [4] Lugli A, Kirsch R, Ajioka Y et al, (2016), Recommendations for reporting tumor budding in colorectal cancer based on the International Tumor Budding Consensus Conference (ITBCC) 2016., *Mod Pathol*, 1299-1311, 30(9), <https://doi.org/10.1038/modpathol.2017.46>
- [5] Hendry S, Salgado R, Gevaert T et al , (2017), Assessing Tumor-Infiltrating Lymphocytes in Solid Tumors:A Practical Review for Pathologists and Proposal for a Standardized Method from the International Immuno-Oncology Biomarkers Working Group: Part 2: TILs in Melanoma, Gastrointestinal Tract Carc, *Adv Anat Pathol* , 311-335, 24(6), <https://doi.org/10.1097/PAP.000000000000162>
- [6] Lang-Schwarz C, Melcher B, Haumaier F, Lang-Schwarz K, Rupprecht T, Vieth M, Sterlacci W, (2018), Budding and tumor infiltrating lymphocytes - combination of both parameters predicts survival in colorectal cancer and leads to new prognostic subgroups. , *Hum Pathol*, 160-167, 79
- [7] Lang-Schwarz C, Melcher B, Haumaier F, Schneider-Fuchs A, Lang-Schwarz K, Krugmann J, Vieth M, Sterlacci W, (2019), Budding, tumor infiltrating lymphocytes, gland formation: scoring leads to new prognostic groups in WHO-low grade colorectal cancer with impact on survival. , *Hum Pathol*, 81-89, 89
- [8] Lang-Schwarz C, Melcher B, Dregelies T, Norouzzadeh Z, Rund-Küffner S, Lang-Schwarz K, Vieth M, Sterlacci W, (2021), Adjuvant Chemotherapy in Stage II and III Colon Cancer: the Role of the „Budding and TILs-(Tumor Infiltrating Lymphocytes) Combination“ as Tumor-Host Antagonists. , *Int J Colorectal Dis*, 1765-1779, 36 (8), <https://doi.org/10.1007/s00384-021-03896-9>
- [9] Lang-Schwarz C, Melcher B, Hartmann A, Bertz S, Dregelies T, Lang-Schwarz K, Vieth M, Sterlacci W, (2021), Programmed death ligand 1 (PD-L1) in colon cancer and its interaction with budding and tumor-infiltrating lymphocytes (TILs) as tumor-host antagonists., *Int J Colorectal Dis*, 2497-2510, 36 (11), <https://doi.org/10.1007/s00384-021-03985-9>

DGP09 Big Data and AI

DGP09.02

Artificial Intelligence helps pathologists improve diagnostic efficiency and accuracy in prostatic biopsy diagnosis.

J. A. Retamero, P. Raciti, D. Klimstra

Paige, Medical, New York, United States of America

The use of Artificial intelligence (AI) for routine diagnostic use in pathology is becoming a reality. The United States Food and Drug Administration authorized Paige Prostate, the first AI system in pathology, in September 2021. AI promises to help pathologists in their diagnostic tasks, but relatively little is known as to how this new technology can actually help pathologists. We review the existing scientific evidence in favour of Paige Prostate and how pathologists aided by this breakthrough technology improve their diagnostic accuracy as well as their efficiency in prostatic biopsy diagnosis.

AI-Assisted Cancer Detection

P. Schöffler

Technical University of Munich, Munich, Germany

AI in Pathology has reached clinical grade and is already commercially available, cleared by the FDA. But how does it work at all? And what do we need to generate future AI that can support pathologists in their daily routines? We explain the concept of multiple instance learning at the example of Paige's Prostate Cancer detection algorithm and outline chances and limitations of future models.

Fast and Robust Deep Tissue Cartography for Colon Sections

V. Bruns¹, M. Benz¹, P. Kuritcyn¹, J. Dexl¹, T. Wittenberg¹, M. Eckstein^{2, 3}, A. Hartmann^{2, 3}, **C. I. Geppert**^{2, 3}

¹Fraunhofer IIS, Erlangen, Germany, ²Institute of Pathology, University Hospital Erlangen-Nürnberg, Friedrich-Alexander-Universität Erlangen-Nürnberg (FAU), Erlangen, Germany, ³Comprehensive Cancer Center Erlangen-EMN (CCC ER-EMN), Erlangen, Germany

Background

Tissue Cartography divides a digitized tissue section by tissue type. Each class is assigned a label color, which is overlaid to the hematoxylin & eosin (H&E) staining. This provides an easy to grasp overview of the tissue section, and important parameters (area, composition, distribution) can be derived.

We developed a 7-class AI model for H&E-stained colon sections [1].

Challenges arise from the huge size of these digitized sections and from the high variance introduced by differences in staining and whole slide scanners. Therefore, we focus on the development of a fast and robust solution.

Methods

A classification model was trained on 2 million patches extracted from 92 annotated sections of a patient cohort comprising both healthy samples and adenocarcinoma of different stages. A set of additional 39 sections was digitized with six different scanners, providing a test set with high variance.

The addressed challenges are encountered using a combination of actions. Firstly, various model architectures of convolutional neural networks (CNNs) are compared in terms of their inference runtime and accuracy [2]. Secondly, robustness is achieved using data augmentation, increasing only the training time, but not the inference time [3]. Thirdly, similar tissue regions are auto-clustered before classification. Based on the observation that a sufficiently small cluster (mean area 0.05 mm²) typically contains tissue of only type, we hypothesized that it is sufficient to classify only a subarea per cluster. This decreases the overall computational cost, yet increases the accuracy since clusters contours (in contrast to patches) follow the tissue morphology.

Results

From a selection of 10 CNN models, an EfficientNet B0 scores best when weighing accuracy and speed equally. Embedding the model in the proposed generic framework of pre-clustering with random patch drawing yields a speedup of 41%, while at the same time raising the accuracy from 94% to 96%. The prediction accuracy drops from over 90% to 40% for slides digitized with other scanners and is brought back up to 90% by employing domain specific data augmentation.

Conclusion

It takes considerable effort to develop AI models that are fast and robust. We provide a generic approach

that is shown to overcome these challenges and should be similarly applicable to other classification tasks in computational pathology.

Literaturangaben

[1] F. Wilm, M. Benz, V. Bruns, S. Baghdadian, J. Dexl, D. Hartmann, P. Kuritcyn, M. Weidenfeller, Th. Wittenberg, S. Merkel, A. Hartmann, M. Eckstein, C. I. Geppert, (2021), Fast whole-slide cartography in colon cancer histology using superpixels and CNN classification, Arxiv (Preprint), 26, <https://arxiv.org/abs/2106.15893>, 2022-03-01

[2] P. Kuritcyn, M. Benz, J. Dexl, V. Bruns, A. Hartmann, C. Geppert, Comparison of CNN models on a multi-scanner database in colon cancer histology, Medical Imaging with Deep Learning, Lübeck

[3] P. Kuritcyn, C. I. Geppert, M. Eckstein, A. Hartmann, V. Bruns, J. Dexl, S. Baghdadian, D. Hartmann, D. Perrin, Th. Wittenberg, M. Benz, (2020), Robust slide cartography in colon cancer histology - Evaluation on a multi-scanner database, Bildverarbeitung für die Medizin

DGP10 Junges Forum II: Pathologie Quo vadis?

DGP10.03

Board certification in Europe - differences in duration, examination and acknowledgement

T. T. Rau, C. Nepl, I. Esposito

Institut für Pathologie, UKD Düsseldorf, Düsseldorf, Germany

Demographisch erwartbar wird Deutschland in den nächsten Jahren einem Mangel an Pathologinnen und Pathologen zu bewältigen haben. Zusätzlich stellen die Aufgaben durch fachlichen Wissenszuwachs, akademischer Pathologie, Mediziner-Ausbildung, Transformations-Prozesse und die Attraktivität der Arbeitsbedingungen wie Vereinbarkeit von Familie und Beruf eine Herausforderung für die pathologischen Gesellschaften dar.

Eine bidirektionale Öffnung für internationale Entsendung und Rekrutierung von PathologInnen könnte möglicherweise Abhilfe schaffen.

In einer vergleichenden Analyse wurden die 30 Länder im Europäischen Wirtschaftsraum einschliesslich Island, Liechtenstein, Norwegen und der Schweiz hinsichtlich einschlägiger Weiterbildungskonzepte, Art und Durchführung der Facharztprüfung sowie Zusatzqualifikationen unter die Lupe genommen. Daran anschliessend wurden Fragen zur Anerkennung von Examina, Titeln und Facharztprüfungen eruiert.

Nach wie vor besteht eine hohe Bandbreite an Weiterbildungsmodalitäten, die eine Vergleichbarkeit und den Quereinstieg neben sprachlicher Hürden erschweren. Die Dauer der Weiterbildung schwankt zwischen 5-6 Jahren. Die Erlangung des Facharztstitels kann über alleinige Ableistung von Pflichtzeiten und -zahlen bis hin zu einem voll strukturierten zweitägigen Assessment erfolgen. In Einzelfällen gehören auch Inhalte der Mikrobiologie und Virologie zum Weiterbildungskonzept. Gesonderte Zusatzqualifikationen bestehen mancherorts hinsichtlich Molekularpathologie und Zytopathologie. Erlangte Examina werden vereinfacht anerkannt, was jedoch nicht zwingend für akademische Titel und Zusatzqualifikationen gilt. Für eine Anerkennung von Zeiten im Ausland muss eine arbeitsvertragliche Beschäftigung an einer Weiterbildungsstätte vorliegen, die allerdings dem Anerkennungs-Vorbehalt der Landesärztekammern unterliegt.

Grundsätzlich erlauben die Abkommen im EWR eine hohe Durchlässigkeit der Systeme anders als beispielsweise mit dem Anglo-amerikanischen und australischen System. Erste Harmonisierungsschritte bestehen mit dem Selbsttest der Europäischen Gesellschaft für Pathologie, der aber im Gegensatz zu anderen Disziplinen noch nicht als «europäischer Facharzttitel» ausgebaut ist.

DGP11 Neues aus der WHO

DGP11.01

Uterine Leiomyosarkome – was sagt die WHO-Klassifikation 2020?

L.-C. Horn

Institute of Pathology, University of Leipzig, Leipzig, Germany

In abnehmender Häufigkeit unterscheidet die WHO-Klassifikation von 2020 das spindelzellige, epitheloide und myxoide LMS des Uterus. Histologische Parameter zur Abgrenzung zum Leiomyom sind: nukleäre Atypien (Kerngrößenschwankungen $>2-3 : 1$), die Mitosezahl (meist >10 Mitosen / 10 HPF bei 0.55 mm Gesichtsfelddurchmesser bzw. 0.24 mm² Fläche) und der Nachweis von Tumorzellnekrosen mit unterschiedlicher Bedeutung in Abhängigkeit vom histologischen Subtyp. Die Mitosezahl wird durch präanalytische, färbetechnische und tumorgeographische Parameter beeinflusst. Ein Grading uteriner LMS ist von der WHO 2020 nicht vorgesehen, wenn von der Klinik gefordert kann es in Anlehnung an das FNCLCC-System der Weichgewebssarkome erfolgen. p53, p16, Ki-67 und WT-1 sind zur Differenzialdiagnose zwischen Leiomyom und LMS derzeit in der Evaluierung. Die Molekularpathologie spielt derzeit (noch) eine untergeordnete Rolle in der Differenzialdiagnostik.

Die WHO-Klassifikation 2020 unterscheidet das spindelzellige, epitheloide und myxoide Leiomyosarkom (LMS) als morphologische Varianten. Diagnostische Parameter zur Unterscheidung zum Leiomyom sind nach wie vor nukleäre Atypien (Kerngrößenschwankungen $>2-3 : 1$), die Mitosezahl (meist >10 Mitosen / 10 HPF bei 0.55 mm Gesichtsfelddurchmesser bzw. 0.24 mm² Fläche) und Tumorzellnekrosen. Die Mitosezahl soll pro mm Gesichtsfelddurchmesser bzw. pro mm² Fläche ermittelt werden. Die genannten morphologischen Kriterien haben in Abhängigkeit vom histologischen Subtyp unterschiedliche Bedeutung. Bei der Ermittlung der Mitosezahl sind präanalytische, färbetechnische und tumorgeographische Aspekte zu beachten. Der STUMP ist nach wie vor die histopathologisch am schlechtesten charakterisierte Entität. Patientinnen mit der Diagnose STUMP sollen ein onkologisches Follow up in Analogie zum LMS erhalten. Immunhistochemische Färbungen mit p53, p16, Ki-67 und WT-1 können zur Abgrenzung von Leiomyomata zum Teil hilfreich sein. Molekularpathologische Untersuchungen spielen in der Differenzialdiagnostik derzeit (noch) eine untergeordnete Rolle.

The 5.th Edition of the WHO (URO5): Prostate Cancer

G. Kristiansen

Universitätsklinikum Bonn, Institut für Pathologie, Bonn, Germany

The fifth edition of the WHO fascicle "Urogenital Tumors" is about to be released. In this presentation, major changes or issues of controversy of the new WHO classification of prostate cancer are presented. The text has been markedly updated and also tightened, the terminology has become more stringent. The term "tumour subtypes" replaces "tumour variants" for distinct clinical or morphological categories within a tumour type, that are morphologically distinct and have prognostic significance.

The term "variant" now denominates genomic rather than morphological features. Former entities like low-grade prostatic intraepithelial neoplasia or the cribriform subtype of high-grade prostatic intraepithelial neoplasia (HGPIN) are no longer regarded as distinct entities.

The importance of intraductal carcinoma of the prostate (IDC-P) has now been recognized, but recommendations who to incorporate it in the Gleason score are diverging.

It can be expected that technical advances in AI based Gleason grading may become relevant in the future but their application is not mandatory at this time.

Even though there is data to support the notion of invasive ductal carcinoma of the prostate as a subtype of acinar carcinoma, in URO5 it is still supported as a separate entity/variant.

Basal cell carcinoma of the prostate is a type of adenoid cystic carcinoma occurring in the prostate and hence has been renamed as "adenoid cystic (basal cell) carcinoma of the prostate".

Prostatic intraepithelial neoplasia–like adenocarcinoma has now been relocated to "acinar adenocarcinoma" because of its clinical behaviour and its genetic alterations, which markedly differ from ductal adenocarcinoma, rendering the old term "PIN-like ductal adenocarcinoma" obsolete.

What is new in the 5th edition of the WHO classification of lymphoid tissue tumours?

G. Ott

Robert-Bosch-Krankenhaus, Abteilung für Klinische Pathologie, Stuttgart, Germany

This paper represents an overview of the new concepts and items in the upcoming 5th edition of the World Health Organization Classification of Haematolymphoid Tumours (WHO-HAEM5) focussing on lymphoid neoplasms. Major changes as compared to the revised 4th edition (WHO-HAEM4R) include a reorganization of entities by a hierarchical (Linnean) system as is adopted throughout the 5th edition of the WHO classification of tumours of all organ systems, the modification of nomenclature for some entities, a revision of diagnostic criteria or subtypes, deletion of certain entities and introduction of new entities. More specifically, both within the B-cell and the T-cell category, tumour-like lesions have been included into the classification that may pose a differential diagnosis to the diagnosis of lymphomas. Within the B-cell system, major changes include the addition of new entities within B-ALL, rendering the grading of follicular lymphoma optional, deletion of the diagnostic term of *B-prolymphocytic leukaemia*, creation of a new umbrella term for lymphomas arising at immune-privileged sites, and the formulation of a new concept for describing and diagnosing patterns of lymphoproliferations arising in the setting of immune deficiency/dysregulation, among others. The mature T-cell and NK-cell neoplasms are grouped into 9 families based on diverse concepts: cell of origin/differentiation state, clinical scenarios, disease localization, and cytomorphology. Lymphomas of T- or NK-cell lineage are not separated as two categories in WHO-HAEM5 because some entities comprise a spectrum of tumours of NK, T, hybrid or indeterminate phenotype, such as in extranodal NK/T-cell lymphoma, EBV+ nodal T- and NK-cell lymphoma, chronic active EBV disease and severe mosquito bite allergy. A common family terminology of nodal T-follicular helper cell lymphomas (nTFHLs) is introduced in WHO-HAEM5, with previously recognized diseases now regarded as entities within this family. Finally, mesenchymal lesions specific to lymph node and spleen, and germline predisposition syndromes associated with the lymphoid neoplasms are described.

DGP12 Strukturierte Befundung - sinnvoll?

DGP12.03

Strukturierte Befundung am Beispiel Prostata

H. Reis^{1, 2, 3}

¹*Dr. Senckenbergisches Institut für Pathologie, Universitätsklinikum Frankfurt, --, Frankfurt, Germany,*

²*University Hospital Frankfurt, Dr. Senckenberg Institute of Pathology, Frankfurt, Germany,* ³*University Medicine Essen, Institute of Pathology, Essen, Germany*

Die Herausforderungen an die Pathologie im Allgemeinen und an die Datenstrukturierung im Speziellen steigen seit Jahren. Zwar werden im Rahmen der pathologischen Befundung erhebliche Datenmengen generiert. Diese sind allerdings häufig nicht in strukturierter Form für weitere Zwecke vorhanden oder müssen durch aufwändige und fehleranfällige Recherche aus den Befunden extrahiert werden.

Da die Daten allerdings für unterschiedliche interne und externe Zwecke, wie beispielsweise im Rahmen von Audits, Tumororganzentren, Meldungen an die Krebsregister, Bedienung unterschiedlicher Konsortien, zur Abrechnung bzw. Leistungserfassung, organisationsintern und auch zur Wissenschaft, benötigt werden, ist eine direkte, strukturierte und qualitativ hochwertige Erfassung von Pathologiedaten von hoher Relevanz und allgemeinem Interesse.

Der Vortrag wird den Prozess des Aufbaus eines strukturierten Befundungssystems am Beispiel des Prostatakarzinoms (Biopsie) zeigen und in den allgemeinen Kontext einordnen. Dabei wird die Eigenentwicklung vor dem Hintergrund internationaler Systeme (ICCR) und kommerzieller Entwicklungen eingeordnet.

DGP12.04

Structured Reporting in Gastrointestinal Pathology

R. Langer

Kepler Universitätsklinikum und Johannes Kepler Universität, Institut für Klinische Pathologie und Molekularpathologie, Linz, Austria

Synoptische oder strukturierte Berichte in der Medizin, speziell in der Pathologie, sind im Gegensatz zu traditionellen narrativen Berichten gekennzeichnet durch ein listen- bzw. laborwertartiges Format und die Verwendung standardisierter Checklisten. Sie sollen zur Vollständigkeit und Verständlichkeit der Berichte und damit letztlich zu einer verbesserten Patientenversorgung bei. Als Grundlage für eine umfassende strukturierte Befundung haben verschiedene Fachgesellschaften für Pathologie Datensätze für alle relevanten Tumortypen veröffentlicht, z.B. die CAP oder die ICCR, die auch die CAP Protokolle mit einbezieht. Mittlerweile sind für alle Gastrointestinale Tumore ICCR Datensätze vor. Anhand dieser Protokolle werden exemplarisch Nutzen und Herausforderungen bei der Implementation von synoptischen Berichten diskutiert.

DGP13 Therapieansprechen: Synergien von Radiologie und Pathologie?

Response evaluation in breast pathology after neoadjuvant treatment

A. Lebeau^{1, 2}

¹Universitätsklinikum Hamburg-Eppendorf, Institut für Pathologie, Hamburg, Germany, ²Gemeinschaftspraxis für Pathologie, Lübeck, Germany

Pathomorphological examination of surgical specimens after NAT provides objective information about the effect of therapy and the option to optimize adjuvant treatment selection. Pathological complete response is a validated and evaluable surrogate end point of survival after neoadjuvant therapy. Thus, standardized evaluation of tumour regression and residual tumour extent is mandatory. In the lecture, the currently most important concepts for quantifying the post-therapeutic tumour residues including the clinically relevant CPS+EG score will be presented and the question of tumour heterogeneity will be highlighted. In addition, the special features of the application of the TNM classification before and after neoadjuvant therapy will be discussed.

Morphological and Molecular Aspects of Therapy Response - the View of the Pathologist

R. Langer

Kepler Universitätsklinikum und Johannes Kepler Universität, Institut für Klinische Pathologie und Molekularpathologie, Linz, Austria

Multimodale Therapiekonzepte haben sich für eine Vielzahl von Tumoren als Standardbehandlung Etabliert. Gewebeveränderungen nach neoadjuvanter Therapie können morphologisch erfasst und charakterisiert werden. Herausforderungen in diesem Bereich betreffen die Makroskopie, die Spezifität von therapie-assoziierten Veränderungen, und die Quantifizierung und Charakterisierung der regressiven Veränderungen für die Etablierung von klinisch validierten Regressionsgraduierungs-Schemata. Auf molekularer und biologischer Seite liefern Gewebeproben und Resektate nach Therapie wichtige Daten über die Tumorbilogie und Response- bzw. Resistenzmechanismen, wobei metabolische und molekulare Veränderungen wertvolle Informationen die über die reine Morphologie hinausgehen.

Grading and Response Assessment of Sarcoma: Potential and Limitations of Radiological Data

W. Kunz

Ludwig-Maximilian-Universität München, Klinik und Poliklinik für Radiologie, München, Germany

In der klinischen Versorgung von Sarkomen spielt die diagnostische und interventionelle Radiologie eine bedeutende Rolle. In der Primärdiagnostik wird je nach Lokalisation oft eine Entnahmestelle für die Biopsie anhand der radiologischen Darstellung gewählt. Die radiologische Information zum Primärbefund kann dabei auch Hinweise auf die Entität und das Grading enthalten. Im Verlauf unter Therapie nutzt man die radiologische Beurteilung ob ein Therapieansprechen oder eine Progression vorliegt; hier gibt es jedoch je nach Entität und Lokalisation deutliche Einschränkungen die pathologische Response abzubilden. Eine weitere Herausforderung sind Muster der Pseudoprogression in der radiologischen Diagnostik. Der Vortrag wird verschiedene klinisch etablierte Aspekte und auch zukünftige Potentiale der Radiologie aufzeigen, insbesondere auch in der Kombination der pathologischen und radiologischen Daten.

Histopathological parameters of lymph node involvement after chemoradiation reveal viable tumor cells but no keratin debris as a prognostic factor in head and neck squamous cell carcinoma

A. Gollietz¹, G. B. Morand^{2, 3}, M. A. Broglie², P. Balermipas⁴, **N. J. Rupp**^{1, 5}

¹Department of Pathology and Molecular Pathology, University Hospital Zurich, Zurich, Switzerland,

²Department of Otorhinolaryngology - Head and Neck Surgery, University Hospital Zurich, Zurich, Switzerland, ³Department of Otolaryngology - Head and Neck Surgery, Sir Mortimer B. Davis – Jewish General Hospital, McGill University, Montreal, Canada, ⁴Department of Radiation Oncology, University Hospital Zurich, Zurich, Switzerland, ⁵Faculty of Medicine, University of Zurich, Zurich, Switzerland

Background

Salvage neck dissection (ND) is required for residual nodal disease after (chemo)radiation in head and neck squamous cell carcinoma (HNSCC). However, little is known about prognostic histopathological features in this situation. The aim of this study was to examine histopathological parameters in ND specimens and correlate them with patient outcome to determine the relevant parameters for histopathological reporting.

Methods

Salvage ND specimen from a cohort of n=75 HNSCC patients were evaluated on H&E stains for the following parameters: viable tumor cells, necrosis, swirled keratin debris, foamy histiocytes, bleeding residues, fibrosis, elastosis, pyknotic cells, calcification, cholesterol crystals, multinucleated giant cells, perineural and vascular invasion. Histological data were correlated with survival outcomes.

Results

Viable tumor cells were present in 30/75 (40%), necrosis in 52/75 (68%), swirled keratin debris in 18/75 (24%), foamy histiocytes in 21/75 (28%), bleeding residues in 15/75 (20%), fibrosis in 59/75 (79%), elastosis in 21/75 (28%), pyknotic cells in 42/75 (56%), calcification in 27/75 (36%), cholesterol crystals in 21/75 (28%), giant cells in 24/75 (32%), perineural invasion in 1/75 (1%) and vascular invasion in 3/75 (4%). Only the presence of viable tumor cells correlated with a worse clinical outcome (OS, TFS; $p < 0.05$).

Conclusion

We could confirm the presence of viable tumor cells as a relevant negative prognostic factor after (chemo)radiation. None of the other parameters correlated with a distinct outcome. Importantly, the presence of (swirled) keratin debris alone should not be considered as presence of viable tumor cells, but as ypN0.

DGP14 Update COVID-19 I (inkl. Ungarischer Workshop)

DGP14.01

The German Registry of COVID-19 Autopsies (DeRegCOVID) & the National Autopsy Network (NATON)

P. Boor

RWTH Aachen University, Aachen, Germany

Background: Autopsy is an important tool for understanding the pathogenesis of diseases, including COVID-19 and post-acute COVID-19 sequelae.

Material and methods: Early in 2020, the German Registry of COVID-19 autopsies (DeRegCOVID) was launched together with the German Society of Pathology and the Federal Association of German Pathologists (www.DeRegCOVID.ukaachen.de). Building upon this, the National Autopsy Network (NATON) started in 2022 as a follow-up of the collaborative autopsy research network DEFEAT PANDEMIcs.

Results: The main objective of DeRegCOVID is to collect data on ideally all autopsies of COVID-19 deceased persons in Germany to meet the need for centralized, coordinated, and structured data collection and reporting in the pandemic. 27 university autopsy centers from forensic medicine, neuropathology, and pathology and 5 non-university autopsy centers contributed data on already more than 1400 autopsies and more than 19000 samples. The respective centers keep rights to their data and biomaterials, which remain decentralized. DeRegCOVID serves as a broker between researchers and autopsy centers. To date, more than 30 publications have been supported by DeRegCOVID and even more were published within the frame of DEFEAT PANDEMIcs and NATON. NATON aims to serve as i/ long-term pandemic preparedness infrastructure for autopsies, ii/ nucleus for collaborative autopsy research with decentralized biobanking, iii/ sustainable platform with broad application areas for the collection of data obtained through autopsies.

Conclusions: The extraordinary cooperation in Germany in the field of autopsies during the COVID-19 pandemic enabled the establishment and successful development of DeRegCOVID and NATON in a unique, national, collaborative autopsy research network. It is a strong signal of the need, willingness and expertise of forensic pathologists, neuropathologists and pathologists to contribute to the joint management of current and future pandemics with autopsy-derived data and samples.

New insights into COVID-19

M. Kühnel¹, C. Werlein¹, M. Ackermann², J. Bauersachs³, P. Boor⁴, P. Braubach¹, S. Freifrau von Stilfried und Rattonitz⁴, A. Haverich⁵, H.-H. Kreipe¹, F. Länger¹, N. Marx⁴, S. Mentzer⁶, L. Neubert¹, M. Reichart⁷, J. L. Robertus⁸, T. Saldit⁷, H. Stark¹, A. Tzankov⁹, S. Verleden¹⁰, T. Welte¹¹, D. Jonigk¹

¹Medizinische Hochschule Hannover, Institut für Pathologie, Hannover, Germany, ²University of Witten/Herdecke, Helios University Clinic Wuppertal, Institute of Pathology and Department of Molecular Pathology, Wuppertal, Germany, ³Medizinische Hochschule Hannover, Klinik für Kardiologie, Hannover, Germany, ⁴RWTH Aachen, Institut für Pathologie, Aachen, Germany, ⁵Medizinische Hochschule Hannover, HTTG Chirurgie, Hannover, Germany, ⁶Harvard Medical School, Laboratory of Adaptive and Regenerative Biology, Boston, United States of America, ⁷University of Göttingen, Institute for X-Ray Physics, Göttingen, Germany, ⁸Royal Brompton & Harefield NHS Foundation Trust, Department of Histopathology, London, United Kingdom, ⁹University Hospital Basel, Institute of Medical Genetics and Pathology, Basel, Switzerland, ¹⁰Antwerp University Hospital, Department of thoracic medicine, Antwerp, Belgium, ¹¹Medizinische Hochschule Hannover, Klinik für Pneumologie, Hannover, Germany

Hintergrund

Die COVID-19 Pandemie stellt den dritten weltweiten Corona-Virus-assoziierten Erkrankungsausbruch der letzten 20 Jahre dar. Klinisch dominiert die pulmonale Beteiligung mit einem akuten Lungenversagen (ARDS) bei schweren Verläufen, jedoch können auch andere Organsysteme wie das Herz-Kreislauf-System, Zentralnervensystem und der Gastrointestinaltrakt betroffen sein. Der Pathomechanismus der Organschädigung sowohl für die Lunge wie auch für die nicht-pulmonalen Organsysteme war zu Beginn der Pandemie weitestgehend unklar.

Methode

Immunhistochemische, elektronenmikroskopische, röntgentomographische und molekularpathologische Analysen an Autopsiegewebe führten zu einem besseren Verständnis der Pathophysiologie von COVID-19 einschließlich der molekularen Regulationsmechanismen.

Ergebnisse

Hierbei hat sich gezeigt, dass die so genannte intussuszeptive Angiogenese (IA) auch bei COVID-19-Patienten nachgewiesen wurde. Bei der IA verändert sich ein bestehendes Gefäß durch Einstülpung des Endothels und Ausbildung eines intraluminalen Septums, wodurch schließlich zwei neue Lumina entstehen. Hierdurch verändert sich die Hämodynamik, unter anderem durch Verlust der laminaren Strömung mit Ausbildung turbulenter inhomogener Flussgeschwindigkeiten. Dies könnte das Risiko für Mikrothromben erhöhen, die in Lunge, Herz, Leber, Nieren, Gehirn und Plazenta nachgewiesen wurden.

Schlussfolgerung

In Autopsiematerial von COVID-19-Patienten konnte ultrastrukturell in verschiedenen Geweben eine veränderte Mikrovaskularität, eine erhöhte IA sowie multifokale Thromben nachgewiesen werden. Es ist anzunehmen, dass diese Veränderungen sowohl für die beobachteten post-akuten interstitiell-fibrotischen Veränderungen wie auch bei long-COVID eine Rolle spielen.

Rapid Identification of Serological Reagents for the Immunohistochemical Detection of Coronavirus-associated Proteins in Formalin-fixed Paraffin-embedded Tissue

A. Jungbluth¹, D. Frosina¹, J. Bagha¹, E. Hernandez¹, M. Szabolcs²

¹Memorial Sloan Kettering Cancer Center, Pathology, New York, United States of America, ²Columbia University Hospital, Pathology, New York, United States of America

Background

Due to the sudden on-set and rapid pandemic course of Severe Acute Respiratory Syndrome Corona-Virus-2 (SARS-CoV2), the medical community was faced with the challenge not only to find proper treatment options, but also to describe the pathological changes associated with coronavirus infection. The latter implies the proper detection of viral proteins in surgical specimens to identify acute and chronic tissue damage in lung and other organs. During the onset of the pandemic, we developed a tissue independent screening method to test serological reagents with the various SARS-CoV2 proteins for their specificity and suitability for IHC of formalin-fixed paraffin embedded tissues.

Methods

To circumvent the problem of the unknown pathobiology of a novel virus in human tissue, we sought a tissue-independent testing method for screening commercially available antibodies. We were able to obtain HEK293 cells transfected with the various viral proteins (Raybiotech, Peachtree Corners, GA, USA). The cells were pelleted and processed like standard surgical specimens. Multi-pellet blocks were generated consisting of HEK293 cells transfected with nucleoprotein (NP), S1 spike protein subunit (S1), S2 spike protein subunit (S2), RNA-binding region as well as untransfected HEK293 cells. Antibodies were tested for their reactivity on the multi-pellet block. After selection on transfected cells, specific antibodies were then tested on autopsy specimen of patients who succumbed to Covid19 infections, Presence of virus was confirmed by rt-PCR and/or in-situ hybridization for viral RNA (RNAscope; ADC/Biotechne).

Results

Anti-SARS-CoV2 monoclonal antibodies were obtained commercially and consecutively tested, until the identification of proper reagents to viral NP, S1, and S2 proteins. A majority of antibodies did not work in IHC and/or generated unspecific reactivity displaying immunostaining with various viral proteins. A total of 10 antibodies were tested, only 3/10 mAbs proved useful for IHC in FFPE material. The reagents were: mAb 001 (anti-NP; SinoBiological) mAb 1A9 (anti-S2; GeneTex), and mAb 1035206 (Anti-S1; Novus). All 3 mAbs gave also strong and consistent staining in FFPE tissue. Immunostaining for viral protein was congruent with ISH localization of viral RNA.

Conclusion

HEK-293 cells transfected with viral proteins are an excellent way to test anti SARS-CoV2 mAbs for

specificity and suitability. A majority of commercial mAbs show strong albeit unspecific staining and are unsuitable for IHC.

COVID-19 associated pathology and categorization of death causes in 100 autopsy cases

A. Kiss^{1,2}, K. Danics², A. Pesti², J. Szilávik³, D. Dobi², T. Varkonyi², T. Glasz², G. Lotz², I. Valyi-Nagy³, Z. Schaff²

¹*Semmelweis Universität Budapest, Institut für Pathologie, Rechts- und versicherungsmedizin, Budapest, Hungary*, ²*Semmelweis University, Institute of Pathology, Forensic and Insurance Medicine, Budapest, Hungary*, ³*Central Hospital of Southern Pest-National Institute of Hematology and Infectious Diseases, Budapest, Hungary, Budapest, Hungary*

Background

Our aim was to analyze the clinicopathological features of severe acute respiratory syndrome coronavirus 2 (SARS-CoV-2) infection in 100 autopsies which were performed on patients in the Institute of Pathology, Forensic and Insurance Medicine at Semmelweis University, Budapest. (Danics et al, *Geroscience*. 2021 Oct;43(5):2265-2287).

Methods

The infection was proved by real-time RT-PCR. 21 patients were from the pandemic's "first wave" (March through July) and 79 from the "second wave" (August through December). Autopsy evaluation analyzed alterations on macroscopy as well as findings on microscopy of scanned and scored sections of formalin-fixed, paraffin-embedded tissue samples (50-80 blocks/case). RNAscope *in situ* hybridization revealed tissue localization of SARS-CoV-2.

Results

Three mortality categories were established regarding the relevance of SARS-CoV-2 infection: (1) "strong" association, (n=57; in which COVID-19 was primary responsible for death; (2) "contributive" association (n=27), in which a pre-existing condition independent of COVID-19 was primary responsible for death, however, with substantial COVID-19 co-morbidity; (3) "weak" association (n=16), in which COVID-19 was minimally or not at all responsible for death. In the first wave "contributive" association dominated the cases, while in the second wave the "strong" association represented 2/3 of the cases. Abnormalities in the lung included diffuse alveolar damage, macrophage infiltration, and vascular and alveolar fibrin aggregates. Macro- and microvascular thrombi and thromboemboli were also detected (lung, kidney, liver). Liver alterations featured sinusoidal dilation and extended space of Disse. Further, endothelial damage and fibrin accumulation and increased vascular permeability was seen. The hearts showed chronic myocardial damage combined with patchy acute myocyte damage in 50 % of patients. Myocarditis was unfrequent, 3 % of cases. Beside 11 end stage renal disease cases the kidneys showed limited glomerular changes, rather associated with acute thrombotic microangiopathy.

Conclusion

Clinicopathological analysis of co-morbidities as well as that of direct pathological signs of COVID-19 allowed accurate categorization of cause of death and COVID-19 association as "strong," "contributive," or "weak." Lung involvement, with reduced ventilatory capacity, was the primary cause of death in the "strong" and "contributive" categories. Liver alterations seem to be characteristic, however, not specific for COVID-19.

Placenta and COVID-19

D. Hargitai¹, Z. Kramer², E. Méray-Mózes¹, T. Barbai², J. Tímár², Z. Schaff², A. Kiss²

¹*Semmelweis Universität Budapest, Klinik für Geburtshilfe und Frauenheilkunde, Budapest, Hungary,*

²*Semmelweis Universität Budapest, II. Institut für Pathologie, Budapest, Hungary*

Aim of the study: Perinatal pathologists reported various pathological alterations in placentas derived from COVID-19 positive pregnancies. The occurrence of massive perivillous fibrin deposition (MPFD) and chronic histiocytic intervillitis (CHI) have been reported to be the most severe consequences of SARS-CoV-2 infection, while many cases showing fetal and/or maternal vascular malperfusion have also been observed. We have collected clinical data and histological findings of COVID-19 affected pregnancies in the different pandemic waves to evaluate the frequency of these entities in our institute.

Materials and Methods: Clinical data were collected from the medical records at Semmelweis University. Histological examination was performed on HE slides, diagnoses were given according to the Amsterdam criteria. Histiocytes were detected with CD68 antibody, SARS-CoV-2 virus particles were revealed by nucleocapsid and spike antibodies. SARS-CoV-2 detection was performed using PCR on either frozen tissues, or on formalin fixed, paraffin embedded samples.

Results: 180 placentas from COVID-19 positive pregnant women were submitted to our institute for pathological examination between April 2020 and March 2022. Data of the first and second wave were evaluated in one group, since the same virus variant was proven to be present. The third, fourth and fifth waves were analyzed separately. During the first and the second waves the most common alteration was maternal vascular malperfusion. In the third and fourth waves fetal vascular malperfusion was the most frequent diagnosis, meanwhile the number of MPFD with CHI increased rapidly, causing intrauterine fetal demise in 7 cases. In the fifth wave 6 cases of fetal vascular malperfusion and 2 cases of maternal vascular malperfusion were diagnosed, however no cases of MPFD with CHI were detected. In nine cases of intrauterine fetal demise both placental and fetal tissue was available: 8 placentas with MPFD were positive for the virus, while fetal tissues proved to be positive in only one case. One intrauterine fetal demise lacked the MPFD alteration of placental tissue, in this case histological signs of severe maternal vascular malperfusion was detected.

Conclusions: SARS-CoV-2 variants caused different pattern of placental alterations. Of these, MPFD with CHI is a life threatening condition, in these cases viral infection in placental tissue causes „suffocation” of the fetus indirectly, hence early detection is crucial.

DGP14 Update COVID-19 II

DGP14.07

Minimally invasive autopsies for the investigation of pulmonary pathology of COVID19 - experiences of a longitudinal series of 92 patients.

P. Noack¹, C. Grosse¹, J. Bodingbauer¹, M. Almeder¹, H. J. Salzer², J. Meier³, B. Lamprecht⁴, R. Langer¹

¹Kepler Universitätsklinikum und Johannes Kepler Universität, Institut für Klinische Pathologie und Molekularpathologie, Linz, Austria, ²Kepler Universitätsklinikum, Klinik für Innere Medizin / Pulmonologie, Linz, Austria, ³Kepler Universitätsklinikum und Johannes Kepler Universität, Klinik für Anästhesiologie und Intensivmedizin, Linz, Austria, ⁴Kepler Universitätsklinikum und Johannes Kepler Universität, Klinik für Innere Medizin / Pulmonologie, Linz, Austria

Background

Autopsies of deceased COVID-19 patients have provided important insights on morphology and pathophysiology of this new disease. Most studies, however, comprise limited case numbers. Factors hampering the investigation of larger series were - and still are - legal and safety issues amongst others. Minimally autopsy (MIA) approaches may be helpful in such situations offering the possibility to obtaining tissue for diagnostic and research purpose with limited risk of infection.

Methods

We report our experiences performing MIA for the collection and analysis of lung tissue of COVID-19 patients who died during the so-called "second wave" between October 2020 and April 2021. MIA were performed by a intercostal approach including removal of a 5cm long piece of rib followed by manual collection of four pieces of lung tissue (5-8 cm size) from each patient. Histology findings were compared with clinical data.

Results

Ninety-two patients (median age 78 years; range 48-98 years; 35 females 57 males) corresponding to 43% of all deceased COVID-19 patients during the study period were included. Diffuse Alveolar Damage (DAD) in various stages was observed in all patients. Eighteen patients had a predominant exsudative DAD pattern, 43 patients a predominant proliferative DAD pattern and 31 patients had a mixed pattern. These findings correlated significantly among the tissue samples within one patient ($p < 0.001$) without significant heterogeneity. Additional suppurative component was present in 46 cases. Fungi were detected in 11 patients. Occurrence of fungi was associated with suppurative component ($p < 0.001$) but not with patterns or degree of DAD. Patients with mixed DAD patterns had initially lower CT values ($p = 0.049$). Younger age was

associated with a predominant DAD proliferative pattern ($p=0.019$) but this was also linked to longer hospitalization times including intensive care unit ($p=0.026$ and $p<0.001$). Results of intravital microbiology tests (i.e., positive bronchioalveolar lavage or blood cultures) did not correlate with DAD pattern, nor presence of fungi or suppurative component.

Conclusion

We observed the expected lung changes in a large longitudinal autopsy series of COVID-19 patients. Our MIA approach can be considered a safe and reliable method for performing postmortal diagnostics in COVID19 cases and other risk situations. The lack of correlation between histological changes indicative of bacterial or fungal superinfection and microbiology could have clinical impact.

Update of a German Autopsy Study of Fatal Cases with SARS-CoV-2 Infection after Vaccination

B. Märkl¹, K. Hirschbühl², T. Schaller¹, R. Claus², E. Sipos¹, L. Rentschler¹, A. Maccagno¹, B. Grosser¹, E. Kling², M. Neidig², T. Kröncke², O. Spring², G. Braun², H. Bösmüller³, M. Seidl⁴, I. Esposito⁴, J. Pablik⁵, J. Hilsenbeck⁵, P. Boor⁶, M. Beer⁷, S. Dintner¹, C. Wylezich⁷

¹UK Augsburg, Institut für Pathologie und Molekulare Diagnostik, Augsburg, Germany, ²UK Augsburg, Augsburg, Germany, ³UK Tübingen, Tübingen, Germany, ⁴UK Düsseldorf, Düsseldorf, Germany, ⁵UK Dresden, Dresden, Germany, ⁶UK Aachen, Aachen, Germany, ⁷Friedrich-Loeffler-Institut, Greifswald, Germany

Background

The introduction of vaccines against SARS-CoV-2 was crucial in coping with the pandemic. It helped to reduce the rate of severe course of the infection and prevented the health systems from collapse. Despite the efficacy of the currently available vaccines, breakthrough infections and vaccination failures, even with severe or fatal courses, are known.

This autopsy study aimed to characterize fatal cases with proofed SARS-CoV-2 infection, considering the administered vaccines, vaccination status, viral variant, viral detection within the organs and antibody titers. The analyses included immunohistochemistry, RNA-ISH, RT-PCR, viral whole-genome sequencing, and serum antibody analyses.

Methods

The autopsies were performed in 17 partially and 31 fully vaccinated individuals. The latter group included nine cases after booster vaccine and one case after recovering from infection and complete vaccination. In 35 cases, complete autopsies were performed, while in 13 cases, the autopsies were restricted to obtaining tissue samples (mainly lungs, heart, liver, kidneys, spleen, and soft tissues). In partially and fully vaccinated cases, the median ages were 72 vs. 79 years, and the male-female ratios were 1:1.25 and 1:0.35, respectively.

Results

COVID-19-pneumonia was the direct cause of death in 12 of 17 partially vaccinated and 21 of 31 in completely vaccinated cases. In these cases, gross and histological morphology were similar to unvaccinated deceased. No influence of the viral variants could be identified. Data concerning circulating antibodies against spike-protein were available in 24 cases in the group of fully vaccinated patients, of which three cases could be classified as vaccination failures because of low titers. A high number of comorbidities was found in all individuals, particularly the rate of malignancies and immunocompromising conditions was increased compared to unvaccinated cases of the Augsburg series. Remarkable low Ct-values were found in nasopharyngeal smear samples. The rate of PCR-based viral RNA detection in non-respiratory samples, including cerebrospinal fluids and CNS samples, significantly increased compared to non-vaccinated cases.

Conclusion

Fatal cases of COVID-19 after vaccination occurred in individuals with severe comorbidities, often immunocompromised and suffering from cancer. The high viral burden in these cases suggests a failure to adequately eliminate the virus despite being vaccinated with development of anti-SARS-antibodies.

Clinical, serological and postmortem findings in SARS-CoV2-vaccine-induced thrombotic thrombocytopenia

V. Warm¹, H. Bösmüller¹, M. Granai¹, K. Althaus², G. Uzun², K. Schwab³, P. Möller⁴, P. Schirmacher⁵, L. Hartmann³, T. Bakchoul², F. Fend¹

¹Universitätsklinikum Tübingen, Allgemeine und Molekulare Pathologie und Pathologische Anatomie, Tübingen, Germany, ²Universitätsklinikum Tübingen, Institut für klinische und experimentelle Transfusionsmedizin, Tübingen, Germany, ³Universitätsklinikum Heidelberg, Pathologisches Institut, Heidelberg, Germany, ⁴Universitätsklinikum Ulm, Institut für Pathologie am Universitätsklinikum Ulm, Ulm, Germany, ⁵Universitätsklinikum Heidelberg, Pathologisches Institut, Tübingen, Germany

Background

Since the appearance of SARS-CoV2 in late 2019, COVID-19 has become a global pandemic. The most effective way to contain infection and severe disease is vaccination against SARS-CoV2. As adverse events after vector-based vaccines, thrombosis with thrombocytopenia similar to autoimmune heparin-induced thrombocytopenia have been reported and were designated vaccine-induced thrombotic thrombopenia (VITT). We report the autopsy and in part serological findings of 3 patients who died from VITT after administration of ChAdOx1 nCoV-19.

Methods

Baseline characteristics, medical history, clinical and laboratory findings and symptoms of 3 patients who died in the course of disease were evaluated and detailed autopsies with histological and immunohistochemical evaluation were performed.

Results

Case 1, a 24-year-old male developed petechiae on the extremities 10 days after vaccination, renal failure and severe headache and seizures. Case 2, a 48-year-old female presented 6 days after vaccination with neurological symptoms and dyspnea. Case 3, a 38-year-old male developed severe headache and nausea and died at home 11 days after vaccination.

Laboratory testing revealed thrombocytopenia and elevated antibody titers against platelet factor 4 in patients 1 and 2. Platelets expressed increased procoagulant markers such as P-selectin. SARS-CoV2 infection was excluded by antibody testing.

The autopsy of case 1 showed a massive cerebral haemorrhage and brain edema, cases 2 and 3 exhibited complete thrombotic obstruction of the cerebral sinuses and subarachnoidal haemorrhage. Furthermore, case 1 and 2 revealed bilateral pulmonary embolism and obstruction of glomerular capillaries by hyaline microthrombi. Immunohistochemical studies to demonstrate platelet and neutrophil activation in situ will be presented.

Conclusion

VITT is a rare adverse event after vector-based vaccination against SARS-CoV2 with an incidence of 1:100.000 and is characterised by PF4-reactive antibodies that lead to platelet activation. This results in disseminated thromboembolic events causing thrombotic occlusions as pulmonary embolism or cerebral sinus thrombosis and in turn thrombocytopenia that can manifest from mild petechiae to severe letal haemorrhage.

Rapid diagnosis of VITT and initiation of therapy are essential for the patients' outcome. Autopsy remains an important tool to identify the underlying pathophysiology of complications of vaccinations and to aid preventive measures.

Stage Dependend Mast Cell densities in Lung Damage of COVID-19 Autopsies

T. Schaller¹, B. Märkl¹, R. Claus², L. Sholl³, J. L. Hornick³, M. P. Giannetti⁴, L. Schweizer⁵, M. Mann⁵, E. Sipos¹, M. Castells⁴

¹University Augsburg, Departement of General Pathology and Molecular Diagnostics, Medical Faculty, Augsburg, Germany, ²University Augsburg, Hematology and Oncology, Medical Faculty, Augsburg, Germany, ³Brigham and Women's Hospital, Harvard Medical School, Boston, MA., Department of Pathology, Boston, United States of America, ⁴Brigham and Women's Hospital, Harvard Medical School, Boston, MA., Division of Allergy and Clinical Immunology, Boston, United States of America, ⁵Max Planck Institute of Biochemistry, Department of Proteomics and Signal Transduction, Martinsried, Germany

Background

SARS-CoV-2 infection results in acute respiratory distress but the pathogenesis of the disease is poorly understood. Recent data suggest that viral RNA is found in mast cells and activated mast cells can release potent inflammatory mediators, including IL-6, and have been implicated in fibrotic lung damage. Mast cells from bone marrow do not express the ACE2 receptor and patients with mast cell activation disorders and asthma do not present disease exacerbations during SARS-CoV-2 infection.

Methods

We evaluated 29 autopsies and post-mortem biopsies from patients who died of COVID-19 and controls. Sections of lung tissue with acute and organizing diffuse alveolar damage (DAD) were selected and mast cells identified by KIT (CD117), tryptase, and chymase immunohistochemistry. RNA in situ hybridization was performed for SARS cellular localization and mass-spectrometry proteomics to identify mast cell proteases. Combination of KIT immunohistochemistry and RNA-ISH analysis was used to evaluate IL6 and TNFalpha expression in exemplary cases.

Results

The majority of patients who died of COVID-19 had increased BMI, diabetes, hypertension and elevated serum CRP and IL-6. Mast cells were positive for tryptase and chymase, indicating a connective tissue MCtc phenotype and chymase protein was abundant. In acute and organizing DAD, mast cells were found in similarly low numbers in low density areas. Conversely, in high density areas, mast cells were significantly increased in organizing DAD compared to acute DAD where mast cells were rather decreased compared to other lesions. SARS-CoV-2 RNA was detectable and might be co-localized in mast cells to a low extent.

Conclusion

Mast cells are skewed towards a MCtc phenotype in autopsy lung samples from COVID-19 deceased. During the early phase of DAD, mast cells are suppressed, which is reversed during the organizing DAD phase of SARS-CoV-2 infection, suggesting a role for mast cells in the lung inflammatory changes. Viral RNA is rarely present in lung mast cells, likely due to lack of ACE-2 receptor.

Impact of P-selectin-PSGL-1 axis on platelet-endothelium-leucocyte interactions in COVID-19

M. Granai, V. Warm, K. Greif, C. Hermann, L. Quintanilla-Martinez, U. Vogel, K. Klingel, F. Fend, H. Bösmüller
Universitätsklinikum Tübingen, Pathologie und Neuropathologie, Tübingen, Germany

Background

The lung is the central target organ in severe SARS-CoV-2 infection, and pulmonary complications the leading cause of death. In critically ill SARS-CoV-2 infected patients, early leukocyte recruitment to the respiratory system was found to be orchestrated by leukocyte trafficking molecules accompanied by secretion of pro-inflammatory cytokines and hypercoagulability[1][2]. The aim of our study is to explore the interplay between pulmonary endothelia and immune compartment in fatal COVID-19 and establish the activation status of platelets and leucocytes in relation with disease stage and in comparison to other causes of ARDS by immunohistochemistry.

Methods

Our study comprised 10 COVID-19 post-mortem lung specimens and 20 control samples (5 ARDS, 5 pneumonia, 10 normal lung) which were stained for the main adhesion molecules for each step of leukocyte migration: E-selectin, P-selectin and PSGL-1 for rolling phase, ICAM1, and VCAM1 for firm adhesion phase and CD11b for intravascular crawling. Image analysis software, QuPath, was used for quantification of positive leukocytes (PSGL-1 and CD11b) and endothelial tissue (E-selectin, P-selectin, ICAM1, VCAM1).

Results

Expression of P-selectin and PSGL-1 was strongly increased in the COVID-19 cohort compared to all control groups (ratio =17,23, $p<0,0001$; ratio=2,75, $p<0,0001$ respectively). Importantly, P-selectin was not only found in endothelial cells but also associated with aggregates of activated platelets adherent to the endothelial surface in COVID-19 cases. In addition, PSGL-1 disclosed positive perivascular leucocyte cuffs, so-called capillaritis. In contrast, VCAM1 and E-selectin were downregulated in COVID-19 compared to pneumonia (ratio=0,12, $p=0,0170$; ratio=0,43, $p=0,0112$ respectively). Moreover, CD11b showed a strongly increased positivity in COVID-19 compared to all controls (ratio=2,89; $p=0,0002$) indicating a proinflammatory immune microenvironment. Interestingly, CD11b exhibited distinct staining patterns at different disease stages.

Conclusion

The striking upregulation of PSGL-1 and P-selectin reveals an interplay of this receptor-ligand pair in COVID-19, increasing the efficiency of initial leukocyte recruitment and platelet activation, thus promoting tissue damage and immunothrombosis. Taken together, our results provide evidence that endothelial activation and unbalanced leukocyte migration play a central role in COVID-19 due to the impairment of P-selectin-PSGL-1 axis.

Literaturangaben

[1] Bösmüller H, Traxler S, Bitzer M, Häberle H, Raiser W, Nann D, Frauenfeld L, Vogelsberg A, Klingel K, Fend F, (2020), The evolution of pulmonary pathology in fatal COVID-19 disease: an autopsy study with clinical correlation, *Virchows Arch.*, 349-357, 477(3)

[2] Bösmüller H, Matter M, Fend F, Tzankov A, (2021), The pulmonary pathology of COVID-19, *Virchows Arch.*, 137-150, 478(1)

Inflammation and vascular remodelling in COVID-19 hearts

C. Werlein¹, M. Ackermann², A. Tzankov³, S. Freifrau von Stilfried und Rattonitz⁴, M. Reichart⁵, A. Haverich⁶, N. Marx⁴, L. Neubert¹, P. Braubach¹, T. Saldit⁵, T. Welte⁷, J. Bauersachs⁸, H.-H. Kreipe¹, H. Stark¹, P. Boor⁴, F. Länger¹, S. Verleden⁹, J. L. Robertus¹⁰, S. Mentzer¹¹, M. Kühnel¹, D. Jonigk¹

¹Medizinische Hochschule Hannover, Institut für Pathologie, Hannover, Germany, ²University of Witten/Herdecke, Helios University Clinic Wuppertal, Institute of Pathology and Department of Molecular Pathology, Wuppertal, Germany, ³University Hospital Basel, Institute of Medical Genetics and Pathology, Basel, Switzerland, ⁴RWTH Aachen, Institut für Pathologie, Aachen, Germany, ⁵University of Göttingen, Institute for X-Ray Physics, Göttingen, Germany, ⁶Medizinische Hochschule Hannover, HTTG Chirurgie, Hannover, Germany, ⁷Medizinische Hochschule Hannover, Klinik für Pneumologie, Hannover, Germany, ⁸Medizinische Hochschule Hannover, Klinik für Kardiologie, Hannover, Germany, ⁹Antwerp University Hospital, Department of thoracic medicine, Antwerp, Belgium, ¹⁰Royal Brompton & Harefield NHS Foundation Trust, Department of Histopathology, London, United Kingdom, ¹¹Harvard Medical School, Laboratory of Adaptive and Regenerative Biology, Boston, United States of America

Background

Cardiac involvement in COVID-19 infection is a common clinical finding and can determine the clinical outcome; however the underlying pathomechanisms are largely unknown.

Methods

Comprehensive analysis of heart-tissue samples of 24 autopsies with confirmed COVID-19 disease was performed and compared them to samples of age-matched Influenza A (n=16) as well as conventional viral myocarditis cases (n=8) and control tissue (n=9). Conventional histopathology, microvascular corrosion casting, scanning electron microscopy, phase-contrast synchrotron x-ray tomography, direct multiplexed measurements of gene expression, multiplexed immunohistochemistry (MPX) and Synchrotron radiation tomographic microscopy were employed.

Results

On conventional histopathology, none of the COVID-19 samples fulfilled the established criteria for lymphocytic myocarditis; however, quantification via MPX showed a significant increase in perivascular CD11b/Tie2+-macrophages in COVID-19 over hospitalisation time not observed in Influenza or conventional viral myocarditis. Ultrastructurally, an altered microvasculature, an increase of intussusceptive angiogenesis as well as multifocal ultrastructurally detectable thrombi (uTh) could be demonstrated, unapparent in conventional morphology. On a molecular level, COVID-19 hearts displayed a distinct expression pattern coding mainly for angiogenesis and epithelial-mesenchymal transition (EMT) and lesser for inflammation as seen in influenza and conventional viral myocarditis cases.

Conclusion

(I) Cardiac involvement in COVID-19 is not a conventional viral myocarditis but a rather qualitative than quantitative increase in a special subpopulation of CD11b+/Tie2+ monocytes/ macrophages contributing to cardiac neoangiogenesis and remodeling in COVID-19 cardiomyopathy. (II) COVID-19 cardiomyopathy is substantially underappreciated upon conventional light-microscopy observation and requires a multimodal approach. (III) Our comparative morphological and transcriptional data indicate that the neovascularization by intussusceptive angiogenesis is the main driver for a specific COVID-19 induced cardiac response facilitated by interactions between the incorporation of blood-borne CD11b+/Tie2+ monocytes/macrophages and damaged and activated endothelial cells in COVID-19 hearts.

AG01 AG Gastroenteropathologie I

AG01.01

Stroma Areactive Invasion Front Areas (SARIFA) in gastric carcinoma as a new biomarker implicating an interaction between adipocytes and tumor cells – a validation study

B. Grosser¹, S. Schiele², A. Probst³, D. Vlasenko⁴, G. Schenkirsch⁵, A. Novotny⁶, W. Weichert⁷, G. Keller⁷, B. Märkl¹

¹*Institut für Pathologie und Molekulare Diagnostik, Universitätsklinikum Augsburg, Augsburg, Germany,*

²*Institut für Mathematik, Universität Augsburg, Augsburg, Germany,* ³*III. Medizinische Klinik, Gastroenterologie, Universitätsklinikum Augsburg, Augsburg, Germany,* ⁴*Klinik für Allgemein-, Viszeral- und Transplantationschirurgie, Universitätsklinikum Augsburg, Augsburg, Germany,* ⁵*Tumordatenmanagement, Universitätsklinikum Augsburg, Augsburg, Germany,* ⁶*Klinik und Poliklinik für Chirurgie, Technische Universität München, München, Germany,* ⁷*Institut für Pathologie, Technische Universität München, München, Germany*

Background

Recently, we presented Stroma Areactive Invasion Front Areas (SARIFA) as a new histological prognostic marker in gastric and colon carcinomas. We defined SARIFA as the direct contact between a cluster of tumor glands/cells comprising at least five tumor cells and inconspicuous surrounding adipose tissue at the invasion front. In our initial study, which included a total of 480 adenocarcinomas of the stomach and the gastroesophageal junction from two different collectives, SARIFA was found to be a negative independent prognostic factor for overall survival (HR 1.638, 95% CI 1.153–2.326, $p = 0.006$; 20% SARIFA positive) with low interobserver variability. Moreover, we provided first evidence for an interaction between adipocytes and tumor cells. Using digital spatial profiling (DSP), the most upregulated genes in SARIFA positive cases were those associated with triglyceride catabolism and endogenous sterols indicating potential underlying mechanisms related to tumor-promoting adipocytes (Martin et al., 2021; Grosser et al., 2022).

Therefore, our next objective was to evaluate the prognostic value of SARIFA in an independent external collective of adenocarcinomas of the stomach and gastroesophageal junction.

Methods

An independent external validation collective consisting of 489 adenocarcinomas of the stomach and the gastroesophageal junction was independently classified according to SARIFA by two pathologists.

Association of SARIFA status with clinicopathological characteristics and overall survival was evaluated.

Results

It was found that 38% of the tumors were SARIFA-positive. Patients who presented SARIFA positive tumors

had a significantly lower overall survival (OS) (median: 24 vs. 56 months; $p = 0.002$, $n = 489$). SARIFA positivity proofed as a negative independent prognostic factor for OS (HR 1.335, 95% CI 1.026-1.736, $p = 0.03$) in Cox regression analyses, which were adjusted for known prognostic parameters (age, pTNM). Regarding the pT stage, only advanced-stage (pT3/4) SARIFA-positive patients showed a worse OS ($p = 0.011$), whereas no differences in terms of survival could be observed during the early stages (pT1/2) ($p = 0.707$). SARIFA positivity was associated with positive lymph nodes and advanced pT stage.

Conclusion

SARIFA combines low interobserver variability, minimal effort, and high prognostic relevance even in an external validation collective and is therefore an extremely promising biomarker specifically in advanced gastric cancer.

The expression and biological effect of RNF43 and LRP1B in gastric cancer is context-dependent.

B. Holm, S. Barsuhn, H.-M. Behrens, S. Krüger, C. Röcken

Institut für Pathologie, UKSH, Campus Kiel, Kiel, Germany

Background

RNF43 and LRP1B function as tumor suppressors in the Wnt signaling pathway and have been described to be frequently mutated in gastric cancer (GC). In this study of a large and well characterized cohort of 446 gastric cancers we explored the significance of RNF43 and LRP1B and their correlations with clinicopathological patient characteristics. In this study we tested the following hypotheses: (1) RNF43 and LRP1B are of tumor biological significance in GC; (2) RNF43 and LRP1B show intratumoral heterogeneity; (3) RNF43-expression and LRP1B-expression correlate with clinicopathological patient characteristics and show differences with regard to histological type of Lauren.

Methods

From the archive of the Department of Pathology, University Hospital Schleswig-Holstein, Campus Kiel we retrieved all patients who had undergone either total or partial gastrectomy for an adenocarcinoma of the stomach or gastroesophageal junction between 1997 and 2009. Immunohistochemical staining was performed on tissue sections of primary tumor using the Bondmax Autostainer and monoclonal antibodies directed against RNF43 and LRP1B. Immunostaining of whole tissue sections was documented with the histoscore. Dichotomized at the median, we separated the cohort into a low/negative and a positive group of RNF43 and LRP1B expression, respectively. Apart from the entire cohort, we also examined the intestinal and diffuse type GCs separately. Statistical analyses were done using SPSS 27.0.

Results

Regarding the entire cohort, the expression of RNF43 and LRP1B correlated significantly with the Lauren phenotype and with each other. LRP1B correlated also with tumor grade. Interestingly, differences were noted regarding RNF43 between the intestinal and diffuse type GCs. Survival analysis of the intestinal type GCs showed that RNF43 low/negative GCs tended to have a better outcome compared with RNF43 high/positive GCs (24.5 months overall survival (OS) and 25.0 months tumor-specific survival (TSS) vs. 14.1 months OS and 17.9 months TSS, respectively). To the contrary, diffuse type GCs with RNF43 low/negative had a worse outcome compared with RNF43 high/positive GCs (12.9 months OS and 18.2 months TSS vs. 17.1 months OS and 21.5 months TSS, respectively).

Conclusion

RNF43 and LRP1B are not easy to use prognostic or predictive biomarkers in GC, its effect on GC biology seems to be context-dependent and might require the simultaneous analysis of several members of the Wnt signaling pathway in relation to the tumor type.

Morphology Matters: A Critical Reappraisal of the Clinical Relevance of Morphologic Criteria From the 2019 WHO Classification in a Large Colorectal Cancer Cohort Comprising 1004 Cases

M. Jesinghaus^{1,2}, M. Schmitt¹, C. Lang², M. Reiser², A. Scheiter³, B. Konukiewicz⁴, K. Steiger², M. Silva², M. Tschurtschenthaler⁵, S. Lange⁵, S. Försch⁶, K. F. Becker², D. Saur⁵, H. Friess⁷, K. Halfter⁸, J. Engel⁸, M. Boxberg², N. Pfarr², D. Wilhelm⁷, W. Weichert²

¹Universitätsklinikum Gießen und Marburg, Institut für Pathologie, Marburg, Germany, ²Technische Universität München, Institut für Pathologie, München, Germany, ³Universitätsklinikum Regensburg, Institut für Pathologie, Regensburg, Germany, ⁴Christian-Albrechts Universität Kiel, Institut für Pathologie, Kiel, Germany, ⁵Technische Universität München, II Medizinische Klinik, München, Germany, ⁶Universitätsklinikum Mainz, Institut für Pathologie, Mainz, Germany, ⁷Technische Universität München, Chirurgische Klinik, München, Germany, ⁸Bayerisches Krebsregister, München, Germany

Background

The 2019 World Health Organization (WHO) classification of colorectal carcinoma (CRC) profoundly reclassified CRC subtypes and introduces tumor budding as a second major grading criterion, while condensing conventional grade into a 2-tiered system. So far it remains largely unexplored how these parameters interact with each other and whether they truly have an independent impact on patient prognosis.

Methods

We reclassified a large single-center cohort of 1004 CRCs spanning two decades for adjusted WHO grade (low vs. high), tumor budding (Bd1/Bd2/ Bd3), and CRC subtype (adenocarcinoma not otherwise specified, micropapillary, mucinous, serrated, medullary, adenoma-like, signet-ring cell, mixed adenoneuroendocrine carcinoma/ neuroendocrine carcinoma, undifferentiated) according to the criteria of the 2019 WHO classification. We investigated the interaction of these parameters, their connection to stage/microsatellite status, and their significance for patient survival in the different subgroups.

Results

Specific subtypes other than adenocarcinoma not otherwise specified represented one third of all CRCs and were unevenly distributed throughout stage and microsatellite subgroups. Subtypes, WHO grade and tumor budding profoundly impacted all survival parameters ($P < 0.001$ for all analyses), with CRC subtypes and tumor budding—but not WHO grade—being stage-independent prognosticators for all survival comparisons. WHO grade had very limited prognostic value in CRC subtypes, while tumor budding retained its strong prognostic impact in most scenarios.

Conclusion

Accurate delineation of CRC subtypes introduced in the 2019 WHO classification provides strong stage-independent prognostic information, arguing that they should be considered in pathology reports and in clinical trials. Of the morphology-based grading schemes included in the 2019 WHO classification, tumor budding outperforms WHO grade.

Delineating the evolutionary trajectories of colorectal cancer development in inflammatory bowel disease

D. Hirsch^{1,2}, M. Brewer², R. Stahl³, K. Ylaya⁴, S. Hewitt⁴, F. Livak⁵, S. Brower³, M. Sanchez⁶, K. Heselmeyer-Haddad², T. Ried²

¹Universitätsmedizin Mannheim, Institut für Pathologie, Mannheim, Germany, ²NIH/NCI, CCR, Genetics Branch, Bethesda, United States of America, ³Englewood Hospital and Medical Center, Department of Surgical Oncology, Englewood, United States of America, ⁴NIH/NCI, CCR, Experimental Pathology Laboratory, Bethesda, United States of America, ⁵NIH/NCI, CCR, Flow Cytometry Core, Bethesda, United States of America, ⁶Englewood Hospital and Medical Center, Institute of Pathology, Englewood, United States of America

Background

Patients with inflammatory bowel diseases (IBD) have an increased risk for developing colorectal cancer (CRC). In contrast to sporadic colorectal tumorigenesis, *TP53* mutations occur early in the progression to CRC. To improve the assessment of malignant progression risk, we aimed to delineate the evolutionary trajectories underlying colorectal tumor development in IBD patients.

Methods

In our initial attempt, we have analyzed 97 samples at different stages of tumor development from 47 patients with IBD-CRC by comparative bulk lesion sequencing. To increase the resolution of our analyses, we have developed a protocol for single cell disintegration and consecutive flow sorting-based enrichment of epithelial cells isolated from formalin-fixed paraffin-embedded tissue samples. This enabled us to study additional 64 colonic samples, covering the spectrum from inflamed, non-dysplastic mucosa to invasive CRC, from an independent cohort of 15 patients with exome sequencing and single cell copy number profiling, to gain insight into the underlying phylogenies.

Results

Overall, IBD-CRCs showed remarkable inter-tumor heterogeneity, however, there was a predilection for *TP53* mutations, and copy number alterations (CNAs) including the gain of 5p were prevalent. Our combined genomic analyses at the population and individual cell level revealed divergent genetic aberration patterns and distinct levels of intra-tumor heterogeneity. In some of the IBD patients, we detected genomic alterations, including but not limited to *TP53* mutations, in colonic mucosa without evidence of dysplasia, indicating occult tumor evolution. Moreover, we observed an unexpectedly high load of CNAs, sometimes confined to small subpopulations of epithelial cells, in a subset of the non-dysplastic, inflamed mucosa samples including e.g., *MYC* amplification. Certain but not all alterations and subclones present in the non-dysplastic mucosa samples were propagated in the associated progressed lesions.

Conclusion

Despite a high degree of both inter- and intra-tumor heterogeneity, our data suggests that detection of genomic aberrations in precursor lesions and before histologic transformation may help predicting malignant progression of IBD. Considering our findings, one of the next crucial steps will be to determine which genetic

alterations actually define clonal expansions that predispose to cancer development and which alterations may just represent innocent bystander mutations, albeit triggering a clonal outgrowth.

TROP2 as a novel marker for cell stiffness in colon cancer cells

K. Huebner¹, A. Nursaitova¹, D. Soteriou², M. Kubankova², M. Kraeter², K. Moeckel², A. Gehring¹, A. Hartmann^{1,3}, J. Guck², R. Schneider-Stock^{1,3}

¹University Hospital, Institute of Pathology, FAU Erlangen-Nürnberg, Erlangen, Germany, ²Max Planck Institute for the Science of Light and Max-Planck-Zentrum für Physik und Medizin, Erlangen, Germany, ³Comprehensive Cancer Center Erlangen-EMN (CCC ER-EMN), University Hospital Erlangen, Friedrich Alexander University Erlangen-Nürnberg, Erlangen, Germany

Background

Metastatic progression is responsible for the majority of colon cancer (CC)-related deaths and its molecular mechanisms are still only poorly understood. For some time cancer cell mechanobiology has been considered to improve our understanding of cancer progression since it is closely linked to tumor cell spreading and invasion. In particular, the tight connection of the cells' mechanical phenotype to their metastatic potential could provide a novel diagnostic tool in cancer research. Since the cancer driver TROP2 has been shown to promote invasion and metastasis, we aimed to identify its role on cell stiffness of CC cells.

Methods

We used real-time deformability cytometry (RT-DC), a novel high-throughput technique, to determine cell stiffness in several CRC cell lines having different mutations in colon cancer specific genes. We modulated their *TROP2* expression status by stable overexpression of *TROP2*, transient *TROP2* silencing as well as CRISPR/Cas9-mediated *TROP2* knockout (KO). We compared the Young's modulus (the power that is necessary to deform a cell) of single cell suspensions grown in 2D cell culture and in 3D using xenografts grown in the chorioallantoic membrane (CAM) model. The *TROP2* expression status was validated by RT-qPCR and immunohistochemistry.

Results

We could show that the mechanical properties of colon cancer cell lines were independent of their mutation status (*p53*, *APC*, *Kras*, *BRAF*); only the Microsatellite instability (MSI) status seemed to trigger a higher deformability compared to microsatellite stable (MSS) cells. Interestingly, tumor cells became always softer when growing as xenografts *in vivo*. We observed that cell lines expressing high levels of *TROP2* presented an increased cell stiffness. In contrast, both transient *TROP2* silencing and stable *TROP2* KO resulted in a softer mechanical phenotype.

Conclusion

The application of RT-DC revealed that TROP2 expression impacts the cell stiffness of CC cells. Our

findings provide valid data to assess the invasive behavior of TROP2 overexpressing tumors and to interpret their behavior at the tumor invasion front.

Identification of novel candidate biomarkers in early adenoma transition

A. Siskova^{1,2}, K. Huebner³, C. Hampel³, G. Ferrero⁴, A. Naccarati^{5,6}, B. Pardini^{5,6}, C. Geppert^{3,7}, J. Prochazka⁸, J. Tureckova⁸, J. Jungwirth^{2,9}, J. Kral¹⁰, L. Vodickova^{1,2,11}, A. Gehring³, K. Erlenbach-Wuenssch^{3,7}, A. Hartmann^{3,7}, P. Vodicka^{1,2,11}, V. Vymetalkova^{1,2,11}, R. Schneider-Stock^{3,7}

¹Department of Molecular Biology of Cancer, Institute of Experimental Medicine of the Czech Academy of Sciences, Prague, Czech Republic, ²Institute of Biology and Medical Genetics, 1st Faculty of Medicine Charles University and General University Hospital in Prague, Prague, Czech Republic, ³University Hospital, Institute of Pathology, FAU Erlangen-Nürnberg, Erlangen, Germany, ⁴Department of Clinical and Biological Sciences, University of Turin, Turin, Italy, ⁵Italian Institute for Genomic Medicine (IIGM), c/o IRCCS Candiolo, Turin, Italy, ⁶Candiolo Cancer Institute-FPO IRCCS, Turin, Italy, ⁷Comprehensive Cancer Center Erlangen-EMN (CCC ER-EMN), University Hospital Erlangen, Friedrich Alexander University Erlangen-Nürnberg, Erlangen, Germany, ⁸Czech Centre for Phenogenomics, Institute of Molecular Genetics, ASCR, Prague, Czech Republic, ⁹Department of surgery, Weiden Clinic, Weiden, Germany, ¹⁰Clinic of Hepatogastroenterology, Institute for Clinical and Experimental Medicine, Prague, Czech Republic, ¹¹Biomedical Centre, Faculty of Medicine in Pilsen Charles University, Pilsen, Czech Republic

Background

Colorectal adenoma, a neoplastic lesion from the epithelium of the intestine, is a precursor of colorectal cancer, the third most common cancer worldwide. Since the molecular mechanisms behind the early transformation into an adenoma are not well understood, we aimed to identify novel candidate genes by whole transcriptomic sequencing (WTS) of a larger cohort of adenomas and their corresponding adjacent tissue.

Methods

We performed WTS on 16 adenoma pairs (NovaSeq6000). Dysregulation of most promising top down- and up-regulated genes was verified by RT-PCR and in an *in vitro* transformation model using normal epithelial cells (HCEC) that underwent three cycles of deadhesion. Gene expression data were correlated with Infinium Whole-Genome Genotyping assay methylation. Functional consequences of the gene signature were analyzed by proliferation assay, immunohistochemistry, and *in vivo* in the chorioallantoic membrane (CAM) assay and an AOM-DSS mice model of colorectal cancer.

Results

The analysis revealed more than 2,000 differentially expressed genes (DEGs) between the adenoma and the adjacent tissue. We have chosen the seven most relevant candidate genes, four up-regulated (*AXIN2*, *ETV4*, *RNF43*, *TACSTD2*), and three down-regulated (*FBLN1*, *GNG7*, *NGFR*) for validation in an independent cohort of 20 adenoma patients. Interestingly, some of the genes were also dysregulated in the *in vitro* transformation model reflecting that cell adhesion and cytoskeleton associated pathways play a major role in early transformation process of adenomas. In the AOM-DSS model the cancer driver TROP2 was significantly overexpressed in colon adenomas.

Conclusion

Our study has identified a novel marker set for precancerous colorectal lesions that should be further analyzed in the context of subsequent tumor transformation and prognostic value.

Neuroendocrine Differentiation in Conventional Colorectal Adenocarcinomas.

B. Konukiewicz¹, A. Kasajima², M. Schmitt², K. Schwamborn², T. Groll², F. Schicktanz², C. Delbridge², L. M. Schütze², D. Wilhelm³, C. Lang², S. Lange⁴, S. Förtsch⁵, P. Jank⁶, K. Steiger², A. von Werder⁴, C. Denkert⁶, W. Weichert², G. Klöppel², M. Jesinghaus⁶

¹Universitätsklinikum Schleswig-Holstein, Campus Kiel, Institut für Pathologie, Kiel, Germany, ²TU München, Institut für Pathologie, München, Germany, ³Klinikum rechts der Isar, Chirurgie, München, Germany, ⁴Klinikum rechts der Isar, II Medizinische Klinik, München, Germany, ⁵Universitätsmedizin Mainz, Institut für Pathologie, Mainz, Germany, ⁶UKGM Marburg, Institut für Pathologie, Marburg, Germany

Background

Kolorektale gemischte adenoneuroendokrine Karzinome sind klinisch aggressiv verlaufende Neoplasien, die sich aus unterschiedlichen Subtypen von Adenokarzinomen in Kombination mit einem morphologisch distinkten neuroendokrinen Karzinom zusammensetzen. Die biologische Relevanz einer Expression von Synaptophysin in konventionellen kolorektalen Adenokarzinomen ohne distinkte neuroendokrine Morphologie ist bisher unklar.

Methods

Es wurde die Expression von Synaptophysin in 1002 konventionellen kolorektalen Adenokarzinomen untersucht. Die Ergebnisse wurden mit den klinisch-pathologischen Charakteristika der Kohorte korreliert und mit Daten von adenoneuroendokrinen Karzinomen verglichen.

Results

Die Expression von Synaptophysin in konventionellen kolorektalen Adenokarzinomen ist assoziiert mit einem verkürzten "disease-free survival" ($p=0,037$), aber nicht mit einem verkürzten "overall-survival" oder "disease-specific survival" in der univariaten Analyse. Die Expression blieb ohne Einfluss in der multivariaten Analyse. "Echte" gemischte adenoneuroendokrine Karzinome zeigten allerdings in der uni- und multivariaten Analyse ein signifikant kürzeres Überleben im Vergleich zu den konventionellen Adenokarzinomen mit- und ohne Synaptophysin Expression ($p<0,001$).

Conclusion

Unsere Studie zeigt, dass die Expression von Synaptophysin in konventionellen Adenokarzinomen im Vergleich zu Synaptophysin-negativen konventionellen Adenokarzinomen nicht mit einem signifikant schlechterem klinischem Outcome assoziiert ist, ganz im Gegensatz zu "echten" gemischten adenoneuroendokrinen Karzinomen. Wir schlussfolgern, dass der Begriff "gemischtes adenoneuroendokrines Karzinom" für solche Neoplasien reserviert sein sollte, die morphologisch eine distinkte neuroendokrine Komponente aufweisen.

AG01 AG Gastroenteropathologie II

AG01.09

SARIFA (Stroma AReactive Invasion Front Areas) proofs to be prognostic biomarker also in pancreatic adenocarcinoma.

P. Grochowski¹, B. Grosser¹, D. Vlasenko², G. Schenkirsch³, T. Schaller¹, B. Märkl¹

¹Universitätsklinikum Augsburg, Institut für Pathologie und molekulare Diagnostik, Augsburg, Germany,

²Universitätsklinikum Augsburg, Klinik für Allgemein-, Viszeral- und Transplantationschirurgie, Augsburg, Germany, ³Universitätsklinikum Augsburg, Comprehensive Cancer Center Augsburg - Onkologisches Zentrum, Augsburg, Germany

Background

SARIFA (Stroma AReactive Invasion Front Areas) is a newly described histological prognostic biomarker, defined as a direct contact between a cluster of tumorous glands/cells and inconspicuous surrounding adipose tissue at the invasion front, which showed its significance in gastric and colon cancer studies previously conducted by our group. The assessment of this parameter is easily applicable, requires no additional staining and shows very low interobserver variability. Despite the progress of oncology in many entities, pancreatic adenocarcinomas (PDA) still belong to the group of hard-to-treat cancers. Because of its functional link to tumour metabolics SARIFA could be an interesting biomarker in PDA. Here we present the results of first analysis of SARIFA-effect in this type of cancer.

Methods

We compiled a collective of patients, who have undergone pancreatic tumour resection by Whipple in the University Hospital Augsburg between years 2005 and 2015. Inclusion criteria were diagnosis of PDA and post-operative survival of at least 30 days. A histology other than PDA was a criterion of exclusion. All available tumour-containing slides have been investigated for the SARIFA-status by two independent observers. SARIFA-positivity has been defined as occurrence of a direct contact between tumorous glands or cells and surrounding adipose tissue at the invasion front by at least 2/3 of given HE-stained tumour slides.

Results

980 slides have been evaluated which corresponds to 176 patients, with mean age of 66 ± 10 and a female:male ratio of 1:1.2 in this collective. SARIFA classification proved to be easily and fast to evaluate and showed a remarkably low interobserver variability. SARIFA positivity was identified in 53 cases (30%). Compared to SARIFA-negative cases it was associated with a significantly reduced overall survival time (median 16.0 versus 22.0 months, $p = 0.018$, $n = 176$).

Conclusion

By overall poor survival rates of patients with a diagnosis of pancreatic cancer, SARIFA could be shown to be a promising prognostic factor. The evaluation of SARIFA-status can be easily applied in pathologic diagnostics of pancreatic cancer. Moreover, based on what could be shown on gastric cancer, it offers a new therapeutic perspective targeting lipid metabolics. Further investigations and statistical analyses are currently ongoing.

Immunological microenvironment of precursor lesions of pancreatic ductal adenocarcinoma (PDAC) in a transgenic mouse model

C. Müller¹, M. Schulte¹, M. Schlensog¹, L. Häberle¹, S. Hänsch², F. Opitz¹, I. Esposito¹

¹*Institute of Pathology, University Hospital Düsseldorf, Moorenstr. 5, 40225 Düsseldorf, Germany, ²Heinrich Heine University, Center for Advanced Imaging, Düsseldorf, Germany*

Background

Pancreatic ductal adenocarcinoma (PDAC) is a highly devastating disease with poor prognosis and rising incidence. It has been shown that the immunological microenvironment (iME) plays a pivotal role in the biological behavior of PDAC; however, the iME of its precursor lesions is still lacking an in-depth characterization. We aim to characterize the iME of normal pancreatic tissue, acinar-to-ductal metaplasia (ADM), pancreatic intraepithelial neoplasia (PanIN) and PDAC in the K-rasLSL.G12D/+;Pdx-1-Cre (KC) and K-rasLSL.G12D/+; Trp53R172H/+; Pdx-1-Cre (KPC) mouse models in order to identify early changes that could influence pancreatic tumorigenesis.

Methods

Tissue Microarrays were constructed using a collective of 41 transgenic mice. 140 tissue cores including matched samples of normal pancreas tissue, precursor lesions (PanIN low grade, n=31 and ADM, n=21) and PDAC (n=70) were analyzed. Immune cells were stained simultaneously with multiplex-based immunofluorescence staining (CD3, CD4, CD8a, FoxP3, PD-1, CD19, F4/80, CD163, Tryptase and Granzyme B). Positive cells were counted by using ImageJ/FIJI software and were normalized to DAPI+ cells and the total area of the lesion. By developing macros, we automatized and standardized cell counting as well as area calculation. The data were analysed statistically (Kruskal-Wallis test followed by Dunn-Bonferroni post-hoc comparison). Cluster and co-localization analyses were performed.

Results

The number of immune cells, mostly found in the stroma around the lesions, was generally higher in PanIN and PDAC tissue compared to normal tissue and, partially, to ADM. PanIN displayed significantly higher numbers of CD19⁺ B cells compared to ADM (p = 0.026). In PDAC, cells of the innate immune response, such as F4/80⁺ macrophages (p = 0.012) and tryptase⁺ mast cells (p = 0.001), were present in significantly higher numbers than in ADM, especially in the tumor periphery. In addition, PDAC samples displayed an immunosuppressive microenvironment, characterized by a tendency towards increased numbers of regulatory T cells.

Conclusion

Our results show that the immunological microenvironment during pancreatic carcinogenesis in mice is highly dynamic and heterogeneous between different precursor lesions.

Clinicopathologic evaluation of intrahepatic cholangiocarcinoma subtypes

T. S. Gerber¹, M. Schindeldecker^{1,2}, F. Bartsch³, L.-K. Heuft³, L. Müller⁴, R. Kloeckner⁴, D. A. Ridder¹, H. Lang³, W. Roth¹, B. K. Straub¹

¹University Medical Center Mainz, Institute of Pathology, Mainz, Germany, ²University Medical Center Mainz, Tissue Biobank, Mainz, Germany, ³University Medical Center Mainz, Department of General, Visceral and Transplant Surgery, Mainz, Germany, ⁴University Medical Center Mainz, Department of Radiology, Mainz, Germany

Background

Intrahepatic cholangiocarcinoma (iCCA) is the second most common primary liver tumor. iCCA constitute especially aggressive carcinomas with high mortality and rising incidence. According to the WHO classification of tumors 2019, iCCA are divided into small and large duct types according to their tumor biology and evolution. Large duct type iCCA share morphological, clinicopathological, and molecular features with perihilar cholangiocarcinoma and have a lower 5-year postoperative survival rate when compared to small duct type iCCA. To further characterize iCCA clinicopathologically, we used a collective of iCCA of overall 200 patients and conducted a comprehensive analysis of clinical and pathological parameters.

Methods

All iCCA were classified into small (n=121) and large duct type iCCA (n=79). Additional properties such as biliary intraepithelial neoplasia and other precursor lesions, growth pattern, margin distance, mucin production, lymphovascular, vascular, and perineural invasion together with immunohistochemistry for E- and N-cadherin, S100, CRP, Ki67, CK7, and CK20 as well as CA19-9, were determined and correlated with clinical and survival data.

Results

In our series, biliary intraepithelial neoplasia (n=52) and intraductal papillary neoplasia of the bile duct (n=9) occurred only in iCCA of the large duct type. The predominant growth pattern of iCCA of the small duct type was mass-forming (98%), sometimes mixed with intraductal growth (18%), and rarely periductal-infiltrating growth (5%). In large duct type iCCA, the periductal-infiltrating pattern was much more common (57%). Lymphovascular invasion, perineural invasion, and lymph node metastases were common features of large duct type iCCA (29%, 41%, and 42% vs. 13%, 17%, and 21%). Mucin formation was observed in 81% of large duct type iCCA compared to 13% in iCCA of the small duct type, which showed only minimal PAS-positive mucin if present at all. Of fifteen patients who initially presented with jaundice, eleven were diagnosed with large duct type iCCA, and only four with small duct type iCCA. N-cadherin, S100, and CRP showed differential expression patterns, but with only limited value.

Conclusion

The diagnosis of the two subtypes of iCCA requires a comprehensive histopathological analysis including all parameters, as no single parameter is sufficient to establish the diagnosis. Additional PAS staining and

adequate embedding of the material may improve iCCA subtyping and thereby help better assess prognosis.

PD-1+ T-cells correlate with Nerve Fiber Density as a prognostic biomarker in patients with resected perihilar cholangiocarcinoma.

D. Liu¹, X. Tan^{1,2}, J. Bednarsch¹, N. T. Gaisa³, P. Boor³, R. D. Bülow³, U. Klinge¹, U. P. Neumann^{1,4}, L. Heij^{1,2,3,5}

¹University Hospital RWTH Aachen, Department of Surgery and Transplantation, Aachen, Germany,

²Maastricht University, NUTRIM School of Nutrition and Translational Research in Metabolism, Maastricht, The Netherlands, ³University Hospital RWTH Aachen, Institute of Pathology, Aachen, Germany, ⁴UMC+ Maastricht, Department of Surgery, Maastricht, The Netherlands, ⁵Erasmus University Medical Center, Institute of Pathology, Rotterdam, The Netherlands

Background

Perihilar cholangiocarcinoma (pCCA) is a hepatobiliary malignancy which a dismal prognosis. Nerve fiber density (NFD) – a novel prognostic biomarker which showed notable prognostic ability in pCCA – describes the density of small nerve fibers without cancer invasion and is categorized into high numbers and low numbers of small nerve fibers (high vs low NFD; [1],[2]). Here, we aim to explore differences in immune cell populations and survival between high and low NFD patients.

Methods

Whole slide multiplex immunofluorescence imaging was applied on 47 pCCA patients focusing on immune cell composition (CD8/CD68/PD1/PDL1/PDL2) in the tumor microenvironment (TME). Calculations of cell counts were conducted in a computer-based manner (TissueFAXS; StrataQUEST). Group comparisons between high and low NFD patients were carried out and oncological outcome investigated (Figure 1).

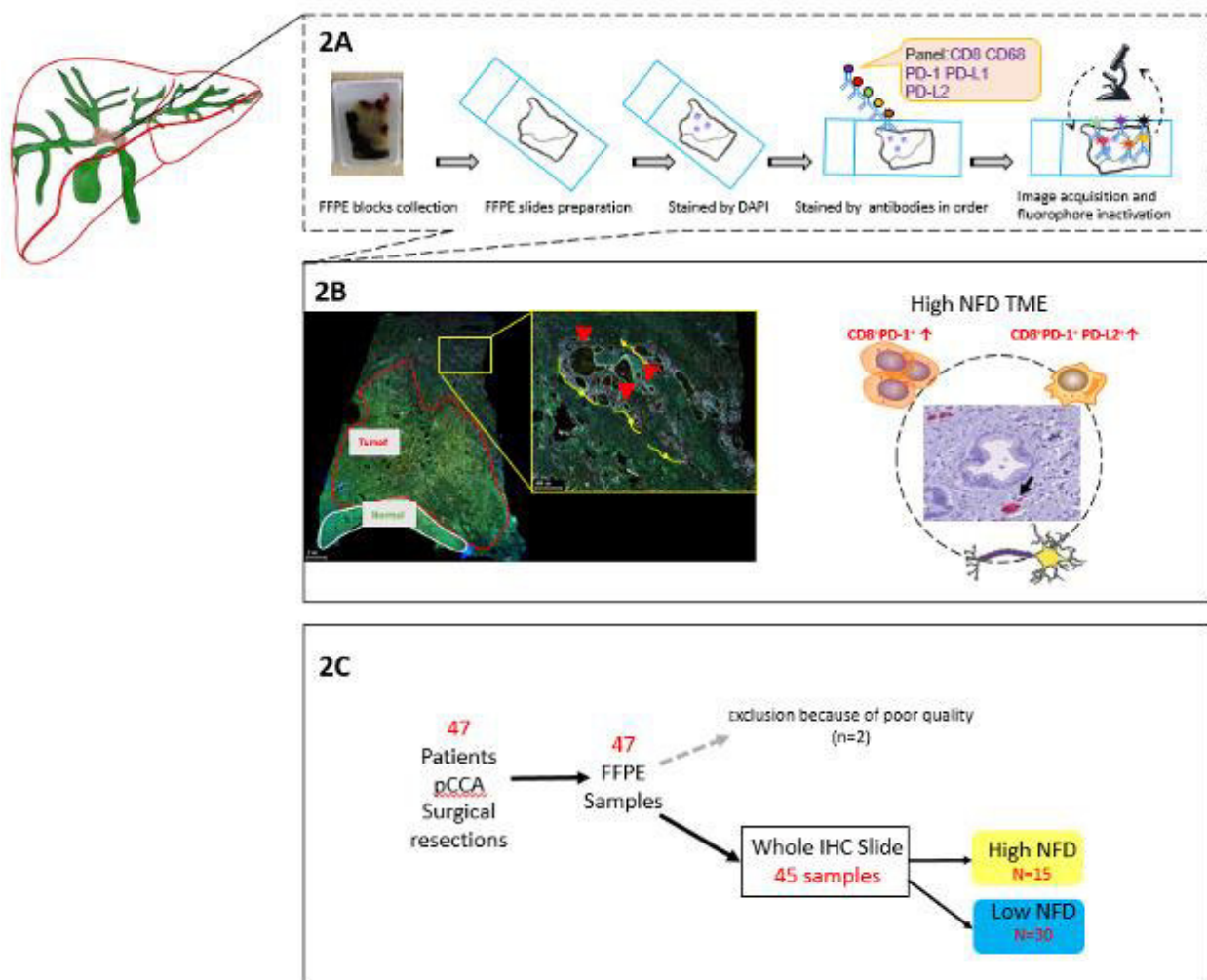


Figure 1: Overview of study workflow. A Slide preparation, staining and scanning. B Slide annotation and computer-based cell counting. C In total we included 47 patients in this study. From 45 patients we were able to analyze the digital scans.

Results

CD8+PD-1 expression was higher in the high NFD than in the low NFD group (12.24×10^{-6} vs. 1.38×10^{-6} positive cells by overall cell count, $p=.017$). High CD8+PD-1 expression was further identified as an independent predictor of overall (OS; Hazard ratio (HR)=0.41; $p=.031$) and recurrence-free survival (RFS; HR=0.40; $p=.039$). Correspondingly, the median OS was 83 months (95% confidence interval (CI): 18 – 48) in patients with high CD8+PD-1+ expression compared to 19 months (95% CI: 5 – 93) in patients with low CD8+PD-1+ expression ($p=.018$ log rank). Also, RFS was significantly lower in patients with low CD8+PD-1+ expression (14 months (95% CI: 6 – 22)) compared to patients with high CD8+PD-1+ expression (83 months (95% CI: 17 – 149), $p=.018$ log rank; Figure 2).

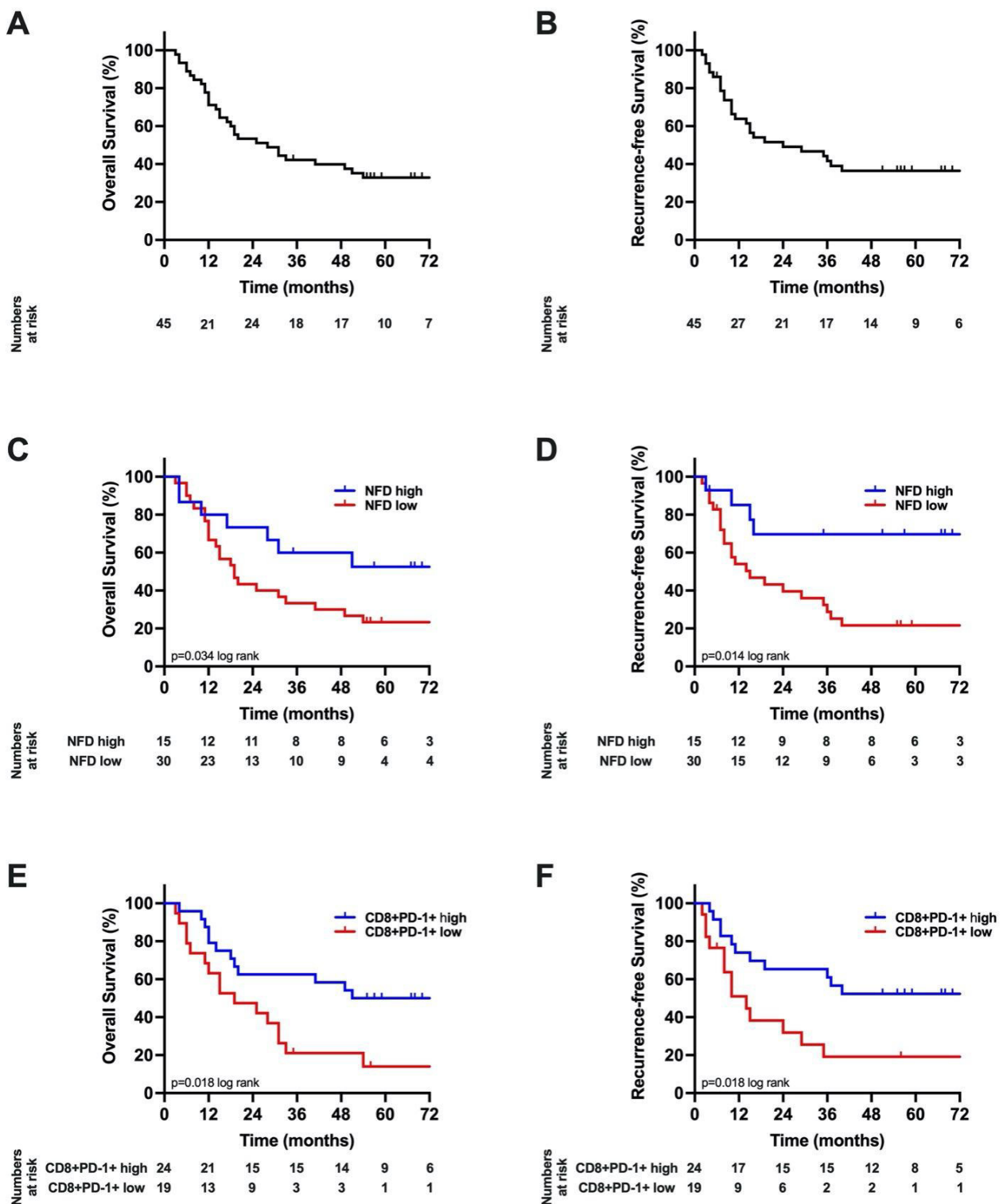


Figure 2: Oncological survival. A OS. B RFS. C OS stratified by NFD. D RFS stratified by NFD. E OS stratified by CD8+PD1+ count. F RFS survival stratified by CD8+PD1+ count.

Conclusion

This is the first analysis correlating immune cell composition with the novel prognostic marker NFD. PD-1+ T-cells were observed to correlate with high NFD as a prognostic biomarker and predict good survival.

Literaturangaben

- [1] Bednarsch, J. Kather, J. Tan, X. Sivakumar, S. Cacchi, C. Wiltberger, G. Czigany, Z. Ulmer, F. Neumann, U. P. Heij, L. R., (2021), Nerve Fibers in the Tumor Microenvironment as a Novel Biomarker for Oncological Outcome in Patients Undergoing Surgery for Perihilar Cholangiocarcinoma, Liver Cancer, 10/3
- [2] Bednarsch, J. Tan, X. Czigany, Z. Liu, D. Lang, S. A. Sivakumar, S. Kather, J. N. Appinger, S. Rosin, M. Boroojerdi, S. Dahl, E. Gaisa, N. T. den Dulk, M. Coolsen, M. Ulmer, T. F. Neumann, U. P. Heij, L. R., (2021), The Presence of Small Nerve Fibers in the Tumor Microenvironment as Predictive Biomarker of Oncological Outcome Following Partial Hepatectomy for Intrahepatic Cholangiocarcinoma, Cancers, 13

The Hippo pathway effector TAZ induces intrahepatic cholangiocarcinoma in mice and is ubiquitously activated in the human disease

K. Evert¹, A. Cigliano¹, M. Sini², S. Ribback², C. Ament¹, K. Utpatel¹, S. Steinmann¹, F. Dombrowski², M. Evert¹, X. Chen³, D. F. Calvisi¹

¹*Institut für Pathologie, Regensburg, Germany*, ²*Institut für Pathologie, Greifswald, Germany*, ³*University of California, Department of Bioengineering and Therapeutic Sciences and Liver Center, San Francisco, United States of America*

Background

Intrahepatic cholangiocarcinoma (iCCA) is a rare and fatal form of liver cancer, accounting for ~10-15% of all primary hepatic tumors, whose incidence has rapidly increased in the United States and Europe in the past decades. Unfortunately, the treatment options are limited and generally ineffective. Therefore, to significantly improve the prognosis of iCCA patients, a better understanding of the molecular pathogenesis of iCCA is imperative.

Methods

Functional interplay between transcriptional co-activator with PDZ-binding motif (TAZ) and AKT was tested by delivering either an activated form of TAZ (TAZS89A) alone or co-delivering activated AKT to the mouse liver using sleeping beauty transposase via hydrodynamic tail vein injection (SBT-HTVI). In addition, the roles of the transcriptional enhanced associate domain (TEAD), Yes-associated protein (YAP), and the NOTCH pathway were addressed in vivo and in vitro using SBT-HTVI, Western blotting, cell culture, qRT-PCR, electron microscopy, and analysis of human tumor samples.

Results

Overexpression of TAZ, a Hippo pathway downstream effector, triggers iCCA development with very low incidence in the mouse liver. Of note, TAZ co-expression with an activated form of the AKT proto-oncogene dramatically increased cholangiocarcinogenesis. These cholangiocellular tumors recapitulated many of the histopathological and molecular features of human iCCA. At the molecular level, the development of AKT/TAZ tumors depended on the binding of TAZ to TEAD transcription factors. In addition, inhibition of the canonical Notch pathway did not hamper carcinogenesis but suppressed the cholangiocellular phenotype of these lesions. Also, the knockdown of YAP, the TAZ paralog, delayed cholangiocarcinogenesis without affecting the tumor phenotype. Furthermore, human preinvasive and invasive iCCAs and mixed hepatocellular carcinoma/iCCA display widespread TAZ activation and downregulation of the mechanisms protecting TAZ from proteolysis.

Conclusion

In summary, we have shown that the TAZ proto-oncogene is widely activated in human iCCA and drives rapid cholangiocarcinogenesis in the mouse liver in association with AKT via the Notch pathway. Therefore,

therapeutic strategies aimed at reactivating the mechanisms limiting TAZ hyperactivation and/or inhibiting TAZ function might be highly beneficial for treating human iCCA.

Mesosopic optical imaging reveals the microarchitecture of hepatic lymphatic vessels

S. Bobe^{1,2}, D. Klump², C. Dierkes², N. Kirschnick², F. Kiefer²

¹*Universitätsklinikum Münster, Gerhard-Domagk-Institut für Pathologie, Münster, Germany*, ²*European Institute for Molecular Imaging, WWU, Münster, Germany*

Background

The liver is the organ with the highest contribution to lymph flow by generating 25-50% of the lymph passing through the thoracic duct. The lymphatic circulation in the liver ensures tissue homeostasis and immune surveillance, but is also involved in pathophysiological processes like metastasis formation and fibrosis. Nevertheless, profound understanding of the three dimensional (3D) structure of hepatic lymph vessels and the mechanisms of hepatic lymphangiogenesis is still missing. Diagnostic routine imaging of the liver includes macroscopic ultrasound, MRI or CT imaging and microscopic examination of histological sections leaving a blind spot in the mesoscale, which covers the range of several millimeters. Visual and functional analyses of lymphatic vessels highly benefit from 3D volumetric imaging, which fully captures complex morphological changes that may appear rather subtle or may even be missed on histological sections. This is however challenging as lymphatic marker molecules are expressed on non-lymphatic hepatic cell types and the dense hepatic tissue causes intense light scattering and absorption.

Methods

Here, we report the successful combination of wholemount immunofluorescence staining, tissue clearing and light sheet fluorescence microscopy (LSFM) for 3D imaging and reconstruction of liver samples of several millimeters in size with a resolution on the micrometer scale.

Results

This technique allowed the detailed characterization of the microarchitecture of lymphatic vessels in the liver, which form a delicate network of finger-like protrusions around portal vein branches and follows as more straight vessels alongside bile ducts and hepatic arterioles. The haplo-insufficient cognate VEGF-C / VEGFR-3 growth factor / receptor pair forms an indispensable signaling axis in lymphangiogenesis. In mouse models with heterozygous deficiency for VEGF-C or VEGFR-3, our LSFM-based mesoscopic imaging approach revealed complex and subtle lymphatic vascular anomalies, which cannot be identified in section-based histology.

Conclusion

Thus, this study demonstrates an indispensable function of the VEGF-C/VEGFR3-signalling pathway for hepatic lymph vessel development and presents a mesoscale optical imaging approach which allows to analyze subtle changes of branched tubular structures in whole liver biopsies. Extension of our workflow to biopsies from various disease samples will improve our understanding of hepatic lymph vessel function in health and disease.

Hepatocellular ballooning in human cirrhotic livers is based on distinct glycogenosis associated with further metabolic and proto-oncogenic aberrations

S. Ribback¹, K. Peters¹, Q. Su², F. Dombrowski¹, P. Bannasch³

¹Universitätsmedizin Greifswald, Institut für Pathologie, Greifswald, Germany, ²Cell Marque, Millipore-Sigma, Rocklin, United States of America, ³Deutsches Krebsforschungszentrum Heidelberg, Heidelberg, Germany

Background

Hepatocellular ballooning frequently occurs in a variety of chronic liver diseases, particularly alcoholic and non-alcoholic steatohepatitis, often associated with Mallory-Denk body and ground glass formation. Cytoplasmic enlargement and “rarefaction” due to ill-defined degenerative changes have been related to these alterations, but their striking resemblance to glycogenotic/steatotic changes characterizing preneoplastic clear cell populations discovered and detailed in various animal models of hepatocarcinogenesis and chronic human liver diseases prone to develop hepatocellular carcinomas remained unrecognized.

Methods

96 cirrhotic human liver specimens were analysed for the appearance of ballooned hepatocytes (BH), especially for their storage of glycogen and lipids, Mallory–Denk-bodies, and ground glass features by light and electron microscopy. Enzyme activities and/or expression of proteins involved in glycolysis, de-novo lipogenesis and proto-oncogenic signaling cascades of AKT/mTOR and Ras/raf-1/MAPK were investigated by cytochemical approaches in serial paraffin and cryostat sections.

Results

BH were found in 43.8% of cirrhotic livers with a mean volume fraction of 14%. Regardless of the underlying etiology, ballooning was mostly associated with excessive storage of glycogen and/or fat, decreased activity of the glucose-6-phosphatase (key enzyme of gluconeogenesis) and increased activity of the glucose-6-phosphate-dehydrogenase (pentose phosphate pathway), and overexpression of proteins involved in glycolysis, lipogenesis and AKT/mTOR and ras/raf-1/MAPK pathway.

Conclusion

BH were frequently detected in human cirrhotic livers, irrespective of the underlying etiology, often with excessive storage of glycogen and/or lipids. Ballooning is due to metabolic and molecular aberrations corresponding to those of preneoplastic glycogenotic hepatocellular lesions well known from experimental hepatocarcinogenesis and chronic human liver diseases prone to develop hepatocellular carcinomas.

These findings suggest that ballooned hepatocytes in human cirrhotic livers are preneoplastic and indicate a high risk for the development of hepatocellular neoplasms.

Identification of DUSP4/6 overexpression as a rheostat to N-Ras induced hepatocarcinogenesis

S. Klemm, K. Utpatel, M. Evert, D. Calvisi, K. Evert, A. Scheiter

Universität Regensburg, Institut für Pathologie, Regensburg, Germany

Background

Upregulation of the mitogen-activated protein kinase (MAPK) cascade is common in hepatocellular carcinoma (HCC). Neuroblastoma RAS viral oncogene homolog (N-Ras) is mutated in a small percentage of HCC and hitherto considered insufficient for hepatocarcinogenesis. We aimed to characterize the process of N-Ras dependent carcinogenesis in the liver and to identify potential therapeutic vulnerabilities.

Methods

N-Ras V12 plasmid was delivered into the mouse liver via hydrodynamic tail vein injection (HTVI) with sleeping beauty transposase. The resulting tumors, preneoplastic lesions, and normal tissue were characterized by NanoString® gene expression analysis, Western Blot, and Immunohistochemistry (IHC). The results were further confirmed by *in vitro* analyses of HCC cell lines.

Results

HTVI with N-Ras V12 plasmid resulted in the gradual formation of preneoplastic and neoplastic lesions in the liver three months post-injection. These lesions mostly showed characteristics of HCC with some exceptions of spindle cell/cholangiocellular differentiation. Progressive upregulation of the Ras/Raf/MEK/ERK signaling was detectable in the lesions by Western Blot and IHC. NanoString® gene expression analysis of preneoplastic and tumorous tissue compared to age-matched controls revealed a gradual overexpression of CD133, Osteopontin, and Dual Specificity Phosphatases 4 and 6 (DUSP4/6), which was further validated by IHC and Western Blotting. *In vitro*, transfection of HCC cell lines with N-Ras V12 plasmid resulted in a coherent upregulation of DUSP4 and DUSP6. Paradoxically, in PLC/PRF/5 cells, this upregulation was accompanied by a downregulation of phosphorylated ERK, suggesting an overshooting compensation.

Conclusion

Contrary to prior assumptions, the G12V N-Ras mutant form is sufficient to elicit hepatocarcinogenesis in the mouse. Furthermore, the upregulation of the MAPK cascade was paralleled by the overexpression of DUSP4 and DUSP6 *in vivo* and *in vitro*. Therefore, DUSP4 and DUSP6 might serve to fine-tune the excessive MAPK-activation, a mechanism that can potentially be harnessed therapeutically.

Direct interaction of the oncogenes YAP and TAZ with the transcription factor HNF1B in hepatocellular carcinoma

F. von Bubnoff¹, M. Wesener¹, J. Schmitt¹, T. Ruppert², P. Schirmacher¹, K. Breuhahn¹, S. Weiler¹

¹*Institute of Pathology, Heidelberg University Hospital, Heidelberg, Germany*, ²*Center for Molecular Biology at Heidelberg University, Core Facility for Mass Spectrometry and Proteomics, Heidelberg, Germany*

Background

Yes-associated protein (YAP) and WW domain containing transcription regulator 1 (WWTR1, TAZ) are the main effectors of the Hippo pathway and act as transcriptional co-activators. Nuclear YAP or TAZ contribute to liver tumor formation and progression via induction of proliferation, cellular stemness and chromosomal instability. However, how YAP and TAZ support tumorigenesis at the molecular level is not fully understood. Here, we investigate the YAP-/TAZ-specific interactome in hepatocellular carcinoma (HCC) with focus on transcriptional regulators.

Methods

HCC cells with inducible expression of YAP and TAZ fused to the biotin ligase BirA were used for BioID proximity-dependent labeling and subsequent mass spectrometry (MS). Potential binding partners were confirmed using co-immunoprecipitation (co-IP) and proximity ligation assay (PLA). Gene silencing was performed by transient transfection of gene-specific siRNAs. Gene expression profiling (EP) after hepatocyte nuclear factor 1 β (HNF1B) silencing was followed by bioinformatic data analysis (\pm 1.5-fold changes with false discovery rates \leq 0.05). Promoter binding sites were identified using HNF1B ChIP sequencing data.[1] HNF1B expression was investigated using a tissue microarray (TMA) consisting of 720 human liver and HCC tissues as well as in mice expressing constitutively active human YAP^{S127A}.

Results

MS revealed that the cholangiocyte-specific transcription factor HNF1B interacts with YAP and TAZ in HCC cells. High HNF1B expression and physical interaction with YAP and TAZ were confirmed in different HCC cell lines. Spatial analysis illustrated prominent nuclear binding of HNF1B with YAP/TAZ and TEAD4, a known YAP/TAZ-interacting transcription factor. In vivo, an induction of murine HNF1B is detectable in YAP^{S127A}-induced hepatocarcinogenesis. EP revealed 323 significantly regulated genes after HNF1B silencing. Promoter binding analysis for HNF1B and TEAD4 suggested the PI3K-pathway effector serum/glucocorticoid regulated kinase 2 (SGK2) as a new potential transcriptional target for the YAP/TAZ/TEAD/HNF1B complex in HCC cells. TMA analysis revealed a subgroup of HCCs expressing nuclear HNF1B.

Conclusion

The cholangiocyte marker HNF1B is expressed in HCC cells and interacts with YAP/TAZ and TEAD4. Elevated expression of HNF1B is a marker for tumor cell dedifferentiation and may represent a mechanism how the Hippo pathway controls other oncogenic pathways such as PI3K signaling in hepatocarcinogenesis.

Literaturangaben

[1] ENCODE Project Consortium, (2012), An integrated encyclopedia of DNA elements in the human genome, Nature, <https://www.encodeproject.org>, 2022-02-26, ENCSR127XTZ (HNF1B) ENCSR800JRG (TEAD4)

AG01 AG Gastroenteropathologie III

AG01.18

Increase of Ki67 during progression of NET G3

A. Kasajima¹, B. Konukiewicz², A. M. Schlitter¹, W. Weichert¹, G. Klöppel¹

¹Technischen Universität München, Institut für Allgemeine Pathologie und Pathologische Anatomie, München, Germany, ²Universitätsklinikum Schleswig-Holstein, Campus Kiel, Christian-Albrechts-Universität zu Kiel, Institut für Pathologie, Kiel, Germany

Background

Neuroendocrine tumors (NETs) G3 are aggressive neuroendocrine neoplasms which occur in many organs but their site-specific distribution and clinical behavior are heterogeneous and have not been well understood. Here, we specifically aimed to clarify their mode of progression.

Methods

We reviewed a large consultation series and found 162 tumor samples of NET G3 obtained from 144 patients diagnosed between 2009 and 2022. The review was based on the 2019 WHO-classification of digestive system tumors.

A NET G3 initially diagnosed in a primary site was defined as “de-novo NET G3”. NETs G3 initially diagnosed as NET G1 or G2 and progressed to NET G3 were defined as “transit NET G3”. Mode of progression could be determined in 70/144 NETs G3. The highest value of the difference between Ki67 indices in a progressing NET G3 was defined as “delta Ki67 value”.

Results

45/144 (31%) and 99/144 (69%) patients were diagnosed either with a primary or metastatic NET G3. Of the 70 NETs G3 with progression data, 54 (77%) and 16 (23%) were grouped as “de-novo” and “transit” NET G3, respectively. The pancreas was the most frequent site of origin of “de-novo” (21/54, 39%) as well as “transit” (7/16, 43%), followed by lung (13/54, 24% for “de-novo”, 4/16, 25% for “transit”). In third place for “de-novo” was the stomach (8/54, 15%) and for “transit” the stomach, small intestine, and rectum (1/16, 6%). The delta Ki67 values of the “transit” NETs G3 were variable (mean 21, range 2-48), with 12 tumors showing low (2 to 25) delta Ki67 values and 4 tumors (3 pancreatic, 1 rectal) high delta values above 40. All tumors with delta values above 40 revealed a change of the p53 expression pattern (wild type to overexpression).

Conclusion

The most frequent sites of origin for NETs G3, both for “de-novo” and “transit” tumors, are the pancreas and the lung. Delta Ki67 values in the “transit” NETs G3 are variable ranging from low (2 to 25) to high (above 40). NETs G3 with high delta Ki67 value showed rapid progression associated with p53 overexpression, suggesting an p53 mutation.

The role of ATF2 in 5-Fluorouracil resistance of colorectal cancer cells

H. Yang¹, K. Huebner¹, C. Hampel¹, K. Erlenbach-Wuenssch^{1,2}, A. Hartmann^{1,2}, V. Mahadevan³, R. Schneider-Stock^{1,2}

¹University Hospital, Institute of Pathology, FAU Erlangen-Nürnberg, Erlangen, Germany, ²Comprehensive Cancer Center Erlangen-EMN (CCC ER-EMN), University Hospital Erlangen, Friedrich Alexander University Erlangen-Nürnberg, Erlangen, Germany, ³Institute of Bioinformatics and Applied Biotechnology (IBAB), Bangalore, India

Background

The Activating transcription factor-2 (ATF2) regulates transcription of various genes, which are involved in cell proliferation, apoptosis, inflammation, and DNA damage response. ATF2 behaves as a double-edged sword in different types of cancer. So far, its role in drug resistance mechanisms in colorectal cancer (CRC) is not known.

Methods

We treated HCT116 (wildtype p53) and HT29 (mutant p53) cells and their corresponding ATF2-CRISPR-knockout (HCT116 ATF2 KO, HT29 ATF2 KO) cells with different doses of 5-Fluorouracil (5FU). Drug effects were measured by Annexin-PI staining, Western Blotting for apoptosis markers, tumor-forming ability assay *in vitro* and the chicken chorioallantoic membrane (CAM) model *in vivo*.

Results

We observed that HCT116 cells lacking ATF2 exhibited 5-FU resistance with significantly reduced DNA damage (γ H2AX) and apoptosis *in vitro* and *in vivo*. 5FU treatment activated the DNA damage response (DDR) pathway. We found elevated levels of pATR^{Thr1989} and pChk1^{ser317} in ATF2 KO cells. Accordingly, Chk1 inhibition sensitized the cells to 5FU. The results of co-immunoprecipitation and proximity ligation assay revealed that ATF2 builds a complex with p-ATR, which phosphorylates Chk1. *In silico* modeling indicated a highly stabilized triple complex consisting of pATR/Chk1/ATF2. In HT29 p53 mutant cells, the dose-dependent increase in cleaved PARP seemed to prevent a further increase in DNA damage suggesting a close association between DNA damage and apoptosis induction. In HCT116 p53^{-/-} cells, we did not see any DDR activation at all.

Conclusion

For the first time, we showed that ATF2 mediates 5FU resistance by affecting the DDR mechanism in a p53-dependent manner. As a scaffold protein, ATF2 seems to affect the efficacy of phosphorylation of the repair protein pChk1 by the damage sensor ATR.

Cytoskeleton associated DAPK links autophagy with EMT

P. Prechtel¹, C. Hampel¹, P. Kunze¹, K. Huebner¹, K. Erlenbach-Wuenssch^{1,2}, A. Hartmann^{1,2}, R. Schneider-Stock^{1,2}

¹*University Hospital, Institute of Pathology, FAU Erlangen-Nürnberg, Erlangen, Germany*, ²*Comprehensive Cancer Center Erlangen-EMN (CCC ER-EMN), University Hospital Erlangen, Friedrich Alexander University Erlangen-Nürnberg, Erlangen, Germany*

Background

The tumor suppressor functions of the death-associated protein kinase (DAPK) relate to apoptosis and autophagy in colorectal cancer. Recently we highlighted its role as an inhibitor of tumor progression. Highly proliferating tumors under nutrient restriction activate autophagy. Experimentally, nutrient restriction initiates an epithelial-mesenchymal transition (EMT), a process at the tumor invasion front. Thus, we questioned the role of DAPK in this scenario.

Methods

We treated HCT116 DAPK WT and two HCT116-derived CRISPR-Cas9 DAPK KO clones with a glucose- and serum-reduced medium and evaluated autophagy and EMT-markers such as p62, LC3 and E-Cadherin by Western Blot analysis and cell-morphology by microscopy. Spheroid formation and CAM experiments were performed to test starvation effects in 3D-conditions and in vivo.

Results

While HCT116 WT cells showed early signs of EMT, their DAPK-deficient clones developed the mesenchymal phenotypes with a significant time delay. When autophagy was inhibited by Bafilomycin co-treatment, tumor cells lacking DAPK showed massive signs of cell death, mostly due to their extraordinary high endogenous autophagic flux.

Conclusion

DAPK-deficient tumor-cells are addicted to autophagy. The strong link between autophagy and EMT might have consequences for therapeutic interventions in DAPK-negative tumors.

Molecular subtyping of gastric cancer according to ACRG using immunohistochemistry – correlation with clinical parameters

E. Pretzsch¹, F. Bösch¹, R. Todorova², H. Nieß¹, S. Jacob¹, M. Guba¹, T. Kirchner², J. Werner¹, F. Klauschen², M. Angele¹, J. Neumann²

¹LMU Klinikum München, AVT Chirurgie, München, Germany, ²LMU Klinikum München, Pathologie, München, Germany

Background

Gastric cancer (GC) is a very heterogenous disease necessitating further stratification for prognostic and therapeutic aspects. Based on the recommendation of the Asian Cancer Research Group (ACRG) that recently established four molecular subtypes (MSI, MSS/EMT, MSS/TP53+, MSS/TP53-) which require molecular expression analysis. The technology required for comprehensive molecular analysis is expensive and not applicable for routine diagnostics. Thus, in this study we established a classification system utilizing immunohistochemistry and morphology-based analyses as surrogate markers in order to reproduce the ACRG molecular subtypes of gastric cancer. To clarify the clinical relevance of the novel classification system, we performed a correlation with established clinical parameters.

Methods

The study cohort consisted of 189 patients with GC (UICC III and IV). Using immunohistochemistry, the following markers were analysed: MLH1, MSH2, MSH6, PMS2 (as a surrogate for microsatellite status), p53, SOX9. We assessed tumor budding as a surrogate for EMT to distinguish between MSS/EMT and MSS/non-EMT groups.

Results

Immunohistochemical and morphologic subtyping classified cases as follows: 10% MSI, 35% MSS/EMT, 16% MSS/TP53+ and 39% MSS/TP53-. Subtypes significantly correlated with the Lauren classification, tumor stage, venous invasion and SOX9 expression ($p < 0.05$). There was no significant correlation between molecular subtype and lymph node growth pattern.

Conclusion

We propose a simple algorithm for molecular subtyping of GC using universally available immunohistochemistry, which correlates with clinical parameters and is cost-effective and applicable in diagnostic routine. This classification might prospectively help to determine patient prognosis, optimize patient care and homogenize patient cohorts for clinical trials.

AG02 AG Uropathologie I

AG02.01

Anti-Angiogenic Properties of A Novel Secreted Neuropilin-2 Isoform In Bladder Cancer

T. Mayr¹, P. L. Dix¹, S.-M. Hasheminasab², C. Hampel³, M. Sylvester⁴, S. Foerster¹, R. Schneider-Stock³, G. Kristiansen¹, M. Muders¹

¹Institut für Pathologie, UK Bonn, Bonn, Germany, ²Institut für Pathologie, Universitätsklinikum Dresden, Dresden, Germany, ³Experimental Tumorpathology, Institute of Pathology, Friedrich-Alexander-University Erlangen-Nuremberg, Erlangen, Germany, ⁴Institute of Biochemistry and Molecular Biology, University of Bonn, Bonn, Germany

Background

The non-tyrosine kinase receptor neuropilin-2 (NRP2) is detected in a number of tumor entities and its upregulation correlates with disease progression. Two membrane-anchored reference isoforms transcribed from the NRP2 gene share extracellular portions, but diverging terminal exons encode unrelated transmembrane and cytoplasmic stretches. Amino-terminal extracellular protein domains are the main features of the soluble dimeric s9NRP2 reference isoform, which is involved in the VEGF-C ligand maturation.

Methods

We used a next-generation sequencing approach to enrich for NRP2 terminal exons identify a novel soluble NRP2 isoform and verified its secretion from cultured cells by mass spectrometry. Western blotting was used to detect soluble NRP2 in human serum samples. Various aspects of VEGF-A₁₆₅ induced angiogenesis were studied in the chicken chorioallantoic membrane assay. Tissue was used to measure messenger and protein levels of the newly discovered isoform.

Results

We identified a novel soluble NRP2 isoform, *NRP2-Mo83*, and verified its secretion from cultured cells. Preliminary data indicate the presence of soluble NRP2-Mo83 protein in human serum samples. While being expressed at variable quantities *in vitro* in a panel of bladder carcinoma cell lines, *NRP2-Mo83* mRNA is downregulated in a small cohort of macrodissected urothelial carcinoma samples. *In vivo*, NRP2-Mo83 counteracts various aspects of VEGF-A₁₆₅ induced angiogenesis in the chicken chorioallantoic membrane assay.

Conclusion

NRP2-Mo83 is presented as a novel soluble NRP2 splice isoform, and its expression at the mRNA and protein level is validated. In accordance with its apparent down-regulation during bladder tumorigenesis,

NRP2-Mo83 is shown to possess anti-angiogenic properties *in vivo* and *in vitro*. The presence of NRP2-Mo83 in serum samples suggest a potential function under non-pathological conditions.

A simplified method for molecular subtype classification of urinary bladder cancer based on RT-qPCR

C. Olah¹, C. Hahnen¹, N. Nagy², J. Musial¹, M. Varadi², G. Nyiro³, B. Györfy^{4, 5}, B. Hadaschik⁶, J. Rawitzer⁷, S. Ting⁷, G. Sjö Dahl⁸, M. J. Hoffmann⁹, T. Szarvas^{1, 2}, **H. Reis**^{7, 10, 11}

¹University Medicine Essen, Department of Urology, Essen, Germany, ²Semmelweis University Budapest, Department of Urology, Budapest, Hungary, ³Semmelweis University, MTA-SE Molecular Medicine Research Group, Budapest, Hungary, ⁴Semmelweis University Budapest, 2nd Department of Pediatrics and Department of Bioinformatics, Budapest, Hungary, ⁵Research Centre for Natural Sciences, Institute of Enzymology, Cancer Biomarker Research Group, Budapest, Hungary, ⁶University Medicine Essen, Department of Urology, Essen, Germany, ⁷University Medicine Essen, Institute of Pathology, Essen, Germany, ⁸Lund University Hospital, Department of Oncology, Clinical Sciences, Lund, Sweden, ⁹Heinrich-Heine-University Hospital Duesseldorf, Department of Urology, Duesseldorf, Germany, ¹⁰Dr. Senckenbergisches Institut für Pathologie, Universitätsklinikum Frankfurt, --, Frankfurt, Germany, ¹¹University Hospital Frankfurt, Dr. Senckenberg Institute of Pathology, Frankfurt, Germany

Background

Both prognostic and predictive information have been associated with transcriptome-based molecular subtypes of muscle-invasive bladder cancer (MIBC). However, these systems are currently not used in clinical routine practice. We therefore aimed to develop a feasible method for molecular subtyping based on a reverse transcription quantitative polymerase chain reaction (RT-qPCR) approach.

Methods

In the first step, we defined a gene set (n=68 genes) that covered both stromal (immune, extracellular matrix, p53-like) and tumor intrinsic (luminal, basal, squamous, neuronal, epithelial-to-mesenchymal, in situ carcinoma) signatures. In the next step, different classifier methods were developed *in silico* using this 68-gene set followed by validation on public data sets (MD Anderson [MDA], The Cancer Genome Atlas [TCGA], Lund, Consensus). In the last step, the 68 gene-expression profiles were analyzed in 104 frozen tissue samples of an institutional MIBC cohort. This was done by a RT-qPCR approach using the TaqMan Array Card platform and samples were classified by our reduced 68-gene marker set.

Results

This reduced marker set combined with the developed classifiers was able to reproduce the prognostic value of each subtype of the MDA, TCGA II, Lund and Consensus subtype classification systems with an overlap of 76%, 79%, 69% and 64%, respectively. We were able to successfully classify 96% (100/104) of our MIBC samples by using RT-qPCR. Our results demonstrate low stromal gene expression levels and neuronal and luminal subtypes to be associated with poor survival.

Conclusion

We developed a robust and feasible method for the molecular subtyping that recapitulates the MDA, TCGA II, Lund and Consensus classification systems [1]. Our data further suggest that stromal signatures might have a higher prognostic value compared to the tumor intrinsic signatures themselves. Therefore, the importance of tumor-stroma interaction during the progression of MIBC is underlined and calls for further research.

Literaturangaben

[1] Olah, C., Hahnen, C., Nagy, N., Musial, J., Varadi, M., Nyiro, G., Gyorffy, B., Hadaschik, B., Rawitzer, J., Ting, S., Sjödaahl, G., Hoffmann, M. J., Reis, H., & Szarvas, T. , (2022), A quantitative polymerase chain reaction based method for molecular subtype classification of urinary bladder cancer-Stromal gene expressions show higher prognostic values than intrinsic tumor genes., *Int J Cancer*, 150(5), 856–867, <https://doi.org/10.1002/ijc.33809>

Identifying proteins interacting with KDM5C in prostate cancer

A.-L. Lemster¹, M. Rezaenia¹, P. Lazar-Karsten¹, L. Gresens¹, M. Sylvester², S. Perner^{1,3}, J. Kirfel¹

¹*University hospital Schleswig-Holstein, Campus Luebeck, Institute of Pathology, Luebeck, Germany,*

²*University of Bonn, Medical Faculty, Institute of Biochemistry and Molecular Biology, Core Facility Mass Spectrometry, Bonn, Germany,* ³*Leibniz Lung Center, Research Center Borstel, Pathology, Borstel, Germany*

Background

Emerging evidence suggested that epigenetic regulators can exhibit both activator and repressor activities in gene transcriptional regulation and disease development, such as cancer. However, how these dual activities are regulated and coordinated in specific cellular contexts remains elusive. KDM5C contains a JmjN domain, a BRIGHT domain, an AIRD (AT-rich interaction) domain, a JmjC domain, a C5HC2 zinc finger, and two PHD (plant homeodomain) fingers. KDM5C binds to histone H3 via its N-terminal PHD finger, which is required for efficient demethylation of histone tails and regulation of gene transcription. We demonstrated that KDM5C plays an essential role in prostate cancer (PCa) development. KDM5C is highly upregulated in metastatic PCa and is directly associated with the invasiveness of prostate tumor cells. To understand the global KDM5C function in PCa, we aim to identify KDM5C interacting proteins or protein complexes.

Methods

Tandem Affinity Purification (TAP) of protein complexes has become an important tool in the field of proteomic research. We used TAP technology as a generic two-step affinity purification protocol to isolate TAP-tagged KDM5C proteins together with associated proteins from PC3 cell lysates. After TAP, the eluate was analyzed by nanoflow liquid chromatography/tandem mass spectrometry (nanoLC-MS/MS) and the proteins were identified.

Results

We constructed different FLAG-HA-tagged mammalian expression vectors expressing either the full-length KDM5C protein (AA 2-1560) or one of two truncated proteins, the N-terminal part of KDM5C (AA 2-829) or the C-terminal part of KDM5C (AA 636-1560). 50 different proteins were identified by mass spectrometry. We discovered that 23 interaction partners bind to the N-terminus of KDM5C, where the enzymatic domains are located, and 9 interaction partners bind C-terminally. 26 out of 50 proteins were located in the nucleus. Interestingly, 29 proteins have been reported to be associated with PCa development. We are planning to confirm the KDM5C interaction by protein-protein interaction assays e.g. pull-down assay or Bioluminescence Resonance Energy Transfer (BRET), and the co-expression of KDM5C and its interacting proteins by IHC staining of a PCa cohort.

Conclusion

Several proteins have been identified to potentially interact with KDM5C in metastatic PCa. These results

may provide deeper insights into the functioning of KDM5C and its role in the development of PCa.

Frequency of *TERT* gene promoter mutations in upper tract urothelial carcinoma

J. Schmelmer^{1,2}, R. Stoehr^{1,2}, B. Wullich^{2,3}, D. Sikic^{2,3}, S. Wach^{2,3}, H. Taubert^{2,3}, H. Heers⁴, P. L. Strissel^{1,2,5}, R. Strick^{2,5}, M. Angeloni^{1,2}, F. Ferrazzi^{1,2,6}, M. Eckstein^{1,2}, A. Hartmann^{1,2}, V. Bahlinger^{1,2}

¹*Institute of Pathology, University Hospital Erlangen, Erlangen, Germany*, ²*Comprehensive Cancer Center Erlangen-EMN (CCC ER-EMN), Erlangen, Germany*, ³*Department of Urology and Pediatric Urology, University Hospital Erlangen, Erlangen, Germany*, ⁴*Department of Urology, University Hospital Gießen and Marburg, Philipps-Universität Marburg, Marburg, Germany*, ⁵*Laboratory for Molecular Medicine, Department of Gynecology and Obstetrics, University Hospital Erlangen-Nürnberg, Erlangen, Germany*, ⁶*Department of Nephropathology, Institute of Pathology, University Hospital Erlangen-Nürnberg, Erlangen, Germany*

Background

Upper tract urothelial carcinoma (UTUC) is a rare cancer entity and accounts for 5-10% of all urothelial tumors. Mutational analysis revealed five different molecular subtypes for this rare cancer entity, which will give more insights into tumor pathogenesis. *TERT* promoter gene mutations are the most common mutations identified in urothelial bladder tumors, however the frequency of these hot spot mutations in UTUC is not well established.

Methods

201 upper tract urothelial carcinomas collected from the Institute of Pathology in Erlangen and Marburg were histomorphologically reevaluated and analyzed. DNA isolation was performed for each tumor using the Maxwell Promega. SNaPshot analysis, including three hot spot regions (-57, -124 or -146), was used to detect mutations among the hotspot regions within the *TERT* gene promoter.

Results

So far, 72.1% (31 out of 43) of the analyzed UTUCs presented as *TERT* promoter mutation carrier, indicating a common alteration observed in urothelial tumors. Additionally, *TERT* promoter mutations were observed independent of the tumor stage. Moreover, the hot spot region -124 was most frequently identified in UTUC samples. More data will be presented during the meeting.

Conclusion

In this ongoing study, and as far as the current low sample size allows any conclusions, the frequencies of *TERT* promoter mutations in UTUC is high and similar to those in urothelial bladder tumors. The high frequency of *TERT* promoter mutations seems to play also an important role in urothelial tumorigenesis of the upper tract and is independent of stage characteristics.

The new WHO classification of testicular tumors - The main changes

F. Bremmer

University Medical Center, Institute of Pathology, Göttingen, Germany

Die 5. Ausgabe der „WHO Klassifikation für Tumoren der ableitenden Harnwege und des männlichen Genitaltraktes“ enthält einige Neuerungen der bestehenden Klassifikationen. Die wesentlichen Veränderungen betreffen den „Primitiven neuroektodermalen Tumor“, dessen Bezeichnung in „Embryonaler Neuroektodermaler Tumor“ (ENET) geändert wurde. Das Seminom wird jetzt in die Germinoma-Tumorfamilie eingeordnet. Die Kriterien für ein Teratom mit somatischer Transformation wurden in „Größenbasiert“ geändert. Karzinoide des Hodens werden nun als „präpubertale testikuläre neuroendokrine Hodenomen“ bezeichnet. Bei der Untersuchung der Malignitätskriterien der Gonadenstromatumoren soll die Mitoserate in mm² angegeben werden (Mitosen/mm²) und nicht mehr als Mitosen/HPF. Der Siegelring-Stromatumor wurde trotz der aktuellen kontroversen Diskussion als neue Entität definiert.

Als weitere neue Entität wurde der „Myoidale Gonaden-Stromatumor“ eingeführt. Zudem wurde der gut differenzierte papilläre Mesotheltumor als eigenständiger Tumor definiert.

Das sertoliformes Zystadenom wurde aufgrund der großen morphologischen Ähnlichkeit zu den Sertolizelltumoren und dem sehr ähnlichen immunhistochemischen Profil aus dem Kapitel der adenexalen Tumoren entfernt und als Untereinheit der Sertolizelltumoren eingeordnet.

Außerdem wurden eigene Kapitel für hämatolymphoide Neoplasien und Weichgewebstumoren der ableitenden Harnwege und des männlichen Genitaltraktes geschaffen.

Der Vortrag soll einen Überblick der wesentlichen Neuerungen geben.

AG02 AG Uropathologie II

AG02.06

Update WHO-classification (5.edition, 2022): Tumors of the urinary system.

R. Knüchel-Clarke^{1, 2}

¹Uniklinik RWTH Aachen,, Pathologie, Aachen, Germany, ²Uniklinik RWTH Aachen, CIO-ABCD, Aachen, Germany

Das Urothel der ableitenden Harnwege ist trotz morphologisch einfacher Grundstruktur das Ausgangsepithel für eine recht hohe Variation von Tumorstadien und manifesten Tumoren, deren Definition durch molekulargenetische Studien einerseits und systematische Sammlung von Subgruppen ständig päzisiert wird. Wesentlich hierbei ist die genaue Definition von Entitäten im Hinblick auf eine Therapiestratifizierung durch den behandelnden Urologen bzw. Uroonkologen.

Die WHO-Klassifikation hat sich als Arbeitsklassifikation weiterentwickelt und die wesentlichen Neuerungen sollen zur Diskussion gestellt werden:

Während das Grading bei Low - und High Grade Bestand hat und auch das Carcinoma in situ klar umrissen bleibt, ist die Dysplasie und der "UPUMP" von der "blauen Seite" des BlueBook entfernt worden.

Getragen von dem Prinzip Low- und High Grade wird die Zytologie mit einem hohen Wert für die sensitive und spezifische Diagnostik des High Grade Tumors verbunden mit der Anwendung des PARIS-Systems für die Urinzytologie klar als wertvoll zum Ausdruck gebracht.

Bei den Tumoren, die direkt vom Urothel ausgehen ist, nachdem z. B. 2016 schon die Müller'schen Tumoren und die Urachuskarzinome als Sonderentitäten erfasst worden sind, eine weitere Entitätspräzisierung, z. B. durch Erfassung der Varianten der Adenokarzinome aufgegriffen worden. Die Liniendifferenzierung der Tumore wird mehr für die Einteilung berücksichtigt und in den Gruppen der aktuelle Stand von Epidemiologie unter Einbeziehung der derzeitigen molekular-pathogenetischen Datenlage erfasst.

Erweiternd für den Blickwinkel des Pathologen und gleichzeitig wichtig und anregend für die Auseinandersetzung mit Tumorherkunft und Therapiemöglichkeiten ist die Entscheidung, in diesem wie auch in anderen Editionen der 5. Auflage der WHO-Klassifikation, organüberschreitende Tumorguppen als Einzelkapitel mit möglichst gleichartiger Nomenklatur zu präsentieren. Dieses erfolgte für die neuroendokrinen Neoplasien, die mesenchymalen und hämatopoetischen Tumoren und die melanozytären Läsionen. Gleichzeitig gibt es keine gesonderten Kapitel mehr für die oberen Harnwege und die Urethra.

Primary pseudomyogenic hemangioendothelioma of the testis with a novel *POTEI-FOSB* gene fusion

A.-K. Gersmann¹, F. Haller², N. Behnert³, A. Richter¹, R. Stöhr², A. Hartmann², P. Ströbel¹, **F. Bremmer¹**

¹University Medical Center, Institute of Pathology, Göttingen, Germany, ²University Hospital Erlangen, Friedrich-Alexander University Erlangen-Nuremberg, Institute of Pathology, Erlangen, Germany,

³Department of Pathology, Pathologie Nordhessen, Kassel, Germany

Background

Pseudomyogenic hemangioendothelioma is a rare endothelial neoplasm of intermediate biological behavior, which often affects young male adults. It usually presents as multifocal tumor nodules in the extremities. The tumor is characterized by an upregulation of FOSB, often based on a *FOSB* gene fusion with *ACTB* and *SERPINE* as fusion partners.

We report the first case of a pseudomyogenic hemangioendothelioma in a 54-year-old man with an isolated tumor manifestation in the left testis. In line with this unusual anatomic location, the tumor harbored a novel *POTEI-FOSB* gene fusion.

Methods

Conventional hematoxylin/eosin staining and immunohistochemical staining of formalin-fixed, paraffin embedded sections were performed to characterize the tumor cells. In addition to that, a next-generation sequencing based fusion analysis with the TruSight RNA Fusion Panel (Illumina, San Diego, USA) was employed to detect gene fusions. Detected gene fusions were visualized from the bam files using the Integrative Genomics Viewer.

Results

The histopathological examination revealed a tumor with a fascicular growth pattern, partially displacing and partially surrounding the seminiferous tubules. It was predominantly composed of spindle cells with a minor component of cells with epithelioid appearance. The tumor cells had eosinophilic cytoplasm, the vesicular nuclei showed mild to moderate atypia and partially contained prominent nucleoli. The stroma had a conspicuous granulocytic infiltrate.

The tumor cells showed an immunohistochemical profile with positivity for pancytokeratine as well as for the endothelial markers CD31 and ERG with negative staining for CD34. Furthermore, the tumor cells showed strong positivity for FOSB.

Accordingly, the RNA fusion analysis revealed a gene fusion involving the genes *POTE Ankyrin Domain Family Member 1 (POTEI)* and *FosB Proto-Oncogene, AP-1 Transcription Factor Subunit (FOSB)*, with genomic breakpoints at chr2:131221120 and chr19:45971680, respectively. On the RNA level, the breakpoints mapped to *POTEI* exon 15 and to *FOSB* exon 1.

Conclusion

Immunohistochemical and molecular analysis confirmed the morphological tentative diagnosis of testicular pseudomyogenic hemangioendothelioma. In line with this unusual anatomic location, the tumor harbored a novel *POTEI-FOSB* gene fusion, which has so far not been described.

***GRHL3* in bladder cancer: a dual role depending on molecular and histological background?**

F. C. Lammert¹, R. Weiskirchen², L. Gan³, R. Knüchel-Clarke¹, M. Rose¹, N. T. Gaisa¹

¹*Institute of Pathology, RWTH Aachen University Hospital, Aachen, Germany*, ²*Institute of Molecular Pathobiochemistry, Experimental Gene Therapy and Clinical Chemistry, RWTH Aachen University Hospital, Aachen, Germany*, ³*IZKF Aachen, Medical Faculty of the RWTH Aachen University, Aachen, Germany*

Background

Grainyhead-like transcription factor 3 (*GRHL3*) belongs to the GRHL transcription factor family known to mediate both tumor suppressive or oncogenic effects based on the given organ or tissue type. So far, the role of GRHL3 in urothelial and/or squamous bladder cancer is still unknown. Therefore, we aimed to investigate GRHL3 expression, function and its orchestrated transcriptomic network with respect to squamous and urothelial bladder cancers.

Methods

We used tissue microarrays of normal urothelium, squamous metaplasia, squamous carcinoma in situ, squamous cell carcinoma (SCC), urothelial carcinoma (UC) and urothelial carcinoma with squamous differentiation (MIX) (n=400 samples) to study immunohistochemical GRHL3 expression and calculated Kaplan Meier curves by SPSS statistics. Additional qRT-PCR was performed on n=189 samples. Findings were validated by using *The Cancer Genome Atlas* (TCGA) BLCA (bladder cancer) data set. Functional *in vitro* analyses (cell growth, XTT proliferation, colony formation, migration, cell-matrix adhesion, and invasion assays) with stable single cell clones overexpressing GRHL3 (GRHL3-pCMV6 clones) with human bladder cell lines SCaBER (SCC model) and EJ28 (UC model) were performed. Transcriptomic networks of cell models were investigated by RNA seq analyses.

Results

GRHL3 mRNA and protein expression was significantly downregulated in squamous bladder cancers while upregulated in urothelial carcinomas. *GRHL3* loss correlated with unfavorable prognosis in squamous bladder cancers. *In vitro*, *GRHL3* overexpression triggered contrary effects in generated models: GRHL3 overexpression blocked growth, colony formation, cell motility, and invasion of squamous SCaBER cells, whereas GRHL3 overexpression in urothelial EJ28 cells mediated oncogenic effects, e.g. invasiveness. RNA seq analyses revealed a putative involvement of Rho GTPase activity affecting actin cytoskeleton and focal adhesion formation.

Conclusion

The presented study provides functional evidence that GRHL3 may act either as tumor suppressor in squamous bladder cancer or oncogene in urothelial bladder cancer depending on the underlying

histopathological and molecular characteristics. However, future studies will be necessary to decipher regulatory networks causative for GRHL3's mode of mechanism.

NeuroSAFE frozen section examination in potentially nerve-sparing radical prostatectomy: Comparison of conventional frozen sections and fluorescence-based confocal microscopy (FCM) - Initial results

J. Köllermann¹, F. J. Koll², H. Reis¹, A. Tschäbunin¹, S. Gretser¹, F. Preisser², B. Höh², M. Wenzel², P. Mandel², F. K.-H. Chun², P. Wild¹

¹Universitätsklinikum Frankfurt / M., Dr. Senckenbergisches Institut für Pathologie, Frankfurt, Germany,

²Universitätsklinikum Frankfurt / M., Klinik für Urologie, Frankfurt, Germany

Background

Die Fluoreszenz-basierte Konfokalmikroskopie (FCM) ermöglicht die digitale Schnellschnittuntersuchung von Gewebe unter Umgehung wesentlicher Laborarbeits-schritte. Die Befundung erfolgt digital. Kürzere Untersuchungszeiten, eine räumlich unabhängige Befundung sowie ein geringerer Personalbedarf machen die Methode attraktiv. Im Rahmen der NeuroSAFE-Prozedur soll die FCM-Technik hinsichtlich Untersuchungsdauer, Bildqualität und Diagnoseübereinstimmung mit der herkömmlichen Gefrier(kryo)technik verglichen werden.

Methods

Im Rahmen eines Pilotprojekts wurde bei 5 Patienten im Rahmen einer Prostatektomie eine NeuroSAFE Untersuchung durchgeführt. Nach Tuschemarkierung des relevanten Präparaterandes erfolgte eine Gewebelamellierung in 4 mm dicke Scheiben und die Untersuchung in Kryotechnik. Nach Auftauen des Gewebes wurden die Scheiben unilateral zusätzlich mittels FCM (Vivascope) in der Pathologie und in Unkenntnis des Kryobefundes untersucht.

Results

Insgesamt wurden 22 Scheiben mit im Mittel 4,4 Scheiben/Fall angefertigt. Die Untersuchungszeit/Fall mittels FCM- bzw. Kryotechnik betrug im Median 43 vs. 20 min. Bezogen auf die Einzelscheiben betrug die Karzinomnachweisrate in beiden Verfahren 32% (7/22). Eine adäquate Randbeurteilbarkeit zeigte sich in 68,2% (15/22; FCM) bzw. 100% (Kryotechnik).

Conclusion

Im Vergleich zur Kryotechnik ergab sich für die FCM-Technik eine Verdopplung der Untersuchungszeit und eine schlechtere Randbeurteilbarkeit. Die Anfertigung von Stufenschnitten bei randkritischem Befund ist nicht möglich. Im Rahmen der NeuroSAFE-Diagnostik ist die FCM- der Kryotechnik derzeit noch unterlegen. Eine Umstellung der Arbeitsabläufe (Untersuchung im OP), sowie eine Reduktion der Probengröße durch gezieltere Probenentnahme bieten bislang von uns noch nicht ausgeschöpfte beispielhafte Optimierungsmöglichkeiten.

Spatial immune phenotypes of distant metastases but not matched primary urothelial carcinomas predicts response to immune checkpoint blockade.

M. Eckstein^{1, 2, 3}, N. Klümper^{2, 4, 5}, L. Landgraf^{1, 3}, P. Strissel^{1, 2, 3, 6}, R. Strick^{2, 3, 6}, D. Sikic^{2, 3, 7}, V. Bahlinger^{1, 2, 3}, J. Breyer^{2, 8}, M. Ritter^{2, 4}, C. Bolenz^{2, 9}, F. Roghmann^{2, 10}, P. Erben^{2, 11}, K. Schwamborn¹², R. Wirtz^{2, 13}, T. Horn¹⁴, B. Wullich^{2, 3, 7}, M. Hölzel⁵, A. Hartmann^{1, 2, 3}, J. Gschwend¹⁴, W. Weichert^{2, 12}, F. Erlmeier^{1, 2, 3, 12}

¹Institut für Pathologie, Universitätsklinikum Erlangen, Erlangen, Germany, ²BRIDGE-Consortium e.V., Mannheim, Germany, ³Comprehensive Cancer Center EMN, Erlangen, Germany, ⁴Klinik für Urologie, Universitätsklinikum Bonn, Bonn, Germany, ⁵Institut für Experimentelle Onkologie, Universitätsklinikum Bonn, Bonn, Germany, ⁶Universitätsfrauenklinik Erlangen, Universitätsklinikum Erlangen, Erlangen, Germany, ⁷Klinik für Urologie und Kinderurologie, Universitätsklinikum Erlangen, Erlangen, Germany, ⁸Department für Urologie, St.-Caritas Krankenhaus Regensburg & Universität Regensburg, Regensburg, Germany, ⁹Klinik für Urologie und Kinderurologie, Universitätsklinikum Ulm, Ulm, Germany, ¹⁰Klinik für Urologie, St. Marien Hospital Herne, Ruhr-Universität Bochum (RUB), Herne, Germany, ¹¹Klinik für Urologie, Universitätsklinikum Mannheim, Mannheim, Germany, ¹²Institut für Pathologie, TU München, München, Germany, ¹³STRATIFYER Molecular Pathology, Köln, Germany, ¹⁴Klinik für Urologie, TU München, München, Germany

Background

PD-L1 status remains the only applied predictive biomarker prior to initiation of immune checkpoint blockade (ICB) in metastatic urothelial carcinoma (mUC), but shows contradictory results. We hypothesize that the use of archived primary tumor material, which often does not accurately reflect metastatic disease status, is a major reason for this unsolved clinical issue.

Methods

We examined PD-L1 expression, spatial infiltration of key immune cell populations (CD3, CD8, CD56, FOXP3, CD68, CD163, CD4, GZMB) and self-antigen presentation (MHC-I) in whole tissue sections from freshly obtained 138 matched pairs of primary tumors (PRIM) and metastases (MET). Expression levels and bioinformatically integrated immune cell phenotypes were correlated with treatment success to chemotherapy and ICB.

Results

PD-L1 status and spatial immunophenotypes differed significantly between matched PRIM and MET. Neither spatially resolved immunophenotypes nor PD-L1 status in PRIM could predict ICB or chemotherapy response or outcomes, whereas in MET our proposed immunophenotypes showed strong predictive and prognostic potential for both systemic treatment modalities (chemotherapy and ICB). Of note, in the presence of our novel "inflamed-cytotoxic" pattern in MET (high presence of GZMB+ cytotoxic CD8+ and CD4+ T cells), 90% of patients showed partial or complete response to ICB, while patients with uninflamed METs or METs with present inflammation but a strongly immunosuppressive microenvironment responded poorly to chemotherapy or ICB.

Conclusion

The tumor immunological microenvironment including PD-L1 expression differs substantially between PRIM and MET of patients with mUC. Spatially resolved immunophenotypes of METs (but not PRIM) can accurately predict ICB therapy response. We conclude that more accurate identification of ICB response will only be possible by analyzing freshly obtained metastatic biopsies in clinical routine.

Epigenetically regulated transcription factor *BNC1* shows oncogenic effects in squamous bladder cancer cells

J. Wirtz¹, A. Kondratkova¹, F. C. Lammert¹, L. Gan², R. Knüchel¹, M. Rose¹, N. T. Gaisa¹

¹University Hospital RWTH Aachen University, Institute of Pathology, Aachen, Germany, ²Medical Faculty of the RWTH Aachen University, IZKF Aachen, Aachen, Germany

Background

The transcription factor (TF) basoonuclin 1 (*BNC1*) is known to orchestrate proliferation and terminal cell differentiation, e.g. of stratified squamous epithelia. In tumorigenesis *BNC1* was shown to be involved in cancer progression, for instance in Epithelial-to-mesenchymal transition (EMT), invasion and metastasis in breast cancer and HNSCC. Recently we revealed *BNC1* overexpression in squamous bladder cancers based on transcriptomic profiles. In this study, we aimed to assess the prognostic impact of *BNC1* expression, to clarify the regulatory mechanisms of *BNC1* gene expression and to investigate the functional role of *BNC1* *in vitro*.

Methods

BNC1 mRNA expression was analyzed by qPCR on n=91 tissue samples comprising normal urothelium (NU), squamous metaplasia (Sq-Met), squamous cell carcinoma (SCC) and urothelial carcinoma (UC). Bisulfite-pyrosequencing was performed to analyze DNA-methylation of the *BNC1* promoter in NU, SCC and UC (overall n=30). All data were *in silico* validated by using the TCGA-BLCA dataset. *In vitro*, stable *BNC1* knockdown (Δ sh-*BNC1*) and control (Δ sh-Mock) single cell clones from the squamous-like SCaBER cell line were generated. Functionally, cell growth, apoptosis, colony formation, and migration assays were performed. Putative target genes of *BNC1* were analyzed by qPCR in Δ sh-*BNC1* clones and controls.

Results

BNC1 overexpression was demonstrated in both, sq-Met and SCC when compared with NU and UC. In parallel, a significant hypomethylation of the *BNC1* promoter region (10.05 ± 4.35 %) was identified in squamous bladder cancers compared to NU tissue. In SCaBER cells with unmethylated *BNC1* promoter, stable knockdown of *BNC1* expression significantly ($p < 0.001$) caused cell and colony growth inhibition by 28.5 ± 3.5 %, while fostering apoptosis. In addition, Δ sh-*BNC1* clones showed reduced migration capacities compared to Δ sh-Mock clones. *CLDN3*, encoding for cell-adhesion protein claudin 3, was identified as putative target gene blocked by *BNC1*, since SCaBER clones lacking *BNC1* expression showed a 2.6-fold ($p < 0.001$) upregulation.

Conclusion

Our findings provide evidence that *BNC1* is epigenetically regulated in bladder cancers, acting as a putative oncogenic driver in squamous differentiated tumor cells and potentially possessing prognostic impact. Ongoing functional studies may help to reveal pathways involved in SCC development and discover novel targets for therapy of squamous bladder carcinoma.

AG03 AG Knochen-, Gelenk- und Weichgewebspathologie I

AG03.02

Chordoma- Overview

T. F. Barth

Institut für Pathologie, Universitätsklinikum Ulm, Ulm, Germany

Chordome sind seltene, primär maligne Knochentumoren des Achsenskeletts und machen ca. 1-4% aller primär malignen Knochentumoren sowie 20% aller primären Wirbelsäulentumoren aus. Der Begriff „Chordom“ reflektiert den morphologischen und immunhistologischen Phänotyp dieser Neoplasie, charakterisiert durch die Expression des Transkriptionsfaktors Brachyury und Vimentin und eine fallweise unterschiedliche Expression von Zytokeratinen und S100 Protein, die sich auch im in der embryonalen Leitstruktur der Chorda dorsalis wiederfindet; folglich wird das Chordom nach WHO als ein Tumor mit notochordaler Differenzierung definiert (ICD-O: 9370/3).

Die jährliche Gesamtinzidenz beträgt ca. 0,84/1.000.000, weshalb Chordome auch zu den sogenannten „orphan diseases“ gezählt werden. Morphologisch zeigen die Chordome ein breites Spektrum von der klassischen Form mit dem typischen physaliforen, also bläschentragenden Zytoplasma bis hin zu hepatoiden, chondroiden, und Nierenzellkarzinom-ähnlichen Varianten. Eine Transformation in ein dedifferenziertes bzw. niedrig differenziertes Chordom wird diskutiert. Die molekulare Charakterisierung von Chordomen sowie die Identifizierung neuer Therapiestrategien erfordern zwingend tragfähige Krankheitsmodelle. Aufgrund der geringen Inzidenz von Chordomen ist die verfügbare Anzahl an stabilen Chordomzelllinien begrenzt. Im Pathologischen Institut der Universität Ulm konnte die weltweit erste und 17 weitere stabile Chordomzelllinien etabliert werden. Durch den Einsatz dieser Linien konnten global erhebliche Fortschritte in der molekularen Charakterisierung von Chordomen erzielt und neue gezielte Therapieansätze in der Behandlung dieser seltenen Neoplasien etabliert werden. Beispiele dafür sind die Definition eines potentiellen Responder Phänotyps von Chordomen auf Grund eines nachgewiesenen rekurrenten Verlustes von *CDKN2A*, der auf eine Therapie mit dem CDK4/6 Inhibitor Palbociclib ansprechen kann und zu einer am NCT in Heidelberg geleiteten Studie in fortgeschrittenen und metastasierten Chordomen geführt hat (NCT PMO-1601). Der Vortrag diskutiert auch diese möglichen neuen Therapieansätze in Chordomen vor dem Hintergrund der aktuell bekannten molekularen Treibermechanismen.

Morphological characteristics of chondrocyte spheroids used for spheroid-based ACI

T. Niedermair¹, N. Reyersbach², V. Ramakrishnan², D. Grevenstein³, **C. Brochhausen¹**

¹Institute of Pathology, University of Regensburg, Regensburg, Germany, ²Institut of Pathology, University of Regensburg, Regensburg, Germany, ³Departement for Orthopaedic Surgery, University Medical Centre of Cologne, Cologne, Germany

Background

Traumatic lesions of articular cartilage often result in osteoarthritis of the knee or hip (OA). One promising technique to treat traumatic cartilage lesions represents the usage of spheroid-based autologous chondrocyte implantation (ACI). A recent study demonstrated excellent histological and immunohistological results from patients after spheroid-based ACI regarding regeneration of hyaline articular cartilage in the defect area[1]. The present study focused on the morphology of the chondrocyte spheroids for a better understanding about their structural characteristics, to find a possible biomarker for good regeneration outcome and a possible automated AI-based image analysis solution.

Methods

Chondrocyte spheroids of 15 patients (unused spheroids after defect treatment) were fixated in formalin. Paraffin-embedded spheroids were used for H&E staining, EPON-embedded spheroids were used for toluidine blue/fuchsin staining followed by histological and ultrastructural analysis (transition electron microscopy/TEM). Histological whole-slide-images (WSI) were prepared using the PreciPoint M8 Scanner (40-fold magnification). Automated image analysis was performed using a neuronal network.

Results

All spheroids revealed a generally round structure. Some Spheroids showed the presence of a superficial zone on the outer surface with flattened cell nuclei and a delimiting layer surrounding the spheroid. Incorporation of lipids were present in some spheroids. Manual and automated count and categorization of cell nuclei both revealed a generally variable cell number within the spheroids with a slightly lower number of clearly defined, homogenously colored nuclei (dense nuclei) compared to nuclei with a clearly defined membrane but partial transparency within the nuclei (ring nuclei). In addition, automated image analysis demonstrated, that the shape of dense nuclei was generally more rounded, whereas ring nuclei were generally more elongated. Ultrastructurally, characteristic changes in chromatin of dense and ring nuclei match the histological findings.

Conclusion

We found histological features of a superficial layer in some spheroids pointing to collagen deposition as under physiological conditions. In addition, a high number of cells demonstrated a rounded chondrocyte-like shape. Further studies need to clarify, how cell number within the spheroids correlates with optimal defect

treatment.

Literaturangaben

[1] Grevenstein D, Mamilos A, Schmitt VH, Niedermair T, Wagner W, Kirkpatrick CJ, Brochhausen C, (2021), Excellent histological results in terms of articular cartilage regeneration after spheroid-based autologous chondrocyte implantation (ACI), *Knee Surg Sports Traumatol Arthrosc*, 29:417–421

CD47 prevents the elimination of diseased fibroblasts in scleroderma

T. Lerbs^{1,2}, L. Cui², T. Chai³, C. Muscat², L. Chung⁴, R. Brown⁴, K. Rieger⁴, T. Shibata², G. Wernig²

¹Universitätsklinikum Bonn, Pathologie, Bonn, Germany, ²Stanford Medical School, Pathology, Stanford, United States of America, ³Stanford Medical School, Institute for Stem Cell Biology and Regenerative Medicine, Stanford, United States of America, ⁴Stanford Medical School, Dermatology, Stanford, United States of America

Background

Scleroderma is a devastating fibrotic autoimmune disease. Current treatments are partly effective in preventing disease progression but do not remove fibrotic tissue. Here, we evaluated whether scleroderma fibroblasts take advantage of the “don’t-eat-me-signal” CD47 and whether blocking CD47 enables the body’s immune system to get rid of diseased fibroblasts.

Methods

We studied patient samples with immunofluorescence stains and ATAC-seq. Then, we used a JUN-inducible skin fibrosis model in which we locally applied doxycycline to induce JUN expression and analyzed skin fibrosis and changes in fibroblast subpopulations through IF stains and flow cytometry. We used qt-PCR to detect changes in hedgehog signaling and applied vismodegib in vivo to determine the contribution of the hedgehog pathway to skin fibrosis. We investigated the effect of JUN on fibroblast proliferation and self-renewal in a niche-independent setting with an adoptive transfer model. To study the effects of blocking CD47, we used the adoptive transfer and in vitro phagocytosis assays. We depleted macrophages through a CD115 antibody in vivo to study whether macrophages drive skin fibrosis. Finally, we treated JUN-inducible mice with an antibody combination against CD47 and IL6 in a prophylactic and a therapeutic setting for skin fibrosis. We used this combination to treat primary scleroderma fibroblasts in the adoptive transfer model.

Results

In patient samples, fibroblasts showed increased JUN expression and increased chromatin accessibility of JUN, IL6, CD47 and CD274. Locally inducing JUN in the skin caused severe skin fibrosis with a loss in adipose tissue, changes comparable to the bleomycin model. During skin fibrosis progression, CD26+ fibroblasts expanded in a hedgehog-dependent manner and blocking hedgehog signaling prevented skin fibrosis. JUN stimulated fibroblast proliferation and transferred increased self-renewal niche-independently. Blocking CD47 eliminated fibroblasts in the niche-independent setting and increased phagocytosis in vitro and depleting macrophages reduced skin fibrosis in vivo. Finally, treating mice with a combination against CD47 and IL6 not only prevented but also removed skin fibrosis and led to the accelerated elimination of primary scleroderma fibroblasts in vivo.

Conclusion

These results provide a rationale for testing a combination against IL6 and CD47 in a clinical setting and show that fibrotic changes in skin fibrosis are a reversible process.

Intercellular effects of EVs from pathologically altered osteoblasts on mesenchymal stem cells

T. Niedermair¹, C. Lukas², S. Li², S. Stöckl², B. Craiovan³, M. Federlin⁴, M. Herrmann⁵, S. Grässel², C. Brochhausen¹

¹*Institute of Pathology, University of Regensburg, Regensburg, Germany*, ²*Department of Orthopaedic Surgery, Experimental Orthopaedics, Centre for Medical Biotechnology (ZMB/Biopark 1), University of Regensburg, Regensburg, Germany*, ³*Center for Orthopaedics and Trauma Surgery, University Hospital Giessen and Marburg GmbH, Marburg, Germany*, ⁴*Department of Conservative Dentistry and Periodontology, University Medical Center Regensburg, Regensburg, Germany*, ⁵*IZKF Group Tissue Regeneration in Musculoskeletal Diseases, University Hospital Wuerzburg and Bernhard-Heine-Centrum for Locomotion Research, University of Würzburg, Würzburg, Germany*

Background

An increasing number of studies demonstrates the impact of exosomes, a specific subgroup of extracellular vesicle (EV), in physiological and pathophysiological processes. By transporting proteins, RNA and DNA, EVs of cells from the musculoskeletal system take part in the control of bone metabolism in health and disease. EVs isolated from mesenchymal stem cells (MSCs) show positive effects on musculoskeletal pathologies as osteoarthritis (OA) and osteoporosis (OP). On the contrary, EVs from pathologically altered bone cells might counteract the effects of therapeutically administered MSC EVs.

Methods

To proof this, we isolated osteoblasts, derived from bone explants of patients with coxarthrosis (CA), OP and a combination of CA and OP and compared vitality and osteogenic cell phenotype *in vitro*. Afterwards, EVs of CA, OP and CA/OP osteoblasts were isolated and their effects on cell metabolism and osteogenic differentiation capacity of bone marrow MSCs (BMSCs) were analyzed.

Results

Cell growth was comparable in osteoblasts from all groups, whereas osteogenic differentiation capacity was slightly different in CA/OP, CA and OP osteoblasts. EVs of CA/OP, CA and OP osteoblasts increased activity of the apoptosis marker caspase 3/7 and decreased activity of the osteogenic marker alkaline phosphatase (ALP) in BMSC cultures. In addition, CA and CA/OP EVs affected BMSC vitality *in vitro*. Further, stimulation with CA EVs decreased deposition of alizarin red stained matrix in BMSC cultures.

Conclusion

The study demonstrates, that musculoskeletal pathologies (CA, OP and CA/OP) are affecting osteogenic bone cell phenotype differently. Furthermore, CA, OP and CA/OP osteoblast-derived EVs result in mostly catabolic changes in BMSC cell metabolism and osteogenic differentiation *in vitro*, independently of the donor pathology. The tissue microenvironment, present when administering MSCs or their EVs as a

therapeutic drug, seem to have an important effect on bone cell metabolism and might affect therapeutic outcome. Further studies should clarify the ultrastructural effects of EVs on target cells to gain a better understanding of the cellular mechanisms in the pathophysiology of bone and under therapeutic conditions.

Murine osteoporotic fracture healing and hyperalgesia are modulated by the peripheral nervous system

T. Niedermair¹, I. Wank², D. Kronenberg³, R. Stange³, A. Hess², S. Grässel⁴, C. Brochhausen¹

¹Institute of Pathology, University of Regensburg, Regensburg, Germany, ²Institute of Experimental and Clinical Pharmacology and Toxicology, Friedrich-Alexander University Erlangen-Nürnberg, Erlangen, Germany, ³Department of Regenerative Musculoskeletal Medicine, Institute of Musculoskeletal Medicine (IMM), University Hospital Münster, Münster, Germany, ⁴Department of Orthopaedic Surgery, Experimental Orthopaedics, Centre for Medical Biotechnology (ZMB/Biopark 1), University of Regensburg, Regensburg, Germany

Background

Various studies already demonstrated the importance of the sensory and sympathetic nervous system on bone metabolism and fracture healing. Loss of sensory neurotransmitters (NT) substance P (SP) and α -calcitonin gene related peptide (α -CGRP) and the sympathetic nervous system impaired fracture healing, biomechanical bone properties and modulated pain-related processes in SP-, α -CGRP-deficient mice and sympathectomized mice under physiological and pathophysiological conditions. Under pathological conditions, such as in osteoporosis, fracture healing is often linked to prolonged or even persisting pain. The present study was conducted to link signals from the sensory and sympathetic nervous system to fracture-induced hyperalgesia and its effects on the cellular healing process.

Methods

Bilateral ovariectomy (OVX) was conducted in wildtype (WT), SP-, α -CGRP-deficient and SYX mice. Externally stabilized femoral fractures were set 28 days after OVX. Two days before, 5 and 21 days after fracture, functional MRI (fMRI) was performed. At day 21, fractured and non-fractured femora were used for μ CT scans and biomechanical tests.

Results

Trabecular thickness (Tb.Th.), bone volume (BV) and BV/total volume (BV/TV) were increased in the callus area of SYX mice 21 days post fracture compared to SP- and α -CGRP-deficient mice. Distal trabecular bone of the non-fractured leg was similar to the other groups. Trabecular number (Tb.N.) and BV/TV were increased and trabecular separation (Tb.Sp.) decreased in non-fractured femora and TV was reduced in fractured femora of SP- and α -CGRP-deficient compared to WT mice. Functional connectivity (FC) of nociceptive and resting-state fMRI differed significantly between WT and NT-deficient mice. Central nociception was modulated by fracture-induced hyperalgesia. Highest differences were measured in α -CGRP-deficient mice. Fracture-induced hyperalgesia and the healing progress are best reflected by FC between sensory and association cortex plus brainstem.

Conclusion

The impact of OVX on bone properties and fracture healing seems to be more intense in the absence of the sympathetic nervous system, as bone microarchitecture was more affected in SYX compared to SP- and α -

CGRP-deficient mice. Longitudinal survey of stimulus-driven and RS FC differed in NT-deficient and WT mice. A prolonged effect on RS FC during fracture healing in α -CGRP-/- mice points to a critical participation of α -CGRP for the resolution of hyperalgesia.

Regulation of *HOXB7*-expression and the impact on the Ras-Raf-MAPK-pathway regarding the viability of chordoma cell lines

L. Haase, P. Möller, T. Barth, K. Mellert

Pathologie Universität Ulm, AG Chordoma, Ulm, Germany

Background

Chordomas are rare tumours of the spine thought to arise from remnants of the Chorda dorsalis. They show a strong expression of the *TBXT* gene coding for the protein Brachyury, a transcription factor of the T-box family.

Previous research revealed an increased expression of genes of the *HOX*-family in sacral tumours in comparison to clival ones, particularly *HOXA7*, *A9*, and *A10*.

In particular, the *HOX* genes of the paralogue group 7 (*HOXA7* and *HOXB7*) are of interest due to indications that *HOXB7* plays a significant role in regulation of *TBXT*.

Based on research by Martin G.R. (1998 Genes Dev), Heinonen H. (2015, Int J cancer) and Wu X. (2006, Cancer Res) we established a hypothetical pathway of *TBXT* regulation in chordoma *via* the *HOXB7*-protein by the Ras-Raf-MAPK-way.

Therefore, we tested the influence of *HOXB7* on the MAPK-kinase way and consequently on *TBXT* in chordoma cell lines.

Methods

We studied the impact of *HOXB7* on five chordoma cell lines. Cellular *HOXB7* levels were either upregulated by transfecting the cells with an *HOXB7* expression vector or downregulated using *HOXB7* specific siRNA. After an incubation time of 24-48 hours proteins were isolated. Western blot analyses were used to determine the amounts of *HOXB7* on the MAPK signalling pathway and Brachyury expression. MTS-assays were used to measure the impact of different amounts of *HOXB7* in chordoma cells on cell viability and proliferation.

Results

HOXB7 overexpression as well as *HOXB7* knockdown was convincingly detected by Western blot analysis. Interestingly, we detected no significant difference in the phosphorylation of the proteins of the MAPK-kinase way, neither in *HOXB7* upregulated nor in *HOXB7* downregulated cells. Consequently, no significant differences were detected in the amount of Brachyury expression in correlation to different amounts of *HOXB7* protein. Further, there was no significant difference regarding the cell viability of chordoma cells after *HOXB7* up- or down regulation.

Conclusion

Our study showed no indication that *HOXB7* regulates the MAPK-way and further *TBXT*. A complete siRNA mediated silencing of *HOXB7* was not achieved. This indicates that minor amounts of HOXB7 protein may suffice in activating the MAPK signalling pathway. This indicates that minor amounts of HOXB7 protein may suffice in activating the MAPK signalling pathway. Furthermore, HOXB7 and HOXA7 are described to share redundant features. Therefore, it is possible that downstream effects are not detectable unless both genes have been silenced.

Ultrastructural Analysis of Mitochondria from Osteoblasts and Osteocytes from Patients with Osteomyelitis

D. Mendelsohn^{1,2}, N. Walter³, T. Niedermair^{1,2}, V. Alt³, M. Rupp³, C. Brochhausen^{1,2}

¹*Institute of Pathology, University Regensburg, Regensburg, Germany*, ²*Central Biobank Regensburg, University and University Hospital Regensburg, Regensburg, Germany*, ³*Department of Trauma Surgery, University Medical Centre Regensburg, Regensburg, Germany*

Background

Osteomyelitis is a challenging disease with high chronification rates, especially with view to the increasing emergence of multiresistant pathogens. The surgical amputation of the afflicted limb often remains as the patients' last resort. Recent studies demonstrated an increase in mitochondrial fission as a possible contributor to the accumulation of intracellular reactive oxygen species and thus, to the induction of cell death of infectious bone cells. The aim of our study is to quantitatively and qualitatively analyze the ultrastructural impact of bacterial infection and its accompanying microenvironmental tissue hypoxia on osteocytic and osteoblastic mitochondria.

Methods

Human bone tissue samples from patients with osteomyelitis were visualized via light microscopy and transmission electron microscopy. Mitochondria in osteoblasts and osteocytes were analyzed and measured ultrastructurally. The results were compared to the control group of non-infectious human bone tissue samples.

Results

Both osteoblastic and osteocytic mitochondria were analyzed and the results depicted swollen hydropic mitochondria including depleted cristae and a decrease in matrix density in the infectious samples as a common finding in both cell types (Figure 1). Furthermore, perinuclear clustering of mitochondria could also be observed regularly. Additionally, increases in relative mitochondrial area and number could be found as a sign for increased mitochondrial fission concordant with previous gene expression studies.

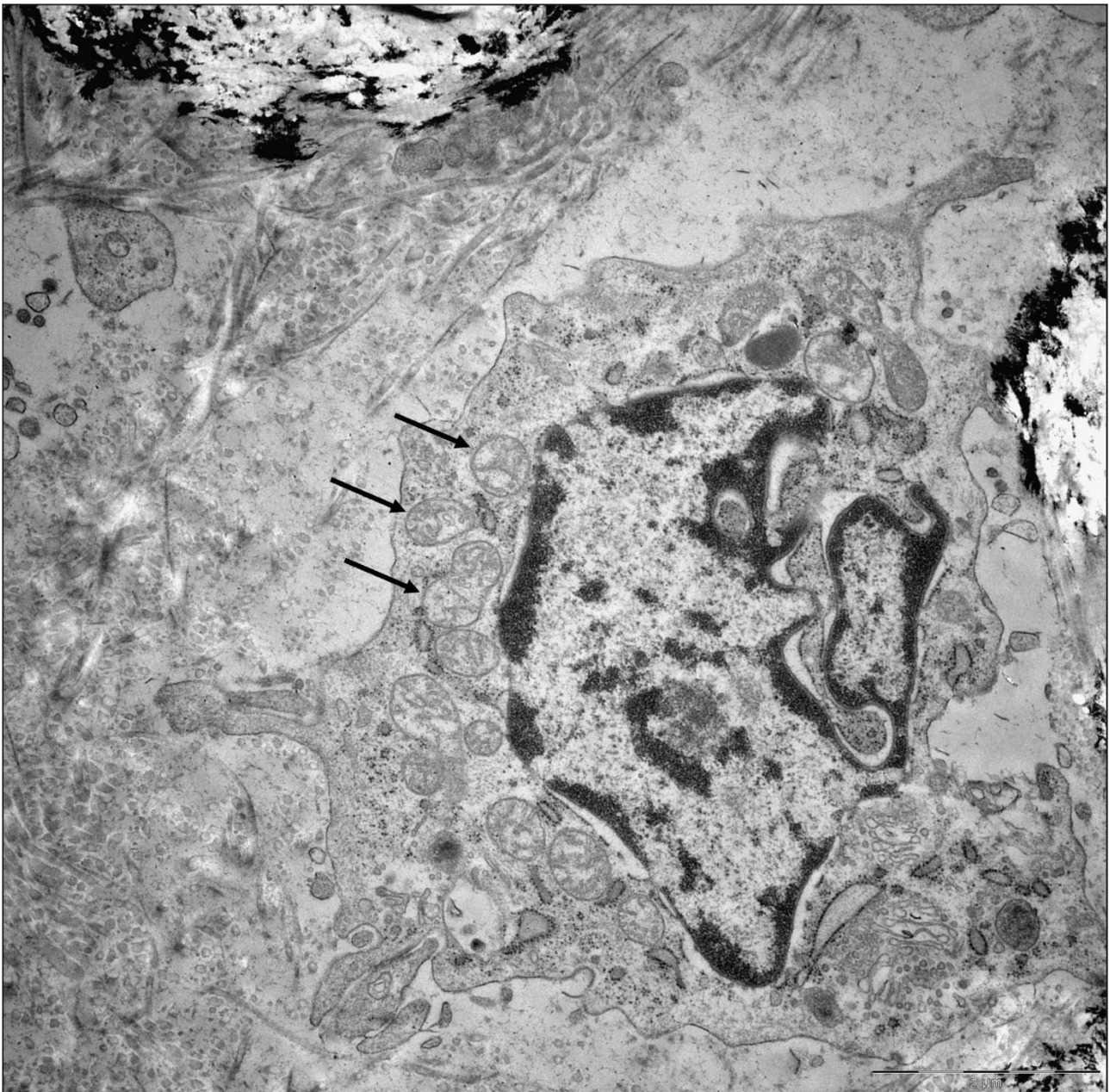


Figure 1: Transmission electron microscopic image of osteocyte from patient with osteomyelitis. Swollen hydropic mitochondria (examples indicated by black arrows) including depleted cristae and decreased matrix density (magnification x 5000)

Conclusion

In conclusion, the results show that mitochondrial morphology is altered during osteomyelitis in a comparable way to mitochondria from hypoxic tissues. This suggests that manipulation of mitochondrial dynamics in a way of inhibiting mitochondrial fission may improve bone cell survival and enhance bone cells regenerative potential to aid in the treatment of osteomyelitis.

AG03 AG Knochen-, Gelenk- und Weichgewebspathologie II

AG03.08

Histomorphometric analysis of 35 giant cell tumors of bone after recurrence as compared to changes following denosumab treatment

S. Arndt¹, W. Hartmann², A. Rókusz³, B. Leinauer¹, A. von Baer⁴, M. Schultheiss⁴, D. Baumhoer⁵, K. Mellert¹, P. Möller¹, M. Sendrói⁶, G. Jundt⁵, T. F. Barth¹

¹Institut für Pathologie, Universität Ulm, Ulm, Germany, ²Sektion für Translationale Pathologie, Gerhard-Domagk-Institut für Pathologie, Universitätsklinikum Münster, Münster, Germany, ³Orthopädie und Institut für Pathologie, Semmelweis Universität, Budapest, Hungary, ⁴Universitätsklinikum Ulm, Klinik für Unfall-, Hand-, Plastische und Wiederherstellungschirurgie, Ulm, Germany, ⁵Knochentumor-Referenzzentrum (KTRZ) am Institut für Pathologie, Universitätsspital Basel und Universität Basel, Basel, Switzerland, ⁶Orthopädie und Institut für Pathologie der Semmelweis Universität, Budapest, Hungary

Background

Giant cell tumor of bone (GCTB) is an osteolytic tumor driven by a *H3F3A*-mutated mononuclear stromal cell that leads to accumulation of osteoclastic giant cells through release of abundant formed RANKL. GCTB frequently recurs after curettage. Treatment of GCTB with the anti-RANKL antibody denosumab heavily impacts on its histology. Reports about malignant transformation following denosumab therapy raise the question whether there is a link between denosumab and malignant transformation.

Methods

We collected tissue from 35 patients with GCTB. 11 patients underwent surgery without antiresorptive therapy and showed local recurrence at least once. 24 of the patients received denosumab, including two cases with malignant transformation after denosumab therapy.

The H.E.-stained slides were analyzed regarding morphological changes. For computer-based quantification of *H3F3A*-mutated tumor cells we used the mutation-specific monoclonal antibody RM263, included KI-67 and SATB2 staining and assessed bone formation.

Results

We compared cell populations of the primary tumor with those of the first recurrence. We detected a drop in the total number of cells ($p=0.028$), that was not statistically significant for the various cell populations. The KI-67 index varied from 5% to 15% in all primary tumors as well as in the recurrences.

The patients treated with denosumab showed an induction of fibrosis and osteoid formation that increased during therapy. The total number of cells was reduced ($p<0.0001$) with almost complete loss of the giant cells. The number of *H3F3A*-mutated tumor cells decreased ($p=0.0002$), while the *H3F3A*-wild-type population remained stable. KI-67 rate dropped from 10% to 1% under denosumab treatment and SATB2-positive cells were reduced.

The two cases with malignant transformation after denosumab treatment revealed a loss of the *H3F3A*-mutated cells while the KI-67 rate raised from 5% to 80%.

Surveying all 35 cases, we noticed a morphological spectrum of GCTB ranging from giant cell rich to giant cell poor tumors. Areas with higher density of giant cells were associated with foci of a higher KI-67 index of the surrounding mononuclear cells.

Conclusion

Denosumab has a strong impact on the content of giant cells and the *H3F3A*-mutated stromal cells when compared to primaries or untreated recurrences and may foster malignant transformation not clonally related to the initial GCTB. The associated mechanisms as well as a potential histological risk stratification remain to be elucidated.

Superficial fibromas with CTNNB1-mutation: subtype of fibromatosis or new entity?

A. Kuntze¹, R. R. Meliss², L. Ermert³, K. Falkenberg¹, A.-C. Puller¹, W. Hartmann¹, E. Wardelmann¹

¹*Gerhard-Domagk-Institute of Pathology, Münster, Germany*, ²*Institute of Pathology and Dermatopathology, Hannover, Germany*, ³*Institute of Pathology, Oldenburg, Germany*

Background

Fibromatoses describe a heterogeneous group of (myo-)fibroblastic tumors. Superficial fibromatoses are common benign tumors arising in aponeuroses of hand, feet or in the penis and show no characteristic genetic alterations. In contrast, desmoid-type fibromatosis is a deeply located infiltrating and locally aggressive neoplasm, predominantly harboring sporadic activating CTNNB1 mutations, resulting in nuclear accumulation of beta-catenin. Less commonly, desmoid-type fibromatosis arises in patients affected with Gardner syndrome, bearing inactivating germline APC mutations, which similarly result in nuclear beta-catenin accumulation. In addition to fibromatosis, this syndrome comes along with Gardner fibromas, less cellular benign fibroblastic tumors located in deep or superficial soft tissues. To our knowledge, a corresponding superficial Gardner-like-fibroma with sporadic CTNNB1 mutation has not been described so far. Recently Aghighi et al. (2021) firstly depicted a superficial tumor with a sporadic CTNNB1 mutation situated in the calf. Here, we present two additional fibromas of the lower extremity harboring somatic CTNNB1 mutations.

Methods

We performed histology, immunohistochemistry for beta-catenin and targeted NGS based molecular DNA analysis (MiSeq system: Illumina; 12.5 pM library pools, 2% PhiX V3 control and MiSeq Reagent v2 chemistry).

Results

The here presented tumors originate from a 61-year-old woman and a 60-year-old man. Compared to desmoid fibromatosis, both are noticeably less cellular and harbor plenty wavy thick and ropy collagen bundles (Figure 1 and 2).

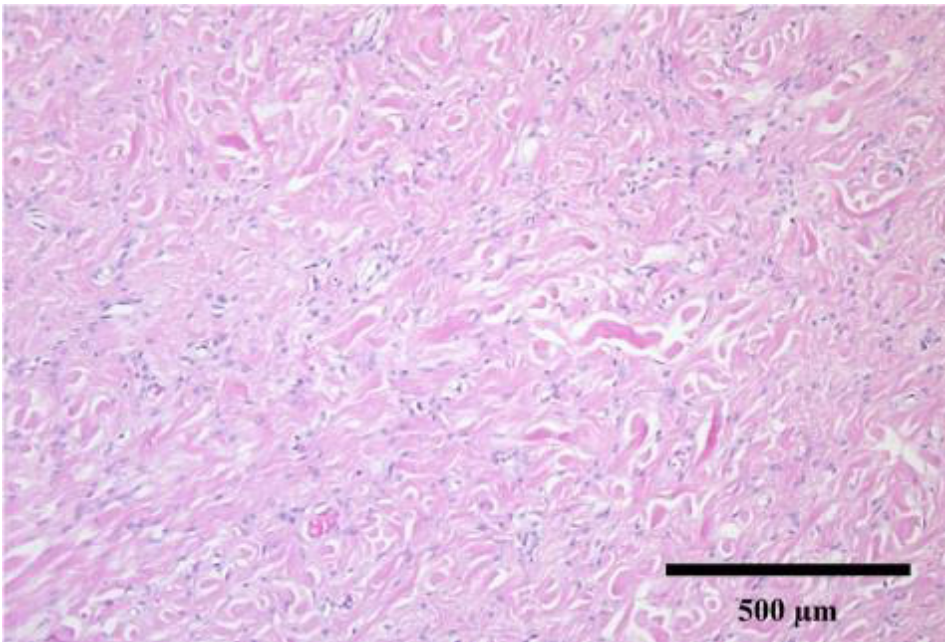


Fig. 1: 1.8 cm dermal tumor consisting of patternless spindle cells with monomorphic ovoid nuclei and interdispersed eosinophilic bundles of plump ropy collagen fibers.

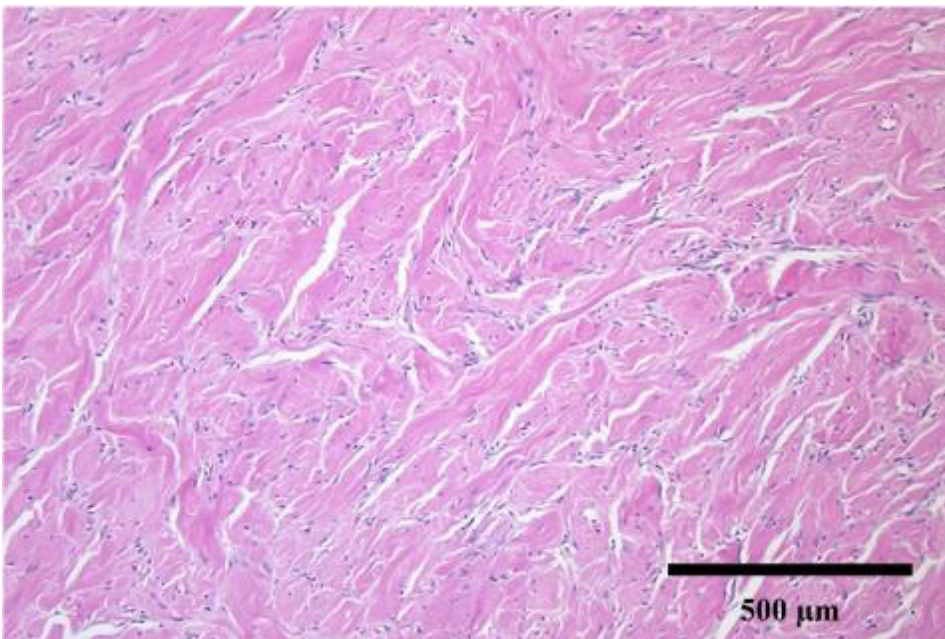


Fig. 2: 2.2 cm subcutaneous tumor composed of loosely arranged bland spindle cells among haphazardly arranged coarse eosinophilic, refractile and wavy collagen bundles.

Conclusion

Based on our findings, we propose to group CTNNB1 mutated superficial fibromas as separate entity with striking morphological differences compared to (desmoid-type) fibromatosis. Instead, they show morphological similarity to Gardner fibromas with which they also share the superficial localization and are driven by comparable molecular alterations. We propose to designate these lesions as corresponding sporadic tumor entity to the germline APC mutation related fibromas.

Identification of Wee1 kinase activity as functional liability in myxoid liposarcoma

L. Heinst¹, R. Berthold¹, I. Isfort¹, S. Wosnig¹, T. Kindler^{2,3}, P. Åman⁴, E. Wardelmann⁵, C. Scholl⁶, S. Fröhling^{7,8}, W. Hartmann¹, M. Trautmann¹

¹*Division of Translational Pathology, Gerhard-Domagk-Institute of Pathology, Münster University Hospital, Münster, Germany*, ²*University Cancer Center, University Medical Center of Mainz, Mainz, Germany*, ³*German Cancer Consortium (DKTK), Mainz, Germany*, ⁴*Sahlgrenska Cancer Center, Department of Pathology and Genetics, Institute of Biomedicine, Sahlgrenska Academy at University of Gothenburg, Gothenburg, Sweden*, ⁵*Gerhard-Domagk-Institute of Pathology, Münster University Hospital, Münster, Germany*, ⁶*Division of Applied Functional Genomics, German Cancer Research Center (DKFZ) and National Center for Tumor Diseases (NCT), Heidelberg, Germany*, ⁷*Division of Translational Medical Oncology, National Center for Tumor Diseases (NCT) and German Cancer Research Center (DKFZ), Heidelberg, Germany*, ⁸*German Cancer Consortium (DKTK), Heidelberg, Germany*

Background

Myxoid liposarcomas (MLS), aggressive soft tissue tumors of adipocyte origin, are genetically characterized by a reciprocal t(12;16) translocation encoding the chimeric *FUS-DDIT3* gene fusion. The resulting FUS-DDIT3 fusion oncoprotein has been shown to play an essential role in MLS tumorigenesis by acting as a transcriptional (dys-)regulator; however, its elusive mode of action and insufficient pharmacologic addressability remain challenging for the therapeutic intervention of MLS. Aiming at the identification of novel FUS-DDIT3-dependent effectors to counteract fusion protein-driven oncogenic transformation, we investigated the functional requirement for the cell cycle checkpoint kinase Wee1 in MLS pathogenesis.

Methods

In vitro analyses assessing Wee1 expression and cellular requirement were performed in multiple MLS cell lines, cell lines derived from other liposarcoma subtypes and a mesenchymal stem cell system. Wee1 kinase activity was modulated by the small-molecule inhibitor Adavosertib (MK-1775) and a RNA interference (RNAi)-based approach with cellular effects analyzed in immunoblots, cell proliferation assays and caspase 3/7 activity-based apoptosis assays.

Results

Genomic RNAi screening in a mesenchymal stem cell system revealed functional dependence of FUS-DDIT3-expressing cells on Wee1 kinase activity. Additionally, FUS-DDIT3-dependent upregulation of Wee1 protein levels and significant reduction of MLS cell viability upon treatment with Adavosertib (MK-1775) was shown. Functional loss of Wee1 kinase activity by small-molecule inhibition and RNAi-mediated depletion induced DNA damage accompanied by unscheduled mitotic entry and apoptosis in MLS cells.

Conclusion

Our results uncovered Wee1 kinase activity as functional vulnerability of FUS-DDIT3-expressing MLS cells and provide first evidence that interference with Wee1 signaling represents a novel strategy for therapeutic intervention in MLS.

IGF-IR-dependent cooperation of FUS-DDIT3 and YAP1 in myxoid liposarcoma

R. Berthold^{1,2}, I. Isfort^{1,2}, C. Erkut³, L. Heinst^{1,2}, I. Grünewald^{1,2}, E. Wardelmann², T. Kindler^{4,5}, P. Åman⁶, T. G. P. Grünewald^{7,8,9,10}, F. Cidre-Aranaz^{7,8}, M. Trautmann^{1,2}, S. Fröhling^{10,11}, C. Scholl³, W. Hartmann^{1,2}

¹*Division of Translational Pathology, Gerhard-Domagk-Institute of Pathology, Münster University Hospital, Münster, Germany*, ²*Gerhard-Domagk-Institute of Pathology, Münster University Hospital, Münster, Germany*, ³*Division of Applied Functional Genomics, German Cancer Research Center (DKFZ) and National Center for Tumor Diseases (NCT), Heidelberg, Germany*, ⁴*University Cancer Center, University Medical Center of Mainz, Mainz, Germany*, ⁵*German Cancer Consortium (DKTK), Mainz, Germany*, ⁶*Sahlgrenska Cancer Center, Department of Pathology and Genetics, Institute of Biomedicine, Sahlgrenska Academy at University of Gothenburg, Gothenburg, Sweden*, ⁷*Division of Translational Pediatric Sarcoma Research, German Cancer Research Center (DKFZ), Heidelberg, Germany*, ⁸*Hopp Children's Cancer Center (KiTZ), Heidelberg, Germany*, ⁹*Institute of Pathology, Heidelberg University Hospital, Heidelberg, Germany*, ¹⁰*German Cancer Consortium (DKTK), Heidelberg, Germany*, ¹¹*Division of Translational Medical Oncology, National Center for Tumor Diseases (NCT) and German Cancer Research Center (DKFZ), Heidelberg, Germany*

Background

Myxoid liposarcoma (MLS) is a fusion gene-driven malignancy with the vast majority of MLS expressing the FUS-DDIT3 fusion oncoprotein. Acting as a transcriptional dysregulator, FUS-DDIT3 has been shown to be essential in MLS pathogenesis, among others via deregulation of IGF-IR/PI3K/AKT signaling and aberrant activation of the Hippo pathway effector YAP1. This study was performed to analyze the oncogenic interplay between FUS-DDIT3, IGF-IR signaling and YAP1, aiming at a deeper understanding of MLS tumorigenesis.

Methods

The expression of IGF-IR, IGF-II and YAP1 was analyzed in a large cohort of MLS specimens by immunohistochemistry. *In vitro* analyses were performed employing human MLS cell lines and a human mesenchymal stem cell system stably expressing FUS-DDIT3. Functional crosstalk between the IGF-IR system, Hippo/YAP1 and FUS-DDIT3 was investigated using RNAi approaches, IGF-II stimulation experiments and small-molecule kinase inhibitors. Co-immunoprecipitation and proximity ligation assays were performed to study nuclear co-localization of FUS-DDIT3 and YAP1. To examine cooperative functions of FUS-DDIT3 and YAP1, RNA-seq analysis, RT-qPCR and adipogenic differentiation assays were conducted.

Results

Immunohistochemical analysis of human MLS tissue specimens showed concurrent expression of IGF-II, IGF-IR and YAP1 in a significant subset of MLS. *In vitro*, FUS-DDIT3-driven IGF-IR signaling, via deregulation of the Hippo pathway, promoted stability and nuclear accumulation of YAP1. Nuclear co-localization of FUS-DDIT3 and YAP1 was detected in FUS-DDIT3-expressing mesenchymal stem cells and MLS cell lines in co-immunoprecipitation and proximity ligation assays. RNA-seq analysis of MLS cells demonstrated FUS-DDIT3 and YAP1 co-regulation of oncogenic gene signatures related to proliferation, cell cycle progression, apoptosis, and adipogenesis. In differentiation assays and RT-qPCR analyses, YAP1 was shown to be functionally involved in FUS-DDIT3-driven disruption of normal adipocytic differentiation.

Conclusion

Our study provides evidence of a FUS-DDIT3-driven network involving IGF-IR signals acting on Hippo/YAP1, and highlights cooperative functions of YAP1 and FUS-DDIT3 in MLS pathogenesis.

Integrated Proteogenomics of Non-Uterine Leiomyosarcomas for Outcome Risk Prediction

M. Ogawa, A. Tanaka, K. Namba, **M. Roehrl**

Memorial Sloan Kettering Cancer Center, Pathology and Laboratory Medicine, New York, United States of America

Background

Non-uterine high-grade leiomyosarcomas (LMS) are rare but frequently lethal neoplasms. LMS often exhibit aggressive behavior, recur locally, and some metastasize to other organs. Thus, better understanding tumor biology is needed to predict individual risk, to tailor treatment, and to improve clinical outcomes. In this study, we used integrated deep proteogenomics at DNA, mRNA, and proteome levels to explore differentially expressed genes and proteins that play a role in driving aggressiveness and metastatic propensity of LMS.

Methods

We selected 40 LMS cases, including 20 low-risk cases (disease-free survival (DFS) of more than 5 years) and 20 high-risk cases (DFS less than 3 years) that were all histologically high-grade and not distinguishable. DNA and mRNA were analyzed using next generation sequencing. Deep unbiased proteomes and phosphoproteomes were analyzed using LC-mass spectrometry. Differential expression analyses and gene pathway enrichment analyses were performed.

Results

Using integrated proteogenomics (quantifying >8,000 proteins and >18,000 transcripts) and comparing high-risk cases to low-risk cases, we discovered 90 differentially expressed genes, 64 up-regulated and 26 down-regulated. In upstream regulator analyses, inflammation-associated genes are associated with high-risk LMS, such as TNF, IL1, IL6, and IFN gamma. In canonical pathway analyses, inflammatory pathways such as tumor microenvironment pathway, IL17 signaling, TREM1 signaling, and HIF1 alpha signaling are also found up-regulated in high-risk LMS tumors.

Conclusion

Our study identified differentially expressed genes and proteins and affected signaling pathways that may drive aggressiveness and metastatic propensity of non-uterine high-grade LMS. We are currently constructing a multiomic outcome risk prediction model for LMS that can help guide adjuvant therapy decisions for LMS patients after surgery.

Interdependency between YAP1 and β -catenin activation in synovial sarcoma

I. Isfort¹, R. Berthold¹, L. Heinst¹, E. Wardelmann², M. Trautmann¹, W. Hartmann¹

¹*Division of Translational Pathology, Gerhard-Domagk-Institute of Pathology, Münster University Hospital, Münster, Germany*, ²*Gerhard-Domagk-Institute of Pathology, Münster University Hospital, Münster, Germany*

Background

Synovial sarcoma (SySa), a rare neoplasm belonging to the group of malignant soft-tissue tumors, is characterized by a specific chromosomal translocation t(X;18). The resulting chimeric SS18-SSX fusion protein represents the major oncogenic driver in SySa tumorigenesis; however, detailed information on its exact pathomechanism and dysregulated signaling pathways remain to be elucidated. Since previous functional analyses uncovered a mechanistic link between SS18-SSX and the activity of the transcriptional co-regulators YAP1/TAZ and β -catenin, this study examined a potential crosstalk between these effectors in SySa.

Methods

Nuclear expression of YAP1/TAZ and β -catenin was analyzed in a large cohort of SySa tumor specimens by immunohistochemistry. *In vitro* experiments were performed with tumor-derived SySa cell lines to study changes in YAP1/TAZ/ β -catenin transcriptional activity upon small molecule inhibitor treatment, RNAi-mediated knockdown or vector-based overexpression. YAP1/TAZ and β -catenin transcriptional activity was determined via TEAD and TCF luciferase reporter assays. Finally, co-immunoprecipitation experiments were performed to investigate the interplay of these co-regulators with the SS18-SSX fusion protein in SySa cell lines.

Results

Immunohistochemically, nuclear YAP1/TAZ/ β -catenin accumulation was found in a vast number of SySa tumor tissues. *In vitro* experiments demonstrated that SS18-SSX stimulates YAP1/TAZ and β -catenin transcriptional activity. Knockdown of YAP1, TAZ or β -catenin and small molecule inhibitor treatment resulted in reciprocal downregulation of TEAD and TCF luciferase reporter activity, while expression of hyperactive variants mutually induced luciferase activity. Co-immunoprecipitation assays showed nuclear co-localization of β -catenin and YAP1 with the SS18-SSX fusion protein in SySa cells.

Conclusion

This study demonstrates that YAP1 and β -catenin co-regulate each other's transcriptional activity, and interact with the SS18-SSX fusion protein in SySa.

VISTA in Soft Tissue Sarcomas: A Perspective for Immunotherapy?

M. Albertsmeier¹, A. Altendorf-Hofmann², L. Lindner³, R. Issels⁴, H.-R. Dürr⁵, M. Angele⁶, F. Klauschen⁷, J. Werner⁶, A. Jungbluth⁸, **T. Knösel**⁹

¹Ludwig-Maximilians Universität, Department für Allgemeine, Viszerale und Transplantationschirurgie, München, Germany, ²Friedrich-Schiller Universität, Department für Allgemeine, Viszerale und Transplantationschirurgie, Jena, Germany, ³Ludwig-Maximilians Universität, Department für Innere Medizin III, München, Germany, ⁴Ludwig-Maximilians-Universität (LMU) München, Department für Innere Medizin III, München, Germany, ⁵Ludwig-Maximilians-Universität (LMU) München, Muskuloskeletale Onkologie, Department für orthopädische Chirurgie, München, Germany, ⁶Ludwig-Maximilians-Universität (LMU) München, Department für Allgemeine, Viszerale und Transplantationschirurgie, München, Germany, ⁷Ludwig-Maximilians-Universität (LMU) München, Institut für Pathologie, München, Germany, ⁸Memorial Sloan Kettering Cancer Center (MSKCC), Department für Pathologie, New York, United States of America, ⁹Ludwig-Maximilians Universität, Institut für Pathologie, München, Germany

Background

VISTA (V domain immunoglobulin suppressor of T cell activation) plays a critical role in antitumor immunity and may be a valuable target in cancer immunotherapy. To date, it has never been studied in a large and well-characterised cohort of soft tissue sarcomas (STS).

Methods

Using immunohistochemistry, we examined VISTA expression in tumour tissues of 213 high-risk STS. We then analysed whether VISTA was associated with other clinicopathological parameters, including tumour-infiltrating lymphocyte (TIL) counts, programmed death receptor-1 (PD1), programmed death ligand-1 (PDL1), CD3, grading and long-term survival.

Results

We observed VISTA expression in 96 (45%) of 213 specimens with distinct patterns ranging from 26% to 63% for histological subtypes. VISTA was associated higher grade (G3 vs G2, $p=0.019$), higher TIL counts ($p=0.033$), expression of PD1 ($p=0.046$), PDL1 ($p=0.031$) and CD3+ ($p=0.023$). In patients without CD3+ TILs, 10-year survival was higher when VISTA was expressed compared to no VISTA expression ($p=0.013$). In multivariate analysis, VISTA expression was independently associated with prolonged survival ($p=0.043$).

Conclusion

VISTA is expressed in different STS subtypes and is associated with increased TILs, PD-1, PD-L1 and CD3 expression. Patients with VISTA+ tumours show improved survival. These results may help define future immunotherapeutic approaches in STS.

Accepted in Cancers 2022 (impact 6,6)

NTRK-rearranged uterine sarcomas: A rare tumor entity with the option of targeted therapy in advanced stages.

G. Mechtersheimer¹, M. Kirchner¹, F. Kommoss¹, C. Flechtenmacher¹, D. Reuss², C. Kölsche¹, A. Stenzinger¹, P. Sinn¹

¹*Pathologische Institut, Allg. Pathologie und Pathologische Anatomie, Heidelberg, Germany*, ²*Pathologische Institut, Abt. f. Neuropathologie, Heidelberg, Germany*

Background

The spectrum of gynecological sarcomas (GySa) is very different from soft tissue sarcomas in general, and the classification and management of GySa continues to diversify. The steadily growing recognition of entity-associated mutations has led to a refined classification of GySa, and NTRK-rearranged spindle cell neoplasm of the female genital tract is a new and emerging entity in this context.

Methods

Three uterine, morphologically undifferentiated spindle cell sarcomas were obtained from the consultation files of the authors. A comprehensive morphological and immunophenotypic characterization of the tumors and targeted RNA-based next-generation sequencing (NGS) for the identification of gene fusions (Archer FusionPlex Sarcoma) was performed. Additional molecular analyses (DNA-based NGS and genome wide DNA methylation analysis) are in progress.

Results

Two tumors were located in the uterine cervix (#1 and #2), the third one in the corpus (#3) of premenopausal, 40-year-old (#1), 28-year-old (#2), and 47-year-old (#3) women. All tumors were characterized by relatively monomorphic spindle cells with intermediate-sized nuclei with focal and moderate nuclear pleomorphism, and abundant eosinophilic cytoplasm, arranged in long intersecting fascicles. Two tumors (#1 and #2) were consistently cellular, while one tumor (#3) showed focally a well vascularized myxoid matrix. Overall, tumor morphology was fibrosarcoma-like. Mitotic activity was brisk, ranging from 12 to 17 mitotic figures per 10 hpf (median: 15 mitotic figures per 10 hpf). Tumor necrosis was present in two tumors (#1 and #3). Immunohistochemically, CD34 and CD10 were positive in at least two tumors and S100 was focally positive in one. All tumors were negative for pan-cytokeratin, estrogen receptor, progesterone receptor, desmin, smooth muscle actin, SOX10, and melan A. Gene fusions involving NTRK were found in all three tumors: EML4::NTRK3(E2N14) in #1, RBPMS::NTRK3 (R5N14) in #2, and LMNA::NTRK1 (L2N11) in #3.

Conclusion

Identification of NTRK rearranged uterine spindle cell sarcomas is important given the potential for targeted treatment. According to the current WHO classification system, these tumors are considered to be of low-

grade malignancy. However, analysis of additional cases with longer clinical follow up is needed to gain more insight into their biological behavior and prognosis.

AG04 AG Hämatopathologie I

AG04.01

Histiocytic and Dendritic Cell Neoplasms (HDCNs)

S. Pileri^{1, 2}

¹European Institute of Oncology, Division of Hematopathology/Hematology Program, Milan, Italy, ²University of Bologna, DIMES, BOLOGNA, Italy

The list of HDCNs has been recently expanded by the inclusion of some conditions (ECD and RDDD), originally thought to represent reactive/inflammatory conditions. Nowadays, HDCNs can be subdivided into two main categories of putative haematopoietic and mesenchymal derivation, respectively (Table 1). They have been traditionally discussed with peripheral B- and T-cell lymphomas, since they essentially consist of terminally differentiated cells. In cases of LCH and ECD, the bone marrow may represent the tumor cell reservoir, given detection of *BRAF-V600E* mutation in hematopoietic stem cells. In HDCNs from a haematopoietic precursor, molecular studies have evidenced mutually exclusive recurrent mutations in the MAPK pathway (mainly affecting *RAS*, *BRAF*, and *MEK*) and less frequently in the PI3K one, representing the rationale for targeted therapies through the usage of MAPK and mTOR inhibitors. None of these mutations is specific for HDCNs, since they can occur in many tumours of different histogenesis. In keeping with their haematopoietic origin, many of the HDCNs can occur in association with myeloid or lymphoid neoplasms, with evidence of a shared clonal origin. ALK+ histiocytosis is characterized by the fusion of *ALK* with different partners (more often *KIF3B*), leading to activation of signaling pathways and sensitivity to ALK-inhibitors. HDCNs of mesenchymal derivation include FDCS, FRCS, and EBV+ FDC/FRC tumour (EBV+FDC/FRCT). FDCS shows mutations more often affecting *CDKN2A*, *NFKB1A*, *TP53*, and *BIRC3*. In a proportion of cases, *BRAF* mutations can also be detected. Gene expression profiling studies and immunohistochemical analyses have revealed constitutive overexpression of PDL1 in LCH and FDCS, which might represent the target for immune checkpoint inhibitors. The systematic collection of these neoplasms is warranted since their treatment is still an unmet clinical need.

Table 1: List of HDCNs

From a haematopoietic precursor: Histiocytic Sarcoma (HS), ALK-positive Histiocytosis, Langerhans Cell Histiocytosis (LCH), Langerhans Cell Sarcoma (LCS), Indeterminate Dendritic Cell Sarcoma (IndCS), Interdigitating Dendritic Cell Sarcoma (IDCS), Disseminated Juvenile Xanthogranuloma (DJXG), Erdheim-Chester Disease (ECD), Rosai-Dorfman-Destombes Disease (RDDD)

From a mesenchymal precursor: Follicular Dendritic Cell Sarcoma (FDCS), Fibroblastic Reticulum Cell Sarcoma (FRCS), EBV-positive Follicular Dendritic Cell/Fibroblastic Reticulum Cell Tumor (EBV+ FDC/FRCT)

Landscape of 4D cell interaction in malignant lymphomas

S. Hartmann¹, S. Scharf², Y. Steiner², A. Loth², E. Donnadieu³, N. Flinner², V. Pöschel⁴, M. Bewarder⁴, J. Bein², U. Brunnberg², A. Bozzato⁴, B. Schick⁴, S. Stilgenbauer⁴, R. M. Bohle⁴, L. Thurner⁴, M.-L. Hansmann²

¹Goethe Universität Frankfurt am Main, Pathologie, Frankfurt, Germany, ²Goethe Universität Frankfurt am Main, Frankfurt, Germany, ³Institut Curie, Paris, France, ⁴Saarland University Medical School, Homburg/Saar, Germany

Background

Profound knowledge exists about the clinical, morphologic, genomic, and transcriptomic characteristics of most lymphoma entities. However, information is currently lacking on the dynamic behavior of malignant lymphomas. The present study aimed to gain insight into the motility of malignant lymphomas and their bystander cells.

Methods

3D Movies of vital lymphoma tissue were acquired with a confocal microscope and analysed with IMARIS software.

Results

Generally, B cells were faster under reactive conditions compared with B cells in malignant lymphomas. In contrast, PD1-positive T cells did not show systematic differences in velocity between reactive and neoplastic conditions in general. However, lymphomas could be divided into two groups: one with fast PD1-positive T cells (Hodgkin lymphoma and mantle cell lymphoma; means 8.4 and 7.8 $\mu\text{m}/\text{min}$) and another with slower PD1-positive T cells. Although the number of contacts between lymphoma cells and PD1-positive T cells was similar in different lymphoma types, important differences were observed in the duration of these contacts. Among the lymphomas with fast PD1-positive T cells, contacts were particularly short in mantle cell lymphoma (mean 54 s), whereas nodular lymphocyte-predominant Hodgkin lymphoma presented prolonged contact times (mean 6.1 min). Short contact times in mantle cell lymphoma were associated with the largest spatial displacement of PD1-positive cells (mean 12.3 μm). Although PD1-positive T cells in nodular lymphocyte-predominant Hodgkin lymphoma were fast, they remained in close contact with the lymphoma cells, in line with a dynamic immunological synapse.

Conclusion

This study shows for the first time systematic differences in the dynamic behavior of lymphoma and bystander cells between different lymphoma types.

Genetic characterization of localized follicular lymphomas reveals novel somatic copy number alterations and somatic mutations using OncoScan and whole-exome sequencing

S. Kalmbach^{1,2}, M. Grau³, M. Zapukhlyak³, E. Leich⁴, A. M. Staiger^{1,5}, K. S. Kurz⁵, M. Engelhard⁶, K. Herfarth⁷, H. Holte⁸, H.-W. Bernd⁹, A. C. Feller⁹, W. Klapper¹⁰, H. Stein¹¹, M.-L. Hansmann¹², S. Hartmann¹², M. C. Vöhringer^{13,14}, G. Lenz³, A. Rosenwald⁴, G. Ott⁵, H. Horn^{1,5}

¹Dr. Margarete Fischer-Bosch Institute of Clinical Pharmacology, Stuttgart, Germany, ²University of Tübingen, Tübingen, Germany, ³Department of Medicine A, Department of Hematology, Oncology and Pneumology, University Hospital Münster, Münster, Germany, ⁴Institute of Pathology, University of Würzburg and Comprehensive Cancer Center Main, Würzburg, Germany, ⁵Department of Clinical Pathology, Robert-Bosch-Krankenhaus, Stuttgart, Germany, ⁶Department for Radiotherapy, University Hospital of Essen, Essen, Germany, ⁷Department of Radiation Oncology, University of Heidelberg, Heidelberg, Germany, ⁸Department of Oncology, Oslo University Hospital, Oslo, Norway, ⁹Hematopathology, Lübeck, Germany, ¹⁰Institute of Pathology, Hematopathology Section and Lymph Node Registry, University Hospital Schleswig-Holstein, Campus Kiel, Kiel, Germany, ¹¹Pathodiagnostik Berlin, Berlin, Germany, ¹²Institute of Pathology, University Hospital Frankfurt, Frankfurt, Germany, ¹³Department of Internal Medicine, Oncology and Hematology, Robert-Bosch-Krankenhaus, Stuttgart, Germany, ¹⁴Department of Oncology and Hematology, Helios Hospital Pforzheim, Pforzheim, Germany

Background

Follicular lymphomas (FLs) represent the majority of indolent B-cell lymphomas. They are predominantly diagnosed in systemic stages III and IV (sFL, approximately 85%), contrasting only 15% of localized FL stages I and II (IFL). Available global genetic analyses of FL are mainly based on sFL samples, but initial comparative analyses of sFL and IFL have indicated genetic differences including a lower frequency of the hallmark t(14;18) translocation and underlying gene expression data.

Methods

Based on the OncoScan CNV Assay and whole-exome sequencing (WES) of a large cohort of IFL, somatic copy number alterations (SCNAs) and somatic mutations were analyzed. Genomic DNAs of 184 IFL from formalin-fixed paraffin embedded and fresh frozen tissue were available for SCNA analysis. WES has been performed on 164 samples, including 140 IFL and a comparative cohort of 24 sFL samples. To call gains, losses and copy-number neutral loss of heterozygosity, SCNA data were evaluated using the Chromosome Analysis Suite (ChAS) software (v4.0) and the Genomic Identification of Significant Targets in Cancer (GISTIC, v2.0) algorithm. WES was measured on the Illumina HiSeq platform with 150 bp paired-end reads. WES analysis employed several tools and public databases to call recurrent somatic mutations, including HISAT2, GATK, Mutect and MutSig2CV.

Results

We identified typical SCNAs for FL, including losses in 1p36, 6q and 10q as well as common gains in 2p16, 6p, 7 and 12q. Moreover, we discovered focal gains and losses affecting only a few specific target genes in 1q23.1, 7p12.2, 11q24 (gains) and in 8p11 (loss). No significant differences in SCNA frequency were identified when comparing IFL and sFL. The most frequently mutated genes were *CREBBP*, *KMT2D*, *BCL2* and *TNFRSF14*, similar to what had been reported for sFL. When comparing IFL and sFL, significant

differences were observed in the mutation frequency of *ARID1A*, with an increased number of mutations in sFL compared to IFL (27% vs. 5%, $p=0.0001$). Notably, we identified different patterns of mutations and SCNAs considering FL with and without BCL2-translocation.

Conclusion

These data underline the increasing importance of a global genetic characterization approach in IFL, since the clinical courses vary considerably among the patients and stages.

Routine application of the Lymph2Cx Assay for the subclassification of diffuse large B-cell lymphoma: report of a prospective real-world series with immunohistochemistry and FISH correlation.

A. Zamo^{1,2}, E. Gerhard-Hartmann^{1,2}, G. Ott³, I. Anagnostopoulos^{1,2}, D. W. Scott⁴, A. Rosenwald^{1,2}, **H. Rauert-Wunderlich^{1,2}**

¹Institut für Pathologie Universität Würzburg, Würzburg, Germany, ²Comprehensive Cancer Center Mainfranken, University Hospital Würzburg, Würzburg, Germany, ³Department of Clinical Pathology, Robert-Bosch-Krankenhaus and Dr. Margarete Fischer-Bosch-Institute of Clinical Pharmacology, Stuttgart, Germany, ⁴BC Cancer, Vancouver, Canada

Background

The subclassification of diffuse large B-cell lymphoma (DLBCL) in germinal center (GCB) and activated B-cell-like (ABC) subtypes has become mandatory in the 2017 update of the WHO classification of lymphoid neoplasms and will probably continue to be used in future classifications. The RNA-based Lymph2Cx assay has been validated as a reliable surrogate of high-throughput gene expression profiling assays for distinguishing between GC and ABC DLBCL and provides reliable results from formalin-fixed, paraffin-embedded (FFPE) material. This test has been previously used in clinical trials, but evidence from real-world routine application is scanty.

Methods

We routinely applied the Lymph2Cx assay to day-to-day diagnostic on a series of 147 consecutive DLBCL cases and correlated our results with the immunohistochemical subclassification using the Hans algorithm and with the fluorescence in-situ hybridization findings using break-apart probes for *MYC*, *BCL2*, and *BCL6*.

Results

The routine use of the Lymph2Cx assay had a high technical success rate (128/147, 94.6%) with minimal rates of assay failure due to poor material and/or RNA quality. The Lymph2Cx assay was discordant with the Hans algorithm in 18% (n=23) of our 128 cases. Discordant cases were mainly classified as GCB by the Hans algorithm and as ABC by Lymph2Cx (n=11, 8.6%). Only 5 cases (3.9%) were classified as non-GCB by the Hans algorithm and as GCB by Lymph2Cx. Additionally, 5.5% of cases (n=7) were unclassified by Lymph2Cx, whereas they were defined as GCB (n=4) or non-GCB (n=3) by the Hans algorithm.

Conclusion

Our data support the routine applicability of the Lymph2Cx assay.

Genome wide methylation profiling allows the separation of blastic variant of nodal marginal zone Lymphoma and primary nodal DLBCL. Work in progress.

F. Spada¹, A. Grunenberg², C. Buske², P. Möller¹, T. F. E. Barth¹

¹*Universitätsklinikum Ulm, Pathologie, Ulm, Germany*, ²*Universitätsklinikum Ulm, Experimentelle Tumorforschung, Ulm, Germany*

Background

Nodal marginal zone Lymphoma (NMZL) is an indolent tumor characterized by small cell morphology; a blastic variant of it is rarely described. The diagnosis of blastic NMZL is made by exclusion due to the lack of specific markers. The main differential diagnosis is diffuse large B-cell lymphoma (DLBCL).

Methods

We compared the clinical data of 41 indolent and 17 blastic NMZL from the German National Registry for Marginal zone B-cell Lymphoma in Ulm and gathered samples of 20 indolent and 20 blastic NMZL*. We hybridized DNA extracted from FFPE tissue and obtained genome wide methylation profiles for 19 indolent and 14 blastic NMZL. We used the Illumina Infinium MethylationEPIC BeadChip. DLBCL methylation data were obtained from the literature, comprising 40 nodal and 24 extranodal DLBCL.

Results

We failed to observe relevant differences in the clinical course of small cell and blastic NMZL. By methylation analysis it was not possible to separate small cell from the blastic NMZL. Methylation based phylogenetic analysis collocated small cell and blastic NMZL between low and intermediate differentiated B-cells, like DLBCL. Clear separation from DLBCL is observed in a supervised analysis ($\sigma/\sigma_{\max} \geq 0.4$, $q \leq 0.001$) for the group of small cell and blastic NMZL as well as in a comparison of nodal DLBCL and blastic NMZL. We identified 2329 CpG loci associated with the promoter region of 502 genes to be significantly differentially methylated between nodal DLBCL and blastic NMZL; however, no enrichment of pathways was detected for these differentiating genes. We further investigated the enrichment in regulatory regions as CpG islands, shelves and shores, but no difference emerged. However, we found an enrichment in Polycomb targeted regions, with a significant ($p < 0.0001$) hypermethylation for nodal DLBCL. In further analysis on the NOTCH pathway, we separated blastic NMZL and nodal DLBCL in a supervised analysis and observed that the overall methylation level for the loci belonging to the NOTCH pathway is significantly higher for blastic NMZL than for nodal DLBCL.

Conclusion

Our aim is a methylation based diagnostic algorithm to distinguish blastic NMZL and primary nodal DLBCL. However, our data underline that the clear separation of the two lymphomas needs an integration of various methylation-based data.

**Cases were kindly contributed by Prof. Dr. A. Rosenwald, Prof. Dr. W. Klapper, Prof. Dr. G. Ott, Prof. Dr. A.*

High prevalence of CHIP mutations in the blood of patients with peripheral bypass graft occlusion

E. Streck¹, **M. Harloff**², S. Schiele³, S. Dintner², G. Müller³, B. Märkl², A. Hyhlik-Dürr¹, R. Claus^{2, 4}

¹Medical Faculty, University of Augsburg, Clinic for Vascular Surgery, Augsburg, Germany, ²Medical Faculty, University of Augsburg, General Pathology and Molecular Diagnostics, Augsburg, Germany, ³Faculty of Mathematics and Natural Sciences, University of Augsburg, Institute of Mathematics, Augsburg, Germany, ⁴Medical Faculty, University of Augsburg, Hematology and Oncology, Augsburg, Germany

Background

Peripheral arterial disease (PAD) caused by atherosclerosis results in reduced arterial blood flow to the limbs. In late stages of disease, atherosclerotic plaques can cause complete arterial occlusion, which may require bypass surgery. Previous studies have reported a relation between clonal hematopoiesis of indeterminate potential (CHIP) and coronary heart disease [1],[2]. CHIP is defined as occurrence of somatic gene mutations in the hematopoietic system without definitive evidence of neoplasia [3]. Here, we investigated whether CHIP in peripheral blood (PB) of PAD patients is associated with acute bypass graft occlusion.

Methods

Genomic DNA from PB of patients with and without bypass occlusion was sequenced using the AmpliSeq for Illumina Myeloid sequencing panel. Patients with a tumor diagnosis, autoimmune diseases, or bypass occlusions caused by technical reasons or infections were excluded. Historical data from CHIP prevalence were used as control [4].

Results

In total, we analyzed the PB of 32 individuals with bypass occlusion and 12 control patients without. Median age was 68 years (range 38-87) in the study group, 87.5% were male. We identified CHIP-related variants in 10/32 individuals (31%) with an average of 1.8 variants per patient. The median VAF was 4% (range 1-40%). The most frequently mutated gene was TET2 (6/17; 35%), followed by DNMT3A (3/17; 18%). Specific mutational combination patterns were not detectable. Detailed analyses of cell subpopulations showed lineage-specific segregation of CHIP with presence of mutations in cells of the myeloid lineage, NK cells, and B cells but not in T lymphocytes. In a small still recruiting control group of peripheral bypass patients without occlusion (n=12), a trend towards lower CHIP frequency was observed. Compared to the general population (> 60 years), the percentage of CHIP-positive individuals with peripheral bypass graft closure tended to be higher.

Conclusion

Based on the observation that CHIP with loss-of-function mutations in the epigenetic modifier TET2 promotes inflammatory processes and atherosclerosis [5], we show an increased prevalence of CHIP, particularly with TET2 mutations, in patients with peripheral bypass graft occlusion. Thus, CHIP could be used as biomarker to identify patients at risk and potentially enable precautionary measures.

Literaturangaben

- [1] Jaiswal S. et al., (2014), Age-Related Clonal Hematopoiesis Associated with Adverse Outcomes, The New England Journal of Medicine, DOI: 10.1056/NEJMoa1408617
- [2] Jaiswal S. et al., (2017), Clonal Hematopoiesis and Risk of Atherosclerotic Cardiovascular Disease, The New England Journal of Medicine, DOI: 10.1056/NEJMoa1701719
- [3] Steensma DP et al., (2015), Clonal hematopoiesis of indeterminate potential and its distinction from myelodysplastic syndromes, Blood, DOI: 10.1182/blood-2015-03-631747
- [4] Arends CM et al., (2018), Hematopoietic lineage distribution and evolutionary dynamics of clonal hematopoiesis, Leukemia, DOI: 10.1038/s41375-018-0047-7
- [5] Fuster JJ et al., (2017), Clonal hematopoiesis associated with TET2 deficiency accelerates atherosclerosis development in mice, Science, Doi: 10.1126/science.aag1381

AG04 AG Hämatopathologie II

AG04.07

What is new in the 5th edition of the WHO classification of lymphoid tissue tumours?

G. Ott

Robert-Bosch-Krankenhaus, Abteilung für Klinische Pathologie, Stuttgart, Germany

This paper represents an overview of the new concepts and items in the upcoming 5th edition of the World Health Organization Classification of Haematolymphoid Tumours (WHO-HAEM5) focussing on lymphoid neoplasms. Major changes as compared to the revised 4th edition (WHO-HAEM4R) include a reorganization of entities by a hierarchical (Linnean) system as is adopted throughout the 5th edition of the WHO classification of tumours of all organ systems, the modification of nomenclature for some entities, a revision of diagnostic criteria or subtypes, deletion of certain entities and introduction of new entities. More specifically, both within the B-cell and the T-cell category, tumour-like lesions have been included into the classification that may pose a differential diagnosis to the diagnosis of lymphomas. Within the B-cell system, major changes include the addition of new entities within B-ALL, rendering the grading of follicular lymphoma optional, deletion of the diagnostic term of *B-prolymphocytic leukaemia*, creation of a new umbrella term for lymphomas arising at immune-privileged sites, and the formulation of a new concept for describing and diagnosing patterns of lymphoproliferations arising in the setting of immune deficiency/dysregulation, among others. The mature T-cell and NK-cell neoplasms are grouped into 9 families based on diverse concepts: cell of origin/differentiation state, clinical scenarios, disease localization, and cytomorphology. Lymphomas of T- or NK-cell lineage are not separated as two categories in WHO-HAEM5 because some entities comprise a spectrum of tumours of NK, T, hybrid or indeterminate phenotype, such as in extranodal NK/T-cell lymphoma, EBV+ nodal T- and NK-cell lymphoma, chronic active EBV disease and severe mosquito bite allergy. A common family terminology of nodal T-follicular helper cell lymphomas (nTFHLs) is introduced in WHO-HAEM5, with previously recognized diseases now regarded as entities within this family. Finally, mesenchymal lesions specific to lymph node and spleen, and germline predisposition syndromes associated with the lymphoid neoplasms are described.

Molecular genetic profiling of hematopoietic malignancies by gene panel sequencing in bone marrow core biopsies and its corresponding aspirates

K. Hirschbühl¹, J. Waidhauser¹, M. Harloff², S. Sommer¹, R. Claus^{1,2}, M. Trepel¹, B. Märkl², **S. Dintner²**

¹University of Augsburg Medical Faculty, Hematology and Oncology, Augsburg, Germany, ²University of Augsburg Medical Faculty, General Pathology and Molecular Diagnostics, Augsburg, Germany

Background

Recent genome profiling studies have generated an advanced understanding of the landscape of somatic mutations in hematopoietic malignancies. An increasing number of genes and variants are known to harbor prognostic and predictive significance. A baseline bone marrow (BM) biopsy is important to rule out the existence of a BM malignancy, and for future comparative use. If a BM examination is performed, both core biopsy (BMCB) and aspirate (BMA) or peripheral blood (PB) samples should be obtained. The BMCB yields important information regarding overall BM cellularity, hematopoietic architecture and fibrosis, the BMA/PB allows a detailed morphologic assessment of dysplasia and the most accurate enumeration of the blast percentage, and both are an important source of genetic information.

Since 2019, we implemented a comprehensive NGS gene panel solution in a strong interdisciplinary collaboration in a team of pathologists and haemato-oncologists. Here, we evaluated the feasibility of a gene panel for molecular genetic profiling of hematopoietic malignancies on BMCB and corresponding BMA/PB to see, if we obtain different genetic information of these fractions.

Methods

The AmpliSeq for Illumina Myeloid panel allowing analysis of molecular aberrations in specimens from hematopoietic malignancies was implemented in our lab. NGS libraries were prepared using standard protocols, and sequencing was performed on the Illumina MiSeq platform.

Results

Until today we analyzed 1589 PB, BMA or BMCB specimens from 813 patients. High quality DNA and RNA could be isolated from 98 % of PB and BMA and 92 % BMCB specimens. In 33 cases genetic analysis was performed on BMCBs. In 20 cases, corresponding samples were assessed and compared for genetic variants. In 9 (45 %) cases matching results could be obtained. In 6 (30 %) cases, BMCB resulted in an important gain of information compared with the corresponding BMA. In 3 (9 %) cases, molecular analysis could only be performed on BMCB, which provided important information for initial diagnosis and therapeutic decision.

Conclusion

Implementing a workflow covering the process from nucleic acid isolation to sequencing based on different type of specimen of hematologic neoplasia is essential. Molecular diagnosis of haematological neoplasms is mainly performed on BMA. In many cases, the complementary analysis of BMCB has expanded the clonal

architecture of the disease or even made a diagnosis possible, especially in cases of punctio sicca.

Efficacy of avapritinib in patients with advanced systemic mastocytosis (AdvSM): hematologic and bone marrow (BM) responses from the phase 2 open-label, single-arm, Pathfinder study

T. I. George¹, K. H. Karner², K. A. Moser², A. Rets², A. Reiter³, D. H. Radia⁴, M. Deininger⁵, H.-M. Lin⁶, S. Dimitrijević⁷, D. J. DeAngelo⁸

¹ARUP Laboratories, University of Utah, Department of Pathology, Salt Lake City, United States of America, ²ARUP Laboratories, University of Utah, School of Medicine, Salt Lake City, United States of America, ³University Hospital Mannheim, Heidelberg University, Department of Hematology and Oncology, Mannheim, Germany, ⁴Guy's & St Thomas' NHS Foundation Trust, London, United Kingdom, ⁵Versiti Blood Research Institute, Milwaukee, United States of America, ⁶Blueprint Medicines Corporation, Cambridge, United States of America, ⁷Blueprint Medicines (Switzerland) GmbH, Zug, Switzerland, ⁸Dana-Farber Cancer Institute, Department of Medical Oncology, Boston, United States of America

Background

Systemic mastocytosis (SM) is a mast cell (MC) neoplasm driven by the *KIT* D816V mutation in ~95% of cases. Diagnosis includes evaluation of MC aggregates, atypical MC morphology, CD25 expression, *KIT* D816V mutation detection, and serum tryptase >20 ng/ml. Avapritinib, an oral, potent, selective inhibitor of *KIT* D816V, reduced BM MC burden in patients with AdvSM in phase 1 EXPLORER. Here, we report on the effect of avapritinib on MC burden, morphology, and immunohistochemistry (IHC) in BM and hematologic parameters in patients with AdvSM from phase 2 PATHFINDER (data cut-off June 23, 2020).

Methods

Patients aged ≥18 years with centrally confirmed AdvSM initiated avapritinib 200 mg once daily. Peripheral blood (PB) smears, bone marrow biopsies (BMBs) and aspirates (BMAs), complete blood counts, and differentials were obtained (screening, Week [W] 8, and W24). MC morphology and reticulin and collagen fibrosis were evaluated histologically. IHC was done on BM sections using standard techniques for tryptase, CD117, CD25, and CD30.

Results

In PATHFINDER (interim analysis), BM MC decreases and elimination of aggregates were observed. Avapritinib decreased overall MC burden in BMBs, associated with a decrease in percentage of MC aggregates. Avapritinib also reduced the proportion of CD25+ and CD30+ MCs in BMBs (Table). In BMAs, avapritinib reduced MC burden and immature and spindle-shaped MCs (Table). Of 5 patients with circulating MCs at screening and post-screening sample measurements (all had SM with associated hematologic neoplasm diagnoses), none had detectable MCs by W8. Cellularity in BMBs decreased by W8. Fibrosis present in BMBs decreased by W24; in patients with increased fibrosis, avapritinib reduced reticulin fibrosis and collagen fibrosis. No significant changes in osteosclerosis scores were noted. In PB, avapritinib reduced eosinophil, leukocyte, neutrophil, and monocyte counts; platelet counts decreased while hemoglobin levels remained relatively consistent (Table).

Table. MC parameters in BM and hematologic parameters

Parameter	Screening	W8	W24
MC parameters, mean % of total (n)^a			
Immature MCs in BMAs	42.8 (n=45)	25.2 (n=33)	13.0 (n=20)
Spindle-shaped MCs in BMAs	45.5 (n=44)	43.2 (n=31)	39.4 (n=17)
Spindle-shaped MCs in BMBs	48.4 (n=60)	37.0 (n=44)	36.3 (n=26)
Expression of CD25 or CD30, mean % of total (n)^a			
CD25+ cells	87.7 (n=59)	37.3 (n=41)	25.3 (n=24)
CD30+ cells	39.2 (n=59)	11.2 (n=40)	5.4 (n=24)
Hematologic parameters, mean (SD), n^a			
Hemoglobin, g/dL	10.7 (1.9), n=62	10.1 (1.8), n=53	10.8 (1.4), n=35
Leukocytes, 10 ⁹ /L	12.1 (10.0), n=62	5.5 (4.6), n=52	5.2 (3.1), n=35
Neutrophils, 10 ⁹ /L	7.4 (7.7), n=61	3.1 (3.0), n=53	2.8 (2.1), n=35
Monocytes, 10 ⁹ /L	1.4 (1.5), n=61	0.6 (0.8), n=51	0.6 (0.4), n=34
Eosinophils, 10 ⁹ /L	1.0 (3.3), n=62	0.1 (0.2), n=51	0.1 (0.2), n=34
Platelets, 10 ⁹ /L	178 (101), n=62	142 (79), n=53	156 (85), n=35

BM, bone marrow; BMA, bone marrow aspirate; BMB, bone marrow biopsy; MC, mast cell; SD, standard deviation; W, week. ^aThe n values correspond to the number of evaluable patients for the described parameter and time point.

Table. MC parameters in BM and hematologic parameters

Conclusion

Avapritinib showed rapid (W8), profound (W24) reductions in neoplastic MC burden with normal morphologic appearance and immunophenotype (over 6 cycles). Normalization of BM cellularity was observed with decreased fibrosis and improved hematologic parameters.

Mutations in distinct molecules of the extracellular matrix are associated with tumor mutational burden and overall survival in multiple myeloma

M. Evers¹, M. Schreder^{2,3}, T. Stühmer⁴, J. Pischmarov¹, F. Jundt^{2,4}, R. Ebert⁵, T. N. Hartmann⁶, M. Rudelius^{1,7}, M. Kuric³, W. Rindt², T. Steinbrunn², C. Langer⁸, S. C. Heredia-Guerrero¹, H. Einsele², R. C. Bargou⁴, A. Rosenwald^{1,4}, E. Leich^{1,4}

¹Institute of Pathology, University of Wuerzburg, Wuerzburg, Germany, ²Department of Internal Medicine II, University Hospital of Wuerzburg, Wuerzburg, Germany, ³First Department of Medicine, Klinik Ottakring, Vienna, Austria, ⁴Comprehensive Cancer Center Mainfranken, University Hospital of Wuerzburg, Wuerzburg, Germany, ⁵Department of Musculoskeletal Tissue Regeneration, University of Wuerzburg, Wuerzburg, Germany, ⁶Department of Internal Medicine I, Medical Center and Faculty of Medicine, University of Freiburg, Freiburg, Germany, ⁷Institute of Pathology, Ludwig-Maximilians-University Muenchen, Muenchen, Germany, ⁸Department of Internal Medicine III, University Hospital Ulm, Ulm, Germany

Background

This study follows up our previous observations that patients with multiple myeloma (MM) present with an accumulation of single nucleotide variants (SNV) in receptor tyrosine kinases (RTKs) and adhesion molecules ([1], [2]). However, the role of SNV in adhesion molecules is unclear. Here, we investigated which type of adhesion molecules are affected by SNV, how the SNV cluster and how they impact other molecular events and survival.

Methods

Mutated adhesion molecules from a whole exome sequencing (WES) dataset (n=43 patients)(1) were analyzed using the STRING-network analysis tool. Subsequently, the mutation frequency and distribution in the clusters revealed by STRING analysis was assessed in our dataset and the CoMMpass WES IA15 study cohort (n=808) of the multiple myeloma research foundation (MMRF). Correlations among molecular parameters (e.g. tumor mutational burden (TMB)) were performed using the Chi-Square/Fisher's exact test. Correlations with overall survival (OS) were done using Kaplan Meier (Log rank) test.

Results

STRING-network analysis revealed a clustering of patient SNV in four main clusters, all associated with the extracellular matrix (ECM): Integrins, collagens, laminins, metalloproteases (ADAM, ADAMTS). Mutation frequencies were similar in both datasets. Overall, 58% of patients in our cohort had mutations in any of the clusters compared to 57% in the MMRF cohort. Collagens were most frequently mutated (30% vs 31%), followed by laminins (26% vs 13%), ADAMTS (21% vs 17%), integrins (21% vs 14%) and ADAMs (9% vs 7%). The mutations were widely spread across all the different genes and there were no typical hotspots. Notably, ECM mutations were significantly enriched in samples with high TMB (>median) in both datasets, while SNV in other gene families, e.g. RTK effectors, were randomly distributed. We observed a shorter OS in patients with mutations in the ECM gene families in the IA15 cohort, especially for patients with integrin mutations. OS was also significantly worse for patients with mutations in certain single integrin genes.

Conclusion

This study for the first time finds an association of high TMB and ECM mutations and that distinct ECM mutations affect MM OS survival. This may suggest a better response of ECM-mutated patients to PD1/PDL1-immunotherapy, though the value of TMB as a prediction for immunotherapy response still remains unclear ([3]).

Literaturangaben

- [1] Leich E, Schreder M, Pischmarov J, Stuehmer T, Steinbrunn T, Rudelius M, et al., (2021), Novel molecular subgroups within the context of receptor tyrosine kinase and adhesion signalling in multiple myeloma, Blood Cancer Journal, 1-5, 11(3), <https://doi.org/10.1038/s41408-021-00442-2>, 2021-03-01
- [2] Leich E, Weissbach S, Klein HU, Grieb T, Pischmarov J, Stuehmer T, et al., (2013), Multiple myeloma is affected by multiple and heterogeneous somatic mutations in adhesion- and receptor tyrosine kinase signaling molecules, Blood Cancer Journal, 102, 3, <https://doi.org/10.1038/bcj.2012.47>, 2021-03-01
- [3] Strickler JH, Hanks BA, Khasraw M, (2021), Tumor Mutational Burden as a Predictor of Immunotherapy Response: Is More Always Better?, Clin Cancer Res., 1236-1241, 27(5), <https://doi.org/10.1158/1078-0432.CCR-20-3054>, 2022-03-01

CD70⁺ subclones drive disease progression in Multiple Myeloma

S. Forster¹, C. Bachmann¹, A. Ochsenbein²

¹*University of Bern, Department for Biomedical Research, Tumor Immunology, Bern, Switzerland,* ²*Inselspital Bern, Department of Medical Oncology, Bern, Switzerland*

Background

Although multiple myeloma is generally considered incurable, an improved understanding of its genetic architecture has recently led to improved treatments, and long-term remissions are achieved in a fraction of patients. However, the majority of myeloma patients develop refractory disease or experience disease relapse despite advanced therapy options. Previous work from the Ochsenbein laboratory indicated that the CD70/CD27 signaling pathway is over-activated in leukemic stem cells of acute and chronic myeloid leukemia, thereby driving disease progression [1,2]. Whether CD70/CD27 signaling plays a role in myeloma progression has not been addressed so far.

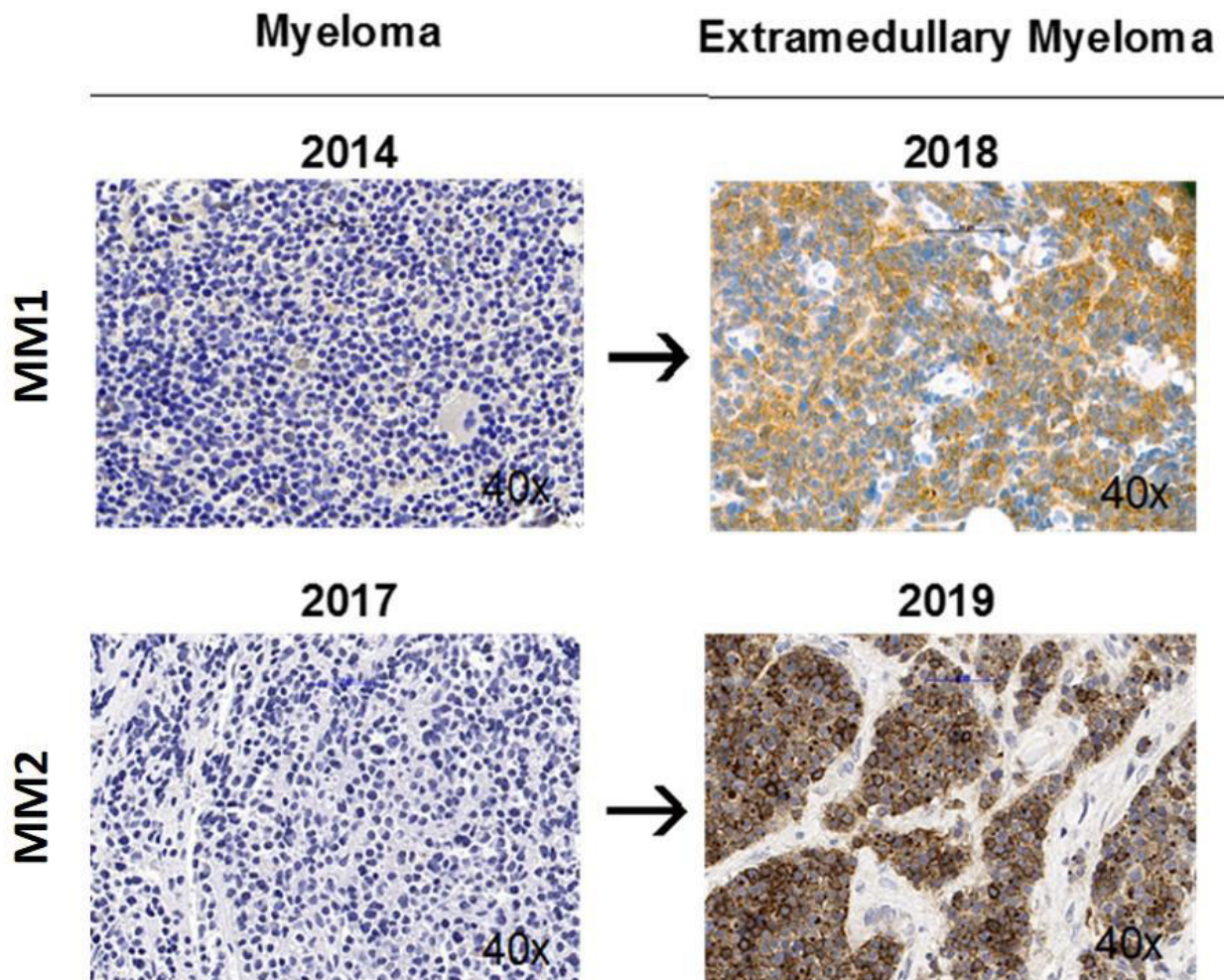
[1] [2]

Methods

A publicly available gene expression dataset of 766 myeloma patients (provided by the Multiple Myeloma Research Foundation, version IA15) was screened for CD70 expression. Expression levels were correlated with overall survival and co-occurrence of clinical and molecular high-risk markers defined by the revised international staging system. In addition, CD70 surface expression levels were analyzed in over 200 myeloma patients at initial diagnosis, after disease relapse or after manifestation of extramedullary disease using a tissue micro array setup and flow cytometry analysis.

Results

Analysis of CD70 gene and protein expression levels in myeloma patients revealed that CD70 is upregulated in ~ 10 to 15% of myeloma patients and that high CD70 expression levels are associated with a worse patient overall survival and increased frequencies of high-risk disease stages. In addition, matched and unmatched comparisons of myeloma patients at initial diagnosis, after relapse or with extramedullary dissemination showed increased CD70 expression levels in end-stage disease states suggesting CD70 upregulation during the course of myeloma progression (Image 01).



Matched comparisons of CD70 expression between multiple myeloma at initial diagnosis and the corresponding relapse with extramedullary manifestation (pictures from two representative patients; 40x magnification)

Conclusion

Summarizing we demonstrate that CD70 is over-expressed in a subset of myeloma patients and that CD70 upregulation is associated with reduced overall survival, unfavorable (high-risk) cytogenetic alterations and disease relapse underlining its potential as a novel prognostic biomarker and therapeutic target in multiple myeloma.

Literaturangaben

- [1] Carsten Riether et al. , (2017), CD70/CD27 signaling promotes blast stemness and is a viable therapeutic target in acute myeloid leukemia, J. Exp. Med., 359–380, 214
- [2] Christian Schürch et al. , (2012), CD27 signaling on chronic myelogenous leukemia stem cells activates Wnt target genes and promotes disease progression. , J. Clin. Invest., 624–638, 122

Functional investigation of the IGF1R-PYK2 signaling network in Multiple Myeloma

S. C. Heredia-Guerrero¹, M. Evers¹, S. Keppler¹, M. Schwarzfischer¹, H. Starz¹, O.-J. Bayrhof², J. Pickert¹, A. Krügl¹, T. Nedeva¹, H. Einsele³, R. C. Bargou², A. Rosenwald¹, T. Stühmer¹, E. Leich¹

¹*Pathologisches Institut, Uni. Würzburg, Würzburg, Germany*, ²*Comprehensive Cancer Center Mainfranken, Würzburg, Germany*, ³*University Hospital Würzburg, Department of Internal Medicine II, Würzburg, Germany*

Background

Our previous NGS study in multiple myeloma (MM) identified a network of Receptor Tyrosine Kinases (RTKs), adhesion molecules and their effectors, affected by point mutations in virtually all cases. RTK mutations were associated with worse overall survival and IGF1R was the most frequently mutated RTK. Among the mutated effectors was the focal adhesion kinase PYK2, which can be regulated by RTKs and/or integrins and is highly expressed in MM compared to normal bone marrow cells[1]. Thus, we aimed to investigate whether IGF1R might be responsible for the activation of PYK2 in MM.

Methods

IGF1R and PYK2 siRNA-knockdown (kd) was done in 7 and CRISPR-Cas knockout (ko) of IGF1R achieved in 2 human MM cell lines (HMCL). Stable transfection of WT and mutant IGF1R (IGF1R^{WTmut1/mut2}) as well as of WT and mutant PYK2 (PYK2^{WT/mut}) was performed in HEK293^{FT} and HMCL, using the Sleeping Beauty system. The impact of IGF1R-kd/ko, and of IGF1R^{WTmut1/mut2} and PYK2^{WT/mut} overexpression, on MEK/ERK-, PI3K-AKT- and PYK2-signaling as well as on proliferation/viability was investigated by Western analysis, cell counting and MTT assays. An *in vitro* drug screen was performed with IGF1R-inhibitor Linsitinib. For immunofluorescence (IF) staining antibodies against IGF1R and PYK2 and high-resolution microscopy were used.

Results

IGF1R-kd reduced PYK2- and AKT-activation in all and MEK/ERK-activation in 6/7 HMCL. We observed a heterogeneous response to Linsitinib, which seemed to be unconnected to the IGF1R-expression/activation or mutation status. Pyk2 was activated upon overexpression of IGF1R in all tested cell lines. IGF1R-ko entailed reduced PYK2 activation/viability/proliferation in one HMCL. In contrast to IGF1R-kd, PYK2-kd did not affect MEK-/ERK- and AKT-signaling in any HMCL. However, IGF1R activation was downregulated upon overexpression of PYK2^{WT/mut} in HEK293 and MM cells. Accordingly, AKT activation was downregulated in MM cells overexpressing PYK2^{mut}. However, MEK/ERK activation was upregulated upon the overexpression of PYK2^{mut} in HEK293 and MM cells. We also noted upregulation of anti-apoptotic proteins in MM cells, specifically after overexpression of PYK2^{mut}. Finally, preliminary IF analysis indicated that IGF1-stimulation led to recruitment of PYK2 to the membrane before but not after IGF1R-ko.

Conclusion

Our results suggest co-regulation of IGF1R and PYK2 in HMCL. However, further investigations are needed to validate and strengthen our hypothesis.

Literaturangaben

[1] Zhang, Yu et al., (2014), Pyk2 promotes tumor progression in multiple myeloma., Blood, 2675-86, doi:10.1182/blood-2014-03-563981, 2022-02-26

AG05 AG Herz-, Gefäß-, Nieren- und Transplantationspathologie

AG05.01

Sudden Cardiac Death UK National Programme Implementation

M. Sheppard, M.D.

St Georges University of London, Molecular & Clinical Sciences Research Institute, London, United Kingdom

Background

Sudden cardiac death (SCD) is defined as natural unexpected death in witnessed cases as an acute change in cardiovascular status with time to death being <1 hour and in unwitnessed cases as person last seen alive <24 hours before being found dead(1) . SCD is frequent in older age groups due largely to ischaemic heart disease in USA, Europe and increasing also in China (2) (3) (4). Death certification is vital to help guide public health services and prevention as well as public health concerns(5). In a recent analysis of USA death certificates from 2018, 34.7% of all death records had an unsuitable underlying cause of death while 19.8% had a nonspecific underlying cause of death (7). The almost universal decline in hospital autopsies has led to significant errors in the cause of death (6) . The declining autopsy rate is highlighted in many studies and even a recent FIFA report on sudden death in young footballers showed that out of 617 cases from 67 countries , only 127 had an autopsy (7) A recent review within Europe highlighted that up to 40% of SCD in people under 50 years cases did not have an autopsy(8). This study did however emphasise that in the United Kingdom we have a high autopsy rate within our coronial system. It is especially important that SCD in younger people is investigated with autopsy as genetic cardiac causes including channelopathies and cardiomyopathies are more frequent which have important implications for their families (9). These cardiac diagnoses in SCD can only be made at autopsy. This highlights that there is still a role for the autopsy in the 21st century in determining the cause of cardiac death which guides future public health planning and prevention .

Methods

We presented our initial results on 453 cases in 2006 (11). Since then we have accumulated 7000 cases into this database, the largest series of autopsy sudden cardiac death with established pathological criteria for diagnosis and wish to expand on our previous series and the evolution of the molecular autopsy which is of vital importance to families and cardiologists who have developed the inherited cardiac conditions speciality within the UK. We also are now embarking on a national programme funded by NHS and BHF which will combine the autopsy diagnosis in SCD with retention of tissue for genetic testing as well as establishing pathways for families to be screened at inherited cardiac clinics throughout UK .

Results

Sudden adult death is main cause with cardiomyopathies

10 years transplant on-call duty. Lessons learned

H. A. Baba¹, A. Potratz¹, M. Schlattjan¹, J. Treckmann², C. Brandtner³, A. Konietzko², T. Benkö², S. Theurer¹

¹Universität Duisburg-Essen, Institut für Pathologie, Essen, Germany, ²Universität Duisburg-Essen, Klinik für Allgemein-, Viszeral- und Transplantationschirurgie, Essen, Germany, ³Deutsche Stiftung Organtransplantation, Essen, Germany

Background

Um den Pool an Organspendern zu erweitern, wird immer häufiger auf marginale Spenderorgane zurückgegriffen. Aus diesem Grund müssen spenderbezogene Gewebeuntersuchungen histopathologisch untersucht werden. Am Institut für Pathologie des Universitätsklinikums Essen wurde aus diesem Grund im April 2010 ein 24 Stunden Rufdienst eingerichtet. Es wird über die Erfahrungen mit dies Rufdienst in den letzten 10 Jahren berichtet.

Methods

Die pathologischen Befunde dieses Rufdienstes von April 2010 bis Dezember 2019 wurden zusammengetragen und mit den klinischen Spenderdaten sowie dem Transplantations outcome in Verbindung gebracht.

Results

In dem Untersuchungszeitraum wurden insgesamt 1.587 Fälle eingeschlossen und insgesamt 1.631 Proben untersucht. 32% der Einsätze (502) erfolgten innerhalb der regulären Arbeitszeit, während 68% der Einsätze (1.067) zwischen 17:00 Uhr und 8:00 Uhr erfolgten. Die häufigste (92%) Fragestellung war die nach der Organqualität, bei 127 (8%) Einsendungen sollte die Frage nach einer Tumorabklärung beantwortet werden. In absteigender Häufigkeit wurden die folgenden Organe untersucht: Leber (84,7%), Niere (6,13%), Lunge (2,45%) sowie Lymphknoten (1,2%). Bezüglich der Organqualität stand die Frage nach Leberverfettung und Fibrose von 1347 Lebern (84,9%) im Vordergrund. In 63,4% fand sich eine makrovesikuläre Verfettung von 0 bis 10%, in 16,9% eine Verfettung von 11-20%, in 7,2% eine Verfettung von 21-30% und in 7,4% eine Verfettung von mehr als 31%.

Von den 127 Tumorabklärungen waren 110 (86,6%) benigne Tumoren und 17 (13,3%) maligne Tumoren. Die häufigsten malignen Tumoren waren Nierenzellkarzinome (7), Adenokarzinome (4), GIST (2). Bei 525 Untersuchungen standen klinische Daten zum Transplantationsverlauf zur Verfügung. Die makrovesikuläre Verfettung korrelierte positiv mit dem BMI des Spenders sowie auch mit dem Vorliegen eines Hypertonus. Logistische Regressionsanalysen zeigen, dass eine erhöhte makrovesikuläre Verfettung in der Spenderleber einhergeht mit einem komplizierten klinischen Verlauf innerhalb der ersten 7 Tage post-Transplantation (unauffällig vs early allograft dysfunction/primary non-function).

Conclusion

Die Vorhaltung eines pathologischen 24 Stunden Rufdienstes ermöglicht es, den Organspender Pool zu erweitern. Die makrovesikuläre Leberzellverfettung ist ein wichtiger Parameter zur Vorhersage eines komplizierten Verlaufes. Die Einführung eines Rufdienstes stellt einen Paradigmenwechsel in der Arbeit des Pathologen dar.

AG05.04

Actual aspects on diagnosis of renal transplants – Banff and beyond

J. H. Bräsen

MHH Pathology, Institute of Pathology, OE 5110, Hannover, Germany

Renal transplantation represents the best therapy for end stage renal disease. Much effort has been put on improvement of longevity of the transplanted organ including comprehensive and regularly updated histological scoring system (Banff classification) for surveillance, but still survival of transplanted kidneys is limited to median 10 years. Molecular analyses have largely increased the understanding of damaging mechanisms within the transplant, especially antibody mediated rejection, which can be difficult to identify using histological methods. Recent changes of the Banff classification and own data from research including the importance of innate immune cells, digital techniques in pathology and molecular analyses will be presented.

Mass spectrometry-based proteomics (LC-MS/MS) without Laser Microdissection (LMD) - a reliable approach to classify cardiac amyloidosis?

J. Luibrand¹, P. Riemenschneider², M. Sulyok¹, S. Mattern², M. A. Jarboui³, M. Ueffing³, B. Maček⁴, F. Fend¹, K. Klingel¹, S. Singer¹

¹Universitätsklinik Tübingen, Allgemeine und molekulare Pathologie und pathologische Anatomie, Tübingen, Germany, ²Universitätsklinik Tübingen, Allgemeine und molekulare Pathologie und pathologische Anatomie, Tübingen, Germany, ³Universitätsklinik Tübingen, Forschungsinstitut für Augenheilkunde, Tübingen, Germany, ⁴Universität Tübingen, Interfakultäres Institut für Zellbiologie, Tübingen, Germany

Background

Amyloidoses represent a diverse group of disorders caused by extracellular deposition of misfolded proteins which can imply different organs including the heart. Correct subtyping of amyloidosis is of utmost importance since the various subtypes (> 30) significantly differ in their respective outcomes and treatment options. In routine diagnostics amyloid deposits are detected by Congo Red staining coupled with apple-green birefringence in polarized light. Amyloid subtyping is widely performed by immunohistochemistry (IHC), which can be challenging and requires long standing experience in the interpretation. Furthermore, subtyping remains limited to the subset of amyloidoses for which antibodies are established/available. Therefore, mass-spectrometry based proteomics (LC-MS/MS) combined with Laser Microdissection (LMD) is now considered for amyloidosis subtyping allowing the identification of virtually all amyloidosis subtypes. However, particularly for very small samples such as endomyocardial biopsies with occasionally very delicate distribution of the amyloid deposits the LMD step is not feasible.

Methods

Here, we tested an LC-MS/MS approach for subtyping cardiac amyloidoses using more than 20 macrodissected (whole specimen) formalin-fixed and paraffin-embedded (FFPE) endomyocardial biopsies.

Results

By using LC-MS/MS of macrodissected samples we could either confirm the amyloidosis subtype as diagnosed by IHC (e.g. AL (lambda/kappa) and ATTR) or could identify subtypes (e.g. ApoAI and ApoAIV) beyond the repertoire of established antibodies in our laboratory.

Conclusion

While a larger cohort and more detailed analyses are required (also regarding the minimal amount of amyloid per sample being sufficient) our results suggest that FFPE LC-MS/MS even without LMD is a valuable approach to classify cardiac amyloidoses.

iNOS expression in postmortem human myocardial infarction hearts for validation of oxidative stress

V. Wilmes¹, C. Niess¹, E. Gradhand², M. A. Verhoff¹, S. Kauferstein¹

¹Institut für Rechtsmedizin, Universitätsklinikum Frankfurt, Goethe-Universität Frankfurt am Main, Frankfurt am Main, Germany, ²Senckenbergisches Institut für Pathologie, Universitätsklinikum Frankfurt, Goethe-Universität Frankfurt am Main, Frankfurt am Main, Germany

Background

Der Myokardinfarkt zählt zu den häufigsten Todesursachen in Deutschland. Der Erforschung der zugrundeliegenden molekularen Vorgänge kommt somit eine entscheidende Rolle zu.

Die Bildung von oxidativ wirksamen Molekülen verursacht oxidativen Stress und kann zu zellulären Veränderungen führen. Oxidativer Stress könnte somit einen wichtigen Faktor im Rahmen eines Myokardinfarkts darstellen. Die induzierbare Stickoxidsynthase (iNOS) stellt hier einen wichtigen Marker dar. iNOS katalysiert die Entstehung von Stickoxid, kann aber auch die Entstehung von radikalem Sauerstoff katalysieren, was Gewebeschädigung und Zelltod zur Folge hat. In dieser Studie sollte ein Beitrag zur Aufklärung der Rolle der iNOS bei Myokardinfarkt geleistet werden.

Methods

Es wurden die mRNA-Expression mittels q-RT-PCR, sowie das Zellexpressionsmuster der iNOS mittels immunhistochemischer Färbungen im infarzierten und nicht infarzierten Myokard untersucht und mit gesunden Kontrollen verglichen. Dazu wurden CD68- und iNOS-Färbungen angewendet.

Results

In den infarzierten Regionen zeigte sich iNOS signifikant hochreguliert im Vergleich zu gesunden Kontrollen, während die iNOS Proteinexpression hauptsächlich in den Makrophagen sichtbar war. Zudem zeigte sich ein deutlicher Anstieg der iNOS Proteinexpression in den infarzierten Herzen.

Conclusion

Unsere Ergebnisse sind ein Hinweis auf erhöhten oxidativen Stress bei Myokardinfarkt. Die durch oxidativen Stress ausgelösten Zellschädigungen könnten in Zusammenhang mit dem Schweregrad des Infarktes stehen. Des Weiteren deuten die Ergebnisse auf eine komplexere Regulation der iNOS Expression hin, die mit der Makrophagenpolarisierung und dem Infarktalter zusammenhängen könnte.

iNOS stellt somit einen wichtigen Marker zur Untersuchung einer kardialen Erkrankung bei Verstorbenen durch oxidativen Stress auf molekularer Ebene dar.

Histopathology of 61 human explanted atrial septal defect occlusion devices without removal of metal/polymer parts

M. Sigler, K. Eildermann, R. Foth, T. Paul

Georg-August-Universität Göttingen, Päd. Kardiologie und Intensivmedizin, Göttingen, Germany

Background

Catheter-based interventional implantation of an occlusion device is currently gold standard for therapy of atrial septal defects (ASD). While implantation technique and closure rates are well described, there are only limited data on biocompatibility. We aimed to evaluate and characterize tissue reactions within and at the surface of ASD occlusion devices.

Methods

Explants were processed using a uniform protocol after surgical removal. Devices were fixed in formalin and embedded in methylmethacrylate. Serial sections were obtained by sectioning with a diamond cutter and grinding, thus saving the metal/tissue interface for histological evaluation. Standard staining and immunohistochemistry was performed using conventional protocols.

Results

61 devices were analyzed (Amplatzer n = 29, Cardioseal/Starflex n= 10, Biostar n= 5, Gore Occluder n= 6, others n= 11). Implants had been in the human body for 1 day to 15 years (mean 3.2 years). Main reason for explantation had been residual shunting in 22, thrombus formation and/or clinical suspicion for embolism or endocarditis in 10, heart surgery otherwise indicated in 8, device dislocation in 7, deformity of the device in 5, damage to the right atrial wall in 3 and other reasons in 6 patients, respectively. Endothelialisation and cellular organisation of tissue within the devices was present in all specimen with implantation times > 6 months. Lymphocytic infiltrations and local foreign body reaction related to textile components were found in almost all explants independent of implantation time. No case of device related endocarditis was identified. Calcifications, partial corrosion of metal wires, and complete degradation of ivalon foam material were seen in explants with implantation time > 7 years.

Conclusion

This is the largest cohort of ASD occlusion devices with complete histological work-up after surgical explantation. We demonstrate timely endothelialisation and tissue organisation, a typical pattern of chronically persisting inflammation. Calcifications and material alterations with partial corrosion or even loss of “permanent” materials were seen in long-term explants. We conclude that patients with ASD occlusion devices should be followed life-long for detection of potential implant-related complications. Our findings may be relevant for the development of new devices.

α -Parvin defines a specific integrin adhesome to maintain podocyte adhesion and the kidney filtration barrier

M. Rogg¹, J. I. Maier¹, C. Van Wymersch¹, M. Helmstädter², A. Sammarco¹, G. Walz², M. Werner¹, **C. Schell¹**

¹*Institute of Surgical Pathology, Faculty of Medicine, Medical Center - University of Freiburg, Freiburg 79106, Germany*, ²*Department of Medicine IV, Faculty of Medicine, Medical Center - University of Freiburg, Freiburg 79106, Germany*

Background

Podocyte detachment from the glomerular basement membrane (GBM) is an established factor driving progression of glomerular kidney diseases. Moreover, co-occurrence of podocyte detachment and mechano-adaptive reinforcement of the actin cytoskeleton - integrin adhesion complex (IAC) – GBM linkage is observed. However, underlying mechanisms determining maintenance of cell-matrix adhesion or initiating detachment remain elusive.

Methods

We generated podocyte specific conditional knockout mice targeting the (IAC) component PARVA (Parva-*fl/fl**hNPHS2Cre). We applied super-resolution microscopy (3D-SIM), electron microscopy (TEM, SEM), multiplex immunofluorescence microscopy (4i), RNA sequencing and classical physiological assays to analyze podocytes *in vivo*. *In vitro*, we used CRISPR/Cas9 genome editing to generate *PARVA* single- and *PARVA* & *PARVB* double knockout podocytes for functional analysis in 2D and 3D environments. Moreover, we used specific ECM ligands, substrate rigidity and micropatterns to investigate IAC function in podocytes.

Results

Loss of PARVA caused rapid podocyte detachment from the GBM leading to focal segmental glomerulosclerosis. Analyzing consequences of PARVA deletion revealed an IAC inherent compensatory mechanism, involving PARVB to sustain efficient mechano-linkage to the actin cytoskeleton *in vitro* and *in vivo*. Exhaustion of this mechanism or sequential genetic deletion of PARVA and PARVB induced a switch in IAC distribution and composition translating into impaired cell-matrix adhesion and loss of the ventral actin cytoskeleton. Degradation of the ILK-Pinch-Parvin (IPP) complex, altered Zyxin distribution and impaired IAC to F-Actin linkage resulted in reduced adaptive capacities to varying extracellular and intracellular mechanical cues, finally leading to cell rounding and detachment.

Conclusion

These observations imply insufficient (mechano-) linkage of an adaptive tensile actin cytoskeleton to integrin adhesion complexes and the GBM as causative mechanism for podocyte detachment in glomerular disease. In contrast, balanced compensatory remodeling of podocyte IACs and the actin cytoskeleton ensure

sufficient adhesion to the GBM and maintenance of the kidney filtration barrier.

AG06 AG Gynäko- und Mammopathologie I

AG06.01

Loss of tumor suppressor TGF- β pathway proteins phosphoSmad2 and Smad4 indicate poor survival in high grade serous ovarian carcinoma

C. A. Kunze¹, W. Zörn¹, I. Hoffmann¹, N. Monjé¹, S. Darb-Esfahani², J. Pohl¹, M.-P. Dragomir^{1,3,4}, W. D. Schmitt¹, E. I. Braicu^{5,6}, H. Kulbe^{5,6}, J. Sehouli^{5,6}, C. Denkert⁷, D. Horst¹, E. Taube¹

¹Charité – Universitätsmedizin Berlin, corporate member of Freie Universität Berlin and Humboldt-Universität zu Berlin, Institute of Pathology, Berlin, Germany, ²Medizinisches Versorgungszentrum Spandau, Institute of Pathology, Berlin, Germany, ³Berlin Institute of Health at Charité – Universitätsmedizin Berlin, Berlin, Germany, ⁴German Cancer Consortium (DKTK), Partner Site Berlin, and German Cancer Research Center (DKFZ), Heidelberg, Germany, ⁵Charité – Universitätsmedizin Berlin, corporate member of Freie Universität Berlin and Humboldt-Universität zu Berlin, Department of Gynecology, Berlin, Germany, ⁶Tumorbank Ovarian Cancer Network (TOC), Berlin, Germany, ⁷Philipps University of Marburg, Institute of Pathology, Marburg, Germany

Background

TGF- β -mediated epithelial to mesenchymal transition (EMT) is a process of transdifferentiation, which plays a role in progression of high grade serous ovarian carcinoma (HGSOC). Major effector molecules of the TGF- β receptor are phosphorylated Smad2 (pSmad2) and Smad4. Since Smad4 is well known as a tumor suppressor we aimed to investigate the impact of these downstream TGF- β proteins in a well-characterized cohort of HGSOC.

Methods

pSmad2 and Smad4 protein expression was determined by immunohistochemistry on tissue micro arrays in a cohort of 604 primary HGSOC retrospectively. Biomarker expression on tumor cells was evaluated with a digital quantitative scoring approach using QuPath image analysis software. Cutoff points for overall survival (OS) of optimal biomarker distribution were determined using the Cutoff-Finder web app. Kaplan-Meier and multivariate Cox regression analyses were performed to evaluate the prognostic power of pSmad2 and Smad4.

Results

High pSmad2 protein expression significantly indicated favorable outcome in patients with primary HGSOC for OS (p=0.000027) and progression free survival (PFS; p=0.022). It remained significant for OS (hazard ratio [HR], 0.693; 95% confidence interval [CI], 0.498-0.966; p = 0.030) in multivariate analysis that included age, tumor stage and residual tumor. High Smad4 protein expression was a significant prognostic marker for favorable outcome in univariate survival analyses (OS p=0.016 and PFS p=0.046). Further we combined the two markers and identified a pSmad2 and Smad4 lacking subgroup with an exceptionally unfavorable prognosis compared to patients with high expression of at least one protein regarding OS (p=0.000014) and

PFS ($p=0.001$). The prognostic power remained independent in multivariate analyses (HR 1.596; 95% CI 1.072-2.375; $p=0.021$ for OS and HR 1.565; 95% CI 1.009-2.427; $p=0.046$ for PFS, respectively).

Conclusion

We show that loss of pSmad2 or Smad4 has an additive effect in identifying subgroups of patients with unfavorable prognosis and that a combined low expression of pSmad2 and Smad4 marks a subgroup with most dismal prognosis. In line with the described tumor suppressive function in other entities, our results point out that loss of Smad proteins in HGSOC leads to an activation of EMT. Restoring this pathway could inhibit the EMT program in this poor prognosis subgroup.

Prognostic value of Regulatory T cells and T helper 17 cells in high grade serous ovarian carcinoma

I. Piwonski¹, S. Marchenko¹, I. Hoffmann¹, B. Sinn¹, C. A. Kunze², N. Monjé², J. Pohl², H. Kulbe³, W. D. Schmitt², S. Darb-Esfahani⁴, E. Braicu^{5, 6}, A.-C. von Brünneck⁷, J. Sehouli^{6, 8}, C. Denkert⁹, D. Horst⁷, K. Jöhrens¹⁰, E. T. Taube⁷

¹Charité Universitätsmedizin Berlin, Institut für Pathologie, Berlin, Germany, ²Charité – Universitätsmedizin Berlin, Institut für Pathologie, Berlin, Germany, ³Charité – Universitätsmedizin Berlin, Tumorbank Ovarian Cancer Network, Berlin, Germany, ⁴Institut für Pathologie Berlin-Spandau und Berlin-Buch, Berlin, Germany, ⁵Charité – Universitätsmedizin Berlin, Institut für Gynäkologie, European Competence Center for Ovarian Cancer, Berlin, Germany, ⁶Charité - Universitätsmedizin Berlin, Tumorbank Ovarian Cancer Network, Berlin, Germany, ⁷Charité - Universitätsmedizin Berlin, Institut für Pathologie, Berlin, Germany, ⁸Charité - Universitätsmedizin Berlin, Institut für Gynäkologie, European Competence Center for Ovarian Cancer, Berlin, Germany, ⁹Philipps-Universität Marburg, Institut für Pathologie, Marburg, Germany, ¹⁰Universitäts Krankenhaus Dresden, Institut für Pathologie, Dresden, Germany

Background

Ovarian cancer is the 8th most frequently diagnosed cancer type for women in 2020, with a mortality rate of 6.7 per 100,000 women in 2018 and therefore the most common cause of death among gynecological malignancies.

Tumor microenvironment and its interaction with the tumor has emerged into research focus with increased attention to the composition of tumor infiltrating lymphocytes (TILs). Especially the influence of subsets of T helper cells like the regulatory T-cells (Tregs) and Th17 cells seem highly dependent on the tumor type. Here we aimed to quantify the composition of Tregs and Th17 cells and their prognostic impact in high-grade serous carcinoma.

Methods

Tregs and Th17 cells were determined by immunohistochemical analysis of CD25 FoxP3 and RORγt, respectively, on tissue micro arrays of a well characterized cohort of 222 patients with high grade serous carcinoma (HGSC). Expression was analyzed with QuPath for quantification and integration with clinical data enabled calculation of prognostic impact. For validation FOXP3 and RORC mRNA expression levels from 502 patients with HGSC in publicly available datasets were evaluated.

Results

An average of 225 Tregs and 71 Th17 cells were detected per spot. Optimal cut-offs were determined with the Cut-off finder tool from the University of Heidelberg. Higher Tregs in stroma ($p = 0.006$), tumor area ($p = 0.0012$) and overall tissue ($p = 0.02$) were associated with a better overall survival. After accounting for the well-known prognostic factors age at diagnosis, residual tumor and FIGO stage, this association remained significant for stromal Tregs ($p=0.02$).

Likewise, survival analysis was performed for Th17 cells. A trend for poorer survival with higher tumor infiltration was observed ($p= 0.089$).

Since the balance of Th17 and Treg cells has been described as relevant for immune response, we analyzed the Th17/Treg ratio and found that it had a positive impact on patient survival ($p=0.025$ for tumor, 0.049 for stroma and 0.016 for overall tissue, respectively). In silico, we were able to validate our findings on mRNA

levels with a significant association for FOXP3 ($p = 0.005$) and a trend for RORC ($p = 0.12$), as well as for the RORC:FOXP3 ratio ($p = 0.15$).

Conclusion

Our results outline a positive prognostic effect for higher Tregs and the ratio of Th17/Tregs in high grade serous ovarian carcinoma. Further research is needed to understand the interplay of Tregs and Th17, especially for high-grade serous ovarian carcinoma.

Desmoplastic stroma reaction and CAF activity contribute to poor therapy response in HGSOC.

M. Wessolly¹, E. Mairinger¹, S. Borchert¹, A. Bankfalvi¹, P. Mach², K. W. Schmid¹, R. Kimmig², F. D. Mairinger¹

¹Universitätsklinikum Essen, Institut für Pathologie, Essen, Germany, ²Universitätsklinikum Essen, Klinik für Frauenheilkunde und Geburtshilfe, Essen, Germany

Background

Known as one of the deadliest gynecological malignancies, high-grade serous ovarian carcinoma (HGSOC) is associated with quick metastatic spread, resistance to adjuvant chemotherapy and poor prognosis. Desmoplastic stroma reaction (DSR) occurring in the tumor microenvironment may be a strong contributing factor. Cancer-associated fibroblasts (CAFs), which are often linked to tumor progression, are central key players in DSR. As platinum-based treatment is still a cornerstone HGSOC treatment, reasons for therapy resistance need to be explored. Here, we present a study unveiling the relation of DSR-associated signaling pathways and poor outcome in a HGSOC cohort.

Methods

The HGSOC cohort encompassed 24 patients. All patients were treated with adjuvant platinum-based chemotherapy. The tumor material was isolated exclusively from the ovaries. The probes were formalin-fixed and embedded into paraffin. RNA was isolated using a Maxwell RSC RNA FFPE kit. For digital gene expression analysis, a custom-designed NanoString nCounter panel was designed, which includes various genes linked to DSR- and CAF-signaling. The analysis was carried out on the NanoString nCounter platform. The explorative data analysis of expression data was conducted in the R programming environment (v. 4.1.2). Furthermore, a validation cohort of 303 epithelial ovarian cancer patients from TCGA served as a control cohort.

Results

All patients showed varying degrees of DSR. Platinum-resistant patients were defined as displaying signs of tumor progression within six months after completion of chemotherapy. Besides poor outcome, these patients were linked to increased gene expression in CAF-linked signaling pathways including MAPK-, TGF- β and PI3K-Akt signaling. The expression of 6 single genes (MMP13, CGA, EPHA3, PITX2, PSMD3, PHLPP1) was linked to resistant patients as well. Strong CAF-signaling and poor outcome was also observed in the control cohort.

Conclusion

The increased activity of PI3K-Akt and MAPK signaling hints towards non-canonical TGF- β signaling, which is employed by CAFs to support the tumor. Of the three above-mentioned genes especially MMP13, EPHA3 and PITX2 are linked to EMT, stroma reorganization and CAF-activity. This study underlines the prognostic

value of DSR and CAF activity in HGSOC as affected patients may not respond to chemotherapy.

Histomorphologic and molecular biomarkers in copy number low and microsatellite instable endometrioid adenocarcinoma – mutual correlations and prognostic impact

F. Stögbauer¹, M. Lautizi^{1, 2}, T. Kacprowski^{3, 4}, H. Bronger^{5, 6}, W. Weichert^{1, 6}, M. Boxberg^{1, 6, 7}

¹*Institut für Pathologie, Technische Universität München, München, Germany*, ²*Lehrstuhl für Experimentelle Bioinformatik - TUM, TUM School of Life Sciences Weihenstephan, Technische Universität München, München, Germany*, ³*Division Data Science in Biomedicine, Peter L. Reichertz Institut für Medizinische Informatik, TU Braunschweig and Hannover Medical School, Braunschweig, Germany*, ⁴*Braunschweig Integrated Centre of Systems Biology (BRICS), Braunschweig, Germany*, ⁵*Klinik und Poliklinik für Frauenheilkunde, Klinikum rechts der Isar, Technische Universität München, München, Germany*, ⁶*Deutsches Konsortium für Translationale Krebsforschung (DKTK), Partnerstandort München und Deutsches Krebsforschungszentrum (DKFZ), Heidelberg, München, Germany*, ⁷*Pathologie München-Nord, München, Germany*

Background

Despite major advances in prognostic stratification of patients with endometrioid adenocarcinoma (EEA), risk assessment of microsatellite instability (MSI) and copy number low (NSMP) cases remains a challenge. Therefore, we aimed to validate recently described morphologic and identify novel molecular biomarkers to improve prognostication.

Methods

Patients with MSI- and NSMP-EEA of the TCGA-UCEC cohort were included (n=227 cases). H&E-stained slides were evaluated regarding histomorphologic parameters (grading, tumor cell budding (TCB), microcystic, elongated, fragmented (MELF) pattern, tumor-stroma-ratio, Klintrup-Mäkinen Score (K/M)). Subsequently, using whole-exome data, mutual correlations of morphologic parameters and somatic mutations were computed. Biomarker genes were identified calculating disease-specific survival (DSS) differences between wildtype and mutated subgroups. The prognostic significance of morphologic and molecular biomarkers was determined in uni- and multivariate analyses. Results were validated in a second independent cohort (MSI/NSMP cases of the CPTAC-cohort, n = 70).

Results

Correlation with somatic mutations discovered n=142 genes for grading (low vs. high), n=57 genes for TCB (absent vs. present) and n=1 gene for K/M (low vs. high). Reactome pathway analyses revealed e.g., associations with collagen organization and interactions with the extracellular matrix. Among morphologic parameters only grading yielded independent impact on DSS in the whole cohort and in the MSI and NSMP subgroups. TCB and MELF were prognostic in the whole cohort and MSI EEA. TSR was prognostic in the whole cohort and the NSMP EEA. Of the significantly altered genes *KMT2D*, *MYH10*, *DNAH11*, *FAT4*, *ANKRD11* and *KIAA1549* showed significant associations with DSS in univariate analyses. After correction (grading, age, FIGO stage) only *FAT4* and *KIAA1549* remained as independent variables in multivariate analyses. Prognostic significance of morphologic and molecular biomarkers could be confirmed in the validation cohort.

Conclusion

Significant mutual correlations between morphologic parameters and molecular alterations were detected. Among the morphologic parameters grading and TCB yielded independent prognostic significance. Uni- and multivariate analyses revealed *FAT4* and *KIAA1549* as potential molecular biomarkers in MSI and NSMP EEA in both the study and the validation cohort. Morphologic and molecular biomarkers could aid in prognostic and therapeutic patient stratification of MSI/NSMP-EEA.

“Recent developments in guidelines in endometrial carcinomas (WHO, ESGO-ESTRO-ESP guidelines, ICCR)”

X. Matias-Guiu

Hospitals Univ. de Bellvitge and Lleida, Pathological Anatomy Service, Barcelona, Spain

During the period 2019-2021, three different guidelines have been updated on endometrial carcinoma, WHO, ESGO-ESTRO-ESP, and ICCR. Of course, they are concordant. This presentation covers the most important issues:

Histological type: The WHO Classification of Tumours distinguishes the following histopathological types of endometrial carcinoma particularly on the basis of their microscopic appearance: 1-Endometrioid carcinoma (EEC), low grade (grades 1,2)/ High grade (grade 3), 2-Serous carcinoma, 3-Clear cell carcinoma, 4-Mixed carcinoma, 5-Undifferentiated carcinoma, 6-Carcinosarcoma, 7- Neuroendocrine carcinomas , 8-Other unusual types.

Histological grade: WHO 2020, recommend binary grading, whereby grade 1 and 2 tumours are classified as low-grade and grade 3 tumours as high-grade

Lympho-vascular space invasion

Molecular classification: The TCGA based molecular classification is able to stratify 4 risk groups using immunohistochemical and molecular analysis. A proposed algorithm tests an endometrial carcinoma first for MSI by immunohistochemistry (or molecular test), followed by analysis of hot spot mutations in POLE of the microsatellite stable tumours and immunohistochemistry for p53 of the microsatellite stable and POLE (hot spot) wild type tumours. The remaining tumours without any of the 3 alterations (MSI, POLE mutation and p53 mutant immunoreactive pattern) are considered copy number low. The prognosis is best for POLE mutant endometrial carcinomas and worst for p53 mutant “serous-like carcinomas, whereas microsatellite instable and copy number low tumours represent an intermediate prognostic group. ESGO-ESTRO-ESP guidelines recommends to use molecular classification for patient risk stratification, in all endometrial cancers, particularly in high grade tumors, but allows omission in low and intermediate risk patients of low grade endometrioid morphology.

Synchronous endometrioid carcinomas of the endometrium and the ovaries: In the three guidelines, it is clearly mentioned that patients with clonally related low-risk tumors be managed conservatively (as if they were two independent primaries) when fulfilling the following criteria: 1) low-grade endometrioid morphology, 2) no more than superficial myometrial invasion, 3) absence of lymphovascular space invasion, and 4) absence of additional metastases

Transcription Factor AP-2beta (*TFAP2B*) - a differentiation marker in breast cancer and human breast epithelial cells

M. Raap, L. Gierendt, H. H. Kreipe, M. Christgen

Medizinische Hochschule Hannover, Institut für Pathologie, Hannover, Germany

Background

Transcription factor AP-2 β (*TFAP2B*) regulates embryonic organ development and is overexpressed in alveolar rhabdomyosarcoma, a rare childhood malignancy. Gene expression profiling has implicated AP-2 β in breast cancer (BC).

Methods

AP-2 β protein expression was assessed in the normal mammary gland epithelium, in various reactive, metaplastic and pre-invasive neoplastic lesions and in two clinical BC cohorts comprising >2000 patients. Human BC cell lines served as functional models to study siRNA-mediated inhibition of AP-2 β .

Results

The normal mammary gland epithelium showed scattered AP-2 β -positive cells in the luminal cell layer. The subpopulation of AP-2 β -positive mammary epithelial cells showed an almost complete, superimposable co-expression with GATA3 and a peculiar intense, ring-like appearing immunoreactivity for CK8/18. Various reactive and pre-invasive neoplastic lesions, including apocrine metaplasia, usual ductal hyperplasia and lobular carcinoma *in situ* (LCIS) showed enhanced AP-2 β expression. In invasive BC cohorts, AP-2 β -positivity was associated with the lobular BC subtype ($P<0.001$), loss of E-cadherin ($P<0.001$), a positive estrogen receptor (ER) status ($P<0.001$), low Ki67 ($P<0.001$), low/intermediate Oncotype-DX recurrence scores ($P<0.001$) and prolonged event-free survival ($P=0.003$). In human BC cell lines, AP-2 β expression was independent from ER-signaling. SiRNA-mediated inhibition of AP-2 β diminished proliferation of lobular BC cell lines *in vitro*.

Conclusion

In summary, AP-2 β is a mammary epithelial differentiation marker. In normal breast epithelium AP-2 β is expressed in the GATA3-positive epithelial subpopulation, which shows a peculiar expression pattern of CK8/18. In breast cancer AP-2 β is preferentially expressed in LCIS and invasive lobular BC. AP-2 β influences tumor cell proliferation and has prognostic implications.

Differential impact of prognostic parameters in hormone receptor-positive lobular breast cancer

M. Christgen¹, O. Gluz^{2, 3}, N. Harbeck^{2, 4}, R. Kates², M. Raap¹, H. Christgen¹, M. Clemens⁵, W. Malter⁶, B. Nuding⁷, B. Aktas⁸, S. Kuemmel^{2, 9}, T. Reimer¹⁰, A. Stefek¹¹, P. Krabisch¹², M. Just¹³, D. Augustin¹⁴, M. Graeser^{2, 3}, F. Baehner¹⁵, R. Wuerstlein^{2, 4}, U. Nitz^{2, 3}, H. Kreipe¹

¹Medizinische Hochschule Hannover, Institut für Pathologie, Hannover, Germany, ²West German Study Group, Moenchengladbach, Germany, ³Ev. Hospital Bethesda, Breast Center Niederrhein, Moenchengladbach, Germany, ⁴University of Munich, Department of Gynecology and Obstetrics, Munich, Germany, ⁵Clinics Mutterhaus der Borromäerinnen, Department of Oncology, Trier, Germany, ⁶Faculty of Medicine and University Hospital of Cologne, Department of Obstetrics and Gynecology, Koeln, Germany, ⁷Evangelical Hospital, Department of Gynecology and Obstetrics, Bergisch Gladbach, Germany, ⁸University of Leipzig, Department of Gynecology, Leipzig, Germany, ⁹Clinics Essen-Mitte, Breast Centre, Essen, Germany, ¹⁰Clinics Suedstadt, Department of Gynecology and Obstetrics, Rostock, Germany, ¹¹Johanniter Clinics Stendal, Breast Center Altmark, Stendal, Germany, ¹²Klinikum Chemnitz, Chemnitz, Germany, ¹³Oncological Practice, Bielefeld, Germany, ¹⁴Breast Centre Ostbayern, Deggendorf, Germany, ¹⁵Genomic Health Inc., Redwood City, Germany

Background

Invasive lobular breast cancer is the second most common breast cancer (BC) subtype. Prognostic parameters (tumor stage, nodal stage, grade, Oncotype DX recurrence score [RS], PR status, Ki67) were retrospectively studied in a large prospective clinical trial encompassing 2585 hormone receptor-positive early BCs (WSG PlanB trial).

Methods

BCs were centrally reviewed and classified as lobular (n=353, 14%) and non-lobular (n=2232, 86%). Median follow-up time was 60 months. Five-year disease-free survival (DFS) estimates were obtained by the Kaplan-Meier method. Prognostic parameters were evaluated using Cox proportional hazard models.

Results

Lobular BC was associated with higher tumor stage, higher nodal stage, lower grade, lower Ki67 and low/intermediate RS. The prevalence of high recurrence scores (RS 26-100) was 3-fold lower in lobular compared to non-lobular BC (8% versus 24%, $P < .001$). Five-year DFS estimates for lobular and non-lobular BC, however, were similar (92.1% and 92.3%, $P = .673$). In multivariate analyses, prognostic parameters for DFS in lobular BC included grade G3 (hazard ratio [HR]=5.06; 95% confidence interval [CI]: 1.91-13.39) and nodal stage pN3 (HR=12.16, 95% CI 3.87-38.24), but not RS. By contrast, prognostic parameters in non-lobular BC included grade G3 (HR=1.65; 95% CI: 1.11-2.44), nodal stage pN3 (HR=3.68; 95% CI: 1.60-8.46) and high RS (HR=2.49; 95% CI: 1.69-3.68).

Conclusion

Lobular BC is associated with low/intermediate RS, although five-year DFS is similar to non-lobular BC. The impact of RS in lobular BC appears to be distinct from that in non-lobular BC. For risk assessment, RS needs to be complemented by clinicopathological parameters for therapy decision making.[1]

Literaturangaben

[1] M. Christgen et al., (2020), Differential impact of prognostic parameters in hormone receptor-positive lobular breast cancer, *Cancer*, 4847-4858, 126

AG06 AG Gynäko- und Mammopathologie II

AG06.08

Highly multiplexed imaging of in situ tumor ecosystems towards precision medicine

B. Bodenmiller

University of Zurich, Department of Quantitative Biomedicine, Zürich, Switzerland

Cancer is a tissue disease. Heterogeneous cancer cells and normal stromal and immune cells form a dynamic ecosystem that evolves to support tumor expansion and ultimately tumor spread. The heterogeneity of this dynamic system is the main obstacle in our attempts to treat and heal the disease. The study of the tumor ecosystem and its cell-to-cell communications is thus essential to enable an understanding of tumor biology, to define new biomarkers to improve patient care, and ultimately to infer for each patient a tailored therapeutic route.

To study and understand the workings of the tumor ecosystem, highly multiplexed image information of tumor tissues is essential. Such multiplexed images will reveal which cell types are present in a tumor, their functional state, and which cell-cell interactions are present. To enable multiplexed tissue imaging, we developed imaging mass cytometry (IMC). IMC currently allows to visualize over 50 antibodies and DNA probes simultaneously on tissues with subcellular resolution. To exploit multiplexed tissue imaging data for research and translation to patients, we have validated hundreds of antibodies, developed multiple computational toolboxes (histocat, cytomapper, steinbock) and introduced novel concepts to describe tissues (cellular neighborhoods, communities and motives). Application of IMC to large patient cohorts of revealed novel spatial biomarkers of disease progression and whether patients might benefit from immunotherapy. Application in an observational clinical trial showed clear clinical usefulness and already indicates benefit for patients.

Implementation of an external quality assessment for *PIK3CA* mutation testing on tumor tissue samples (2021) - lessons learned.

R. Erber¹, L. Dimitrova², C. Schmidt¹, R. Stöhr¹, F. Haller¹, M. Rübner³, P. A. Fasching³, M. W. Beckmann³, M. Hummel⁴, F. Rodepeter⁵, C. Denkert⁵, U. Lehmann⁶, A. Hartmann¹

¹*Institute of Pathology, University Hospital Erlangen, Friedrich-Alexander-Universität Erlangen-Nürnberg (FAU), Comprehensive Cancer Center Erlangen-EMN, Erlangen, Germany,* ²*Qualitätssicherungs-Initiative Pathologie QuIP GmbH, Berlin, Germany,* ³*Department of Gynecology and Obstetrics, University Hospital Erlangen, Comprehensive Cancer Center Erlangen-EMN (CCC ER-EMN), Friedrich-Alexander-Universität Erlangen-Nürnberg (FAU), Erlangen, Germany,* ⁴*Charité-Universitätsmedizin Berlin, Corporate Member of Freie Universität Berlin, Humboldt-Universität zu Berlin and Berlin Institute of Health, Institute of Pathology, Berlin, Germany,* ⁵*Institute of Pathology, UKGM—University Hospital Marburg, Philipps-University Marburg, Marburg, Germany,* ⁶*Institute of Pathology, Hannover Medical School, Hannover, Germany*

Background

Alpelisib, an alpha-specific PI3K inhibitor, is approved for treatment of postmenopausal women/men with *PIK3CA* mutated hormone receptor (HR)-positive, human epidermal growth factor receptor growth factor receptor-2 (HER2)-negative, locally advanced/metastatic breast carcinoma (BC) at disease progression after endocrine therapy. Formalin-fixed paraffin-embedded BC tissue or liquid biopsy can be used for *PIK3CA* mutation analysis. We performed an external quality assessment (EQA) to ensure quality of pathological laboratories regarding *PIK3CA* mutation testing using FFPE BC tissue. Here, we would like to provide insight into EQA preparations and lessons learned.

Methods

For the EQA, n=10 cases were required. Each case required tissue sections for pretesting (1 lead panel + 2 panel institutes) and n=63 EQA test sets, which included 1 tissue section each for hematoxylin&eosin staining and 2 tissue sections each for DNA isolation/*PIK3CA* mutation analysis.

Results

After retrospective identification (starting 02/2021) of n=38 cases of HR-positive HER2-negative BC with sufficient FFPE tissue [inclusion criteria: Diagnosis/treatment at Erlangen University Hospital (UKER); signed informed consent; tumor size ≥18 mm, ≥2 FFPE blocks with adequate tumor cell content], *PIK3CA* mutation analysis was performed for ≥2 FFPE blocks each from n=21/38 cases (04-08/2021) at the lead panel institute (UKER) using a real-time qualitative polymerase chain reaction (PCR) based assay. Due to intratumoral heterogeneity of *PIK3CA* status (n=5/21) and other reasons, n=15/21 cases could be tested for the presence of a *PIK3CA* mutation by the two panel institutes (University Hospital Marburg, Hannover Medical School) using different next generation sequencing panels (NGS) (09/2021). For n=3 cases, NGS panels gave aberrant results compared to PCR assay and led to exclusion of these cases from EQA. Of the final n=12/15 cases with matching *PIK3CA* results, n=10 were selected for inclusion in the EQA according to the number of spare FFPE blocks. The EQA was divided into the “DACH region” (Germany, Austria, Switzerland) and “international” (non-DACH region). Of the n=13 participants from DACH region (12/2021), n=11 successfully passed the EQA (84.6%). International testing is ongoing due to import issues.

Conclusion

In summary, adequate project/time/shipment management and human resources must be planned for when organizing an EQA. For *PIK3CA* mutation testing in FFPE BC tissue, intratumoral heterogeneity must also be considered.

The age-specific differences in histopathological tumor characteristics and TNM classification of breast carcinomas in Quality assured Mamma Diagnostic (QuaMaDi) Program in the State of Schleswig-Holstein in Germany

L.-J. Kramp¹, M. Mathiak-Buchhorn¹, H.-M. Behrens¹, K. W. F. Schäfer^{2, 3}, M. T. van Mackelenbergh³, C. Röcken¹

¹*Universitätsklinikum Schleswig-Holstein, Campus Kiel, Institut für Pathologie, Kiel, Germany,*

²*Universitätsklinikum Schleswig-Holstein, Campus Kiel, Klinik für Radiologie und Neuroradiologie, Kiel,*

Germany, ³Universitätsklinikum Schleswig-Holstein, Campus Kiel, Klinik für Gynäkologie und Geburtshilfe, Kiel, Germany

Background

We explored the hypothesis that high quality standards in diagnostic mammography can lead to an early diagnosis of breast cancers and identifies at risk populations outside screening programs. The histopathological features and distribution of TNM classification were examined in relation to patient age in a large group of women with breast cancers participating in the Quality Assured Mamma Diagnostic (QuaMaDi) Program of the State of Schleswig-Holstein [1].

Methods

Surgical pathological reports were studied for clinicopathological characteristics, receptor status, molecular subtype and tumor stage. Analysis was conducted by dividing the study population into 3 age groups: women under 50 years (pre-screening), 50-69 years (peri-screening) and over 70 years (post-screening).

Results

7.111 biopsies and 2.887 resection specimens were included. Breast cancer was diagnosed in 4.241 (59.7%) cases, one fourth of them in women < 50 years (Figure 1).

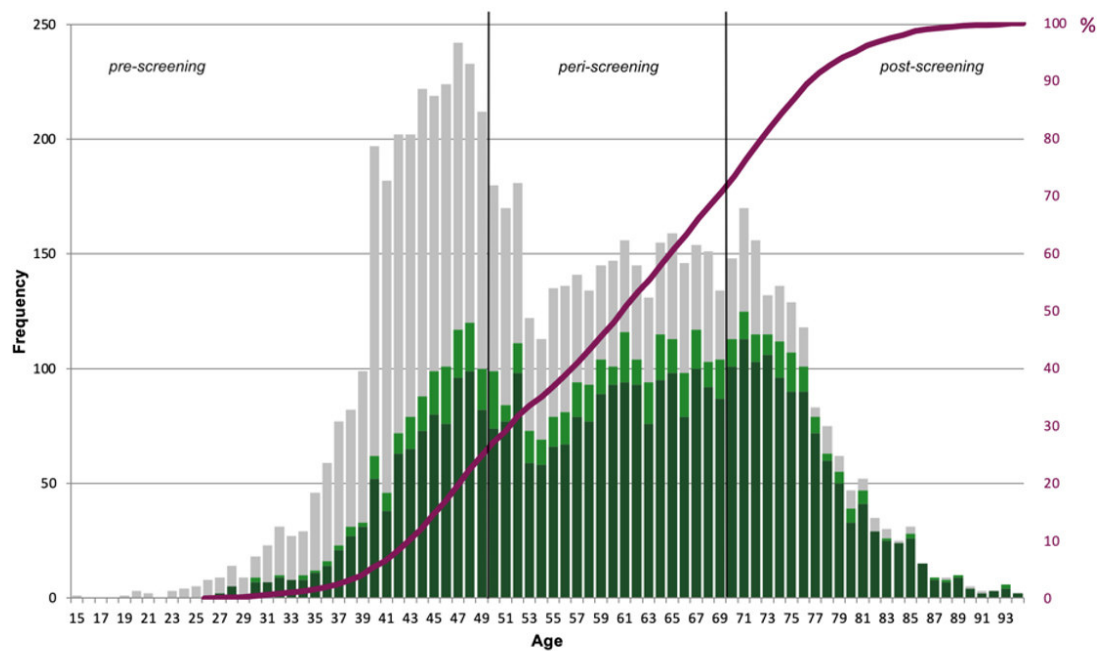
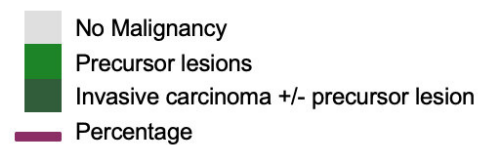


Figure 1: Absolute age distribution of 7.111 histological submissions at the time of diagnosis in the period from 01/01/2005 to 31/12/2016, color-divided by the presence or absence of malignancy. The black vertical lines mark the age groups pre-, peri-, and post-screening. The red curve describes the cumulative proportion of the incidence of invasive breast carcinoma and precursor lesions in relation to age at diagnosis.



Elderly women (>70 years) had more well-differentiated, estrogen receptor (ER)-positive and HER2-negative carcinomas, whereas younger women (<50 years) tended to have more poorly differentiated, ER negative, and HER2-positive carcinomas. 47% of breast carcinoma were luminal B tumors and were most common regardless of age (Table 1).

Table 1: Comparison of histological submissions, which contain one biopsy (= 1 biopsy), based on the age groups pre-, peri- and post-screening.

		Total	Age group			p-value
		n (%)	pre-screening (< 50 years) n (%)	peri-screening (50-69 years) n (%)	post-screening (≥ 70 years) n (%)	
Localization	Total number [n]	6.329				0.007⁽¹⁾
C50.1	109 (1.7)	34 (1.4)	39 (1.5)	36 (2.7)		
C50.2	383 (6.1)	149 (6.2)	162 (6.2)	72 (5.4)		
C50.3	205 (3.2)	80 (3.3)	76 (2.9)	49 (3.7)		
C50.4	1.377 (21.8)	530 (22.1)	586 (22.5)	261 (19.7)		
C50.5	305 (4.8)	128 (5.3)	120 (4.6)	57 (4.3)		
C50.6	36 (0.6)	5 (0.2)	22 (0.8)	9 (0.7)		
C50.8	1.197 (18.9)	463 (19.3)	493 (18.9)	241 (18.2)		
C50.9	2.717 (42.9)	1.008 (42.1)	1.110 (42.6)	599 (45.2)		
B-classification	Total number [n]	4.433				0.000⁽¹⁾
B1	151 (3.4)	78 (4.5)	55 (3.3)	18 (1.7)		
B2	1.408 (31.8)	879 (50.5)	406 (24.7)	123 (11.7)		
B3	283 (6.4)	151 (8.7)	93 (5.6)	39 (3.7)		
B4	53 (1.2)	12 (0.7)	24 (1.5)	17 (1.6)		
B5a	260 (5.9)	73 (4.2)	123 (7.5)	64 (6.1)		
B5b	2.232 (50.3)	536 (30.8)	930 (56.5)	766 (73.2)		
B5c	46 (1.0)	10 (0.6)	16 (1.0)	20 (1.9)		
B5d	0 (0.0)	0 (0.0)	0 (0.0)	0 (0.0)		
Carcinoma	Total number [n]	3.084				
Invasive ductal carcinoma/ invasive carcinoma NST	2.318 (75.2)	573 (81.3)	1.062 (75.4)	683 (70.3)		0.000 ⁽²⁾
Invasive lobular carcinoma	486 (15.8)	82 (11.6)	234 (16.6)	170 (17.5)		0.000 ⁽²⁾
Invasive carcinoma with medullary features/ medullary carcinoma/atypical medullary carcinoma	59 (1.9)	24 (3.4)	22 (1.6)	13 (1.3)		0.175 ⁽²⁾
Other invasive carcinomas	221 (7.1)	26 (3.7)	90 (6.4)	105 (10.9)		
Tubular carcinoma	50 (1.6)	8 (1.1)	27 (1.9)	15 (1.5)		0.004 ⁽²⁾
Invasive papillary carcinoma/ solid papillary carcinoma	36 (1.2)	4 (0.6)	12 (0.9)	20 (2.1)		0.005 ⁽²⁾
Metaplastic carcinoma	6 (0.2)	0 (0.0)	2 (0.1)	4 (0.4)		0.135 ⁽²⁾
Mucinous carcinoma	65 (2.1)	7 (1.0)	17 (1.2)	41 (4.2)		0.000 ⁽²⁾
Other subtypes	36 (1.2)	5 (0.7)	16 (1.1)	15 (1.5)		0.046 ⁽²⁾
Metastases	18 (0.6)	1 (0.1)	12 (0.9)	5 (0.5)		0.006 ⁽²⁾
Other malignant tumors	9 (0.3)	1 (0.1)	4 (0.3)	4 (0.4)		0.368 ⁽²⁾
Multiple malignant carcinomas	1 (0.0)	0 (0.0)	0 (0.0)	1 (0.1)		0.386 ⁽²⁾
In situ-lesions	Total number [n]	529				
Atypical epithelial proliferation of ductal type/ DCIS non high grade /ADH	300 (56.7)	85 (55.2)	150 (56.6)	65 (59.1)		0.000 ⁽²⁾
Ductales carcinoma in situ high grade	171 (32.3)	49 (31.8)	83 (31.3)	39 (35.5)		0.000 ⁽²⁾
Lobular intraepithelial neoplasia	16 (3.0)	4 (2.6)	11 (4.2)	1 (0.9)		0.007 ⁽²⁾
Flat epithelial Atypia	23 (4.3)	13 (8.4)	9 (3.4)	1 (0.9)		0.008 ⁽²⁾
Multiple in situ-carcinoma	19 (3.6)	3 (1.9)	12 (4.5)	4 (3.6)		0.021 ⁽²⁾
Elston & Ellis grading system	Total number [n]	1.602				0.025⁽¹⁾
G1	463 (28.9)	96 (25.3)	186 (28.9)	181 (31.3)		
G2	899 (56.1)	212 (55.8)	358 (55.6)	329 (56.9)		
G3	240 (15.0)	72 (18.9)	100 (15.5)	68 (11.8)		
Estrogen receptor status	Total number [n]	3.503				0.000⁽¹⁾
Negative	508 (14.4)	150 (18.3)	229 (14.1)	127 (11.9)		
Positive (weak expression)	145 (4.1)	45 (5.5)	64 (4.0)	36 (3.4)		
Positive (moderate expression)	661 (18.9)	228 (27.9)	286 (17.7)	147 (13.8)		
Positive (strong expression)	2.191 (62.5)	395 (48.3)	1.040 (64.2)	756 (70.9)		
Progesterone receptor status	Total number [n]	3.497				0.099⁽¹⁾
Negative	950 (27.2)	226 (27.7)	448 (27.7)	276 (25.9)		
Positive (weak expression)	237 (6.8)	43 (5.3)	123 (7.6)	71 (6.7)		
Positive (moderate expression)	838 (24.0)	178 (21.8)	395 (24.4)	265 (24.9)		
Positive (strong expression)	1.472 (42.1)	369 (45.2)	651 (40.3)	452 (42.5)		
HER2-Status	Total number [n]	3.068				0.000⁽¹⁾
Negative	2.656 (86.6)	585 (83.1)	1.189 (84.9)	882 (81.6)		
Positive	412 (13.4)	119 (16.9)	212 (15.1)	81 (8.4)		
Positive (% within HER2-Status)		119 (28.9)	212 (51.5)	81 (19.7)		
Ki-67-index (grouped)	Total number [n]	927				0.160⁽¹⁾
≤ 10	110 (11.9)	22 (10.0)	41 (11.3)	47 (13.7)		
10-20	219 (23.6)	43 (19.5)	83 (22.9)	93 (27.1)		
20-25	105 (11.3)	25 (11.3)	42 (11.6)	38 (11.1)		
25-50	299 (32.3)	75 (33.9)	119 (32.8)	105 (30.6)		
> 50	153 (16.5)	48 (21.7)	63 (17.4)	42 (12.2)		
Unclassifiable	41 (4.4)	8 (3.6)	15 (4.1)	18 (5.2)		
IHC based molecular subtypes	Total number [n]	1.322				0.000⁽¹⁾
Triple-negative (ER- PR- HER2-)	301 (22.8)	99 (28.2)	123 (22.1)	79 (19.1)		
Luminal A	297 (22.5)	60 (17.1)	108 (19.4)	129 (31.2)		
Luminal B	622 (47.0)	160 (45.6)	277 (49.7)	185 (44.7)		
HER2-positive	102 (7.7)	32 (9.1)	49 (8.8)	21 (5.1)		

⁽¹⁾ Fishers exact test

⁽²⁾ Chi square test

70.4% of resected specimen had pT1 stage. Nodal negative were 71.2% [2].

Conclusion

In QuaMaDi breast cancer was diagnosed at an early and potentially curable stage of disease due to high-quality standards in diagnostic mammography. In addition, regardless of age, an increased number of prognostically unfavorable molecular subtypes were detected. Thus, QuaMaDi helps to identify at risk populations. QuaMaDi significantly improves diagnostic mammography and complements mammography screening programs and the program should be continued.

Literaturangaben

[1] Katalinic, A, Bartel, C, Raspe, H, Schreer, I, (2007), Beyond mammography screening: quality assurance in breast cancer diagnosis (The QuaMaDi Project), *British Journal of cancer*, 157-161, 96(1),
<https://www.nature.com/articles/6603506>, 2022-02-06

[2] Kramp, LJ, Mathiak, M, Behrens, HM, Schäfer, FW, van Mackelenbergh, M, Röcken, C, (2022), The age-specific differences in histopathological tumor characteristics and TNM classification of breast carcinomas in Quality assured mamma diagnostic (QuaMaDi) program in the state of Schleswig-Holstein in Germany, *Journal of Cancer Research and Clinical Oncology*, 387–400, 148(2),
<https://link.springer.com/article/10.1007%2Fs00432-021-03841-x>, 2022-02-06

Class II tumor suppressor genes in breast cancer can be classified according to intrinsic molecular subtypes and may be suitable for risk classification of *ductal carcinoma in situ* (DCIS)

C. Kunze¹, S. Villwock¹, D. C. Dehelean¹, L. Hilgers¹, S. von Stillfried¹, F. Steib¹, S. Mühl², R. Knüchel-Clarke¹, C. Kuhl³, E. Wardelmann², E. Dahl^{1, 4}

¹*Institute of Pathology, University Hospital RWTH Aachen, Aachen, Germany*, ²*Institute of Pathology, University Hospital Münster, Münster, Germany*, ³*Department of Diagnostic and Interventional Radiology, University Hospital RWTH Aachen, Aachen, Germany*, ⁴*RWTH centralized Biomaterial Bank (RWTH cBMB), Medical Faculty of the RWTH Aachen University, Aachen, Germany*

Background

Since the introduction of systematic mammography screening, the incidence of *ductal carcinoma in situ* (DCIS) has increased by more than 5-fold. Currently, guidelines recommend at least local treatment for all DCIS similar to that of invasive cancers. However, it is well established that a substantial proportion of DCIS will not progress to invasive cancer even if left untreated. Unfortunately, we are currently unable to predict which DCIS will progress, causing considerable overtreatment. Class II tumor suppressor genes (C2TSGs) inactivated by promoter DNA hypermethylation are important and early players in breast cancer initiation and progression. Here we present a novel strategy how prognostic C2TSGs may be applicable for DCIS risk classification.

Methods

Identification and filtering procedures for novel putative C2TSGs from the Cancer Genome Atlas (TCGA) database were described in last years DGP contribution by Dehelean et al. (see ViPa2021 abstract book). Molecular classification of these C2TSGs according to the intrinsic breast cancer subtypes was performed using the webinterface RosettaSX (www.rosettasx.com). Loss of expression of the proteins encoded by C2TSGs was analyzed by immunohistochemistry using tissue microarrays generated from 143 DCIS identified from Aachen and Münster. DCIS expression patterns were compared to pathological and clinical data using SPSS.

Results

We found that epigenetically silenced tumor suppressor genes (C2TSGs) in invasive breast cancer samples can be broken down in three subgroups showing loss of expression in accordance with intrinsic molecular subtypes. While genes belonging to group 1 are lost in TNBC and luminal B tumors, genes belonging to group 2 are only lost in TNBC, and those belonging to group 3 are only lost in luminal B tumors. Analyzing protein distribution of members of each group in DCIS revealed strikingly different expression patterns, indicating that such epigenetic features may provide prognostic information about DCIS and their potential regarding progression to invasive cancer.

Conclusion

A molecular classification of DCIS according to expression loss of epigenetically silenced tumor suppressor genes (C2TSGs) in line with potential later intrinsic molecular subtypes may be helpful for further DCIS risk classification and thus future therapy stratification.

Funding

This project has received funding from the EU Horizon 2020 program under grant agreement No. 667211 (Biomarker team within the HYPMED project)

Impact of TROP-2 and its cellular localization on prognosis of breast cancer – an analysis of 1164 tumors from a prospective clinical trial

C. C. Westhoff¹, J. Rüschhoff², P. Jank¹, B. V. Sinn³, A. Pehl¹, R.-P. Henke⁴, A. Hattesohl¹, F. Marmé⁵, J. Furlanetto⁶, S. Loibl⁶, C. Denkert¹

¹Philipps-University Marburg and University Hospital Marburg (UKGM) — Universitätsklinikum Marburg, Institut für Pathologie, Marburg, Germany, ²Elisabeth Krankenhaus, Kassel, Germany, ³Charité - Universitätsmedizin Berlin, Institut für Pathologie, Berlin, Germany, ⁴Klinikum Oldenburg, Oldenburg, Germany, ⁵Medizinische Fakultät Mannheim, Universität Heidelberg, Universitätsfrauenklinik Mannheim, Mannheim, Germany, ⁶German Breast Group, Neu-Isenburg, Germany

Background

TROP-2 (trophoblast cell surface antigen 2) is involved in regulating cancer growth and invasion in different tumour types. TROP-2 is also a potent therapeutical target, being addressed by antibody drug conjugates (ADC). This study evaluates the impact of TROP-2 on breast cancer (BC) prognosis in high-risk, node-positive BC of the German adjuvant intergroup node-positive (GAIN) cohort.

Methods

Tumor samples from patients included in the GAIN trial were used. Tissue microarrays (TMA) were generated from formalin-fixed paraffin embedded (FFPE) pretherapeutic surgical resection tissue with one spot per patient (n= 1362). Immunohistochemical staining was performed with human TROP-2 antibody AF650. Membranous and cytoplasmic expression of TROP-2 in invasive tumor cells was assessed in percent. The Cutoff Finder web application was used for identification of the best cutoff point according to disease-free survival (DFS) and overall survival (OS). For n=1269 patients, data on hormone receptor (HR) and HER2 status were available. The association of membranous (m)TROP-2 expression with molecular intrinsic subgroups, TNM stages, age, proliferation and HR status was statistically tested.

Results

For 1164 TMA spots valid TROP-2 evaluation was available, with 62.2% luminal/HER2-negative (n=724), 22.3% HER2+/HRany (n= 260) and 15.5% triple-negative BC (TNBC) (n=180). The Cutoff Finder identified 2% as best cutoff for mTROP-2 expression across all molecular subgroups, whereas no defined cutoff was identified for cytoplasmic TROP2-expression. mTROP-2 < 2% was significantly associated with luminal/HER2-negative tumors (p=0.017) and poor differentiation (G3, p=0.007). In multivariate Cox regression analysis, mTROP-2 ≥ 2% in invasive tumor cells was associated with improved DFS and OS (for DFS hazard ratio (hr) 0.448 [95%CI 0.313-0.643], p<0.001, for OS hr 0.433 [95%CI 0.275-0.680], p<0.001). Detailed data for the different molecular subtypes will be presented.

Conclusion

Our results show that mTROP2 is commonly expressed in breast cancer and that an increased expression of TROP2 is associated with better survival in breast cancer. The results are relevant for biomarker strategies for future therapeutic concepts. In the SASCIA trial, investigating Sascituzumab TROP2 is prospectively

assessed.

E-cadherin to P-cadherin switching in lobular breast cancer with tubular elements

M. Christgen¹, S. Bartels¹, J. L. van Luttikhuisen², J. Bublit², L. Rieger¹, H. Christgen¹, H. Stark¹, B. Sander¹, U. Lehmann¹, D. Steinemann², P. W. Derksen³, H. Kreipe¹

¹*Medizinische Hochschule Hannover, Institut für Pathologie, Hannover, Germany*, ²*Medizinische Hochschule Hannover, Humangenetik, Hannover, Germany*, ³*University Medical Center Utrecht, Department of Pathology, Utrecht, The Netherlands*

Background

Loss of E-cadherin due to mutation of the *CDH1* gene is a characteristic feature of invasive lobular breast cancer (ILBC). Beta-catenin, which binds to E-cadherin, is simultaneously downregulated, reflecting disassembly of adherens junctions (AJs) and loss of cell adhesion. E-cadherin to P-cadherin expression switching can rescue AJs and cell adhesion. However, P-cadherin has not been implicated in ILBC, so far.

Methods

We characterized thirteen ILBCs with exceptional histomorphology, which we termed ILBCs with tubular elements. The *CDH1* status was determined by next generation sequencing and whole-genome copy number (CN) profiling. Expression of various cadherins was assessed by immunohistochemistry.

Results

ILBCs with tubular elements were ER-positive (13/13) and HER2-negative (13/13) and harbored deleterious *CDH1* mutations (11/13) accompanied by loss of heterozygosity due to deletion of chromosome 16q22.1 (9/11). E-cadherin expression was lost or reduced in non-cohesive tumor cells and in admixed tubular elements (13/13). Beta-catenin expression was lost in non-cohesive tumor cells, but was retained in tubular elements (11/13), indicating focal rescue of AJ formation. N-cadherin and R-cadherin were always negative (0/13). Strikingly, P-cadherin was commonly positive (12/13) and immunoreactivity was accentuated in tubular elements. In a reference cohort of invasive mammary carcinomas, P-cadherin-positive cases (36/268, 13%) were associated with triple-negative non-lobular breast cancer ($P < 0.001$). Compared with ILBCs from the reference cohort, P-cadherin expression was more common in ILBCs with tubular elements (12/13 versus 7/84, $P < 0.001$).

Conclusion

In summary, E-cadherin to P-cadherin switching occurs in a subset of ILBCs. P-cadherin is the molecular determinant of a mixed-appearing histomorphology in ILBCs with tubular elements.[1]

Literaturangaben

[1] M. Christgen et al., (2020), E-cadherin to P-cadherin switching in lobular breast cancer with tubular elements, *Mod Pathol*, 2483-2498, 33

Inter-observer agreement for the histological diagnosis of invasive lobular breast cancer – An international concordance study

M. Christgen¹, L. D. Kandt¹, W. Antonopoulos², S. Bartels¹, M. R. van Bockstal³, M. Bredt¹, M. J. Brito⁴, H. Christgen¹, C. Colpaert⁵, B. Cserni⁶, G. Cserni⁷, M. E. Daemrich⁸, R. Danebrock⁹, F. Dedeurwaerdere¹⁰, C. H. M. van Deurzen¹¹, R. Erber¹², C. Fathke¹³, H. Feist¹⁴, M. Fiche¹⁵, C. A. Gonzalez¹⁶, N. ter Hoeve¹⁷, L. Kooreman¹⁸, T. Krech^{19, 20}, G. Kristiansen²¹, J. Kulka²², F. Laenger¹, M. Lafos¹, U. Lehmann¹, M. D. Martin-Martinez²³, S. Mueller¹, E. Pelz²⁴, M. Raap¹, A. Ravarino²⁵, T. Reineke-Plaass¹, N. Schaumann¹, A.-M. Schelfhout²⁶, M. de Schepper²⁷, J. Schlue¹, K. Van de Vijver²⁸, W. Waelpu²⁹, A. Wellmann³⁰, M. Graeser^{31, 32}, O. Gluz^{31, 32}, S. Kuemmel^{31, 33}, U. Nitz^{31, 32}, N. Harbeck^{31, 34}, C. Desmedt³⁵, G. Floris³⁶, P. W. Derksen¹⁷, P. J. van Diest¹⁷, A. Vincent-Salomon³⁷, H. Kreipe¹

¹Medizinische Hochschule Hannover, Institut für Pathologie, Hannover, Germany, ²University Clinics Heidelberg, Institute of Pathology, Heidelberg, Germany, ³Cliniques Universitaires Saint-Luc, Brussel, Belgium, ⁴Champalimaud Foundation, Pathology and Breast Unit, Lisboa, Portugal, ⁵Universitair Ziekenhuis Leuven, Department of Pathology, Leuven, Belgium, ⁶TNG Technology Consulting GmbH, Budapest, Hungary, ⁷University of Szeged, Department of Pathology, Budapest, Hungary, ⁸Group Practice for Pathology Schweinfurt, Schweinfurt, Germany, ⁹Johannes Wesling Clinics Minden, Institute of Pathology, Minden, Germany, ¹⁰AZ Delta, Laboratorium voor pathologie, Roeselare, Belgium, ¹¹Erasmus MC Cancer Institute, Department of Pathology, Rotterdam, The Netherlands, ¹²University Hospital Erlangen, Institute of Pathology, Erlangen, Germany, ¹³Martin-Luther-University Halle-Wittenberg, Institute of Pathology, Halle (Saale), Germany, ¹⁴Diakonissenkrankenhaus Flensburg, Institute of Pathology, Flensburg, Germany, ¹⁵Aurigen SA, Institute of Pathology Aurigen, Lausanne, Switzerland, ¹⁶University College Dublin, Conway Institute of Biomolecular and Biomedical Research, Dublin, Ireland, ¹⁷University Medical Center Utrecht, Department of Pathology, Utrecht, The Netherlands, ¹⁸Maastricht University Medical Center, Institute of Pathology and GROW, Maastricht, The Netherlands, ¹⁹University Clinics Hamburg-Eppendorf, Institute of Pathology, Hamburg, Germany, ²⁰Gemeinschaftspraxis Prof. Dr. med.R.H. Krech, Osnabrueck, Germany, ²¹University Clinics Bonn, Institute of Pathology, Bonn, Germany, ²²Semmelweis University Budapest, 2nd Department of Pathology, Budapest, Germany, ²³Institut de Pathologie et Genetique Gosselies, Gosselies, Belgium, ²⁴Institute of Pathology Viersen, Viersen, Germany, ²⁵University of Cagliari, Institute of Pathology, Cagliari, Italy, ²⁶OLV Ziekenhuis Aalst, Department of Pathology, Aalst, Belgium, ²⁷University Hospitals Leuven, Department of Pathology, Leuven, Belgium, ²⁸Cancer Research Institute Ghent, Ghent, Belgium, ²⁹UZ Brussel, Brussel, Belgium, ³⁰Institute of Pathology Celle, Celle, Germany, ³¹West German Study Group, Moenchengladbach, Germany, ³²Ev. Hospital Bethesda, Breast Center Niederrhein, Moenchengladbach, Germany, ³³Clinics Essen-Mitte, Breast Centre, Essen, Germany, ³⁴University of Munich, Department of Gynecology and Obstetrics, Munich, Germany, ³⁵KU Leuven, Laboratory for Translational Breast Cancer, Leuven, Belgium, ³⁶KU Leuven, Department of Imaging and Radiology, Leuven, Belgium, ³⁷PSL Research University, Pathology-Genetics-Immunology Department, Paris, France

Background

Invasive lobular breast cancer (ILC) is a special breast cancer (BC) subtype and is driven by loss of E-cadherin. Correct classification of ILC is important for patient treatment. This study assessed the agreement among pathologists for the diagnosis of ILC.

Methods

Two sets of hormone receptor (HR)-positive/HER2-negative BCs were independently reviewed by participating pathologists. In set A (61 cases), participants were provided with hematoxylin/eosin (HE)-stained sections. In set B (62 cases), participants were provided with HE-stained sections and E-cadherin immunohistochemistry. Tumor characteristics were balanced. Participants classified specimens

as non-lobular BC *versus* mixed BC *versus* ILC. Pairwise inter-observer agreement and agreement with a reference diagnosis was determined with Cohen's kappa statistics. Subtype calls were also correlated with the *CDH1*/E-cadherin mutation status.

Results

Thirty-five pathologists completed both sets, providing 4305 subtype calls. Pairwise inter-observer agreement was moderate in set A (median $k=0.58$), and substantial in set B (median $k=0.75$, $P<0.001$). Agreement with the reference diagnosis was substantial in set A (median $k=0.67$), and almost perfect in set B (median $k=0.86$, $P<0.001$). The median frequency of *CDH1*/E-cadherin mutations in specimens classified as ILC was 65% in set A, and 73% in set B ($P<0.001$). Cases with variable subtype calls included E-cadherin-positive ILCs harboring *CDH1* missense mutations, and ILCs with tubular elements due to E- to P-cadherin switching.

Conclusion

Subtyping of BC as ILC achieves almost perfect agreement with a reference diagnosis, if assessment is supported by E-cadherin immunohistochemistry. *CDH1* missense mutations, and E- to P-cadherin switching in ILC with tubular elements are sources of discordant classification.[1]

Literaturangaben

[1] M. Christgen et al., (2021), Inter-observer agreement for the histological diagnosis of invasive lobular breast carcinoma, J Pathol Clin Res, In press

AG07 AG Dermatopathologie

AG07.01

Dermatopathology of COVID-19 infection and vaccine-related cutaneous manifestations.

M. T. Fernández Figueras

*Hospital Universitari General de Catalunya. Grupo Quironsalud & Universitat Internacional de Catalunya,
Director of the Department of Anatomic Pathology, Catalunya, Spain*

The COVID-19 pandemic has been associated to a rise in dermatological disorders caused by the infection or its vaccination. Among COVID-19 patients, many developed distinctive cutaneous lesions, other presented a secondary activation or reactivation of immune-related processes, viral infections, or neoplasia and finally some developed drug eruptions. The distinctive cutaneous dermatological manifestations of COVID-19 infection have been divided into 5 main clinical groups:

1. Chilblains tend to involve younger individuals with a robust interferon response and is associated to an excellent outcome. These lesions are almost indistinguishable from idiopathic perniosis or chilblain lupus although tend to present more frequently intense vascular damage with fibrin deposition, purpura, and thrombosis, as well as higher basal vacuolar change.
2. Livedoid and necrotic lesions were initially misinterpreted as belonging to the same spectrum of chilblains. However, they are typical of older individuals and associated with cytokine storm systemic thrombotic events and poor prognosis. Typically, these lesions present extensive areas of ischemia with microthrombi occluding small and medium sized vessels. Inflammation is minimal in these biopsies.
3. Vesicular eruptions can range from widespread lesions that can have a varicella-like appearance (showing often peculiar form of keratinocyte ballooning and apoptosis) to lesions involving mostly the trunk that are identical to Grover disease.
4. Urticarial lesions were observed often in patients with poor prognosis and microscopically showed combination of histological patterns (lichenoid, urticarial, spongiotic, etc). Eosinophilia was common, raising the differential diagnosis with drug eruption
5. Maculopapular eruptions are a heterogeneous group of lesions with morbilliform, purpuric, pityriasis-rosea-like, erythema multiforme-like patterns and others. Oral lesions, also frequent, were histologically non-specific.

Regarding vaccination, the COVID-arm is one the most prevalent reactions with a CD4 infiltrate, spongiosis and in some cases eosinophilia. Also, some individuals presented spongiotic lesions of V-REPP (vaccine-related eruption of papules and plaques), bullous pemphigoid-like lesions or dermal hypersensitivity reactions as well as manifestations similar to those triggered by the COVID-19 infection.

Histopathological and immunohistochemical study of PRAME expression in different benign, dysplastic and malignant primary and metastatic melanocytic lesions

M. Abbas¹, O. Bettendorf², J. de Jonge³

¹Uniklinikum Münster, Gerhard-Domagk Institut für Pathologie, Münster, Germany, ²Institut für Pathologie und Zytologie, Schüttorf, Germany, ³Institut für Pathologie und Zytologie, Pathologie, Schüttorf, Germany

Background

Immunotherapy is a revolutionary strategy of cancer treatment. There is an antibody-based targeting Therapies that targeting growth-factor receptors such as against EGFR, Her2-neu and CD20. Because of developing resistance, there is immunotherapy using immune checkpoint inhibitors against PDL1 and cytotoxic T-lymphocyte-associated antigen 4 (CTLA-4). PRAME (PReferentially expressed Antigen in MElanoma) is one of cancer testis antigens (CTAs). Adoptive T-cell-therapy is modulated against CTAs with regard to their restricted expression in somatic normal tissues, re-expression in many cancer types and immunogenic nature. The study is an attempt to get insight of the practical use of immunotherapy against PRAME in malignant lesions.

Methods

100 cases with different subtypes of benign nevi, dysplastic nevi, primary and metastatic malignant melanoma were examined histopathologically and submitted to immunohistochemical study with focussing in PRAME expression. Other markers were added (HMB-45, Melan-A, P16 and Ki67) to ensure the diagnosis and to compare with the PRAME expression. 10 control cases were added including dermatofibroma, atypical fibroxanthoma and papillary renal cell carcinoma

Results

PRAME expression was positive in all cases in situ melanoma. It is expressed in 68% of primary malignant melanoma and 50% in metastatic melanoma. 70% of dysplastic nevi were negative. It is expressed also in atypical fibroxanthoma but it is negative in all examined papillary renal cell carcinoma

Conclusion

We suggest PRAME immunohistochemistry (IHC) as a marker to predict the liability for immunotherapy in the malignant melanocytic lesions and in situ melanoma. A cocktail of immunohistochemical markers should be used in the diagnosis of difficult cases and to avoid misdiagnosis and pitfalls

Mutational Profiling in Spindle Cell and Desmoplastic Melanoma

S. E. Weißinger^{1, 2}, J. C. Thierauf^{3, 4}, J. K. Lennerz⁵

¹*Institute of Pathology, Alb Fils Kliniken GmbH, Göppingen, Germany,* ²*Institute of Pathology, Universityhospital Ulm, Ulm, Germany,* ³*Massachusetts General Hospital, Molecular Pathology Unit, Boston, United States of America,* ⁴*University Heidelberg, Heidelberg, Germany,* ⁵*Massachusetts General Hospital, Center for integrated diagnostics, Boston, United States of America*

Background

Spindle cell (SM) - and desmoplastic melanoma (DM) are subtypes of melanoma which differ in clinical, histomorphological, and genetic features from other types of melanomas. The genomic profile, especially of spindle cell melanoma, has rarely been examined.

Methods

To evaluate the genomic profile of SM and DM, we analyzed six SM and six DM formalin fixed and paraffin embedded patient samples from a previous described cohort of spindle cell- and desmoplastic melanomas[1][2]. Furthermore, we performed anchored multiplex PCR for next generation sequencing (NGS) to detect fusion transcripts, single nucleotide variants, insertions, deletions, and copy number variations in a panel of 39 different genes, including *BRAF* or *NRAS* as potentially therapeutically relevant target genes.

Results

NGS revealed mutations in *BRAF*, co-occurring with alterations in *TP53*, *PTEN* or *KRAS* in 2/12 (17%) of the cases. *NRAS* and/or *PIK3CA* mutations could be found in 2/12 (17%) of the cases, whereas a mutually exclusive mutation in *TP53* could be detected also in 2/12 (17%) of the cases. We did not identify *KIT* mutations or fusion transcripts. Furthermore, there was no significant difference in mutational signature between SM and DM; however, in this cohort, *BRAF* mutations occurred more frequently in SM (2/6) than in DM (0/6).

Conclusion

Genetic distinction of SM and DM will require more comprehensive approaches. Prognostically relevant and/or targetable genetic alterations were found in 75% (9/12) of the cases, arguing for mutational profiling, when clinically indicated.

Literaturangaben

[1] Weissinger, S.E. et al, (2014), A diagnostic algorithm to distinguish desmoplastic from spindle cell melanoma, Off. J. U. S. Can. Acad. Pathol. Inc, Mod. Pathol.

[2] Weissinger, S.E. et al, (2017), Performance Testing of RREB1, MYB, and CCND1 Fluorescence In Situ Hybridization in Spindle-Cell and Desmoplastic Melanoma Argues for a Two-Step Test Algorithm., Int. J. Surg. Pathol.

AG08 AG Thoraxpathologie I

AG08.01

Does alveolar fibroelastosis recur after lung transplantation

P. Braubach¹, C. Werlein¹, P. Tittmann¹, J.-C. Kamp^{1,2}, F. Länger¹, S. Dettmer³, C. Müller⁴, J. Gottlieb², D. Jonigk¹

¹Medizinische Hochschule Hannover, Institut für Pathologie, Hannover, Germany, ²Medizinische Hochschule Hannover, Klinik für Pneumologie, Hannover, Germany, ³Medizinische Hochschule Hannover, Abteilung für Radiologie, Hannover, Germany, ⁴Medizinische Hochschule Hannover, Klinik für Pädiatrische Pneumologie, Hannover, Germany

Background

Alveolar fibroelastosis (AFE) is a distinct form of interstitial pulmonary fibrosis and most likely a stereotypic reaction to injury. It is characterized by fibrous obliteration of the alveolar spaces accompanied by hyperelastosis of the remaining alveolar septa.

AFE is the dominant form of interstitial fibrosis found in the restrictive form of chronic allograft dysfunction (rCLAD) which is associated with a poor prognosis. Besides this, AFE can also be found in primary and secondary pleuroparenchymal fibroelastosis and as additional pattern in other forms of interstitial lung diseases where it also often heralds poor outcome. From informal review of lung resections, we have learned that AFE type scarring can be observed in contexts of repeated acute inflammation – for example cystic fibrosis. Failed clearing of fibrinous exudate after lung injury – e.g. by dysfunctional matrix-metalloproteinase type enzymes - is hypothesized to be a cause for the AFE type fibrotic remodelling. Therefore, we hypothesized that if host derived factors play an important role in the development of AFE an association between AFE in the recipient lung and the transplanted lung might be observable.

Methods

To investigate a potential association between AFE in donor lung and lung transplant we compiled a unique collective of patients from over 30 years of lung transplantation at Hannover Medical School receiving both a lung transplantation and a re-lung transplantation.

Results

We characterized presence and distribution of AFE in both the explanted donor lung and the explanted lung transplant. In this we also provide the most in-depth morphological characterization of AFE distribution and phenotype in rCLAD to date.

Conclusion

The results from this study will give evidence to answer the clinically relevant question: Does alveolar fibroelastosis recur after lung transplantation.

The challenge of long-term cultivation of human precision-cut lung slices

E. Preuß

Medical School Hannover, Hannover, Germany

Background

Human precision-cut lung slices (PCLS) have been established as a fast and reliable high-throughput tool for numerous toxicological, pharmacological or immunological studies and they have the potential to reduce the number of animals needed to analyze new therapeutics. However, in contrast to animals, the maximal cultivation time is limited. Even though in most studies a cultivation period of less than one week is considered sufficient e.g. in asthma research, more complex diseases that involve actual remodeling of the pulmonary architecture, such as fibrotic pulmonary diseases, require longer cultivation periods. So far, data regarding long-term cultivation of human PCLS is very limited.

Methods

To evaluate whether PCLS are suitable for long-term studies, we cultivated over 1.500 human PCLS from 16 different donors with different pathological backgrounds under standardized, serum-free conditions for up to 28 days and assessed the preservation of viability, the integrity of different tissue compartments and the transcriptome to an unprecedented extent.

Results

In doing so, we could show that even though viability was fine over the whole course of cultivation, the different compartments of the PCLS (airways, alveoli and vasculature) suffer from different degrees of cell loss during long-term cultivation. A rather unexpected finding was the significantly increasing manifestation of keratinizing squamous metaplasia of the alveolar epithelium, already starting to manifest within the first week of cultivation. Interestingly, the manifestation of squamous metaplasia was twice as frequent in PCLS from fibrotic as from control lung tissue, offering the opportunity of studying dysregulated repair mechanisms of the abnormal mesenchyme in pulmonary fibrosis.

Conclusion

Overall, our study provides a comprehensive overview of histomorphological and -pathological changes that occur during long-term cultivation of PCLS

Lung Pathology of postCOVID

K. Steinestel¹, A. Czech¹, F. Kirchhoff², P. Boor³, C. Hackenbroch⁴, W. Bloch⁵, D. Gagiannis⁶

¹Bundeswehrkrankenhaus Ulm, Pathologie und Molekularpathologie, Ulm, Germany, ²Universität Ulm, Molekulare Virologie, Ulm, Germany, ³Universitätsklinikum Aachen, Institut für Pathologie, Aachen, Germany, ⁴Bundeswehrkrankenhaus Ulm, Radiologie, Ulm, Germany, ⁵Deutsche Sporthochschule Köln, Köln, Germany, ⁶Bundeswehrkrankenhaus Ulm, Klinik I Innere Medizin, Sektion Pneumologie, Ulm, Germany

Background

Coronavirus disease 2019 (COVID-19) emerged to a worldwide pandemic in 2020 and there is uncertainty about possible long-time sequelae. About 10% of patients present with persistent fatigue, muscle weakness, lung diffusion impairment and chest imaging abnormalities >12 weeks not only after severe, but also after mild and moderate course of SARS-CoV-2 infection (defined by the WHO as postCOVID condition). The aim of this study was to evaluate lung pathology in a cohort of 51 postCOVID patients.

Methods

We prospectively enrolled 51 previously healthy patients (without a history of autoimmune disease) and with persistent respiratory symptoms after mild/ moderate SARS-CoV-2 infection without hospitalization (median age, 40 yrs). We performed full clinical evaluation including pulmonary function tests, high-resolution computed tomography (HR-CT) and serology for ANA/ENA (indirect immunofluorescence/ immunoblot). In 43 patients, transbronchial biopsies (TBBs) were taken for histopathological and ultrastructural assessment of interstitial lung disease (ILD). Broncho-alveolar lavage (BAL) fluid samples are currently analyzed by legendplex immunoassay.

Results

HRCT patterns were heterogeneous including ground glass opacities, bronchial wall thickening and enlarged peripheral pulmonary arteries. Autoantibodies (ANA titers $\geq 1:320$ and/or positive immunoblot for specific ENAs: Scl-70, PM-Scl, dsDNA, SS-B and Histone) were detected in 15/51 patients. In 32/43 cases, histopathological assessment of TBBs revealed interstitial lymphocytosis (NSIP-like) with alveolar hemorrhage and/or fibrinous exudate. CD4/CD8 ratio in tissue and BAL was 2.6 and 2.5, respectively. Ultrastructural assessment showed interstitial collagen deposition.

Conclusion

The majority of patients with postCOVID condition shows small airway inflammation and interstitial collagen deposition. The observed histopathologic and serologic parallels between postCOVID and connective tissue disease-associated ILD (CTD-ILD)/ interstitial pneumonia with autoimmune features (IPAF) indicate a possible use of antiinflammatory or antifibrotic therapies in the setting of persistent pulmonary symptoms after SARS-CoV-2 infection.

Comparative analysis of fibroblastic foci in patients with idiopathic pulmonary fibrosis and pulmonary sarcoidosis

L. Neubert^{1,2}, J. C. Kamp^{2,3}, H. Stark^{1,2}, J. B. Hinrichs^{2,4}, C. Boekhoff¹, A. D. Seidel¹, F. Ius^{2,5}, A. Haverich^{2,5}, J. Gottlieb^{2,3}, T. Welte^{2,3}, P. Braubach^{1,2}, F. Laenger^{1,2}, M. M. Hoeper^{2,3}, M. P. Kuehnelt^{1,2}, D. D. Jonigk^{1,2}

¹Medizinische Hochschule Hannover, Institut für Pathologie, Hannover, Germany, ²Deutsches Zentrum für Lungenforschung (DZL), Biomedical Research in Obstructive Lung Disease Hannover (BREATH), Hannover, Germany, ³Medizinische Hochschule Hannover, Klinik für Pneumologie, Hannover, Germany, ⁴Medizinische Hochschule Hannover, Institut für Diagnostische und Interventionelle Radiologie, Hannover, Germany, ⁵Medizinische Hochschule Hannover, Klinik für Herz-, Thorax-, Transplantations- und Gefäßchirurgie, Hannover, Germany

Background

Fibroblastic foci (FF) are characteristic features of usual interstitial pneumonia / idiopathic pulmonary fibrosis (UIP/IPF) and thought to represent a key mechanism of pathogenesis. Hence, FF have a high impact on UIP/IPF diagnosis in current guidelines. However, FF also occur in other fibrotic pulmonary diseases while there is a gap in knowledge regarding the underlying molecular mechanisms.

In this work, we analyzed the compartment-specific gene expression of FF in IPF and sarcoidosis in order to elucidate molecular similarities and differences.

Methods

N=6 IPF patients and n=6 sarcoidosis patients were used for laser capture microdissection, mRNA expression analysis, and immunostaining. Biological pathways were analyzed using two different gene expression databases. As control samples, we used healthy downsizing tissue from n=21 lung transplants.

Results

The mRNA expression analysis revealed a significantly altered expression signature for 136 out of 760 genes compared to healthy controls based on Holm-Bonferroni corrected p-values while half of these showed a similar regulation in both IPF as well as sarcoidosis. Based on false discovery rates, only 2 of these genes remained differentially expressed. Direct comparison of sarcoidosis and IPF did not show any differentially regulated genes. These results were in line with the immunostaining results. Biological pathway analysis revealed a similar activity pattern of several fibrosis-related pathways in both diseases, slightly pronounced in IPF.

Conclusion

These results suggest that the molecular mechanisms behind the development of FF are similar in sarcoidosis and IPF, suggesting a re-evaluation of current guidelines and encouraging further studies on the use of anti-fibrotic agents in sarcoidosis.

AG08 AG Thoraxpathologie II

AG08.05

Fluorescence in situ hybridization and functional analysis of the KMT2A-MAML2 gene fusion in thymic epithelial tumors and in the thymic carcinoma cell lines 18889c and MP57

M. Rose¹, S. Küffer¹, D. Müller¹, K. Reuter-Jessen¹, S. Okada^{1,2}, A. Marx³, P. Ströbel¹

¹Universitätsmedizin Göttingen, Pathologie, Göttingen, Germany, ²Kyoto Prefectural University of Medicine, Division of Thoracic Surgery, Department of Surgery, Kyoto, Japan, ³Universitätsmedizin Mannheim, Pathologie, Mannheim, Germany

Background

Thymic epithelial tumors (TET) have been described to have a unique genomic landscape with the lowest mutational burden among adult cancers. The recurrent gene fusion involving the lysine methyltransferase 2A (*KMT2A*) and mastermind-like transcriptional coactivator 2 (*MAML2*) genes is a unique aberration in the B2 and B3 type thymoma however, a clinical or functional relevance of the KMT2A-MAML2 fusion protein in TET has not yet been described.

Methods

For the identification of KMT2A and MAML2 translocations 160 thymoma and thymic carcinoma were screened using fluorescence in situ hybridization (FISH) break apart probes from Zytovision on tissue microarrays (TMA). Samples with detected translocations were validated using the myeloid and the solid cancer next generation sequencing panel from Archer. Phenotypic analyses and RNA seq were performed with the thymic carcinoma cell line 1889c and MP57, the thymic cell line HS67 and the human embryonal kidney cell line HEK293 overexpressing the KMT2A-MAML2 fusion protein.

Results

FISH analysis revealed frequent translocation events of both KMT2A and MAML2 in all TET subtypes including A, AB, B2 and B3 TH. The overexpression of the KMT2A-MAML2 fusion protein in cell lines lead to an increased expression of E-cadherin with diminished levels of vimentin and showed a decreased migration capacity in comparison to controls. In contrast, no difference in cell proliferation or in response to Cisplatin or Etoposide could be observed. The MAML2 target and stem cell maintenance gene HES1 showed an increased expression in cell lines expressing the fusion construct.

Conclusion

Single translocations of KMT2A and MAML2 in different subtypes indicate increased recombination events

with unknown gene fusions in TET. The overexpression of the KMT2A-MAML2 fusion protein induces a differential expression of EMT markers and HES1 indicating a function in cellular plasticity and differentiation. However, the specific KMT2A-MAML2 translocation was only observed in one type B3 thymoma. The identification of different translocation partners of KMT2A and MAML2 will extend the genomic landscape of TET and will lead to new insights in the biology of thymoma and thymic carcinomas. The influence of MAML2 on HES1 indicates a functional relevance in tumor dedifferentiation and may have clinical relevance for patients with disease refractory to conventional therapeutic modalities.

CDK7 is a prognostic biomarker for non small cell lung cancer

C. Kümpers¹, T. Jagomast¹, C. Heide², F.-O. Paulsen³, S. Schierholz⁴, E. Dreyer¹, J. Kirfel¹, S. Perner^{1, 5}

¹Institut für Pathologie UKSH Campus Lübeck, Lübeck, Germany, ²Schön Klinik Neustadt, Klinik für Chirurgie, Neustadt i.H., Germany, ³Zentrum für Onkologie UKE Hamburg, Hamburg, Germany, ⁴Klinik für Thoraxchirurgie UKSH Campus Lübeck, Lübeck, Germany, ⁵Pathologie Forschungszentrum Borstel, Borstel, Germany

Background

Non-small cell lung cancer (NSCLC) remains, despite promising progress of personalized therapy approaches, the leading cause of cancer-related death globally. Cyclin dependent kinase 7 (CDK7) is an kinase involved in transcription, overexpressed in a broad spectrum of cancer types and found to be associated with an unfavourable prognosis. In this study we aimed to investigate the protein expression of CDK7 in a high cohort of NSCLC incorporating adenocarcinomas (adNSCLC) and squamous cell carcinomas (sqNSCLC) and to correlate its expression with clinicopathological data and survival.

Methods

We performed immunohistochemical staining of CDK7 on our cohort of NSCLC including 258 adNSCLC and 101 sqNSCLC and measured protein expression via a semi automated read out. According to the median value of CDK7 the cohort was stratified in a CDK7 high and low expressing group, respectively, and results were correlated with clinico-pathological data.

Results

CDK7 was significantly higher expressed in sqNSCLC than in adNSCLC. In the group of sqNSCLC, CDK7 expression was significantly higher in sqNSCLC with lymph node metastases than in sqNSCLC with N0 stage. We found a significantly worse overall survival and disease-free survival for patients with CDK7 high expressing NSCLC without identifying CDK7 being an independent prognostic factor.

Conclusion

Since a high CDK7 expression seems to be linked with a poor prognosis it might serve as a promising novel prognostic biomarker and its assessment could be implied in future routine diagnostic workup of NSCLC samples. Considering that CDK7 inhibitors are currently tested in several trials for advanced solid malignancies, it may also be a new target for future anti cancer therapy.

Activation of AKT signaling promotes resistance to FGFR1 inhibition in squamous-cell lung cancer

O. Elakad¹, B. Häupl^{2, 3, 4}, V. Labitzky⁵, S. Yao¹, S. Küffer¹, A. von Hammerstein-Equord⁶, B. C. Danner⁶, M. Jücker⁷, H. Urlaub⁸, T. Lange⁵, P. Ströbel¹, T. Oellerich^{2, 3, 4}, **H. Bohnenberger¹**

¹University medical center Göttingen, Institute of Pathology, Göttingen, Germany, ²Goethe University Frankfurt, Department of Medicine II, Hematology/Oncology, Frankfurt, Germany, ³German Cancer Research Center and German Cancer Consortium, Heidelberg, Germany, ⁴Goethe University Frankfurt, Frankfurt Cancer Institute, Frankfurt, Germany, ⁵University Medical Center Hamburg-Eppendorf, Institute for Anatomy and Experimental Morphology, Hamburg, Germany, ⁶University medical center Göttingen, Department of Thoracic and Cardiovascular Surgery, Göttingen, Germany, ⁷University Medical Center Hamburg-Eppendorf, Center for Experimental Medicine, Institute of Biochemistry and Signal Transduction, Hamburg, Germany, ⁸Max Planck Institute for Biophysical Chemistry, Bioanalytical Mass Spectrometry Group, Göttingen, Germany

Background

Lung cancer is the primary reason for cancer-related deaths worldwide. Gene amplification of Fibroblast growth factor receptor 1 (*FGFR1*) is one of the most frequent and drugable genetic alterations in squamous-cell lung cancer (SQCLC), hence selective tyrosine kinase inhibitors have been developed to target *FGFR1*. Clinical trials in phases I and II have proven safety and activity of these inhibitors in SQCLC with a disease-control rate of 26–39 %. Some patients have profited from the treatment for more than 14 months. However, resistance mechanisms originally existing in patients or acquired during treatment have so far limited treatment efficiency in clinical trials.

Methods

In the present study, we aimed to investigate resistance-signaling pathways of *FGFR1* inhibition in *FGFR1*-amplified SQCLC cells. Therefore, we performed a wide-scale phosphoproteomic mass-spectrometry analysis of SQCLC cells with *FGFR1* amplification and intrinsic, pharmacologically or mutationally induced resistance against *FGFR1* inhibition to identify signaling pathways that lead to resistance *FGFR1* inhibition resistance.

Results

We compared *FGFR1*-amplified SQCLC cell lines with either intrinsic or induced opposing response to *FGFR1* inhibition by phosphoproteomic mass-spectrometry. Were able to quantify 11,052 phosphosites and we found a strong and significant phosphorylation of AKT1 and its downstream target PRAS40 at its activatory phosphosites in the resistant cell lines. Co-inhibition of AKT and *FGFR1* re-sensitized resistant lung cancer cells synergistically to *FGFR1* inhibition. Furthermore, we were able to demonstrate a strong intrinsic variation of AKT phosphorylation by immunohistochemical staining of phosphorylated AKT in tissue samples from SQCLC patients.

Conclusion

In conclusion, we used a phosphoproteomic approach to investigate resistance-signaling pathways of *FGFR1* inhibition in squamous cell lung cancer. In addition to providing a huge data library of resistance-

associated phosphorylation patterns, we identified a common resistance pathway that includes the activation of AKT. Examination of AKT activation could help to predict response to *FGFR1* inhibition and combination with AKT inhibitors might move the way toward an effective therapy for *FGFR1*-dependent lung-cancer patients in cases of resistance to treatment.

Proteomics to connect lung cancer molecular phenotype to tumor genotype and histopathology

J. Lehtiö

Karolinska Institutet and SciLifeLab, K7 Onkologi-Patologi, Stockholm, Sweden

The explosion of genomics data has improved our understanding of cancer greatly in recent years. However, the knowledge on how combination of cancer genomic aberrations in particular tumors affect the functional proteome is still very limited. This is a major hinder for selection of anti-cancer drug combinations in precision medicine as well as predicting immunotherapy response. Proteome data represents the combined effect of epigenetic, transcriptional and translational regulation and will therefore provide an important molecular phenotype data layer for multi-omics analysis.

To allow effective systems biology analysis including proteomics, we have generated tools that take advantage of massive genomics and transcriptomics data by incorporating sequence information to the proteomics data-analysis pipeline. This will allow protein level analysis of gene variants as well as detection of novel protein coding regions. In cancer, genomics instability creates so called neoantigen when non-canonical proteins and peptides are translated. Our proteogenomics methods offers a view into tumor neoantigen space. In same analysis, in-depth quantitative proteome data on tumor tissue provides information both on cancer driving pathways and molecular insights in immune evasion mechanisms. Proteogenomics driven multi-omics view of lung cancer is presented by analysis of several lung cancer cohorts (REF01). We could define proteome-based lung cancer subtypes by mass spectrometry based in-depth proteomics of 141 cases. Interestingly, these subtypes differ on tumor neoantigen burden as well as types of neoantigens with interesting differences in likely immune evasion mechanisms. A lung adenocarcinoma subtype associated with poor prognosis, immune-cold phenotype, despite high neoantigen burden, was identified. This subtype was enriched in STK11 mutations and we could demonstrate that this activated immune evasion mechanism via expression of FLG1 immune inhibitory ligand. To allow clinical application, we developed a DIA based classifier for lung cancer subtyping. The classifier was tested in two additional tumor cohort, in a similar early-stage lung cancer cohort of 208 cases and using a late-stage biopsy cohort of 80 samples.

Literaturangaben

[REF01] Lehtio J., et al, (2021), Proteogenomics of non-small cell lung cancer reveals molecular subtypes associated with specific therapeutic targets and immune-evasion mechanisms, *Nature Cancer*, 1224–1242 , <https://doi.org/10.1038/s43018-021-00259-9>

AG09 AG Kopf-Hals-Pathologie

AG09.01

CDK7 Expression implies a poor prognosis in HNSCC

J. Ribbat-Idel¹, T. Jagomast¹, L. Klapper¹, P. Kuppler¹, A. Offermann¹, E. Dreyer¹, K.-L. Bruchhage², C. Idel², S. Perner^{1,3}

¹Universität zu Lübeck und UKSH Campus Lübeck, Institut für Pathologie, Lübeck, Germany, ²Universität zu Lübeck und UKSH Campus Lübeck, Klinik für Hals-, Nasen- und Ohrenheilkunde, Lübeck, Germany,

³Forschungszentrum Borstel, Leibniz Lungenzentrum, Pathologie, Borstel, Germany

Background

Head and neck squamous cell carcinoma (HNSCC) are among the most common cancers worldwide and are associated with a poor prognosis. Therefore, international research efforts continue to identify new prognostically relevant markers. pMED1 and CDK7 are proteins which have been observed to be differentially expressed in other cancer types and to have prognostic impact. CDK7 phosphorylates pMED1. Here, we present a study about their expression and prognostic implications in HNSCC.

Methods

We accessed our large and well characterized cohort which consist of tumor tissue and clinical data of 419 HNSCC patients. We performed immunohistochemical staining of CDK 7 and pMED1 and employed a semi-automated read out to measure protein expression. Results were correlated with clinical and pathological data.

Results

A higher expression of the CDK7 and was found to be linked up to a poor overall survival and disease-free survival. It proved to be an independent prognostic factor when compared to e. g., p16. CDK7 showed a higher expression in immune cell infiltrated tumors.

Conclusion

Since a higher CDK7 expression seems to predict a poor prognosis in both overall and disease-free survival it may be suitable as a novel prognostic factors in routine diagnostic workup for future patients. Also, as in vitro studies were able to identify a CDK 7 inhibitor it may also be a promising target for future anti cancer therapy.

Revealing differences of local PD-L1 mRNA expression and corresponding protein occurrence in head and neck tumour

J. Lischka, M. Großer, U. Sommer, G. B. Baretton, P. Hönscheid, K. Jöhrens

Institut für Pathologie des Universitätsklinikums Carl Gustav Carus Dresden, Dresden, Germany

Background

Targeted blockade of PD-1/PD-L1 axis has become increasingly important in cancer therapy e.g. of breast or head and neck cancer. Gold standard in predictive diagnosis is immunohistochemistry (IHC) with detection of PD-L1 expression. The data on the influence of PD-L1 protein expression on prognosis of patients treated with checkpoint inhibitors disputed. However, detection of PD-L1 by IHC is obligatory for therapy of some tumour entities. Depending on the approved drugs, the scores and threshold values vary for the same entity. In harmonisation studies, the similarities of different immunohistochemical PD-L1 antibodies were investigated for different tumor entities. Here, various assays have shown different staining properties. A determination of PD-L1 mRNA expression, complementary to diagnostics by IHC, could represent a biomarker for better patient selection.

The aim of this study is to validate the IHC assays in addition to harmonisation studies by visualising isoform-specific PD-L1 mRNA expression in tumour tissue of head and neck squamous cell carcinomas (HNSCCs).

Methods

Detection of isoform-specific PD-L1 mRNA expression is performed by chromogenic in situ hybridization (CISH) and quantitative reverse transcriptase polymerase chain reaction (qRT-PCR) on formalin-fixed, paraffin-embedded tumour tissue of HNSCCs ($n = 20$). Automated staining of immunohistochemical antibodies SP142, SP263, E1L3N, 28-8, and 22C3 was performed on the same tissue block as part of a harmonisation study.

Results

Tumours with low PD-L1 mRNA expression had a lower CPS_{IHC} than tumours with high PD-L1 mRNA expression of protein-coding transcript variants for all antibodies ($p_{\text{E1L3N}} = 0.0074$, $p_{\text{SP263}} = 0.0046$, $p_{\text{SP142}} = 0.0101$, $p_{\text{28-8}} = 0.0155$, $p_{\text{22C3}} = 0.019$). Detection of the PD-L1 probe to visualize PD-L1 mRNA expression in tumour whole tissue also showed correlations with IHC. Here, scoring of tumour cells by TPS_{IHC} of antibody SP142 showed the strongest correlation to TPS_{CISH} ($r_{\text{SP142}} = 0.4702$; $p_{\text{SP142}} = 0.049$). In some samples, there was thus a discrepancy between IHC, qRT-PCR and CISH.

Conclusion

Further studies investigating the prognostic value of PD-L1 mRNA expression on survival of patients with HNSCCs treated with checkpoint inhibitors are needed to investigate the value of PD-L1 mRNA expression as a predictive biomarker, especially in cases where IHC and PD-L1 mRNA Expression show different results.

Who's Driving? Switch of Drivers in Immunotherapy-Treated Progressing Sinonasal Melanoma

S. N. Freiburger^{1, 2}, P. Turko³, M. Hüllner^{2, 4}, R. Dummer^{2, 3}, G. B. Morand^{5, 6}, M. P. Levesque^{2, 3}, D. Holzmann⁵, **N. J. Rupp**^{1, 2}

¹Department of Pathology and Molecular Pathology, University Hospital Zurich, Zurich, Switzerland, ²Faculty of Medicine, University of Zurich, Zurich, Switzerland, ³Department of Dermatology, University Hospital Zurich, Zurich, Switzerland, ⁴Department of Nuclear Medicine, University Hospital Zurich, Zurich, Switzerland, ⁵Department of Otorhinolaryngology - Head and Neck Surgery, University Hospital Zurich, Zurich, Switzerland, ⁶Department of Otolaryngology - Head and Neck Surgery, Sir Mortimer B. Davis – Jewish General Hospital, McGill University, Montreal, Canada

Background

Mucosal melanoma can be driven by various driver mutations in genes such as *NRAS*, *KIT*, or *KRAS*. However, some cases present with only weak drivers, or lacking known oncogenic drivers, suggesting immunotherapy over targeted therapy. While resistance mechanisms to immunotherapy in cutaneous melanoma have been uncovered, including alterations in *JAK1/2*, *B2M*, or *STK11*, a switch of oncogenic drivers under immunotherapy has not yet been observed.

Methods

Clinico-pathological data including FDG-PET/CT imaging data from n=3 cases of metastatic sinonasal melanoma treated with immunotherapy, and n=3 metastatic sinonasal melanoma treated with radiotherapy only were collected. Different tissue specimen (primary tumor, metastatic manifestations) were subjected to a melanoma-specific next generation sequencing panel ("MelArray"), and immunohistochemistry. In addition, liquid biopsies were investigated by an ultra-sensitive cfDNA assay (Oncomine™ Colon cfDNA Assay).

Results

Three cases of metastatic sinonasal melanoma switched oncogenic drivers from *KRAS*, *KIT*, or no driver to *NRAS* during or after immunotherapy, thereby showing progressive disease. One of the cases presented with three spatially separate driver mutations in the primary tumor, whereas the *NRAS* clone persisted under immunotherapy. In comparison, three different control cases receiving radiotherapy only did not show a change of the detectable molecular drivers in their respective recurrences or metastases.

Conclusion

In summary, these data provide an important rationale for longitudinal molecular testing, based on evidence for an unforeseen recurrent event of molecular driver switch to *NRAS* in progressing sinonasal melanoma. These findings provide the basis for further studies on a potential causal relation of emerging *NRAS* mutant clones and immunotherapy.

This work has been published [1]

Literaturangaben

[1] Freiburger SN, Turko P, Hüllner M, Dummer R, Morand GB, Levesque MP, Holzmann D, Rupp NJ, (2021), Who's Driving? Switch of Drivers in Immunotherapy-Treated Progressing Sinonasal Melanoma. , Cancers (Basel), May 31;13(11):2725. doi: 10.3390/cancers13112725. PMID: 34072863; PMCID: PMC8198298., <https://pubmed.ncbi.nlm.nih.gov/34072863/>

Molecular alterations underlying tumor cell budding in head and neck cancer

I. Ourailidis^{1,2}, F. Stögbauer³, S. Beck¹, W. Weichert³, P. Schirmacher¹, A. Stenzinger¹, M. Boxberg³, J. Budczies¹

¹Heidelberg University Hospital, Institute of Pathology, Heidelberg, Germany, ²Heidelberg University, Faculty of Biosciences, Heidelberg, Germany, ³Technical University Munich, Institute of Pathology, Munich, Germany

Background

Several studies have demonstrated a negative prognostic impact of tumor cell budding (TCB) in head and neck squamous cell carcinoma (HNSCC), but the underlying molecular mechanisms of TCB formation in HNSCC are not well understood.

Methods

The study cohort included 286 HPV- and 45 HPV+ HNSCC from TCGA for which both digitalized H&E-stained slides and molecular data were available. Corresponding mutation, methylation, and gene expression data were obtained from the Genomic Data Commons data portal. Tumor buds were defined as clusters of up to four tumor cells separated from the tumor mass. For each tumor, the number of tumor buds was evaluated in ten digital high-power fields by a senior pathologist. Association of TCB with gene expression and methylation was analyzed using Spearman correlations, while the comparison of TCB between mutated and non-mutated samples was performed using unpaired two-samples Wilcoxon tests. Lists of altered genes were compiled correcting the p-values with the Benjamin-Hochberg method and controlling the FDR at 5%. The HPV- and HPV+ samples were analyzed separately.

Results

Significant association of TCB with mutations was detected for two genes: *NSD1* mutations correlated negatively with TCB in HPV- HNSCC, while *TP53* mutations correlated positively with TCB in HPV+ HNSCC. Methylation of 126 (1%) genes was associated with TCB in HPV- HNSCC, while methylation of 511 (3%) genes was associated with TCB in HPV+ HNSCC. Expression of 422 (2%) genes was associated with TCB in HPV- HNSCC, while expression of 786 (4%) genes was associated with TCB in HPV+ HNSCC. Among these genes, those annotated to the epithelial mesenchymal transition (EMT) were highly significantly enriched in both HPV- HNSCC (5.5-fold enrichment) and HPV+ HNSCC (2.7-fold enrichment). The enrichment analysis of the genes correlating with TCB additionally revealed that genes implicated in cell-cell and cell-extracellular matrix adhesion were also highly significantly enriched in both HPV- and HPV+ HNSCC.

Conclusion

TCB correlated with mutations of only two genes and in an HPV-specific pattern. A plethora of genes correlated with TCB on the level of methylation and gene expression. Our data-driven approach reveals a comprehensive molecular characterization of TCB in HNSCC for the first time, showing a major impact of

EMT and cell adhesion pathways. These genes should be further analyzed and prioritized for the evaluation of therapeutic targeting.

Current Advances in the Morphological and Molecular Classification of Salivary Gland Tumors

N. J. Rupp^{1, 2}

¹Department of Pathology and Molecular Pathology, University Hospital Zurich, Zurich, Switzerland, ²Faculty of Medicine, University of Zurich, Zurich, Switzerland

This presentation will provide an overview of the current classification of salivary gland tumors. In particular, molecular alterations in established entities, as well as their variants, will be addressed. In addition, new and emerging entities such as microsecretory adenocarcinoma, sclerosing microcystic adenocarcinoma, and mucinous adenocarcinoma will be outlined.

AG10 AG Zytopathologie

AG10.01

Molekulare Zytologie: Chancen und Herausforderungen

V. Tischler

Institut für Pathologie, Universitätsklinikum Bonn, Bonn, Germany

In unterschiedlichen Tumorentitäten, wie beispielsweise dem nicht-kleinzelligen Lungenkarzinom (NSCLC), ist die (wiederholte) Gewinnung von Proben zur Diagnose und zur Untersuchung von prädiktiven Markern aufgrund der anatomischen Verhältnisse in manchen Fällen schwierig. Hier werden häufig sehr kleine oder zytologische Proben gewonnen. Wie bereits gezeigt wurde, lassen sich zytologische Proben exzellent für die prädiktive Markeranalytik mittels Fluoreszenz in-situ Hybridisierung und Next Generation Sequencing einsetzen. Auch beim zytologischen Probenmaterial ist wie beim formalinfixierten Paraffin eingebetteten Gewebe eine strikte Qualitätskontrolle sowie eine Standardisierung der Laborprozesse von großer Bedeutung. Weitere Vorteile der zytologischen Proben sind die einfache und schnelle Überprüfung der Repräsentativität, zum Beispiel im Rahmen einer Rapid On-site Evaluation (ROSE), sowie die Möglichkeit zur Anfertigung von zwei- oder dreidimensionalen präklinischen Zellkulturmodellen. Somit kann das zytologische Probenmaterial in Ergänzung zur prädiktiven Markeranalytik direkt für funktionelle genomische Testungen, z.B. bei unklaren Variantenkonstellationen, expandiert werden. Hieraus können beispielsweise ergänzende Informationen für die Therapieentscheidung gewonnen werden.

AG10.02

Non-cellular findings in cytological preparations

M. Engels

Uniklinik Köln, Institut für Pathologie, Köln, Germany

Abstract: Nichtzelluläre Elemente in zytologischen Präparaten

Einleitung: Es gibt in zytologischen Präparaten eine Vielzahl von unterschiedlichen Phänomenen, die nicht die zu untersuchenden Zellen betreffen. Diese Befunde im Hintergrund können ablenkend, verwirrend und irreführend sein. Eine systematische Darstellung kann helfen, diese Phänomene korrekt einzuordnen und zu bewerten.

Überblick: Zu folgenden Befunden werden Beispiele aus unterschiedlichen Probensorten bei benignen und malignen Veränderungen gezeigt: Kristalle, Konkrement, Schleim und amorphes Material im Hintergrund, Kontamination, Artefakte.

Diskussion: Die meisten beschriebenen Veränderungen nicht spezifisch. Es ist aber wichtig, sie zu kennen, um falsch-positive Diagnosen zu vermeiden. In einigen Fällen können Phänomene im Hintergrund wertvolle diagnostische Hinweise geben.

Add-on Opportunistic Screening for Oral Cancer and Precursors in Patients with Fanconi Anemia using Brush Biopsy-Based Cytology

M. Schramm¹, B. E. Silva de Araujo¹, M. Markgraf¹, R. Dietrich², I. K. de Santana Almeida Araujo¹, N. Pomjanski¹, A. Böcking¹, S. Biesterfeld¹, E. Velleuer^{1,3}

¹Heinrich Heine University, Institute of Pathology, Department of Cytopathology, Düsseldorf, Germany,

²German Fanconi Anemia Support Group, Eschau, Germany, ³HELIOS Klinikum, Centre for Child and Adolescent Health, Krefeld, Germany

Aims: Fanconi anemia (FA) is a rare inherited DNA instability disorder that is associated with bone marrow failure and a highly elevated risk of neoplasia, especially a 500-fold to 700-fold higher risk of head and neck squamous cell carcinoma compared with the general population. Two thirds of them arise in the oral cavity, preceded by visible lesions. The latter are frequent and often multiple but not necessarily linked to malignancy that make repeated tissue-biopsies not feasible. In close collaboration with the German FA support group, we aimed to introduce an alternative strategy using brush biopsy-based oral cytology for the detection of those lesions that are necessary to treat.

Methods: In an ongoing prospective study, since 2006 the oral cavities of more than 900 international FA affected individuals have been inspected systematically. Visible suspect lesions were sampled with cytobrushes for conventional or liquid-based cytology and DNA ploidy analysis, if necessary. The results were correlated to a long-term clinicopathological follow-up, if available. Cytogenetic changes in oral samples with a low number of suspect cells were analyzed with a multicolor Fluorescent in situ Hybridization (FISH) assay. We initially tested 13 promising DNA probes using FA oral squamous cell carcinoma (OSCC) cell lines [1]. Finally, probes for *CCND1*, *TERC*, *MYC* and centromere of chromosome 6 were combined to a multicolor FISH assay and the diagnostic accuracy was analyzed on 160 oral lesions for cutoff determination and 153 for validation.

Results and Conclusions: The diagnostic accuracy of conventional cytology and DNA ploidy analysis of 737 evaluable oral lesions was analyzed including 86 lesions with at least high-grade oral epithelial dysplasia. 63% of OSCC and precursors were detected at a noninvasive or early stage. For cytology and if necessary additional DNA ploidy analysis the sensitivity and specificity were 100% and 92.2%, respectively. Negative cytology or the lack of DNA aneuploidy identify benign lesions with high accuracy and thus reduce the need for invasive diagnostic biopsies [2]. The validation of the multicolor FISH assay showed a good diagnostic accuracy, but some false positive results were observed. The majority of those patients had syn- or metachrone oral (pre)cancer, possibly indicating the detection of a genetically altered field rather than a lesion that warrant immediate treatment.

Literaturangaben

[1] Silva de Araujo, B. E., Velleuer, E., Dietrich, R., Pomjanski, N., Santana Almeida Araujo, I. K., Schlensog, M., Wells, S. I., Dorsman, J. C., Schramm, M., (2022), Detection of cytogenetic changes and

chromosomal aneuploidy with fluorescent in situ hybridization in cytological specimens of oral cancers in Fanconi anemia—Proof of concept., *Clinical and Experimental Dental Research*, 108-116, 8(1)

[2] Velleuer, E., Dietrich, R., Pomjanski, N., de Santana Almeida Araujo, I. K., Silva de Araujo, B. E., Sroka, I., Biesterfeld, S., Böcking, A., Schramm, M., (2020), Diagnostic accuracy of brush biopsy-based cytology for the early detection of oral cancer and precursors in Fanconi anemia., *Cancer Cytopathol.*, 403-413, 128(6)

AG11 AG Molekularpathologie I

AG11.02

EGFR exon 20 insertion mutations in NSCLC: spectrum, frequency and results of the first German proficiency test

M. Ihle¹, M. Grassow-Narlik², K. Ilm², S. Merkelbach-Bruse¹

¹*University Hospital Cologne, Faculty of Medicine and University Hospital Cologne, 50924 Köln, Germany,*

²*Quality in Pathology – QulP, 10117 Berlin, Germany*

Background

Amivantamab (Rybrevant, Janssen-Cilag), a bispecific monoclonal antibody targeting EGFR and MET, has recently been approved by FDA and EMA as monotherapy for patients with advanced or metastatic NSCLC harboring EGFR exon 20 insertion (EGFRex20ins) mutation after failure of platinum-based therapy. Herein, data from routinely processed diagnostic pathology NSCLC specimens were retrospectively investigated to gain more insights into the distribution of EGFRex20ins mutations. Furthermore, we describe the conditions and results of a proficiency test for EGFRex20ins mutation detection in NSCLC in either tissue or liquid biopsies. The goal was to evaluate the accuracy of EGFRex20ins mutation testing across multiple centers and across different starting material.

Methods

In routine diagnostics from 2013 until 2021, over 30,000 NSCLC patients were routinely tested for EGFR exons 18-21 by next generation sequencing. Description of variants was done according to the HGVS guidelines. Frequencies of detected EGFRex20ins mutations were determined and served as basis for the selection of samples for the tissue and liquid biopsy part of the proficiency testing.

Results

We found 203 NSCLC samples harboring an EGFRex20ins mutation. Over 66 different EGFRex20ins mutations were evaluated. The most common were the following duplications: p.A767_V769dup, p.S768_D770dup, p.N771_H773dup. 32 out of 37 (86.5%) institutes participated successfully in the tissue part of the proficiency test and 12 out of 19 (63.2%) in the liquid biopsy part respectively. Next generation sequencing was the method of choice in both parts. Not all the compared commercial, mutation specific PCR assays were able to detect all mutations in the tissue and the liquid biopsy part due to insufficient sensitivity or the limited mutation spectrum covered.

Conclusion

This study shows the large heterogeneity of insertion mutations in a wide region of exon 20 of the *EGFR* gene. Furthermore, EGFRex20ins mutations can be reliably detected in tissue as well as in liquid biopsies if the test is validated and suitable for the detection of this heterogeneous field of mutations. This study underlines the need for external quality assessment in routine molecular testing of advanced NSCLC to guarantee optimal personalized treatment.

Disclaimer/Acknowledgment: Study was supported by Janssen-Cilag GmbH

Immuno-histomorphological comparison regarding heterogeneity between primary lung carcinomas and corresponding lymph node metastases

T. Kolb, P. Möller, T. F. Barth, R. Marienfeld

Universitätsklinikum Ulm, Pathologie, Ulm, Germany

Background

Pulmonary adenocarcinoma is classified into different histological growth patterns according to the 2004 WHO classification - lepidic, acinar, papillary, micropapillary and solid growth patterns. There is increasing evidence that each growth pattern indicates a distinct biological profile and is associated with a different prognosis. In addition, NSCLC is often diagnosed at a late stage, and lymph node metastases are mostly used for accurate staging of the primary tumor. Furthermore, another mechanism utilized by tumor cells to evade immune surveillance is the activation of immune checkpoint proteins like programmed cell death 1 (PD-1) and T cell immunoglobulin and ITIM domain (TIGIT), which impair the anti-tumor immunity by activation. However, as primary tumor and metastases display a different molecular setup, we investigated the heterogeneity of the primary tumor and the corresponding metastases, regarding the expression of the PD-1 and TIGIT axes in contrast of the different histologic growth patterns.

Methods

We performed immunohistochemical staining of 96 tumor segments from 11 resected tumor samples to evaluate the expression of PD-L1, PD-1, Nectin-2, PVR, and TIGIT in distinct growth patterns between the primary tumor and the metastasis.

Results

We determined heterogeneity between and within different tumor segments regarding morphological growth patterns. Furthermore, expression of immune checkpoint proteins varied between different growth patterns within the primary tumor as well as in the metastasis. Of note, we detected TIGIT not only on tumor infiltrating lymphocytes but also on cells of adenocarcinoma in primary and metastatic site, whereas non-neoplastic lung tissue was consistently TIGIT-negative.

Conclusion

The immune checkpoint protein distribution in histologic subtypes of primary and metastatic site of pulmonary adenocarcinoma displays an considerable intra- and intertumoral heterogeneity implying the requirement of a multiregional analysis when determining the expression status of PD-1:PD-L1 as well as the TIGIT:PVR/Nectin-2 checkpoint proteins as predictive markers.

Spatial patterns of specific immune cells populations in the tumor microenvironment as biomarkers in lung adenocarcinoma

E. Romanovsky¹, C. Massa², D. Kazdal¹, M. Kirchner¹, P. Schirmacher¹, A. Stenzinger¹, B. Seliger², J. Budczies¹

¹*Institute of Pathology, Heidelberg University Hospital, General Pathology and Pathological Anatomy, Heidelberg, Germany,* ²*Martin Luther University Halle-Wittenberg, Institute for Medical Immunology, Halle, Germany*

Background

Image analysis allows the detection of spatial patterns of specific immune cell populations in tissue slices. However, these spatial patterns have not been sufficiently researched in terms as potential biomarkers. In this study, we investigate the intra-tumor and the inter-tumor variability of immune cells patterns in lung adenocarcinoma (LUAD).

Methods

A total of 56 tissue blocks from a cohort of 19 LUAD tumors was analyzed using multispectral imaging (MSI). For each of the tumors, a tissue slice crossing the entire tumor was cut into tissue blocks and 2-4 of the tissue blocks were selected and analyzed. The levels of five immune cell populations (B cells, CD4+ and CD8+ T cells, macrophages, Tregs) was evaluated using cell segmentation data from MSI. Cell counting, morphometric analysis, spatial point pattern analysis, and distance analysis were performed, and biomarkers including information on the spatial arrangement of the immune cell populations were defined. The inter-tumor and intra-tumor variability were analyzed using analysis of variance and assessed for significance using the F statistics. Altogether, we evaluated 20 biomarkers for each of five cell types, resulting in 100 tested hypotheses. P-values were corrected using the Benjamini-Hochberg method and the false discovery rate was controlled at 10%.

Results

Of 100 biomarkers tested, 61 showed significantly higher inter-tumor variability compared to the intra-tumor variability. The cell proportions and the mean of the distances of tumor cells to the next immune cell were significant for all immune cell populations studied. The highest ratio between inter-tumor and intra-tumor variability was shown by the mean of the distances of tumor cells to the next B cell, as it possessed the highest F value ($F=22.58$, $p=1.07 \times 10^{-14}$). The second highest F values showed CD8+ T cell proportion in tumor tissue ($F=7.56$, $p=1.57 \times 10^{-7}$) and mean of the distances of tumor cells to the next CD8+ T cell ($F=9.16$, $p=9.49 \times 10^{-9}$).

Conclusion

Biomarkers reflecting spatial patterns of immune cells were reproducible over different tissue blocks of tumor. These biomarkers should be further analyzed for their prognosticity and predictivity.

Biomarker testing in lung cancer patients- upscaling the fast track analysis

J. Fassunke, F. Saur, T. Röhrlich, U. Siebolts, S. Merkelbach-Bruse

Uniklinik Köln, Institut für Pathologie, Köln, Germany

Background

Several molecular alterations that have been defined as “driver mutations” in non-small-cell lung cancer (NSCLC) help to identify patients most likely to respond to targeted therapies. Since the results of molecular diagnostics are of immediate clinical relevance, we perform a rapid analysis (also called “fast track” analysis) for therapeutically targetable alterations e.g. *EGFR* exons 19 and 21, *KRAS* exon 2, *ALK*, *ROS1*, *NTRK*, and *BRAF*. Analyses are carried out with a mixture of technologies and are currently lacking three new targetable alterations, *EGFR* exon 20 insertions, *MET* exon 14 skipping mutations and *RET* translocations. Additionally, the information of the exact *KRAS* mutation status is missing due to the screening technique used. For sufficient analysis of lung cancer samples, additional biomarkers have to be added to our fast-track portfolio. At the same time the assay should allow for the combined analysis of several alterations with one technology. The method should provide information rapidly and at the same time be cost and material saving.

Methods

We collected 45 DNA samples with *KRAS* (n=17), *BRAF* (11) and *EGFR* (17) mutations and 39 RNA samples with *ALK* (n=11), *RET* (9) and *ROS1* (12) translocations and *MET* (7) exon 14 skipping, which had been previously tested by parallel sequencing in our laboratory. All samples, including wildtype samples for each DNA and RNA assay, were analyzed for the presence of mutations by allele-specific real-time PCR using the Easy PGX system (Diatech Pharmacogenetics, Jesi, Italy) on the thermocycler EasyPGX qPCR instrument 96 (Diatech Pharmacogenetics). The running time of the real time analysis was 2 h and the minimum of 40 ng DNA or RNA was used for each biomarker. Data were analyzed with the Aria software version 1.4 (Diatech Pharmacogenetics).

Results

The majority of DNA and RNA samples were directly analysed correctly by the Aria analysis software. Seven DNA and five RNA samples were correctly determined by reanalyzing the raw data. In total, 97 % yielded the correct result. No false-positive results were obtained. One sample each could not be detected correctly.

Conclusion

Allele-specific real-time PCR with the Diatech Easy PGX system is a reliable alternative technology for fast track analysis.

The immune microenvironment in EGFR- and ERBB2-mutated lung cancer

M. Kirchner¹, K. Kluck¹, R. Brandt¹, A.-L. Volckmar¹, R. Penzel¹, D. Kazdal¹, V. Endris¹, H. Seker-Cin¹, O. Neumann¹, H. Goldschmid¹, J. Glade¹, M. Allgäuer¹, M. Kriegsmann¹, P. Schirmacher¹, M. Thomas^{2,3}, J. Budczies^{1,3,4}, P. Christopoulos^{2,3}, A. Stenzinger^{1,3,4}

¹*Institut für Pathologie, Allgemeine Pathologie, Heidelberg, Germany*, ²*Universitätsklinik Heidelberg, Thoraxklinik und Nationales Centrum für Tumorerkrankungen (NCT), Heidelberg, Germany*, ³*Translationales Lungenforschungszentrum Heidelberg (TLRC-H), Heidelberg, Germany*, ⁴*Deutsches Konsortium für Translationale Krebsforschung (DKTK) und Deutsches Krebsforschungszentrum (DKFZ), Heidelberg, Germany*

Background

Targeted therapies have improved survival and quality of life for patients with non-small-cell lung cancer with actionable driver mutations. However, epidermal growth factor receptor (EGFR) and human epidermal growth factor receptor 2 gene (HER2, also known as ERBB2) exon 20 insertions (Ex20mut) are characterized by a poor response to currently approved tyrosine kinase inhibitors and immunotherapies. The underlying immune biology is not well understood. To characterize the tumor microenvironment of EGFR- and ERBB2-mutated lung adenocarcinomas (ADC) we performed messenger RNA expression profiling.

Methods

Messenger RNA expression profiling was conducted on the NanoString nCounter gene expression platform using the PanCancer Human IO 360 Panel. We included ADCs with ERBB2 (n = 19) and EGFR exon 20-insertion mutations (n = 13) and compared these to tumors with classical EGFR mutations (n = 40, affecting EGFR exons 18, 19 or 21) and EGFR/ERBB2 mutation-negative lung ADC (EGFR/ERBB2wt, n = 26) focusing on immunologically relevant transcripts. Tumor-infiltrating immune cells were estimated from gene expression profiles.

Results

Cytotoxic cells were significantly lower in EGFR-mutated tumors regardless of the affected exon, while Th1 cells were significantly lower in EGFR-Ex20mut compared to EGFR/ERBB2wt tumors. We assessed the differentially expressed genes of ERBB2-Ex20mut and EGFR-Ex20mut tumors compared to EGFR-Ex18/19/21mut and EGFR/ERBB2wt tumors. Of these, the genes GUSB, HDAC11, IFNGR2, PUM1, RASGRF1 and RBL2 were up-regulated, while a lower expression of CBLC, GBP1, GBP2, GBP4 and MYC was observed in all three comparison groups. The omnibus test revealed 185 significantly (FDR = 5%) differentially expressed genes and we found these four most significant gene expression changes in the study cohort: VHL and JAK1 were overexpressed in ERBB2-Ex20mut and EGFR-Ex20mut tumors compared

to both EGFR-Ex18/19/21mut and EGFR/ERBB2wt tumors. RIPK1 and STK11IP showed the highest expression in ERBB2-Ex20mut tumors.

Conclusion

Targeted gene expression profiling is a promising tool to read out the characteristics of the tumor microenvironment from routine diagnostic lung cancer biopsies. Significant immune reactivity and specific immunosuppressive characteristics in ERBB2-Ex20mut and EGFR-Ex20mut lung ADC with at least some degree of immune infiltration support further clinical evaluation of immune-modulators as partners of immune checkpoint inhibitors in such tumors.

AG11 AG Molekularpathologie II

AG11.08

Genomic Large Rearrangements (LRs) in HRR genes in high-grade ovarian carcinomas

M. Romey¹, K. M. Timms², J. Teply-Szymanski¹, B. Swedlund², F. Rodepeter¹, M. Jones², A. Hattesoht¹, M. Comeaux², A. Grass¹, C. Solimeno², P. Jank¹, G. Simister², C. Denkert¹

¹Philipps-Universität Marburg und UKGM Standort Marburg, Pathologie, Marburg, Germany, ²Myriad Genetics, Salt Lake City, United States of America

Background

The concept of synthetic lethality has recently entered clinical practice for ovarian cancer patients. Since then, assessing Homologous Recombination Deficiency (HRD) and Genomic Instability (GI) has emerged as a standardized diagnostic evaluation to allow for targeted treatment with PARP inhibitors. Gene variants classified as LRs are defined as DNA segment rearrangements from gains or losses of partial exons, up to gains or losses that encompass the entire gene. We evaluated the prevalence of LRs in a real-life cohort of high-grade ovarian cancer patients, with a focus on their distribution across the GIS range.

Methods

From January to November 2021, 1163 ovarian cancer tumor samples were screened using the Myriad myChoice CDx HRD assay, followed by next-generation sequencing. Library preparation was performed with a hybrid capture approach with probes covering 15 Homologous Recombination Repair (HRR) genes including BRCA1, BRCA2, and 26,523 SNPs across the whole genome. Each patient's HRD status was evaluated by measuring the BRCA1/2 mutational status and the Genomic Instability Score (GIS), with a predefined cut-point of ≥ 42 for a positive score. Sequencing data was analyzed by Myriad's proprietary algorithm to determine the mutational status of BRCA1/2 and the other HRR genes, followed by an additional manual review of each sample by two independent reviewers for tumor HRR-gene LRs.

Results

LRs could be found in 88/1163 (7.5 %) of ovarian cancer samples, with a GIS ranging from 11 to 94. Out of those, 37 samples scored a GIS below the cut-point of 42 (42 %). In total, 93 LRs were found, with 5 samples showing more than one rearranged HRR gene, each recording a GIS above 42. RAD51B (24), CDK12 (16), BRCA1 (14), ATM (8) and BRCA2 (7) were found to make up 74 % of all observed LRs. Interestingly, rearrangements in BRCA1 were mostly present in higher GIS samples (median GIS = 64.5), while LRs in other HRR genes such as RAD51B were observed across the whole GIS range (median GIS = 53), and CDK12 LRs were rather present in lower GIS samples (median GIS = 32).

Conclusion

Genomic LRs are observed in ovarian cancer samples across the whole GIS range, but occurrence is significantly skewed towards 5 of the 15 HRR genes. LRs in BRCA1 are predominantly found in GIS-high samples, whereas LRs in CDK12 mainly occur in GIS-low ovarian cancer samples.

***TP53* mutations are associated with primary endocrine resistance in luminal early breast cancer**

I. Grote¹, S. Bartels¹, L. Kandt¹, L. Bollmann¹, H. Christgen¹, M. Gronewold¹, M. Raap¹, U. Lehmann¹, O. Gluz^{2,3,4}, U. Nitz^{2,3}, S. Kümmel^{2,5,6}, C. zu Eulenburg², M. Braun⁷, B. Aktas^{8,9}, E.-M. Grischke¹⁰, C. Schumacher¹¹, K. Lüdtke-Heckenkamp¹², R. Kates², R. Würstlein¹³, M. Gräser^{2,3}, N. Harbeck^{2,13}, M. Christgen¹, H. Kreipe¹

¹Medizinische Hochschule Hannover, Institut für Pathologie, Hannover, Germany, ²Westdeutsche Studiengruppe, Mönchengladbach, Germany, ³Johanniter Ev. Krankenhaus Bethesda Mönchengladbach, Brustzentrum, Mönchengladbach, Germany, ⁴Universitätsklinik Köln, Frauenklinik und Brustzentrum, Köln, Germany, ⁵Evangelische Kliniken Essen-Mitte, Interdisziplinäres Brustkrebszentrum, Essen, Germany, ⁶Charité, Frauenklinik, Berlin, Germany, ⁷Rotkreuzklinikum München, Brustzentrum, München, Germany, ⁸Universitätsklinikum Essen, Klinik für Frauenheilkunde und Geburtshilfe, Essen, Germany, ⁹Universitätsklinikum Leipzig, Klinik für Frauenheilkunde, Leipzig, Germany, ¹⁰Universitätsklinikum Tübingen, Universitäts-Frauenklinik, Tübingen, Germany, ¹¹St. Elisabeth-Krankenhaus Köln-Hohenlind, Brustzentrum, Köln, Germany, ¹²Niels-Stensen-Klinik, Brustzentrum Osnabrück, Georgsmarienhütte, Germany, ¹³Universitätsklinikum München (LMU), LMU Brustzentrum, München, Germany

Background

Hormonal blockade provides an effective growth suppressive therapy for the majority of breast cancers (BC). However, about 20%–30% of luminal BC, local or distant recurrence during or after endocrine treatment. Mechanisms of primary non-responsiveness to endocrine treatment in luminal early breast cancer are currently far from being understood.

Methods

In this study, 622 hormone-receptor positive and *ERBB2* non-amplified early BC cases treated with short-term preoperative endocrine therapy (pET) from the WSG ADAPT trial (NCT01779206) were analyzed for alterations of genes which had been implicated in endocrine resistance in metastatic BC.

For this molecular analysis, endocrine proliferative response (EPR) to short-term pET was categorized in four categories corresponding to optimal response (post-pET Ki67 <10%) versus slightly, moderately, and severely impaired proliferative response (post-pET Ki67 10%–19%, 20%–34%, and ≥35%, respectively). Gene mutations commonly described in previously treated advanced breast cancer (*ARID1A*, *BRAF*, *ERBB2*, *ESR1*, *GATA3*, *HRAS*, *KRAS*, *NRAS*, *PIK3CA*, and *TP53*) were analyzed by next generation sequencing. Amplifications of *CCND1*, *FGFR1*, *ERBB2* and *PAK1* were determined by digital PCR or fluorescence in situ hybridization.

Results

The frequency of *TP53* mutations increased significantly with increasing EPR category ($P < 0.0001$). This was independent from the Oncotype DX Recurrence Score group and was seen in patient subsets treated with either tamoxifen or aromatase inhibitors ($P = 0.0005$ each).

In addition, *ERBB2*-amplified BC cases ($n = 8$) were also associated with impaired EPR. Despite the small number, we observed a statistically significant correlation between *ERBB2* amplification status and impaired EPR ($p = 0.0015$).

Conclusion

Our findings indicate that impaired EPR to pET is suitable to identify cases with primary endocrine resistance and appears to reflect the genetic risk in in early luminal breast cancer.

References:

Grote I, Bartels S, Kandt L, Bollmann L, Christgen H, Gronewold M *et al*. TP53 mutations are associated with primary endocrine resistance in luminal early breast cancer. *Cancer Med*. 2021 Dec;10(23):8581-8594. doi: 10.1002/cam4.4376.

Implementation of HRD analysis in daily routine diagnostics-overall performance and pitfalls

J. Siemanwoski, V. Welter, B. Schömig-Markiefka, U. Siebolts, S. Merkelbach-Bruse

Hospital, Pathology, Cologne, Germany

Background

20% of ovarian cancer samples without BRCA1/2 mutations but with genomic instability showed also good response rates for poly (ADP-ribose) polymerase (PARP) inhibitors. Therefore, HRD positivity has been added as new biomarker for PARPi response and different assays were developed identifying those genomic scars by analyzing the effects of defective homologous recombination associated genes. The Myriad myChoice assay and the Foundation Focus CDx BRCA LOH assay were already used in clinical studies. Alternative assays still need to be validated with clinical samples and regarding their performance in a daily routine setting. In this study we used the HRD Focus Assay (Amoy Dx) that simultaneously analyses and detects around 24 000 SNPs for genomic scar evaluation as well as *BRCA1* and *BRCA2* mutations to highlight issues of challenging samples, correct data interpretation and limitations of this system concurrently.

Methods

Within the last month more than 100 ovarian cancer routine diagnostic samples were analyzed both for their genomic scar score (GSS) and *BRCA1/2* mutational status. Prior analysis, DNA was extracted from formalin-fixed, paraffin-embedded tumor tissue (FFPE). For the combinational estimation of GSS and *BRCA1/2* library preparation was done using the HANDLE HRD Focus Panel (AmoyDx). After sequencing using the Nextseq (Illumina), data analysis was performed on the ANDAS Server (AmoyDx).

Results

According to the manufacturer, samples with a tumor cellularity below 30% and low rates of DNA (< 50 ng) resulting in low rates of SNP effective depth (<200) should not be used. Indeed, our results during validation revealed that those parameters could change the GSS, drastically. Therefore, around 5 % had to be excluded from analysis due to low DNA concentration or low cellularity. Additionally, around 7 % were not interpretable due to low rates of SNP effective depth.

Conclusion

In contrast to the results from clinical studies we found more samples being GSS positive without *BRCA* mutation than the stated 20%. In future studies a possible false positive rate of GSS should be analyzed more detailed in a clinical setting with direct comparison to the response rate of the combinational therapy using PARP inhibitors. In order to verify the HRD status other HRD panels or RAD51C staining could be used.

Additionally, we could show that correct data interpretation depends on the overall test performance

regarding coverage of SNP regions and cellularity.

AG11.11

Assessing and evaluating the scope and constraints of Idylla molecular assays by using different source materials in routine diagnostic settings.

S. Boppudi¹, E. Faust¹, S. Scheil-Bertram¹, A. Fisseler-Eckhoff^{1, 2}

¹*Helios Dr.Horst Schmidt Kliniken, Institute of Pathology and cytology, Wiesbaden, Germany,*

²*Gemeinschaftspraxis für Pathologie, Wiesbaden, Germany*

Background

For cancer patients' treatment, diagnostics concerning tumor type and determination of molecular markers in short turnaround time is very critical. The fully automated, real-time PCR based molecular diagnostic Idylla assays (Biocartis, Mechelen, Belgium) are well established in many laboratories for qualitative detection, short turnaround time and routine screening of clinically relevant oncogenic mutations in EGFR, BRAF, KRAS, NRAS genes and MSI testing. According to the manufacturer, all IVD-assays are recommended to use only with FFPE tissue samples of 5-10µM dissections with at least 10% tumor content. This study also evaluated the performance of the Gene Fusion assays cartridges (RUO). In this current study, we have tested the performance and accuracy of these assays with other different tissue/source materials like isolated DNA/RNA, cryomaterial etc. along with the recommended FFPE material.

Methods

In this current study, the different source materials used as input material in the assay cartridges are (1) gDNA/RNA isolated from FFPE tissues, cryomaterial, frozen tissue cuts, and HE stained slides. (2) tissue scratched from normal 5µM and 2µM FFPE sections (3) tissue scratched from HE slides (4) direct input of cryomaterial fluid (5) direct input of tissue section fluid. Along with different input materials, the study also included archival FFPE tissue sections dating from 15 years back. The study also aimed for performance check of the IVD-Idylla assays cartridges when tested for different pan-tumor samples individually.

Results

All the assays tested with tissue scratched from FFPE/HE sections showed above 96% of accuracy, sensitivity, and specificity individually. This study indicates that minimum of 8ng/µl gDNA concentration is required with at least 10µl input (80ng) for certainty of results. For use of fluids, a direct input of 20µl is recommended for better performance. The Idylla assays also performed exceptionally well on the archival tissues showing above 94% efficiency. The use of IVD-labeled assays for other solid tumors was also remarkable with more than 95% sensitivity and specificity.

Conclusion

The performance test and accuracy of Idylla assays with different tissue/source materials along with the recommended FFPE material showed high efficiency with certain limitations. For use of Idylla assays, both qualitative and quantitative applicability of different tumor materials could produce efficient results in different diagnostic settings.

Results of studies to validate HRD analysis using the Qiaseq HRD assay from Qiagen

W. Dietmaier, F. Keil, M. Klier-Richter, A. Scheiter, K. Utpatel

Universität Regensburg, Institut für Pathologie, Regensburg, Germany

Background

Homologous repair deficiency (HRD) is a new biomarker to assess the potential benefit of a PARP inhibitor therapy in various tumor entities, especially in high-grade serous ovarian carcinoma (HGSC). Several assays are commercially available to study HRD by NGS, but their diagnostic suitability needs to be validated. Data from validation studies of the Targeted DNA Panel (Qiagen) including HRD and 15 HRR related genes (Qiagen) are presented here.

Methods

Twelve ovarian cancer cases with known HRD status were analyzed using the Targeted DNA HRD Panel (Qiagen). Sequencing was performed on the NextSeq platform (Illumina). FASTQ data were generated from the primary data using the Docker engine (Illumina) and analyzed using CLC Genomics Workbench (21.0.5) to calculate HRD scores. The accuracy of the results was investigated by comparison with results from pre-studied tumor samples with already known HRD values and HRD status data generated externally by MyChoice® HRD Plus CDx assay (Myriad Genetics) as part of routine diagnostic studies.

Results

Analysis to calculate concordance of HRD scores yielded a correlation coefficient (Pearson) of 0.9481. The proportion of true positive HRD statuses was 100% (n=2), and the proportion of false negatives was 0%. This results in an analytical sensitivity of 100%. The proportion of true-negative statuses was 100% (n=10), and the proportion of false-positive statuses was 0% resulting in an analytical specificity of 100%. Precision studies showed deviations of HRD score values of +/-2 when using the same starting DNA. The overall HRD statuses of all 12 samples were consistent with the externally determined examinations, respectively.

Conclusion

Our data of HRD analyses with the Qiaseq-HRD-Assay (Qiagen) show a high concordance in the HRD values and a complete concordance in the HRD statuses with HRD results of pre-studied tumor samples with already known HRD values and HRD statuses generated externally by MyChoice® HRD Plus CDx assay (Myriad Genetics) in the examined group of 12 ovarian cancer cases.

AG11 AG Molekularpathologie III

AG11.13

Targeted and explorative mass spectrometry show kallikrein 6 and 10 overexpression in PDAC and suggest a collective cell migration for pancreatic cancer

J. Werner^{1,2}, P. Bernhard¹, K. Fröhlich¹, M. Fahrner¹, J. Eberhard², P. Bronsert¹, F. Rückert², O. Schilling¹

¹*Institute for Surgical Pathology, University of Freiburg, Freiburg, Germany, Freiburg, Germany,* ²*Surgical Clinic of Mannheim, University of Heidelberg, Mannheim, Germany, Mannheim, Germany*

Background

Pancreatic ductal adenocarcinoma (PDAC) represents one of the most lethal malignancies worldwide and therefore urgently needs new diagnostic and therapeutic strategies. The secreted proteases kallikrein (KLK) 6 and 10 were shown to be significantly upregulated in PDAC and are hence assumed to play critical roles in the progression of pancreatic cancer. In this project, we performed both targeted and shotgun mass spectrometry (MS) to investigate KLK6 and 10 protein expression in PDAC, and further generated a complete proteome profiling of PDAC to better understand the disease-related proteome biology.

Methods

Macrodissected FFPE tissue samples of PDAC (n=14), chronic pancreatitis (n=7), normal (n=5) and non-malignant adjacent pancreas (n=11) were prepared following an optimized single-pot solid-phase-enhanced sample preparation (SP3) protocol prior to targeted and explorative MS analysis. Data analysis was performed with Skyline and DIA-NN with subsequent differential expression analysis using the multigroup limma approach for pairwise comparisons.

Results

The targeted results showed that KLK6 and 10 protein levels were significantly increased in PDAC compared to all controls, strongly suggesting that the aforementioned proteins contribute to its malignancy. Explorative analysis showed significant downregulation of proteins involved in translation and ER-related proteins in both PDAC and chronic pancreatitis, which illustrates the impaired function of the exocrine pancreas. In chronic pancreatitis, we observed a significant upregulation of proteins involved in wound healing and the humoral immune response, which underlines its inflammatory properties. PDAC revealed significantly overexpressed proteins involved in cell adhesion, which stands in contrast to the EMT theory and suggests a collective cell migration rather than single-cell dissemination. In PDAC we further observed a significant upregulation of proteins involved in the glycolysis in line with a downregulation of the mitochondrial energy metabolism, illustrating the Warburg Effect in pancreatic cancer.

Conclusion

KLK6 and 10 are significantly overexpressed in PDAC compared to all controls and may therefore represent promising targets for new biomarkers and/or new therapeutic targets in pancreatic cancer. We further identified interesting protein representatives in PDAC, which might contribute to its malignancy. To validate our findings, future studies with larger patient cohorts will be needed.

The role of TROP2 methylation in colon cancer cells

A. Gehring¹, K. Huebner¹, J. Prochazka², K. Erlenbach-Wuenssch^{1,3}, R. Grutzmann^{3,4}, A. Hartmann^{1,3}, R. Schneider-Stock^{1,3}

¹University Hospital, Institute of Pathology, FAU Erlangen-Nürnberg, Erlangen, Germany, ²Czech Centre for Phenogenomics, Institute of Molecular Genetics, ASCR, Prague, Czech Republic, ³Comprehensive Cancer Center Erlangen-EMN (CCC ER-EMN), University Hospital Erlangen, Friedrich Alexander University Erlangen-Nürnberg, Erlangen, Germany, ⁴Department of Surgery, Friedrich Alexander University Erlangen-Nürnberg, Erlangen, Germany

Background

TROP2 is a transmembrane glycoprotein, which is encoded by the TACSTD2 gene. Its overexpression in colon cancer cells is associated with poor prognosis and aggressiveness. Just recently, FDA and EMA approved a TROP2 antibody-drug conjugate for treatment of triple negative breast cancer. TROP2 is majorly regulated by promotor methylation which is associated with transcriptional silencing. There is not much known yet about the epigenetic regulation of TROP2 in colon cancer cells. Thus, we aimed to evaluate the role of promoter hypermethylation for TROP2 expression in colon cancer.

Methods

Eight different colon cancer cell lines were analyzed regarding their TROP2 expression by Western blotting. Their promotor methylation status was analyzed by Pyrosequencing. We also analyzed the promotor methylation in human tissue samples, comparing tumor and non-tumor samples. Their corresponding TROP2 expression status was determined by immunohistochemistry staining. TROP2 low or no expressing cell lines were treated with the DNA methyltransferase 1 inhibitor (DNMT1i) 5-Azacytidine to re-express TROP2. Next, CRISPR/Cas9 TROP2 knockout (KO) clones were generated to functionally analyze their migratory potential in a wound healing assay.

Results

TROP2 expression in the tumor cell lines was strongly correlated with their TROP2 promoter methylation status. Tumor tissues having generally higher TROP2 expression than their corresponding non-tumor samples and mostly showed a demethylated TROP2 promoter. Treatment with a DNMT1i led to demethylation of the TROP2 promoter accompanied by an increase in TROP2 mRNA and protein expression. TROP2 KO cells exhibited a lower migratory potential.

Conclusion

TROP2 is a trigger for tumor cell migration and its expression in colon cancer cells is epigenetically regulated by promoter hypermethylation.

AG11.15

A helpful tool to estimate the disease-causing value of unknown gene fusion.

M. Wessolly¹, F. Mölder^{1,2}, T. Herold¹, J. Köster², K. W. Schmid¹, H.-U. Schildhaus¹, S. Borchert¹, F. D. Mairinger¹

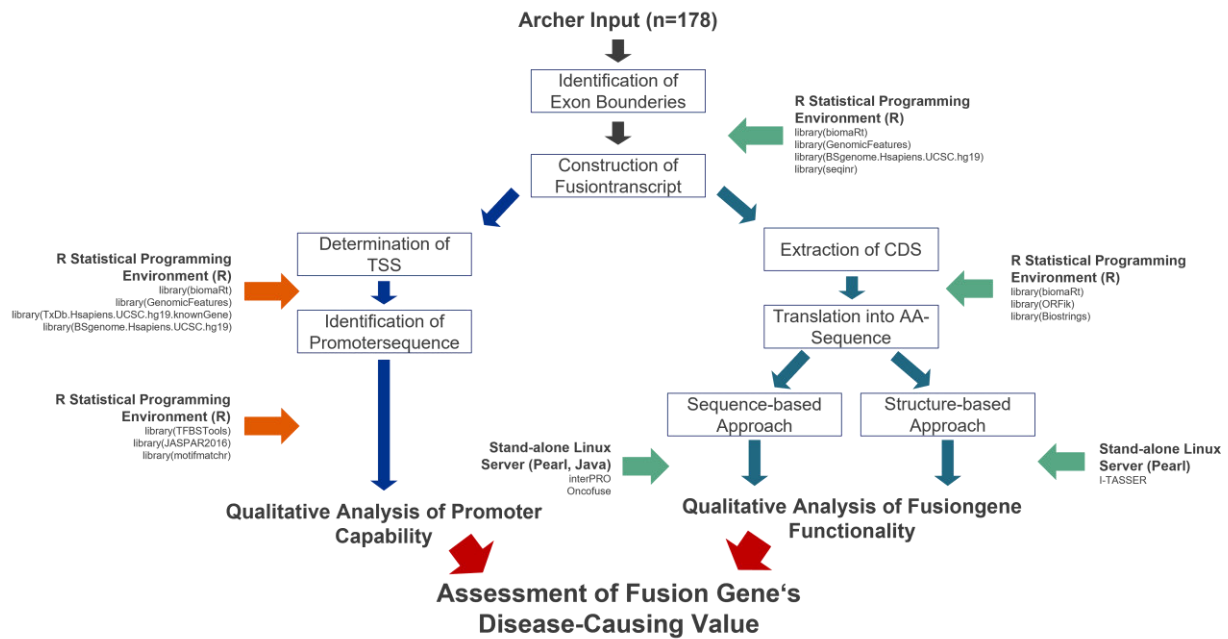
¹*Universitätsklinikum Essen, Institut für Pathologie, Essen, Germany*, ²*Universitätsklinikum Essen, Genominformatik, Institut für Humangenetik, Essen, Germany*

Background

Gene fusions are genomic events that may result in new oncogenes and serve as drivers in various malignancies. Though specific driver mutations resulting from fusions, like EML4-ALK in Non-small cell lung carcinoma or EWSR1-FLI1 in Ewing sarcoma, already play a crucial role for diagnostic and therapeutic decisions, newly identified gene fusions by novel RNA sequencing techniques have remained elusive regarding their therapeutic relevance. Here we want to present a bioinformatical pipeline specifically developed to evaluate gene fusion transcripts based on transcript sequence and thereby providing a tool easily usable by clinicians and pathologists alike.

Methods

Gene names, reference sequences as well as the two genomic breakpoints provided by any RNA sequencing approach (e.g. ArcherDX) are needed as an input. From this, a fusions transcript is constructed based on exonic sequences from each fusion partner. Additionally, the promotor potency of each partner is assessed by evaluating the amount of matched transcription factor binding motifs. Furthermore, the fusion databases TCGA, ChiTarRS, ChimerKB and COSMIC are researched, whether a specific fusion has already been reported. These analysis steps are conducted in the R programming environment (v. 4.1.2). A java script-based standalone application of InterPro is used to estimate which protein domains either retained or lost their function due to the fusion process. In parallel, first impressions of a fusions' functional influence can be gained by running a java script-based application of Oncofuse.



This figure gives a brief overview of our conducted methodology.

Results

Transferring this methodology to 178 sequenced fusions, they can be distinguished based on their promotor activity and expression gain. Involved fusion partners could be linked to various cell growth and differentiation pathways including MAPK-and PI3K-Akt signaling. Many of them were characterized as oncogenes and retained primarily their kinase function during the fusion process.

Conclusion

This tool allows a quick and reliable evaluation of unknown fusions and how to put them into context with known oncogenes. By knowing which functions are retained during the fusion progress, this tool may also be helpful to predict the therapeutic relevance of specific fusions.

Implications for molecular testing of FGFR2 fusions in cholangiocarcinoma

O. Neumann^{1, 2, 3}, T. Burn^{4, 5}, M. Allgäuer¹, M. Ball^{1, 6}, M. Kirchner¹, T. Albrecht¹, A.-L. Volckmar¹, S. Beck¹, V. Endris¹, H. Goldschmid¹, U. Lehmann⁷, H. Seker-Cin¹, S. Uhrig^{8, 9}, S. Rössler¹, J. Budczies^{1, 2}, S. Fröhling^{2, 3, 8, 10}, T. Longerich^{1, 11}, A. H. Wagner^{12, 13}, A. Vogel¹⁴, P. Schirmacher^{1, 2, 3, 11}, A. Stenzinger^{1, 2, 3, 6}, D. Kazdal^{1, 2, 3, 6}

¹Universitätsklinikum Heidelberg - Institut für Pathologie, Heidelberg, Germany, ²Zentrum für Personalisierte Medizin Heidelberg (ZPM), Heidelberg, Germany, ³Deutsches Krebskonsortium (DKTK), Heidelberg, Germany, ⁴Ehemals Incyte Research Institute, Wilmington, DE, United States of America, ⁵Jetzt Tyra Biosciences, Carlsbad, CA, United States of America, ⁶Deutsches Zentrum für Lungenforschung (DZL), Translational Lung Research Center (TLRC), Heidelberg, Germany, ⁷Medizinische Hochschule Hannover, Institut für Pathologie, Hannover, Germany, ⁸Deutsches Krebsforschungszentrum (DKFZ), Heidelberg, Germany, ⁹Computational Oncology Group, Molecular Precision Oncology Program, (NCT), Heidelberg, Germany, ¹⁰Nationales Centrum für Tumorerkrankungen (NCT), Translationale Medizinische Onkologie, Heidelberg, Germany, ¹¹Leberkrebszentrum Heidelberg, Heidelberg, Germany, ¹²Nationwide Children's Hospital, Columbus, Steve und Cindy Rasmussen Institut für Genomische Medizin, Columbus, United States of America, ¹³The Ohio State University College of Medicine, Abteilung für Kinderheilkunde und Biomedizinische Informatik, Columbus, United States of America, ¹⁴Medizinische Hochschule Hannover, Gastroenterologie, Hepatologie und Endokrinologie, Hannover, Germany

Background

Cholangiocarcinoma (CCA) is a primary malignancy of the biliary tract with a poor prognosis. Recently, several actionable genetic aberrations with significant enrichment in intrahepatic CCA have been identified, including FGFR2 gene fusions with a prevalence of 10-15%. Recent clinical data indicate that these fusions can be treated with drugs in advanced/metastatic disease in the second-line setting, and efficacy in earlier lines of therapy is currently being evaluated in clinical trials. This scenario warrants standardized molecular profiling of these tumors.

Methods

To this end, we undertook a detailed analysis of the original genetic data from the FIGHT-202 trial. We describe the genetic landscape and architecture of *FGFR2* fusions in iCCA including their annotation, clinical reporting, and implications for the selection of appropriate diagnostic tools.

Results

By comparing different detection methods and presenting representative cases, we have described the genetic landscape and architecture of FGFR2 fusions in iCCA and highlighted biological and technical aspects to be considered in their detection. We elaborated parameters, including a proposed annotation, that should be provided in a molecular diagnostic FGFR2 report to allow a full understanding of the analysis performed and the information provided.

Conclusion

Covering and dissecting these aspects in detail will support molecular pathologists, pathologists, and clinicians in diagnostics, reporting of results and decision making.

AG11.17

Two years of targeted therapy- a single center molecular tumor board observational study

A. Scheiter¹, F. Hierl¹, F. Keil¹, F. Lüke^{2,3}, T. Pukrop², W. Dietmaier¹, M. Evert¹, K. Utpatel¹

¹Universität Regensburg, Institut für Pathologie, Regensburg, Germany, ²Universitätsklinikum Regensburg, Klinik und Poliklinik für Innere Medizin III, Regensburg, Germany, ³Fraunhofer-Institut für Toxikologie und Experimentelle Medizin ITEM-R, Regensburg, Germany

Background

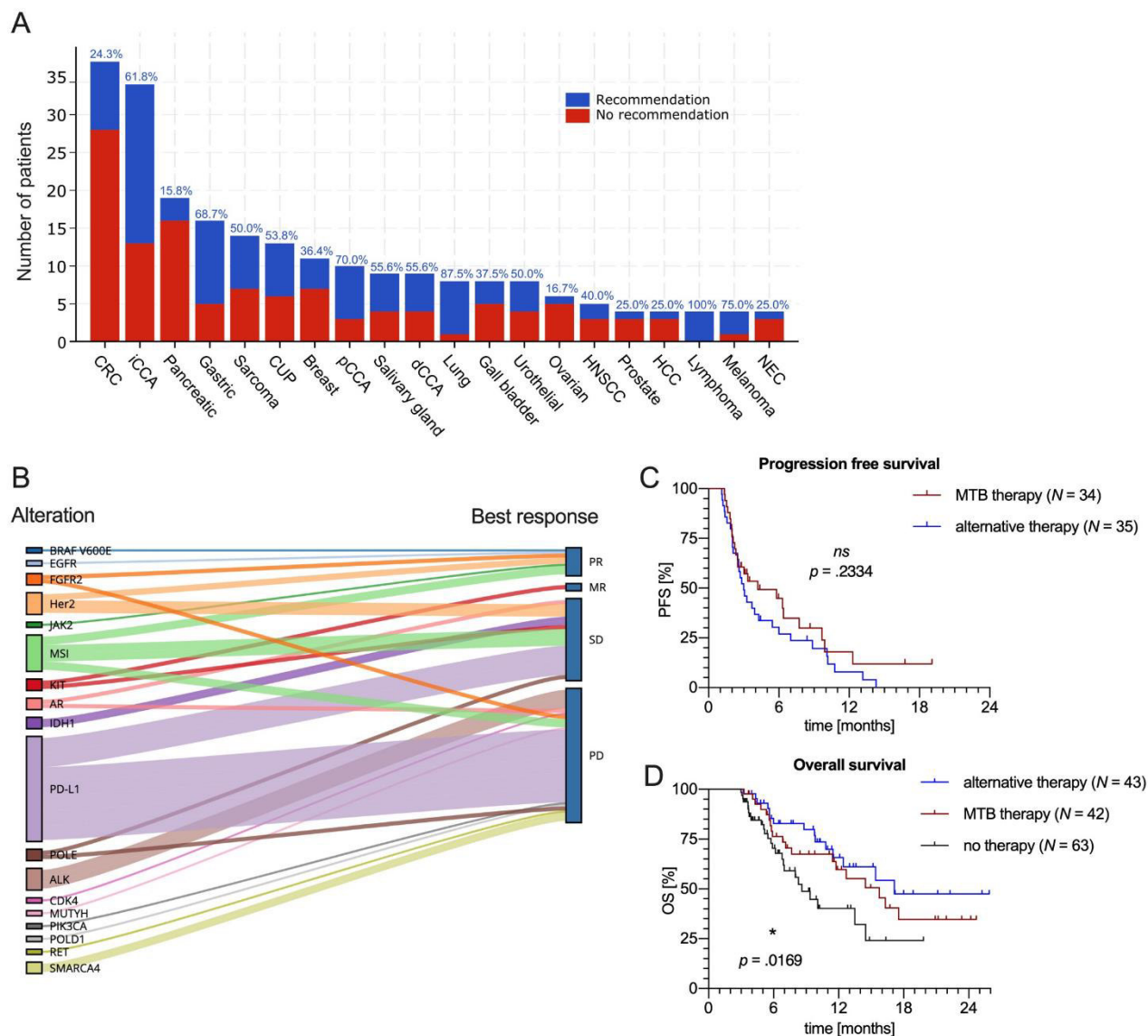
Molecular tumor board (MTB) guided therapies are not yet recognized as standard of care, since there have been conflicting reports in the past on their potential benefit. Given the lack of evidence, a constant evaluation of MTB informed treatments is compulsory. Here, we present an analysis of two-years MTB experience in a comprehensive cancer center.

Methods

Data were obtained from patients enrolled in our prospective MTB observational study. The enrollment criteria included: advanced cancers under last-line treatment, or rare cancers without established therapy, estimated life expectancy of more than 6 months and openness towards experimental treatments. Next-generation DNA sequencing using the TSO500 panel on a NextSeq platform (Illumina) in conjunction with immunohistochemistry for Her2, PD-L1 as well as mismatch repair proteins and PCR-based fragment-sizing for MSI evaluation were employed.

Results

A total of 251 patients comprising numerous cancer entities (A) were included from 2019 to 2021. Pathogenic or likely pathogenic mutations were detected in 210 patients (83.7%). 125 patients received a therapy recommendation (49.8 %) with a preponderance of intrahepatic cholangiocarcinoma (61.8%) and gastric adenocarcinoma (68.7%), as opposed to a recommendation rate of only 24.3% in colorectal cancer and 15.8% in pancreatic cancer. 47 patients (B) received an MTB-recommended therapy (18.7%). Partial response was observed in 6, mixed response in 1, stable disease in 11 and progressive disease in 18 patients. Median overall survival (OS) for patients without therapy, with MTB therapy and with an alternative therapy was 8.6, 15.8 and 17.1 months respectively ($p = 0.0169$, Log-rank test, C). No significant difference for progression free survival (PFS) was seen in favor of MTB therapy as opposed to alternative therapies with a median PFS of 4.2 months vs. 3.0 months ($p = 0.2334$, D).



(A) Stacked bar chart of therapy recommendations per cancer entity. (B) Alterations + responses. PR, partial remission; MR, mixed response; SD, stable disease; PD, progressive disease. (C) PFS (Alternative = guideline + physician's choice) (D) OS

Conclusion

Certain entities, including cholangiocarcinoma and gastric cancer displayed a high proportion of recommendations, while the analysis of colorectal and pancreatic cancer rarely yielded targetable alterations. Albeit only a fraction of recommended therapies was administered, clinical benefit could frequently be derived. Thus, MTB informed therapies can well be considered as a last bastion of defense.

AG12 AG Kinder- und Fetalpathologie I

AG12.01

Placental pathology in sudden intrauterine death (SIUD) in SARS-CoV-2 positive oligosymptomatic women

G. G. R. Hiller¹, L.-C. Horn¹, I. Krücken¹, M. Niedermair², K. Perac², C. Pietsch³, C. Brambs⁴, A.-K. Höhn¹

¹Universitätsklinikum Leipzig, Institut für Pathologie, Leipzig, Germany, ²Klinikum Wels-Grieskirchen, Institut für Klinische Pathologie, Molekularpathologie und Zytodiagnostik, Wels-Grieskirchen, Austria,

³Universitätsklinikum Leipzig, Institut für Medizinische Mikrobiologie und Virologie, Leipzig, Germany,

⁴Luzerner Kantonsspital, Frauenklinik, Luzern, Switzerland

Background

Pregnant women are also susceptible for SARS-CoV-2. Although the infection of the placenta may be rare, occasionally pregnancy may be affected by intrauterine failure. The knowledge of placental morphology on sudden intrauterine demise is still limited.

Methods

Fetal and placental tissue of two cases of sudden intrauterine death in the second trimester were analysed morphologically and by immunohistochemistry and RT-PCR in detail.

Results

Both mothers were positively tested for the Alpha variant of SARS-CoV-2 but were oligosymptomatic for COVID-19. Unexpected sudden intrauterine death (SIUD) occurred at the 15.2nd and 27.3rd weeks of gestation.

One fetus presented intrauterine growth restriction but no malformation nor inflammatory changes were observed at both autopsies. In contrast to the placentas, all tested fetal tissue was negative for SARS-CoV-2 by immunohistochemical and RT-PCR analyses. Macroscopically the placentas presented increased consistency with a white, reticular cutting surface occupying about 95% of the whole placenta.

Histologically only very focal histiocytic chronic intervillitis was seen. Massive perivillous fibrin deposits with extensive necroses of the villous trophoblast were present in more than 90% of the placental tissue. Immunohistochemical staining was strong and diffusely positive for SARS-CoV-2 in the villous trophoblast and rarely within villous stromal cells. Placental SARS-CoV-2 infection was confirmed by RT-PCR.

Conclusion

Sudden intrauterine death may occur in COVID-19 oligosymptomatic mothers. Acute placental failure is responsible for SIUD, morphologically presented by massive perivillous fibrin deposits and extensive necroses of the villous trophoblast which is positive for SARS-CoV-2 by immunohistochemical staining and RT-PCR. Detailed histopathological examination of placental and fetal tissue to verify SARS-CoV-2 is

mandatory to determine the pathogenesis and understand the functionality of that disease.

Placental pathology associated with SARS-CoV-2 infection - case series conducted at the Institute for Surgical Pathology, Medical Centre, University Freiburg

L. Reil¹, M. Kunze², T. Menter³, M. Bohlmann⁴, M. Werner¹, S. Huber-Schumacher¹

¹Institut für Klinische Pathologie, Universitätsklinikum Freiburg, Freiburg, Germany, ²Klinik für Frauenheilkunde, Universitätsklinikum Freiburg, Freiburg, Germany, ³Institut für Medizinische Genetik und Pathologie, Universitätsspital Basel, Universität Basel, Basel, Switzerland, ⁴Zentrum für Gynäkologie und Geburtshilfe, St. Elisabethen-Krankenhaus Lörrach gGmbH, Lörrach, Germany

Background

Coronavirus disease 2019 (COVID-19), caused by severe acute respiratory syndrome coronavirus 2 (SARS-CoV-2), during pregnancy can lead to placental infection and may severely damage the placenta and even lead to intrauterine foetal demise (IUID). “SARS-CoV-2 placentitis” is defined by the triad of increased perivillous fibrin deposition, necrosis of trophoblast and chronic histiocytic intervillitis (CHI).

The aim of the presented study was to collect data on placental changes in SARS-CoV-2 positive pregnant women in relation to clinical symptoms and a review of literature.

Methods

In 2021, there were over 2 000 births at the University Medical Centre in Freiburg, of which 140 were COVID-19 cases. In this case series, we analysed 50 placentas of women, who had experienced COVID-19 during pregnancy or active infection during childbirth between January 2021 and February 2022.

Placentas were examined macroscopically and histologically according to standardised protocols for pathological changes, including signs of maternal and foetal malperfusion characteristic for SARS-CoV-2. In cases of “SARS-CoV-2 placentitis” further immunohistochemical studies were performed, including the detection of SARS-CoV-2 antigens.

Results

Histopathological prominent CHI, increased perivillous fibrin deposition and trophoblast necrosis were only observed in seven cases, which resulted in acute placental insufficiency and in five cases in IUID. The majority of our cases did not display any prominent CHI or trophoblast necrosis, with varying degrees of intervillous fibrin deposition. Only a few cases demonstrated signs of foetal vascular malperfusion.

Conclusion

Our case series results are in line with current literature, which showcase distinct, but rare placental damage known as “SARS-CoV-2 placentitis” in COVID-19 cases. However, the majority of placentas of SARS-CoV-2-infected mothers did not display any significant histopathological changes.

AG12.03

Review of placentas submitted for histological examination with regard to their clinical indication and correlation with the histological findings

L. Strahler, Dörthe Brüggmann(Geburtshilfe-Universitätsklinikum Frankfurt a.M.), Franz Bahlmann(Geburtshilfe-Bürgerhospital Frankfurt a.M.), Steffen Kunzmann(Neonatologie-Bürgerhospital Frankfurt a.M.), Elise Gradhand(Pathologie-Universitätsklinikum Frankfurt a.M.)

Senckenbergisches Institut für Pathologie, Kinder- und Perinatalpathologie, Frankfurt am Main, Germany

Background

Currently in Germany, there is no official guideline for submitting placentas for histopathological examination. Placentas are usually sent for histological examination by obstetricians under locally established indications. However, the practice of submitting placentas varies between different centers. We examine the cohort of placentas sent to us and compare it with a control group of placentas with an inconspicuous course of birth, without clinically established indications.

Methods

A placenta request form was used, which was based on established international guidelines. A total of 236 placentas from 2019-2021 were evaluated. 127 placentas from singleton and twin pregnancies with clinical indications and control group of 109 placentas from singleton and twin pregnancies without clinical indications. They underwent standardized histopathologic examination. Clinical information (gestational age, birth weight, maternal BMI, pregnancy history, APGAR score) and indication were taken from the request form and later statistically correlated with histological diagnoses.

Results

In the group of placentas from singleton pregnancies with clinical indication, 10 (13.7%) placentas are without detectable histopathological findings. In contrast, 63 (86.3%) placentas show pathology. In the control group, 29 (74.4%) placentas are histologically unremarkable. In 10 (25.6%) placentas in this group, there is pathological change. The group of placentas from twin pregnancies with clinical indications presents pathology in 33 (61.1%) placentas. Again, 21 (38.9%) placentas show no pathological findings. In the control group, 21 (30%) placentas present pathology. In contrast, 49 (70%) placentas are pathologically unremarkable.

Conclusion

One of the most important findings of the study is that the largest proportion of submitted singleton placentas with clinical indication have pathological placental findings and thus can be very helpful for further management of the child and mother and potentially future pregnancies. Placental examination based on clinically established indications regularly provides information about pregnancy and peripartum conditions for mother and child and is therefore often an underestimated diagnostic tool in obstetrics.

AG12.04

Meta-analysis on COVID-19-pregnancy-related placental pathologies shows no specific pattern

J.-T. Suhren¹, A. Meinardus¹, K. Hussein², N. Schaumann¹

¹Institut für Pathologie, Medizinische Hochschule Hannover, Hannover, Germany, ²MVZ Pathologie Hildesheim Hannover-Zentrum GmbH, Hildesheim, Germany

Background

Coronavirus disease 2019 (COVID19) pneumonia may occur during pregnancy, but fetal infection rarely occurs. There are several reports on placenta pathology, which indicate COVID19-typical changes in a subfraction of cases, in particular chronic histiocytic intervillitis (CHIV). Therefore, the aim of this meta-analysis was to clarify whether there is a typical COVID19-associated pattern of placenta lesions.

Methods

Systematic literature search was performed. Publications of ≥ 10 cases with COVID-19-positive pregnancies and histological placenta examinations were evaluated (30 publications from 2019-2021; 1452 placenta cases).

Results

No COVID-19-specific placenta pathology pattern was found. Both vascular and inflammatory lesions, including CHIV, manifested in similar frequencies as in non-COVID19 placentas.

Conclusion

There are no typical placenta pathologies associated with COVID19. The most important prognostic factor appears to be COVID19-pneumonia-associated maternal hypoxia with secondary fetal brain damage rather than placenta pathologies.

Prognosis of postoperative clinical course of neonates after surgical intervention for necrotizing enterocolitis - is the histological examination of the surgical specimen helpful?

O. Schickedanz¹, E. Gradhand¹, U. Rolle²

¹*Dr. Senckenbergisches Institut für Pathologie, Kinderpathologie, Frankfurt am Main, Germany,*

²*Universitätsklinikum Frankfurt, Kinderchirurgie & Kinderurologie, Frankfurt am Main, Germany*

Background

Necrotizing enterocolitis (NEC) is a common disease of premature infants. Besides the attempt of conservative antibiotic therapy, surgical excision of the necrotic intestinal segment, as sparingly as possible, represents the common practice. We want to investigate whether there is a correlation between the histopathological findings and the postoperative clinical course of the operated children. So far, no studies on a possible correlation have been published in the literature.

Methods

We re-assessed the surgical specimen of 57 infants with intestinal perforations or the diagnoses of NEC during the years 2010-2019. We examined the H+E slides with regard to the vitality of the mucosa of the central resection segment and the resection margins and correlated these with clinical parameters: survival, NEC recurrence, other postoperative complications (Ileus, malrotation, anasomatic insufficiency, stenosis). We divided the children's cases into groups with none, one or two avital resection margins. The groups were further subdivided according to the clinical parameters of death, NEC recurrence and other postoperative complications.

Results

Of the original 72 cases examined, 57 cases were finally included. Of the 57 children, 5 (8.8%) died postoperatively, 9 (15.8%) had another NEC, 29 (50.1%) remained recurrence-free, and 14 (24.5%) had other postoperative complications. A chi-square test was used to determine whether there was an association between the histopathologic vitality of the resection margins and the postoperative course. The hypothesis was accepted with a significance of 25.9%. According to our data, there has been no statistical correlation between the viability of the resection margins of the NEC specimens and clinical survival. Further histological parameters with potential clinical relevance were assessed. For example, we also examined the resected specimens for peritonitis. Of 57 children, only 14 (24.6%) had extensive acute peritonitis.

Conclusion

This study assesses whether there is a correlation between the histologic findings of surgical NEC specimens and the clinical outcome and potential prognosis of the infants. There is a tendency for correlation between certain histological parameters and clinical outcome. We also found that certain histologic features could explain the pathomechanism of NEC occurrence in individual cases. This information could support clinical

care and potentially improve clinical outcomes.

Case Report: Autopsy of a 4-month-old infant with Waterhouse-Friderichsen syndrome and lymphocytic interstitial pneumonia due to co-infection with SARS-CoV-2 and *Neisseria meningitidis*

F. Kellers, E. Jüttner, C. Röcken, K. Heß

Department of Pathology, University Hospital Schleswig-Holstein, Kiel, Germany

Background

Severe or fatal outcomes following SARS-CoV-2 infection in infants are rare. When compared to adults, children often have a milder course and favorable prognosis.[1] Co-infections with SARS-CoV-2 and other respiratory pathogens are common in children, but do not aggravate the course of the disease in most cases.[2] Consequently, histopathological examinations of tissue alterations due to COVID-19 in infants have not been performed to a large extent.

Methods

We present an autopsy case of a four-month-old patient that was diagnosed with COVID-19 14 days prior to hospital admission for meningococcal meningitis, and died of septic shock in multiorgan failure despite escalated intensive therapy. Cerebrospinal fluid (CSF) had been obtained before antibiotic treatment was started. Autopsy was performed five days post mortem. Swabs were taken for bacterial culture and PCR analyses. Tissue samples were fixed in 4 % formaldehyde and processed according to our standard protocols. Analyses on H&E and immunohistochemical (IHC) stained slides were performed on paraffin-embedded tissue and reviewed by board certified surgical pathologists and neuropathologists.

Results

Autopsy revealed features of Waterhouse-Friderichsen syndrome such as hemorrhagic infarction of adrenal glands, signs of disseminated intravascular coagulation and septic shock. Immunohistochemical investigation of the central nervous system revealed acute meningitis, hypoxic ischemic brain damage and edema. Moreover, the lung displayed lymphocytic interstitial pneumonia, which was supported by IHC staining. *Neisseria meningitidis* serogroup B was retrieved from CSF but was not detectable on meninges or lung post mortem. SARS-CoV-2 was detected by PCR test in the lung tissue taken post mortem.

Conclusion

In this case of co-infection with SARS-CoV-2 and *Neisseria meningitidis*, fatal pathological findings due to meningococcal disease were confirmed. Although the infant had presented with mild symptoms and clinical recovery regarding COVID-19, we confirmed lymphocytic interstitial pneumonia after 14 days. Cases of infants and children with a severe course of COVID-19 are rare, and mostly attributed to patients with comorbidities.[3] However, in this case histological examinations showed significant tissue alterations attributed to SARS-CoV-2 infection despite clinical recovery. In a setting of bacterial co-infection a severe course of disease is possible.

Literaturangaben

- [1] Ludvigsson JF. , (2020), Systematic review of COVID-19 in children shows milder cases and a better prognosis than adults, *Acta Paediatr*, 1088-1095, 109(6), <https://www.ncbi.nlm.nih.gov/pubmed/32202343>
- [2] Li Y, Wang H, Wang F, Lu X, Du H, Xu J, et al., (2021), Co-infections of SARS-CoV-2 with multiple common respiratory pathogens in infected children: A retrospective study, *Medicine (Baltimore)*, e24315, 100(11), <https://www.ncbi.nlm.nih.gov/pubmed/33725930>
- [3] Williams N, Radia T, Harman K, Agrawal P, Cook J, Gupta A, (2021), COVID-19 Severe acute respiratory syndrome coronavirus 2 (SARS-CoV-2) infection in children and adolescents: a systematic review of critically unwell children and the association with underlying comorbidities, *Eur J Pediatr*, 689-697, 180(3), <https://www.ncbi.nlm.nih.gov/pubmed/32914200>

AG12 AG Kinder- und Fetalpathologie II

AG12.07

Development of 3D spheroid models highlights the therapeutic potential of combining BH3 mimetics with Natural Killer (NK) cells as a novel therapeutic strategy in pediatric rhabdomyosarcoma

V. Särchen¹, S. Shanmugalingam¹, S. Kehr¹, L. M. Reindl², V. Greze², S. Wiedemann¹, C. Boedicker¹, M. Jacob¹, K. Bankov³, N. Becker³, S. Wehner², T. M. Theilen⁴, **S. Gretser**³, E. Gradhand³, C. Kummerow⁵, E. Ullrich², M. Vogler¹

¹Goethe-University Frankfurt, Institute for Experimental Cancer Research in Pediatrics, Frankfurt am Main, Germany, ²Goethe-University Frankfurt, Children's Hospital, Frankfurt am Main, Germany, ³Goethe-University Frankfurt, Dr. Senckenberg Institute of Pathology, Frankfurt am Main, Germany, ⁴Goethe-University Frankfurt, Department of Pediatric Surgery and Pediatric Urology, Frankfurt am Main, Germany, ⁵School of Medicine, Department of Biophysics, Center for Integrative Physiology and Molecular Medicine, Homburg, Germany

Background

The induction of apoptosis is a direct way to eliminate tumor cells and improve cancer therapy. Apoptosis is tightly controlled by the balance of pro- and antiapoptotic Bcl-2 proteins. BH3 mimetics neutralize the antiapoptotic function of Bcl-2 proteins and are highly promising compounds inducing apoptosis in several cancer entities including pediatric malignancies. However, the clinical application of BH3 mimetics in solid tumors is impeded by the frequent resistance to single BH3 mimetics and the anticipated toxicity of high concentrations or combination treatments. One potential avenue to increase the potency of BH3 mimetics is the development of immune cell-based therapies to counteract the intrinsic apoptosis resistance of tumor cells and sensitize them to immune attack.

Methods

Rhabdomyosarcoma cell lines (RH30, RD) were cultured in regular monolayer culture as well as 3D spheroid culture and treated with apoptosis inducing agents (BH3 mimetics, Bcl-XL Inhibitor A1331852, Bcl-2 Inhibitor ABT-199 or Mcl-1 Inhibitor S63845). In following experiments, the cell lines were co-treated with BH3 mimetics and enriched NK cells, which were isolated from Buffy coats of healthy donors. To quantify susceptibility to the treatments, cell viability as well as cell death analysis were performed.

Results

First, we were able to establish spheroid cultures of rhabdomyosarcoma cells that served as models for drug testing. In this model, we could show that RH30 and RD displayed increased PI uptake by combined treatment with A1331852 and S63845, confirming that simultaneous inhibition of Mcl-1 and Bcl-XL induced cell death in tumor spheroids. Furthermore, we were able to demonstrate that activated allogeneic Natural

Killer (NK) cells migrated into tumor spheroids and displayed cytotoxicity against rhabdomyosarcoma. Next, we investigated whether treatment of tumor spheroids with subtoxic concentrations of BH3 mimetics could increase the cytotoxicity of NK cells. Notably, the cytotoxic effects of NK cells were enhanced by the addition of BH3 mimetics. Treatment with either the Bcl-XL or the Mcl-1 inhibitor increased the cytotoxicity of NK cells and reduced spheroid size, while the Bcl-2 inhibitor had no effect on NK cell-mediated killing.

Conclusion

This is the first study to describe the combination of BH3 mimetics targeting Bcl-XL or Mcl-1 with NK cell-based immunotherapy in rhabdomyosarcoma cell lines, highlighting the potential of BH3 mimetics in immunotherapy.

Non-Hodgkin lymphoma in children and adolescents: Important aspects of diagnosis and new insights into the biology of mature B-cell neoplasia.

I. Oschlies

Universitätsklinikum Schleswig-Holstein, Campus Kiel, Institut f Pathologie, Sektion Hämatopathologie, Kiel, Germany

Non-Hodgkin-Lymphome (NHL) gehören zu den häufigeren im Kinder- und Jugendalter auftretenden Neoplasien. Das Spektrum der NHL ist in dieser Altersgruppe relativ limitiert und umfasst Burkitt-Lymphome, großzellig anaplastische Lymphome (ALCL), Gewebemanifestationen von Precursorzellneoplasien sowie weniger häufige Entitäten wie das diffuse großzellige B-Zell-Lymphom (DLBCL), das primär mediastinale großzellige B-Zell Lymphom (PMBCL) und seltene T-Zell-Lymphome. Im letzten Jahrzehnt wurden zudem einige B-Zell-Lymphome als typische Entitäten des jungen Lebensalters näher beschrieben und als provisorische Entitäten in der WHO-Klassifikation 2017 benannt. Diese Erkrankungen werden auch in die bevorstehende aktualisierte WHO-Klassifikation übernommen werden. Hierzu gehören das Burkitt-ähnliche Lymphom mit *11q*-Alteration, das großzellige B-Zell-Lymphom mit *IRF4*-Rearrangierung und das follikuläre Lymphom des pädiatrischen Typs. Im Vortrag werden die genannten B-Zell-Neoplasien unter Berücksichtigung jüngerer Forschungserkenntnisse vorgestellt und ihr Stellenwert im diagnostischen Alltag diskutiert. Zudem sollen einige pragmatisch diagnostische Algorithmen aufgezeigt werden, die bei der Einordnung lymphatischer Infiltrate oder lymphomverdächtiger Befunde bei Kindern und Adoleszenten möglichst zielführend sind.

AG13 AG Geschichte und Ethik der Pathologie - Special topic: Aufbau und Erhalt pathologischer Sammlungen

AG13.01

Rudolf Virchow and His Pathological Specimens

T. Schnalke

Berliner Medizinhistorisches Museum der Charité, Berlin, Germany

Human specimens are stored in greater numbers in many institutes of pathology but also in medical historical collections and museums until today. A broad discussion is going on regarding the handling of these sensitive objects. Thus, it seems worthwhile to take a closer look at the culture and history of medical collecting and fabricating of such specific items. In my contribution I will address concepts, aims, and results, which the world famous Berlin pathologist Rudolf Virchow followed and realized while setting up one of the largest specimen collection at his time and finally creating his own Pathological Museum at the Charité in 1899. The following questions will be raised: When and how did Virchow develop his ideas of a dynamic body museum? How did he practically proceed with dissecting and making specimens? What system structured his collecting activities? How did he plan to arrange the specimens in his showcases? But also the other way around: How did his understanding of collecting and presenting shape his primary activities: his research orientated viewing, as well as directing of his scientific attention at the dissection table?

Präparate menschlicher Herkunft lagern bis heute in zahlreichen Pathologischen Instituten, aber auch in medizinhistorischen Sammlungen und Museen. Der Umgang mit den in jeder Hinsicht sensiblen Objekten wird breit diskutiert. Vor diesem Hintergrund lohnt ein genauerer Blick zurück in Kultur und Geschichte des einschlägigen medizinischen Sammelns und Präparierens. In meinem Beitrag verfolge ich Konzepte, Ziele und Ergebnisse, die der weltweit geachtete Berliner Pathologe Rudolf Virchow mit seinen Bemühungen um den Aufbau einer pathologischen Präparatesammlung und letztlich mit Gründung seines Pathologischen Museums 1899 an der Charité verfolgte und umsetzte. Dabei stellen sich insbesondere folgende Fragen: Wann und wie entwickelte Virchow seine Idee eines dynamischen Körpermuseums? Wie ging er praktisch vor beim Sezieren und Präparieren? Welche Systematik verfolgte er beim Sammeln? Wie wollte er seine Präparate in den Schauvittrinen arrangieren? Aber auch im Umkehrschluss: Wie formte die Vorstellung vom Sammeln und Zeigen seine primäre Tätigkeit – den forschenden Blick und die wissenschaftliche Aufmerksamkeit am Seziertisch?

The Military Pathological Collection of the Bundeswehr Medical Service

K. Steinestel¹, V. Hartmann²

¹Bundeswehrkrankenhaus Ulm, Pathologie und Molekularpathologie, Ulm, Germany, ²Sanitätsakademie der Bundeswehr, München, Germany

Die Wehrpathologische Lehrsammlung des Sanitätsdienstes der Bundeswehr ist an der Sanitätsakademie der Bundeswehr in München beheimatet. Sie zeigt über 3000 Exponate, welche bis in die Zeit des Ersten Weltkrieges zurückreichen und insbesondere im Ersten und Zweiten Weltkrieg im Rahmen von Feldsektionen Gefallener entnommen und präpariert wurden. Basis der Sammlung, welche v. a. die Einwirkungen von Stich-, Hieb- und Schussverletzungen sowie von Granat- und Minensplittern wie von chemischen Waffen auf den menschlichen Organismus zeigt, sind die Präparate des in München tätigen Militärpathologen Max Borst (1869-1946). Nach 1958 wurde die Wehrpathologische Sammlung als Teil der Feldprosektur (FPros) 291 unter Oberfeldarzt Dr. Dr. Fischer aufgestellt. Diese hatte den Auftrag, klinische und forensische Obduktionen an Soldaten vorzunehmen sowie histologische Untersuchungen für die Bundeswehrkrankenhäuser und die Landgerichtsärzte München II, Landshut und Deggendorf durchzuführen. Die FPros 291 erweiterte bis zu ihrer Auflösung 1978 die Sammlung, welche anschließend an die Abteilung für Studien und Wissenschaften der Sanitätsakademie der Bundeswehr in der Ernst-von-Bergmann-Kaserne im Norden Münchens überführt wurde. Seither steht die Sammlung dem Lehr- und Ausbildungsbetrieb von Sanitätsoffizieren und Sanitätspersonal sowie einem interessierten Fachpublikum zur Verfügung. Insgesamt haben seit 1978 über 93.000 Fachbesucher die Wehrpathologische Lehrsammlung des Sanitätsdienstes der Bundeswehr besucht.

AG13.03

How to handle unknown fluids in fluid-preserved collections

K. König

Karl-Sudhoff-Institut für Geschichte der Medizin und der Naturwissenschaften, Universität Leipzig, Leipzig, Germany

Historische Feuchtpräparatsammlungen sind ein problembehafteter Schatz an vielen pathologischen Instituten. Die Sammlungen werden zwar als pflegeintensiv wahrgenommen, dennoch ist die Pflege, die den Sammlungen zuteilwird, alles andere als intensiv. Die Gründe hierfür sind neben der regulären Arbeitsbelastung der MitarbeiterInnen vielfältig. Insbesondere die Unkenntnis über die Verwendungen der einzelnen Konservierungslösungen sorgt dafür, dass entweder gar nichts getan, oder die verlorene Flüssigkeit mit Ethanol oder Formaldehyd aufgefüllt wird.

Im Rahmen des Vortrags werden die gängigsten historischen Konservierungslösungen und eine sich daraus ableitende „Universallösung“ für solche Problemfälle, die in Kooperation mit der Pathologisch-anatomischen Sammlung in Wien entwickelt wurde, vorgestellt.

AG13.04

Integration of historical macro-pathological specimens in current medical digital teaching

P. Eichhorn

Pathologisches Institut, Universitätsklinikum Erlangen, Erlangen, Germany

Eine der wertvollsten Eigenschaften historischer makro-pathologischer Präparate in der Lehre ist die Tatsache, dass sie oft einen Blick auf unbehandeltes Gewebe und damit einen unvoreingenommenen Zugang zu einem Fall bzw. einer konkreten Diagnose ermöglichen. In einem vorangegangenen Projekt wurden solche historischen Präparate bereits erfolgreich in die curriculare Lehre integriert. Vor dem Hintergrund, dass digitale Lehrangebote einen zunehmend größeren Stellenwert erfahren sowie aus den Erfahrungen, die mit den physischen Präparaten in den Präsenzkursen gesammelt werden konnten, wird nun in einem Anschlussprojekt an einer Integration dieser Präparate in die digitale Lehre gearbeitet. Das grundsätzliche Problem einer Digitalisierung solcher Präparate ist, dass deren große Stärke, nämlich die Möglichkeit einer stereoskopischen und frei beweglichen Betrachtung, verloren geht. Um diesen Umstand so weit möglich zu kompensieren, werden die Präparate aus bis zu 36 verschiedenen Winkeln fotografiert und die so generierten Bilddaten anschließend zu einer 360°-Ansicht montiert. Diese werden den Studierenden auf einer Online-Plattform zur Verfügung gestellt. In einem zweiten Schritt sollen die digitalisierten Präparate nicht nur als „nackte“ Präparate, sondern in Form von virtuellen Fallgeschichten präsentiert werden. Neben der Fallbeschreibung und den Bildern der makroskopischen Präparate wird auch ein direkter Link zu den entsprechenden histologischen Präparaten, die unabhängig von diesem Projekt auf derselben Internetplattform zur Verfügung gestellt werden, integriert. So ist es möglich, einen didaktischen Weg von Anamnese bzw. Fallbeschreibung über die Makroskopie hin zur Histologie zu gehen. Auch wenn belastbare Zahlen erst durch eine Evaluation nach Abschluss des Projektes zur Verfügung stehen werden, fällt die bisher erfahrene Resonanz der Studentenschaft positiv aus.

Soft tissue tumors and its aid technologies for diagnosis over time: immunohistochemistry and fluorescence-in-situ-hybridization.

T. Braunschweig¹, K. Schierle²

¹Institut für Pathologie - University Clinic RWTH Aachen, Aachen, Germany, ²Institut für Pathologie - SLK-Kliniken Heilbronn GmbH, Heilbronn, Germany

Background

The diagnosis and nature of tumors of soft tissue origin, sarcomas, is still challenging and subject of changes in classification and subgrouping over time until today. As in the beginning the tumor site and gross impression was most important, with Rudolf Virchow histological features, histomorphology and substance analyses took over to be the common basis of diagnosis for around 100 years. In the 60s to the 80s of the 20th century, progress in supporting technologies took place and immunohistochemistry (IHC) found its way to routine diagnostics in laboratories of pathology in the 80th as also fluorescence-in-situ-hybridization (FISH) in the 90th.

Methods

By internet search in different archives as pubmed, "Internet Archive" and "Karlsruhe Virtueller Katalog" and on specific journal pages (e.g. "Cancer Research", "Virchows Archiv"), publications could be sorted, recapitulated and merged.

Results

Soft tissue tumors are already named a subgroup by its tissue of origin and histological features by Rudolf Virchow in 1863 (13th lecture). In his lectures he shows in detail that their subgrouping (not naming it classification back that time) is based on their histomorphological characteristics and the more differentiated or specialized tissue component as e.g. a tumor consisting of connective tissue and muscle cells/tissue is more likely named a muscle tumor. Subsequently, soft tissue tumors were diagnosed by their tumor components based on histological/substantial-chemical features in the 19th and first half of 20th century. In the second half of the 20th century, ultrastructural features of soft tissue tumors were included in subgrouping of tumors by introducing electron microscopy in the 50s, in the 1960s-1970s labeled antibodies were introduced in detecting specific antigens but it lasted until the beginning of 1980s that immunohistochemistry was part of routine diagnostics. In the 1990s, molecular pathology raised as a new discipline in laboratories of pathology, even if mutations in tumors could be already recognized since the 1970s. As an elegant methodology to combine the fast detection of mutations and histology, fluorochrome-labeled DNA probes became part of the repertoire in the diagnosis of soft tissue tumors in research in the 1990s and in routine by the beginning of 2000s.

Conclusion

Still, IHC and FISH are standards in the evaluation of sarcomas while the introduction of next-generation

sequencing in routine diagnostics in the 2010s was expected to and might replace these.

AG14 AG Informatik, digitale Pathologie und Biobanking I

AG14.02

Deep learning-based prediction of upper tract urothelial cancer molecular subtypes from histopathological slides

M. Angeloni^{1,2}, S. Lindner^{1,2}, S. Foersch³, P. Volland^{1,2}, C. I. Geppert^{1,2}, H. Heers⁴, S. Wach^{2,5}, H. Taubert^{2,5}, D. Sikic^{2,5}, B. Wullich^{2,5}, R. Stoehr^{1,2}, R. Strick^{2,6}, P. L. Strissel^{2,6}, M. Eckstein^{1,2}, A. Hartmann^{1,2}, F. Ferrazzi^{1,2,7,8}, V. Bahlinger^{1,2,8}

¹Institute of Pathology, University Hospital Erlangen-Nürnberg, Friedrich-Alexander-Universität Erlangen-Nürnberg, Erlangen, Germany, ²Comprehensive Cancer Center Erlangen-EMN (CCC ER-EMN), Erlangen, Germany, ³Institute of Pathology, University Medical Center Mainz, Mainz, Germany, ⁴Department of Urology and Pediatric Urology, University Hospital Gießen and Marburg, Marburg, Germany, ⁵Department of Urology and Pediatric Urology, University Hospital Erlangen, Friedrich-Alexander Universität Erlangen-Nürnberg, Erlangen, Germany, ⁶Laboratory for Molecular Medicine, Department of Gynecology and Obstetrics, University Hospital Erlangen-Nürnberg, Friedrich-Alexander-Universität Erlangen-Nürnberg, Erlangen, Germany, ⁷Department of Nephropathology, Institute of Pathology, University Hospital Erlangen-Nürnberg, Friedrich-Alexander-Universität Erlangen-Nürnberg, Erlangen, Germany, ⁸These authors contributed equally as senior authors, -, Germany

Background

Upper tract urothelial carcinoma (UTUC) is a rare tumor entity that accounts for 5-10% of all urothelial tumors, for which there is great need for better patient stratification. In recent years the increasing use of high-resolution whole-slide images (WSIs) opened the way to deep learning-based approaches as powerful tools to identify candidate prognostic and/or predictive cancer biomarkers. Here, we propose a deep-learning workflow to predict immunohistochemistry (IHC)-based subtypes from WSIs of UTUC patients.

Methods

Luminal/basal subtyping of a cohort of 100 tumor samples \geq pT2 was performed relying on hierarchical clustering of the expression of three luminal (FOXA1, GATA3, CK20) and three basal (CD44, CK5, CK14) IHC markers evaluated on tissue microarrays. H&E slides were digitalized and tumor areas manually annotated in QuPath. A Python-based pipeline was developed to automatically generate, filter, and stain-normalize tiles. A transfer-learning approach was employed for subtype prediction by fine-tuning a ResNet50 pre-trained on ImageNet. To assess the performance of our approach, a stratified random split of WSIs into 70% training/30% validation was repeated three times.

Results

Our approach achieved a mean validation accuracy of 0.83 [0.81-0.87] at patient level, with a mean AUROC of 0.8 [0.72-0.92]. We are currently performing the evaluation with an independent test set. Class activation maps highlighted dense nuclei with small stroma bridges as morphological luminal distinctive features, and dense stroma and keratinization as basal characteristics. Furthermore, using tiles-level predictions to build

WSI classification maps, potentially heterogeneous WSIs, i.e. with co-presence of both subtypes, could be identified.

Conclusion

Taken together, our deep-learning workflow appears able to predict IHC-based subtypes in UTUC directly from H&E slides. In addition, the identification of potentially heterogeneous slides might offer a valid support to help pathologists in pre-selecting samples for further investigation and stratify UTUC patients for targeted therapy. Expression analysis is being performed to validate our findings.

AG14.03

Deep Learning outperforms conventional laboratory staining methods in predicting molecular subtypes of gastric adenocarcinoma.

N. Flinner¹, S. Gretser¹, A. Quaas², K. Bankov¹, C. Doering¹, R. Buettner², J. Rueschoff³, P. Wild¹

¹University Hospital Frankfurt, Dr. Senckenberg Institute of Pathology, Frankfurt, Germany, ²University Hospital Cologne, Köln, Germany, ³Targos Molecular Pathology GmbH, Kassel, Germany

Background

Gastric cancer (GC) is one of the most lethal cancer types. Four distinct molecular subtypes (EBV, MSI, GS and CIN) are defined by the TCGA, each responding differently to immune- or chemotherapy.

Methods

The four molecular subtypes were characterized for a GC cohort from Colone (in analogy to others) using in-situ techniques. OncoScan arrays for a smaller subset were performed for validation.

In addition, we used the TCGA data for training of an ensemble cNN to predict the molecular subtypes using a bagging approach: each individual cNN was trained with 84 randomly selected WSI's (21 per class) from a bigger dataset. This dataset included additional patients for MSI, GS and CIN classes, but not for EBV. This procedure ensures that each cNN was trained with slightly different datasets. The Colone cohort was used for independent testing.

Results

Significant differences in GS subtype identification were observed between the staining approach and the results from the OncoScan arrays. In addition the OncoScan arrays agreed more frequently with deep learning compared to the in-situ staining approach. For the three remaining classes, the ensemble cNN performed well for the external Colone dataset. The bagging approach reduced the error rate from 47% to 33% , compared to individual cNN's; while random guessing would result in error rates of 75% for this problem. In addition, the bagging ensemble also outperformed a vanilla ensemble, which was trained with an invariant dataset. Predictions revealed cases positive for two or more subtypes, challenging the original subtype definition.

Conclusion

A staining-based approach is not suitable for determining the molecular subtype in GC and is outperformed by Deep Learning.

Vendor Agnostic vs. Proprietary User Interfaces for AI Solutions in Digital Pathology

K. Strohmenger¹, C. Jansen¹, D. Romberg², T. Evans³, S. Manthey¹, P. Hufnagl^{1, 4}, N. Zerbe¹

¹Charité – Universitätsmedizin Berlin, corporate member of Freie Universität Berlin and Humboldt Universität zu Berlin, Institute of Pathology, Berlin, Germany, ²Fraunhofer MEVIS, Institute for Digital Medicine, Bremen, Germany, ³Technische Universität Berlin, Distributed Artificial Intelligence Laboratory, Berlin, Germany, ⁴HTW University of Applied Sciences, Center for Biomedical Image and Information Processing (CBMI), Berlin, Germany

Background

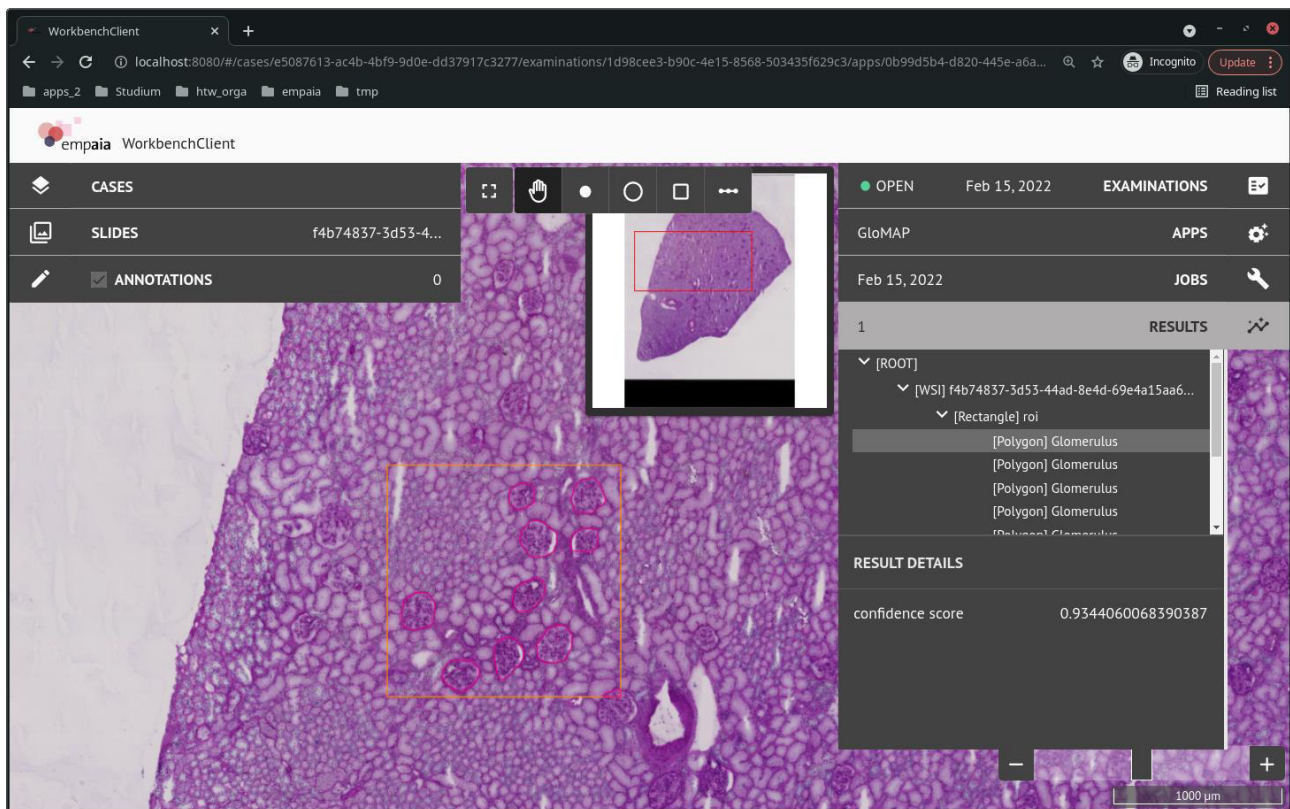
The integration of new artificial intelligence (AI) applications into existing pathology systems faces two major challenges: First, application programming interfaces (APIs) of such systems, if they are accessible at all, are often proprietary and closed-source. Therefore, the integration of any third party application depends on the system manufacturers to actively support the process. Second, regulatory laws require these apps to go through a conformity assessment procedure for each system into which they are integrated. This is especially true when the user interface (UI) changes, even if the algorithm remains the same [1].

Methods

The EMPAIA project already features a vendor agnostic, browser based Workbench UI to view whole slide images (WSIs), draw annotations, start different AI apps or view their results (see figure). This is made possible by formalizing an app's input and output via the EMPAIA App Description (EAD) syntax. The EAD is also the basis for the EMPAIA App API to provide a standardized interface for WSI and annotation data for the computational part of an app, which is run in a separate compute environment [2]. Furthermore, the EMPAIA platform is currently extended to allow AI vendors to provide their own UIs for their apps within the EMPAIA Workbench.

Results

Five AI apps from different vendors are already adapted to run on the EMPAIA platform. The vendor's feedback has helped to improve the EAD syntax, the App API, the vendor agnostic Workbench UI, but also to identify requirements to enable usage of proprietary UIs. Seven additional AI apps and their UIs are currently integrated into the extended Workbench.



Viewing an AI app's results in the vendor agnostic EMPAIA Workbench UI. The right side shows a tree view, depicting relations between annotations and assigned primitive values, i.e. a confidence score.

Conclusion

The appeal of a vendor agnostic UI is a streamlined appearance and a reduced development process of AI apps, as only their computational part has to be implemented. The latter is especially useful in research context. However, to minimize efforts and costs for conformity assessments required for clinical usage, AI vendors should be able to provide their own UIs. Moreover, a dedicated UI tailored specifically for an app is often better suited for visualizing the results in an appropriate way, thus providing a better user experience.

Literaturangaben

- [1] (2017), Regulation (EU) 2017/746 of the European Parliament and of the council of 5 April 2017 on in vitro diagnostic medical devices and repealing directive 98/79/EC and commission decision 2010/227/EU, Official Journal of the European Union, 117, <https://eur-lex.europa.eu/legal-content/EN/TXT/?uri=CELEX:32017R0746>, 2022-02-07
- [2] Daniel Romberg, Klaus Strohmenger, Christoph Jansen, Tobias Küster, Nick Weiss, Christian Geißler, Tomasz Soltysinski, Michael Takla, Peter Hufnagl, Norman Zerbe, Andre Homeyer, (2022), EMPAIA App Interface: An open and vendor-neutral interface for AI applications in pathology, Computer Methods and Programs in Biomedicine, 215, <https://www.sciencedirect.com/science/article/pii/S0169260721006702>, 2022-02-07

Going digital in Pathology – Where to store the big data?

P. Schüffler, K. Steiger, W. Weichert

Technical University of Munich, Munich, Germany

Background

Digital pathology has the potential to generate data sets at petabyte scale due to the large size of high-resolution tissue scans. While data sets are needed for the development of high-performing state-of-art artificial intelligence (AI) in pathology, the cost-efficient storage can be challenging for many pathology institutes. In this talk, we motivate the effort to digitize and store large-scale pathology data sets with an example of clinical-grade AI for prostate cancer detection and explore three options to store the data: on premises, in a private data center and in the cloud, each evaluated for pathology departments of five different sizes (from 50k – 1000k slides per year), and with the practical example of the digital transformation in our pathology department.

Methods

Over the last year, our department installed a workflow for clinical digital pathology, including two GT450 Dx scanners (Leica Biosystems, Buffalo Grove, Illinois), to meet the digitizing rate of 200k slides per year. Digital slides are currently stored persistently on a dedicated network attached storage system (NAS). Alternative approaches include the local data center or cloud-based storage. We compare the estimated costs for five different pathology department sizes processing 50k, 100k, 200k, 500k, or 1000k slides per year. For each size, we project the estimated storage costs for 1, 2, 3, 5 and 10 years.

Results

Currently in our department, 6k slides per month are being digitized, with increasing throughput. For a fast solution, on-premises storage systems have been acquired sufficient for one year's digital scans, with an average cost of 0,22 EUR per GB, or 25.792 EUR to 515.840 EUR after one year depending on department size. After that year, a transition is planned to use our institution's data center instead. Cloud storage is typically multi-tiered and the costs comprise storage time and access frequency. Assuming two months of hot storage after scanning, we calculate an average cost of 0,15 EUR per GB, or 18.375 EUR to 367.502 EUR after one year depending on department size.

Conclusion

Large-scale data sets in pathology are needed to build clinical-grade pathology AI.

On-premises storage is suitable for a quick-start solution, while data centers and cloud are scalable for long-term providing cost-efficient storage due to professional tiering. Still, cloud storage must fulfill requirements to protect patient's privacy and data security.

High resolution multiclass semantic segmentation in prostate

A. Turzynski

Gemeinschaftspraxis für Pathologie, Lübeck, Germany

Background

Semantic segmentation with deep learning methods represents a powerful tool for informational distillation of image content. A neural network to segment 14 different diagnostic elements in H&E-stained prostate tissue is presented.

Methods

Whole slide images were annotated by immunohistochemistry, image processing, conventional stains or manual annotation and correction. The classes included: nuclei, nucleoli, epithelium, basal cells, gland lumina, corpora amylacea, stroma, striated muscle, fat tissue, inks (black, red, green and yellow) and background. For each class binary segmentation networks using the U-net backbone were trained. The predictions of these models were used to create a set of 14 classes pseudo-masks from a H&E dataset of prostate tissue (prostatectomies and diagnostic cores). A U-net using the convolutional blocks of EfficientnetB2 was trained to simultaneously predict the 14 classes in patches (512x512 pixels, 0.5 µm/pixel) finally visualized as pseudo-color images.

Results

The trained segmentation network reaches a high accuracy (mean IoU-score: 0.871, mean F1-score: 0.894) in segmenting the diagnostic relevant classes in prostate tissue (fig. 1,2). Misrecognitions are mainly restricted to the minority classes (striated muscles, inks, fat, lumina). The overall processing of large patches of 3072x3072 px (1.5x1.5 mm tissue, 36 tiles) including pre- and postprocessing takes only 2.63 seconds in one go.

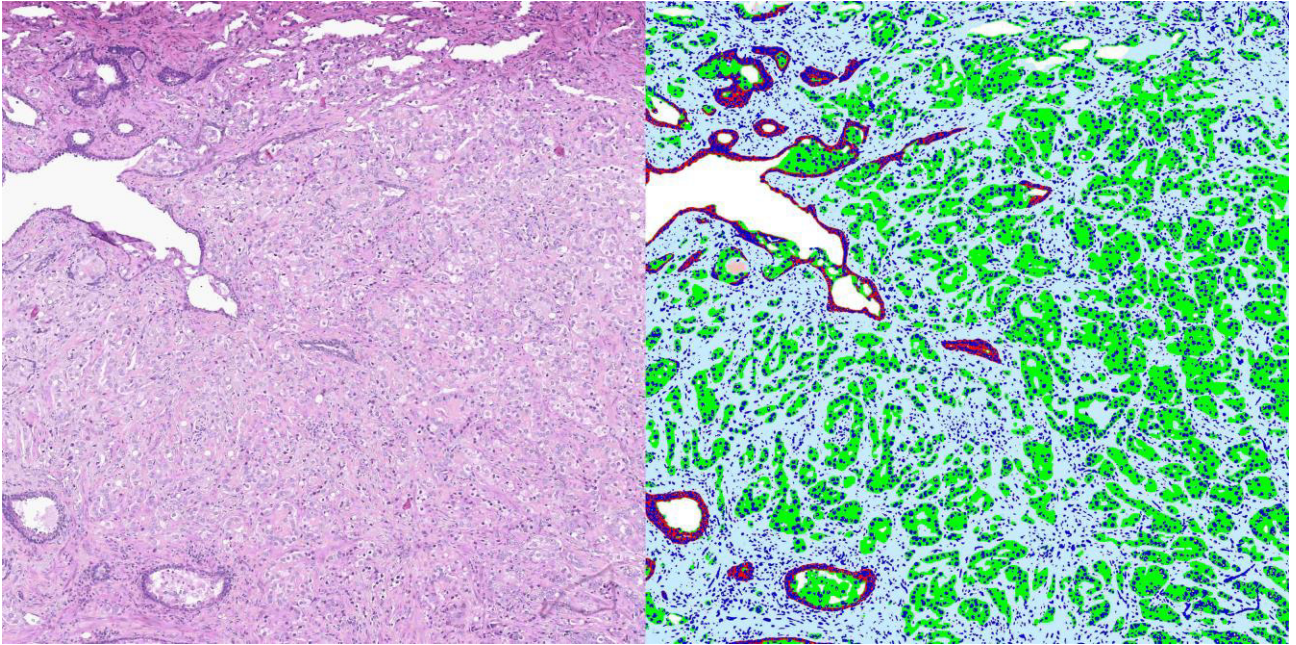


Fig. 1: Semantic segmentation in prostate cancer (stroma: light blue, nuclei: deep blue, nucleoli: yellow, basal cells: red, non basal epithelium: green, lumina:white, corpora amylacea: brown).

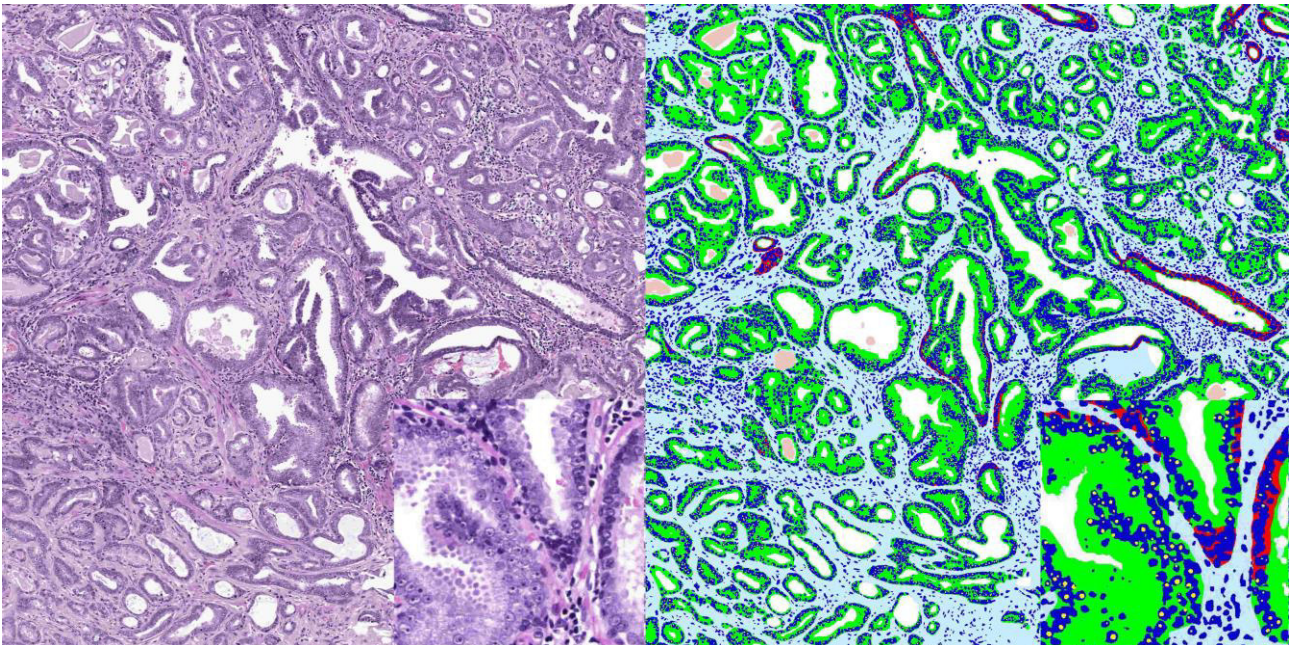


Fig. 2: Semantic segmentation in prostate cancer. Insets: higher magnifications to demonstrate the nucleoli. Pseudo-color encoding see fig.1.

Conclusion

Accurate high resolution multiclass segmentation is achievable in H&E-stained prostate tissue. The segmentation of diagnostic items can serve as basis for subsequent diagnostic decision networks thus enabling an automated criteria-based diagnostic pathway.

Quality aspects for benchmark datasets for AI solutions in pathology

A. Homeyer¹, C. Geißler²

¹*Fraunhofer MEVIS, Bremen, Germany*, ²*Technische Universität Berlin, DAI-Labor, Berlin, Germany*

Background

Artificial intelligence (AI) solutions that automatically extract information from digital tissue images have shown great promise for improving pathological diagnosis. For their practical application, it is crucial to estimate the performance of AI solutions on cases from routine laboratory work. However, compiling appropriate test or "benchmark" data sets is a major challenge, and to date there are very few relevant studies or literature.

Methods

The BMWK-funded EMPAIA project brought together relevant stakeholders, including pathologists, AI solution developers, and researchers, in an open committee to discuss these challenges and develop solutions. Based on literature research and own experience with the development and productization of AI solutions, the committee has developed recommendations for collecting benchmark data sets for AI solutions in pathology.

Results

Various aspects were considered, e.g.: What are the regulatory requirements in different countries? How can the enormous variability in histology be covered adequately? How should rare subgroups be represented? How large must the dataset be? How can bias in a benchmark dataset be detected?

Conclusion

The recommendations help pathologists and developers compile appropriate benchmark datasets for demonstrating the safety and utility of AI solutions and for obtaining regulatory approval.

Unsupervised image analysis and linear expression of focal adhesion kinase (FAK) as a prognostic digital biomarker in colon cancer and precursor lesions

R. Huss^{1,2}, T. T. Arndt³, B. Grosser¹, S. Miller¹, F. Sommer⁴, G. Müller³, B. Märkl¹

¹Universitätsklinikum Augsburg, Institut für Pathologie und Molekulare Diagnostik, Augsburg, Germany,

²Universitätsklinikum Augsburg, Institut für Digitale Medizin, Augsburg, Germany, ³Institut für Mathematik der Universität Augsburg, Lehrstuhl für Rechnerorientierte Statistik und Datenanalyse, Augsburg, Germany,

⁴Universitätsklinikum Augsburg, Klinik für Allgemeine, Viszeral- und Transplantationschirurgie, Augsburg, Germany

Background

The discovery and development of prognostic and predictive biomarker on tissue specimens has been quite a diverse undertaking in the field of precision pathology. Pathologists have been trained to report different categories of staining intensities (0, 1+, 2+, 3+) combined with quantitative measures and considering explicit staining pattern to meet constantly changing thresholds. Recently, pathologists are assisted by digital clinical decision support tools (CDS) that aid those tedious and time-consuming tasks. Most CDS result from the supervised transfer of pre-existing analog read-outs into a digital framework. Here we report the unsupervised detection of a linear expression of a potential biomarker that separates invasive colon cancer from early lesions.

Methods

Focal adhesion kinase (FAK) is a non-receptor tyrosine kinase associated with the site of integrin clusterin to mediate cell growth, proliferation, survival and migration. FAK phosphorylation and overexpression has been seen in invasive and metastatic cancer and is – among others - linked to Src signaling and p53 mutation. There is further evidence that targeting FAK renders cancers to immune therapies. We stained multiple cores of invasive colon cancer (n = 28) and precursor lesions (n= 23) with an anti-FAK antibody (*kindly provided by FAKnostics*) and applied colour deconvolution to isolate different intensities on the TMAs. After some preprocessing steps (colour deconvolution, median filter, subtract background, etc) mean values were computed for the darker and lighter parts of the image. The fraction of these mean values gives a linear expression score (mean value of 1.0 represents equal expression of stroma and epithelium).

Results

The linear and unsupervised expression analysis of FAK-stained TMAs revealed a mean expression score of 0.67 in invasive colon cancer cores as compared to a mean colour value of FAK expression in precursor lesions of 0.83. This result correlates with the expected overexpression of FAK in invasive cancer vs. non-invasive lesions (almost 2-fold). However, there are a few cases of adenoma that also show high FAK expression levels and might represent high-risk lesions. Further analysis of those cases is warranted.

Conclusion

Here we demonstrate that an unsupervised image analysis of immunohistochemistry stained tissue samples

can separate invasive colon cancer from non-invasive lesions as a potential prognostic and possibly predictive algorithm that might serve as a linear digital biomarker.

AG14 AG Informatik, digitale Pathologie und Biobanking II

AG14.10

Evaluation of an artificial intelligence approach to assist the detection of melanoma metastasis in lymph nodes

D. Otero Baguer¹, P. Jansen², N. Duschner³, M. Iske¹, M. Schmidt¹, J. Le'Clerc Arrastia¹, D. Schadendorf², E. Hadaschik², J. Schaller³, K. G. Griewank², P. Maass¹

¹University of Bremen, Center for Industrial Mathematics, Bremen, Germany, ²Uniklinik Essen, Essen, Germany, ³MVZ Dermatopathologie Duisburg Essen, Essen, Germany

Background

The detection of melanoma metastasis in lymph node samples has become an essential tool for predicting prognosis and allocating treatment. For this purpose, lymph nodes are excised and the tissue slices are examined histopathologically. The examination involves using IHC and H&E staining to highlight relevant structures and support the diagnostic process. It is a time-demanding task that requires analyzing several glass slides and small metastasis are challenging to detect. These cases significantly increase the workload for pathologists. This work aims to develop an artificial intelligence (AI) approach, based on deep artificial neural networks, to support the detection and assessment of melanoma metastasis in lymph nodes.

Methods

We use a data set with more than 1000 whole slide images (WSI) that include H & E and IHC stainings for the study. The samples come from three different laboratories in Germany and were digitized using Leica and Hamamatsu scanners. Annotation of the WSI was done in an efficient semi-automatic process between pathologists and the AI. Based on a few entirely manually annotated samples, the AI model was trained to make initial suggestions for segmentation. Following annotations then required only minor adjustments by the pathologists, from which the model could in turn also learn. The neural network is a modified version of the U-Net architecture with a Res-Net backbone and it was trained using a deep supervision strategy.

Results

The model has been already deployed in one of the laboratories and is currently being tested in a prospective setting. Preliminary results show high sensitivity and specificity of the model, which indicates that the method is indeed helpful and very promising. It is able to detect metastasis of small, medium, and large sizes and has proven to increase the confidence of the whole process.

Conclusion

The system that was developed in this work not only makes the whole process less time-consuming for the pathologists but also represents a second opinion that can reveal metastasis areas that could have been overlooked. Additionally, we were able to close the gap between research and daily routine and integrated

the system as a module of our digital pathology platform DigiPath-Viewer, which is currently being used on a daily basis in one of the involved laboratories.

Fast-track AI-assisted immunohistochemical stain evaluation and statistical analysis of TMAs

K. Kurowski^{1, 2, 3}, C. Schell^{1, 2}, O. Schilling¹, M. Werner^{1, 2, 3}, P. Bronsert^{1, 2, 3}

¹Medical Center – University of Freiburg and Faculty of Medicine, Institute for Surgical Pathology, Freiburg, Germany, ²Medical Center – University of Freiburg and Faculty of Medicine, Tumorbank Comprehensive Cancer Center Freiburg (CCCCF), Freiburg, Germany, ³Medical Center – University of Freiburg and Faculty of Medicine, Core Facility for Histopathology and Digital Pathology, Freiburg, Germany

Background

Spatial resolved biomarker examination constitutes a major pillar in cancer research. The procedures to gain substantial results, beginning from slide preparation to statistical correlation and visualization are highly time- and cost intensive. To diminish this obstacle, a pipeline for Tissue Micro Array (TMA) construction, AI-based immunohistochemical (IHC) stain estimation and script-based statistical analysis was implemented into existing workflows.

Methods

Five components were streamlined. **1.** centralizing of ELSI confirm data, derived from structured histopathological and clinical reports, **2.** additionally collected FFPE tissue specimens, **3.** the Tissue Micro Arrayer TMA Grandmaster (3DHitech), **4.** the AI-assisted image analysis program QuPath (Version 0.3.0) and **5.** the statistical software R-Studio comprising the graphical user interface. TMA design was planned encompassing replicates of representative tumor regions and - in order to bypass batch effects - layout randomization. QuPath scripts comprised evaluation of subcellular tumor compartments and the surrounding stroma tissue. R-Scripts included data preparation (merging clinical and TMA information), pre-analyses (distribution, cut-off finder, descriptive analyses), statistical testing (uni- and multivariate analyses) and graphical data-visualization.

Results

Streamlining the semi-automated TMA construction with an AI-assisted subcellular IHC-stain estimation and a subsequent script-based statistical analysis enables a fast and objective correlation of tumormarker-expression with clinico-pathological variables. It allows a significant reduction in work time and work force, consecutively leading to a substantial cost-reduction. The usage of TMA-sections bypasses experimental variability between patient-samples and batch effects are minimized. The inter-tissue comparability and result validity of the respective experiment is therefore maximized. The results can be analyzed separately or correlated with the immunohistochemical findings. Of note, constructed TMAs can further be analyzed using advanced techniques (e.g. MALDI-TOF, CyTOF, spatial transcriptomics) or provided to other researchers.

Conclusion

The presented pipeline for the semi-automated construction, stain evaluation and statistical analysis of TMAs represents a time- and cost-effective as well as an easily applicable and reproducible procedure, which is not only restricted to IHC based analyses.

Pre-Scan QC – Preliminary Results for Artefact Detection in Slide Overview Images

T. Eixelberger¹, T. Niedermair², K. Evert², B. Müller³, D. Vermeulen³, K. Steiger⁴, C. Delbridge⁴, W. Heimberg⁵, M. Mayer⁵, P. Schöffler⁴, W. Weichert⁴, M. Evert², C. Brochhausen-Delius², **V. Bruns**¹

¹Fraunhofer IIS, Erlangen, Germany, ²Institute of Pathology, University Regensburg, Regensburg, Germany, ³PreciPoint GmbH, Freising, Germany, ⁴Institute of Pathology, Technical University Munich (TUM), München, Germany, ⁵HTI Automation GmbH, Ebersberg, Germany

Background

Quality Control (QC) is a challenge in Pathology labs. The transition into a digital workflow introduces whole-slide-scanning as a new processing step. The fact that all slides are being digitized presents an opportunity to introduce a computer-assisted QC. In the PathoScan project funded by the Bavarian Ministry of Economic Affairs, Regional Development and Energy (FKZ ESB074/005), we develop a QC component. Following the paradigm that errors should be detected early on in the workflow, it analyzes images captured by the scanner's overview camera before the actual microscopic scan. Alternatively, it could be employed in the wet lab.

Methods

Initially, a requirements analysis was conducted by assembling a list of potential artefacts. Each item was then assessed in terms of its (1) frequency of occurrence, (2) impact on the ability to diagnose and (3) estimated technical difficulty of detecting this artefact type automatically. The following modules have been realized until now: segmentation of cover slip, tissue, tissue folds, marker, glass breakage and enclosed air. Detecting the cover slip allows for determining whether it is properly positioned or reaches over the glass slide edge. Relating the tissue to the cover slip furthermore permits to detect when a tissue is not entirely covered by it. The current dataset comprises 198 glass slides with a size of ca. 4700x1700 pixels and resolution of approximately 16 µm/px taken with the PreciPoint M8's overview camera. Due to the limited size of the data set, deep learning was not used for the analysis, but methods including local binary patterns, adaptive thresholding and K-means.

Results

As a reference, cover slips, tissue islands, marker and tissue folds were manually contoured while the remaining artefact types were labeled on a slide level. The cover slip is detected with a mean error of 1.6 px and tissue islands with a Dice score of 0.93. Slides on which tissue touches or overlaps the cover slip are identified with an accuracy of 0.80, a sensitivity of 0.90 and a precision of 0.80.

Conclusion

Our preliminary results on a medium size data set are promising. In a scenario where re-preparation of problematic slides involves a manual second look (at the cost of a higher delay), the analysis can well be tuned towards a high sensitivity and lower specificity. Future work will involve further accuracy improvements, an evaluation on a larger dataset as well as the addition of further modules such as detection

of over- and under-staining.

Syntax and Semantics for interoperable, standard-based, Anatomic Pathology Structured Reports (APSR)

G. Haroske¹, T. Rüdiger², A. Essenwanger³, S. Thun³, für das KDS-Team Pathologiebefundbericht der Medizininformatik-Initiative

¹*Berufsverband Deutscher Pathologinnen und Pathologen (BDP), Kommission Digitale Pathologie, Berlin, Germany*, ²*Klinikum Karlsruhe, Institut für Pathologie, Karlsruhe, Germany*, ³*Berlin Institute of Health at Charite (BIH), Core Facility Digitale Medizin und Interoperabilität, Berlin, Germany*

Background

Pathology Reports are highly complex collections of observations on patient-derived specimens that have been made observable through special procedures. In terms of structure and content, they follow more or less professionally agreed specifications. The degree of their comprehensibility for clinical doctors as well as the machine evaluability determines the degree of their interoperability.

Methods

As part of the Medical Informatics Initiative (MII), an interdisciplinary team developed a core data set for structured pathology reports based on the IHE profile APSR, created an information model and profiled resources from the HL7 standard FHIR (Fast Healthcare Interoperability Resources). In this profiling process, the terminology bindings to international medical reference terminologies LOINC and SNOMED CT were also made. Art-Decor and Simplifier were the main software tools used for interdisciplinary collaboration.

Results

The information model for the pathology report is closely based on the IHE profile APSR and takes into account the reusability of profiles from other core data sets of the MII. A DiagnosticReport was chosen as the core of the FHIR profiling, which combines all profiles for the service request, the bioprobes sent in, and the patient as well as the actual pathological-anatomical observations in a systematic way. This DiagnosticReport provides human-readable text in the usual manner of a pathology report and can be queried and searched for specific content by computer systems. In order to create a medical document [Ref01] from a FHIR resource, namely the pathology report in its usual written and signed form, the DiagnosticReport was referenced as an entry in the only section of an FHIR composition, the Diagnostic Report Section. The necessary terminology bindings and cardinalities of the elements in the FHIR resources have been made. For the wide variety of conceivable specific individual observations, the terminological rules for those semantics were described, according to which these observations are to be coded.

Conclusion

With the FHIR profiling for the core data set "Pathology report" of the MII, an implementable standard-based tool for pathology systems is available, which generally defines a syntax and semantics for this purpose. The semantic annotation of a standardized pathology vocabulary, e.g. from ICCR proposals or national S3 guidelines, remains a major challenge for digital pathology in German-speaking countries.

Literaturangaben

[Ref01] Haroske, G., Moerz, M., Oemig, F. , (2022), Document standards for pathology reports in digital medicine, Pathologie 41(1), 52-59

Deep learning-assisted differential detection of pancreatic intraepithelial neoplasia and characterization of inflammatory structures in proximity

R. S. J. Sarker¹, J. Rao¹, K. Steiger¹, A. Muckenhuber¹, P. Schöffler¹, **L. Dan¹**, **J. Israel¹**, W. Weichert¹, D. K. Das², T. Thomas², U. Joshi²

¹*Institute for Pathology, Comparative Experimental Pathology (CEP), Faculty of Medicine, Technical University Munich, Munich, Germany,* ²*AIRA Matrix Private Limited, Mumbai, India*

Background

With a 5-year survival rate of 5%, pancreatic ductal adenocarcinoma (PDAC) represents the fourth leading cause of cancer-related deaths worldwide. The most common PDAC precursor lesions are pancreatic intraepithelial neoplasia (PanIN). Diagnosis of PanIN from a histopathological image remains the 'gold standard' in pathology, as the existing imaging modalities cannot accurately identify them pre-operatively. To address this challenge, we propose a deep learning-based method for the detection and grading of PanIN lesions. Secondly, since inflammatory processes have emerged as key mediators of pancreatic cancer development and progression, therefore, we also attempted to profile the inflammatory structures in neighborhoods of PanINs.

Methods

Whole slide images, WSI (n=59) were acquired by digitizing hematoxylin and eosin-stained human pancreatic sections using an Aperio AT2 slide scanner, at 40x magnification. A deep neural network model (DeepLabv3) was trained on WSI tiles (size 1024x1024) to classify lesions into high or low-grade PanINs. The training and testing data set comprised of 10 and 27 WSI respectively. The outputs were compared to pathologists' annotation. Next, the detected PanIN lesions were imported to the open-source software, QuPath. To characterize the inflammatory structures, a semantic segmentation model from the Tissue Image Analytics, TIA Toolbox¹ was used to obtain a probability map of inflammatory tissue regions. The slides were classified into PanIN high grade-rich (HG) or low-grade-rich (LG) using area metrics.

Results

Concordance of the algorithm with pathologist annotation results to detect high/low-grade PanIN showed 91.56% sensitivity and 85.68% specificity. The classification filter identified 4 slides as significantly HG-rich and 14 slides as significantly LG-rich. Using QuPath scripting functionality, the classified slides were further analyzed for the metrics of inflammation regions in modifiable proximity of HG or LG lesions respectively (e.g. area, cell count, and distance to lesion).

Conclusion

This algorithm provides quantification-based segmentation and classification of PanIN, facilitating early detection of precursors to PDAC. The next step is to evaluate this data on inflammations in PanIN HG-rich versus LG-rich tissue sections. Our approach promises a comprehensive, early detection solution for PDAC precursors and a potential characteristic inflammatory pattern associated with each type of PanIN in patients.

Literaturangaben

[TIAToolbox] 1. Pocock, J., Graham, S., Vu, Q. D., Jahanifar, M., Deshpande, S., Hadjigeorgiou, G., Shephard, A., Bashir, R. M. S., Bilal, M., Lu, W., Epstein, D., Minhas, F., Rajpoot, N. M., & Raza, S. E. A. , (2021), TIAToolbox: An End-to-End Toolbox for Advanced Tissue Image Analytics, <https://doi.org/10.1101/2021.12.23.474029>

AG14.15

Extracting HCC-related Data from histological reports by using a Dependency Grammar

J. Dörenberg¹, N. Gaisa², J. Bednarsch³, L. R. Heij^{2,3}, E. Dahl^{1,2}

¹University Hospital RWTH Aachen, RWTH centralized Biomaterialbank, Aachen, Germany, ²University Hospital RWTH Aachen, Institute of Pathology, Aachen, Germany, ³Universital Hospital RWTH Aachen, Department of Surgery and Transplantation, Aachen, Germany

Background

Integrated AI-based analysis of clinical and experimental cancer data is an area of high interest but requires the availability of structured data. Personalized therapy of hepatocellular carcinoma (HCC) may especially benefit from such big data approaches. However, most pathologists in Germany still write their report in floating text. To make these important documents of cancer data available for AI-based research it is required to extract information from histological report texts and provide them in a structured form.

Methods

An AI-based approach is used to analyse the sentence structure of the reports. This information is then used to filter the report texts for required information. The Dependency Grammar (DG) parser Supar parses the sentences of the reports into a tree structure of grammatical relations by using an LSTM-based Neural Net which the developers already trained on a non-medical corpus^[1]. Each relation entry is subsequently lemmatized using Germalemma. Afterwards, the relations are filtered for the required information by using regular expressions and the Ontology database UMLS^[2]. Finally, these information are provided in a table.

Results

Before applied to an actual information extraction task, the DG parser was evaluated on a corpus of 200 sentences randomly taken from breast biopsy reports and achieved UAS=0.94, LA=0.92 and LAS=0.9. On 10 HCC reports the tool extracted different information. 98% of the information were extracted correctly (Fig1). The tool can be configured for an arbitrary set of required information in a decent amount of time. The data are extracted with high accuracy.

Number of HCCs	Fibrosis	Vascular invasion	Tumor diameter	Inflamm.	Inflamm. degree	Distance to resection area	Desmet stage	Steatosis	Cirrhosis	
1			1,4cm			1mm			TRUE	Correct
1		TRUE	5,5cm			0,3cm				Wrong
1	TRUE		4,2cm	TRUE		0,3cm			FALSE	
1		TRUE	5,5cm			0,3cm				
1	TRUE	TRUE	8,5cm	TRUE			3			Not given in record
1			16cm			0,1cm				
1	TRUE	TRUE	4,2cm	TRUE		1,5mm		TRUE	FALSE	
1										
1		FALSE	9,5cm			1cm				
1		FALSE	8,5cm	TRUE				TRUE		
1	TRUE		3,6cm			0,2cm	1-2			

Fig1: Data set extracted by the tool. Each row represents one report. The green entries were extracted correctly, the red information

was not found. All other information was not given in the reports.

Conclusion

The tool extracts data from histological reports with high accuracy. The test data for testing parsing and information extraction performance are currently limited. More test data are going to be annotated which warrant further evaluation. So far, the filter cannot handle distinct language patterns such as hyphenation. The tool will be optimized and evaluated on a larger data set of our HCC cohort and further data from arbitrary clinical data sets ensuring high performance on arbitrary clinical data sets. Thus, the tool provides arbitrary information from histological reports for any clinical research.

Literaturangaben

- [1] Timothy Dozat and Christopher D. Manning, (2017), Deep Biaffine Attention for Neural Dependency Parsing, Conference paper at ICLR
- [2] Oliver Bodenreider, (2003), The Unified Medical Language System (UMLS): integrating biomedical terminology, Nucleic Acids Research, 267D-270, Volume 32

Poster

P01 Postersitzung Gastroenteropathologie I

P01.01

Differentiation of inflammatory alterations in esophageal biopsies using FFPE proteomics (LC-MS/MS).

S. Mattern¹, P. Riemenschneider¹, J. Luibrand¹, A. Dickemann¹, M. Franz-Wachtel², B. Macek², F. Fend¹, S. Singer¹

¹Universitätsklinikum Tübingen, Allgemeine und Molekulare Pathologie und Pathologische Anatomie, Tübingen, Germany, ²Eberhard Karls Universität Tübingen, Interfakultäres Institut für Zellbiologie (IFIZ) - Proteom Centrum, Tübingen, Germany

Background

Esophageal inflammation is a common finding with different causes. Gastroesophageal reflux disease (GERD) is the most common cause, but in some cases, it is difficult to differentiate this from other more severe underlying diseases. Especially chronic inflammatory bowel diseases, particularly Crohn's disease, should be identified to provide the appropriate treatment.

Methods

We analyzed and compared paraffin-fixed paraffin-embedded (FFPE) biopsy samples of esophageal manifestations of Crohn's disease and inflammatory alterations in GERD by using a mass spectrometry proteomic approach (LC-MS/MS).

Results

We identified a proteomic signature being characteristic for esophageal manifestation of Crohn's disease compared to GERD. Proteins that were increased or only detectable in Crohn's disease were e.g. HLA-DRA, HLA-DRB1, ISG15, PSMB10, TAPBP, THY1 and also WARS. Other Proteins like e.g. EIF6, PSMB6, TTR, NAA50 and APOH were elevated or only detectable in biopsies of GERD patients.

By performing an enrichment analysis of the elevated proteins using the STRING Database we identified among enriched GO terms/Pathways: „Inflammatory bowel disease“, „NOD-like receptor signaling pathway“, „Antigen processing and presentation“ and „Proteasome“, among others.

Conclusion

Proteomic analysis on FFPE biopsies allows differentiation between esophageal manifestations of Crohn's disease and GERD which could help determine the correct diagnosis in borderline cases and thus improve therapy and patient management.

Putative tumor biological significance of *PCLO* in gastric cancer – Results from a large Central European cohort

M. Bernhardt, H.-M. Behrens, S. Krüger, C. Röcken

Institut für Pathologie, Kiel, Germany

Background

A recent multi-regional whole exome sequencing of nine gastric adenocarcinomas (GC) had shown that 29 of 48 (60.4%) tumor samples harbored mutations of *PCLO*. [1] In addition, previous studies provided evidence that *PCLO* is one of the ten most frequently mutated genes in GC. [2] However, its putative significance in GC biology is currently unknown. To fill this gap of information, we studied the expression of *PCLO* in a large and well characterized cohort of GC patients and correlated the expression with diverse clinicopathological patient characteristics.

Methods

466 whole tissue sections of patients with therapy-naïve GC were stained with an anti-*PCLO* antibody. The immunostaining of tumor cells showed no (0), weak (1+), moderate (2+), or strong (3+) staining intensity. The HScore was calculated according to the formula: $HScore = [0 \times \text{percentage of immunonegative tumor cells}] + [1 \times \text{percentage of weakly stained tumor cells}] + [2 \times \text{percentage of moderately stained tumor cells}] + [3 \times \text{percentage of strongly stained tumor cells}]$, resulting in a possible HScore between 0 and 300. Staining of stroma and vessels was assessed as present or absent for each case. The HScore dichotomized at the median was correlated with diverse clinicopathological patient characteristics.

Results

The tumor cells of 175 GCs expressed *PCLO*. 291 were immunonegative. HScore results ranged between 0-190, the maximum of 190 points were reached twice. Stromal cells expressed *PCLO* in 106 GCs and vessel walls in 84 GCs. *PCLO* was found more commonly in H. pylori-positive, intestinal, and high-grade GCs. The expression decreased with increasing tumor size (T category). No correlation was found with any other clinicopathological patient characteristic. The median overall (16.0 ± 1.8 months vs. 14.0 ± 1.4) and tumor specific (17.9 ± 3.6 vs. 15.0 ± 1.6) survival of patients with *PCLO*-positive GCs was, although not significantly better compared with negative cases. Based on our findings we hypothesize that *PCLO* is a tumor suppressor gene. Loss of *PCLO* favours tumor progression. Furthermore, this could also explain, why in some cases different mutations of *PCLO* were found in the same tumor.

Conclusion

Mutation of *PCLO* is probably a late, subclonal event.

Literaturangaben

- [1] Röcken C, Amallraja A, Halske C, Opasic L, Traulsen A, Behrens H-M, Krüger S, Liu A, Haag J, Egberts J-H, Rosenstiel P, Meißner T. , (2021), Multiscale heterogeneity in gastric adenocarcinoma evolution is an obstacle to precision medicine. , Genome medicine
- [2] Wang H, Shen L, Li Y, Lv J., (2020), Integrated characterisation of cancer genes identifies key molecular biomarkers in stomach adenocarcinoma. , Journal of clinical pathology

Elevated microsatellite instability at selected tetranucleotide repeats (EMAST) in gastric cancer: a distinct microsatellite instability type with potential clinical impact?

A.-L. Herz¹, S. Wisser¹, M. Kohlruss¹, J. Slotta-Huspenina¹, M. Jesinghaus^{1,2}, B. Grosser^{1,3}, M. Jesinghaus^{1,2}, K. Steiger^{1,4}, A. Novotny⁵, A. Hapfelmeier^{6,7}, T. Schmidt^{8,9}, M. Gaida^{10,11}, W. Weichert^{1,4}, **G. Keller¹**

¹Technical University of Munich, Institute of Pathology, München, Germany, ²University Hospital Marburg, Institute of Pathology, Marburg, Germany, ³University Hospital Augsburg, Institute of Pathology, Augsburg, Germany, ⁴German Cancer Consortium, Partner Site Munich, Institute of Pathology, München, Germany, ⁵Technical University of Munich, Department of Surgery, München, Germany, ⁶Technical University of Munich, Institute of Pathology, Institute for AI and Informatics in Medicine, München, Germany, ⁷Technical University Munich, Institute of General Practice and Health Services Research, München, Germany, ⁸University of Heidelberg, Department of Surgery, Heidelberg, Germany, ⁹University Hospital Köln, Department of Surgery, Köln, Germany, ¹⁰University of Heidelberg, Institute of Pathology, Heidelberg, Germany, ¹¹University Medical Center Mainz, Institute of Pathology, Mainz, Germany

Background

Elevated microsatellite instability at selected tetranucleotide repeats (EMAST) is a type of microsatellite instability (MSI), which occurs preferentially at microsatellite markers with tetranucleotides as the repeat unit. The aim of our study was to investigate the clinical impact of EMAST in the context of neoadjuvant chemotherapy (CTx) in gastric/gastro-esophageal adenocarcinomas (1).

Methods

We analysed 583 resected tumours (272 without and 311 after CTx) and 142 tumour biopsies before CTx. If at least two or three of five tetranucleotide repeat markers tested showed instability, the tumours were defined as EMAST (2+) or EMAST (3+) respectively. Expression of mismatch repair proteins including MSH3 was analysed using immunohistochemistry (1). Microsatellite instability (MSI) and Epstein-Barr virus positivity were determined using standard assays (2).

Results

EMAST (2+) and (3+) was detected in 17.8% and 11.5% of the tumours respectively. The frequency of EMAST (2+) or (3+) in high MSI (-H) tumours was 96.2% or 92.5% respectively, demonstrating a high overlap with this molecular subtype and the association of EMAST and MSI status was significant (each overall $p < 0.001$). EMAST (2+ or 3+) alone in MSI-H and EBV negative tumours, demonstrated only a statistically significant association of EMAST (2+) positivity and negative lymph node status (42.3% in EMAST (2+) and 28.8% in EMAST negative, $p = 0.045$). EMAST alone in neither definition was significantly associated with overall survival (OS) of the patients. The median OS for EMAST (2+) patients was 40.0 months (95% CI 16.4-63.6) and 38.7 months (95% CI 26.3-51.1) for the EMAST negative group ($p = 0.880$). The median OS for EMAST (3+) patients was 46.7 months (95% CI 18.2-75.2) and 38.7 months (95% CI 26.2-51.2) for the negative group ($p = 0.879$). No statistically significant association with response to neoadjuvant CTx was observed ($p = 0.992$ and $p = 0.433$ for EMAST (2+) and (3+)) (1).

Conclusion

In conclusion, our results demonstrate a nearly complete intersection between MSI-H and EMAST and they indicate, that EMAST alone is not a distinct instability type associated with noticeable clinical-pathological characteristics of gastric carcinoma patients (1).

Ref.:

(1) Herz et al. J Pathol Clin Res, online January 2022

(2) Kohlruss et al. J Pathol Clin Res 2019, 5:227-239

Paradox inflammatory manifestation of acute appendicitis in anti-inflammatory Januskinase inhibitor-based therapy with Tofacitinib (Xeljanz™) for ulcerative colitis

F. Weber¹, K. Eger², D. Jechorek², C. March³, R. S. Croner⁴, **F. Meyer**⁴

¹Universitätsklinikum Magdeburg A.ö.R., Klinik für Allgemein-, Viszeral-, Gefäß- und Transplantationschirurgie, Magdeburg, Germany, ²Universitätsklinikum Magdeburg A.ö.R., Institut für Pathologie, Magdeburg, Germany, ³University Hospital, Dept. of Radiology and Nuclear Medicine, Magdeburg, Germany, ⁴University Hospital, Dept. of General, Abdominal, Vascular and Transplant Surgery, Magdeburg, Germany

Background

Aim: Because of **i)** clinical management experiences derived from this challenging clinical case & **ii)** selective references from the scientific medical literature, an unusual counterfactual scientific case report is illustrated.

Methods

Scientific case report

Results

Case description: *Medical history* (currently): A 52-year-old male had spasmodic pain in the right lower abdomen for 2 days. No fever, no bowel movement changes, no vomiting (in the past: steroid-resistant ulcerative colitis under imm.-suppr. therapy [10 months Adalimumab, 9 months Vendolizumab, for 6 months Tofacitinib], fructose intolerance, no abd. surgery, medication: Xeljanz™ [Tofacitinib, 5 mg 2x1; JAK-inhibitor; PFIZER PHARMA GmbH, Berlin, Germany]; Mutaflor™ [1x1; Ardeypharm GmbH, Herdecke, Germany]).

Clinical findings: Pressure pain in the right lower abdomen w/ local muscular defense (Mc-Burney/Lanz+), no peritonism, Psoas-sign+.

Diagnostic measures: - Labs: standard value of white blood cell count, CrP: 25 mg/L.

- Transabdominal ultrasound: hypertrophic "appendix vermiformis" with target-phenomenon & occlusive fluid.

Decision-making: Indication for lap. exploration.

Treatment: Under periop. single-shot antibiotic with Unacid™, urgent lap. appendectomy was performed with additional lavage & placement of local drainage. In surgery, the diagnosis of appendicitis was validated.

Clinical course: Uncomplicated postop. phase. Sufficient analgesia, removal of local drainage on the 2nd postop. Dismissal on 4th day after surgery in ambulant medical care.

Histopathology: Validation of ulcero-phlegmonoösis, acute-purulent appendicitis with fibrinous-purulent mesenteriolitis.

Further course of action: Imm.-suppr. therapy was continued.

Conclusion

Based on the paradoxon that an acute inflammatory disease (acute appendicitis) developed in case of an ongoing imm.-suppr/anti-inflammatory treatment using a JAK-inhibitor for ulcerative colitis, such uncommon clinical case is reported even though this side effect is formally known. This might be the manifestation of **i)** an immunomodulatorily reduced or at least altered mucosal defence incl. an elevated risk for opportunistic infections as specific visceral “side effect“ of the JAK-inhibitor &/or as a consequence of **ii)** an induced alternative inflammatory mechanism/proinflammatory signal transduction as well as an intestinal drainage defect in the segment of right colic artery with consecutive collection of necrotic cells & activation of inflammatory mediators.

Proteome-based (LC-MS/MS) characterization of microsatellite stable (MSS) and instable (MSI) colorectal cancer

A. Dickemann¹, P. Riemenschneider¹, S. Mattern¹, J. Luijbrand¹, M. Kloor², I. Bonzheim¹, M. Franz-Wachtel³, B. Macek³, F. Fend¹, S. Singer¹

¹Universitätsklinikum Tübingen, Allgemeine und Molekulare Pathologie und Pathologische Anatomie, Tübingen, Germany, ²Universitätsklinikum Heidelberg, Pathologisches Institut, Heidelberg, Germany, ³Eberhard Karls Universität Tübingen, Interfakultäres Institut für Zellbiologie (IFIZ) - Proteom Centrum, Tübingen, Germany

Background

Colorectal adenocarcinoma (CRC) remains one of the most frequent causes of cancer-related deaths worldwide. Among highly relevant molecular parameters for disease management and outcome of CRC is the microsatellite status. Microsatellite instability (MSI) is characterized by genetic hypermutability caused by insufficient DNA-mismatch repair (MMR) due to defective MMR proteins such as MLH1, PMS2, MSH2, and MSH6. The MSI-status is defined by the stability of 5 microsatellite markers: BAT25 and BAT26, D2S123, D5S346, and D17S250. Tumors without an unstable marker are classified as microsatellite stable (MSS), tumors with 1 instable marker as MSI-Low(L) and tumors with 2 or more instable markers as MSI-High(H).

Methods

To gain deeper insights in proteome-wide alterations of the respective CRC subgroups (MSS, MSI-H, MSI-L) liquid chromatography and tandem mass spectrometry (LC-MS/MS) was performed on 22 CRCs FFPE-specimens.

Results

By this approach we could identify 4882 protein groups across all samples. Proteins differentially expressed by comparing the MSI-H and MSS group included upregulated proteins linked to inflammation and antigen presentation (e.g. S100A8, S100A9, TAP1 and HLA-subtypes) and downregulated, predominantly mitochondrial proteins (e.g. DIABLO and SDHB) at least in part linked to the Warburg effect, among other alterations. The comparison between MSI-L and MSS CRCs revealed again mitochondrial proteins (e.g. ALDH1B1 and COX6C) to be decreased and other factors, such as RAB27A and TMEM25, to be increased.

Conclusion

While our analyses are still ongoing the results so far suggest that the MSI status (including MSI-L) of CRCs is associated with characteristic proteomic alterations. FFPE LC-MS/MS may therefore serve as an alternative approach to evaluate the MSI status in CRC specimen and may improve our understanding of MSI-related (colo-rectal) cancer biology.

Murine Organoids as a Model System for Quantitative Evaluation of Tumor Antigen Presentation

P. K. Ziegler¹, M. Ghalamkaran¹, F. R. Greten², P. J. Wild¹

¹*Universitätsklinikum Frankfurt, Dr. Senckenbergisches Institut für Pathologie, Frankfurt a.M., Germany,*

²*Georg-Speyer-Haus, Institut für Tumorbologie und experimentelle Therapie, Frankfurt a.M., Germany*

Background

Tumor neoantigens are recognized the Achilles heel of cancer cells displaying their distorted genomic base to the immune system. Neoantigens arise from i.e. mutated proteins and can act as inducers of anti-tumor immunity. In general, a high number of non-synonymous mutations (tumor mutational burden, TMB) acts as positive predictive feature of immune-checkpoint inhibitor therapy, however, a large number of cancers with high TMB or MSI lack T cell infiltration for unknown reasons.

Methods

In order to study antigen-presentation by tumor cells we make use of an orthotopic tumor transplantation model combined with the expression of ovalbumin, a well-characterized model antigen widely used in immunological studies. Murine intestinal organoids have been modulated to reflect mutations frequently found in human colorectal cancer, namely *APC*, *TP53*, *KRAS*, *TGFBR2* and additional *AKT*-activation. Following orthotopic transplantation into the rectum of MHC-matched recipient mice these organoids rapidly engraft, form tumor masses and frequently metastasize into draining lymph nodes and the liver.

Results

The model antigen ovalbumin has been characterized to give rise to specific MHC-I and -II restricted antigens, which can be detected using transgenic T cells or tetramers. For *in vivo* assays, in order to circumvent immunologic rejection in transplantation experiments the expression of ovalbumin is controlled by a tetracycline-dependent promoter. Organoids are being transplanted into mouse rectum and tumor formation is monitored by endoscopy. Once sizeable tumors have been detected tumor tissue is examined by histology, IHC and flow cytometry. *In vitro* antigen-specific T cells response can be assessed using a co-culture system of ovalbumin-expressing tumor organoids and antigen-specific T cells.

Conclusion

Tumor antigen presentation is crucial for tumor suppressive effects by the adaptive immune system. While the level of tumor-specific antigens, i.e. neoantigens, can be assessed by routine molecular pathological techniques, the level of antigen presentation within the tumor tissue or in draining lymph nodes remains largely unknown. Here we describe a murine model system to quantify the level of antigen presentation in an experimental setting. This model can be used for detection of the molecular features of tumor cells to alter the level of antigen-presentation and to evaluate future therapeutic strategies to enhance adaptive anti-tumor immunity.

Expression patterns of HSP90, HSP70 and MLKL in human colon cancer

E. C. Keller¹, E. Drecoll², R. Langer³, W. Weichert¹, P. J. Jost⁴, **J. Slotta-Huspenina¹**

¹Institute of Pathology, Technical University of Munich, Munich, Germany, ²Ernst von Bergmann Institute of Pathology, Potsdam, Germany, ³Institute of Pathology, Johannes Kepler University, Linz, Austria, ⁴Division of Oncology, Department of Internal Medicine, Medical University of Graz, Graz, Austria

Background

Necroptosis is an immunogenic form of regulated necrosis and has been implicated in various cancer entities, including colon cancer. Mixed lineage kinase domain-like protein (MLKL) plays a crucial role in the execution of tumor necrosis factor (TNF)-induced necroptosis. Upon phosphorylation, MLKL forms oligomers and translocates to the plasma membrane to execute cell death. Recently, heat shock protein 90 (HSP90) has been identified to be required for MLKL oligomerization. Likewise, HSP70 has been shown to be needed for MLKL polymerization. Thus, the aim of this study was to shed light on the expression profiles of HSP90, HSP70 and MLKL in colon cancer.

Methods

Tumoural MLKL, HSP70 and HSP90 expression was determined by immunohistochemistry on tissue micro arrays comprising 375 primary resected colon carcinomas of all stages. Expression levels were semi-quantitatively determined by calculating the immunoreactive score (IRS, 0-12). For HSP90 and HSP70 expression of this cohort, see [1] and [2]. Statistical analysis was carried out using Excel and Graphpad Prism.

Results

MLKL expression ranged from negative to high and was positive (IRS 1-12) in 79.7% of cases (299/375). HSP90 and HSP70 were positive in 71.6% (260/363) and 72.4% (265/366), respectively. While HSP90 expression significantly correlated with high MLKL expression ($r=0.305$, $p<0.001$), there was no significant association of HSP70 with MLKL ($p=0.099$). Based on expression patterns (positivity defined as $IRS>0$, negativity as $IRS=0$), 290 colon carcinoma cases revealed a MLKL+/HSP90+ (79.9%) and 66 a MLKL+/HSP90- (22.7%) pattern. MLKL+/HSP70+ pattern was observed in 211 (72.5%) and MLKL+/HSP70- pattern in 80 cases (27.4%).

Conclusion

HSP90 and HSP70 are frequently co-expressed with MLKL in human colon cancer. However, a substantial number of MLKL-positive cases do not show expression of HSP90 or HSP70 (22.7% and 27.4%). The absence of HSPs in these cases might point towards impairment of MLKL polymerization and therefore necroptosis-execution. This also has implications for the application of HSP70 inhibitors, such as necroptosis-blocking compound 1 (NBC1).

Literaturangaben

- [1] K. Bauer, U. Nitsche, J. Slotta-Huspenina, E. Drecoll, C. Hann von Weyhern, R. Rosenberg, H. Höfler, R. Langer, (2012), High HSP27 and HSP70 expression levels are independent adverse prognostic factors in primary resected colon cancer, *Cellular Oncology*, 197-205, 35
- [2] E. Drecoll, U. Nitsche, K. Bauer, S. Berezowska, J. Slotta-Huspenina, R. Rosenberg, R. Langer , (2014), Expression analysis of heat shock protein 90 (HSP90) and Her2 in colon carcinoma, *International Journal of Colorectal Disease*, 663-671, 29

The impact of cancer-associated fibroblasts on the biology and progression of colorectal carcinomas

L. Henrich¹, K. Greimelmaier², M. Wessolly¹, N. Klopp³, E. Mairinger³, J. Wohlschlaeger³, S. Berger³, Y. Krause³, K. W. Schmid³, H. U. Schildhaus³, F. D. Mairinger¹, S. Borchert³

¹Pathologie Universitätsklinikum Essen, Translationale Tumorforschung, Essen, Germany, ²Institut für Pathologie- Diakonissenkrankenhaus Flensburg, Flensburg, Germany, ³Pathologie Universitätsklinikum Essen, Essen, Germany

Background

Colorectal cancer (CRC) is the third most common cancer and the second leading cause of cancer-related death. CRC is known for its tumor microenvironment (TME), which promotes tumorigenesis and metastasis and consists of FAP-positive fibroblasts (cancer-associated fibroblasts, CAFs) as major components. The importance of CAFs in tumorigenesis and increased malignancy has been widely documented, but many questions remain unanswered. The exact biological background of CAFs, as well as their relationship to the tumor microenvironment, has not yet been investigated in detail. This work deals with the biology and progression of CAFs and their impact on CRC.

Methods

A cohort of 155 CRC of different localisations (distal, proximal, rectum, sigma), polyps, chronic inflammation, and healthy samples were included. The patient's age, sex, location, TNM classification, inflammation status, and the immune-expression of the markers CD3, p53, BCAT, Ki67 were known. Cases consist of formalin-fixed, paraffin-embedded (FFPE) tissue for RNA and DNA isolation. Digital gene expression analysis (NanoString) was performed using a panel covering different signaling pathways (MAPK, PI3K/Akt, TGF- β , WNT, p53, etc.). Moreover, targeted amplicon-based NGS was performed to determine CRC mutational profile. CAF density and activity via FAP scoring as well as MSI status has been determined immunohistochemically.

Results

FAP expression was found in 81 patients out of 150 samples. In 63 of 64 (98.4 %) CRC cases, 11 of 40 adenomas (27,5 %), and 7 out of 18 inflammations (38.9 %) FAP expression could be detected. No expression of FAP was found in the healthy or control group. 13 out of 74 key genes examined showed a significant association with the occurrence of FAP-positive fibroblasts. GSEA shows prominent enrichment of pathways associated with PI3K as well as MAPK signaling, but also immune response pathways such as Natural killer cell-mediated cytotoxicity seems to be activated via CAFs. No significant differences between single subtypes based on their MSI, TP53, RAS, and BRAF status could be detected.

Conclusion

The results confirmed an interplay between CAFs and cancer cells, promoting growth, invasiveness, angiogenesis, and metastasis. TGF- β , CDKs, and the Wnt signaling pathway, which support proliferation, growth, and apoptosis, were particularly affected. In conclusion, CAFs play a major role in CRC and impact

the tumor microenvironment at all stages of development.

Peritoneal tumor lesions - representative case series on rare diagnoses at a tertiary center

F. Weber¹, C. March², K. Eger³, R. S. Croner⁴, **F. Meyer⁴**

¹Universitätsklinikum Magdeburg A.ö.R., Klinik für Allgemein-, Viszeral-, Gefäß- und Transplantationschirurgie, Magdeburg, Germany, ²University Hospital, Dept. of Radiology and Nuclear Medicine, Magdeburg, Germany, ³Universitätsklinikum Magdeburg A.ö.R., Institut für Pathologie, Magdeburg, Germany, ⁴University Hospital, Dept. of General, Abdominal, Vascular and Transplant Surgery, Magdeburg, Germany

Background

Aim: Exemplary demonstration of 8 cases with rare peritoneal tumor (Tu) lesions (PTLs) & their histol. results in abd. surgery emphasizing boil. diversity.

Methods

Representative scientific case reports

Results

(selective cases): **1)** Intraop. incidental finding of a jejunal PTLs during gynecol. surgery of endometrium carcinoma (Ca) leading to segm. resection & reconstruction w/ side-to-side jejunojejunostomy (histol. investigation, jejunal diverticulum with pancr. metaplasia).

2) During expl. laparotomy, in case of suspected ovarian Tu, multiple 8- to 15-mm PTLs were resected along with radical hysterectomy - medical history (hx), mastectomy for breast cancer (histologically, no Tu in the gynecol. specimen detectable, rather primary perit. Ca).

3) In lap. hernioplasty of incarcerated trocar hernia, a suspicious inflamed fatty Tu-like tissue was resected from the descending colon (histologically, acute epiploic appendagitis).

4) In expl. laparotomy for pseudomyxoma peritonei (PCI: 32) of unknown origin, 4 PTLs were resected for further Tu classification displaying parts of a mucinous adeno-Ca (histol. investigation confirmed pseudomyxoma).

5) In lap. appendectomy, partial resection of the greater omentum was combined (histol. finding of the appendix: lipofibrosis of the appendix w/ necrotic fat tissue consistent with a twisted "appendix epiploicae").

6) In expl. laparotomy for chronic subileus (medical hx, appendectomy & resection of the ileum with ileoileostomy), small PTLs were detected & interpreted as scarring adhesion of the jejunum (histol. preparation displayed plant food ingredients w/ older necrosis of fat tissue).

7) Abd. CT scan displayed an oval paracolic mass (no diverticulitis) diagnosed as "appendagitis epiploicae" of the descending/sigmoid colon.

8) Common surg. intervention of urology & abd. surgery comprising subtotal peritonectomy, right hemicolectomy, partial resection of the urinary bladder & hyperthermic intraperit. chemotherapy incl. fresh frozen section (later def. histol. investigation, primary serous papillary adeno-Ca of the peritoneum).

Conclusion

PTL can comprise diverse origins & entities. Histol. investigation & close cooperation of the pathologist & surgeon can be considered a substantial prerequisite for def. diagnosis-finding, following decision-making & further therap. steps using various modi, however, associated with still limited clin. experiences on the appropriate diagn. & (peri-)therap. management due to their rareness.

Rare case of diverticulitis of the ascending colon in Western countries

M. Shehabeldin¹, C. Paasch², R. S. Croner³, **F. Meyer³**

¹University Hospital, Division of Pediatric Surgery, Dept. of General, Abdominal, Vascular and Transplant Surgery, Magdeburg, Germany, ²University Hospital, Dept. of General and Abdominal Surgery, Brandenburg (Havel), Germany, ³University Hospital, Dept. of General, Abdominal, Vascular and Transplant Surgery, Magdeburg, Germany

Background

Pain of the right lower abdomen comprises a broad spectrum of differential diagnoses.

Aim: To illustrate the rare diagnosis of diverticulitis of the ascending colon occurring in a patient with right-side abdominal pain

Methods

Scientific case report

Results

Case presentation: *Medical history and clinical finding:* A 40-years old female patient was admitted as an emergency case to the hospital due to pain for four days with increasing intensity at the right lower abdomen.

Diagnostic measures (initially): - Laboratory parameters (SI): CrP serum level - 158.73 mg/L, white blood cell count [leucocytes] - 11.4 GpT/L

- Abdominal ultrasound showed thickening of the intestinal wall indicating an inflammation around an identified diverticulum of the ascending colon and small fluid accumulation indicating a covered perforation.

- Abdominal CT-scan confirmed ultrasound finding of inflammatory intestinal wall thickening of a diverticulum at the ascending colon with characteristics of a covered perforation.

Diagnosis: Diverticulitis of the ascending colon

Therapy: The patient was admitted to the hospital. Initially, i.v. antibiotic and analgesic therapies were initiated accomplished by i.v. infusion. After temporary "n.p.o.", oral nutrition was carefully initiated, which was well tolerated. In addition, the patient also received nutritional counseling regarding diverticulum.

Course: Under the therapeutic measures, general condition of the patient and the local pain symptoms proved rapidly. The infection parameters were regressive; i.v. antibiotic therapy was continued until day 5 to protect. The patient was able to defecate without any problems. For further course, colonoscopy was recommended.

Conclusion

Right-hemicolon diverticulitis is a rare diagnosis based on diverticulosis, which itself shows a high and age-dependent prevalence. In Western industrial countries, approximately 1.5 % of all diverticulitis cases originate at the ascending colon.

This diagnosis needs to be also taken into account in case of right-side lower abdominal pain as one of the possible differential diagnoses in its broad profile from a surgical perspective.

Although, there is only a low level of evidence, diverticulitis of the ascending colon is not commonly associated with nausea, vomiting and fever as in appendicitis, which itself occurs more frequently in rather younger patients.

Therapeutic measures are similar to those established for a diverticulitis of the sigmoid colon, which was also successful in the presented case.

Representative spectrum of various appendix vermiformis-associated lesions (case series)

K. Boettge¹, C. Paasch¹, C. Schildberg¹, R. S. Croner², **F. Meyer²**

¹University Hospital, Dept. of General and Abdominal Surgery, Brandenburg (Havel), Germany, ²University Hospital, Dept. of General, Abdominal, Vascular and Transplant Surgery, Magdeburg, Germany

Background

Acute appendicitis is considered one of the most frequent causes of abdominal pain and - in the majority - reason for the indication of surgical intervention in adults and children.

In addition to the acute inflammation of appendix vermiformis, there are numerous appendix-related differential diagnoses. The appropriate awareness of and knowledge on that appear essential for clinical care, in particular, under the today's option to treat uncomplicated acute appendicitis with antibiotics.

Aim: Exemplary illustration of 8 cases with rare appendix vermiformis-associated manifestations of diverse diagnoses (AVAM) to reflect daily clinical, in particular, surgical practice.

Methods

Representative scientific case series (design) - including patient-related (etiology, incidence), diagnosis-associated (sex ratio, symptomatology), perioperative, therapeutic (in particular, surgical intervention-related) aspects and early postoperative outcome details, such as morbidity (characterized by general/special complications) and mortality (hospital, 30 d) for each specific diagnosis/entity.

Results

(corner points):

- The spectrum of AVAM is broad - all specific diagnoses and entities can mimic acute appendicitis with regard to clinical symptomatology, laboratory parameter profile and (partially) imaging.
- AVAM are dominated by inflammatory and neoplastic entities.
- Specific attention is focussed onto chronic appendicitis, appendicopathy, mucinous appendix carcinoma, acute appendicitis in a femoral or inguinal hernia, twisted "appendix epiploica", single metastasis of gastric cancer at the appendix, appendagitis epiploica, subhepatic appendicitis, perityphlitic infiltration, neuroendocrine tumor lesion of the appendix, pseudomyxoma peritonei in case of mucinous appendix carcinoma.
- All determined entities required surgical intervention - only in one exceptional case, conservative therapeutic approach was imaginable in definitive diagnosis-finding.

Conclusion

AVAM can have diverse origin and comprise various entities. The competent, consequent, correct and early diagnosis-finding appears decisive with regard to therapy, early postoperative course and (in case of malignant diseases) prognosis.

Histopathology and close interdisciplinary cooperation are - due to AVAM rareness - a substantial prediction

for a timely diagnosis-finding, prompt therapeutic decision-making and practical realization as well as - if necessary - subsequent therapeutic steps, possibly using variable modes.

Acute Epiploic Appendagitis - a rare differential diagnosis of acute abdomen

L. Harling¹, K. Eger², C. March³, R. S. Croner¹, **F. Meyer¹**

¹University Hospital, Dept. of General, Abdominal, Vascular and Transplant Surgery, Magdeburg, Germany,

²University Hospital, Institute of Pathology, Magdeburg, Germany, ³University Hospital, Dept. of Radiology and Nuclear Medicine, Magdeburg, Germany

Background

Acute epiploic appendagitis is a rather rare differential diagnosis of unclear or acute abdomen.

Aim: To describe the extraordinary diagnosis of acute epiploic appendagitis based on experiences obtained in the successful clinical case management & secondly, on selective references from medical scientific literature.

Methods

Scientific case report

Results

Case summary: - *Medical history*: A 29-year-old female was admitted with abdominal pain in the left lower quadrant - she reported a laparoscopic ovarian cyst removal 3 years prior.

- *Physical examination of the abdomen* revealed tenderness in the left lower quadrant without a palpable mass.

- Leading *diagnosis* was found using transabdominal ultrasound & confirmed by an abdominal CT scan.

- *Therapeutic approach* comprised explorative laparoscopy (because of the incarcerated hernia), adhesiolysis, removal of a tip of the greater omentum out of the hernial sac, closure of the hernial orifice, & removal of an unclear, inflamed, & bloody fatty tissue from the wall of the descending colon (*histopathological investigation*, acute epiploic appendagitis) flanked by conservative treatment of diverticulitis of the sigmoid colon.

- The further *clinical course* was uneventful (discharge, on the 3rd postoperative day) with favorable *long-term outcome* characterized by no further complaints for 15 months.

Conclusion

Acute epiploic appendagitis is an inflammatory, usually self-limiting condition of the epiploic appendages of the colon. It typically manifests with abdominal pain in the lower left quadrant. Imaging is an important diagnostic tool to determine whether the patient has in fact acute epiploic appendagitis recognizing the characteristic oval lesions with the surrounding inflammation & central fat attenuation on CT as well as the hyperechoic oval lesions with a hypoechoic peripheral band on ultrasound images as crucial. Nevertheless, it is often overlooked in patients & confused with its differential diagnoses, such as appendicitis or diverticulitis. In the described case, the patient was initially diagnosed with an incarcerated abdominal hernia &, therefore,

she subsequently underwent surgery. The inflamed epiploic appendage was discovered in laparoscopic exploration, removed, & confirmed through the histopathology report, an approach to be performed with great caution, namely, on one hand, not to **i)** misinterpret an inflamed diverticula or covered perforation of it as well as - on the other hand - **ii)** overlook a peritoneal tumor lesions.

Uncomplicated diverticulitis of the sigmoid colon in ongoing immunosuppressive and anti-inflammatory treatment of a female patient with rheumatoid arthritis (RA)

L. Harling, I. P. Aswandi, R. S. Croner, **F. Meyer**

University Hospital, Dept. of General, Abdominal, Vascular and Transplant Surgery, Magdeburg, Germany

Background

Aim: Based on clin. case-specific management experiences & references from the literature, the paradox case configuration of an acute infl. reaction as an unusual complication or visceral side effect of an anti-infl./imm.-suppr. medication for the basic disease, RA, is described.

Methods

Scientific case report

Results

Case description: *Med. history (hx)*: A 47-years old female patient with RA (medication: Prednisolon [inhibits infl. reaction], Leflunomid ["Disease Modifying Anti-Rheumatic Drug" {DMARD} - prevents proliferation of activated lymphocytes, suppresses endogenous immune system]) came to the emergency room because of pain in the lower abdomen for 3 hours

Clin. finding: Abdomen, soft & diffuse tenderness on palpation in both lower quadrants (*punctum maximum* in the left lower abdomen, sparse boborygmus, no peritonism)

Diagnostics: - Lab parameters: White blood cell count, 10.5 Gpt/L; CrP, 71.22 mg/L

- Plain film of the abdomen: Gas-filled intestine (left colonic flexure) with gas-fluid level in the small intestine; coprostasis (descending colon & rectum); no free air

- Ultrasound: Appendix vermiformis not detectable, a few enlarged mesenteric lymph nodes, slight thickening of the terminal ileum – most likely a secondary sign as in appendicitis, no free fluid or hint for a complication

- CT scan: Uncomplicated diverticulitis of the sigmoid colon (wall thickening) with diverticulosis & surrounding infl. reaction of the fatty tissue

Decision-making: Conservative therapy

Therapy: i.v. antibiotics & analgetics - on the 3rd day, questionable skin reaction to Ciprobay & Clont leading to the change onto Tazobac; pro re nata medication for nausea & vomiting in administering Novaminsulfon leading to a change onto Paracetamol

Clin. course: Initiation of oral nutrition; under administration of prokinetics, regular defecation

Prospect: Physical rest, mild diet, colonoscopy within the non-inflamed interval of 6 weeks, follow-up control of clin. findings & labs by the family practitioner - in case of clin. impairment (fever, discomfort, progressive pain), immediate follow-up visit; gynecological verification & test for allergies

Conclusion

Older (rather not applicable in this case) & imm.-suppr. patients do have frequently only slight or atypical complaints.

The patient under Prednisolon & Leflunomid therapy for RA needs to be classified imm.-suppr. with an associated increased infectious risk as well as imm.-suppr. drug & steroid intake can be considered risk factors for a perforation.

P01 Postersitzung Gastroenteropathologie II

P01.14

Lipid droplets and associated proteins in viral hepatitis

S. Schelbert^{1, 2}, V. Dries^{3, 4}, U. Drebber³, H. R. Witzel¹, M. Schindeldecker¹, A. Weinmann⁵, R. Bartenschlager⁶, P. Schirmacher⁷, W. Roth¹, B. K. Straub¹

¹University Medical Center of the Johannes Gutenberg University, Institute of Pathology, Mainz, Germany, ²University Hospital, Institute of Pathology, Würzburg, Germany, ³University Hospital, Institute of Pathology, Köln, Germany, ⁴Synlab Pathology, Mannheim, Germany, ⁵University Medical Center of the Johannes Gutenberg University, Department of Internal Medicine I, Mainz, Germany, ⁶Molecular Virology, Department of Infectious Diseases, Ruprecht-Karls-University, Heidelberg, Germany, ⁷University Hospital, Institute of Pathology, Heidelberg, Germany

Background

Chronic hepatitis B and C conveys a high risk for the development of liver cirrhosis and hepatocellular carcinoma. Lipid metabolism plays a key role for chronic hepatitis C, as lipid droplets (LDs) are necessary to generate infectious HCV particles [1]. LDs are dynamic organelles, that are regulated by amphiphilic proteins of the perilipin-family with respect to LD-formation, maintenance, and degradation [2]. Perilipin 1 and 2 are constitutively localized on the LD-surface [2]. Aim of this project was to study LD-histopathology in chronic hepatitis.

Methods

The study was conducted based on a well characterized clinicopathologic collective of 231 liver biopsies from patients with chronic hepatitis C. In addition, liver biopsies and resection specimens from patients with chronic hepatitis B, acute hepatitis E, autoimmune hepatitis (AIH), primary sclerosing cholangitis and normal liver parenchyma were examined in control.

Results

As already shown by other studies [3], steatosis correlated with the HCV genotype and livers of patients infected with HCV genotype 3a showed a higher degree of steatosis than those with genotype 1b ($p = 0.014$). Viral load did not significantly correlate with the degree of steatosis in our collective. Most interestingly, 36 % of the liver biopsies from patients with HCV showed perilipin-positive steatotic foci not detected by conventional microscopy. These perilipin-positive steatotic foci were also found in 18 % of livers of patients with HBV, 20 % of normal liver tissue and 25 % of livers with AIH. Perilipin 1 and 2-positive steatotic foci only partially overlapped with virus infected areas as indicated by HBs-staining. Ultrastructural analysis of these foci showed a sharp boundary between hepatocytes rich in LDs and hepatocytes which contained only a small number of LDs in the cytosol. The foci partially showed a deviation of glutamine synthetase staining, but no elevated Ki67-proliferation index, and no staining for LFABP, HSP70, glypican 3

or other markers shown for hepatocellular tumours.

Conclusion

We could identify perilipin-positive steatotic foci in a high proportion of livers with chronic liver disease, most prominent, but not restricted to viral hepatitis, which may be areas of focal metabolic dysregulation. However, it is not yet clear, whether these foci represent a reactive / degenerative process or even an (early) preneoplastic one.

Literaturangaben

- [1] Miyanari, Yusuke; Atsuzawa, Kimie; Usuda, Nobuteru; Watashi, Koichi; Hishiki, Takayuki; Zayas, Margarita; Bartenschlager, Ralf; Wakita, Takaji; Hijikata, Makoto; Shimotohno, Kunitada, (2007), The lipid droplet is an important organelle for hepatitis C virus production, *Nature cell biology*, 961 - 969, 9
- [2] Sztalryd, Carole; Brasaemle, Dawn L., (2017), The perilipin family of lipid droplet proteins: Gatekeepers of intracellular lipolysis, *Biochimica et biophysica acta - Molecular and cell biology of lipids*, 1221 - 1232
- [3] Asselah, T.; Rubbia-Brandt, L.; Marcellin, P.; Negro, F., (2006), Steatosis in chronic hepatitis C: why does it really matter?, *Gut*, 123 - 130, 1

Impact of ALDH1A1 on patient overall survival in intrahepatic cholangiocellular carcinoma and the tumor stroma

K. Kurowski¹, M.-A. Pantea¹, M. Foell¹, O. Schilling¹, M. Werner¹, S. Fichtner-Feigl², B. Bengsch³, P. Bronsert¹, P. A. Holzner², S. Timme¹

¹Universitätsklinikum Freiburg, Institut für Klinische Pathologie, Freiburg, Germany, ²Universitätsklinikum Freiburg, Klinik für Allgemein und Viszeralchirurgie, Freiburg, Germany, ³Universitätsklinikum Freiburg, Klinik für Innere Medizin II Gastroenterologie, Hepatologie, Endokrinologie und Infektiologie, Freiburg, Germany

Background

Aldehyde dehydrogenase 1A1 (ALDH1A1), belonging to the aldehyde dehydrogenase family, is characterised by its anti-oxidative effects and a stem cell marker. ALDH1A1 overexpression has been described with increased tumor malignancy and poor patients overall survival in various malignomas. Considering ALDH1A1 expression in intrahepatic cholangiocarcinoma (iCC), inconclusive results regarding patients' prognosis are published.

Methods

69 patients (35 male / 34 female) suffering from iCC, operated and histo-pathologically diagnosed at the University Medical Centre Freiburg were included into the study. All samples were processed according to standardised protocols. TMAs, consisting of three tumor samples / cores per patient were stained for ALDH1A1. ALDH1A1 expression was analysed subcellularly within the cytoplasm of the tumor cells and the surrounding tumor stroma via QuPath and statistically correlated with clinico-pathological data using RStudio.

Results

Clinical parameters with a significant impact on overall survival (OS) were pT-classification ($p=0.03$), regional lymphnode metastasis ($p<0.0001$), lymph and blood vessel invasion ($p<0.0001$ and $p=0.048$ respectively) and microscopically positive resection margin ($p=0.013$).

In tumor as well as in tumor surrounding stroma cells, a high ALDH1A1 expression correlated with a significantly longer OS (ALDH1A1 expression tumor $p = 0.0068$; ALDH1A1 expression stroma $p = 0.008$). Conducting gender specific analyses, ALDH1A1 over expression revealed a significantly prolonged OS in the female subpopulation for both tumor ($p = 0.0077$) and stroma cells ($p = 0.043$).

Conclusion

Although high ALDH1A1 expression predicts a worse prognosis in many malignancies, a high expression in iCC seems to be correlated with a longer OS. Hereby not only the expression in tumor cells, but also in surrounding stroma cells impacts the OS in iCC patients significantly, which is firstly described in this study. Interestingly, splitting the cohort by gender, a significantly prolonged OS was shown exclusively in the female subgroup with high ALDH1A1 expression, which has to be further investigated.

Epigenetic differences between HCC and iCCA reveal clinically relevant targets as potential biomarkers for individualized therapy

N. Abedin¹, **K. Bankov**², S. Gretser², Y. Fu², K. Filipski^{3, 4, 5, 6}, P. N. Harter^{3, 4, 5, 6}, C. Döring², S. Zeuzem¹, P. Wild²

¹University Hospital Frankfurt, Medical Clinique 1, Frankfurt, Germany, ²University Hospital Frankfurt, Dr. Senckenberg Institute of Pathology, Frankfurt, Germany, ³University of Frankfurt, Neurological Institute (Edinger Institute), Frankfurt, Germany, ⁴Frankfurt Cancer Institute (FCI), Frankfurt, Germany, ⁵University Hospital Frankfurt, University Cancer Center (UCT) Frankfurt, Frankfurt, Germany, ⁶German Cancer Research Center (DKFZ), Heidelberg, German Cancer Consortium (DKTK), Partner Site Frankfurt/Mainz, Frankfurt, Germany

Background

Liver malignancies, i.e. hepatocellular carcinoma (HCC) and intrahepatic cholangiocarcinoma (iCCA) are associated with a poor prognosis and low survival rate. Due to a lack of specific biomarkers and asymptomatic progression, diagnosis mostly occurs at an advanced stage and is associated with poor prognosis. With limited curative treatment options and systemic therapies hardly improving survival, it is vital to develop safe and accurate biomarkers. Although immune checkpoint blockade has proven to be an efficient therapeutic option for a variety of cancers, most malignant liver diseases are not responsive to this therapy.

Methods

To identify new potential targets in HCC and iCCA and gain knowledge in the immune suppressive mechanisms in these malignancies, we conducted a gene expression analysis using the nCounter[®] NanoString system and the nCounter[®] Immune Exhaustion Panel. Total RNA and DNA was extracted from FFPE-tissue of patients diagnosed with HCC, and iCCA. DNA was used to analyse the DNA methylation patterns using the Human Methylation EPIC array (Illumina) of all samples in order to study the epigenetic regulation of potential targets.

Results

The unsupervised hierarchical clustering of gene expression and DNA methylation analysis showed that HCC cases clearly separated from the iCCA cases. The differential gene expression analysis revealed several targets that were significantly dysregulated in iCCA compared to HCC. ITGB8, B7-H4 and MST1R and Arg1 were identified as immune-modulatory target transcripts and further transcripts have been classified as metabolite interconversion enzyme (PC00262). Additionally, these transcripts proved to be differentially methylated between the mentioned groups.

Conclusion

Our study revealed differentially regulated immune exhaustion targets between HCC and iCCA. We assume

that the expression of the selected transcripts is further regulated by promoter methylation and results in attracting and activating immune suppressive cells. Metabolite interconversion enzymes are discussed to be essential for the activation or inactivation of anticancer drugs and could potentially affect drug treatment outcome, thereby representing potential biomarkers. Previous studies examining the function of these targets showed that they all significantly contribute to tumor progression and in some cases exert immunomodulatory effects. Further validation studies need to be conducted to assess clinical relevance.

A clinicopathologic and immunohistochemical analysis of precursor lesions of pancreatic ductal adenocarcinoma.

R. Vesce, A. Yavas, L. J. Häberle, I. Esposito

Institut für Pathologie, Universitätsklinikum Düsseldorf, Düsseldorf, Germany

Background

Pancreatic ductal adenocarcinoma (PDAC) has a dismal prognosis. The only chance for cure is complete surgical resection, which can be performed only in a subset of patients because of the fast disease progression and spreading. New solutions allowing for an early detection are needed.

Over the years, precursor lesions of PDAC have been identified. These include pancreatic intraepithelial neoplasias (PanIN) and intraductal papillary mucinous neoplasms (IPMN).

We aim to demonstrate that the immunohistochemical (IHC) analysis of these precursors could be an opportunity to develop marker panels, which could allow us to identify patterns associated with the risk of progression.

Methods

We performed an evaluation of IHC marker expression in a collective of PDAC precursors, including 39 IPMN (gastric and intestinal type) and 27 PanIN, in addition to their invasive cancers, when present (n=23). Our IHC panel consists of markers that are relevant for subtyping (MUC1, MUC2, MUC5AC, MUC6, CDX2), markers associated with biological behaviour (p16, p53, GATA6, Smad4, ki67), as well as new markers (TFF3, MUCL3), which have been identified by additional molecular studies.

Results

Positive apical MUC1 expression was associated with PDAC ($p<0.001$) and high-grade (HG) precursors ($p=0.004$).

MUC2 and CDX2 were expressed exclusively in intestinal type IPMN. TFF3 also showed a significant correlation with intestinal phenotype ($p<0.001$).

MUC5AC and MUC6 were expressed homogenously in our cohort; MUC6 was mostly associated with low-grade (LG) PanIN and LG gastric IPMN ($p<0.001$). In addition, MUC6 expression was decreased in HG precursors associated with PDAC ($p=0.01$).

P16 and GATA6 expression was significantly decreased in PDAC compared to the pre-invasive lesions ($p=0.002$; $p=0.01$). Altered expression of p53 was observed in 53% and loss of Smad4 in 43% of PDAC cases. Normal expression of p16, p53 and Smad4 was observed in 90% and normal expression of GATA6 in 68% of precursors.

Ki67 was increasingly expressed in PDAC and associated HG precursors, compared to LG precursors ($p<0.001$); in addition, a higher proliferation rate was observed in LG intestinal IPMN, compared to LG PanIN and LG gastric IPMN ($p<0.001$).

Conclusion

Precursor lesions of pancreatic cancer present distinct morphology and marker expression, possibly being associated with different biological behaviour. However, these results are preliminary; further molecular analyses are being performed to further substantiate these observations.

Resistin activating key signaling pathways in pancreatic ductal adenocarcinoma

A. Hausen¹, H. Witzel¹, S. Allmang¹, N. Marnet¹, S. Heinrich², W. Roth¹, M. M. Gaida¹

¹*Institut für Pathologie, Mainz, Germany*, ²*Klinik für Allgemein-, Viszeral- und Transplantationschirurgie, Mainz, Germany*

Background

Pancreatic ductal adenocarcinoma (PDAC) exhibits a poor prognosis and its mortality closely parallels incidence. Therefore, the asymptomatic behavior till advanced stages and early infiltration of the adjacent peripancreatic fat tissue are attributable phenomena. Visceral fat tissue is considered as highly metabolically and secretory active due to the release of cytokines, interleukins, as well as adipokines like resistin. We studied the effect of resistin on PDAC signaling.

Methods

We performed immunohistochemical stainings to detect the resistin receptors Toll-like receptor 4 (TLR4) and Adenylyl cyclase-associated protein 1 (CAP1) in non-neoplastic pancreatic tissue, low-grade and high-grade pancreatic intraepithelial neoplasia (PanIN), PDAC, as well as lymph node metastasis each in the sequence of 113 individual patients. Next, the expression of the resistin receptors CAP1 and TLR4 in PDAC cell lines (AsPC1, BxPC3, T3M4, Panc1) and the following activation of the ERK-, STAT3-, and p38-signaling pathway after incubation with recombinant resistin was examined using Western blot. The detection of downstream targets of PDAC cell lines after resistin treatment for 24 hours was performed by a proteome profiler and qPCR.

Results

The expression of resistin receptors CAP1 and TLR 4 receptors was observed in non-neoplastic pancreatic tissue, low-grade and high-grade PanIN, PDAC, and lymph node metastasis as well as PDAC cell lines. Furthermore, a time dependent activation of the ERK-, STAT3-, and p38-signaling pathway in PDAC cell lines after resistin incubation was shown. Resistin incubation influenced protein translation of further downstream proteases.

Conclusion

Thus, our data showed the influence of resistin on PDAC in the activation of signaling pathways and induction of downstream proteases.

Leptin and tumor plasticity in pancreatic ductal adenocarcinoma

A. Hausen¹, H. Witzel¹, S. Allmang¹, N. Marnet¹, S. Heinrich², W. Roth¹, M. M. Gaida¹

¹*Institut für Pathologie, Mainz, Germany*, ²*Klinik für Allgemein-, Viszeral- und Transplantationschirurgie, Mainz, Germany*

Background

Pancreatic ductal adenocarcinoma (PDAC) is a devastating disease with a five-year survival rate of less than 9 %. Among others, the early and diffuse tumor infiltration of the adjacent peripancreatic fat tissue is attributable for the poor prognosis. Indeed, visceral fat tissue is highly secretory active and releases a variety of adipokines and other substances influencing the tumor metabolism and micromilieu. This study investigates the interactions between the adipokine leptin and PDAC.

Methods

Immunohistochemistry was performed to visualize the leptin receptor in non-neoplastic pancreatic tissue, low-grade and high-grade pancreatic intraepithelial neoplasia (PanIN), PDAC, as well as lymph node metastasis each sampled as “sequence” of 113 individual patients. Furthermore, leptin receptor expression in human PDAC cell lines (AsPc1, BxPC3, T3M4) as well as the consecutive activation of the ERK-, STAT3-, and p38-signaling pathway after incubation with recombinant leptin was examined using Western blot. To analyze effects on the downstream products of PDAC cell lines after leptin exposure, we performed a proteome profiler followed for cancer-associated proteases followed by confirmation of candidates using qPCR.

Results

Leptin-receptor is expressed in non-neoplastic pancreatic tissue, low-grade PanIN, high-grade PanIN, PDAC, lymph node metastasis, as well as PDAC cell lines. Additionally, a time dependent activation of the ERK-, STAT3-, and p38-signal pathway as well as a upregulation of metalloproteases like ADAMTS13 translation was observed.

Conclusion

Our data indicate an activation of PDAC cells with the leptin followed by induction of key signaling pathways and downstream proteases.

Proteomic Analysis of Primary PDAC and Metastasis

J. P. L. Goncalves, **C. Bollwein**, A. M. Schlitter, W. Weichert, K. Schwamborn

Technische Universität München, Institut für Pathologie, München, Germany

Background

The survival rate of patients affected with pancreatic ductal adenocarcinoma (PDAC) is lower than 10%. That is due to the inexistent symptoms during the initial stage of tumor development. At the time of diagnosis, patients often already present with distant metastasis. The development of distant metastasis is not yet fully understood, and treatment of the primary lesion is not always successful in treating the metastasis. Herein we demonstrate that proteomic analysis by mass spectrometry imaging of primary PDAC and distant metastasis provide significant information to further understand the disease development.

Methods

One mixed tissue microarray (TMAs) containing multiple sample cores from primary PDAC and distant metastasis from 13 patients was employed as sample set. From 5 of these patients, it was possible to include samples from both primary and corresponding metastasis. The samples were subjected to on-tissue tryptic digestion, followed by matrix application (alpha-cyano-4-hydroxycinnamic acid) using an automated sprayer (HTX Technologies). Samples were then analyzed utilizing a RapifleX MALDI-TOF mass spectrometer (Bruker Daltonics). Subsequently, the matrix was removed, sections were stained by hematoxylin and eosin and scanned using the Aperio slide scanner for histopathological annotation. Data analysis was performed by using the SCiLS Lab (Bruker Daltonics) and statistical analysis was performed on R. Further samples pairs of primary PDAC and distant metastasis were used as an external validation dataset.

Results

The built classification models presented very high accuracy in differentiating between primary and metastasis. Random forest and support vector machine both presented accuracies over 93% and sensitivities over 95%, while linear discriminant analysis yielded 90% accuracy and 98% sensitivity. When employing the built classification methods on an external dataset with samples of primary PDAC and corresponding distant metastasis of five different patients, we confirmed that the developed method is applicable to further sample sets, with very satisfactory outcomes. As per feature analysis, we have also observed that collagens seem to play a pivotal role in the development of distant metastasis.

Conclusion

In this pilot study, we have shown that mass spectrometry imaging can be employed to further understand the meanders of PDAC distant metastasis development.

CPA1 and CELA3B are highly specific markers for the diagnosis of pancreatic acinar cell carcinoma

M. Lennartz¹, S. Weidemann¹, N. Gorbokon¹, A. Menz¹, F. Büscheck¹, A. M. Luebke¹, A. Hinsch¹, V. Reischwich¹, D. Höflmayer¹, C. Fraune¹, K. Möller¹, C. Bernreuther¹, P. Lebok^{1,2}, G. Sauter¹, W. Wilczak¹, S. Minner¹, S. Steurer¹, E. Burandt¹, D. Dum¹, R. Simon¹, T. Krech^{1,2}, T. S. Clauditz¹, F. Jacobsen¹, R. Uhlig¹

¹UKE, Institut für Pathologie, Hamburg, Germany, ²Klinikum Osnabrück, Institut für Pathologie, Osnabrück, Germany

Background

Acinar cell carcinoma accounts for about 1% of all pancreatic neoplasms. Because of the intermediate prognosis of these tumors - between the unfavorable prognosis of ductal adenocarcinoma and the good prognosis of neuroendocrine neoplasia - the reliable detection of these rare tumors is important. The correct diagnosis is often difficult due to the variable morphology of acinar cell carcinomas. The immunohistochemical detection of components of the secretory granules of the pancreas therefore plays an important role in confirming the diagnosis. Relevant proteins include carboxypeptidase A1 (CPA1, an acinar cell zinc metalloproteinase), chymotrypsin-like elastase family member 3B (CELA3B or elastase-3B, a pancreatic enzyme), and pancreatic secretory granule membrane major glycoprotein (GP2, the most common membrane protein of the zymogen granules of the pancreatic acinar cells).

Methods

Since little is known about the expression of these proteins in tumors, CPA1, CELA3B and GP2 were analyzed immunohistochemically in tissue microarrays from more than 10,000 tumors from 130 tumor types and 76 different normal tissues.

Results

In normal tissues, all 3 markers showed strong expression in pancreatic acinar cells. Additional (weaker) staining was found for CEL3B on the apical membrane of the superficial epithelium of the ileum and colon, and for GP2 in the Brunner's glands of the duodenum and focally also in the gastric antrum, gallbladder epithelium and bronchial glands. 10,036 tumors (14 acinar cell carcinomas of the pancreas, 116 other tumors) could be successfully analyzed for all 3 markers. Of 14 acinar cell carcinomas, 14 (sensitivity 100%) were positive for CPA1, 13 (92.8%) for CELA3B and 12 (85.7%) for GP2. Among 10,022 "non-acinar cell carcinomas" there was positivity for CPA1 in 0 (specificity for acinar cell carcinoma: 100%), CELA3B in 5 (one acinar cell carcinoma of the salivary gland, 2 mucoepidermoid carcinoma of the salivary gland and 2 adenocarcinoma of the colon; specificity 99.9%) and GP2 in 108 (22 tumor types; specificity 98.9%) of the tumors. 12 of the 14 acinar cell carcinomas were positive for CPA1, CELA3B and GP2.

Conclusion

In summary, the results of our study on more than 10000 tumors identify CPA1 (sensitivity and specificity 100%) and CELA3B (sensitivity 92.6%, specificity 99.9%) as very promising new markers for the difficult diagnosis of pancreatic acinar cell carcinoma.

The impact of adjuvant therapy on outcome in UICC stage I pancreatic cancer

M. Günther¹, S. Böck², V. Heinemann², J. Werner³, J. Engel^{4, 5, 6}, S. Ormanns¹

¹Medizinische Fakultät, LMU München, Pathologisches Institut, München, Germany, ²LMU Klinikum, Medizinische Klinik und Poliklinik 3, München, Germany, ³LMU Klinikum, Klinik für Allgemein-, Viszeral-, und Transplantationschirurgie, München, Germany, ⁴Medizinische Fakultät der LMU, Institut für Medizinische Informationsverarbeitung Biometrie und Epidemiologie, München, Germany, ⁵Tumorzentrum München, München, Germany, ⁶Münchner Krebsregister, München, Germany

Background

Adjuvant chemotherapy has become standard of care for pancreatic ductal adenocarcinoma (PDAC) as it improves patient outcome. However, its clinical meaning in early-stage, UICC I tumors remains uncertain.

Methods

We examined the effect of adjuvant therapy on disease-free survival (DFS) and overall survival (OS) of UICC stage I PDAC patients treated at an academic tertiary care center between 2000 and 2016.

Results

Among 124 patients (69 male, 55 female; median age 68 years, range 41 – 84 years) with UICC stage I disease, adjuvant therapy improved both DFS (19.8 vs 12.8 months, HR 0.59, 95%CI 0.37 - 0.94, P=.03) and OS (40.9 vs 20.3 months, HR 0.54, 95%CI 0.35 - 0.84, P=.005). Multivariate analyses and propensity score matching confirmed the prognostic impact of adjuvant therapy independent of localization, differentiation and R-status.

Conclusion

Every patient with UICC I PDAC should receive adjuvant chemotherapy as it may improve outcome significantly. Our findings support the concept of PDAC as systemic disease from early stages on.

Left hepatic lobe within an epigastric hernia

C.-J. Schiffner, R. S. Croner, **F. Meyer**

University Hospital, Dept. of General, Abdominal, Vascular and Transplant Surgery, Magdeburg, Germany

Background

Aim: An extraordinary hernia finding (left liver & intestine within the hernia sac) is illustrated as teaching case example in the category "IMAGE & CASE".

Methods

Scientific "Case report"

Results

Case presentation: *Medical history (hx) - current:* Enlarging soft bulging of the upper abdomen with no local pain (*own:* recurrent blood on stool & abdominal pain; colonoscopy w/ biopsy revealed carcinoma [Ca] of the descending colon w/ following left hemicolectomy [histopathological investigation: pT3b pN0 [0/22] L0 V0 cM0]). After 2 re-laparotomies within 2 days because of an anastomotic insufficiency, transversostoma was created, which was never excised for re-establishing the GI Passage since the patient did not agree; in addition, previous alcohol abuse).

Clinical finding: Male patient of middle age with previous median laparotomy cut (after surgical intervention for colon Ca) with a palpable epigastric fascia gap of appr. 12x20 cm (width x length), no tenderness on palpation, slight indolent resistance - hepatic margin within the hernia sac w/ no hint for incarceration (*Diagnosis*).

Diagnostics: - In 2020, follow-up CT scan revealed hepatic tumor lesions (secondary finding: incisional hernia w/ left lobe & intestine within the hernia sac).

- CT-guided puncture of the hepatic tumor (Tu) lesions showed metastases of the moderately differentiated adeno-CA of the colon.

- Molecular genetics revealed KRAS-mutation, NRAS-wild type, MMRp status.

Therapy: Radiation & one cycle of FOLFOX-based chemotherapy regimen were initiated resulting in increasing size of Tu lesions. Subsequently, therapy was aborted due to a liver abscess. In 9/2020, "atypical right hemihepatectomy" (resection of the segments V-VII & one third of VIII) incl. Vicryl mesh implantation ("onlay" position) for laparotomy closure was performed.

Outcome/follow-up investigation: The patient has been Tu-free since X/2020 - due to his medical hx, the patient resigned stoma excision & sufficient hernia repair with a mesh.

Conclusion

The liver can be considered an unusual hernia content of an incisional hernia in the spectrum of rare hernia findings (e.g., Tu lesions of peritoneal carcinomatosis within an inguinal hernia sac etc.) or association with accompanying findings (e.g., incisional hernia & rectus diastasis etc.). The hernia was not adequately sutured

as part of partial liver resection w/ a partially resorbable mesh in “sublay” position for prevention of further possible complications taking into account the patient’s medical hx.

Unusual inflammation as appendicitis epiploicae in immunosuppressants after liver transplantation

I. Trautwein¹, M. Petersen¹, C. March², R. S. Croner³, **F. Meyer³**

¹Universitätsklinikum Magdeburg A.ö.R., Klinik für Allgemein-, Viszeral-, Gefäß- und Transplantationschirurgie, Magdeburg, Germany, ²University Hospital, Dept. of Radiology and Nuclear Medicine, Magdeburg, Germany, ³University Hospital, Dept. of General, Abdominal, Vascular and Transplant Surgery, Magdeburg, Germany

Background

Inflammatory reactions caused by immunosuppression appear a particular interesting disease due to its very specific etiopathogenesis.

Methods

Scientific case report

Results

Case: Medical history (hx) - current: A 68-years old male patient underwent abdominal CT scan because of pain in the left lower abdomen w/ the suspicious diagnosis of diverticulitis leading to initiation of antibiotics by 24 hours prior to the transferral (for previous liver transplantation: LTx) (- own: **1**) Medication - Januva 1x100 mg, Pantozol 1x40 mg, Salofalk 500 mg 3x2, Movicol 1 bag or if needed, Cellcept® [Mycophenolate mofetil] 2x500 mg, Prograf® [Tacrolimus] 2x1 mg, Delix 1x2.5 mg; **2**) Additional diagnoses: Art. hypertonus, diab. mellitus, diverticle of the urinary bladder; **3**) Previous surgical interventions: Orthotopic LTx because of hepatocellular carcinoma [HCC] due to alcohol-induced liver cirrhosis [2013], resection of the liver segments IV/V because of HCC [2011], herniated intervertebral disc [2018]).

Clinical finding: - In general: Patient in good physical condition & normosome nutritional status, cardiopulmonarily compensated & orientated.

- Abdomen: Soft abdominal wall, distinct pressure pain in the left lower abdomen, no muscular defense, no peritonismus.

Diagnostics: - Labs: CrP 38,0 mg/L; white blood cell count within normal range

- CT scan: Diverticulosis; appendicitis epiploica in the left lower abdomen w/ oval fat-isodense structure near the sigmoid colon w/ surrounding inflammatory imbibition & pronounced intestinal wall / differential diagnosis: Diverticulitis of the sigmoid colon.

Diagnosis: 1st episode of an uncomplicated diverticulitis of the sigmoid colon

Decision-making: Conservative therapy

Therapy: Initially, n.p.o., following initiation of oral nutrition, initiation of a calculated antibiotic therapy with Cefuroxim/Clont, infusion therapy, analgetics

Clinical course: Improvement of clinical finding & lab parameters, oral nutrition & discharge w/ no pathological finding on the 7th day.

Further measures: Clinical & lab parameter controls by the family practitioner, nutrition counseling &

colonoscopy within 3 months.

Conclusion

In the described case, there was one of the 105 & 99 side effects of the immunosuppressive medication Mycophenolate mofetil & Tacrolimus listed as “colonic inflammation” & “gastrointestinal inflammation”, respectively, or an inflammatory response of a susceptible (gastro-)intestinal mucosa or the whole intestinal wall caused by LTx-associated immunosuppr. medication.

P02 Postersitzung Uropathologie

P02.01

Response to adjuvant chemotherapy of luminal and basal phenotypes and molecular subtyping of “double-negative” muscle-invasive bladder cancer

F. Koll¹, A. Schwarz², J. Köllermann², S. Banek¹, L. Kluth¹, C. Wittler¹, K. Bankov², C. Döring², N. Becker², F. Chun¹, P. Wild², H. Reis²

¹Universitätsklinikum Frankfurt, Klinik für Urologie, Frankfurt, Germany, ²Universitätsklinikum Frankfurt, Dr. Senckenbergisches Institut für Pathologie, Frankfurt, Germany

Background

Molecular subtypes of muscle-invasive bladder cancer (MIBC) have been proposed to be predictive of response to neoadjuvant chemotherapy. However, data to provide guidance to select patients for adjuvant chemotherapy based on molecular subtypes is sparse. In this study we use CK5/6 and GATA3 protein expression to surrogate “luminal” and “basal” molecular subtypes and investigate the impact on survival after adjuvant chemotherapy. For “double-negative” patients (without expression of CK5/6 or GATA3) we used transcriptomic data to call molecular subtypes.

Methods

We analyzed 181 MIBC samples with immunohistochemistry (IHC) for expression of CK5/6 and GATA3 and performed uni- and multivariant survival analysis for 110 patients undergoing radical cystectomy. CK5/6 and GATA3 (double) negative cases were further analyzed for mRNA expression profiles using the HTG transcriptome panel with 19398 mRNA targets. Gene expression data was used to assign molecular consensus subtypes.

Results

Micropapillary histological subtype was associated with GATA3 expression (100%) and squamous histological subtype with expression of CK5/6. Besides pathological tumor and lymph node stage, the absence of CK5/6 and GATA3 expression (double-negative) was associated with increased risk of death (HR 4.96; 95%CI 1.6-15.6, p=0.006). Molecular subtyping according to the consensus classification revealed NE-like (30%), stroma-rich (30%) and Ba/Sq (40%) subtypes of double negative cases. In the multivariate Cox-regression analysis, administration of adjuvant chemotherapy was associated with significant survival benefit (HR 0.15 95%CI 0.1-0.3, p<0.001).

Conclusion

Immunohistochemical markers used in pathological routine might facilitate identification of basal and luminal phenotypes and histological subtypes strongly correlate with IHC-markers. However, a two-sided IHC-based surrogate-marker system might not sufficiently reflect the (molecular) heterogeneity of MIBC. That is exemplarily demonstrated by our data in cases without IHC-expression for CK5/6 and GATA3 displaying heterogenous molecular and morphological subtypes. The molecular subtypes of MIBC themselves require validation to guide treatment decisions to advance individualized therapy decision.

Proteomic analysis of non-muscle invasive and muscle invasive bladder cancer highlights distinct subgroups

T.-L. J. Dinh^{1, 2, 3}, M. Cosenza-Contreras^{1, 2, 3}, A. Huynh¹, N. Pinter¹, K. Kurowski¹, I. Glavynskiy¹, L. Braun¹, G. Espadas^{4, 5}, E. Brombacher^{2, 6, 7, 8}, F. Hause¹, T. Werner^{1, 8}, C. Kreutz^{6, 7}, M. Werner¹, E. Sabido^{4, 5}, P. Bronsert^{1, 9}, M. Grabbert¹⁰, C. Schell¹, O. Schilling^{1, 9}

¹University of Freiburg, Institute for Surgical Pathology, Faculty of Medicine,, Freiburg i. Br., Germany,

²University of Freiburg, Faculty of Biology, Freiburg i. Br., Germany, ³University of Freiburg, MelnBio Graduate School, Freiburg i. Br., Germany, ⁴Center for Genomic Regulation, Proteomics Unit, Barcelona, Spain, ⁵Universitat Pompeu Fabra, Barcelona, Spain, ⁶University of Freiburg, Institute of Medical Biometry and Statistics, Freiburg i. Br., Germany, ⁷Centre for Integrative Biological Signalling Studies, Freiburg i. Br., Germany, ⁸University of Freiburg, Spemann Graduate School of Biology and Medicine, Freiburg i. Br., Germany, ⁹German Cancer Consortium and German Cancer Research Center, Heidelberg, Denmark, ¹⁰Medical Center, University of Freiburg, Department of Urology, Freiburg i. Br., Germany

Background

Urothelial bladder cancer ranks among the top ten malignancies worldwide with approximately 20% of cases presenting as a muscle-invasive entity with worse prognosis. We investigated the proteome biology of non-muscle invasive and muscle invasive bladder cancer (NMIBC / MIBC) with a cohort comprising 17 NMIBC and 51 MIBC cases.

Methods

Protein was extracted from formalin-fixed, paraffin embedded (FFPE) samples after macrodissection and analyzed by data-independent acquisition (DIA), yielding an average proteome coverage of >6000 quantified proteins per sample.

Results

Comparison of MIBC vs. NMIBC highlighted an enriched proteome signature of extracellular matrix (ECM) and immune response components in MIBC together with depletion of lipid metabolism components. Moreover, semi-tryptic data analysis suggests elevated levels of proteolytically truncated proteins in MIBC, indicative of increased endogenous proteolytic processing.

Unsupervised clustering of the MIBC proteomes produced three distinct clusters with signatures of metabolism, immune-functionality, and ECM. We could see resemblance of these clusters to mRNA subtypes identified by Robertson et al. in 2017, namely luminal-papillary, basal-squamous, and luminal-infiltrated. The metabolic subgroup shows an enrichment of proteins associated with immune exclusion and non-muscle invasive properties, such as PPARGgamma, FOXA1 and GATA3. In line with this observation, the metabolic cluster has a rather immune excluded phenotype and clusters close to NMIBC in principal component analysis, indicative of proteomic similarities. Cox regression analysis suggests a tendency for prolonged progression free survival (PFS) for the metabolic cluster, whereas a trend for shortened PFS was observable for the ECM cluster and proteins of both endoplasmic reticulum and Golgi complex.

Conclusion

Currently, we are investigating genome-proteome correlations, the function of cell surface proteases, and co-regulated proteins of tumour and stroma using patient-derived bladder cancer xenografts.

In summary, our study provides a deep insight into the proteome biology of early and advanced bladder cancer. In addition, we could identify clusters that resemble clinically relevant mRNA expression subtypes of MIBC.

Molecular subtypes associate with the immunological microenvironment in upper tract urothelial carcinomas

V. Bahlinger^{1,2}, M. Angeloni^{1,2}, P. Volland^{1,2}, I. Rosch^{1,2}, R. Stoehr^{1,2}, C. I. Geppert^{1,2}, B. Wullich^{2,3}, D. Sikic^{2,3}, S. Wach^{2,3}, H. Taubert^{2,3}, H. Heers⁴, P. L. Strissel^{1,2,5}, R. Strick^{2,5}, F. Ferrazzi^{1,2,6}, A. Hartmann^{1,2}, M. Eckstein^{1,2}

¹*Institute of Pathology, University Hospital Erlangen, Erlangen, Germany*, ²*Comprehensive Cancer Center Erlangen-EMN (CCC ER-EMN), Erlangen, Germany*, ³*Department of Urology and Pediatric Urology, University Hospital Erlangen, Erlangen, Germany*, ⁴*Department of Urology, University Hospital Gießen and Marburg, Philipps-Universität Marburg, Marburg, Germany*, ⁵*Laboratory for Molecular Medicine, Department of Gynecology and Obstetrics, University Hospital Erlangen-Nürnberg, Erlangen, Germany*, ⁶*Department of Nephropathology, Institute of Pathology, University Hospital Erlangen-Nürnberg, Erlangen, Germany*

Background

Molecular classification systems in bladder tumors are widely known. It is not clear yet to which extent similar classification approaches (i.e. immune phenotypes, molecular protein subtypes) are transferable to the rarer urothelial carcinoma arising from the upper urinary tract (UTUC). Additionally, compared to bladder tumors, the impact of tumor immunological microenvironment (TIME) is not well understood. To investigate these open questions, we performed immunohistochemical analysis (IHC) of molecular subtype markers and quantified spatial immune cell infiltration in UTUC.

Methods

201 UTUC were histologically reevaluated and used for analysis. A limited marker panel of three luminal (CK20, FOXA1, and GATA3) and three basal markers (CD44, CK14 and CK5) was used for subtype estimation. CD3, CD8, CD45, PD-1 and PD-L1 were automatically analyzed using QuPath. Descriptive statistical methods and uni-/multi-variable survival models were employed for the analysis. Hierarchical clustering analysis (Ward's method) was used to identify molecular subtypes.

Results

With this limited marker panel, four molecular classes could be identified for the entire UTUC cohort, namely: "luminal" (n = 66; 32.8%), "CK20-positive" (n = 53; 26.4%), "urothelial-like" (n = 42; 20.9%) and basal (n = 40; 20.0%). Basal tumors turned out to have the worst patient survival (log-rank p-value = 0.0036). When reducing the initial cohort to the pT2+ samples, the "CK20-positive" subtype was no longer present and no differences in patient survival could be observed across the different subtypes. IHC-derived molecular subtypes in UTUC significantly associate with immune classes: 50% of basal tumors expressed high levels of PD-L1 on tumor cells and present the evasion group, whereas 40.0% of uninfamed tumors were classified as luminal (p=0.0005).

Conclusion

IHC-derived molecular classification systems in UTUC seem to resemble those established for bladder tumors. "Urothelial-like" and "CK20-positive" groups are exclusive for UTUC and could highlight a different biological background of urothelial tumors as well as a combination of a heterogeneous stage cohort in

UTUC samples. Detected immunophenotypes showed the same association as in bladder tumors, with basal tumors showing more immune infiltration and luminal tumors being predominantly uninfamed. Gene expression analysis will be performed to better understand the associations detected by IHC analyses.

High NECTIN4 protein levels in urothelial high-risk non-muscle-invasive bladder cancer

S. Garczyk^{1,2}, S. Degener³, F. Bischoff^{1,2}, T. Schnitzler^{1,2}, A. Salz^{1,2}, R. Golz⁴, A. Buchner⁵, G. B. Schulz⁵, U. Schneider^{1,2}, **R. Schlößer**^{1,2}, N. T. Gaisa^{1,2}, R. Knüchel^{1,2}

¹University Hospital RWTH Aachen, Institute of Pathology, Aachen, Germany, ²Center for Integrated Oncology Aachen Bonn Cologne Duesseldorf (CIO ABCD), Aachen Bonn Cologne Duesseldorf, Germany, ³Helios University Hospital Wuppertal, Department of Urology, Wuppertal, Germany, ⁴Helios University Hospital Wuppertal, Institute of Pathology, Wuppertal, Germany, ⁵Ludwig-Maximilians-University Munich, Department of Urology, Munich, Germany

Background

Patients suffering from high-grade non-muscle-invasive bladder cancer (HG NMIBC) are at high risk (HR) of developing fatal muscle-invasive disease. Problematically, bladder-preserving treatments for these patients are limited and additional therapies are needed. NECTIN4, a type I transmembrane protein, is overexpressed by the majority of advanced urothelial carcinomas and recently, the antibody-drug conjugate (ADC) enfortumab vedotin, targeting cancer-associated NECTIN4, has been approved by the the U.S. Food and Drug Administration (FDA) for the treatment of advanced urothelial carcinoma. However, data on the expression of NECTIN4 and its therapeutic potential for HR NMIBC are limited.

Methods

NECTIN4 protein levels were systematically studied by immunohistochemistry in cohorts of carcinoma *in situ* (pTis)/pT1HG (N=182 samples), HG papillary tumors from mixed-grade lesions (mixed pTaHG) (N=87 samples) and papillary HG tumors without a history of low-grade disease (pure pTaHG/pT1HG) (N=99 samples) from overall 226 patients in comparison to protein levels in normal urothelial controls (26 samples, 22 patients). An immunohistochemical score (H-score) was applied, taking cytoplasmic and membranous NECTIN4 protein expression into account. Samples were finally classified as “negative” (H-score 0-14), “weak” (H-score 15-99), “moderate” (H-score 100-199) and “strong” (H-score 200-300).

Results

The percentage of NECTIN4 positivity across HG NMIBC subgroups was high (91%, N=368 samples), with 77% exhibiting moderate/strong expression. NECTIN4 levels differed between HG NMIBC subgroups: non-invasive parts of pTis/pT1HG and pure pTaHG/pT1HG samples showed NECTIN4 positivity in 96% and 99%, with 88% and 83% moderate/strong expressing specimens, respectively, whereas NECTIN4 levels detected in mixed pTaHG lesions were significantly lower (72% positivity, 48% with moderate/strong NECTIN4 levels). Compared to NECTIN4 protein levels in normal urothelial samples (62% positivity, 4% with moderate/strong NECTIN4 levels), NECTIN4 expression in non-invasive parts of pTis/pT1HG and of pure pTaHG/pT1HG lesions was significantly enriched (for both comparisons $P < 0.001$), but not in HG tumors from mixed-grade papillary lesions.

Conclusion

NECTIN4-directed ADCs might be a promising treatment strategy for HR NMIBC patients, especially for

those exhibiting CIS/T1HG and pure TaHG/T1HG tumors without a history of low-grade disease.

Nectin4 expression in muscle-invasive bladder cancer

D.-C. Wagner¹, S. Foersch¹, A. Freude¹, E. Juengel², M. Brandt², A. Haferkamp², W. Roth¹, S. Porubsky¹

¹*Universitätsmedizin der Johannes Gutenberg-Universität Mainz, Institut für Pathologie, Mainz, Germany,*

²*Universitätsmedizin der Johannes Gutenberg-Universität Mainz, Klinik und Poliklinik für Urologie und Kinderurologie, Mainz, Germany*

Background

The cell adhesion molecule nectin4 is expressed during embryonal development, widely downregulated in adult cells, but reexpressed in several tumors including muscle-invasive bladder cancer (MIBC). The antibody-drug conjugate enfortumab vedotin specifically binds and clears nectin4-expressing cells and is hence a promising approach for patients with MIBC that progressed on prior lines of therapy. Nectin4 is also an immune checkpoint ligand that binds the inhibitory T cell receptor TIGIT and contributes to immune cell exhaustion. The aim of this study was to investigate the relationship between nectin4, PD-L1 and TIGIT expression in MIBC as well as its prognostic value and potential to predict response to PD-1/PD-L1 antibodies.

Methods

Immunohistochemical staining for nectin4, PD-L1, CD8 and TIGIT was performed in tissue microarrays containing 328 cases of MIBC resected in the Department of Urology, University Hospital Mainz between 1995 and 2013. H-scores for nectin4 and PD-L1, as well as densities of CD8+ and TIGIT+ cells were automatically determined using the software platform QuPath. Optimal cut-off values were evaluated using maximally selected rank statistics. The aforementioned work flow was repeated in a second cohort of 22 patients that have been treated with PD-1/PD-L1 antibodies.

Results

Nectin4 expression was present in 87.5% of patients and did not correlate with PD-L1 expression or densities of CD8+ or TIGIT+ cells ($r=-0.14$, -0.04 and 0.04). A total of 53% of patients were double positive for nectin4 and PD-L1, whereas 40% and 7% were only positive for nectin4 and PD-L1, respectively. Nectin4 and PD-L1 positivity, as well as a high density of CD8+ and TIGIT+ cells were associated with significantly better overall survival (OS). Multivariate analysis identified nectin4 positivity (hazard ratio (HR) 0.6; $p=0.01$) and high TIGIT+ cell density (HR 0.68; $p=0.025$) as positive prognostic factors for OS. Nectin4 expression was equally distributed among responders and non-responders to PD-1/PD-L1 antibodies, however, OS after therapy was significantly improved in patients with nectin4 positive tumors (median OS not reached vs. 1.0 year; HR 0.056; $p<0.01$).

Conclusion

In MIBC, nectin4 (i) is an independent prognostic marker, (ii) seems to be expressed independent of adaptive anti-tumor immunity and (iii) predicts improved survival following established immune checkpoint

therapy.

Expression of the enfortumab vedotin target Nectin-4 strongly decreases during metastatic progression of urothelial carcinoma.

N. Klümper^{1, 2, 3}, D. Ralser⁴, L. Landgraf^{5, 6}, P. Strissel^{2, 5, 6, 7}, R. Strick^{2, 6, 7}, C. Bolenz^{2, 8}, J. Breyer^{2, 9}, P. Erben^{2, 10}, V. Bahlinger^{2, 5, 6}, M. Ritter^{1, 2}, F. Roghmann^{2, 11}, D. Sikic^{2, 6, 12}, K. Schwamborn¹³, T. Horn¹⁴, B. Wullich^{2, 6, 12}, R. Wirtz^{2, 15}, A. Hartmann^{2, 5, 6}, M. Hölzel³, J. Gschwend¹⁴, W. Weichert^{2, 13}, F. Erlmeier^{2, 5, 6, 13}, **M. Eckstein**^{2, 5, 6}

¹Klinik für Urologie, Universitätsklinikum Bonn, Bonn, Germany, ²BRIDGE-Consortium e.V., Mannheim, Germany, ³Institut für Experimentelle Onkologie, Universitätsklinikum Bonn, Bonn, Germany, ⁴Klinik für Gynäkologie und gynäkologische Onkologie, Universitätsklinikum Bonn, Bonn, Germany, ⁵Institut für Pathologie, Universitätsklinikum Erlangen, Erlangen, Germany, ⁶Comprehensive Cancer Center EMN, Erlangen, Germany, ⁷Universitätsfrauenklinik Erlangen, Universitätsklinikum Erlangen, Erlangen, Germany, ⁸Klinik für Urologie und Kinderurologie, Universitätsklinikum Ulm, Ulm, Germany, ⁹Department für Urologie, St.-Caritas Krankenhaus Regensburg & Universität Regensburg, Regensburg, Germany, ¹⁰Klinik für Urologie, Universitätsklinikum Mannheim, Mannheim, Germany, ¹¹Klinik für Urologie, St. Marien Hospital Herne, Ruhr-Universität Bochum (RUB), Herne, Germany, ¹²Klinik für Urologie und Kinderurologie, Universitätsklinikum Erlangen, Erlangen, Germany, ¹³Institut für Pathologie, TU München, München, Germany, ¹⁴Klinik für Urologie, TU München, München, Germany, ¹⁵STRATIFYER Molecular Pathology, Köln, Germany

Background

With the recent advent of antibody-drug-conjugates (ADC), the armamentarium of effective therapeutic options for patients with metastatic urothelial carcinoma (mUC) has been expanded. Enfortumab Vedotin (EV), an ADC targeting the surface protein Nectin-4, and the Anti-Trop-2 ADC Sacituzumab Govitecan have already been approved based on promising clinical data, but there is as yet no predictive biomarker for rational patient selection. It is known that primary tumors (PRIM) and corresponding distant metastases (MET) in mUC differ greatly with respect to the expression of therapeutically relevant markers such as PD-L1. However, there are no data yet on the evolution of Nectin-4 and Trop-2 expression from matched PRIM and MET.

Methods

To address the question of whether ADC target protein expression differs during tumor evolution and metastatic spread, we examined Nectin-4 and Trop-2 protein expression on a large cohort of matched PRIM and MET from patients with mUC (N=138) using immunohistochemistry (IHC).

Results

Trop-2 was homogeneously and strongly expressed in both the PRIM and the corresponding MET (Mean H-score > 285). Only a minority of 2.2% of the samples were Trop-2 negative (neuroendocrine tumors). In contrast, Nectin-4 expression was significantly lower in PRIM (Mean H-score = 110) and 16.8% of PRIM were completely Nectin-4 negative. Of note, Nectin-4 expression significantly decreased from PRIM to MET during tumor development (Wilcoxon matched pairs $p < 0.0001$), and one out of three MET (35.0%) had no remaining Nectin-4 expression.

Conclusion

The expression of Nectin-4 decreases substantially during metastatic tumor evolution, which may influence the response to EV. It should be critically evaluated whether patients without Nectin-4 expression in MET can benefit from EV.

Somatostatin receptor (SSTR) mRNA expression reveals distinct subtypes of neuroendocrine-like bladder cancer and bears potential for radioligand therapies

S. Bertz¹, R. P. Baum^{2,3}, R. Hake⁴, S. Eidt⁴, P. Grabowski⁵, M. Eckstein¹, A. Lupp⁶, M. Pavel⁷, A. Agaimy¹, M. Buettner-Herold⁸, A. Hartmann¹, R. Wirtz⁹

¹Universitätsklinikum Erlangen, Pathologisches Institut, Erlangen, Germany, ²Curanosticum Wiesbaden-Frankfurt, Wiesbaden, Germany, ³ICPO Foundation, Ravensburg, Germany, ⁴Institut für Pathologie am St Elisabeth-Krankenhaus Köln-Hohenlind, Köln, Germany, ⁵Charité Universitätsmedizin Berlin, corporate member of Freie Universität Berlin, Humboldt-Universität zu Berlin, and Berlin Institute of Health, Institut für Hämatologie, Onkologie and Tumorummunologie, Campus Benjamin Franklin, Berlin, Germany, ⁶Universitätsklinikum Jena, Institut für Pharmakologie and Toxikologie, Jena, Germany, ⁷Universitätsklinikum Erlangen, Medizinische Klinik I, Endokrinologie, Erlangen, Germany, ⁸Universitätsklinikum Erlangen, Pathologisches Institut, Nephropathologische Abteilung, Erlangen, Germany, ⁹STRATIFYER Molecular Pathology GmbH, Köln, Germany

Background

Molecular profiling identified a new subtype of highly aggressive bladder cancer, named “neuroendocrine-like” due to its histopathological appearance with frequent small and large cell neuroendocrine differentiation. These tumors harbor p53 mutations (94%) and RB1 mutations/deletions (94%). They poorly respond to chemotherapy and immunotherapy. However, little is known about the presence of somatostatin receptor (SSTR) expression or other radioligand targets such as FAP or CXCR4, which could be used for theranostic approaches.

Methods

For this pilot study paraffin fixed pretreatment tissue of 26 patients with neuroendocrine small or large cell bladder cancer and urothelial carcinomas (UC) with neuroendocrine differentiation were analyzed. RNA from FFPE tissues was extracted with commercial kits and relative gene expression of SSTR1-3, radioligand receptors (FAP, CXCR4) and proliferation markers (MKI67, TOP2A, RACGAP1) were quantified by standardized RT-qPCR systems (STRATIFYER Molecular Pathology GmbH, Cologne). Spearman correlation, Cluster analysis, Kruskal-Wallis and MannWhitney tests were done by JMP 9.0.0 (SAS software).

Results

SSTR2 mRNA expression was found in all tumors to varying extent with approximately 25% reaching a level of neuroendocrine tumors from other sites of origin. SSTR1 mRNA was found in 50% and SSTR3 in one of the tumors. Despite relatively small cohort size SSTR2 expression tended to be negatively associated to the proliferation marker MKI67 and RACGAP1 ($r=-0.3641$, $p=0.0675$ and $r=-0.2745$, $p=0.01747$), while SSTR1 tended to be positively associated with the proliferation marker TOP2A and RACGAP1 ($r=0.3372$, $p=0.0921$ and $r=0.3778$, $p=0.0571$). Cluster analysis revealed three distinct subtypes of neuroendocrine-like bladder cancers, which either express SSTR1 and SSTR2 with increased proliferative activity or only express SSTR2 with lower proliferative activity. The third group did not express significant SSTR levels but frequently had elevated levels of the new radioligand target FAP.

Conclusion

“Neuroendocrine-like” bladder cancers variably express somatostatin receptors, which are the classical targets of radioligand therapies, particularly in well differentiated neuroendocrine tumors of other origin. They can be subclassified into SSTR1 positive, SSTR2 positive and FAP positive subtypes, which might indicate alternative treatment options for this aggressive tumor type, which cannot be effectively treated by standard chemotherapy and immunotherapy approaches.

Tumor budding in pT1 high grade urothelial carcinoma of the urinary bladder: an independent parameter to estimate the risk of progression

S. Bultmann¹, M. Lein², S. Braun¹, J. Köllermann³

¹*Institut für Pathologie, Sana Klinikum Offenbach, Offenbach, Germany*, ²*Klinik für Urologie und Kinderurologie, Sana Klinikum Offenbach, Offenbach, Germany*, ³*Dr. Senckenbergisches Institut für Pathologie, Universitätsklinikum Frankfurt, Frankfurt am Main, Germany*

Background

The pT1 high grade urothelial carcinoma of the urinary bladder shows a heterogeneous clinical course. Therefore, the therapeutic range extends from bladder-preserving concepts to radical cystectomy (so-called early cystectomy). Established histologic parameters are of limited help in making treatment decisions. Therefore, there is a clinical need for additional histological criteria for prognostic assessment, especially for estimating the risk of progression. Tumor budding (TB) is a histological prognostic factor already established in colorectal cancer [1]. First promising results have also been obtained in urothelial carcinoma [2]. The objective was to determine the value of TB for estimating the risk of progression in pT1 high grade urothelial carcinoma of the urinary bladder.

Methods

Transurethrally obtained resection material from 259 patients with initial diagnosis of pT1 high grade urothelial carcinoma was retrospectively examined microscopically. The median follow-up was 49 months (rank: 6 - 168). TB was defined as sprouting of tumor cells in the form of single cells and/or clusters (< 5 tumor cells) into the stroma. At least 10 budding foci in a tumor area at 200× magnification were considered positive findings [2]. In addition to TB, established histologic parameters (grading, angioinvasion, concomitant CIS) and additive histologic factors (substaging, infiltration extent and pattern) were collected.

Results

A positive TB finding was found in 54 cases (20.8%). In univariate analysis using the Kaplan-Meier method and log-rank test, the positive finding was associated with significantly shorter progression-free survival ($p < 0.001$; Fig. 1). Multivariate Cox regression analysis also showed an independent increased risk of progression for TB (HR 2.1; $p=0.036$).

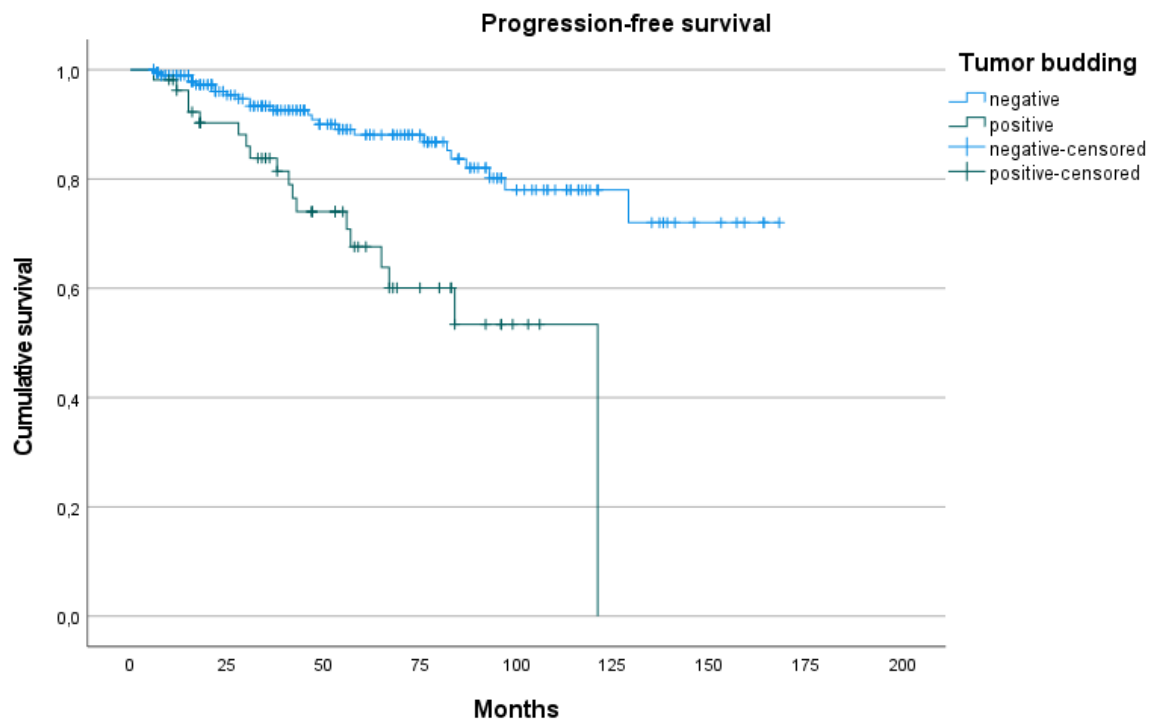


Figure 1: Kaplan-Meier curve of tumor budding in relation to progression-free survival. $p < 0.001$ (log-rank test).

Conclusion

TB is an independent risk factor for aggressive progression in pT1 high grade urothelial carcinoma. It is easily determinable independent of tissue sample orientability. Therefore, its use in routine diagnostics for risk group stratification, especially for the question of early cystectomy seems promising.

Literaturangaben

- [1] Tariq Sami Haddad et al., (2021), Improving tumor budding reporting in colorectal cancer: a Delphi consensus study, *Virchows Archiv*, 479:459–469
- [2] Keishiro Fukumoto et al., (2016), Tumor budding, a novel prognostic indicator for predicting stage progression in T1 bladder cancers, *Cancer Sci*, 107:1338–1344

MALDI mass spectrometry imaging - Prognostic pathways and metabolites for renal cell carcinomas

F. Erlmeier¹, N. Sun², J. Shen², A. Feuchtinger², A. Buck², V. Prade², T. Kunzke², P. Schraml³, H. Moch³, M. Autenrieth⁴, W. Weichert⁵, A. Hartmann¹, A. Walch²

¹Universitätsklinikum Erlangen-Nürnberg, Pathologisches Institut, Erlangen, Germany, ²Research Unit Analytical Pathology, Helmholtz Zentrum München – German Research Center for Environmental Health, München, Germany, ³Department of Pathology and Molecular Pathology, University Hospital Zurich, Zürich, Switzerland, ⁴Department of Urology, Rechts der Isar Medical Center, Technical University of Munich, München, Germany, ⁵Institute of Pathology, Technical University Munich, Munich, München, Germany

Background

Renal cell carcinoma (RCC) is the seventh most common cancer type and accounts for more than 80% of all renal tumors. For RCC prognostic biomarkers are still missing. High mass resolution matrix-assisted laser desorption/ionization (MALDI) mass spectrometry imaging (MSI) is a suitable method for biomarker detection for several tumor entities. In summary, we analyzed a large, multicenter cohort including the three most common RCC subtypes (clear cell RCC (ccRCC), papillary RCC (pRCC) and chromophobe RCC (chRCC)) by MALDI for prognostic biomarker detection.

Methods

We performed MALDI-fourier-transform ion cyclotron resonance (FT-ICR)-MSI analysis for renal carcinoma tissue sections from 782 patients. Therefore, SPACiAL pipeline was integrated for automated co-registration of histological and molecular features. Kaplan-Meier analyses with overall survival as endpoint were executed to determine the metabolic features associated with clinical outcome.

Results

Specific nucleotides, such as guanosine monophosphate or cyclic GMP, and ribose phosphate indicated strong impacts on patient outcomes in RCC in common. Kaplan – Meier significant metabolites specific for subtype ccRCC consisted of nucleotides, glutathione disulfide and a lysophospholipid. For chRCC subtype specific Kaplan – Meier significant metabolites included nucleotide and derivatives, oxidative phosphorylation, acrylaminosugars, pentose phosphates, lipids and fatty acids. Additionally, Kaplan – Meier significant metabolites specific for subtype pRCC comprised glucosamine as aminosugar and 2-sulfinoalanine from cysteine and methionine metabolism.

Conclusion

In summary, several pathways and metabolites with prognostic power for RCC in general and also for different RCC subtypes were detected. For RCC in general the cyclic Guanosinmonophosphate (cGMP) pathway could be a powerful prognostic relevant pathway. The Glutathion pathway was enriched in clear cell

RCC. For pRCC the cysteine pathway was specific. Beside this, the chRCC shows an enrichment of the uridinmonophosphat pathway. In conclusion, MALDI is a high potential technique for biomarker detection in several tumor entities.

The role of CD103+ tissue resident T-lymphocytes in ccRCC and distant metastases

C. Sanders¹, A. S. M. Hamad¹, S. Ng², R. Hosni¹, J. Ellinger³, N. Klümper³, M. Ritter³, C. Stephan⁴, K. Jung⁴, G. Kristiansen¹, S. Hauser³, M. Toma¹

¹*Institut für Pathologie, Universitätsklinikum Bonn, Bonn, Germany*, ²*Institut für experimentelle Onkologie, Universitätsklinikum Bonn, Bonn, Germany*, ³*Institut für Urologie, Universitätsklinikum Bonn, Bonn, Germany*, ⁴*Institut für Urologie, Charité Berlin, Berlin, Germany*

Background

Klarzellige Nierenzellkarzinome (ccRCC) sind immunogene Tumoren, was sich in deren Therapieansprechen auf Immuncheckpoint-Inhibitoren widerspiegelt. Über den Einfluss des Immunzellinfiltrates auf die Prognose klarzelliger Nierenzellkarzinome gibt es widersprüchliche Angaben. Die Datenlage zur Zusammensetzung der Immunzellinfiltration in Fernmetastasen und ihren Einfluss auf die Prognose ist dürrtig. Ziel dieser Studie war die Charakterisierung des Immunzellinfiltrates in ccRCC und Fernmetastasen in Zusammenschau mit klinisch-pathologischen Parametern.

Methods

Die Infiltrationsdichte von CD3-, CD4-, CD8-, CD20- und CD103-positiven Lymphozyten wurde immunhistologisch bestimmt und in 25 Primärtumoren, deren gepaarten Metastasen (n=25) und 25 nicht-metastasierten ccRCC quantifiziert. Die Validierungskohorte für CD8+ und CD103+ Lymphozyten bestand aus 241 weiteren ccRCC. Die mRNA-Expression von CD103/ITGAE wurde im TCGA-KIRC-Datensatz untersucht und mit klinisch-pathologischen Daten korreliert.

Results

Tumoren mit dichtem Immunzellinfiltrat zeigten signifikant häufiger Fernmetastasen ($p < 0,05$). Schlechter differenzierte Tumoren wiesen eine höhere Infiltrationsdichte von CD103+ Lymphozyten als gut differenzierte Tumoren auf. Eine hohe Infiltrationsdichte von CD103+ und CD103+/CD8+ Zellen in Primärtumoren war mit einem kürzeren Gesamtüberleben assoziiert, sowohl in der immunhistochemisch ausgewerteten Kohorte als auch in der TCGA-Kohorte. Im Gegensatz zu anderen Immunzellen war die Infiltrationsdichte in Fernmetastasen verglichen mit dem Primarius signifikant erhöht. Die Lungenmetastasen wiesen eine Akkumulation von CD103+ Lymphozyten im Vergleich zu den Metastasen anderen Lokalisationen auf.

Conclusion

Unsere Ergebnisse weisen auf die besondere Rolle CD103+ positiver Immunzellen in der Tumorumgebung von primären ccRCC und ihrer Fernmetastasen hin.

Targeting CDK7 - Characterization of the CDK7-MED1 Signaling Axis in Prostate Cancer Tissue

F.-O. Paulsen^{1,2}, **K. Duan**¹, F. Becker¹, D. Roth¹, V. Jörg^{1,3}, E. Dreyer¹, A. Offermann¹, S. Perner^{1,2,4}

¹Luebeck University Hospital Schleswig-Holstein, Institute of Pathology, Lübeck, Germany, ²University Medical Center Hamburg-Eppendorf, Department of Oncology, Hematology and Bone Marrow Transplantation with Division of Pneumology, Hamburg, Germany, ³University Medical Center Hamburg-Eppendorf, Department of Medicine, Hamburg, Germany, ⁴Research Center Borstel - Leibniz Lung Center, Pathology, Borstel, Germany

Background

Recently, Cyclin-dependent kinase (CDK) 7 was shown to phosphorylate Mediator-complex subunit 1 (MED1) in prostate cancer, resulting in its activation and orchestrated AR activity. Hyperactive AR-signaling contributes to the development of castration resistant prostate cancer (CRPC) and therapeutic options to successfully inhibit the AR-axis are scarce. Several CDK7 inhibitors are being tested as therapeutical options in Phase I/II trials for solid cancers, including advanced PCa. Aim of this study was to characterize the expression of CDK7 in human PCa tissues and its relationship to phosphorylated MED1, and to further its implication on PCa aggressiveness in human tissue, to potentially deploy clinical testing of CDK7 inhibitors in advanced PCa.

Methods

Immunohistochemistry was performed on 595 PCa tissue samples including 394 primary tumor foci obtained by radical prostatectomy, 64 locally advanced or recurrent tumor foci from 38 patients obtained by transurethral resection of the prostate (pTUR), 65 lymph node metastases (LNM) from 57 patients, 35 distant metastases (DM) from 32 patients and 36 benign prostatic samples. Expression data of CDK7 and pMED1 were correlated with clinic-pathological data including biochemical disease-free survival (DFS) and expression of AR and ERG-status.

Results

CDK7 is expressed in the majority of PCa tissues and expression levels are significantly higher in tissues of LNM, pTUR and DM compared to primary tumors. CDK7 and pMED1 expression show strong correlation ($r = 0.6936$, $p < 0.0001$). High expression of CDK7 associates with shorter disease-free survival (5-year DFS 63.0% vs. 85.0%). High CDK7 and pMED1 levels correlate with nuclear AR expression in tumor tissues. CDK7 positive tumors harbor higher Ki67 expression-indices and show more frequently positive ERG status.

Conclusion

In conclusion, CDK7 is frequently expressed in human PCa, correlates with an aggressive phenotype, and predicts disease recurrence after radical prostatectomy. CDK7-mediated phosphorylation of MED1 is a

potential mechanism leading to hyperactivation of AR-signaling. Therapeutical inhibition of CDK7 might be a potential approach to overcome resistance to androgen deprivation therapy in PCa and clinical testing should be deployed.

PSMA as prognostic biomarker – results of internal prostate needle biopsies

A. Weingart¹, D. Kang¹, M. C. Roesch², A. S. Merseburger², V.-W. Sailer¹, A. Offermann¹, S. Perner^{1,3}

¹*University Hospital Schleswig-Holstein, Campus Luebeck, Institute of Pathology, Luebeck, Germany,*

²*University Hospital Schleswig-Holstein, Campus Luebeck, Department of Urology, Luebeck, Germany,*

³*Leibniz Lung Center, Research Center Borstel, Borstel, Germany*

Background

Prostate cancer (PCa) is the most common cancer in men and characterized by heterogeneous courses of disease. To address the challenge of risk stratification of PCa patients reliable biomarkers are urgently needed. The prostate-specific membrane antigen (PSMA) has recently developed as an independent prognostic biomarker by our group and others. Aim of the study was to retrospectively assess the correlation between PSMA and pathological parameters of patients diagnosed with PCa in our university hospital from 2018-2021.

Methods

In this study, we evaluated the IHC staining intensity of PSMA on 211 prostate punch biopsies. This intensity score was subsequently correlated with established prognostic histopathological biomarkers performing Pearson's Chi-squared or Fisher's exact test.

Results

We found strong correlations between the PSMA expression and the Gleason Grade Group as well as the maximum tumor infiltration level. The correlation of PSMA expression with the two most reliable prognostic markers for PCa in the absence of correlations with five further markers indicates that PSMA might be an independent marker for prognosis of PCa.

Conclusion

This study confirms that PSMA expression is a promising parameter for risk stratification with the potential to improve therapeutic management of PCa patients. Additional studies including clinical data are needed for further validation of PSMA as novel biomarker for the stratification of patients.

Analysis of histological inflammation and atrophy in correlation with mpMRI changes in men without prostate cancer

C. López-Cotarelo¹, M. Thomas², R. Al-Monajjed², M. Boschheidgen³, T. Rau¹, G. Antoch³, P. Albers², L. Schimmöller³

¹Institut of Pathology, Heinrich Heine University and University Hospital of Duesseldorf, Düsseldorf, Germany, ²University Dusseldorf, Medical Faculty, Department of Urology, Düsseldorf, Germany, ³University Dusseldorf, Medical Faculty, Department of Diagnostic and Interventional Radiology, Düsseldorf, Germany

Background

Multiparametric magnetic resonance imaging (mpMRI) has become a significant part for detection of prostate cancer (PCA). However, the use of mpMRI to classify non-neoplastic prostatic changes is still unclear. Thus, the aim of this study was to analyze mpMRI prostatic changes in correlation to the histopathology in men without prostate cancer.

Methods

In total 72 patients, aged 53±8 years with mpMRI followed by PCA negative targeted (TB) and 12-core systematic (SB) MRI/US fusion-guided prostate biopsy between 2015 and 2021 were enrolled. Needle biopsy specimens were characterized regarding presence of histological inflammation and non-neoplastic glandular lesions. Inflammation and atrophy were quantified for every biopsy core. MpMRI findings in the peripheral zone (PZ) and index lesion (IL) were assessed regarding the grade of diffuse changes in T2W, ADC-value, and positivity of dynamic contrast enhancement (DCE). The study endpoint was the correlation between MRI characteristics and histopathological intensities of prostatitis and atrophy.

Results

The mean PSA, PI-RADS classification, volume, and PSAD of patients were 5.4 ng/ml (4.0–7.9), 3 (2–4), 43 ml (33–57), and 0.13 ng/mL² (0.10–0.19). Changes in T2W, the ADC value, and positive or negative DCE showed a significant correlation with the atrophy intensity in SB (p=0.02, p=0.003, p=0.002). Prostatitis and atrophy linearly increased with the PI-RADS classification (2 to 4). Younger (≤50y) vs. older men (>50y) had lower PSA 4.4 vs. 7.8 ml/ng (p=<0.001), prostate volume 40 vs. 59 ml (p=0.001), and PI-RADS (2-3) vs. 3 (3-4) (p=0.005). Atrophy was detected less in younger men (p=0.006). T2W changes were similar in both groups (p=0.493). ADC and DCE positivity were higher in younger men (p=0.005 and p=0.09 not significant).

Conclusion

PI-RADS correlated with atrophy and prostatitis, whereas T2W or DCE changes alone were not significantly correlated with histopathological verified prostatitis. Men above 50y showed more atrophy and was accompanied with progredient benign prostatic hyperplasia.

The SDF-1/CXCL12 polymorphism rs1801157 does not influence the risk for penile cancer development in Caucasians

R. Stöhr¹, O. Wendler², J. Giedl¹, N. Gaisa³, G. Richter⁴, V. Campean⁵, M. Burger⁶, B. Wullich⁷, S. Bertz¹, L. Tögel¹, A. Hartmann¹

¹Universitätsklinikum Erlangen, Institut für Pathologie, Erlangen, Germany, ²Universitätsklinikum Erlangen, Hals-Nasen-Ohren-Klinik – Kopf- und Halschirurgie, Erlangen, Germany, ³Uniklinik RWTH Aachen, Institut für Pathologie, Aachen, Germany, ⁴Institut für Pathologie, Hameln, Germany, ⁵Institut für Pathologie, Ansbach, Germany, ⁶Universitätsklinikum Regensburg, Lehrstuhl für Urologie am Caritas-Krankenhaus St. Josef, Regensburg, Germany, ⁷Universitätsklinikum Erlangen, Urologische und Kinderurologische Klinik, Erlangen, Germany

Background

The stromal cell derived factor 1 (SDF1 or CXCL12), which belongs to the C-X-C chemokine family, is produced in many tissues. CXCL12 and other chemokines play important roles in inflammation processes due to their pro-inflammatory characteristics, acting as chemoattractant to immune cells. The CXCL12 gene has a polymorphism at its' 3'- untranslated region (rs1801157). The variant allele seems to have important regulatory functions, being associated with higher CXCL12 plasmatic levels. The immune system plays a crucial role in the infection resolution. High-risk HPV presence may not be eliminated and persists through several years, inducing an inflammatory microenvironment leading to the development of pre-cancerous lesions. Recent case-control studies gave evidence that rs1801157 is associated with increased risk for various cancers as well as susceptibility to HPV infection and development of high-grade cervical squamous intraepithelial lesions. The aim of the presented study was the evaluation of a possible influence of rs1801157 on penile cancer risk.

Methods

DNA was isolated from archival non-cancerous and tumorous tissue of 104 penile SCC cases. Distribution of rs1801157 (g.17289G>A) of the CXCL12 gene was determined by RFLP analysis. HPV detection in the SCC tissue was done by usage of GP5+/6+ primers followed by subtype-specific PCR. For comparison rs1801157 genotype distribution data of 191 Caucasian controls taken from the 1000Genomes project were used.

Results

The distribution of rs1801157 followed the Hardy-Weinberg equilibrium in both cases and controls. HPV DNA was detected in 37% of the penile SCC cases. Overall, there was no significant difference in the distribution of rs1801157 neither between cases and controls ($p=0,814$) nor between HPV positive and negative penile SCC cases ($p=0,876$). There was also no association between rs1801157 genotypes and age of disease onset ($p=0,650$).

Conclusion

Our data argue against an influence of the CXCL12 rs1801157 SNP on risk for development of penile SCC in Caucasians. Even in combination with HPV status the SNP appears not to modify disease risk in HPV positive cases as it was reported for HPV-associated lesions in other organs.

P03 Postersitzung Knochen-, Gelenk- und Weichgewebspathologie

P03.01

Case report: IgG4-related pseudotumor with multinucleated giant cells in the axilla

A. Maccagno¹, B. Märkl¹, A. Agaimy², E. Mayr³, L. Füzesi¹

¹Universitätsklinikum Augsburg, Pathologie und Molekulare Diagnostik, Augsburg, Germany,

²Universitätsklinikum Erlangen, Pathologie, Erlangen, Germany, ³Universitätsklinikum Augsburg, Orthopädie und Unfallchirurgie, Augsburg, Germany

Background

IgG4-related pseudotumors (IgG4-RPT) are a subgroup of the IgG4-associated diseases (IgG4-RD): they are solid, more or less bounded lesions with typical lymphoplasmacytic infiltrate rich in IgG4 plasma cells, storiform fibrosis and sometimes, but not always, obliterative phlebitis. This condition was originally described as an autoimmune pancreatitis in 2001 (Hamano et al.), but in later years this condition was described virtually in any organ system, sparing the soft tissues. Many of these pathological pictures (such as Riedel's thyroiditis and retroperitoneal fibroses) were even known since many decades but have only relatively recently been recognized as variants of the spectrum of IgG4-RD.

Methods

We report the case history of a IgG4-RPT in the axilla with unusual presence of multinucleated giant cells.

Results

A 62-year-old woman presents with a sometimes slightly painful mass of a few centimeters in the axillary cavity, which has slightly increased in size over the previous months. The surgical preparation shows a yellow lesion with blurred margins and firm consistency. The histological examination revealed a tumor consisting of intense fibroblastic proliferation, numerous multinucleated giant cells, focal cholesterol crystals and many foam cell macrophages as well as dense lymphoid infiltrates with CD3-positive T-lymphocytes but most of all many CD20-positive cells in follicular structures without evidence of foreign material. A low proliferative index was observed with KI-67. Stainings for cytokeratins, MDM2, langerin and beta-catenin showed no reactivity. Surprisingly, the lesion showed numerous IgG- and IgG4-positive plasma cells as well as an IgG4-IgG-ratio of more than 0.4, thus fulfilling the criteria for the diagnosis of an IgG4-associated pseudotumor.

Conclusion

This is, to our knowledge, the first description of a case of an IgG4-related pseudotumor diagnosed in soft tissue (in this case axillary adipose tissue). Multinucleated giant cells have already been described in IgG4-

RPT, although very rarely. Their presence associated with fibroblastic proliferation and lymphoplasmacytic infiltration should always lead to the assumption of IgG4-RPT in the differential diagnosis, regardless of anatomical location.

Effects of sensory and sympathetic neurotransmitter on histological callus maturation during osteoporotic fracture healing

T. Niedermair¹, R. H. Straub², S. Grässel³, C. Brochhausen¹

¹*Institute of Pathology, University of Regensburg, Regensburg, Germany, ²Laboratory of Experimental Rheumatology and Neuroendocrine Immunology; Department of Internal Medicine; University of Regensburg, Regensburg, Germany, ³Department of Orthopaedic Surgery, Experimental Orthopaedics, Centre for Medical Biotechnology (ZMB/Biopark 1), University of Regensburg, Regensburg, Germany*

Background

Bone, bone marrow and periosteum are innervated by sensory and sympathetic nerve fibers. By releasing neurotransmitters into the periphery, the sensory and sympathetic nervous system can modulate vascularization, bone regeneration and fracture healing. Under physiological conditions, deficiency in sensory neuropeptide Substance P (SP) and sympathetic nerve fibers impaired bone structural properties in a murine tibial fracture model using SP-deficient and sympathectomized mice.

Methods

In the present analysis, we could demonstrate an impact of sensory and sympathetic neurotransmitter on fracture healing under pathophysiological conditions. Therefore, female wildtype (WT), SP-deficient, α -calcitonin gene-related peptide (α -CGRP)-deficient and sympathectomized (SYX) mice underwent bilateral ovariectomy as a model for postmenopausal osteoporosis. After 28 days, intramedullary fixed femoral fractures were set. To analyze callus maturation, area of callus tissue types, mesenchymal, cartilaginous and bony callus, was assessed histologically up to 21 days post fracture. In addition, status of macrophages and CD4- and CD8-positive cells was analyzed. Bone resorption markers in serum were measured to allow a better assessment of the histologically obtained results.

Results

SP-deficiency increased hypertrophic cartilage area 9 days post fracture while sympathectomy delayed bony callus tissue maturation. Destruction of sympathetic nerve fibers further decreased the presence of CD4-positive cells in the callus tissue during early fracture healing and decreased the presence of CD8-positive cells 21 days post fracture. Additionally, Alkaline phosphatase level was increased in serum of SYX mice 16 days post fracture. Histological analysis of macrophage profile revealed an increased presence of M2 macrophages (Arg1-positive) in the callus tissue of α -CGRP-deficient mice during the inflammatory phase (day 5 post fracture) of murine femoral fracture healing.

Conclusion

Polarization of M2 macrophages was promoted in α -CGRP-deficient mice but callus tissue maturation was

unaffected. Loss of sensory neuropeptide SP accelerated the remodeling of hypertrophic callus tissue. Destruction of sympathetic nerve fibers affected late stage bony callus remodeling during fracture healing in SYX mice. This study shows, that the histological assessment of callus maturation is a valuable tool to analyze the impact of SP, α -CGRP and the sympathetic nervous system on fracture healing in a murine femoral fracture model.

Whole-Exome Sequencing of Chordoma including a Case with 4 Recurrences over 15 Years

S. Ullmann¹, A. Roessner¹, J. Schreier¹, D. Schanze², C. Lohmann³, M. Röpke³, D. Jechorek¹, S. Franke¹

¹Medical Faculty, Otto-von-Guericke University, Department of Pathology, Magdeburg, Germany, ²Medical Faculty, Otto-von-Guericke University, Department of Human Genetics, Magdeburg, Germany, ³Medical Faculty, Otto-von-Guericke University, Department of Orthopedics, Magdeburg, Germany

Background

Currently surgical excision is the only curative therapeutic option for chordoma patients. With R0-resection often being difficult a high recurrence rate has been described[1]. In recent years few NGS studies in primary chordomas have been published[2]. However there isn't much tumor tissue data about molecular genetic alterations in recurrences or metastases of chordomas[3]. Therefore we have analysed an unusual case with four recurrences over a time span of 15 years and compared the results with primary chordomas. Our aim was to identify genomic differences between the recurrences and the primary chordomas and describe a possible genomic evolution in the recurrences.

Methods

DNA from the 16 Chordomas was extracted from formalin- fixed, paraffin-embedded (FFPE) tissue samples. After thorough quality checking the DNA was analysed by whole- exome sequencing (WES). Inter alia the expression of brachyury p53, Ki 67, and SMARCB1 was investigated by immunohistochemical techniques.

Results

Our results were consistent with current literature of primary chordomas, showing alterations in common tumorsuppressor-genes like APC, p53, ARID and and BRCA2 as well as DNA-repair-genes such as MLH1 and MSH6. Intriguingly our study found an increase in quantity of mutations over time, most of all in chromatin regulatory genes like SET2D, KMT, KDM but also in BRCA2, BRAF and rarer genes like LYST, HYDIN and a wide variety of zinc finger genes. The number of SNVs and InDels did not show significant differences between the primary tumor and the recurrences.

Conclusion

In the primary tumors our WES study essentially revealed a pattern of molecular alterations in accordance with the data which has been published so far[3]. In the recurrence case a high number of aberrations in chromatin regulatory genes was found pointing to a possible importance of these alterations for recurrence development[4]. Overall the progress in tumor mutation burden as well as copy number variations in the 4 chordoma recurrences over 15 years were more limited compared to the genetic evolution of carcinomas with long time recurrences[5]. This could indicate different molecular genetic traits of chordoma in comparison to carcinomas.

Literaturangaben

[1] Walcott, B. P. et al, (2012), Chordoma: current concepts, management, and future directions., The

Lancet Oncology 13, e69-e76, 10.1016/S1470-2045(11)70337-0 (2012)

[2] Tarpey, P. S. et al., (2017), The driver landscape of sporadic chordoma., Nat Commun 8, 890; 10.1038/s41467-017-01026-0

[3] Seeling, C. et al., (2021), Molecular features and vulnerabilities of recurrent chordomas., CR 40, 244; 10.1186/s13046-021-02037-y

[4] Wang, L. et al., (2016), Genomic aberrations frequently alter chromatin regulatory genes in chordoma., Genes, chromosomes & cancer 55, 591–600, 10.1002/gcc.22362

[5] Xu, B. et al., (2020), Case report: 16-yr life history and genomic evolution of an ER+ HER2- breast cancer., Cold Spring Harbor molecular case studies 6, 10.1101/mcs.a005629

Pitfall of Differential Diagnostic Challenge: Keratin-positive Abdominal Gastrointestinal Stromal Tumors (GIST).

S. Miller¹, L. Füzesi¹, T. Tornóczy², K. Kovács², B. Märkl¹

¹*University Hospital of Augsburg, Department of Pathology and Molecular Diagnostics, Augsburg, Germany,*

²*Medical School and Clinical Center, University of Pécs, Department of Pathology, Pécs, Hungary*

Background

Gastrointestinal stromal tumors (GIST) are characteristically composed either of spindle cells or of epithelioid cells or show a mixed histomorphology. However, other soft tissue tumors can also reveal an epithelioid cytomorphology, e.g. epithelioid sarcomas, angiomatous tumors, fibrosarcomas or even melanomas. This leads to a differential diagnostic challenge both in small biopsy specimens and in large tumors with uncertain imaging of abdominal organ origin. Additionally, the overlapping immunohistochemistry in epithelioid tumors can result in a misleading diagnosis. The main aim of this study was to refer to some special aspects of differential diagnosis.

Methods

Case report of a 31-year-old woman, who was diagnosed with an about 20 cm sized abdominal tumor and additional peritoneal metastases, after imaging most likely to match ovarian origin. Macroscopic and histomorphological analyses as well as immunohistochemical stains and molecular analyses were conducted. The results were then compared with the current literature.

Results

The tumor biopsy revealed an epithelioid cytomorphology with a high mitotic index of 68/50HPF. First immunohistochemical analyses were neither convincing for ovarian (CK7-, EMA-, inhibin-, estrogen and progesterone receptor-) nor for melanocytic origin (HMB45-, SOX10-, S100- and melanA-) and did not match with other cell lineages (CD34-, SMA-, CD99-, CD10-). Vimentin-, panCK-, CK5- and BAP1-positivity as well as E-cadherin-negativity led to the working diagnosis of an abdominal malignant mesothelioma. Grossly, the postoperative tumor specimen showed cystic and solid areas with a lobulated surface and no contact to the small bowel. The right ovary showed superficial metastases and the left ovary was free of metastases. In additional immunohistochemical analyses, the tumor cells were positive for c-KIT and for DOG1. The diagnosis of a cytokeratin positive epithelioid GIST could be stated by the mutation of cKIT genes, in accordance with the literature.

Conclusion

In the differential diagnosis of abdominal epithelioid malignant lesions, also an epithelioid GIST should be taken into account. A possibly misleading phenomenon in epithelioid GIST is the occasional cytokeratin positivity, which has been observed in 0,5 - 3,5 % of cases. Another interesting aspect is the cKIT mutation, whereby the cytokeratin-negative epithelioid GIST is frequently PDGFRA mutated.

Soft tissue tumors and its aid technologies for diagnosis over time: immunohistochemistry and fluorescence-in-situ-hybridization.

T. Braunschweig¹, K. Schierle²

¹Institut für Pathologie - University Clinic RWTH Aachen, Aachen, Germany, ²Institut für Pathologie - SLK-Kliniken Heilbronn GmbH, Heilbronn, Germany

Background

The diagnosis and nature of tumors of soft tissue origin, sarcomas, is still challenging and subject of changes in classification and subgrouping over time until today. As in the beginning the tumor site and gross impression was most important, with Rudolf Virchow histological features, histomorphology and substance analyses took over to be the common basis of diagnosis for around 100 years. In the 60s to the 80s of the 20th century, progress in supporting technologies took place and immunohistochemistry (IHC) found its way to routine diagnostics in laboratories of pathology in the 80th as also fluorescence-in-situ-hybridization (FISH) in the 90th.

Methods

By internet search in different archives as pubmed, "Internet Archive" and "Karlsruhe Virtueller Katalog" and on specific journal pages (e.g. "Cancer Research", "Virchows Archiv"), publications could be sorted, recapitulated and merged.

Results

Soft tissue tumors are already named a subgroup by its tissue of origin and histological features by Rudolf Virchow in 1863 (13th lecture). In his lectures he shows in detail that their subgrouping (not naming it classification back that time) is based on their histomorphological characteristics and the more differentiated or specialized tissue component as e.g. a tumor consisting of connective tissue and muscle cells/tissue is more likely named a muscle tumor. Subsequently, soft tissue tumors were diagnosed by their tumor components based on histological/substantial-chemical features in the 19th and first half of 20th century. In the second half of the 20th century, ultrastructural features of soft tissue tumors were included in subgrouping of tumors by introducing electron microscopy in the 50s, in the 1960s-1970s labeled antibodies were introduced in detecting specific antigens but it lasted until the beginning of 1980s that immunohistochemistry was part of routine diagnostics. In the 1990s, molecular pathology raised as a new discipline in laboratories of pathology, even if mutations in tumors could be already recognized since the 1970s. As an elegant methodology to combine the fast detection of mutations and histology, fluorochrome-labeled DNA probes became part of the repertoire in the diagnosis of soft tissue tumors in research in the 1990s and in routine by the beginning of 2000s.

Conclusion

Still, IHC and FISH are standards in the evaluation of sarcomas while the introduction of next-generation sequencing in routine diagnostics in the 2010s was expected to and might replace these.

P04 Postersitzung Hämatopathologie

P04.01

Molecular analysis of blastic plasmacytoid dendritic cell neoplasm reveals two distinct age-dependent subgroups and a role for clonal hematopoiesis in elderly patients

T.-C. Schade¹, D. Nann¹, G. Ott², A. Rosenwald³, A. Zamo³, W. Klapper⁴, I. Oschlies⁴, H. Stein⁵, A. Feller⁶, S. Cogliatti⁷, S. Dirnhofer⁸, S. Forchhammer⁹, J. Weller¹⁰, P. Sander¹, A. Rau¹, E. Kohler¹, F. Mihalik¹, R. Braun¹, J.-P. Geppert¹¹, A. Chott¹², I. Bonzheim¹, L. Quintanilla-Martinez¹, F. Fend¹

¹Institut für Pathologie Tübingen, AG Hämatopathologie, Tübingen, Germany, ²Robert-Bosch-Krankenhaus Stuttgart, Pathologie, Stuttgart, Germany, ³Institut für Pathologie Würzburg, Würzburg, Germany, ⁴Institut für Pathologie Universitätsklinikum Schleswig-Holstein, Kiel, Germany, ⁵Pathodiagnostik Berlin MVZ GmbH, Referenzzentrum für Hämatopathologie Berlin, Berlin, Germany, ⁶Institut für Hämatopathologie Lübeck, Lübeck, Germany, ⁷Institut für Pathologie, Kantonsspital St. Gallen, St. Gallen, Switzerland, ⁸Institut für Pathologie, Universitätsklinikum Basel, Basel, Switzerland, ⁹Universitätsklinikum Tübingen, Universitäts-Hautklinik, Tübingen, Germany, ¹⁰Universitätsklinikum Tübingen, Hämatologie, Tübingen, Germany, ¹¹Institut für Pathologie und Dermatohistologie Tübingen, Tübingen, Germany, ¹²Institut für Pathologie und Mikrobiologie, Klinik Ottakring Wien, Wien, Austria

Background

Blastic plasmacytoid dendritic cell neoplasm (BPDCN) is a rare hematologic malignancy with frequent primary presentation in the skin and poor survival. The molecular pathogenesis of BPDCN remains poorly explored. Collecting archival cases from the Austrian, German and Swiss reference centers for hematopathology, we performed an in-depth analysis of the mutational profile of BPDCN and investigated a potential association with clonal hematopoiesis (CH).

Methods

Formalin-fixed and paraffin-embedded BPDCN samples were collected from hematopathology centers in Germany (Berlin, Kiel, Lübeck, Stuttgart, Munich, Tübingen, Würzburg), Switzerland (Basel, St. Gallen), and Austria (Vienna). All cases were immunohistochemically stained for CD123, CD56 and TCL1 and molecularly studied using amplicon-based NGS on FFPE samples to detect mutations and translocations common in myeloid disorders (OncoPrint Myeloid Assay, ThermoFisher).

Results

60 samples of 41 of patients (age range 7y – 84y, M:F= 1.4:1) were included. 34 extramedullary BPDCN manifestations (30 skin, 4 other sites), 16 BPDCN infiltrates in the bone marrow (BM), 8 matched tumor-free BM samples and two BM biopsies with CMML were evaluated. A total of 118 mutations were identified in 23 genes with an average of 2.9 mutations per patient. Age-related differences in mutational profile were

observed. Patients over the age of 50 years (n=34) frequently had mutations in *TET2* (76%), *SRSF2* (26%), *NRAS* (24%), *KRAS* (15%), *ASXL1* (15%), *ZRSR2* (15%) and *PTPN11* (12%). In patients younger than 50 years (n=7) *TET2*, *SRSF2*, *ASXL1* and *ZRSR2* mutations were absent. In contrast, mutations were found in *KRAS* (43%), *NRAS* (14%), *U2AF1* (14%), *IKZF1* (14%), *BCOR* (14%), *STAG2* (14%) and a *KMT2A-MLLT10* fusion. Children under 13 years of age (n=2) lacked mutations in the tested genes. All patients with *TET2* mutations carried the same mutations in the examined BM samples, irrespective of the presence or absence of BM involvement.

Conclusion

BPDCN shows a distinct age-dependent genetic profile. Mutations in *TET2* and *ASXL1* were found exclusively in patients >50y and were associated with CH, whereas younger patients showed mainly *RAS* mutations, and children lacked mutations in the examined genes altogether. This implies important age-dependent differences in molecular pathogenesis of BPDCN irrespective of the identical phenotype. The genetic profile of pediatric BPDCN will be explored further.

PTP1B Δ 6 und PTP1B Δ 2-4 – Functional analyses of the oncogenic variants of PTP1B

J. Wildfeuer, M. Zahn, P. Möller, R. Marienfeld

Universitätsklinikum Ulm, Pathologie, Ulm, Germany

Background

Overactivation of the Janus kinase (JAK)/ Signal Transducer and Activator of Transcription (STAT) signaling pathway is critical for the survival and proliferation of Hodgkin/Reed-Sternberg (HRS) cells, the malignant cells of the classical Hodgkin lymphoma (cHL). Under physiological conditions, protein-tyrosine phosphatase 1B (PTP1B) is a negative regulator of the JAK/STAT signaling pathways. By contrast, previous studies of our group showed that exon deletions in PTP1B in cHL cell lines have a positive effect on the JAK/STAT signaling pathway. Moreover, both oncogenic variants, the splice variant PTP1B Δ 6 (lack of exon 6) and the mutant PTP1B Δ 2-4 (lack of exons 2-4) augment cell proliferation and confer resistance against cytotoxic reagents. However, the molecular mechanisms underlying these positive effects displayed by both oncogenic PTP1B variants are not fully understood. Thus, we performed protein interaction studies to get an insight into these molecular mechanisms.

Methods

A determination of the interactome of the oncogenic variants PTP1B Δ 6 and PTP1B Δ 2-4 was performed with stably transfected HEK-293T cells using the SILAC method. Subsequent mass spectroscopic analysis identified potential interaction partners. The accuracy of results from potential interaction partners was further verified by co-immunoprecipitation.

For a first insight into whether the two variants PTP1B Δ 6 and PTP1B Δ 2-4 affect other signaling pathways besides the JAK/STAT pathway, a transcriptome analysis of stably transfected L428 and HEK-293T was performed.

Results

Our preliminary results revealed that PTP1B Δ 6 has three times more potential interaction partners than wildtype PTP1B. Some interacting proteins specific for PTP1B Δ 6 were identified. In contrast, PTP1B Δ 2-4 showed half the number of interaction partners compared to the wildtype. All possible interaction partners of the wildtype PTP1B were also detected in PTP1B Δ 6 and PTP1B Δ 2-4, but quantitative differences of the different protein-protein interactions have been found.

Preliminary results regarding the transcriptome are currently under evaluation.

Conclusion

Preliminary results of the common interaction partners for PTP1B Δ 6 and PTP1B Δ 2-4 are eminent. Moreover, these protein-protein interactions have to be further validated and the functional relevance of the PTP1B Δ 6 specific interaction partners has to be resolved.

SOCS1 (Silencer of Cytokine Signaling 1) expression in B-cell derived cell lines and tissue.

S. E. Weissinger¹, M. Zahn¹, **R. Marienfeld**¹, C. Tessmer², G. Moldenhauer², P. Möller¹

¹Pathologie Universitätsklinikum Ulm, Ulm, Germany, ²German Cancer Research Center (DKFZ), Antibody Unit, Genomics and Proteomics Core Facilities, Heidelberg, Germany

Background

Mutations in the *Silencer of cytokine signaling 1 (SOCS1)* gene were identified in a variety of B-cell neoplasms, like diffuse large B-cell lymphoma (DLBCL) or classical Hodgkins lymphoma (cHL) with a high frequency. Moreover, progression-free and overall survival of DLBCL and cHL are highly affected by truncating SOCS1 mutations. Currently, a reliable immunohistochemistry protocol to identify B-cell lymphoma with truncated SOCS1 proteins is lacking. Therefore, we aimed to establish a routine staining procedure using two SOCS1 antibodies, binding either the N-terminus (#4H1) or the C-terminus (#424C) of SOCS1, were used as 'test pair'.

Methods

Immunohistochemical SOCS1 staining using either an N- (#4H1) or C-terminal (#424C) directed SOCS1 antibody on tonsil tissue, B-cell derived cell lines and lymphoma tissue were performed. HEK293T cells were transfected with plasmids encoding the *SOCS1* variants *SOCS1_{fs}*; (c.349_359del11, frame shift), *SOCS1_{del}* (c.393_407del15, in frame) and *SOCS1_H* (c.431_512del82, frame shift with premature STOP codon) or *SOCS1_{WT}* and cell blocks generated. Next to immunohistochemistry total cell proteins were extracted and SOCS1 protein status was detected by immunoblot. Karpas1106, a SOCS1 deficient cell line, served as negative control. Epitope Mapping and cross-reactivity analysis was performed by PEPperPrint GmbH (Heidelberg, Germany).

Results

Epitope mapping revealed a very strong binding for #424C to a consensus motif of 8 aa, concordant to aa 195-202 of SOCS1 and a consensus motif of 6 aa for #4H1 concordant to aa 50-55 of SOCS1. While staining using #424C was highly specific, anti-SOCS1 antibody #4H1 showed various cross-reactions with other proteins resulting in a 'pancellular' immunohistochemical staining pattern in FFPE tissue. Like #424C, #4H1 identified SOCS1 wildtype and SOCS1 mutations in immunoblot experiments but also recognized an unknown protein with high intensity. Furthermore, due to a lack of the C-terminal epitope recognized by #424C *SOCS1_{fs}* and *SOCS1_H* mutants were not detected using this antibody[†].

Conclusion

The newly developed anti-SOCS1 monoclonal antibody #424C appears to be valuable method for the detection of SOCS1 in tissue samples. However, a combined staining of tissue section using #424C and #4H1 to define SOCS1 and truncating SOCS1 mutation is hampered by the non-specific binding of #4H1.

† Weissinger SE, *et al.*, 2022, doi: 10.1111/ejh.13730.

Progressive cauda syndrome with paraparesis and sensory symptoms due to extranodular high grade large B-cell lymphoma with extensive intravascular component (autopsy case report)

I. Kleinlein¹, A. Maccagno¹, K. Koch², W. Klapper², M. Naumann³, M. Christ³, B. Märkl¹, A. Bayas³

¹Pathology, Faculty of Medicine, University of Augsburg, Germany, ²Institute of Pathology, University Medical Center Schleswig-Holstein, Kiel, Germany, ³Neurology, Faculty of Medicine, University of Augsburg, Germany

Background

Lymphoma can cause various neurological manifestations that might affect any part of the nervous system. Involvement of the PNS is one of the major constituents of neurological disorders associated with lymphoma.[23884813][17577023][30111607]

Methods

We report an autopsy case of a 78-year-old male, suffering from rapidly progressive sensory symptoms and paraparesis, who died 6 weeks later because of fulminant multi-organ failure. Laboratory findings were not indicative with elevated cerebrospinal fluid (CSF) lactat and protein and only initially borderline cell count (5/μl in CSF, normal at control). Known pre-existing conditions included non-insulin dependent diabetes mellitus (NIDDM) and history of tuberculosis.

Results

Post-mortem examination revealed extranodal high grade large B-cell lymphoma with an extensive intravascular component (highly similar to intravascular large B-cell lymphoma/IVLBCL) in several organs, in particular in PNS (cauda equina and nerve roots), with thrombembolism and ischemic colitis. An additional extravascular component was present in bone marrow. Both components showed similar expression of CD20, CD19, CD5 and clonality of IgH locus, but no staining of CD23, CD34, Tdt or KIT.

Conclusion

In conclusion, progressive cauda syndrome with paraparesis and sensory symptoms has been caused by PNS infiltration. In the literature, only few similar cases have been reported, but with a mainly intravascular component.[8490846][18614371][22088211]

In view of the variable presentation with non-specific constitutional and neurological symptoms and lack of reliable ancillary tests for intravascular lymphoma affecting the nervous system, this case emphasizes the value of autopsies in clarifying the cause of death and revealing this rare differential diagnosis in a case of otherwise unexplained cauda syndrome.

Literaturangaben

- [8490846] Glass J, (1993), Intravascular lymphomatosis. A systemic disease with neurologic manifestations, Cancer, PubMed
- [17577023] Ponzoni M, (2007), Definition, diagnosis, and management of intravascular large B-cell lymphoma: proposals and perspectives from an international consensus meeting, Journal of Clinical Oncology, PubMed
- [18614371] Grove C S, (2008), Intravascular lymphoma presenting as progressive paraparesis, Journal of Clinical Neuroscience, PubMed
- [22088211] de Fino C, (2012), Intravascular large B-cell lymphoma presenting as slowly progressive paraparesis with normal MRI features , Journal of the Neurological Sciences, PubMed
- [23884813] Tomita M, (2013), Clinicopathological features of neuropathy associated with lymphoma, Brain, PubMed
- [30111607] Ponzoni M, (2018), Intravascular large B-cell lymphoma: a chameleon with multiple faces and many masks, Blood, PubMed

Molecular analysis of myeloid sarcoma reveals a mutational profile similar to AML, but with some differences and enables separation from BPDCN

T.-C. Schade¹, D. Nann¹, P. Sander¹, A. Rau¹, E. Kohler¹, R. Braun¹, F. Mihalik¹, J. Slotta-Huspenina², I. Bonzheim¹, L. Quintanilla-Martinez¹, F. Fend¹

¹*Institut für Pathologie Tübingen, AG Hämatopathologie, Tübingen, Germany*, ²*Institut für Allgemeine Pathologie und Pathologische Anatomie der Technischen Universität München, München, Germany*

Background

Myeloid sarcoma (MS) is a rare extramedullary manifestation of myeloid blasts either in the setting of AML or *de novo*. To date, little is known about the spectrum of genetic alterations and mechanisms governing extramedullary homing in MS. We performed an in-depth analysis of the mutational profile of MS and compared the results to literature data of AML to identify potential differences.

Methods

Formalin-fixed and paraffin-embedded MS samples and in part matched bone marrow trephines were collected from the archives of the institutes of pathology, University Hospital Tübingen and Technical University of Munich. All cases had been extensively phenotyped during diagnostic workup and were analyzed using amplicon-based NGS on RNA and DNA to detect mutations in 40 genes and translocations in 29 genes common in myeloid disorders (OncoPrint Myeloid Assay, ThermoFisher).

Results

46 samples of 32 of patients (age range 6y – 89y, M:F= 1.3:1) were included in the study. 34 extramedullary MS manifestations (9 skin, 14 other sites), 5 matched AML infiltrates in the bone marrow (BM), 3 matched tumor-free BM samples and 4 matched BM biopsies with MDS, MPN or CMML were evaluated. A total of 111 mutations were identified in 28 genes with an average of 3.5 mutations per patient. Overall, MS showed similar distribution of mutations compared to published data in AML, but mutational frequencies in *TET2* (38% vs. 5-25%), *NRAS* (38% vs. 15%) and *IDH1* (19% vs. 6-10%) were elevated in MS. Furthermore, we identified 5 AML-specific translocations in our cases, demonstrating the suitability of FFPE material for RNA-based analysis. Comparison with a cohort of 41 blastic plasmacytoid dendritic cell neoplasms (BPDCN, data submitted in a different abstract) revealed distinct mutational profiles, namely absence of *NPM1* mutations and AML-specific translocations in BPDCN.

Conclusion

MS shows a spectrum of genetic alterations comparable to AML, but *TET2*, *NRAS* and *IDH1* mutations

appear to be more common in extramedullary MS than in AML. The mutational spectrum is distinct from BPDCN, which may be difficult to separate from cutaneous MS. Furthermore, our study demonstrates that detection of fusions, which is crucial for risk assessment, can be performed robustly on FFPE material.

Time-dependent altered changes of neoplastic features in JAK2-mutated cells upon JAK1/JAK2 inhibition

M. Bauer¹, C. Vaxevanis², C. Massa², B. Seliger^{2,3}, C. Wickenhauser¹

¹Universitätsklinikum Halle (Saale), Institut für Pathologie, Halle (Saale), Germany, ²Universitätsklinikum Halle (Saale), Institut für Medizinische Immunologie, Halle (Saale), Germany, ³Fraunhofer Institute, Cell Therapy and Immunology, Leipzig, Germany

Background

Constitutive activation of the JAK/STAT signaling pathway due to mutations in the *JAK2* gene plays a central role in MPN initiation and progression. The selective JAK1/JAK2 inhibitor ruxolitinib has been approved for MPN treatment providing a good control of clinical symptoms despite its limited impact on the clearance of neoplastic hematopoiesis. Therefore, effects of short-term and long-term JAK/STAT inhibition and their reversibility were analyzed in *in vitro* models regarding therapy related changes of MPN cells by determination the growth rate, the expression of immune relevant and maturation markers.

Methods

The JAK2 V617-mutated HEL (sAML) and SET-2 (MPN) cell lines were treated with ruxolitinib for 1-15 weeks. CD34, CD33, HLA-I, and PD-L1 expression, cell viability and proliferation were determined at distinct time points of continuous ruxolitinib treatment by flow cytometry. The cytokine secretion was measured with LEGENDplex™ Human Inflammation Panel. RNA expression of different genes of the JAK/STAT signaling pathway was analyzed by qPCR.

Results

Short-term treatment of HEL and SET-2 cells for one week resulted in a reduced cell proliferation and secretion of IL8, TGF- β and CCL2, as well as diminished expression of immune modulatory markers and activation of JAK/STAT signaling pathway, which was completely reversible after treatment stop. In contrast, continuous treatment with ruxolitinib over 15 weeks demonstrated a time-dependent increased proliferation of both cell lines associated with a decreased number of vital cells, a continuous increase in HLA class I, PD-L1, but also of pSTAT1 and pTYK expression, as well as a reduced frequency in CD34-positive blasts. Long-term ruxolitinib treatment resulted in a stable CD34^{neg}, PD-L1^{high}, HLA-I^{high}, cytokine^{neg} phenotype of HEL cells, whereas the phenotype of SET-2 cells was partially reversible with regard to maturation und expression of immunogenicity markers.

Conclusion

Selective JAK1/JAK2 inhibition in the JAK2-mutated MPN cell line was completely reversible with regard to maturation, HLA-I and PD-L1 expression and the CD34 phenotype, while the proportion of CD33⁺ and CD33⁺CD34⁺ subpopulations changed irreversible after 15 weeks treatment of HEL cells. However, the initially suppressed JAK/STAT signaling pathway recovered after 15 weeks treatment with in particular higher pTYK2 expression levels, which might provide a rational for the design of novel (combination) therapies.

P05 Postersitzung Herz-, Gefäß-, Nieren- und Transplantationspathologie

P05.01

Monstrous pseudoaneurysm of the subclavian artery secondary to clavicle fracture

U. Barth¹, D. Granowski¹, M. Lehmann¹, S. Stephan-Falkenau², F. Meyer³

¹Helios Klinik Jerichower Land, Klinik für Allgemein-, Gefäß- und Viszeralchirurgie, Burg, Germany, ²MVZ am Helios Klinikum Emil von Behring, Berlin-Zehlendorf, Institut für Gewebediagnostik/Pathologie, Berlin, Germany, ³Klinik für Allgemein-, Viszeral-, Gefäß- & Transplantationschirurgie, Universitätsklinikum Magdeburg A.ö.R., Magdeburg, Germany

Background

The clavicular vascular nerve bundle is usually well protected by the clavicle and the first rib. Injuries of the subclavian artery with development of corresponding bleeding complications or formation of pseudoaneurysms are extremely rare and then associated with a high morbidity and mortality, which according to literature data can be 15-34 %.

Methods

Based on a representative case report of a monstrous pseudoaneurysm of the subclavian artery after a clavicle fracture, the diagnostic options and possible therapeutic approaches are discussed.

Results

A 57-year-old female patient suffered a fall trauma to the left shoulder. However, the patient did not present to a doctor. In the course, however, a pulsating tumour of the left clavicular region developed with formation of increasing congestive oedema of the left arm, venous subcutaneous bypass circulation and dermatitis of the left arm. The native X-ray of the left shoulder region and bone reconstruction of the native computed tomography (CT) scan documented extensive osteolysis, which took a longitudinal extension of about 5 to 6 cm compared to the opposite side. The corresponding CT angiography (CTA) showed the monstrous aneurysm in the area of the left shoulder, originating from the left subclavian artery and displacing the surrounding structures. This led to the decision-making: open vascular surgical excision of the pseudoaneurysm from the infraclavicular site and direct vascular suture after temporary cessation of arterial perfusion using catheter balloons at the proximal and distal pseudoaneurysm site of subclavian artery. In the postoperative follow-up, there was no neurological deficit of the left arm indicating plexus damage, regular perfusion of the left arm and reduced swelling confirming regular postoperative result.

Conclusion

A large pseudoaneurysm of the subclavian artery with osteolysis of the middle clavicle secondary to fracture is a rare clinical finding requiring interdisciplinary vascular surgery/traumatology/plastic surgery management. Due to the increasing establishment and safe handling of endovascular techniques, open surgical therapy has taken a back seat. However, open vascular surgical reconstruction also offers advantages in individual cases, especially when compression symptoms lead to vascular and nervous complications due to the sheer size of the aneurysm.

Impact of various factors and parameters onto the early postoperative and long-term outcome of vascular surgical and image-guided treatment of suture aneurysms

P. Romancik¹, **F. Meyer**², A. Hribaschek¹, U. Redlich³, Z. Halloul⁴, J. Tautenhahn¹

¹Municipal Hospital ("Klinikum Magdeburg gGmbH"), Dept. of Vascular Surgery, Magdeburg, Germany,

²University Hospital, Dept. of General, Abdominal, Vascular and Transplant Surgery, Magdeburg, Germany,

³Municipal Hospital ("Klinikum Magdeburg gGmbH"), Dept. of Diagnostic and Interventional Radiology, Magdeburg, Germany, ⁴University Hospital, Division of Vascular Surgery, Dept. of General, Abdominal, Vascular and Transplant Surgery, Magdeburg, Germany

Background

Suture aneurysms (SA) have increasingly become a relevant focus of secondary care due to the favorable long-term outcome and survival. The aim of the study was to detect the occurrence of SA in retrospective case series and based on periinterventional/-operative management experiences.

Methods

Eighty-six consecutive patients with 106 SA were documented as part of this retrospective (1.4.2010 - 1.9.2016) unicenter observational study who either had undergone image-guided or vascular surgical treatment. The cases were characterized with patient- (age, sex ratio), finding-characteristics (SA site/size), image-guided interventional/vascular surgical approach and outcome aspects (patency rate, SA recurrency, morbidity, mortality).

Results

- The majority of SA occurred after implantation of an aorto-bifemoral prosthesis (43.4 %) and at the groin (81.1 %).
- The mean time interval to SA manifestation in the groin was 55.4 months and 51.6 months to manifestation of recurrent SA ($p = 0.683$).
- Though Thromboendarterectomy (TEA) has been reported as risk factor for SA generation in the literature, there was no significant difference for the frequency of SA occurrence comparing former vascular surgical interventions with *versus* without former TEA ($p = 0.325$).
- The mean diameter of the inguinal SA was 46.4 mm and of recurrent SA at the groin 54.5 mm ($p = 0.34$). This might be a hint of in compliant patients or of an insufficient postinterventional/-operative follow-up care.
- After treatment of SA, there was no complication in 56.6 % of cases ($n = 60$). All subjects who underwent image-guided intervention showed no complication.
- In the spectrum of postoperative complications, the most frequent problems were lymphocele with no need for surgical intervention (20.8 %), hematoma with need of surgical intervention (8.5 %) and postoperative explantation of alloplastic materials (3.8 %). The 30-days mortality in all SA was 2.8 %.
- Emergency operations for SA showed a significantly higher probability of a postoperative complication ($p = 0.038$).

Conclusion

In SA treatment, image-guided techniques may become more important due to a lower complication rate and limited invasiveness. However, open reconstruction remains the standard procedure for SA at the groin (implantation of an interponate). Postoperatively, patients need to be notified on the importance of a life-long vascular surgical follow-up.

P05.03

NUP133 controls nuclear pore assembly, transcriptome composition and cytoskeleton regulation in podocytes

M. Rogg, J. I. Maier, M. Ehle, A. Sammarco, M. Werner, **C. Schell**

Institute of Surgical Pathology, Faculty of Medicine, Medical Center - University of Freiburg, Freiburg 79106, Germany

Background

Steroid-resistant nephrotic syndrome (SRNS) frequently leads to glomerular kidney disease and end stage renal disease. SRNS is caused by an increasing number of more than 50 hereditary monogenic mutations selectively affecting podocytes - epithelial cells of the glomerular filtration barrier. Recently, mutations in several components of the nuclear pore complex (NPC) including NUP133 and NUP107 have been reported to cause hereditary SRNS. However, a comprehensive understanding of underlying mechanisms leading to selective disease manifestation in podocytes remained rather elusive.

Methods

CRISPR/Cas9 mediated genome editing was employed to generate a novel *in vitro* genetic model of hereditary podocytopathy caused by *NUP133*. We comprehensively analyzed transcriptome composition, nuclear pore assembly and actin cytoskeleton function due to NUP133 loss of function or introduction of disease causing mutations.

Results

Loss of NUP133 translated into degradation of the NUP133 interactor NUP107 leading to impaired assembly of the NPC. This NPC defect resulted in marked alterations of the podocyte specific transcriptome disturbing several susceptible and essential signaling pathways. Further, detailed analysis revealed several alterations of regulators and effectors of small RhoGTPase signaling pathways. Finally, impaired cytoskeleton regulation by small RhoGTPase signaling resulted in decreased generation of cell protrusions as exemplified by defective cell spreading. Surprisingly, comparative analysis of SRNS-related *NUP133* mutations revealed only mild defects on NPC assembly.

Conclusion

Mild impairment of NPC assembly might be the primary consequence of mutant variants leading to a partial loss of function like phenotype and disease manifestation in susceptible cell types like podocytes. Mechanistically, disturbed small RhoGTPase signaling in *NUP133* mutant podocytes impairs generation of cell protrusions and thereby establishment of the complex foot process architecture of podocytes.

Alteration of glycocalyx on endothelium of peritubular capillaries in chronic kidney disease

K. Ermert¹, **B. M. Klinkhammer**¹, E. M. Buhl², J. Floege³, P. Boor^{1, 2, 3}

¹Universitätsklinikum der RWTH Aachen, Pathologie, Aachen, Germany, ²Universitätsklinikum der RWTH Aachen, Elektronenmikroskopie, Aachen, Germany, ³Universitätsklinikum der RWTH Aachen, Nephrologie, Aachen, Germany

Background

The glycocalyx is a carbohydrate-rich gel-like mesh, which covers the luminal surface of cells, including the endothelium. The glycocalyx is involved in many regulatory functions of the endothelium, including vascular permeability. In chronic kidney disease (CKD), peritubular capillaries undergo anatomical, structural and functional alterations such as rarefaction, increased tortuosity and increased permeability. Here, we hypothesized that the glycocalyx of peritubular capillaries might be affected in CKD and investigated morphological and ultrastructural pathological alterations of the glycocalyx in different murine CKD models and human kidney tissue.

Methods

We stained the glycocalyx of peritubular capillaries in kidney tissue of murine and human CKD specimen using different fluorescently labelled plant-derived lectins. Next, we established the Lanthanum Dysprosium Glycosamino Glycan adhesion (LaDy GAGa) staining technique to visualize the ultrastructure of the glycocalyx using transmission electron microscopy and to perform quantitative analyses. Finally, we analyzed the expression and regulation of glycocalyx components in primary murine endothelial cells.

Results

Fluorescence stainings using different lectins with high affinity to components of the renal glycocalyx revealed a reduced binding to the endothelium in CKD. We found a similar change in a human kidney tissue. The LaDy GAGa staining technique visualized the ultrastructure of the glycocalyx and enabled quantitative analyses. We found a significant reduction of the glycocalyx thickness and density in two different models of renal fibrosis and CKD, i.e. unilateral ureteral obstruction and ischemia-reperfusion injury. Additionally, mRNA expression of proteins involved in glycocalyx biology, synthesis and turnover, i.e., syndecan 1 and glypican 1, which are main components of the glycocalyx, and exostosin 2, involved in the synthesis of the glycocalyx, were significantly upregulated in endothelial cells isolated from murine CKD models.

Conclusion

Visualization of glycocalyx using specific ultrastructural analyses allows qualitative and quantitative analyses, revealing significant pathological alterations in the glycocalyx of peritubular capillaries in CKD.

Large-scale segmentation and feature extraction for digital nephropathology

D. L. Hölscher¹, N. Bouteldja¹, Y.-C. Lan¹, A. Sadr¹, S. von Stillfried¹, **R. D. Bülow**¹, P. Boor^{1,2}

¹Uniklinik RWTH Aachen, Institut für Pathologie, Aachen, Germany, ²Uniklinik RWTH Aachen, Medizinische Klinik II, Aachen, Germany

Background

Pathology often relies on manual scoring, which is work-intensive and remains subjective and prone to errors. Nephropathology in particular relies on semi-quantitative assessment of histology, thus constituting a perfect use case for development of precision histology tools. Deep Learning-based segmentation and quantification of whole slide images (WSI) enable extraction of interpretable morphometric data from histology, thus contributing to precision pathology. Here, we developed a framework for automated histology segmentation and quantification including a wide spectrum of non-neoplastic kidney diseases.

Methods

We trained two U-Net based Convolutional Neural Networks (CNNs) for: i) detection of kidney tissue and ii) instance segmentation of relevant histological structures, i.e. glomeruli, tubules and arteries. In total, we analysed 1103 WSI from four cohorts, including two external datasets for multi-center validation. 35 morphometric features from 51,445 glomeruli, 4,016,792 tubules and 362,471 arteries were extracted, generating 30 million morphometric data points that were associated with clinical and pathology data.

Results

Both the kidney tissue and the structure segmentation CNN showed accurate results on WSI-level despite variable injury patterns such as crescents, segmental sclerosis, tubular atrophy or arteriosclerosis. Morphometric analysis of glomeruli revealed an increase in glomerular area e.g., in membranous glomerulonephritis and all cases characterized with nephrotic range proteinuria independent of the underlying disease. The glomerular tuft circularity was decreased in pauci-immune glomerulonephritis, especially in cases with severe loss of kidney function. Cases with arterial hypertension showed an increase in arterial wall diameter compared to cases without hypertension across diseases. Principal component analysis of multiple glomerular, tubular and interstitial features identified morphological alterations of glomeruli and the tubulointerstitium that are associated with renal functional decline. Automated extraction of histological structures with large morphometric deviations compared to normal can be used for fast track assessment of severely damaged regions.

Conclusion

Segmentation and large-scale quantitative feature extraction enables reproducible quantitative analysis of

kidney histology, opening new possibilities for precision nephropathology.

All-Body-Cavity (ABC)-Scopy: A Feasibility Study for an Endoscopic Method of Minimal Invasive Autopsies

L. Rentschler¹, T. Schaller¹, K. Hirschbühl², B. Märkl¹, I. Kleinlein¹, S. Dintner¹, S. Wolf³, C. Golling³, D. Vlasenko³

¹University Hospital of Augsburg, General Pathology and Molecular Diagnostics, Augsburg, Germany,

²University Hospital of Augsburg, Hematology and Oncology, Augsburg, Germany, ³University Hospital of Augsburg, General, Visceral and Transplantation Surgery, Augsburg, Germany

Background

Autopsies are of major importance in evaluating the cause of death as well as the extent and characteristics of diseases. The decrease in autopsy numbers in many western countries during the past decades has been partially attributed to the invasiveness and disfigurement of the deceased body due to the autopsy. To address this trend, various methods of minimal or non-invasive autopsy for postmortem examination have been developed. In this study, an endoscopic approach was compared to traditional autopsies. The approach was tested for accuracy of relevant post-mortem diagnoses and the usability of the collected tissue for histologic and molecular examinations.

Methods

In this series, the All-Body-Cavity-scopy (ABC-scopy) was performed in 10 cases on patients scheduled for autopsy at the University Hospital, Augsburg. Each endoscopic autopsy involved a laparoscopic evaluation and at least a unilateral thoracoscopic evaluation of the accessible organs. This was followed by exemplary or guided excision biopsies of liver, spleen, kidney, pancreas, lung, heart, and any conspicuous findings or clinically reported abnormalities. Following the ABC-scopy, a conventional autopsy was performed and further tissue samples collected. The tissue samples gained in each method were separately histologically examined by senior pathologists. Found diagnoses were compared for relevant deviations. To test the feasibility of the gained tissue for potential molecular diagnostics, RNA and DNA were extracted from FFPE material and evaluated for integrity on a 2100 Bioanalyzer (Agilent).

Results

With a median duration of 125 minutes for a 2-person team, the ABC-scopy provided a high accuracy and thoroughness of postmortem diagnoses in the accessible organs. Out of 10 autopsies, major deviations were found in only one case. Excision biopsies were collected up to a size of 5 x 2,5 x 2,5 cm for solid parenchymatous organs (e.g. liver) and up to 9 x 6 x 3 cm for softer tissue (e.g. lung). The tissue collected during the ABC-scopy was at least of similar or often better quality than the tissue collected in conventional autopsies.

Conclusion

The ABC-scopy could be shown as a feasible approach for minimal invasive postmortem evaluation of high diagnostic value. Specifically, the larger size of the excision biopsies, which enables representative histology, differentiates this method from minimal invasive methods that use needle biopsies or diagnostic

imaging only.

Adrenal tropism of SARS-CoV-2 and adrenal findings in patients with severe fatal COVID-19: a post-mortem case series

T. Paul¹, S. Ledderose¹, B. Märkl², T. Paul¹, M. Stern³, O. Keppler³, T. Kirchner¹, A. Walch⁴, M. Rudelius¹

¹Ludwig Maximilians Universität München, Pathologie, München, Germany, ²Universität Augsburg, Pathologie, Augsburg, Germany, ³Max von Pettenkofer Institut München, Virologie, München, Germany, ⁴Helmholtz Zentrum München, Pathologie, Neuherberg, Germany

Background

Progressive respiratory failure and hyperinflammatory response is the primary cause of death in the coronavirus disease 2019 (COVID-19) pandemic. Despite mounting evidence of disruption of the hypothalamus-pituitary-adrenal axis in COVID-19, relatively little is known about the tropism of severe acute respiratory syndrome coronavirus 2 (SARS-CoV-2) to adrenal glands and associated changes.

Methods

We examined adrenal glands obtained during autopsy from 21 patients who died from COVID-19 and compared them with ten adrenal glands obtained from patients who died from influenza A (H1N1) infection. For ten COVID-19 patients an additional analysis of the hypothalami and pituitary glands was completed. The specimens were studied with multiplex immunohistochemistry and multispectral image analysis, in-situ hybridization and imaging mass spectrometry. In addition, infection experiments with adrenal cortical carcinoma cell lines with SARS-CoV-2 were performed

Results

Here we demonstrate adrenal viral tropism and replication in COVID-19 patients. Adrenal glands showed inflammation accompanied by inflammatory cell death. Histopathologic analysis revealed widespread microthrombosis and severe adrenal injury. Adrenal cortical carcinoma cell lines showed productive viral replication. In addition, activation of the glycerophospholipid metabolism and reduction of cortisone intensities were characteristic for COVID-19 specimens.

Conclusion

In our autopsy series adrenal viral tropism of SARS-CoV-2 associated with adrenal inflammation accompanied by inflammatory cell death suggests that SARS-CoV-2 facilitates the induction of adrenitis as a direct consequence of productive viral infection. Given the central role of adrenal glands in immunoregulation and taking into account the significant adrenal injury observed, monitoring of developing adrenal insufficiency might be essential in acute SARS-CoV-2 infection and long-COVID19 patients.

P06 Postersitzung Gynäko- und Mammopathologie

P06.01

Struma ovarii – associated with hyperthyroidism

G. G. R. Hiller¹, A.-K. Höhn¹, A. Dannemann², J. Einenkel², A. Pilny³, L.-C. Horn¹

¹Universitätsklinikum Leipzig, Institut für Pathologie, Leipzig, Germany, ²Sana Kliniken Leipziger Land, Klinik für Frauenheilkunde und Geburtshilfe, Borna, Germany, ³Universitätsklinikum Leipzig, Klinik und Poliklinik für Frauenheilkunde, Leipzig, Germany

Background

20-25% of ovarian neoplasms are germ cell tumors and the majority of them account for mature teratomas. Thyroid tissue is a common finding in ovarian teratomas (>50%), the term struma ovarii (SO) is dedicated to ovarian neoplasms that either entirely or predominantly (>50%) consist of thyroid tissue, which accounts for 1-3% of all ovarian teratomas. SO associated with hyperthyroidisms is a very rare complication.

Methods

We present the case of a giant struma ovarii associated with an ectopic hyperthyroidism.

Results

A 52-year-old woman presented with abdominal pain and a history of bowels resection because of neuroendocrine carcinoma years before. Clinical examination presented a large ovarian tumor, suspicious for malignancy and a serum level of Ca-125 of 80 U/ml. The resection specimen presented an ovarian tumor of 763 g and 16.0 x 9.5 x 9.5 cm with multicystic brownish cutting surface with cysts ranging from 0.2 up to 8.5 cm. The tumor was initially misdiagnosed as suspicious for endometrial ovarian carcinoma on frozen section, but diagnosed as benign SO on final sections which was confirmed by immunostaining. Six weeks before the patient presented with hyperthyroidisms and thrombosis of the V. brachialis. The signs of hyperthyroidism disappeared after tumor resection.

Conclusion

Usually, SO present with non-specific symptoms, such as abdominal pain/distension or vaginal bleeding or it is an incidental finding in patients with pelvic discomfort. A few patients have ascites or ascites with hydrothorax (pseudo-Meigs syndrome). Ectopic hyperthyroidism caused by SO is extremely rare. The case demonstrates an unusual large benign SO causing ectopic hyperthyroidism, which was initially misdiagnosed as ovarian cancer on frozen section.

Squamous cell carcinoma arising from a mature cystic ovarian teratoma – histomorphologic and molecular findings

G. G. R. Hiller¹, A.-K. Höhn¹, A. Pilny², U. Obeck¹, M. Stiller¹, M. Martin³, L.-C. Horn¹

¹Universitätsklinikum Leipzig, Institut für Pathologie, Leipzig, Germany, ²Universitätsklinikum Leipzig, Klinik und Poliklinik für Frauenheilkunde, Leipzig, Germany, ³Universitätsklinikum Leipzig, Klinik und Poliklinik für Diagnostische und Interventionelle Radiologie, Leipzig, Germany

Background

20-25% of ovarian neoplasms are germ cell tumors and the majority of them account for mature cystic teratomas. Malignant transformation with the presence of somatic type neoplasms is very rare. Up to 80% of those malignancies present as SCC, that carry a poor prognosis. Pathogenetic informations are very limited.

Methods

We present the case of a squamous cell carcinoma arising from a mature cystic ovarian teratoma and its histomorphologic and molecular findings.

Results

A 59-year-old postmenopausal woman clinically presented with abdominal pain and large bowels compression. Colonoscopic guided biopsy represented a non-small cell carcinoma suspicious for squamous cell carcinoma 25cm from the anus. CT-imaging revealed pelvic mass with infiltration of the right ureter and colon sigmoideum and elevated serum levels of CA-125 of 155 U/ml suggesting cystic teratoma with malignancy. The exenteration specimen represented a (mature) cystic ovarian teratoma of 14.9 x 9.5 x 8.5 cm containing an 9.0 x 8.3 x 4.8 cm poorly differentiated keratinising squamous cell carcinoma (SCC) with pseudo-sarcomatous growth and infiltration of the rectosigmoid and the mesoreter on the right side, but no lymph node involvement, staged pT3c pN0 (0/86). The invasive tumor was accompanied by squamous carcinoma in situ. Both lesions were negative for p16 but represented aberrant p53-staining. On molecular level there was a negativity for HPV-DNA, but TP53-mutation.

Conclusion

Malignant transformation in mature cystic teratomas account for about 0.2-0.3% but should not be missed during histopathological workup and have to be separated from SCC in association with ovarian endometriosis. Within somatic type malignant tumors with mature ovarian teratomas about 80% account for SCC. As in the present case, some SCC are accompanied by carcinoma in situ. Older age, large tumor size (>15.0cm and >12cm, respectively) and the presence of solid component within the teratoma are discussed as suitable predictors for malignant transformation. Alteration for TP53 may be involved within malignant transformation. Somatic type SCC within mature ovarian teratomas present with poor prognostic outcome.

Epithelial-mesenchymal transition (EMT) in vulvar cancer

L.-C. Horn¹, C. E. Brambs², C. Eckey¹, G. G. R. Hiller¹, M. Höckel³, M. Mende⁴, A. K. Höhn¹

¹*Institute of Pathology, University of Leipzig, Leipzig, Germany*, ²*Luzerner Kantonsspital, Department of Obstetrics and Gynecology, Luzern, Switzerland*, ³*Department of Obstetrics & Gynecology, University of Leipzig, Leipzig, Germany*, ⁴*IMISE University of Leipzig, Leipzig, Germany*

Background

Epithelial-mesenchymal transition (EMT) is associated with increased metastatic spread and poor prognosis. Data on vulvar carcinoma are limited.

Methods

32 squamous cell carcinoma of the vulva (16 with and 16 without inguinal lymph node metastases) and their lymph node deposits were evaluated for immunohistochemical expression of EMT-markers (vimentin, cyclin D1, e-cadherin), p16, p53 and Ki-67. Results of EMT-immunostaining was compared to lymph node involvement and expression of p53 and p16. The micro-anatomical staining pattern for EMT markers comparing the tumor center with the front of invasion was analysed in each tumor.

Results

There was no difference in the expression of EMT-markers between node negative and node positive tumors. Staining for vimentin and cyclin D1 was seen within tumor cells at the front of invasion in 100% and 84.4% of the tumors, respectively. The majority of cases (68.7%) showed negative or reduced staining for e-cadherin in this micro-anatomical localization. Tumor cells within the lymph node metastases showed positive staining for e-cadherin in 75% and for cyclin D1 in 49% of the cells but were negative for vimentin in 13 out of 16 cases (81.3%). Tumors with aberrant p53-staining represented a non-significant higher vimentin but significantly higher cyclin D1 expression at the front of invasion than those with p53 wild-type pattern.

Conclusion

The present study shows no differences in the expression of EMT-markers between node positive and negative vulvar cancers. The evaluation of immunostaining within the micro-anatomical context indicates that an EMT-phenotype is restricted to the tumor cells at the front of invasion. Paired analyses of vulvar carcinomas and their lymph node deposits suggest mesenchymal-epithelial transition (MET). Immunohistochemical staining results may suggest that EMT is more prevalent in vulvar cancer with aberrant p53 staining.

Carbonic anhydrase XII as biomarker and therapeutic target in ovarian carcinomas

L. Hiepp¹, D. Mayr¹, K. Gärtner², E. Schmoeckel¹, F. Klauschen¹, A. Burges³, S. Mahner³, R. Zeidler^{2,4}, B. Czogalla³

¹*Institute of Pathology, Ludwig-Maximilians-University, Munich, Germany*, ²*Helmholtz Center Munich – German Research Center for Environmental Health, Munich, Germany*, ³*Department of Obstetrics and Gynecology, University Hospital, Ludwig-Maximilians-University, Munich, Germany*, ⁴*Department of Otorhinolaryngology, University Hospital, Ludwig-Maximilians-University, Munich, Germany*

Background

Carbonic anhydrase XII (CA XII) is an ectoenzyme involved in pH regulation. Overexpression of CA XII is reported for many neoplasms. CA XII not only enables the maintenance of tumor cell function but also promotes tumor spreading by acidifying the extracellular milieu [1]. Consequently, CA XII is considered an attractive target molecule for new strategies in cancer treatment [2]. As such progress is highly demanded for ovarian carcinomas (OCs), the study aimed to provide deeper information about their CA XII expression profile.

Methods

Tissue specimens of 487 patients were included retrospectively. Immunohistochemical analysis of the CA XII expression in neoplastic and non-neoplastic epithelial ovarian cells was conducted using the specific anti-CA XII antibody 6A10 [2]. Due to its first application on paraffin-embedded slides, a modified staining protocol was established. The immunoreactive score (IRS) was used for staining evaluation. Results were correlated with clinicopathological parameters. Furthermore, 24 samples of ascites fluid with tumor cells were analyzed by flow cytometry.

Results

CA XII expression is found in 390 (99.5%) out of 392 OCs. Most carcinomas (72.2%) exhibit detectable amounts of CA XII in more than eighty percent (PP4) of the tumor cells. Median IRS is 8. Invasive carcinomas express more CA XII than semi-malignant borderline ovarian tumors (n = 19), which in turn show higher expression levels than non-neoplastic epithelial ovarian cells (n = 19). Within the OC tissue, strong CA XII expression is associated with poorer grading. High CA XII expression at the time of diagnosis shows a trend towards shorter overall survival in a stratified subgroup of high-grade serous OCs. Analysis of ascites-derived tumor cells demonstrates strong CA XII expression in all (22 out of 22) cases of OCs. Two additionally analyzed cases of borderline ovarian tumors remain negative.

Conclusion

Binding of the antibody 6A10 reveals an upregulation of CA XII in OCs. The described correlation of CA XII expression with tumor dignity and grading indicates that CA XII plays a role for their aggressive behavior. Particularly considering the results obtained from ascites analysis, CA XII could serve as a diagnostic marker for the presence of vital cancer cells. 6A10 binds to their surface and could be used therapeutically due to its inhibitory potential [3][4].

Literaturangaben

- [1] Ivanov, Sergey et al., (2001), Expression of hypoxia-inducible cell-surface transmembrane carbonic anhydrases in human cancer, *American Journal of Pathology*, 905-919, 158(3)
- [2] Battke, Christina et al., (2011), Generation and characterization of the first inhibitory antibody targeting tumour-associated carbonic anhydrase XII, *Cancer Immunology, Immunotherapy*, 649-658, 60(5)
- [3] Gondi, Gabor et al., (2013), Antitumor efficacy of a monoclonal antibody that inhibits the activity of cancer-associated carbonic anhydrase XII, *Cancer Research*, 6494-6503, 73(21)
- [4] von Neubeck, Bettina et al., (2018), An inhibitory antibody targeting carbonic anhydrase XII abrogates chemoresistance and significantly reduces lung metastases in an orthotopic breast cancer model in vivo, *International Journal of Cancer*, 2065-2075, 143(8)

Differentiated High-Grade Squamous Intraepithelial Lesion of the Uterine Cervix (d-HSIL, d-CIN 3) as a Distinct Precursor Lesion in Keratinising HPV-negative Squamous Cell Carcinoma of the Uterine Cervix

L.-C. Horn¹, A. Dannemann², **G. G. R. Hiller**¹, A. K. Höhn¹, J. Einenkel³, U. Obeck¹, M. Stiller¹, C. E. Brambs⁴

¹*Institute of Pathology, University of Leipzig, Leipzig, Germany*, ²*Sana Country Hospital,, Department of Obstetrics & Gynecology,, Borna, Germany*, ³*Sana Country Hospital,, Borna, Germany*, ⁴*Luzerner Kantonsspital, Department of Obstetrics and Gynecology,, Luzern, Switzerland*

Background

Although HPV-negative precursor lesions have been recently described, morphologic and molecular features of HPV-independent squamous precursor lesions are very limited

Methods

Detailed histopathological and immunohistochemical analyses of p16, p53 and CK 17 were performed, as was a molecular evaluation for HPV-DNA and p53-mutation of a cervical squamous cell carcinomas associated with uterine prolapse with the definition of a hitherto not well-described precursor lesion and molecular tumorigenic pathway.

Results

Histopathologically, the keratinizing squamous cell carcinoma (SCC) with infiltrative growth and their adjacent precursor lesions were negative for p16, showed an aberrant p53-expression and diffuse and strong staining for CK 17 on immunohistochemistry. On the molecular level, both the SCC and the precursor were negative for HPV-DNA but harbored a *TP53*-mutation. The precursor lesions were characterized by epithelial thickening with superficial keratinization, the presence of basal and parabasal keratinocytes with mitotic figures beyond the basal layer, thus showing features similar to those seen in differentiated types of vulvar intraepithelial lesions (d-VIN), suggesting the terminology of cervical d-HSIL (syn. d-CIN 3). An HPV-independent pathogenetic pathway with a p53-alteration was identified for that case.

Conclusion

That specific SCC represent a keratinized, HPV-independent tumor harboring a *TP53*-mutation. For the first time, a precursor lesion of HPV-independent SCC of the uterine cervix was been described with a d-VIN-like morphology, and a separate tumorigenic pathway was defined.

Evaluation of P16/Ki67 (CINtecplus) and L1-Capsid compared with HPV-Genotyping in cervical cytology in women above 35 years old with focussing in patients with Group IIp (ASC-US, Atypical squamous cell of undetermined significance)

M. Abbas¹, I. Erduran², J. de Jonge³, O. Bettendorf²

¹Uniklinikum Münster, Gerhard-Domagk Institut für Pathologie, Münster, Germany, ²Institut für Pathologie und Zytologie, Schüttorf, Germany, ³Institut für Pathologie und Zytologie, Pathologie, Schüttorf, Germany

Background

Cervical cancer is the second or third most common cancer in women with around 0.5 million cases worldwide. There were many new subgroups in the new nomenclature (2015) like IIa and IIp with subdivisions of IIID into IIID1 and IIID2. Group IIp (ASC-US) was for a long time under controversial discussions. By the beginning of 2020, there is a new method of cervix screening in women, which is called Ko-Test (conventional cytology and HPV-test for high risk groups (HPV-HR-Test)), there are now new controversial discussions about the importance of this group and about the importance of conventional cytological smears in women >35 years old. Our work is focussing on this group IIp in women above 35 years old, to evaluate the importance of conventional cytological smears with the optional use of immunocytochemistry (CINtecplus and L1-Capsid) to evaluate the abnormal cells and grading the dysplasia, if present, in comparison with the HPV-HR-Test.

Methods

In the Institut für Pathologie und Zytologie-Schüttorf-Germany from the beginning of year 2020 till the beginning of year 2021 about 146.800 samples for women above 35 years old. Conventional cytological examination was done in parallel with HPV-HR-Test. 555 cases were subgrouped as IIp. Immunocytochemical examination was added in 24.3% of the cases.

Results

After performing the immunocytochemical examination in these cases, there were about 3.7% with CIN II and CIN III (HSIL). In HPV-HR-Test, there were 26.4% positive. 33.7% of the negative HPV-HR were immunocytochemically suspect of positivity and 0.5% were surely positive. 13.6% of the HPV-16-negative cases were histologically diagnosed as HSIL and about 20.9% were histologically either LSIL or HSIL. 14.6% of HPV-18-negative cases were histologically diagnosed as HSIL and 19.5% were histologically either LSIL or HSIL.

Conclusion

The results of this study with this number of cases ensure the need of conventional cytological examination as well as the additive immunocytochemistry in suspicious cases of group IIp to ensure the diagnosis and to exclude the higher dysplasia. The problem by this examination is the need of human power (CTA and certified cytopathologist) as well as the continuous training. The advantage of HPV-subtyping is that

machinary work with screeing too much number of cases in little time but it is not accurate and can give false way to treat the cases. HPV-HR-Test is only not enough as a method of screening, because it maybe misleading.

Molecular classification of endometrioid endometrial carcinoma with minimal deviation-like pattern (MDA-like ECX)

G. G. R. Hiller¹, A.-K. Höhn¹, J. Eienkel², R. Handzel³, I. Krücken¹, L.-C. Horn¹

¹Universitätsklinikum Leipzig, Institut für Pathologie, Leipzig, Germany, ²Sana Kliniken Leipziger Land, Klinik für Frauenheilkunde und Geburtshilfe, Borna, Germany, ³Universitätsklinikum Leipzig, Klinik und Poliklinik für Frauenheilkunde, Leipzig, Germany

Background

Endometrial carcinoma (EC) is the most common gynecologic malignancy worldwide, the fourth most common cancer in women within the United States and the sixth most common worldwide. The vast majority of EC represent endometrioid histology, including its variants from the most common conventional patterns to rarer patterns as microcystic elongated and fragmented pattern (MELF) and minimal deviation-like pattern (MDA). Especially in MDA-type endometrioid EC the knowledge about molecular subtyping is limited.

Methods

Examining cases of MDA-type endometrioid EC regarding its clinicopathologic features and morphologic appearance in hysterectomy specimens with molecular examination of p53-, mismatch repair protein-expression and *POLE*-mutational status, according to ProMISE-classification.

Results

Eighteen cases of endometrioid adenocarcinoma of MDA-type or with a component of minimal deviation pattern of at least 10% have been diagnosed at our institution in the years 2005 to 2020. MDA-like pattern of invasion was defined as regular, rounded and often widely spaced glands invading the myometrium without or with minimal accompanying desmoplastic stromal or inflammatory response. The mean age of the patients was 71.2 years (range 46-88 years), 7/18 patients showed at least one risk factor of the classic "triple syndrome" obesity, diabetes and hypertension. Six out of the 18 cases showed aberrant p53-expression, 3/18 presented loss of MMR-protein-expression, 1/18 showed *POLE*-mutation and 8/10 were of no special molecular profile (NSMP).

Conclusion

Four groups of carcinomas with descending prediction have been described by The Cancer Genome Atlas (TCGA) according to their molecular characterization: 1 - *POLE*-mutated, 2 - MMR-deficient, 3 - p53 wildtype, 4 - p53-mutated. These groups can also be used to characterize endometrial carcinoma independent of their histomorphological subtype. Within the group of MDA-like EC about half of the cases show a specific mutation while the other half is of no specific molecular profile. Finally, on molecular level, endometrioid ECX with MDA-type infiltration pattern fall in range with other subtypes of endometrial

endometrioid carcinomas and are capable to be classified according to the ProMISE-classification system.

Breast Cancer: Characterization of Hormone Receptor Status Using Mass Spectrometry Imaging

J. P. L. Goncalves, C. Bollwein, W. Weichert, **K. Kristina Schwamborn**

Technische Universität München, Institut für Pathologie, München, Germany

Background

Breast cancer diagnosis and subsequential treatment choice revolve around the characterization of the status of different receptor proteins: estrogen receptor (ER), progesterone receptor (PR), and human epidermal growth factor 2 (HER2). Triple-negative breast cancer (TNBC) is usually associated with poor outcomes due to lower response rates to traditional treatment approaches. In this study, we have evaluated the proteomic content by imaging mass spectrometry to better understand the molecular signatures of each protein receptor.

Methods

Tissue microarrays comprising samples from breast cancer samples (n=1194) were subjected to on-tissue tryptic digestion and incubated in a humid environment followed by matrix application (alpha-cyano-4-hydroxycinnamic acid) using an automated sprayer (HTX Technologies). Samples were analyzed utilizing a Bruker RapifleX MALDI-TOF mass spectrometer. Subsequently, the matrix was removed, sections were stained by hematoxylin and eosin and scanned using the Aperio slide scanner for meticulous histopathological annotation. The receptor statuses were also all re-evaluated by the same pathologist to avoid inter-personal bias. Data analysis was performed using SCiLS Lab (Bruker) and statistical analysis was performed on R.

Results

The classification accuracy yields promising results for the individual receptors (90,6% for ER; 81.21% for PR and; 77,7% for HER2). However, the classification of TNBC samples yields an accuracy of 96%, indicating that this subtype has other available targets for diagnosis and possible treatment. From the analysis of the individual molecular features, we were able to identify a very promising protein, which is overexpressed in TNBC: Vimentin. This protein could be used as a target for treatment, and for a quicker validation of TNBC diagnosis.

Conclusion

Mass spectrometry imaging can not only be utilized to characterize hormone receptor status in breast cancer but also to identify candidate target proteins for treatment.

Co-expression of Transcription Factor AP-2beta (*TFAP2B*) and GATA3 in human mammary epithelial cells with intense, apicobasal immunoreactivity for CK8/18

M. Raap¹, L. Gierendt¹, C. Werlein¹, E. Kühnle², H. H. Kreipe¹, M. Christgen¹

¹Medizinische Hochschule Hannover, Institut für Pathologie, Hannover, Germany, ²Medizinische Hochschule Hannover, Gynäkologie, Hannover, Germany

Background

AP-2b is a new mammary epithelial differentiation marker which is preferentially expressed in lobular carcinoma *in situ* and invasive lobular breast cancer. In normal breast epithelium AP-2b is expressed in a scattered subpopulation of luminal cells. So far, these cells have not been further characterized.

Methods

Co-expression of AP-2b protein and luminal epithelium markers (GATA3, CK8/18), hormone receptors (estrogen receptor (ER), androgen receptor (AR)) and stem cells markers (CK5/14, CD44) were assessed by double- immunofluorescence in the normal mammary gland.

Results

The subpopulation of AP-2b-positive mammary epithelial cells showed an almost complete co-expression with GATA3 and a peculiar intense, ring-like appearing immunoreactivity for CK8/18. Confocal imaging revealed an apicobasal staining for CK8/18 in AP-2b-positive cells, which was not seen in AP-2b-negative cells. A partial co-expression with hormone receptors (ER, AR) and no co-expression with candidate stem cell markers (CK5/14, CD44) were seen.

Conclusion

In summary, AP-2b is a luminal mammary epithelial differentiation marker, which is expressed in the GATA3-positive subpopulation of luminal epithelial cells. These AP-2b-positive/GATA3-positive cells also show a peculiar CK8/18-expression which may indicate a previously unknown functionally specialized mammary epithelial cell population.

Breast cancer tumor microenvironment in sub-Saharan Africa reveals features associated with worse survival among West African Patients

M. Bauer¹, M. Y. Nigussie², Z. D. Woldesonbet², T. Yalew³, E. van den Berg⁴, J. I. Nikulu⁵, C. B. Traore⁶, S. S. Manraj⁷, O. J. Ogunbiyi⁸, I.-O. A. Ekanem⁹, I. Festus¹⁰, D. Mohenou¹¹, B. Effi¹², C. Adebamowo¹³, C. Dzamalala¹⁴, ABC-DO-Studiengruppe¹⁵, V. McCormack¹⁵, C. Wickenhauser¹, B. Seliger^{16, 17}, E. Kantelhardt¹⁸

¹Universitätsklinikum Halle (Saale), Institut für Pathologie, Halle (Saale), Germany, ²School of Medicine, College of Health Sciences, Tikur Anbessa Specialized Hospital, Addis Ababa University, Department of Microbiology, Immunology & Parasitology, Addis Ababa, Ethiopia, ³Tikur Anbessa Specialized University Hospital, College of Health Sciences, Addis Ababa University, Department of Pathology, Addis Ababa, Ethiopia, ⁴National Health Laboratory Services, Department of Histopathology, Johannesburg, South Africa, ⁵Unité Pilote du GFAOP, Ligue congolaise contre le cancer, Lubumbashi, Congo, the Democratic Republic of the, ⁶Service de Laboratoire, Anatomie, Cytologie, Pathologique, Bamako, Mali, ⁷Vistoria Hospital, Central Health Laboratory, Candos, Mauritius, ⁸University College Hospital, Department of Pathology, Ibadan, Nigeria, ⁹Calabar Cancer Registry, Department de Pathologie, Calabar, Nigeria, ¹⁰National Hospital, Abuja Hospital, Abuja, Nigeria, ¹¹Abidjan Hospital, Service d'anatomiecytologie pathologique, Abidjan, Côte d'Ivoire, ¹²Alassane Ouattara University, Department of Anatomic Pathology, School of Medicine, Bouake, Côte d'Ivoire, ¹³Institute of Human Virology, Abuja, Nigeria, Institute of Human Virology, Abuja, Nigeria, ¹⁴Blantyre Hospital, Department of Pathology, Blantyre, Malawi, ¹⁵IARC, Environment and Lifestyle Epidemiology Branch, Lyon, France, ¹⁶Universitätsklinikum Halle (Saale), Institut für Medizinische Immunologie, Halle (Saale), Germany, ¹⁷Fraunhofer Institute, Cell Therapy and Immunology, Leipzig, Germany, ¹⁸Universitätsklinikum Halle (Saale), Institut für Epidemiologie, Halle (Saale), Germany

Background

The incidence of breast cancer (BC) in sub-Saharan Africa (SSA) is steadily increasing. Next to advanced tumor stages, limited therapeutic options and frequently aggressive intrinsic subtypes in SSA, an unfavorable tumor microenvironment (TME) has been suggested in these patients. In order to get insights into regional differences, the composition of the TME and the expression of immune-relevant markers in BC samples from different regions in SSA were compared and their prognostic value investigated.

Methods

The TME of 1237 BC tissue samples from ten countries in SSA was analyzed by scoring the tumor infiltrating lymphocytes (TILs) combined with immunohistochemistry (IHC) and RNA expression profiling for (i) immune cell subpopulation composition and their spatial distribution as well as for (ii) the immunogenicity of BC. These data were correlated to clinical parameters, pathological features including intrinsic BC subtypes and patients' survival.

Results

While only minor regional differences were found in TIL density, which were associated with the BC patients' survival, higher numbers of CD163⁺ macrophages and CD3⁺CD8⁺ T cells accompanied by higher levels of IL-10, but lower levels of IFN- γ were detected in BC of West Africa. Furthermore, BC patients of West Africa were characterized by a significantly reduced immunogenicity due to a downregulation of HLA class I antigens and components of the antigen presenting machinery (APM) as well as Janus kinase/signal

transducer and activator of transcription (JAK/STAT) signaling pathway, which was also correlated with a worse patients' prognosis.

Conclusion

This study highlights a regional diversity of the TME composition and HLA class I-mediated immune escape mechanisms in BC specimen of SSA with a reduced immunogenicity and immune suppressive microenvironment in BC of West African women.

P08 Postersitzung Thoraxpathologie

P08.01

Cancer or Systemic Vasculitis: a solitary pulmonary nodule in a patient with Granulomatosis with Polyangiitis mimicking malignancy

N. Reitsam, B. Märkl, T. Schaller

Universitätsklinikum Augsburg, Institut für Pathologie und Molekulare Diagnostik, Augsburg, Germany

Background

Granulomatosis with Polyangiitis (GPA) is a rare multisystem disorder first described by Friedrich Wegener in 1936 [1]. GPA is characterized by necrotizing granulomatous inflammation and small-vessel vasculitis. In Germany, the annual incidence is 34 GPA cases per million people per year [2]. With respiratory involvement in up to 90% of the cases [3], much is known about the pulmonary imaging findings in GPA [4]. Yet, none of these findings is absolutely specific, and GPA lesions may be misdiagnosed with cancer.

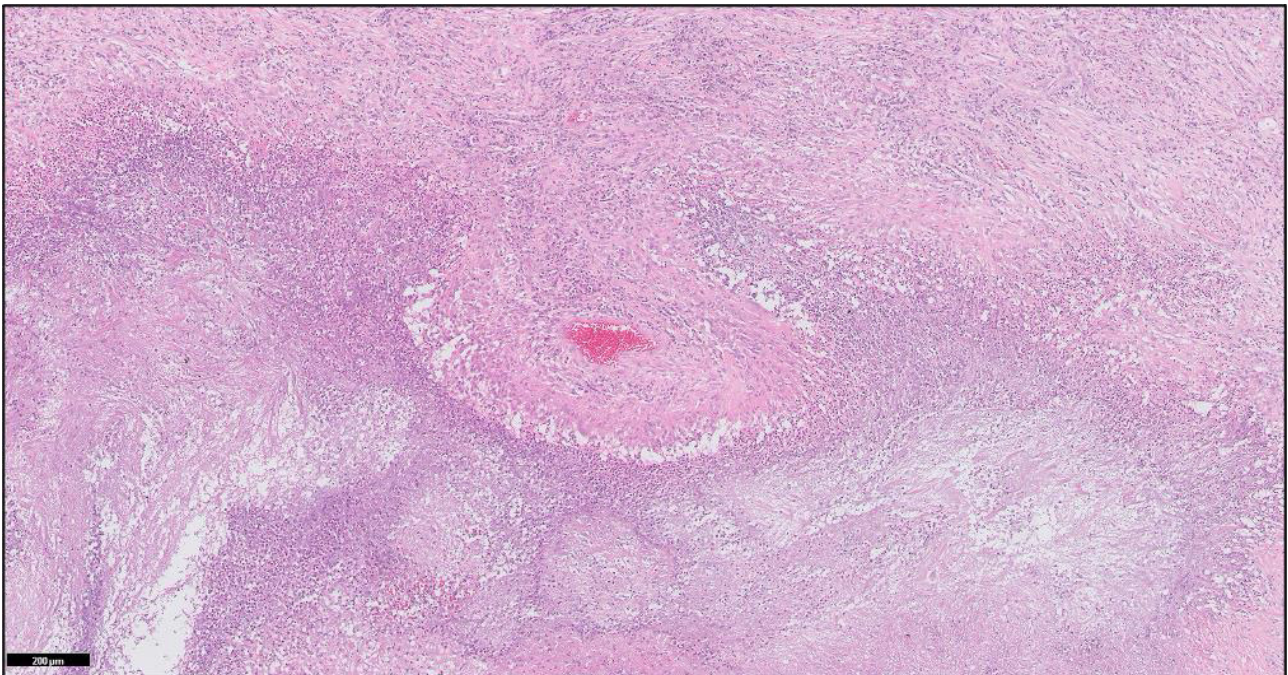
Here, we present the case of a 58 year-old man suffering from GPA since 1990 with a previously diagnosed nose, muscle and kidney involvement. Due to a terminal renal failure, kidney transplant was planned and a CT scan was performed in preparation. The CT scan showed a solitary nodule of unclear dignity in the right upper lobe of the lung. The patient's medical history was notable for a papillary urothelial carcinoma (pTa, G2). In the follow-up PET-CT the lesion was progredient in size, showed an increased 18F-FDG uptake and was highly suspicious for malignancy. Assuming a malignant origin, a video-assisted thoracoscopic wedge resection was performed.

Methods

We performed HE staining on frozen sections as well as on FFPE tissue. Additionally, PAS, EVG, FE and Ziehl-Neelsen stains were carried out to confirm the diagnosis.

Results

The frozen section analysis and the FFPE tissue stains both revealed a characteristic geographic pattern of 'dirty' basophilic necrosis as well as granulomatous inflammation composed of lymphocytes, plasma cells, neutrophils and giant cells immediately adjacent to a vessel, being consistent with the patient's previously known GPA.



Granulomatosis with Polyangiitis showing a necrotizing granuloma with 'dirty' basophilic necrosis and extensive inflammation directly adjacent to a blood vessel (HE stain, frozen section).

Conclusion

Although granulomatous inflammation on biopsy is only 1 out of 4 diagnostic criteria for GPA [5], histologic examination of suspicious lesions is often indispensable as GPA lesions can mimic infections or cancer. Hence, systemic vasculitis should always be considered as a potential non-neoplastic differential diagnosis for pulmonary lesions. Compared to a malignant diagnosis, a GPA relapse is no contraindication for organ transplant, which will hopefully be beneficial for our patient.

Literaturangaben

- [1] Wegener F, (1936), Über generalisierte, septische Gefäßerkrankungen, Verh Dtsch Path Ges, 202-210, 29
- [2] Hellmich B, Lamprecht P, Spearpoint P, et al, (2021), New insights into the epidemiology of ANCA-associated vasculitides in germany: Results from a claims data study, Rheumatology (Oxford), 4868-4873, 60
- [3] Hoffman GS, Kerr GS, Levitt RY, et al, (1992), Wegener granulomatosis: An analysis of 158 patients, Ann Intern Med, 488-498, 116
- [4] Allen SD, Harvey CJ, (2007), Imaging of wegener's granulomatosis, Br J Radiol, 757-765, 80
- [5] Leavitt RY, Fauci AS, Bloch DA, et al, (1990), The american college of rheumatology 1990 criteria for the classification of wegener's granulomatosis, Arthritis Rheum, 1101-1107, 33

Severe adverse events of immune checkpoints inhibitors: 3 autopsy cases

F. J. Farfán López¹, I. Kleinlein¹, L. Rentschler¹, A.-K. Gantner², J. Geisendörfer², B. Märkl¹

¹*Universitätsklinikum Augsburg, Institut für Pathologie und molekulare Diagnostik, Augsburg, Germany,*

²*Universitätsklinikum Augsburg, II Medizinische Klinik, Augsburg, Germany*

Background

PDL1 upregulation in tumor cells allows evading the immune system attack. Checkpoint inhibitors block the binding between PDL1 ligand and its receptor PD1, favoring the effect of T cells and improving antitumor immunity. Despite the good results, mild side effects due to activation of the immune system have been reported in many patients. In about 1% of cases, these effects are serious, producing encephalitis, myocarditis or pneumonitis.

Methods

We present three autopsy cases corresponding to three males aged 70 to 73 years.

Results

The first patient developed myositis and myocarditis after treatment with Nivolumab for metastatic melanoma. The myocarditis is similar to the inflammation described in cardiac transplant rejection, but with a greater presence of CD3 lymphocytes and macrophages as well as myocytes and PDL1+ macrophages. The second case corresponds to a patient with a history of metastatic melanoma treated with Nivolumab for four cycles, presenting encephalitis. Neurologic immune-related adverse events most frequently affect the PNS. Clinical presentations are usually multifocal and sometimes occurs, as in this case, a fulminant evolution. The third case was a patient with lung adenocarcinoma treated with three cycles of Atezolizumab, with post-treatment pneumonitis. Immune-related pneumonitis is characterized by CD8+ lymphocytic infiltration and organized pneumonitis. It also requires the exclusion of pneumonitis due to another cause. Less commonly, acute fibrinous pneumonitis or diffuse alveolar damage may occur, which can be fatal. In all three cases the reactive inflammatory process was the cause of death.

Conclusion

Checkpoint-inhibitor therapy has gained importance in the treatment of various tumors such as metastatic melanoma, lung or urothelial tumors, with very promising results but with rare and potentially serious side effects.

Tumor spread through airspaces (STAS): a comprehensive analysis of clinicopathological features in a real-world lung adenocarcinoma cohort

A. Stehle^{1,2}, E. Belker³, K. Bankov¹, N. Tekeli-Camci⁴, A. Burchardt², M. Kinzler², W. Gleiber², M. Demes¹, W. Schreiner³, B. Vrugt⁵, G. Rohde^{2,4}, P. Wild¹

¹Goethe University Hospital, Dr. Senckenberg Institute of Pathology, Frankfurt, Germany, ²Goethe University Hospital, Medical Clinic I, Frankfurt, Germany, ³Goethe University Hospital, Department of Thoracic Surgery, Frankfurt, Germany, ⁴St. Elisabethen Hospital, Department of Oncological Pneumology, Frankfurt, Germany, ⁵Cantonal Hospital Münsterlingen, Institute of Pathology, Münsterlingen, Switzerland

Background

Tumor spread through airspaces (STAS) is a new pattern of invasion in lung cancer but its role as a prognostic biomarker remains controversial.[1] We aimed to decipher the potential mechanism underlying the morphological STAS pattern.

Methods

We retrospectively reviewed 200 lung adenocarcinoma (LUAD) tissue samples resected between 2008 and 2018. STAS was visually assessed by H&E whole-slide-images. Expression of E-Cadherin, N-Cadherin, Vimentin, b-Catenin, Mucin-21 (MUC21), lysine-methyltransferase-9-alpha (KMT9a) and metastasis-associated protein 1 (MTA1) was analyzed by immunohistochemistry using a tissue microarray. Univariate and multivariate analyses were applied to determine associations between STAS and clinicopathological parameters. Overall- (OS) and recurrence-free (RFS) survival was assessed and compared by Kaplan-Meier method and log-rank test.

Results

77 (38,5%) LUADs were STAS positive. STAS was associated with micropapillary histopathology ($p<0.001$), nodal positivity ($p=0.013$), lymphovascular invasion ($p=0.008$) and distant and locoregional recurrence ($p=0.038$). There was no difference in OS but small (diameter < 3cm) UICC I-III STAS positive LUADs had significantly worse RFS($p=0.025$). In our cohort no associations between STAS and E-Cadherin, N-Cadherin, Vimentin, b-Catenin or MTA1, as surrogates of induction of epithelial-mesenchymal transition, were detected. STAS was significantly associated with MUC21-expression, a molecule linked to cell incohesiveness[2]($p=0.004$) and with KMT9a, a regulator of cancer cell proliferation and survival [3]($p=0.043$).

Conclusion

In conclusion, our data gives further evidence that STAS is associated with aggressive tumor phenotypes and our findings corroborate its potential to serve as an independent negative prognostic factor in LUAD. In our cohort STAS positive tumors did not show EMT features supporting the controversial debate that EMT

might be an associated risk factor but not the underlying mechanism of STAS.[4] The implementation of STAS in routine pathology practice to date is limited. Hence further studies need to be conducted to elucidate the underlying biological mechanisms responsible for STAS and the resulting therapeutic implications.

Literaturangaben

[1] Shih AR, Mino-Kenudson M., (2020), Updates on spread through air spaces (STAS) in lung cancer, *Histopathology*, 173-180, 77/2

[2] Yoshimoto T, Matsubara D, Soda M, et al., (2019), Mucin 21 is a key molecule involved in the incohesive growth pattern in lung adenocarcinoma., *Cancer Science*, 3006-3011, 110/9

[3] Baumert HM, Metzger E, Fahrner M, et al. , (2020), Depletion of histone methyltransferase KMT9 inhibits lung cancer cell proliferation by inducing non-apoptotic cell death, *Cancer Cell International*, 1-13, 20/1

[4] Jia M, Yu S, Yu J, Li Y, Gao H, Sun PL., (2020), Comprehensive analysis of spread through air spaces in lung adenocarcinoma and squamous cell carcinoma using the 8th edition AJCC/UICC staging system., *BMC Cancer*, 1-11, 20/1

Whole-exome sequencing confirms proteasomal processing alterations as a novel mechanism of immune escape, stratifying patients for immune checkpoint blockade

M. Wessolly¹, M. Wiesweg², S. Borchert¹, H. Beckert³, S. Stephan-Falkenau⁴, E. Mairinger¹, A. Mathilakathu¹, J. Kollmeier⁵, C. Aigner³, C. Taube³, J. Wohlschlaeger⁶, T. Bauer⁵, T. Mairinger⁴, K. W. Schmid¹, M. Schuler², H. Reis¹, **F. D. Mairinger¹**

¹Universitätsklinikum Essen, Institut für Pathologie, Essen, Germany, ²Universitätsklinikum Essen, Westdeutsches Tumorzentrum, Essen, Germany, ³Universitätsklinikum Essen, Ruhrlandklinik - Westdeutsches Lungenzentrum, Essen, Germany, ⁴Helios Klinikum Emil von Behring, Institut für Gewebediagnostik, Berlin, Germany, ⁵Helios Klinikum Emil von Behring, Lungenklinik Heckeshorn, Berlin, Germany, ⁶Diakonissenkrankenhaus Flensburg, Institut für Pathologie, Flensburg, Germany

Background

Lung cancer reigns supreme as the deadliest cancer type worldwide and poses a serious issue for the public health. Although ICB is an effective therapy, the main problem of primary resistance remains. Currently, biomarkers are PD-L1 protein expression, but also tumor mutational burden (TMB) has been suggested. In previous works, we identified altered epitope processing as an important mechanism for tumor immune escape. We seek to verify the existence and clinical impact of altered epitope processing in comparison to TMB using whole-exome sequencing (WES) in a well-defined cohort of patients.

Methods

Therapy naïve FFPE samples of 72 patients with advanced or metastatic NSCLC (any histology) who received ICB were used for analysis. All samples underwent both WES and digital gene expression analysis (PanCancer Immune Profiling panel). Probability for proteasomal cleavage of mutated and wild-type sequences, Epitope binding affinity of predicted fragments and TCR affinity of fragments identified as still presented and MHC class I molecules were calculated using the deep-learning algorithms NetChop, NetMHC and NetCTL, respectively. Finally, activation of TCR signalling has been predicted using the ImmunogenicityScore.

Results

18/54 (33.3%) showed mutations associated with altered proteasomal processing and were classified as processing escapes. A significantly shortened OS after ICB time for the processing escape group could be found ($p=0.008$, HR: 2.85, 95% CI: 1.27-6.41), with a median survival of 7.8 months (95% CI: 5.4 – 14.6), whereas in the non-processing group, median survival has not been reached (95% CI: 9.76 – NA). The one-year survival rate differs between 26.4% and 63.1%. Also TTF significantly shortened for the processing escape group ($p=0.002$, HR: 2.78, 95% CI: 1.41-5.46), with a median TTF of 3.9 months (95% CI: 2.8 – 7.3) versus 15.1 months (95% CI: 7.3 – NA). The one-year TTF rate differs between 15.7% and 60.2%.

Conclusion

We could validate the effect of a processing escape phenotype on patients survival and outcome after ICB. The determination of processing escapes revealed a clear trend for both shortened TTF and OS after ICB in

the processing escape group. We could show the negative impact through selection of mutations leading to non-immunogenic epitopes on patients response to ICB. This has to be considered for further adaptations of diagnostic processes to overcome therapy resistance.

P11 Postersitzung Molekularpathologie

P11.01

Laser microdissection (LMD) as a valuable tool for analyzing intratumoral molecular heterogeneity in colorectal cancer

N. Maag, A. Arndt, K. Steinestel

Bundeswehrkrankenhaus Ulm (BwKrhs Ulm), Institut für Pathologie und Molekularpathologie, Ulm, Germany

Background

Colorectal cancer (CRC) is the third common cause of death from cancer. Oncogenic driver mutations in *RAS/RAF* oncogenes are frequent in CRC. However, the presence of different subclones within a single tumor can lead to treatment failure regarding anti-EGFR-directed antibody therapies. The identification of different subclones and their mutational profiles within a single tumor and the analysis of morphologically distinct tumor areas might help to unravel novel aspects of tumor biology and therapy resistance. Here, we used laser microdissection (LMD) to investigate tumor heterogeneity in CRC.

Methods

We established LMD and purified DNA from several morphologically distinct tumor areas (n=13) in CRCs from two patients and compared the results from routine testing with our newly established LMD approach. LMD enables the comparative analysis of small tumor areas by cutting histologically selected elements under microscopic control using a laser beam.

Results

In some cases, potential low level mutations (PLLM) could not be detected using the routine method of manually dissecting the tumor area since they were either masked by high level mutations (HLM) or wildtype sequence. Using the LMD method enabled the identification of concomitant PLLM in *NRAS* and *BRAF* genes of the identical patient sample. It could be shown that the LMD technique successfully circumvented technical limitations of the routine method and enabled the microscopic selection and collection of small tumor areas with differential morphology. This approach allowed for a highly selective concentration of PLLM from local areas within a large tumor mass rather than an overlay of mutations from different areas of the tumor. The analysis of one CRC patient showed an area with wildtype *KRAS* in close proximity to a *KRAS*-HLM area in the primary tumor and wildtype *KRAS* in a metastasis tissue sample from the same patient.

Conclusion

In summary, LMD improved spatial resolution in the molecular analysis of CRC tumor tissue compared to routine methods. Our results confirm the presence of molecular heterogeneity in CRC that should be kept in

mind when interpreting sequencing results, since low frequency mutations can have an impact on the effectiveness of targeted therapy.

Identification of a tumor-based protein biomarker panel to predict the time to recurrence for intrahepatic cholangiocarcinoma

T. Werner^{1,2,3}, K. L. Budau¹, K. Kurowski¹, M. Cosenza Contreras^{1,3,4}, N. Pinter¹, M. Werner¹, C. Sigel⁵, L. Tang⁵, P. Bronsert¹, O. Schilling^{1,3}

¹Institut für Klinische Pathologie / Universitätsklinikum Freiburg, Freiburg, Germany, ²Spemann Graduate School for Biology and Medicine (SGBM), Freiburg, Germany, ³Faculty of Biology / University of Freiburg, Freiburg, Germany, ⁴MelnBio Graduate School, Freiburg, Germany, ⁵Department of Pathology / Memorial Sloan Kettering Cancer Center, New York, United States of America

Background

Pathological classification of intrahepatic cholangiocarcinoma (iCCA) remains challenging, given this cancer's inaccessibility to diagnostic probing and insufficient molecular characterization. Although iCCA frequently reappear after initial surgery, only few and imprecise tools are available to predict highly individual times-to-recurrence (TTR). In our study, we investigated a cohort of iCCA patients to characterize proteomic profiles, which could be used as predictive markers for the TTR.

Methods

We macrodissected 80 tumor samples and measured via liquid-chromatography mass-spectrometry (LC-MS/MS) based proteomics in data independent acquisition mode (DIA).

Results

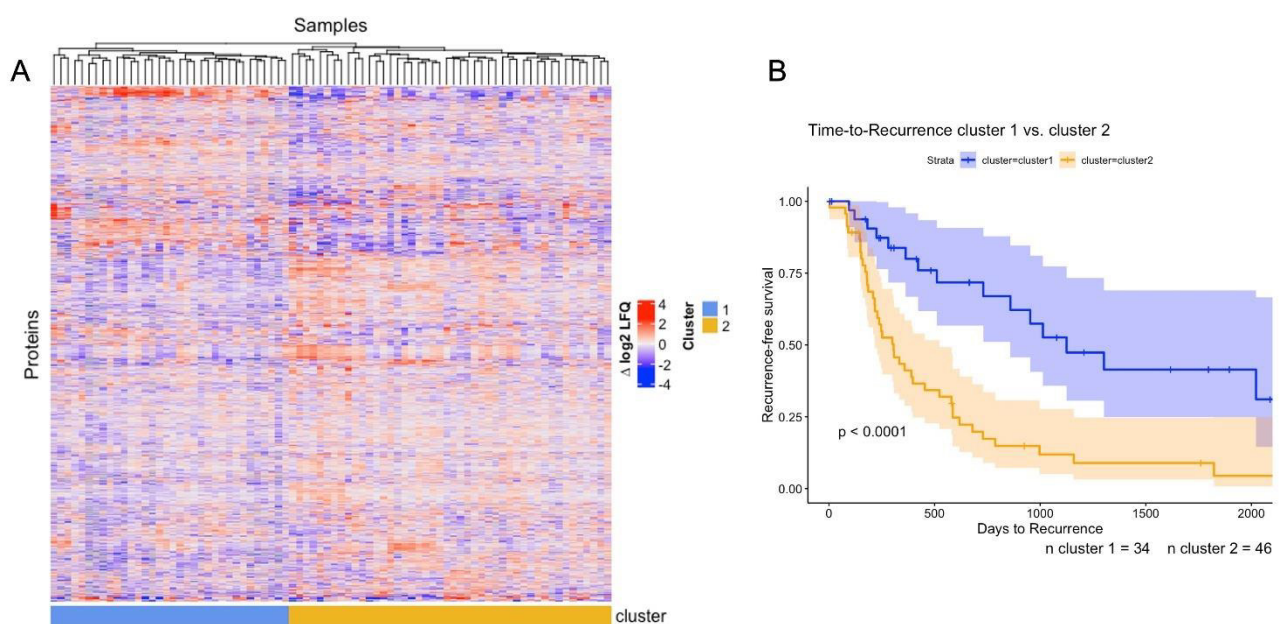


Figure 1: Heatmap of hierarchical clustering result (A) and comparison of recurrence-free survival between both clusters (B)

In a hierarchical clustering analysis, we could define two patient subgroups, which showed significantly diverging TTR distributions. Enrichment analysis revealed extracellular matrix (ECM) constituents to be upregulated in cluster 1, which is associated with a beneficial prognosis, and increased RNA and protein synthesis and processing in cluster 2. In a second, independent analysis, we iteratively applied Cox' proportional hazards model (CPHM) to identify single proteins whose expression correlates with TTR distribution. Gene set enrichment analysis of protein hits with a positive hazard ratio, which indicates increased risk for early recurrence, revealed an involvement in cell cycle advancement, and RNA and protein biosynthesis. Conversely, proteins associated with low hazard ratios and low risk were mostly linked to the ECM.

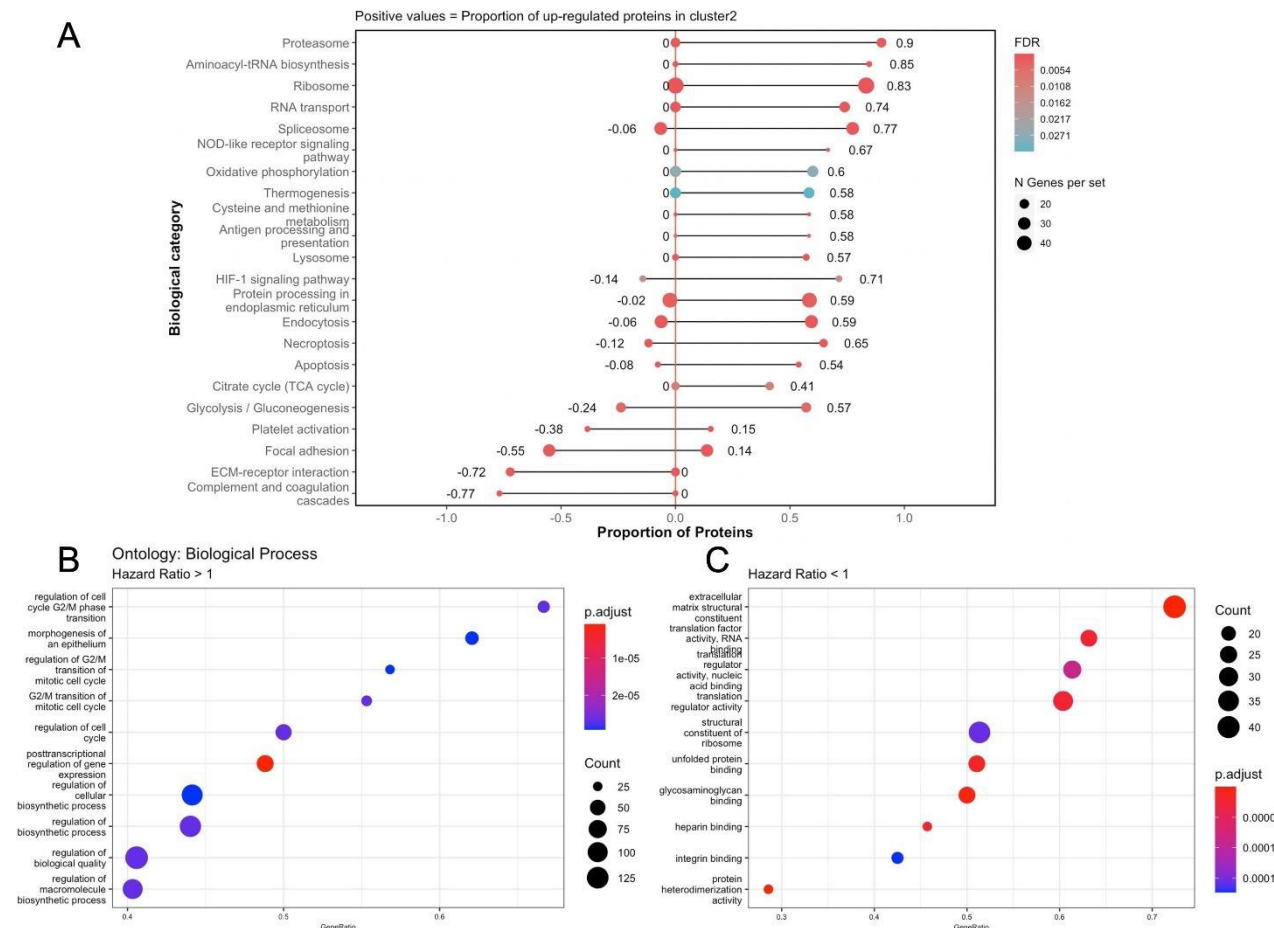


Figure 2: Gene Ontologies of differentially regulated proteins among cluster 1 and 2 (A) and of low (B) and high-risk (C) protein hits from CPHM

Conclusion

A comparison of significant protein hits from both approaches revealed largely identical proteins were detected as determinants of the TTR, with ECM proteins playing a particular role in disease progression. Six of these proteins were selected as a marker candidate panel to estimate the TTR. These include cluster1 / low risk associated proteins Vitronectin, Biglycan, and Histone 1.0, and cluster 2 / high risk related proteins SKI, Fructose-bisphosphate aldolase A, and L-lactate dehydrogenase, all of which will be further validated via immunohistochemistry and a second, independent iCCA cohort.

Literaturangaben

- [1] Banales et.al., (2020), Cholangiocarcinoma 2020: the next horizon in mechanisms and management, Nature Reviews Gastroenterology and Hepatology, 557-588, <http://dx.doi.org/10.1038/s41575-020-0310-z>
- [2] Kelley et.al., (2019), Systemic therapies for intrahepatic cholangiocarcinoma, Journal of Hepatology, 353-363, 2, <https://doi.org/10.1016/j.jhep.2019.10.009>

[3] Gillet et.al., (2016), Mass Spectrometry Applied to Bottom-Up Proteomics: Entering the High-Throughput Era for Hypothesis Testing, Annual Review of Analytical Chemistry, 449-472, <https://www.annualreviews.org/doi/10.1146/annurev-anchem-071015-041535>

P11.03

Isotachophoresis in comparison to bead based extraction of nucleic acids from FFPE tissue and its use for routine diagnostics.

R. Pappesch, S. Merkelbach-Bruse

Uniklinik Köln, Pathologie, Köln, Germany

Background

Extraction of nucleic acids can be time-consuming, labor-intensive and limited in terms of overall throughput. Semi-automated processes were the key for high throughput, which is most important for implementation in routine diagnostics. However, there are still problems regarding sample yield when it comes to formalin-fixed paraffin-embedded (FFPE) small biopsies. Recent years have brought advances in next generation sequencing (NGS) for detection of genomic aberrations. Nevertheless, some extraction methods cannot provide the quality and quantity of nucleic acids necessary for downstream applications. In this study, 12 samples were either extracted with a bead based extraction method (Promega, Madison, USA) or with an Isotachophoresis based method (Purigen Biosystems, Pleasanton, USA). with regard to implementation in routine diagnostics.

Methods

For DNA, RNA or TNA isolation, three to six sections of 10 µm thickness were cut from FFPE tissue blocks and compared in terms of concentration and usability for downstream applications. For the bead-based method, we used either the Maxwell 16 FFPE Tissue RSC RNA Purification Kit, the FFPE Tissue LEV DNA Purification Kit (Promega) on the Maxwell RSC or 16 Instrument (Promega) following the manufacturers protocol. For the Isotachophoresis-based method, we sent the same amount of material to Purigen and they used either the FFPE to pure DNA, FFPE to pure RNA or the FFPE Complete Kit on the Ionic Purification System (Purigen). For preparing libraries the FusionPlex® Lung for Illumina® (ArcherDX) panel and a custom GeneRead DNAseq Targeted Panel V2 (Qiagen, Hilden, Germany) panel have been used.

Results

Isotachophoresis based extraction delivered a higher yield out of small biopsies in comparison to the bead based system. There were no problems in preparing NGS libraries, and both methods delivered NGS results in equal quality. Comparing protocols, the extraction methods need approximately the same amount of time for extraction. However, where the Ionic Purification System is able to only extract 8 samples in one run or 4 for TNA extraction, the Maxwell system can manage up to 16 samples.

Conclusion

Both systems are capable to provide high quality nucleic acids for downstream applications in a sufficient amount. However, Isotachophoresis is a promising alternative for small biopsies and therefore should be considered in routine diagnostics.

Tryptic peptide mass spectrometry imaging of solid tumors via reproducible data analysis workflows

M. Föll^{1,2}, M. Stillger^{1,3}, L. Moritz¹, V. Volkmann¹, K. Enderle-Ammour¹, A. Frey¹, M. Dieterle¹, K. Wilhelm⁴, D. Guo², O. Vitek⁵, A. Jud⁶, S. Fichtner-Feigl⁶, M. Werner^{1,7,8}, P. Hönscheid^{7,9}, P. Bronsert^{1,7,8}, O. Schilling^{1,7}

¹University Medical Center Freiburg, Institute of Surgical Pathology, Faculty of Medicine, Freiburg, Germany, ²Northeastern University, Khoury College of Computer Sciences, Boston, United States of America, ³University of Freiburg, Faculty of Biology, Freiburg, Germany, ⁴University Medical Center Freiburg, Center for Surgery, Department of Urology, Faculty of Medicine, Freiburg, Germany, ⁵Northeastern University, Khoury College of Computer Sciences, Boston, Germany, ⁶University Medical Center Freiburg, Department of General and Visceral Surgery, Faculty of Medicine, Freiburg, Germany, ⁷German Cancer Consortium (DKTK) and Cancer Research Center (DKFZ), Heidelberg, Germany, ⁸University Medical Center Freiburg, Tumorbank Comprehensive Cancer Center Freiburg, Freiburg, Germany, ⁹University Hospital Carl Gustav Carus, Institute Pathology, Dresden, Germany

Background

Mass spectrometry imaging (MSI) enables the measurement of tryptic peptides directly from thin tissue sections of formalin-fixed and paraffin-embedded (FFPE) tissues archived at pathologies. MSI allows studying solid tumors in a spatially resolved manner and thus gives new insights into tumor biology by measuring intra-tumor heterogeneity and the spatial composition of the tumor microenvironment. Furthermore, it classifies tissues according to tumor subtype or prognostic measures. For tryptic peptide MSI experiments, typically interactive proprietary software is used, which hinders reproducible data analysis.

Methods

We previously established a comprehensive suite of MSI data analysis tools in the open source bioinformatic cloud platform Galaxy (<https://usegalaxy.eu>). From the modular tools standardized workflows can be assembled. Workflows as well as complete analysis histories can be shared in Galaxy and meet the criteria of FAIR (findability, accessibility, interoperability, and reusability) research data. We have used Galaxy to analyze tryptic peptide MALDI-TOF imaging datasets of 39 urothelial carcinoma, >50 pancreatic cancer and 6 colorectal cancer patients.

Results

Based on the tryptic peptide distribution and composition, tissues in the urothelial carcinoma dataset could be classified with high accuracy into tumor and surrounding stroma tissues as well as into muscle-infiltrating and non-muscle infiltrating urothelial cancers. Immunohistochemistry confirmed an increased histone H2A abundance in the tumor compared to the stroma tissues and increased vimentin and decreased cytokeratin 7 in muscle-infiltrating vs. non-muscle infiltrating urothelial carcinomas. In the pancreatic cancer experiment, two tumor subtypes, pancreatic ductal adenocarcinoma and endocrine pancreatic cancers could be discriminated with a classification accuracy above 80%. In primary colorectal cancers and patient matched liver metastasis, organized intratumor heterogeneity was discovered by MSI but both entities showed high degree of similarity and no evidence of metastasis forming clusters could be found. By sharing the complete analysis histories in Galaxy and additionally the raw data via the PRIDE repository when publishing, we make our MSI studies fully reproducible and transparent and advocate open science.

Conclusion

Tryptic peptide MSI on FFPE tissues in combination with reproducible data analysis workflows set the foundation for research and future clinical applications in pathology.

Pan-cancer in silico analysis of the Tripartite family members (TRIM)

K. Duan¹, A. Weingart¹, A. Offermann¹, S. Perner^{1, 2, 3}

¹Luebeck University Hospital Schleswig-Holstein, Institute of Pathology, Lübeck, Germany, ²University Medical Center Hamburg-Eppendorf, Department of Oncology, Hematology and Bone Marrow Transplantation with Division of Pneumology, Hamburg, Germany, ³Research Center Borstel - Leibniz Lung Center, Pathology, Borstel, Germany

Background

Intracellular protein degradation via molecular processes including ubiquitination plays a pivotal role in various biological processes. The tripartite motif-containing (TRIM) protein family as part of the ubiquitin system has been gradually associated with tumors in recent years. Aim of this study was to investigate the relationship between the expression and genetic status of the TRIM family genes and the outcome of diverse cancer types.

Methods

mRNA expression data of 21 tumor entities from the TCGA were used. Differential expression genes (DEGs) analysis between tumor and normal tissues was performed by using edgeR package (R language). After obtaining patient survival information, Univariate Cox Regression (UCR) analysis, Receiver Operating Characteristic (ROC), Area Under Curve (AUC), and Grouped Survival (GS) analysis was performed. Kaplan-Meier curves were generated for significant differentially expressed TRIMs. In the end, the genomic alteration profile of TRIM family members was obtained from cBioPortal and analyzed.

Results

The TCGA dataset comprises 65 TRIM family members. In general, mRNA alterations of TRIMs are tumor-specific. Glioblastoma and pancreatic adenocarcinoma contain most and least differential expressed TRIMs, respectively. TRIM59 was over-expressed in 15 tumor entities, whereas TRIM63 was under-expressed in 9 tumor entities. 18 TRIMs have the potential to predict patient's endpoint events. Our analysis revealed a quite heterogenic alteration profile of both higher and lower expressed TRIMs displaying genetic alteration frequencies ranging from 0% to almost 22%. Strikingly, the the amplification frequency of TRIM59 in squamous cell carcinomas of diverse regions (cervical, head and neck squamous, lung) as well as in endocervical and esophageal adenocarcinoma exceeded 10%, and correlated highly significantly with an increase in mRNA expression.

Conclusion

This pan-cancer study revealed the association between the gene expression of TRIM family members and carcinogenesis, combined with patient prognosis and genomic alterations. The results of this analyses

provide a solid foundation for further research on whether TRIM family proteins can be used as novel prognostic markers or therapeutic targets for various cancer entities.

Peptide Mass Spectrometry Imaging (MSI) of Pancreatic Cancers and the Application of a Powerful and User-friendly Analysis Pipeline

M. N. Stillger^{1, 2}, M. C. Foell¹, M. P. Dieterle³, M. Werner^{1, 3}, P. Hoenscheid⁴, P. Bronsert^{1, 3, 5}, O. Schilling^{1, 3, 6}

¹*Institute for Surgical Pathology, Freiburg im Breisgau, Germany*, ²*Faculty of Biology - University of Freiburg, Freiburg im Breisgau, Germany*, ³*Faculty of Medicine, Albert-Ludwigs-University of Freiburg, Freiburg im Breisgau, Germany*, ⁴*Institute Pathology, University Hospital Carl Gustav Carus, Technical University Dresden and National Center for Tumor Diseases Partner Site Dresden, Dresden, Germany*, ⁵*Core Facility for Histopathology and Digital Pathology, University Medical Center, Freiburg im Breisgau, Germany*, ⁶*German Cancer Consortium (DKTK) and German Cancer Research Center (DKFZ), Heidelberg, Germany*

Background

Mass Spectrometry Imaging (MSI) allows analyzing tissue specimens for the spatial distribution of hundreds of biomolecules such as proteins, peptides, lipids and metabolites. It's a powerful tool for clinical pathology as it can assist in generating diagnoses and prognoses via the measurement of molecular and morphological tissue properties. The frequent pancreatic ductal adenocarcinomas (PDAC) show limited therapy options and patients suffer from late diagnosis due to vague symptoms. The rather rare endocrine pancreatic cancers (PNET) are further subdivided into several subtypes, which mostly show better prognosis than PDAC. We applied MSI of peptides to identify m/z features distinguishing between PDAC and different PNET subtypes including more and less aggressive subtypes. Using open source analysis tools that were previously implemented in the Galaxy environment, we established a powerful analysis pipeline that provides an easy to handle user interface and complies to guidelines for reproducible and transparent analyses.

Methods

We performed MSI on a cohort of PDAC and diverse PNET cases aiming at identifying spatial peptide clusters, which define the specific tumor areas and distinguish between PDAC and PNET. FFPE specimens of ~150 patients were assembled in 13 TMAs and measured on a rapifleX device (Bruker Daltonics). Data analysis was performed using MSI data analysis packages implemented in the Galaxy environment. To perform supervised classification analysis, tumor regions were annotated and filtered with an established co-registration pipeline.

Results

First analysis, focussed on the data preprocessing and quality assessment revealed a good data quality and identified ~ 750 m/z features that were used for supervised classifications. The classifier distinguishing PDAC and PNET showed an accuracy above 85 % and consisted of ~ 150 m/z features to define PDAC and PNET. By the aid of LC-MS/MS data, we want to identify the m/z features of interest and report the corresponding peptides.

Conclusion

To conclude, we provide a powerful analysis workflow for transparent and reproducible MSI data analysis in Galaxy and show its applicability to a large clinical dataset. Furthermore, first results highlight the power of

MSI to study peptide profiles and establish a spatial classifier to distinguish between PDAC and PNET cancers using small FFPE tumor samples from TMAs.

Imipramine induces GSDME-mediated pyroptosis through upregulating NRP1

Y. Niu, M. Muders

University Hospital Bonn, Rudolf Becker Laboratory for Prostate Cancer Research, Center of Pathology, Bonn, Germany

Background

Pyroptosis is one form of inflammatory regulated cell death. The Gasdermin protein family are recently identified as the executors of pyroptosis by forming Gasdermin pores on the cytoplasmic membrane. Many chemotherapy agents and natural extracts have been shown to be able to induce pyroptosis. However, whether the tricyclic antidepressant imipramine takes part in pyroptosis induction remains unknown.

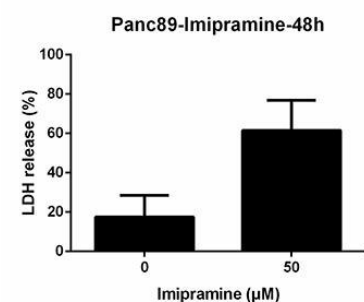
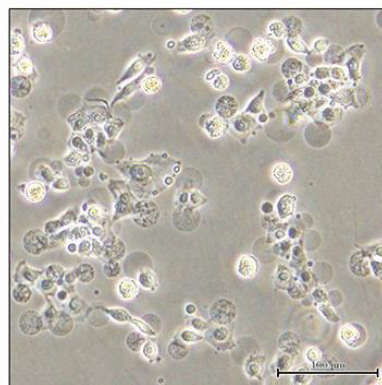
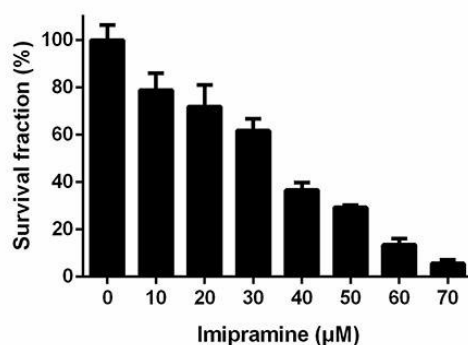
Methods

Cell survival was assessed by MTS assay. Pyroptosis was determined by cell morphological changes, lactate dehydrogenase (LDH) release, and the cleavage of gasdermin E (GSDME). Immunoblot and quantitative reverse transcription PCR (qPCR) were adopted to examine the expression of proteins and mRNAs, respectively.

Results

Imipramine inhibited the survival of Panc89 pancreatic ductal adenocarcinoma cells in a dose-dependent manner. Meanwhile, large bubbles formed by swollen cytoplasm and significantly enhanced LDH release were observed after 50 μ M imipramine treatment in Panc89 cells (Figure 1).

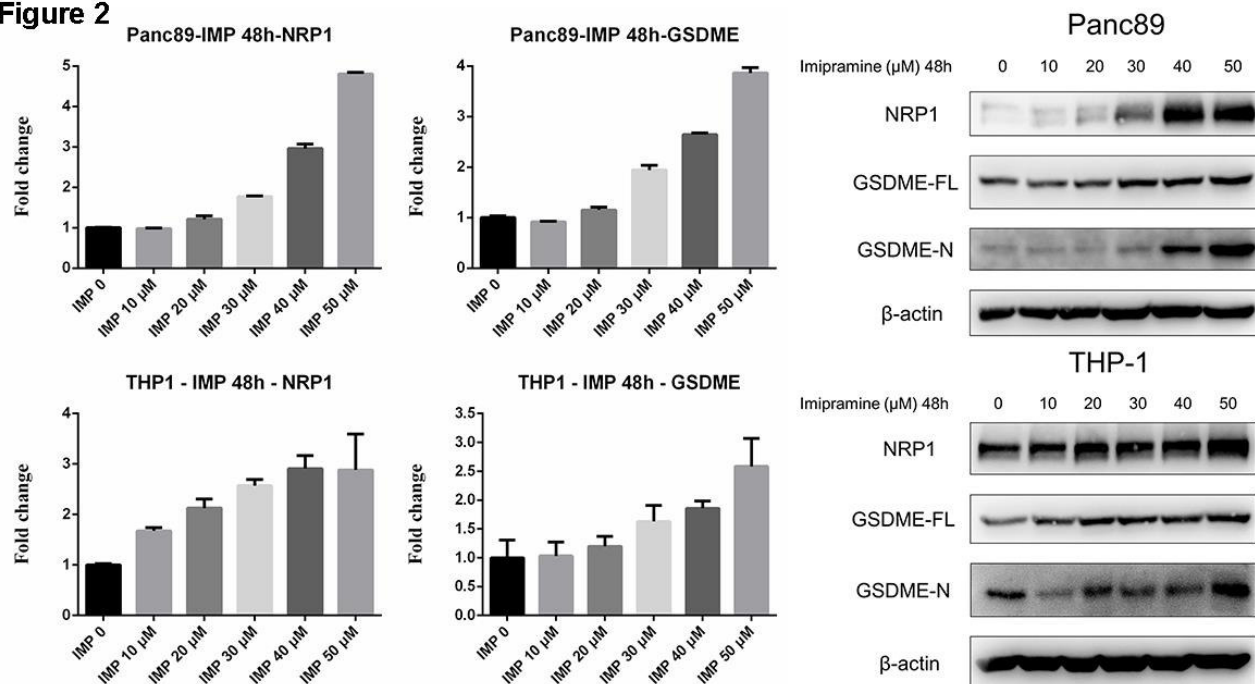
Figure 1 Panc89-Imipramine-48h



Imipramine induced pyroptotic cell death in Panc89 cells

Furthermore, we found that imipramine upregulated both mRNA and protein levels of GSDME, as well as the cleavage of GSDME, which is the evidence of pyroptosis. Interestingly, imipramine also improved the mRNA and protein level of neuropilin-1 (NRP1), which is a cell-surface receptor of semaphorins and VEGFs. Similar effects were also found in the PMA-treated THP-1 macrophages (Figure 2).

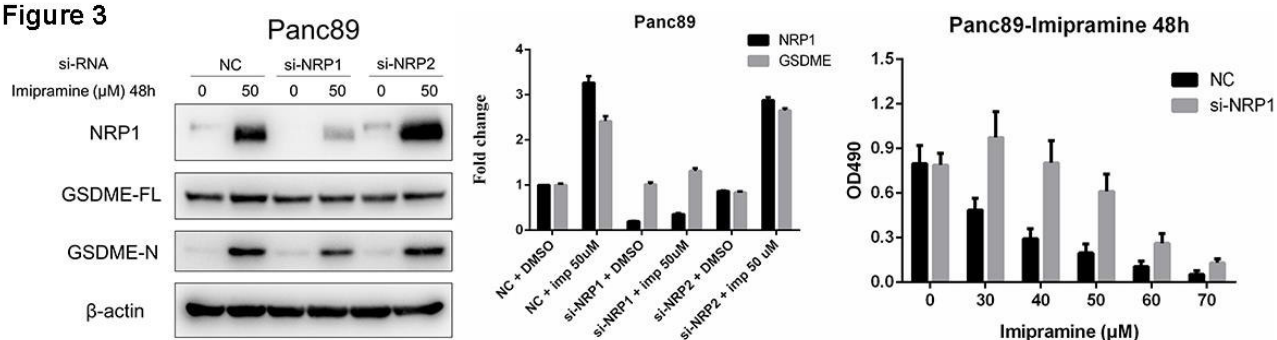
Figure 2



Imipramine promoted GSDME expression and cleavage, as well as NRP1 level

Next, we found that imipramine-induced increase of GSDME expression and cleavage was significantly suppressed by the knockdown of NRP1 using siRNA, but not by the knockdown of NRP2, the other member of the neuropilin family. Silencing NRP1 also suppressed the cell death induced by imipramine treatment (Figure 3).

Figure 3



NRP1 was involved in the GSDME-mediated pyroptosis induced by imipramine

Conclusion

Our study suggested that NRP1 might play an important role in the GSDME-mediated pyroptosis induced by imipramine.

Carcinoembryonic antigen-related cell adhesion molecule 6 (CEACAM6) promotes metastatic spread to the lung in advanced prostate cancer

A. Saraji¹, K. Hempel¹, J. Stegmann-Frehse¹, K. Duan¹, A. Offermann¹, R. Krupar², C. Watermann¹, D. Jonigk³, J. Kirfel¹, S. Perner¹, V. Sailer¹

¹*Pathology of the University Hospital Schleswig-Holstein, Campus Luebeck, Luebeck, Germany*, ²*Research Center Borstel, Leibniz Lung Center, Borstel, Germany*, ³*Institute of Pathology, Hannover Medical School, Hannover, Germany*

Background

Most patients with prostate cancer (PCa) will survive their disease, but in the event of metastatic spread treatment options are rare. Patients seldom develop lung metastases, therefore PCa lung metastases are insufficiently characterized and the molecular mechanisms that lead to lung metastases remain to be unraveled. We recently performed comprehensive transcriptome analysis of PCa lung metastases and identified carcinoembryogenic antigen cell adhesion molecule 6 (CEACAM6) as a potential driver of metastatic spread. Here, we show the biological significance of CEACAM6 in PCa cell proliferation and apoptosis.

Methods

CEACAM6 was silenced by siRNA in PC3 cells and western blot was used to determine CEACAM6 protein expression in PC3 cells. Furthermore, siRNA-*CEACAM6* PC3 cells were monitored *in vitro* for functional assessment including cell viability and proliferation assay by CCK8 method followed by measuring the ratio of apoptosis by performing caspase-3 assay. Non-treated and scrambled (scr) RNA PC3 cells were used as control.

Results

Following a specific knockdown of *CEACAM6* in PC3 cells, the expression of CEACAM6 protein was significantly decreased in comparison to scrambled RNA and untreated PC3 cells as controls (Fig.1 A-B). Furthermore, cell viability and cell counts decreased in CEACAM6 silent PC3 cells compared to untreated cells (Fig.2 A-B). In contrast, caspase-3 activity was highly elevated in siRNA-*CEACAM6* PC3 compared to controls (Fig.3).

Conclusion

CEACAM6 as a cell adhesion molecule has been implicated in promoting metastatic disease in several solid

tumors such as colorectal or gastric cancer. We recently showed that CEACAM6 is highly upregulated in PCa lung metastases and hence performed functional validation experiments to elucidate upon its role in PCa progression. Our findings show that CEACAM6 might play an important role in fostering metastatic spread to the lung of PCa patients via enhancing proliferation and suppressing apoptosis. CEACAM6 might therefore pose an attractive therapeutic target.

Literaturangaben

- [1] Siegel RL, et al., (2019), CA Cancer J Clin.
- [2] Ritch C et al., (2018), F1000Res.
- [3] Bubendorf et al., (2000), Hum Pathol.
- [4] Blumenthal RD et al., (2007), BMC Cancer
- [5] Rujian Zhu et al., (2019), Transl Androl Urol.

TMB in limited FFPE tissue specimens, pleural effusions and bronchoalveolar lavages of NSCLC cases

S. Wolter¹, G. Kayser¹, C. F. Waller², M. Werner^{1,3}, S. Laßmann¹

¹Universitätsklinikum Freiburg, Institut für Klinische Pathologie, Freiburg, Germany, ²Universitätsklinikum Freiburg, Klinik für Innere Medizin I: Hämatologie, Onkologie und Stammzelltransplantation, Freiburg, Germany, ³Deutsches Konsortium für Translationale Krebsforschung (DKTK), Partnerstandort Freiburg, Freiburg, Germany

Background

Tumor mutation burden (TMB) is a predictive biomarker read-out from NGS-based comprehensive genomic profiling. Here, we used the TSO500 panel (Illumina) in matched Formalin-fixed and Paraffin-embedded (FFPE) tissue specimens and pleural effusions (PE) and/or bronchoalveolar lavages (BAL) of non-small cell lung cancer (NSCLC) patients to explore low-input scenarios of routine molecular diagnostics.

Methods

This retrospective technical study included matched FFPE tissue specimens (n=10), PEs (n=7) and/or BALs (n=4) of ten NSCLC patients. Library preparation, sequencing (NextSeq550Dx) and data analysis (onboard-analysis using the TSO500 Local App) was performed according to Illuminas workflows. Resulting metadata and TMB values were correlated between matched NSCLC sample pairs.

Results

As expected from morphology and tumor cell content (10-80%), (tumor-) DNA yields were highly variable (2-367ng total DNA, no yield for 2 samples). Input amounts of 100ng, 40ng or <40ng (tumor-) DNA resulted in ranges of 1081-1491ng, 941-1325ng and 44-685ng library, respectively. Despite not passing every quality control, all libraries were further processed. Libraries generated from 100ng, 40ng and <40ng (tumor-) DNA, yielded 79-84MR, 73-87MR and 16-79MR passing filters, respectively. Total (tumor-) DNA input also directly affected median target coverage (100ng: 426-940x, 40ng: 125-485x, <40ng: 2-50x). Technically QC-valid TMB values were obtained in 18/21 samples, with 3 BAL sample failures. TMB values of matched pairs of FFPE tissue/PE (n=7 cases) and FFPE/BAL (n=1 case) showed different (>4Mut/Mb) TMB values in 6/8 cases and similar TMB values in 2/8 cases. Nevertheless, TMB was rated as "low" in all 6/6 cases with different TMB values and 1/2 cases with matched TMB values. Only 1/8 cases, displayed a matched sample concordant "high" (>10Mut/Mb) TMB value. Finally, TMB was "low" in the remaining 2/10 cases with only FFPE tissue samples.

Conclusion

This study* demonstrates feasibility of TMB measurement in different types of limited samples of NSCLC cases if morphological (tumor cell content) and technical factors influencing TMB measurement by the NGS workflow are considered. Besides widely accepted TMB measurement in tissue specimens, also pleural effusions, but not bronchoalveolar lavages, qualify as alternative material.

*Supported by a research grant of Bristol-Myers Squibbs.

P11.10

A comprehensive validation of targeted next-generations sequencing panels to detect gene fusions and variants, including MSI, in pan-tumor samples

M. Walker, M. Prinz, W. Weichert, N. Pfarr

Institute of Pathology, Technical University Munich (TUM), Munich, Germany

Background

Genomic alterations bear a growing meaning for an additional target in cancer treatment. Different molecular strategies exist to identify genomic alteration in tumor cells. Molecular approaches reaches from targeted hotspot gene regions, using conventional PCR and subsequent Sanger sequencing, to gene specific panels, using next-generations sequencing. Gene specific panels covers most known and therapeutically relevant alterations for a specific entity such as lung specific panel detecting alterations in *EGFR*, *BRAF* etc. Still, there is a crucial need of broader panels to enable detection of alternative mutations in a tumor entity. This additional information offers cancer patient to be treated with an Off-Label-Use drug, which was not considered so far for this specific tumor entity.

Methods

Here we tested two different broader NGS-based panels using Archer Anchored Multiplex PCR (AMP™) technology to identify gene fusions as well as variants including MSI on a pan-tumor level. The tested DNA-based panel includes 71 genes and MSI sites. The tested RNA-based panel includes 136 genes. Both panels are designed to work with difficult samples such as formalin-fixed, paraffin-embedded tissues. We tested samples derived from different tumor entities, including a variety of genomic alterations. Furthermore, we included samples with varying tumor cellularity to test the detections limit. We compared twenty-four FFPE samples for each tested panel to an in-house standard NGS-based method.

Results

Taken together, we detected all gene fusions with the tested RNA-based panel. One of two MET Exon 14 Skipping variants where not identified. All previously identified mutations using our standard NGS-based method could be confirmed using the DNA-based panel. The MSI/MSS status of almost all samples, except one, were concordant with the method used for comparison.

Conclusion

The tested RNA-based panel offers a good possibility to test not only for entity specific and already characterized gene fusions, but also uncharacterized or rare gene fusions. Additionally the fusion panel covers a broad range of fusions from a batch of different entities. The tested DNA-based panel provides the possibility to test mutation status as well as MSI/MSS status within one assay and furthermore, it covers most of the therapeutically relevant alterations in most cancer entities.

P11.11

Comparison of two distinct methods for the detection of *PIK3CA* somatic mutations in formalin-fixed and paraffin-embedded tissue of patients with breast cancer: Real-Time PCR versus Next-Generation Sequencing (NGS)

C. Schmitt¹, R. Schmitt¹, J. Jeroch², A. Jeute¹, P. Wild^{1, 2}, M. Demes^{1, 2}

¹*Dr. Senckenbergisches Institut für Pathologie, Universitätsklinikum Frankfurt, Molekularpathologie, Frankfurt, Germany,* ²*Universitätsklinikum MVZ GmbH - Wildlab, Molekularpathologie, Frankfurt, Germany*

Background

40 % of patients with hormone receptor (HR)-positive and human epidermal growth receptor 2 (HER2)-negative breast cancer harbour a mutation in *PIK3CA*. A *PIK3CA* gene mutation results in the constitutive activation of the enzymatic activity of the p110alpha subunit enabling growth factor-independent proliferation. Treatment with alpelisib–fulvestrant prolonged progression-free survival among patients with *PIK3CA*-mutated, HR-positive, HER2-negative advanced breast cancer who had received endocrine therapy previously. The detection of alterations in the Gen *PIK3CA* needs a valid method with a high sensitivity and specificity.

Methods

The DNA of 22 FFPE samples was extracted and analysed regarding the *PIK3CA* status. To verify the results obtained by the AmoyDx® *PIK3CA* Five Mutations Detection Kit, the NGS-based OCA v3 panel (ThermoFisher) was applied.

The results were compared in order to establish a valid, time-saving and cost-effective method in routine diagnostics. The AmoyDx® Real-Time PCR was performed on the LightCycler480II (Roche) and the OCA panel was analysed with the Ion S5™ system including the Ion Reporter™ software for variant detection and interpretation. Discrepant results were assessed by a third method.

Results

The respective results obtained by the AmoyDx® Assay and the OCA v3 Panel showed a good concordance. One AmoyDx® *PIK3CA* run may include a maximum of 10 samples. One OCA S5 run may contain a maximum of 14 samples. The AmoyDx® workflow has a much shorter turnaround time and is much cheaper as compared to the OCA S5 method.

Conclusion

We demonstrate consistent detection of *PIK3CA* somatic mutations with the AmoyDx Assay in genomic DNA extracted from FFPE material with a detection sensitivity of approximately 1-2% mutant allele fraction and validate these results using Next-Generation Sequencing. We propose this single gene analysis as a simple, fast and inexpensive diagnostic tool to determine the *PIK3CA* mutation status for the indication of an alpelisib therapy.

Towards Cohort-Wide Translational Proteome Studies: Reproducible Proteomic Workflows and Their Application to Skin and Cancer Diseases

M. Fahrner^{1, 2, 3}, C. Barbieux⁴, M. Bonnet des Claustres⁴, A. Jud⁵, M. Föll^{1, 6}, B. Grüning⁷, P. Bronsert^{1, 8, 9}, C. Zamboglou^{10, 11, 12}, H. Röst¹³, S. Fichtner-Feigl^{5, 11}, A. Grosu^{10, 11}, A. Hovnanian⁴, M. Werner^{1, 8, 9}, O. Schilling^{1, 11, 14}

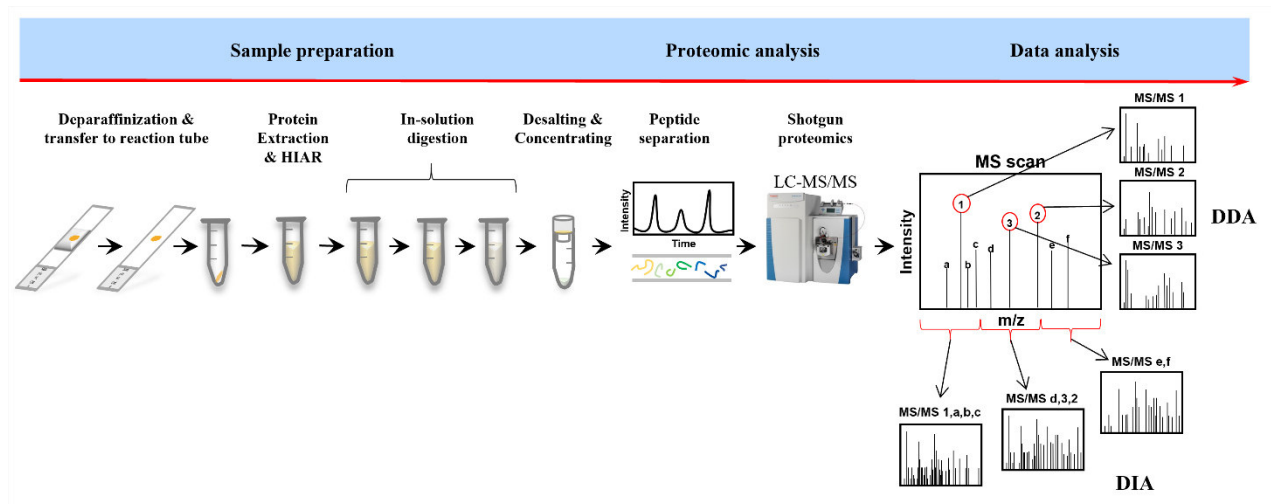
¹*Institute for Surgical Pathology, Medical Center – University of Freiburg, Faculty of Medicine, University of Freiburg, Freiburg, Germany,* ²*Faculty of Biology, Albert-Ludwigs-University Freiburg, Freiburg, Germany,* ³*Spemann Graduate School of Biology and Medicine (SGBM), University of Freiburg, Freiburg, Germany,* ⁴*INSERM UMR 1163, Laboratory of Genetic Skin Diseases, Imagine Institute, Paris, France,* ⁵*Department of General and Visceral Surgery, Medical Center – University of Freiburg, Faculty of Medicine, University of Freiburg, Freiburg, Germany,* ⁶*Khoury College of Computer Sciences, Northeastern University, Boston, United States of America,* ⁷*Department of Computer Science, University of Freiburg, Freiburg, Germany,* ⁸*Tumorbank Comprehensive Cancer Center Freiburg, Medical Center - University of Freiburg, Freiburg, Germany,* ⁹*Core Facility Histopathology and Digital Pathology Freiburg, Medical Center - University of Freiburg, Freiburg, Germany,* ¹⁰*Department of Radiation Oncology, Medical Center - University of Freiburg, Faculty of Medicine, University of Freiburg, Freiburg, Germany,* ¹¹*German Cancer Consortium (DKTK) and German Cancer Research Center (DKFZ), Freiburg, Germany,* ¹²*German Oncology Center, European University of Cyprus, Limassol, Cyprus,* ¹³*Donnelly Centre, University of Toronto, Toronto, Canada,* ¹⁴*BIOSS Centre for Biological Signaling Studies, University of Freiburg, Freiburg, Germany*

Background

Molecular pathology largely relies on Genomic and Transcriptomic approaches for comprehensive and sensitive translational studies. Continuous instrument and method development in quantitative mass spectrometry-based proteomics enable reproducible in-depth proteome investigations in a variety of patient-derived samples, including body fluids and tissue specimens. This has paved the way for the more recently emerged field of clinical proteomics, focusing on the thorough analysis of the proteome composition and alteration thereof in a variety of diseases.

Methods

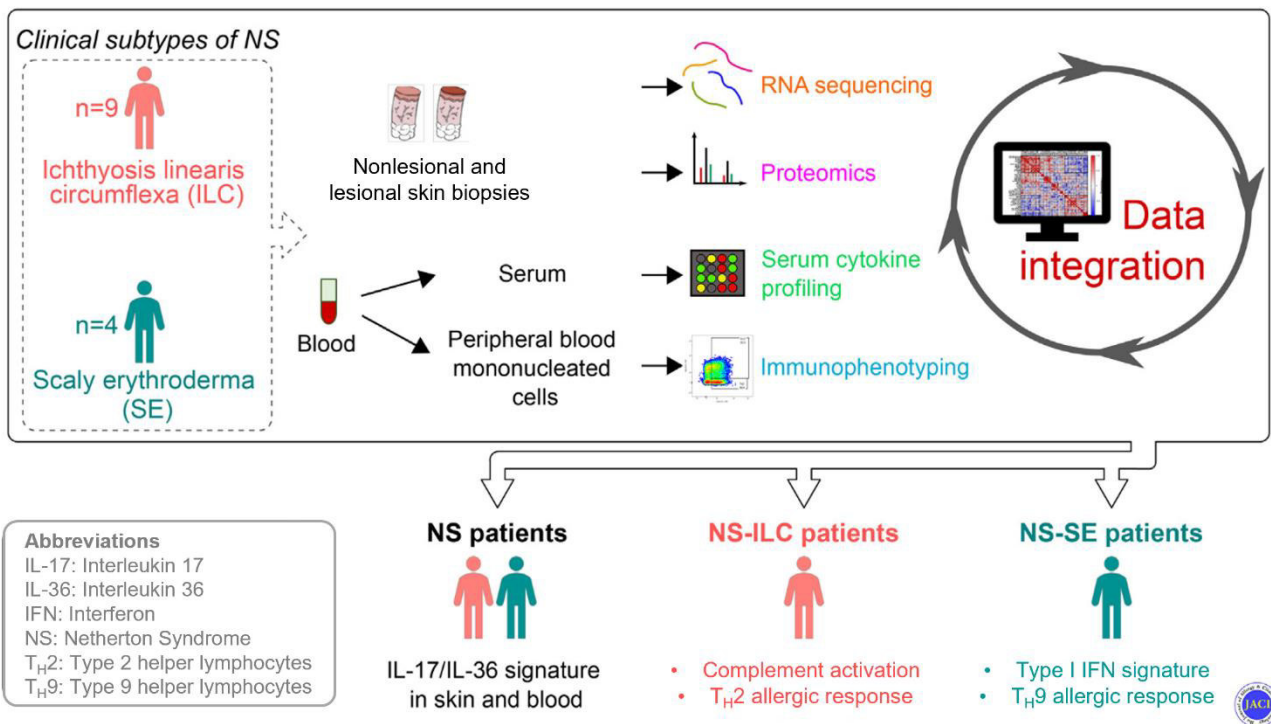
We applied MS-based quantitative proteomic workflows to perform cohort-wide translational proteomics in different malignancies and the rare skin disease Netherton syndrome.



Quantitative mass spectrometry-based proteomics using patient-derived tissue specimens.

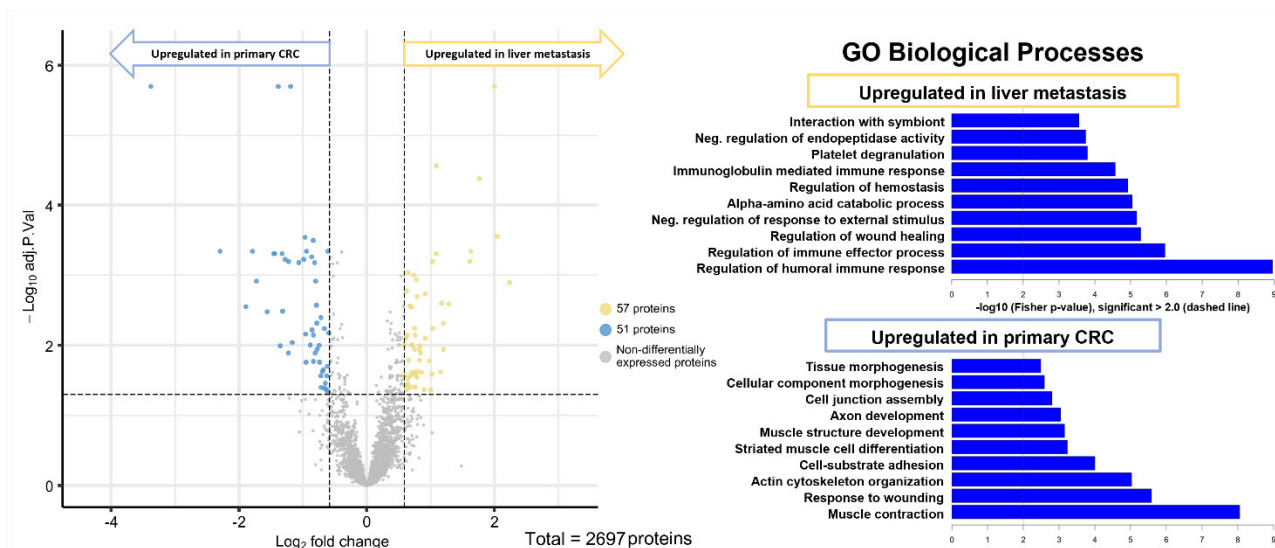
Results

A multi-omics approach reveals a shared immune signature in Netherton syndrome and distinct allergic responses between two clinical subtypes for which this study proposes a pathophysiologic model that paves the way towards novel therapeutic targets and improved medical treatment [1].



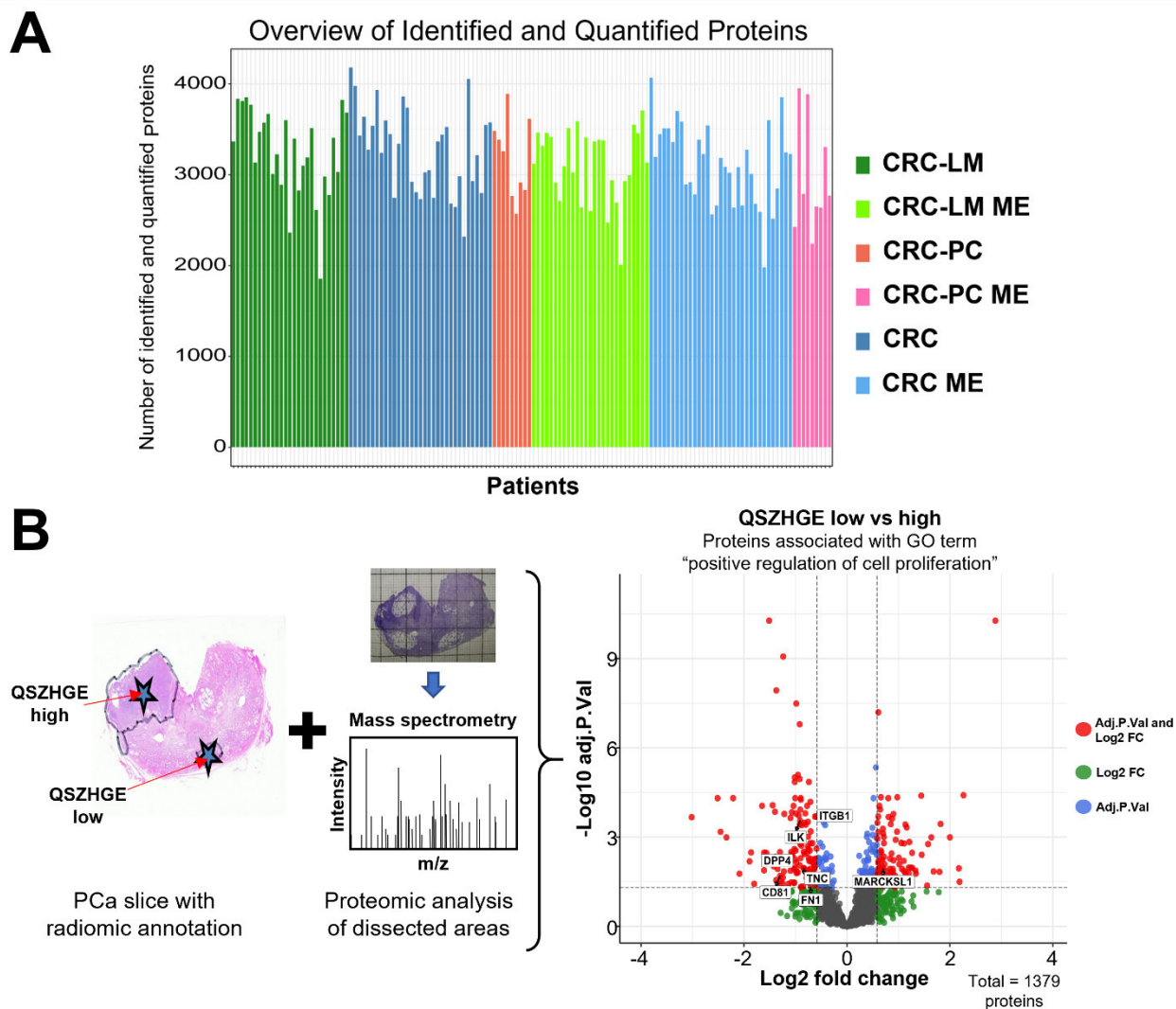
Netherton syndrome (NS) subtypes share IL-17/IL-36 signature with distinct type I IFN, Th2 and Th9 allergic responses.

A pilot study investigating metastasizing colorectal carcinoma (CRC) revealed distinct proteome fingerprints pointing to an enhanced immune response in the liver metastases as compared to the primary CRC [2].



Translational proteome study reveals distinct proteome biology in primary CRC and corresponding liver metastasis.

We performed further translational proteomics to investigate metastasizing CRC (including tumor microenvironment) and the correlation of radiomic features with localized protein profiles in prostate cancer.



(A) Number of identified proteins in the in-depth proteomic analysis of metastasizing CRC. (B) Radioproteomic research in prostate cancer, correlating localized protein profiles with extracted radiomic features.

Conclusion

We contributed robust translational proteomic workflows to advance molecular and pathobiological understanding in a variety of diseases. This technology bears great potential for applications in molecular pathology.

Literaturangaben

[1] Claire Barbieux, Mathilde Bonnet des Claustres, Matthias Fahrner, Evgeniya Petrova, Lam C. Tsoi, Olivier Gouin, Florent Leturcq, Pascale Nicaise-Roland, Christine Bole, Vivien Béziat, Emmanuelle Bourrat, Oliver Schilling, Johann E. Gudjonsson, Alain Hovnanian, (2021), Netherton syndrome subtypes share IL-17/IL-36 signature with distinct IFN-alpha and allergic responses., *Journal of Allergy and Clinical Immunology*, <https://doi.org/10.1016/j.jaci.2021.08.024>

[2] Matthias Fahrner, Peter Bronsert, Stefan Fichtner-Feigl, Andreas Jud, Oliver Schilling, (2021), Proteome biology of primary colorectal carcinoma and corresponding liver metastases., *Neoplasia*, <https://doi.org/10.1016/j.neo.2021.10.005>

P11.13

Subcellular mitochondrial alterations in hepatocytes and brown adipose tissues from ChREBP knock out mice during long term choline deficient diet

M. Yasser, H. Leiner, F. Dombrowski, S. Ribback

Universitätsmedizin Greifswald, Institut für Pathologie, Greifswald, Germany

Background

Carbohydrate-response-element-binding protein (ChREBP) emerged as central metabolic-regulator [1]. It expressed abundantly in liver & brown adipose tissue (BAT), acts also as master regulator for lipid-metabolism [2] & could play an active role in diet specific disorders or NAFLD (non-alcoholic-fatty-liver-disease) [2]. Choline recognized as essential nutrient because of its wide-ranging roles in human-metabolism & its deficiency is reasoned to have impact on liver disease [3].

Here, we studied long-term choline deficiency effect on ChREBP-knockout (KO), liver specific ChREBP KO (ACF) & C57Bl/6J (wild type, WT) in our CD-HFD (choline-deficient-high-fat-diet) mouse model. We destined to investigate mitochondrial structural conditions by transmission-electron-microscopy (TEM) for determining metabolic differences in our mouse model. Since, ChREBP act as lipogenic regulator, thus investigating ChREBP-background-effect on energy metabolism could be one of NAFLD pathogenetic mechanisms & aid our understanding in metabolic mitochondrial dysfunction.

Methods

Liver tissues were examined by histology & TEM. 48-week-old male C57Bl/6J WT, KO & ACF mice (n=3/group, body weight>20g) were anesthetized & abdominally perfused.

Liver & BAT from interscapular (iBAT) & supraclavicular (scBAT) regions was taken & fixed in 1% osmium tetroxide, ethanol gradient-dehydrated, embedded in epoxy-resin & sectioned by Leica ultratome. These 500-750nm semi-thin-sections were stained with H&E & toluidine blue for light-survey. While ultrathin sections (70-90nm) stained with uranyl acetate & examined by Libra-120 electron microscope (Carl-Zeiss).

Results

Our preliminary results found that, mitochondria from scBAT of ACF mouse have a vesicular-swollen appearance with disorganization & rupture of cristae compared to WT. Also, mitochondria from ACF liver have bundles of separated cristae & electron-dense deposits. Interestingly, Megamitochondria formation were also observed in ACF mouse livers. Remaining mouse groups analysis together establishing status of UCP1 (mitochondrial uncoupling protein-1) that acts as main thermogenesis modulator & its downstream targets by RT-PCR & western is ongoing.

Conclusion

Mitochondrial matrix regulation & permeability transition is essential for maintaining energy homeostasis. Any changes in structural integrity have stimulatory effect on cell metabolic requirements & leads to metabolic diseases. Thus, it's enthralling to study mitochondrial-morphometric-parameters in liver & BAT samples.

Literaturangaben

[1] Nuernberger V, Mortoga S, Metzendorf C, Burkert C, Ehricke K, Knuth E, Zimmer J, Singer S, Nath N, Karim M, Yasser M, Calvisi D, Dombrowski F, Ribback S, (2021), Hormonally Induced Hepatocellular Carcinoma in Diabetic Wild Type and Carbohydrate Responsive Element Binding Protein Knockout Mice, Multidisciplinary Digital Publishing Institute (MDPI), Cells, 2787, 10, <https://doi.org/10.3390/cells10102787>, Institut for Pathologie, University of Greifswald, Greifswald, Germany

[2] Daniel PV, Mondal P, (2020), Causative and sanative dynamicity of ChREBP in Hepato-Metabolic disorders, Elsevier, European Journal of Cell Biology, 151128, <https://doi.org/10.1016/j.ejcb.2020.151128>, Indian Institute of Technology Mandi, India

[3] Zeisel SH, Da Costa KA, (2009), Choline: an essential nutrient for public health, Oxford University Press Oxford, UK, Nutrition reviews, 615--623, <https://doi.org/10.1111/j.1753-4887.2009.00246.x>, Department of Nutrition, University of North Carolina, NC, USA

P12 Postersitzung Kinder- und Fetalpathologie

P12.01

Intrauterine fetal demise in extensive SARS-CoV-2-associated placental maternal vascular malperfusion in the setting of SARS-CoV-2 placentitis

M.-L. Eich¹, T. Menter², N. F. Mokwa³, B. Grüttner³, A. M. ... Müller⁴

¹Uniklinik Köln, Pathologie, Köln, Germany, ²Universitätsspital Basel, Pathologie, Basel, Switzerland, ³Uniklinik Köln, Klinik für Frauenheilkunde und Geburtshilfe, Köln, Germany, ⁴Uniklinik Köln, Praxis für Pathologie/Zentrum für Kinderpathologie an der Uniklinik Köln, Köln, Germany

Background

Recently an increasing numbers of reports about SARS-CoV-2 associated intrauterine fetal demise or neonatal deaths were reported in the literature. Most common findings compromise combination of maternal and fetal malperfusion, villitis and/or intervillitis.^{1,2}

Methods

Macroscopic and microscopic of the placenta was performed including standard morphology and immunohistochemistry. Furthermore PCR analysis of the placental tissue was conducted.

Results

Clinical history

A 36 years old patient was admitted to the delivery room with premature labor at 31 weeks of gestation. Three weeks before she has been infected with SARS-CoV-2 suffering only from mild symptoms. Ultrasound showed a mild hydrops and no fetal heart actions. As she had suffered from two previous abortions. Thrombophilia diagnostics were conducted before the pregnancy showing heterocygous factor VII deficiency.

Pathological findings

Macroscopic evaluation showed a 303 g and 23 x 12 x 2 cm measuring placenta. Microscopically the placental parenchyma was subtotally infarcted, showed fibrin deposits, extensive trophoblast necrosis, and intervillous thrombus. Vital areas showed an infiltrate with CD68-positive macrophages.

Immunohistochemically, syncytiotrophoblasts were positive for SARS-CoV-2 S-Antigen und N-Antigen. Furthermore, a C4d activation could be proven.

Placental swab and PCR of the placental parenchyma, umbilical cord and amnion-chorion membrane

showed SARS

Conclusion

We report a case of a placenta with extensive maternal vascular malperfusion, chronic histiocytic intervillitis and trophoblast necrosis corresponding to SARS-CoV-2-placentalitis^{1,2} in context of fetal demise at 31 weeks of gestation. Maternal vascular malperfusion has been described in cases of SARS-CoV-2 infection, however the manifested severity of this case in the setting of a severe SARS-CoV-2-placentalitis in a patient with only mild SARS-CoV-2-infection is rare. It emphasizes the need of a maternal prophylactic anticoagulation also in cases of mild courses of disease.

Adrenocortical carcinoma (ACC) in an infant with Cushing's syndrome and virilization

S. Turial¹, H. Krause¹, F. Meyer², M. Zenker³, D. Jechorek⁴, A. Redlich⁵

¹Universitätsklinikum Magdeburg A.ö.R., Abteilung für Kinderchirurgie, Klinik für Allgemein-, Viszeral-, Gefäß- und Transplantationschirurgie, Magdeburg, Germany, ²University Hospital, Dept. of General, Abdominal, Vascular and Transplant Surgery, Magdeburg, Germany, ³Universitätsklinikum Magdeburg A.ö.R., Institut für Humangenetik, Magdeburg, Germany, ⁴Universitätsklinikum Magdeburg A.ö.R., Institut für Pathologie, Magdeburg, Germany, ⁵Universitätsklinikum Magdeburg A.ö.R., Kinderhämатologie-onkologie, Universitätskinderklinik, Magdeburg, Germany

Background

Aim: To describe the rare case of an infant with ACC including its typical clinical signs and pitfalls in diagnostics and therapy based on **i)** the clinical management experiences obtained in the clinical care and **ii)** selective references from the scientific medical literature.

Methods

Scientific case report

Results

Case:

- *Medical history*: Eight-months old girl was presented with virilization based on Cushing's syndrome.
- *Diagnostics*: By initial hormonal assessments, a non-circadian-rhythm excessive hypercortisolism and a decreased expression of corticotropin (ACTH) were identified. Imaging studies (cerebral and abdominal MRI, thoracic CT scan and abdominal ultrasound) displayed a right-side adrenal mass of approximately 5 cm in diameter. No metastases or further relevant pathologies were noticed.
- *Therapy*: Complete resection (R0) of the mass including lymphadenectomy was achieved by open adrenalectomy (preserving the affected kidney).
- *Clinical course*: Postoperative follow-up of 9 months was uneventful.
- *Further therapeutic consequences /outlook*: Due to only local ACC, R0 resection status and postoperative normalization of steroid profiles (COG stage I), there was no need for postoperative chemotherapy.

Conclusion

Preoperative biopsy, incomplete resection and intraoperative tumor spillage are associated with poor prognosis. Therefore, careful and complete surgical resection is valued to be the only potentially curative treatment for ACC. Preoperative metastatic spread of ACC is universally considered a highly unfavorable prognostic factor. In adrenal masses with signs of steroid hormone excess, attempts for taking a biopsy or puncture of the tumor mass are strictly to be avoided. Steroid profiling before surgery and preservation of tumor samples for the GPOH-“tumorbox” should be considered at the time of surgery to provide a “Liquid-biopsy” (ctDNA) for follow-up purposes. In terms of surgical approaches, the role of laparoscopic resection for ACCs remains controversial. In case of necessity for the postoperative chemotherapy, in Germany, the

NN1/NN2 protocol (according to the GPOH-MET) is recommended.

The adjuvant mitotane (pesticide, adrenocorticolytic agent) used for patients with COG stage III and IV disease seems to be the most beneficial medication.

Lipoblastoma as a representative example of rare soft tissue tumor lesions in infants with its challenging diagnostic and surgical management

S. Turial¹, H. Krause¹, A. Surov², D. Jechorek³, **F. Meyer⁴**, Z. Halloul⁵

¹Universitätsklinikum Magdeburg A.ö.R., Abteilung für Kinderchirurgie, Klinik für Allgemein-, Viszeral-, Gefäß- und Transplantationschirurgie, Magdeburg, Germany, ²Universitätsklinikum Magdeburg A.ö.R., Klinik für Radiologie und Nuklearmedizin, Magdeburg, Germany, ³Universitätsklinikum Magdeburg A.ö.R., Institut für Pathologie, Magdeburg, Germany, ⁴University Hospital, Dept. of General, Abdominal, Vascular and Transplant Surgery, Magdeburg, Germany, ⁵University Hospital, Division of Vascular Surgery, Dept. of General, Abdominal, Vascular and Transplant Surgery, Magdeburg, Germany

Background

Aim: To illustrate a rare case of a soft tissue tumor(Tu) mass of the right groin diagnosed as lipoblastoma based on specific references of the med. literature & the experiences obtained in the case-specific care

Methods

Scientific case report

Results

CASE: - *Med. history (hx)*: Swelling of the right groin increasing after physical activities. Fam. med. hx, breast Ca (grandmother).

- *Clin. findings*: 22-months-old girl with an elastic swelling of 2x3 cm in size at the right groin.

- *Diagnostics*: **1)** Lab parameters: White blood cell count, 11.1 (normal range, 3.7-9.8) Gpt/L.

2) US-guided Bx: Appropriate puncture specimen w/o complications

3) Histology: Lipomatous lesion w/ lipoblast-like cells & muscle tissue; Ki67-index, 1% (no MDM2 expression).

4) MRI revealed a partially liquid, partially fat-equivalent Tu-like lesion of 44x34x48 mm in size within the adductor group of thigh muscles occupying the medial myofascial compartment of the right leg incl. **i)** a finger-shaped tail up to the left hip (no intraarticular Tu extension) & like a Tu cone to the right obturator internus muscle, **ii)** displacement of the nerve & vessels to the lat. site w/ no hint for osseus infiltration, & **iii)** blood supply from the right common fem. artery (additionally, cystiforme ovarian lesion of 9x7 mm in size at the left side).

- *Therapy* (surg. intervention, 92 min): R0 resection (by pediatric & vasc. surgeons) of the mass w/ a gentle capsule (orienting Tu margin) incl. surrounding muscle fibers (for Tu-free resection margin), lymphadenectomy as part of the resected Tu conglomerate & additional excision of the dermal puncture site at the right groin (+ preserving all vessels)

- *Histol. investigation* (surg. specimen): Confirmation of lipoblastoma

- *Clin. course*: Postop. time period showed development of a wound seroma w/ fever prompting to surg. wound revision & initiation of antibiotics. After an episode of an infection of the upper resp. tract, a wound abscess needed to be surgically opened, at the init. phase with exposed vasc. segment of the right groin prompting for antiseptic wound dressing, later on treated with vacuum-assisted closure (VAC).

- *Further therap. consequences/outlook*: Regular clin. & US-based contr. investigations in an outpatient clinic setting & clin. data documentation in the "Soft Tissue Sarcoma Registry" (CWS-SoTiSar).

Conclusion

Careful & complete surg. resection is valued to be the only potentially curative treatment incl. continuous follow-up investigations (clin. finding & imaging controls).

Poster

P14 Postersitzung Informatik, digitale Pathologie und Biobanking

P14.01

Snomed CT – a promise for structured reporting and interoperability

T. Rüdiger¹, G. Haroske², S. Campbell³, J. Campbell⁴, L. Tutina⁵, I. Green⁵, Snomed CT Pathology and Laboratory Medicine Clinical Reference Group

¹*Städtisches Klinikum Karlsruhe, Pathologie, Karlsruhe, Germany*, ²*Berufsverband Deutscher Pathologinnen und Pathologen, Kommission Digitale Pathologie, Berlin, Germany*, ³*Department of Pathology and Microbiology, Omaha, United States of America*, ⁴*University of Nebraska Medical Center, Internal Medicine, Omaha, United States of America*, ⁵*Snomed International, London, United Kingdom*

Background

Interoperability is the ability of different information systems to cooperatively access data to treat patients more efficiently. Pathology reports provide crucial data about many disorders and guide treatment. To make pathology reports interoperable, they need to be bound to a reference terminology that can be understood, also by a machine.

Snomed CT could serve as a reference terminology, that is expressive and granular enough to be used in primary documentation. Snomed CT was acquired by the German Ministry of Health in 2020 and is a major building block in the concept of the Medizininformatik-Initiative.

The key element of Snomed CT is the concept. A concept represents an idea in medicine. Every idea must be represented by one and only one concept, thus the representation is unequivocal. In addition to a unique concept identifier, descriptions are assigned, each representing a synonym for the same idea. Relationships link concepts to other concepts whose meaning is related. These relationships provide formal definitions and other properties of the concept. In addition to hierarchical (is-a) relationships, attribute relationships represent other aspects of the meaning of a concept e.g., a disorder to its finding site.

In addition to such precoordinated concepts, Snomed CT provides a compositional grammar to build postcoordinated expressions that refine concepts by additional attributes and their values. From a point of the formal representation, these are equivalent to precoordinated (predefined) concepts and can be used to define finely granular data in a report.

The OWL description logic allows to represent the relationships in a form that inferences can be made and used by computer software.

Methods

Based on ICCR cancer protocols, the possibilities are evaluated to represent the content in Snomed CT, such building an interoperable representation of the pathology report.

Results

Snomed CT provides the expressional richness and granularity to serve as basis for interoperable reports. Some vocabulary is missing to adequately describe all specimens. In addition, Snomed CT can provide a foundation to contextually access knowledge resources in a structured way.

Conclusion

The Pathology and Laboratory Medicine Clinical Reference Group of Snomed CT will address gaps in the terminology to allow Snomed CT to both be used in reports and in the workflow of pathology.

Deep learning quantified stroma and lymphocyte are independent predictors for overall survival in pancreas cancer

X. Tan^{1,2}, M. Rosin¹, S. Appinger¹, B. Grootkoerkamp³, L. Häberle^{4,5}, G. Wiltberger^{1,5}, M. Doukas⁶, I. Esposito^{4,5}, U. P. Neumann^{1,5,7}, L. R. Heij^{1,5,6,8}

¹University Hospital RWTH Aachen, Department of Surgery and Transplantation, Aachen, Germany, ²Maastricht University, NUTRIM School of Nutrition and Translational Research in Metabolism, Maastricht, The Netherlands, ³Erasmus MC Cancer Institute, Department of Surgery, Rotterdam, The Netherlands, ⁴University Hospital Duesseldorf, Institute of Pathology, Duesseldorf, Germany, ⁵Center for Integrated Oncology Aachen Bonn Cologne Duesseldorf (CIO ABCD), Duesseldorf, Germany, ⁶Erasmus MC Cancer Institute, Department of Pathology, Rotterdam, The Netherlands, ⁷Maastricht University Medical Center, Department of Surgery, Maastricht, The Netherlands, ⁸University Hospital RWTH, Institute of Pathology, Aachen, Germany

Background

Stroma in percentage (SIP) has proved to be a potential predictive marker for patients in pancreatic cancer (PDAC). However, assessment of SIP can be discrepant between pathologists. The application of a deep learning method in routine digital slides provides a novel opportunity for pathological assessment of SIP.

Methods

We applied our image pipe-line, utilized on a U-Net model, on clinical data from 4 cohorts, total amount of patients 800. SIP and lymphocyte in percentage (LIP) were predicted. Categories were classified into SIP-low, SIP-intermediate and SIP-high. Categories for LIP: LIP-low and LIP-high. Our main outcome was the 5-year overall survival (OS) predicted by SIP and LIP.

Subgroups:

group 1: SIP-intermediate and LIP-high

group 2: SIP-intermediate and LIP-low or SIP-Low and High and LIP-high, not both subgroups in optimal condition

group 3: SIP-Low and High and LIP-low

Results

Total accuracy reached 83.23%: average accuracy for tumor prediction 89.57%, lymphocyte prediction 75.54%, and stroma prediction 81.97%. The predicted SIP and LIP were prognostic factors in PDAC patients. In each cohort, SIP-intermediate or LIP-high had a better 5-year OS compared to the groups with worse outcome, as well as in the results for all the cohorts.

The Aachen cohort (AC), patients in group 1 (n=58) showed a median 5-year OS of 28 months (95% CI: 25–39), and group 2 (n=125) showed 19 months (95% CI: 15–22) and group 3 (n=61) showed 11 months (95% CI: 7–13 (p < 0.001 log rank)). The Duesseldorf cohort (DUS), showed a median 5-year OS of 31 months (95% CI: 22–44) in group1 (n=36), 18 months (95% CI: 16–25) in group2 (n=68) and 9 months (95% CI: 7–12) in group 3 (n=73 (p < 0.001 log rank)). The Rotterdam cohort (EMC), showed a median 5-year OS of 33

months (95% CI: 27–58) in group 1 (n=19), 24 months (95% CI: 20–31) in group 2 (n=51) and 15 months (95% CI: 12-17) in group 3 (n=67 ($p < 0.001$ log rank)). The TCGA cohort, showed a median 5-year OS of 35 months (95% CI: 23–59) in group 1 (n=27), 18 months (95% CI: 16–24) in group 2 (n=37) and 8 months (95% CI: 5-12) in group 3 (n=28 ($p < 0.001$ log rank)).

Conclusion

We identify SIP as an important novel prognostic biomarker in PDAC patients, demonstrating the intermediate stroma group having a better outcome. This allows PDAC patient stratification for oncological outcome.

Comparison of manual and automated digital image analysis systems for quantification of cellular protein expression

T. Jagomast¹, C. Idel², L. Klapper¹, P. Kuppler¹, L. Proppe³, S. Beume³, M. Falougy⁴, D. Steller⁴, S. Hakim⁴, A. Offermann¹, M. C. Roesch⁵, K.-L. Bruchhage², S. Perner¹, J. Ribbat-Idel¹

¹*Institut für Pathologie, Universität zu Lübeck, Lübeck, Germany*, ²*Klinik für Hals-, Nasen- und Ohrenheilkunde, Universität zu Lübeck, Lübeck, Germany*, ³*Klinik für Gynäkologie, Universität zu Lübeck, Lübeck, Germany*, ⁴*Klinik für Kiefer- und Gesichtschirurgie, Universität zu Lübeck, Lübeck, Germany*, ⁵*Klinik für Urologie, Universität zu Lübeck, Lübeck, Germany*

Background

Quantifying protein expression in immunohistochemically stained histological slides is an indispensable tool for oncologic research. The use of computer-aided evaluation of immunohistochemically stained slides contributes to objectify measurements. However, some programs rely on manual digital image analysis meaning the region of interest must be annotated by the user. Others have built-in machine learning algorithms that enable workflows with automated digital image analysis and automatically detect the region of interest. We aimed to verify if software supporting automated digital image analysis would produce results that match with software employing manual digital image analysis.

Methods

Cancer patient cohorts of tissue microarrays were immunohistochemically stained. To consider different distributions of staining within cellular sub-compartments and tumor architectures the study encompassed nuclear and cytoplasmatic markers as well as adenocarcinomas and squamous cell carcinomas. Focusing on cancer cells we quantified the chromogenic intensity and calculated the positive index using manual and automated digital image analysis. We then investigated if the data derived from the two programs were reasonably comparable and amended our findings in the context of a biomarker study.

Results

Within all cohorts, we were able to show a high correlation for the chromogenic intensity between manual and automated digital image analysis with Pearson correlation coefficients >0.9 ($p < 0.001$). The measurements for the positive index revealed high agreement. Moreover, we could show that the cell detections of the programs were comparable as well and both proved to be sufficiently exact when compared to manual counting. Regarding the realized biomarker study, we were able to reproduce all significant clinical findings with both procedures.

Conclusion

Manual and automated digital image analysis show a high correlation regarding immunohistochemistry data acquired from different tumor architectures. The two workflows proved to be suitable to stratify patients for evaluation with clinical data in a biomarker study. Automated digital image analysis might be preferable as it is time-saving and can be easily reproduced. Therefore, it might accelerate biomarker research and enable high throughput approaches to be processed in less time.

Results have been published: DOI: 10.14670/HH-18-434

A machine learning approach to classify whole slide images by formalin-fixed paraffin-embedded or frozen section origin

L. Dan, J. Israel, S. R. Sarker, F. Stögbauer, W. Weichert, K. Steiger, P. Schöffler

Technical University of Munich, München, Germany

Background

The development of artificial intelligence (AI) in pathology often requires large-scale datasets of digital pathology slides. Therefore, many pathology departments digitize their archives retrospectively. However, these archives can host slides that are unlabeled or mislabeled regarding their fixation type, which poses a problem for the quality of datasets. For example, frozen section (FS) slides provide lower tissue quality than formalin-fixed, paraffin-embedded (FFPE) slides, and thus need to be excluded from training data. At scale, this is mostly feasible with automatic classification.

We developed a new deep learning (DL) algorithm for the automatic classification of FFPE and FS slides in order to increase the quality of future training datasets in computational pathology. Although initially developed for pancreatic tissue slides, we show that our model can be transferred to other tissues without loss in performance.

Methods

Our dataset consists of 24 training, 4 validation and 16 test slides of pancreatic cancer cases and 92 additional test slides across 15 other topographies, resulting in overall 71 FS and 65 FFPE slides, each scanned at 40x magnification (0.25 μm /pixel).

From each training slide, 2500 tissue patches (500x500 px) were extracted ignoring image artifacts such as pen marks and tissue folds. Patches were then used to fine-tune a pretrained VGG-19 convolutional neural network. The trained model was then evaluated on the hold-out test set. Moreover, to investigate the transferability to other organs, the model was tested on slides with mixed topographies.

Results

On the 16 pancreatic test slides, we achieved an accuracy of 98.92% and an AUC of 0.9886 at tile level, and an accuracy of 100.0% at slide level. Applied to the 92 mixed test slides, the classifier scored an accuracy of 97.46% and an AUC of 0.9765 at tile level, and predicted all but one slide correctly (including 25 correctly predicted slides that were priorly mislabeled), corresponding to a slide level accuracy of 98.91%.

Conclusion

Our preliminary results indicate that this classification problem can be reliably solved using DL. Even though our model was trained on pancreatic slides, the stable performance across 15 other topographies implies that key features of FS/FFPE remain the same. Moving on, we will conduct further tests on larger datasets and perform re-training if needed.

Once the reliability of the classifier is verified, it can be integrated as a pre-processing step in computational pipelines.

Vascular remodeling is a crucial event in the early phase of hepatocarcinogenesis in rodent models for liver tumorigenesis.

M. Tulessin¹, R. S. J. Sarker¹, J. Griger², W. Weichert¹, K. Steiger¹, C. Mogler¹

¹*Technische Universität München, Institut für Pathologie, München, Germany*, ²*Technische Universität München, Institut für Molekulare Onkologie und Funktionelle Genomik, München, Germany*

Background

The investigation of hepatocarcinogenesis is one of the major fields of interest in the oncology research and rodent models are commonly used to unravel the pathophysiology of onset and progression of hepatocellular carcinoma (HCC). HCC is a highly vascularized tumor and vascular remodeling is one of the hallmarks in tumor progression. To date, only few detailed data exist about the vasculature and vascular remodeling in rodent models used for hepatocarcinogenesis. The aim of this study was, therefore, to perform a comprehensive characterization and comparison of the vasculature in mouse models used for hepatocarcinogenesis studies.

Methods

In this study, formalin fixed paraffin-embedded samples of 25 genetically engineered mice (GEMM) for liver tumorigenesis were used. The vasculature of hepatocellular carcinoma (HCC) and preneoplastic foci of cellular alteration (FCA) were comprehensively characterized by using immunohistochemistry techniques (CD31, Collagen IV, α SMA, Desmin and LYVE1). Computational image analysis was performed to evaluate selected parameters including microvessel density, pericyte coverage, vessel size, intratumoral vessel distribution and architecture using Aperio ImageScope software (Version 12.4.0.7018, Leica Biosystems) and Definiens software programs (Version XD 64 2.7, Definiens AG, Munich, Germany).

Results

262 FCA lesions and 36 HCC lesions were investigated so far. Analysis included microvessel density (MVD) using CD31 and Collagen IV stainings and pixel analysis of α SMA and Desmin as well as an analysis of LYVE1 staining. Furthermore, the size of the vessels were used to automatically define into 3 groups of vessels (small, medium and large). HCC presented with a significant lower number of vessels, but larger vessel size and increased coverage leading to a higher degree of maturation, whereas FCA lesions were presented with a higher microvessel density and a higher amount of smaller but more immature vessels.

Conclusion

Our results clearly demonstrate, that vascular remodeling is present in early stages of liver tumorigenesis making mouse models with a histological spectrum of FCA and HCC as an attractive tool for angiogenesis research.

Ex vivo fluorescence confocal microscopy on diagnostic ultrasound-guided core needle biopsies of the liver: A feasibility study from a tertiary hospital

M. N. Kinzler¹, N. Abedin¹, A. Tschäbunin², S. Gretser², F. Schulze², A. A. Schnitzbauer³, S. Zeuzem¹, P. J. Wild^{2, 4}

¹Department of Internal Medicine I, University Hospital Frankfurt, Goethe University Frankfurt am Main, Frankfurt am Main, Germany, ²Dr. Senckenberg Institute of Pathology, University Hospital Frankfurt, Goethe University Frankfurt am Main, Frankfurt am Main, Germany, ³Department of General, Visceral, Transplant and Thoracic Surgery, University Hospital Frankfurt, Goethe University Frankfurt am Main, Frankfurt am Main, Germany, ⁴Wildlab, University Hospital Frankfurt MVZ GmbH, Frankfurt am Main, Frankfurt am Main, Germany

Background

Ex vivo fluorescence confocal microscopy (FCM) is a rapidly emerging tool providing virtual H&E images of native tissue in real time. This method has been established in dermatohistological examinations and is currently extended to further organ tissues. Preliminary data concerning the suitability of FCM for precise diagnosis in liver specimens were recently published. However, data reporting reliable information about macro- and micro-vesicular steatosis of liver parenchyma remain scarce so far. First, we therefore aimed to investigate the potential of FCM micro-imaging technique in our tertiary hospital to assess different levels of steatosis in both core needle biopsies and surgical specimens with regard to its feasibility in the context of liver transplant surgery where a timely feedback on the extent of macro-vesicular steatosis is of special interest. The second aim of this study was to evaluate the time from biopsy to final FCM image acquisition in the raw clinical setting of a university hospital.

Methods

Thus, we determined the time required from ultrasound-guided core needle biopsies in the Department of Internal Medicine to histopathological assessment of the digital scan.

Results

Our results indicate FCM as a suitable technique precisely representing different levels of steatosis compared to conventional histology. In contrast to 24h within the routine diagnostic, digital scans can be reliably obtained < 10 minutes after ultrasound-guided liver biopsy. Here, we used the VivaScope 2500M-G4 (VivaScope, Munich, Germany) for FCM image acquisition. FCM images were compared to conventional histology by an expert hepatobiliary pathologist. Pre-treatment of the native tissue with 70% ethanol and acridine orange (fluorescent dye) did not alter the conventional downstream diagnostic including immunohistological staining and molecular pathology like next-generation sequencing. Adequate amounts of DNA could be extracted from both native and FFPE tissue.

Conclusion

In conclusion, we provide real world data about FCM as a fast, precise and reliable method to histopathological assess liver specimens in the context of transplant surgery and ultrasound-guided biopsies.

The Explainability Paradox: Challenges for xAI in Digital Pathology

T. Evans¹, C. O. Retzlaff¹, C. Geißler¹, M. Kargl², M. Plass², H. Müller², T.-R. Kiehl³, N. Zerbe³, A. Holzinger²

¹*Technical University of Berlin, DAI-Labor, Berlin, Germany*, ²*Medical University Graz, Graz, Austria*, ³*Charité – Universitätsmedizin Berlin, corporate member of Freie Universität Berlin and Humboldt- Universität zu Berlin, Institute of Pathology, Berlin, Germany*

Background

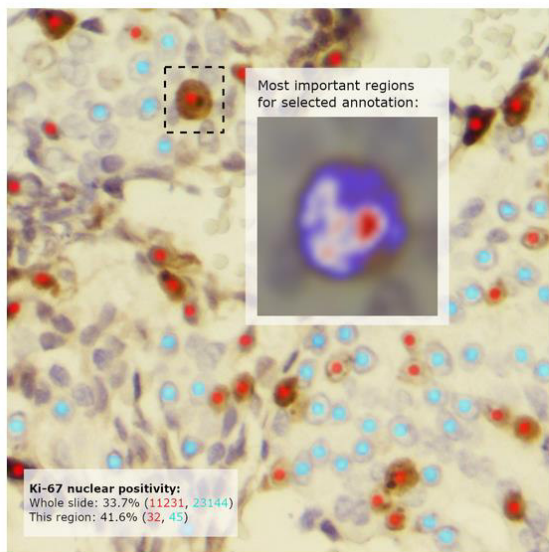
Explainability is identified as a critical component for the safety, approval and acceptance of AI systems for use in pathology [cui2021]. Despite the cross-disciplinary challenge of building explainable AI (xAI), few user-centric studies in this domain have been carried out [antoniadi2021].

We conducted the first mixed-methods study of user interaction with state-of-the-art explainability methods in digital pathology, revealing challenging dilemmas faced by developers of xAI systems, and proposing empirically-based principles for their safe and effective design.

We present a summary of this research, as recently published in the Future Generation Computer Systems Special Issue on Explainable AI for Healthcare.

Methods

Data was gathered in parallel from a structured online questionnaire and semi-structured expert interviews, and analyzed using a grounded theory-based methodology.



Hide explanation

Local saliency map

Show the most relevant pixels for the classification of a selected annotation

I find the explanation intuitively understandable *

Strongly disagree 1 2 3 4 5 6 7 Strongly agree

The explanation helps me to understand factors relevant to the algorithm *

Strongly disagree 1 2 3 4 5 6 7 Strongly agree

The explanation helps me to decide whether I can trust the generated annotations *

Strongly disagree 1 2 3 4 5 6 7 Strongly agree

The explanation provides me with valuable information for my work *

Strongly disagree 1 2 3 4 5 6 7 Strongly agree

Additional comments

Page 5 of 9

Previous

Next

An xAI example as presented to a study participant for evaluation

Results

The fast pace of routine work in pathology places a high premium on user interface elements that impose a minimal cognitive load. This in turn creates pressure for xAI methods to generate simple, user-intuitive explanations.

With their simplicity, such explanations bring with them a source of potential bias, as users resolve their inherent ambiguity based on prior beliefs and expectations. This creates the risk of instilling a false sense of confidence and/or unrealistic expectations of AI systems.

Conclusion

These results imply challenging balances to strike between user desiderata for medical xAI and the sources of bias that these are liable to introduce.

The decision to include explainability in AI systems should be treated critically, carefully weighing risk against requirement. Where xAI is deemed appropriate, explanations should be explicit rather than implicit, and developed in close feedback with users and other stakeholders.

Above all, our findings emphasize the importance of an interdisciplinary approach to xAI development and research, such that social and psychological aspects of the human-AI interaction can be accounted for, mitigated, and/or taken advantage of.

Literaturangaben

[antoniadi2021] Antoniadis, Anna Markella and Du, Yuhan and Guendouz, Yasmine and Wei, Lan and Mazo, Claudia and Becker, Brett A. and Mooney, Catherine, (2021), Current Challenges and Future Opportunities for XAI in Machine Learning-Based Clinical Decision Support Systems: A Systematic Review, MDPI, Applied Science, 11, <https://www.mdpi.com/2076-3417/11/11/5088/htm>

[cui2021] Cui, Miao and Zhang, David Y., (2021), Artificial intelligence and computational pathology, Nature, Laboratory Investigation, 412--422, 101, <https://www.nature.com/articles/s41374-020-00514-0>

Deep Learning in Pancreatic Tissue: Automatic identification of anatomical structures and diseases.

M. Kriegsmann¹, K. Kriegsmann², **G. Steinbuss**², C. Zgorzelski³, A. Hausen⁴, M. Gaida⁴

¹*Institut für Pathologie, Universitätsklinikum Heidelberg, Heidelberg, Germany*, ²*Universitätsklinikum Heidelberg, Innere Medizin V, Heidelberg, Germany*, ³*Institut für Pathologie, Universitätsklinikum Heidelberg.de, Heidelberg, Germany*, ⁴*Institut für Pathologie, Universität Mainz, Mainz, Germany*

Background

Identification of pancreatic tissue structures and reliable identification of ductal adenocarcinoma (PDAC) and precursor lesions in histological tissue slides can be challenging. Thus, the development of additional methods for the identification of anatomical and pathological tissue structures are desirable. Deep learning has been suggested to address this problem. Therefore we investigated if classification of different tissue structures, including PDAC and precursor lesions is possible by deep learning techniques.

Methods

We scanned and annotated tissue microarrays from 201 patients with PDAC. 81165 image patches were extracted and assigned to a training, validation and test cohort. A EfficientNet classifier was subsequently trained and optimized to detect 11 different tissue classes.

Results

Our algorithm achieved an accuracy of up to 92% on the test set after the introduction of a quality control threshold. SmoothGrad heatmaps were implemented for explainability of the algorithm. Results were successfully transferred to scanned whole slide images.

Conclusion

The application of deep learning approaches have great potential for routine diagnostics and research in pancreatic tissue, when conducted under the supervision of a trained pathologist.

Federated Learning for Breast Cancer Classification

U. Kurt, A. Kazi, N. Navab, P. Schöffler

Technical University of Munich, Computer Science, Munich, Germany

Background

In pathology, integration of external datasets is complicated due to data privacy and data sovereignty reasons. In addition to that, time and resource necessities of diagnosis require an artificial intelligence method to solve problems. In federated learning methods, data is not centrally collected and stored. Instead, a global model is trained and validated by sharing its parameters with the connected local dataset without sharing any sensitive information. In this work, we try to bring the concept of federated learning to digital pathology. We apply a federated learning model to a publicly available breast cancer classification BACH[1] and show the results for classification task.

Methods

As shown in Figure 1, Federated learning clients' trained weight information is then aggregated to improve the prediction capacity of the global model[2]. Thanks to that, individually learned information is also shared among all clients. A 2-client federated learning diagram can be seen in Figure 2.

For this project, we leverage ICIAR 2018 - BACH dataset. This dataset consists of 400 hematoxylin and eosin (H&E) stained breast histology microscopy images. Images divided into four different classes(normal, benign, in situ carcinoma, and invasive carcinoma) and an example image from each class can be seen by Figure 1. Each image of size 2048x1546 pixels is divided into twelve 512x515 pixels image patches then patches are resized to 512x512 pixels. Dataset was divided into training-validation-test datasets. Test dataset will be kept apart for only test purposes while clients are using training and validation datasets on training.

In the light of state-of-the-art image classification, ResNet101 and DenseNet121 models pre-trained on ImageNet were used as an ensemble model in this project.

Results

Overall accuracy is calculated by dividing the number of correctly predicted classes by the number of all images. Local model of client 1 showed an overall validation accuracy of 82.29%, and client 2 showed an overall validation accuracy of 78.75%. The final global model achieved an overall accuracy of 83.33% on hold test dataset.

Conclusion

The federated learning approach is a very promising technique to collect valuable information from multiple sites and create a global competence model without the necessity of any sensitive data sharing. Using more than two clients and including more different datasets for different clients will

be the next aims of this project for better simulation of the real-world situation.

Diagnosis of signet ring cell carcinoma of the upper gastrointestinal tract using deep learning

S. FörSCH, F. Hartmann, A. Fernandez, W. Roth

Universitätsmedizin Mainz, Institut für Pathologie, Mainz, Germany

Background

Bösartige Neoplasien des oberen Gastrointestinaltrakts sind häufig vorkommende Malignome und mit einer hohen Morbidität und Mortalität assoziiert. Eine besondere Herausforderung in der histopathologischen Diagnostik stellen Siegelringzellkarzinome bzw. diffuse Magenkarzinome dar. Hier könnten Verfahren der künstlichen Intelligenz (KI), insbesondere das Deep Learning (DL) dazu beitragen, die histopathologische Diagnostik entscheidend zu verbessern.

Methods

Zunächst wurde eine Kohorte von Patient*innen mit siegelringzellig differenzierten Magenkarzinomen zusammengestellt. Hiernach erfolgte die sorgfältige Annotation der tumorösen Areale, sowie weiterer Gewebebestandteile (Epithel, Immunzellen, Muskelgewebe, Fettgewebe). Anschließend wurde ein tiefes Konvolutionsnetzwerk auf die Erkennung dieser fünf verschiedenen Gewebebestandteile trainiert.

Results

Die Klassifikation der fünf verschiedenen Gewebebestandteile -inklusive von Arealen mit Siegelringzellen- gelang mit einer Gesamtgenauigkeit von knapp 97%. Die Fläche unter der Grenzwertoptimierungskurve lag bei 0,994, die unter der Präzisions-Recall-Kurve bei 0,990. Die Performanz war vergleichbar für alle fünf Klassen.

Conclusion

KI und DL ermöglichen die Erkennung von Siegelringzellkarzinomen und anderen Gewebebestandteilen mit guter bis exzellenter Genauigkeit. Wird ein Model wie von uns beschrieben in ein klinisches Unterstützungssystem integriert, kann dies hochwahrscheinlich dazu beitragen, die Befundung dieser schwierig zu diagnostizierenden Tumoren entscheidend zu verbessern. Eine solche Unterstützungsmöglichkeit wird in weitergehenden Studien systematisch evaluiert werden.

P14.11

Enabling stain independence for deep learning-based segmentation and quantification in kidney histopathology

N. Bouteldja¹, D. L. Hölscher¹, B. M. Klinkhammer¹, R. D. Buelow¹, J. Lotz², N. Weiss², C. Daniel³, K. Amann³, P. Boor^{1,4}

¹*Institute of Pathology, RWTH Aachen University Hospital, Aachen, Germany*, ²*Fraunhofer Institute for Digital Medicine MEVIS, Bremen, Germany*, ³*Institute of Pathology, University Erlangen, Erlangen, Germany*,

⁴*Department of Nephrology and Immunology, RWTH Aachen University Hospital, Aachen, Germany*

Background

Many image analysis applications in digital pathology require a large amount of annotated data to cope with various sources of variability in the image domain. Since manual data annotations are time-consuming, the desire for methods tackling variabilities with low efforts is increasing. In this work, we deal with the variability of using different histological stainings to depict molecular changes, since deep learning (DL) models are typically trained and thus applicable to only a single stain.

Methods

Here, we compare our proposed concept based on stain augmentation with two additional major methodologies including image registration and stain translation to enable a stain-independent analysis of an already existing, stain-specific DL model without manual overhead. That model segments six major renal structures from periodic acid-Schiff (PAS)-stained kidney tissue of various species.

Results

Validation on different immunohistochemical stainings in mice and humans showed that stain augmentation significantly outperformed all other methods. It demonstrated high segmentation performances for all structures in each stain, even in held-out stains not seen during training, that were also comparable to the original PAS performance. Applications in animal models and patient biopsies showed the feasibility of analyzing inflammation and fibrosis using compartment-specific quantifications of immunohistochemical stains.

Conclusion

Our benchmark study on stain independence in digital pathology suggests that stain augmentation is an effective and currently matchless technique to make DL models stain-independent without manual efforts. Applied to our segmentation model, it enables the association between molecular, anatomical, and structural information leveraging new possibilities for automated and extensive histomorphometry.

Nuclei Detection and Segmentation using Instance-Segmentation Networks

V. Ramakrishnan^{1,2}, L. Barragan³, J. Daza⁴, A. Artinger^{1,2}, T. Niedermair^{1,2}, T. Itzel³, P. Arbelaez³, A. Teufel⁴, C. Brochhausen^{1,2}

¹Institute of Pathology, University of Regensburg, Regensburg, Germany, ²Central Biobank Regensburg, University and University Hospital Regensburg, Regensburg, Germany, ³Center for Research and Formation in Artificial Intelligence (CinforIA), Universidad de Los Andes, Bogota, Colombia, ⁴Medical Clinic II - Medical Faculty Mannheim (UMM), Universität Heidelberg, Mannheim, Germany

Background

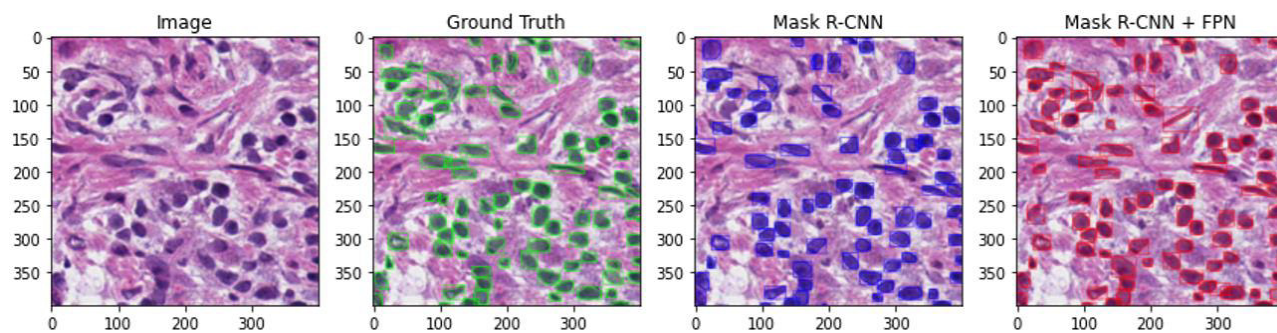
Computational pathology offers useful tools to examine cell nuclei, which are highly relevant for numerous pathologies. Nuclei detection is used to detect individual nuclei as separate objects, while semantic segmentation is used to identify nuclear boundaries. Currently, detection is achieved by using post-processing techniques like watershed segmentation on results of semantic segmentation networks. An instance segmentation network, which enables simultaneous detection and segmentation of nuclei using an end-to-end approach, is rarely used for this application. Here, we show that a popular instance segmentation network, a Mask R-CNN with Feature Pyramidal Network (FPN), can produce results comparable to the current state-of-the-art on semantic segmentation of nuclei along with simultaneously detecting them.

Methods

Kumar dataset is a public dataset with over 22,000 annotated nuclei in 30 training samples and over 8250 annotated nuclei in 14 validation samples (H&E images from seven organs: breast, liver, kidney, prostate, bladder, colon, and stomach). Each image is of a 1000x1000 resolution. Mask R-CNN is efficient in detecting fewer objects, which is why a patch-based analysis is first researched upon. To evaluate its performance, the FPN variant of a Mask R-CNN was trained on patches of the Kumar dataset using an Adam optimizer. Data augmentation techniques are used to consider rotation invariance and invariance due to blending parameters like contrast and saturation.

Results

After smart training and apt augmentation techniques on the FPN variant of Mask R-CNN, we observed a dice score of 83%, which exceeds the state-of-the-art dice score of 82.6% on the Kumar dataset. This highlights the fact that one can replace the commonly used semantic segmentation algorithms with an instance segmentation for nuclei detection due to its end-to-end trainable nature, eliminating the need for post-processing. This network can additionally identify occlusions in cell nuclei and analyze nuclear properties like number, area, and eccentricity.



Nuclei detection and segmentation using Mask R-CNN + FPN

Conclusion

The enhanced Mask R-CNN can accelerate research in digital pathology and might, in the future, be possibly integrated as a diagnostic tool to help pathologists in nuclear analyses in a user-friendly perspective.

Paving the way for cross-border biobank cooperation: The Bavarian-Czech Biobank Landscape Project

D. Seidler^{1, 2}, **M. Snitilá**^{1, 2}, J. Kinkorová^{3, 4}, O. Topolčan^{3, 4}, C. Brochhausen^{1, 2}

¹Universität Regensburg, Institut für Pathologie, Regensburg, Germany, ²Zentrale Biobank Regensburg, Regensburg, Germany, ³University Hospital Pilsen, Department of Immunochemistry, Pilsen, Czech Republic, ⁴Charles University and University Hospital Pilsen, Biobank of the Faculty of Medicine, Pilsen, Czech Republic

Background

International cooperation is essential for the exchange of experiences and for the scientific progress of biobanks and in precision medicine. The Central Biobank Regensburg and the Biobank of the Faculty of Medicine in Pilsen carried out various projects in the Bavarian-Czech area through the BRoTHER consortium, which have enormously supported the research in precision medicine of both partners. Aim of the present project was to establish a landscape of biobanks in Bavaria and the Czech Republic to support cross-border biobank-cooperation. The project was funded by the Bavarian-Czech Academic Agency.

Methods

The partners prepared a questionnaire that was sent out to the biobanks in Bavaria and the Czech Republic. The results provide an overview of the Bavarian-Czech biobank landscape and enable the start of a conversation about similarities and differences between the biobanks. In a digital reader, the biobanks are able to inform themselves about biobanks in the cross-border region and find partners for joint projects or knowledge exchange.

Results

Out of the 19 biobanks contacted, 14 responded with an interest in possible cross-border cooperation. The survey results were summarized and published in a 36-page reader that introduced the characteristics of every participating biobank. In this presentation of the biobanks, the individual institutions are introduced and it is shown how they are organized, which samples are stored and which storage facilities were used. The participating biobanks can thus get an overview of the biobanks in Bavaria and the Czech Republic and directly find the contact details of all biobanks. In a joint web meeting, the biobanks had the chance to talk about the project results and started networking.

Conclusion

The results of the project showed that most biobanks do not know a lot about the biobank-scene across the border. The biobanks acknowledged this lack of information and reported that a basis for networking is highly appreciated. The biobanks are mostly anchored in different national and international networks, but the contact to biobanks the neighboring regions is still to be established. The Bavarian-Czech Biobank Landscape project provided this basis for future cooperation. Getting to know and exploring the biobank-scene of both regions is the first step for a wide range of knowledge exchange, sample exchange and research projects that will enormously strengthen German-Czech cooperation in the field of high-

performance medicine.

3D Visualization of Blood Vessels

V. Ramakrishnan^{1,2}, R. Schoenmehl^{1,2}, F. Guertler^{1,2}, T. Niedermair^{1,2}, A. Artinger^{1,2}, C. Brochhausen^{1,2}

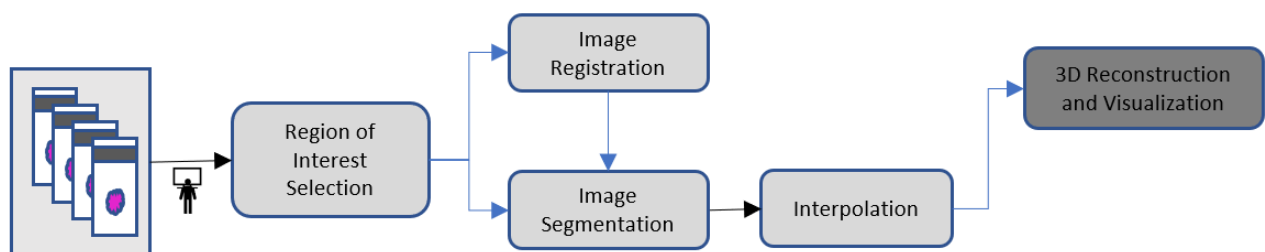
¹*Institute of Pathology, University of Regensburg, Regensburg, Germany*, ²*Central Biobank Regensburg, University and University Hospital Regensburg, Regensburg, Germany*

Background

Angiogenesis is essential for many physiological and pathological processes such as wound healing or tumor growth. A promising method to optimize the understanding of the underlying processes is to use a pipeline of computer vision and deep learning algorithms, which can successfully reconstruct blood vessels of histopathological sections as a 3D model. This allows visualization of blood vessels and their branches from different tissues and facilitates counting and analyses.

Methods

The present study used parallel histologically stained slides from 5 µm thickness of a granulation tissue sample to reconstruct a reliable 3D model using image registration, image segmentation, interpolation, and reconstruction.

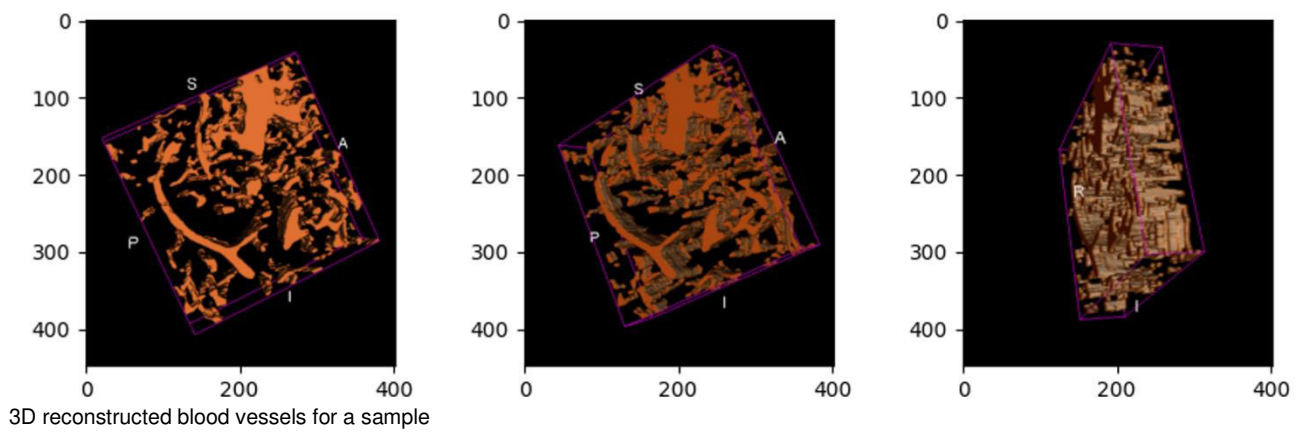


Pipeline for 3D reconstruction

A specific region of interest is chosen on each of 8 - 10 parallel consecutive slides, where the visualization of blood vessels is needed. Image registration is used to align images that are misoriented due to translation, rotation, scale, skew, folding, etc. A coarsely registered stack of images using an intensity-based pyramidal image registration was finetuned using a deformable network based on spatial transformation. The resulting transformation matrices and flow vectors are applied on the binary segmented masks, segmented using a UNeT neural network. Bilinear interpolation is used to predict the intermediate binary masks, which can be reconstructed in 3D using any common 3D visualization tool.

Results

Two samples of granulation tissue, one stained with HE and the other with CD31, were successfully reconstructed and visualized in 3D (figure 2). The segmentation algorithms resulted in a dice score of over 80% using UNeT. The dice score across the complete stack, increased from 3% before registration to 26% after registration, highlighting the importance of registration. After 3D reconstruction, blood vessels could be visualized with their branches.



Conclusion

In summary, 3D reconstruction of blood vessels will be a helpful tool in analyzing angiogenesis. In the future, we will skeletonize the 3D model to automatically evaluate the branching of blood vessels.

Multimodal deep learning model for prognosis prediction in clear cell renal cancer

S. Schulz¹, A.-C. Woerl^{1, 2}, F. Jungmann³, C. Glasner¹, P. Stenzel¹, S. Strobl¹, A. Fernandez¹, D.-C. Wagner¹, A. Haferkamp⁴, P. Mildenerberger³, W. Roth¹, S. Foersch¹

¹Pathologie, UM Mainz, Mainz, Germany, ²Informatik, JGU Mainz, Mainz, Germany, ³Radiologie, UM Mainz, Mainz, Germany, ⁴Urologie, UM Mainz, Mainz, Germany

Background

Clear-cell renal cell carcinoma (ccRCC) constitutes the vast majority of renal malignancies and is associated with substantial mortality. So far, TNM stage and histopathological grading have mostly been used to determine a patient's prognosis and there are few prognostic biomarkers used in clinical routine for this entity. Clinical management of ccRCC involves multiple disciplines such as radiology, urology, oncology, and pathology, each generating complex medical data. Here, artificial intelligence (AI) approaches could be highly useful in extracting meaningful information to improve prognosis prediction. This could be used to benefit a patient's clinical outcome e.g. via an individual adjustment of follow-up schedules or of treatment intensity.

Methods

In order to train a multimodal deep learning model (MMDLM) two cohorts of metastatic and non-metastatic ccRCC patients were used: (1) The Cancer Genome Atlas (TCGA) cohort including 230 patients and (2) the Mainz cohort including 18 patients with ccRCC. For each patient the MMDLM was trained on multiscale histopathological images, CT/MRI scans, and genomic data from whole exome sequencing. The outcome was evaluated by means of Harrell's concordance index (C-index) and also various performance parameters for predicting the 5-year survival status (5YSS). Different visualization techniques were employed to render our model more transparent.

Results

The MMDLM performed very well in predicting the prognosis of ccRCC patients with a mean C-index of 0.7791 and a mean accuracy of 83.43%. Multimodal training based on a combination of different data sources yielded significantly better results in comparison to unimodal training using only one source at a time. Additionally, the MMDLM's prediction proved to be an independent prognostic factor outperforming other clinical parameters such as grading or T stage. Findings of the TCGA cohort were tested on the Mainz cohort with similar results.

Conclusion

Multimodal deep learning models integrating multiscale histopathologic with radiologic image data sources can contribute to prognosis prediction in ccRCC and potentially help to improve the clinical management of this disease.

Patient-level proteomic network prediction by explainable artificial intelligence

P. Keyl¹, M. Bockmayr², G. Dernbach², D. Heim², G. Montavon¹, K.-R. Müller², F. Klauschen²

¹*Technische Universität Berlin, Berlin, Germany*, ²*Charité - Universitätsmedizin Berlin, Berlin, Germany*

Background

Understanding the pathological properties of dysregulated protein networks in individual patients' tumors is the basis for precision therapy. Functional experiments are commonly used, but cover only parts of the oncogenic signaling networks, whereas methods that reconstruct networks from omics data usually only predict average network features across tumors. Here, we show that the explainable AI method Layer-wise relevance propagation (LRP) can infer protein interaction networks for individual patients from proteomic profiling data.

Methods

A neural network is trained to predict individual protein abundances based on the abundances of arbitrary sets of other proteins from the same patient. Subsequently, LRP is applied to predict the relevance of each protein for this prediction. This relevance score is then used as an estimate of the interaction strength between every pair of proteins

Results

On synthetic data, LRP reconstructs average and individual interaction networks with an AUC of 0.99 and 0.93, respectively, and outperforms state-of-the-art network prediction methods for individual tumors. Using data from The Cancer Proteome Atlas, we identify known and potentially novel oncogenic network features, among which some are cancer-type specific and show only minor variation among patients, while others are present across certain tumor types but differ among individual patients.

Conclusion

Layer-wise relevance propagation allows for the prediction of sample-wise interaction networks based on a proteomic dataset. This approach may in the future support predictive diagnostics in precision oncology by inferring "patient-level" oncogenic mechanisms.

Connecting a customized data management system to the GBA Sample Locator using an ETL process

A. Artinger^{1,2}, V. Ramakrishnan^{1,2}, J. Eicher³, I. Gatz³, T. Nidermair^{1,2}, C. Brochhausen^{1,2}

¹*Institute of Pathology, University Regensburg, Regensburg, Germany*, ²*Central Biobank Regensburg, University and University Hospital Regensburg, Regensburg, Germany*, ³*Institute of Artificial Intelligence and Informatics in Medicine, Chair of Medical Informatics, University Hospital rechts der Isar, Technical University of Munich, Munich, Germany*

Background

Today's medical research requires large amounts of biospecimen and data. To ensure their best availability, the German Biobank Alliance (GBA) has developed the Sample Locator, which facilitates the query of all sites for available biomaterial with associated data [1]. Researchers can request for the number of patients and biospecimens that are eligible for their research purpose and can directly contact the respective biobanks. To enable this data query, the data from all sites must be put into a uniform format. The HL7 FHIR® standard is used for this purpose. At the Regensburg site, an ETL process was established to map the data from the biobank system to the FHIR format according to the GBA data set.

Methods

Data is exported as CSV files from the biobank system because there is no direct database access. The ETL process is implemented as a Maven project written in Java language. We use the HAPI FHIR package to use the defined FHIR structures and to validate the converted FHIR resources against the GBA implementation guide [2]. The FHIR version used is R4.

Results

First, we had to adapt the data management system to be able to fill the GBA dataset. This was easily implemented, as our customized biobank data management system can be adapted at any time. However, in consequence no existing mapping program can be used to automatically convert the data into the desired format. Therefore, we developed an ETL process that filters the necessary data from CSV files exported from the biobank system. The ETL process stores the data in an internal data model consisting of containers that summarize the individual patients' cases. Then, we form the FHIR resources starting with the patients and adding the observations and specimens connected to the patients. All resources are summarized in a FHIR bundle, validated against the GBA implementation guide, and exported as a JSON file.

Conclusion

In the present project we developed a system that automatically converts and validates data from CSV files into FHIR format for uploading directly to a FHIR store, which is customized to our system. With minor adjustments it can also be used for other sites with the same data management system.

Literaturangaben

[1] Schüttler C, Huth V, von Jagwitz-Biegnitz M, Lablans M, Prokosch H, Griebel L, (2020), A Federated

Online Search Tool for Biospecimens (Sample Locator): Usability Study, J Med Internet Res 2020, 22(8): e17739, <https://www.jmir.org/2020/8/e17739/>, 2022-04-07

[2] <https://www.bbmri.de>, (2022), BBMRI.de/GBA Implementation Guide, <https://samplify.github.io/bbmri-fhir-ig/index.html>, 2022-04-07

Autorenindex

(fett = Erstautor*innen)

Abbas, M.	AG07.04, P06.06
Abedin, N.	P01.16 , P14.06
Ackermann, M.	DGP14.12
Adebamowo, C.	P06.10
Agaimy, A.	P02.07, P03.01
Aigner, C.	P08.04
Aktas, B.	AG06.07, AG11.09
Al-Monajjed, R.	P02.13
Albers, P.	P02.13
Albertsmeier, M.	AG03.14
Albrecht, T.	AG11.16
Allgäuer, M.	AG11.06, AG11.16
Allmang, S.	P01.18, P01.19
Almeder, M.	DGP14.07
Alt, V.	AG03.07
Altendorf-Hofmann, A.	AG03.14
Althaus, K.	DGP14.09
Åman, P.	AG03.10, AG03.11
Amann, K.	P14.11
Ament, C.	AG01.13
Anagnostopoulos, I.	AG04.04
Angele, M.	AG01.21, AG03.14
Angeloni, M.	AG02.04, AG14.02 , P02.03
Antoch, G.	P02.13
Antonopoulos, W.	AG06.14
Appinger, S.	P14.02
Arampatzi, P.	DGP05.03
Arbelaez, P.	P14.12
Arndt, A.	P11.01
Arndt, S.	AG03.08
Arndt, T. T.	AG14.08
Artinger, A.	P14.12, P14.14, P14.17
Aswandi, I. P.	P01.13
Augustin, D.	AG06.07
Autenrieth, M.	P02.09
Bachmann, C.	AG04.11
Baehner, F.	AG06.07
Bagha, J.	DGP14.03
Bahlinger, V.	AG02.04, AG02.10, AG14.02, P02.03 , P02.06
Bakchoul, T.	DGP14.09
Balermipas, P.	DGP13.05
Ball, M.	AG11.16
Banek, S.	P02.01
Bankfalvi, A.	AG06.03
Bankov, K.	AG12.07, AG14.03, P01.16, P02.01, P08.03
Bannasch, P.	AG01.15
Barbieux, C.	P11.12
Baretton, G. B.	AG09.02
Bargou, R. C.	AG04.10, AG04.12
Barragan, L.	P14.12
Barsuhn, S.	AG01.02
Bartels, S.	AG06.13, AG06.14, AG11.09
Bartenschlager, C.	DGP02.05
Bartenschlager, R.	P01.14
Barth, T.	AG03.06, DGP05.06, DGP05.08, AG04.05, DGP05.01, DGP05.07, AG03.08, AG11.03
Barth, U.	P05.01
Bartsch, F.	AG01.11
Bauer, M.	P04.06, P06.10, P06.10

Bauer, T.	P08.04
Bauersachs, J.	DGP14.12
Baum, R. P.	P02.07
Baumhoer, D.	AG03.08
Bayas, A.	P04.04
Bayrhof, O.-J.	AG04.12
Beck, S.	AG09.04, AG11.16
Becker, F.	P02.11
Becker, K. F.	AG01.03
Becker, N.	AG12.07, P02.01
Beckert, H.	P08.04
Beckmann, M. W.	AG06.09
Bednarsch, J.	AG01.12, AG14.15
Beer, M.	DGP14.08
Behnert, N.	AG02.07
Behrens, H.-M.	AG01.02, AG06.10, P01.02
Bein, J.	AG04.02
Belker, E.	P08.03
Bensch, B.	P01.15
Benz, M.	DGP05.02, DGP09.04
Berger, S.	P01.08
Bernd, H.-W.	AG04.03
Bernhard, P.	AG11.13
Bernhardt, M.	P01.02
Bernreuther, C.	P01.21
Berthold, R.	AG03.10, AG03.11 , AG03.13
Bertz, S.	P02.07 , P02.14
Bette, S.	DGP05.01
Bettendorf, O.	AG07.04, P06.06
Beume, S.	P14.03
Bewarder, M.	AG04.02
Bischoff, F.	P02.04
Bloch, W.	AG08.03
Bobbe, S.	AG01.14
Böck, S.	P01.22
Bockmayr, M.	DGP05.05, P14.16
Bodingbauer, J.	DGP14.07
Boedicker, C.	AG12.07
Boekhoff, C.	AG08.04
Boettge, K.	P01.11
Bohle, R. M.	AG04.02
Bohlmann, M.	AG12.02
Bohnenberger, H.	AG08.07
Bolenz, C.	AG02.10, P02.06
Bollmann, L.	AG11.09
Bollwein, C.	P01.20, P06.08
Bonnet des Claustres, M.	P11.12
Bonzheim, I.	P01.05, P04.01, P04.05
Boor, P.	AG01.12, AG08.03, DGP14.08, DGP14.12, P05.04, P05.05, P14.11
Boppudi, S.	AG11.11
Borchert, S.	AG06.03, AG11.15, P01.08, P08.04
Bösch, F.	AG01.21
Boschheidgen, M.	P02.13
Bösmüller, H.	DGP05.04, DGP14.08, DGP14.09, DGP14.11
Bottner, J.	DGP07.04
Bouteldja, N.	P05.05, P14.11
Boxberg, M.	AG01.03, AG06.04, AG09.04
Bozzato, A.	AG04.02
Brada, M. D.	DGP07.03
Braicu, E.	AG06.02, AG06.01
Brambs, C.	AG12.01, P06.03, P06.05
Brandt, M.	P02.05
Brandt, R.	AG11.06
Braubach, P.	AG08.01 , AG08.04, DGP14.12

Braun, G.	DGP14.08
Braun, L.	P02.02
Braun, M.	AG11.09
Braun, R.	P04.01, P04.05
Braun, S.	P02.08
Braunger, M.	DGP02.05
Braunschweig, T.	, AG13.05
Bredt, M.	AG06.14
Bremmer, F.	AG02.07
Breuhahn, K.	AG01.17
Brewer, M.	AG01.04
Breyer, J.	AG02.10, P02.06
Brito, M. J.	AG06.14
Brochhausen, C.	AG03.02, AG03.04, AG03.05, AG03.07, P03.02, P14.12, P14.13, P14.14, P14.17, AG14.12
Broglie, M. A.	DGP13.05
Brombacher, E.	P02.02
Bronger, H.	AG06.04
Bronsert, P.	AG11.13, AG14.11, P01.15, P02.02, P11.02, P11.04, P11.06, P11.12
Brower, S.	AG01.04
Brown, R.	AG03.03
Bruchhage, K.-L.	AG09.01, P14.03
Brunnberg, U.	AG04.02
Brunner, J. O.	DGP02.05
Bruns, V.	AG14.12, DGP05.02, DGP09.04
Bublitz, J.	AG06.13
Buchner, A.	P02.04
Buck, A.	P02.09
Budau, K. L.	P11.02
Budczies, J.	AG09.04, AG11.04, AG11.06, AG11.16
Buelow, R. D.	P14.11
Buettner, R.	AG14.03
Buettner-Herold, M.	P02.07
Buhl, E. M.	P05.04
Bülow, R. D.	AG01.12, P05.05
Bultmann, S.	P02.08
Burandt, E.	P01.21
Burchardt, A.	P08.03
Burger, M.	P02.14
Burges, A.	P06.04
Burn, T.	AG11.16
Büschek, F.	P01.21
Buske, C.	AG04.05
Calvisi, D. F.	AG01.13, AG01.16
Campbell, J.	P14.01
Campbell, S.	P14.01
Campean, V.	P02.14
Capper, D.	DGP07.05
Castells, M.	DGP14.10
Chai, T.	AG03.03
Chen, X.	AG01.13
Chott, A.	P04.01
Christ, M.	P04.04
Christgen, H.	AG06.07, AG06.13, AG06.14, AG11.09
Christgen, M.	AG06.06, AG06.07 , AG06.13 , AG06.14 , AG11.09, P06.09
Christopolous, P.	AG11.06
Chun, F.	P02.01
Chun, F. K.-H.	AG02.09
Chung, L.	AG03.03
Cidre-Aranaz, F.	AG03.11
Cigliano, A.	AG01.13
Clauditz, T. S.	P01.21
Claus, R.	AG04.06, AG04.08, DGP14.08, DGP14.10

Clemens, M.	AG06.07
Cogliatti, S.	P04.01
Colpaert, C.	AG06.14
Comeaux, M.	AG11.08
Cosenza-Contreras, M.	P02.02, P11.02
Craiovan, B.	AG03.04
Croner, R. S.	P01.04, P01.09, P01.10, P01.11, P01.12, P01.13, P01.23, P01.24
Cserni, B.	AG06.14
Cserni, G.	AG06.14
Cui, L.	AG03.03
Czech, A.	AG08.03
Czogalla, B.	P06.04
Daemmrich, M. E.	AG06.14
Dahl, E.	AG06.11, AG14.15
Dan, L.	AG14.14, P14.04
Danebrock, R.	AG06.14
Daniel, C.	P14.11
Dannemann, A.	P06.01, P06.05
Danner, B. C.	AG08.07
Darb-Esfahani, S.	AG06.01, AG06.02
Das, D. K.	AG14.14
Daza, J.	P14.12
de Jonge, J.	AG07.04, P06.06
de Schepper, M.	AG06.14
DeAngelo, D. J.	AG04.09
Dedeurwaerdere, F.	AG06.14
Degener, S.	P02.04
Dehelean, D. C.	AG06.11
Deiningner, M.	AG04.09
Delbridge, C.	AG01.07, AG14.12
Demes, M.	P08.03, P11.11
Denkert, C.	AG01.07, AG06.01, AG06.02, AG06.09, AG06.12, AG11.08
Derksen, P. W.	AG06.13, AG06.14
Dernbach, G.	P14.16
Desmedt, C.	AG06.14
Dettmer, S.	AG08.01
Dexl, J.	DGP09.04
Dickemann, A.	P01.01, P01.05
Dierkes, C.	AG01.14
Dieterle, M.	P11.04, P11.06
Dietmaier, W.	AG11.12 , AG11.17
Dietrich, O.	DGP05.03
Dimitrijević, S.	AG04.09
Dimitrova, L.	AG06.09
Dinh, T.-L. J.	P02.02
Dintner, S.	AG04.06, AG04.08, DGP14.08, P05.06
Dirnhofer, S.	P04.01
Dix, P. L.	AG02.01
Doering, C.	AG14.03
Dombrowski, F.	AG01.13, AG01.15, P11.13
Donnadieu, E.	AG04.02
Dörenberg, J.	AG14.15
Döring, C.	P01.16, P02.01
Doukas, M.	P14.02
Dragomir, M.-P.	AG06.01
Drebbler, U.	P01.14
Drecoll, E.	P01.07
Dreyer, E.	AG08.06, AG09.01, P02.11
Dries, V.	P01.14
Duan, K.	P02.11, P11.05 , P11.08
Dum, D.	P01.21
Dummer, R.	AG09.03
Dürr, H.-R.	AG03.14

Duschner, N.	AG14.10
Dzamalala, C.	P06.10
Eberhard, J.	AG11.13
Ebert, R.	AG04.10
Eckey, C.	P06.03
Eckstein, M.	AG02.04, AG02.10 , AG14.02, DGP05.02, DGP09.04, P02.03, P02.06, P02.07
Effi, B.	P06.10
Eger, K.	P01.04, P01.09, P01.12
Ehle, M.	P05.03
Eich, M.-L.	P12.01
Eicher, J.	P14.17
Eidt, S.	P02.07
Eildermann, K.	AG05.07
Einenkel, J.	P06.01, P06.05, P06.07
Einsele, H.	AG04.10, AG04.12
Eixelberger, T.	AG14.12
Ekanem, I.-O. A.	P06.10
Elakad, O.	AG08.07
Ellinger, J.	P02.10
Enderle-Ammour, K.	P11.04
Endris, V.	AG11.06, AG11.16
Engel, J.	AG01.03, P01.22
Engelhard, M.	AG04.03
Erben, P.	AG02.10, P02.06
Erber, R.	AG06.09 , AG06.14, DGP08.02
Erduran, I.	P06.06
Erkut, C.	AG03.11
Erlenbach-Wuensch, K.	AG01.06, AG01.19, AG01.20, AG11.14
Erlmeier, F.	AG02.10, P02.06, P02.09
Ermert, K.	P05.04
Ermert, L.	AG03.09
Espadas, G.	P02.02
Esposito, I.	AG01.10, DGP14.08, P01.17, P14.02
Essenwanger, A.	AG14.13
Evans, T.	AG14.04, P14.07
Evers, M.	AG04.10 , AG04.12
Evert, K.	AG01.13 , AG01.16, AG14.12
Evert, M.	AG01.13, AG01.16, AG11.17, AG14.12
Fahrner, M.	AG11.13, P11.12
Falkenberg, K.	AG03.09
Falougy, M.	P14.03
Farfán López, F. J.	P08.02
Fasching, P. A.	AG06.09
Fassunke, J.	AG11.05
Fathke, C.	AG06.14
Faust, E.	AG11.11
Federlin, M.	AG03.04
Feist, H.	AG06.14
Feller, A.	P04.01, AG04.03
Fend, F.	AG05.05, DGP05.04, DGP14.09, DGP14.11, P01.01, P01.05, P04.01, P04.05
Fernandez, A.	P14.15, P14.10
Ferrazzi, F.	AG02.04, AG14.02, P02.03
Ferrero, G.	AG01.06
Festus, I.	P06.10
Feuchtinger, A.	P02.09
Fiche, M.	AG06.14
Fichtner-Feigl, S.	P01.15, P11.04, P11.12
Filipski, K.	P01.16
Fisseler-Eckhoff, A.	AG11.11
Flechtenmacher, C.	AG03.15
Flinner, N.	AG04.02, AG14.03
Floege, J.	P05.04

Floris, G.	AG06.14
Foell, M.	P01.15
Foell, M. C.	P11.06
Foerster, S.	AG02.01
Föll, M.	P11.04 , P11.12
Forchhammer, S.	P04.01
Försch, S.	AG01.03, AG01.07, P14.10 , AG14.02, P02.05, P14.15
Forster, S.	AG04.11
Foth, R.	AG05.07
Franke, S.	P03.03
Franz-Wachtel, M.	P01.01, P01.05
Fraune, C.	P01.21
Freiberger, S. N.	AG09.03
Freifrau von Stilfried und Rattonitz, S.	DGP14.12
Freude, A.	P02.05
Frey, A.	P11.04
Friess, H.	AG01.03
Fröhlich, K.	AG11.13
Fröhling, S.	AG03.10, AG03.11, AG11.16
Frosina, D.	DGP14.03
Fu, Y.	P01.16
Fuhr, V.	DGP05.03
Furlanetto, J.	AG06.12
Füzesi, L.	P03.01, P03.04
Gagiannis, D.	AG08.03
Gaida, M. M.	P01.03, P01.18, P01.19, P14.08
Gaisa, N.	AG14.15, P02.14, AG01.12, AG02.08, AG02.11, P02.04
Gan, L.	AG02.08, AG02.11
Gantner, A.-K.	P08.02
Garczyk, S.	P02.04
Gärtner, K.	P06.04
Gatz, I.	P14.17
Gehring, A.	AG01.05, AG01.06, AG11.14
Geisendörfer, J.	P08.02
Geißler, C.	AG14.07, P14.07
George, T. I.	AG04.09
Geppert, C.	AG01.06, AG14.02, DGP05.02, DGP09.04, P02.03
Geppert, J.-P.	P04.01
Gerber, T. S.	AG01.11
Gerhard-Hartmann, E.	AG04.04
Gersmann, A.-K.	AG02.07
Ghalamkaran, M.	P01.06
Giannetti, M. P.	DGP14.10
Giedl, J.	P02.14
Gierendt, L.	AG06.06, P06.09
Glade, J.	AG11.06
Glasner, C.	P14.15
Glavynskyi, I.	P02.02
Gleiber, W.	P08.03
Gluz, O.	AG06.07, AG06.14, AG11.09
Goldschmid, H.	AG11.06, AG11.16
Golliez, A.	DGP13.05
Golling, C.	P05.06
Golz, R.	P02.04
Goncalves, J. P. L.	P01.20, P06.08
Gonzalez, C. A.	AG06.14
Gorbokon, N.	P01.21
Gottlieb, J.	AG08.01, AG08.04
Grabbert, M.	P02.02
Grabowski, P.	P02.07
Gradhand, E.	AG05.06, AG12.05, AG12.07
Graeser, M.	AG06.07, AG06.14
Granai, M.	DGP05.04 , DGP14.09, DGP14.11

Granowski, D.	P05.01
Gräser, M.	AG11.09
Grass, A.	AG11.08
Grässel, S.	AG03.04, AG03.05, P03.02
Grassow-Narlik, M.	AG11.02
Grau, M.	AG04.03
Green, I.	P14.01
Greif, K.	DGP05.04, DGP14.11
Greimelmaier, K.	P01.08
Gresens, L.	AG02.03
Greten, F. R.	P01.06
Gretser, S.	AG02.09, AG12.07, AG14.03, P01.16, P14.06
Grevenstein, D.	AG03.02
Greze, V.	AG12.07
Griewank, K. G.	AG14.10
Griger, J.	P14.05
Grischke, E.-M.	AG11.09
Grochowski, P.	AG01.09
Groll, T.	AG01.07
Gronewold, M.	AG11.09
Grootkoerkamp, B.	P14.02
Großer, M.	AG09.02
Grosse, C.	DGP14.07
Grosser, B.	AG01.01 , AG01.09, AG14.08, DGP14.08, P01.03
Grosu, A.	P11.12
Grote, I.	AG11.09
Grunenberg, A.	AG04.05
Grünewald, I.	AG03.11
Grünewald, T. G. P.	AG03.11
Grüning, B.	P11.12
Grüttner, B.	P12.01
Grutzmann, R.	AG11.14
Grützmann, R.	DGP05.02
Gschwend, J.	AG02.10, P02.06
Guba, M.	AG01.21
Guck, J.	AG01.05
Guertler, F.	P14.14
Günther, M.	P01.22
Guo, D.	P11.04
Gyorffy, B.	AG02.02
Haase, L.	AG03.06, DGP05.08
Häberle, L. J.	AG01.10, P01.17, P14.02
Hackenbroch, C.	AG08.03
Hadaschik, B.	AG02.02
Hadaschik, E.	AG14.10
Haferkamp, A.	P02.05, P14.15
Hahnen, C.	AG02.02
Hake, R.	P02.07
Hakim, S.	P14.03
Halfter, K.	AG01.03
Haller, F.	AG02.07, AG06.09
Halloul, Z.	P05.02, P12.03
Hamad, A. S. M.	P02.10
Hampel, C.	AG01.06, AG01.19, AG01.20, AG02.01
Handzel, R.	P06.07
Hänsch, S.	AG01.10
Hansmann, M.-L.	AG04.02, AG04.03
Hapfelmeier, A.	P01.03
Harbeck, N.	AG06.07, AG06.14, AG11.09
Harling, L.	P01.12, P01.13
Harloff, M.	AG04.06, AG04.08
Haroske, G.	AG14.13, AG14.13 , P14.01
Harter, P. N.	P01.16

Hartmann, A.	AG01.05, AG01.06, AG01.19, AG01.20, AG02.04, AG02.07, AG02.10, AG06.09, AG11.14, AG14.02, DGP05.02, DGP09.04, P02.03, P02.06, P02.07, P02.09, P02.14
Hartmann, F.	P14.10
Hartmann, L.	DGP14.09
Hartmann, S.	AG04.02 , AG04.03
Hartmann, T. N.	AG04.10
Hartmann, W.	AG03.08, AG03.09, AG03.10, AG03.11, AG03.13
Hasheminasab, S.-M.	AG02.01
Hattesoehl, A.	AG06.12, AG11.08
Häupl, B.	AG08.07
Hause, F.	P02.02
Hausen, A.	P01.18, P01.19 , P14.08
Hauser, S.	P02.10
Haverich, A.	AG08.04, DGP14.12
Heers, H.	AG02.04, AG14.02, P02.03
Heidel, C.	AG08.06
Heidenreich, S.	DGP05.03
Heij, L.	AG01.12
Heij, L. R.	AG14.15
Heim, D.	P14.16
Heimberg, W.	AG14.12
Heinemann, V.	P01.22
Heinrich, S.	P01.18, P01.19
Heinst, L.	AG03.10 , AG03.11, AG03.13
Helmstädter, M.	AG05.08
Hempel, K.	P11.08
Henke, R.-P.	AG06.12
Henrich, L.	P01.08
Herbst, C.	DGP02.04
Heredia-Guerrero, S. C.	AG04.10, AG04.12
Herfarth, K.	AG04.03
Hermann, C.	DGP05.04, DGP14.11
Hernandez, E.	DGP14.03
Herold, T.	AG11.15
Herrmann, M.	AG03.04
Herz, A.-L.	P01.03
Heß, K.	AG12.06
Heselmeyer-Haddad, K.	AG01.04
Hess, A.	AG03.05
Heuft, L.-K.	AG01.11
Hewitt, S.	AG01.04
Hiepp, L.	P06.04
Hierl, F.	AG11.17
Hilgers, L.	AG06.11
Hiller, G. G. R.	P06.03, P06.05, AG12.01, P06.01, P06.02, P06.07
Hilsenbeck, J.	DGP14.08
Hinrichs, J. B.	AG08.04
Hinsch, A.	P01.21
Hirsch, D.	AG01.04
Hirschbühl, K.	AG04.08 , DGP14.08, P05.06
Höckel, M.	P06.03
Hoenscheid, P.	P11.06
Hoeper, M. M.	AG08.04
Hoffmann, I.	AG06.01, AG06.02
Hoffmann, M. J.	AG02.02
Höflmayer, D.	P01.21
Höh, B.	AG02.09
Höhn, A. K.	P06.03, P06.05
Höhn, A.-K.	AG12.01, P06.01, P06.02, P06.07
Holm, B.	AG01.02
Hölscher, D. L.	P05.05 , P14.11
Holte, H.	AG04.03
Hölzel, M.	AG02.10, P02.06
Holzinger, A.	P14.07

Holzmann, D.	AG09.03, DGP07.03
Holzner, P. A.	P01.15
Homeyer, A.	AG14.07
Hönscheid, P.	AG09.02, P11.04
Horn, H.	AG04.03
Horn, L.-C.	AG12.01, P06.01, P06.02, P06.03, P06.05 , P06.07
Horn, T.	AG02.10, P02.06
Hornick, J. L.	DGP14.10
Horst, D.	AG06.01, AG06.02
Hosni, R.	P02.10
Hovnanian, A.	P11.12
Hribaschek, A.	P05.02
Huber-Schumacher, S.	AG12.02
Huebner, K.	AG01.05 , AG01.06, AG01.19, AG01.20, AG11.14
Hufnagl, P.	AG14.04
Hüllner, M.	AG09.03
Hummel, M.	AG06.09
Huss, R.	AG14.08, DGP02.04, DGP02.05
Hussein, K.	AG12.04
Huynh, A.	P02.02
Hyhlik-Dürr, A.	AG04.06
Idel, C.	AG09.01, DGP07.04, P14.03
Ihle, M.	AG11.02
Ihrler, S.	DGP07.05
Ilm, K.	AG11.02
Isfort, I.	AG03.10, AG03.11, AG03.13
Iske, M.	AG14.10
Israel, J.	AG14.14, P14.04
Issels, R.	AG03.14
Itzel, T.	P14.12
Ius, F.	AG08.04
Jacob, M.	AG12.07
Jacob, S.	AG01.21
Jacobsen, F.	P01.21
Jagomast, T.	AG08.06, AG09.01, DGP07.04, P14.03
Jahrsdörfer, B.	DGP05.06
Jank, P.	AG01.07, AG06.12, AG11.08
Jansen, C.	AG14.04
Jansen, P.	AG14.10
Jarboui, M. A.	AG05.05
Jechorek, D.	P01.04, P03.03, P12.02, P12.03
Jeroch, J.	P11.11
Jesinghaus, M.	AG01.03 , AG01.07, P01.03, P01.03
Jeute, A.	P11.11
Jöhrens, K.	AG06.02, AG09.02
Jones, M.	AG11.08
Jonigk, D.	AG08.01, DGP14.12, P11.08, AG08.04
Jörg, V.	P02.11
Joshi, U.	AG14.14
Jost, P. J.	P01.07
Jücker, M.	AG08.07
Jud, A.	P11.04, P11.12
Juengel, E.	P02.05
Jundt, F.	AG04.10
Jundt, G.	AG03.08
Jung, K.	P02.10
Jungbluth, A.	AG03.14, DGP14.03
Jungmann, F.	P14.15
Jungwirth, J.	AG01.06
Jurmeister, P.	DGP05.05, DGP07.05
Just, M.	AG06.07
Jüttner, E.	AG12.06

Kacprowski, T.	AG06.04
Kalmbach, S.	AG04.03
Kamp, J. C.	AG08.04, AG08.01
Kandt, L.	AG11.09
Kandt, L. D.	AG06.14
Kang, D.	P02.12
Kantelhardt, E.	P06.10
Kargl, M.	P14.07
Karner, K. H.	AG04.09
Kasajima, A.	AG01.07, AG01.18
Kates, R.	AG06.07, AG11.09
Kaufenstein, S.	AG05.06
Kayser, G.	P11.09
Kazdal, D.	AG11.04, AG11.06, AG11.16
Kazi, A.	P14.09
Kehr, S.	AG12.07
Keil, F.	AG11.12, AG11.17
Keller, E. C.	P01.07
Keller, G.	AG01.01, P01.03
Kellers, F.	AG12.06
Keppler, O.	P05.07
Keppler, S.	AG04.12
Keyl, P.	P14.16
Kiefer, F.	AG01.14
Kiehl, T.-R.	P14.07
Kimmig, R.	AG06.03
Kindler, T.	AG03.10, AG03.11
Kinkorová, J.	P14.13
Kinzler, M.	P08.03, P14.06
Kirchhoff, F.	AG08.03
Kirchner, M.	AG03.15, AG11.04, AG11.06 , AG11.16
Kirchner, T.	AG01.21, P05.07
Kirfel, J.	P11.08, AG02.03, AG08.06, DGP07.04
Kirschnick, N.	AG01.14
Klapper, L.	AG09.01, DGP07.04, P14.03
Klapper, W.	AG04.03, P04.01, P04.04
Klauschen, F.	AG01.21, AG03.14, DGP05.05, DGP07.05, P06.04, P14.16
Kleinlein, I.	P04.04 , P05.06, P08.02
Klemm, S.	AG01.16
Klier-Richter, M.	AG11.12
Kling, E.	DGP14.08
Klinge, U.	AG01.12
Klingel, K.	AG05.05, DGP05.04, DGP14.11
Klinkhammer, B. M.	P05.04, P14.11
Kloeckner, R.	AG01.11
Kloor, M.	P01.05
Klopp, N.	P01.08
Klöppel, G.	AG01.07, AG01.18
Kluck, K.	AG11.06
Klump, D.	AG01.14
Klümper, N.	AG02.10, P02.06 , P02.10
Kluth, L.	P02.01
Knösel, T.	AG03.14
Knüchel-Clarke, R.	AG02.11, P02.04, AG02.08, AG06.11
Koch, K.	P04.04
Kohler, E.	P04.01, P04.05
Kohlruss, M.	P01.03
Kolb, T.	AG11.03
Koll, F.	P02.01 , AG02.09
Köllermann, J.	AG02.09 , P02.01, P02.08
Kollmeier, J.	P08.04
Kölsche, C.	AG03.15
Kommoss, F.	AG03.15

Kondratkova, A.	AG02.11
Konukiewicz, B.	AG01.03, AG01.07 , AG01.18
Kooreman, L.	AG06.14
Köster, J.	AG11.15
Kovács, K.	P03.04
Krabisch, P.	AG06.07
Kraeter, M.	AG01.05
Kral, J.	AG01.06
Kramp, L.-J.	AG06.10
Krause, H.	P12.02, P12.03
Krause, Y.	P01.08
Krech, T.	AG06.14, P01.21
Kreipe, H.	AG06.07, AG06.13, AG06.14, AG11.09, AG06.06, P06.09, DGP14.12
Kreutz, C.	P02.02
Kriegsmann, K.	P14.08
Kriegsmann, M.	AG11.06, P14.08
Kristiansen, G.	AG02.01, AG06.14, P02.10
Kristina Schwamborn, K.	P06.08
Kröncke, T.	DGP14.08
Kronenberg, D.	AG03.05
Krückel, I.	AG12.01, P06.07
Krüger, S.	AG01.02, P01.02
Krügl, A.	AG04.12
Krupar, R. F. A.	DGP08.01 , P11.08
Kubankova, M.	AG01.05
Kuehnel, M. P.	AG08.04
Kuettel, S.	AG06.07, AG06.14
Küffer, S.	AG08.05, AG08.07
Kuhl, C.	AG06.11
Kühnel, M.	DGP14.12
Kühnle, E.	P06.09
Kulbe, H.	AG06.01, AG06.02
Kulka, J.	AG06.14
Kümmel, S.	AG11.09
Kummerow, C.	AG12.07
Kümpers, C.	AG08.06
Kuntze, A.	AG03.09
Kunze, C. A.	AG06.01 , AG06.02, AG06.11
Kunze, M.	AG12.02
Kunze, P.	AG01.20
Kunzke, T.	P02.09
Kuppler, P.	AG09.01, P14.03
Kuric, M.	AG04.10
Kuritsyn, P.	DGP09.04
Kurowski, K.	AG14.11 , P01.15 , P02.02, P11.02
Kurt, U.	P14.09
Kurz, K. S.	AG04.03
Labitzky, V.	AG08.07
Laenger, F.	AG06.14, AG08.04
Lafos, M.	AG06.14
Lammert, F. C.	AG02.08 , AG02.11
Lamprecht, B.	DGP14.07
Lan, Y.-C.	P05.05
Landgraf, L.	AG02.10, P02.06
Lang, C.	AG01.03, AG01.07
Lang, H.	AG01.11
Lang-Schwarz, C.	DGP08.03
Lange, S.	AG01.03, AG01.07
Lange, T.	AG08.07
Langer, C.	AG04.10
Länger, F.	AG08.01, DGP14.12
Langer, R.	DGP14.07, P01.07
Laßmann, S.	P11.09

Lautizi, M.	AG06.04
Lazar-Karsten, P.	AG02.03
Le'Clerc Arrastia, J.	AG14.10
Lebok, P.	P01.21
Ledderose, S.	P05.07
Lehmann, M.	P05.01
Lehmann, U.	AG06.09, AG06.13, AG06.14, AG11.09, AG11.16
Leich, E.	AG04.03, AG04.10, AG04.12
Lein, M.	P02.08
Leinauer, B.	AG03.08
Leiner, H.	P11.13
Leitheiser, M.	DGP05.05
Lemster, A.-L.	AG02.03 , DGP07.04
Lennartz, M.	P01.21
Lennerz, J. K.	AG07.05
Lenz, G.	AG04.03
Lerbs, T.	AG03.03
Levesque, M. P.	AG09.03
Li, S.	AG03.04
Lin, H.-M.	AG04.09
Lindner, L.	AG03.14
Lindner, S.	AG14.02
Lischka, J.	AG09.02
Liu, D.	AG01.12
Livak, F.	AG01.04
Lohmann, C.	P03.03
Loibl, S.	AG06.12
Longerich, T.	AG11.16
López-Cotarelo, C.	P02.13
Loth, A.	AG04.02
Lotz, J.	P14.11
Lüdtke-Heckenkamp, K.	AG11.09
Ludwig, C.	DGP05.06
Luebke, A. M.	P01.21
Luibrand, J.	AG05.05 , P01.01, P01.05
Lukas, C.	AG03.04
Lüke, F.	AG11.17
Lupp, A.	P02.07
Maag, N.	P11.01
Maass, P.	AG14.10
Maccagno, A.	DGP14.08, P03.01 , P04.04
Maček, B.	AG05.05, P01.01, P01.05
Mach, P.	AG06.03
Mahadevan, V.	AG01.19
Mahner, S.	P06.04
Maier, J. I.	AG05.08, P05.03
Mairinger, E.	AG06.03, P01.08, P08.04
Mairinger, F. D.	AG06.03, AG11.15, P01.08, P08.04
Mairinger, T.	P08.04
Malter, W.	AG06.07
Mandel, P.	AG02.09
Mann, M.	DGP14.10
Manraj, S. S.	P06.10
Manthey, S.	AG14.04
March, C.	P01.04, P01.09, P01.12, P01.24
Marchenko, S.	AG06.02
Marienfeld, R.	AG11.03, P04.02, P04.03
Märkl, B.	AG01.01, AG01.09, AG04.06, AG04.08, AG14.08, DGP02.04, DGP02.05,
DGP14.08 , DGP14.10, P03.01, P03.04, P04.04, P05.06, P05.07, P08.01, P08.02	
Marmé, F.	AG06.12
Marnet, N.	P01.18, P01.19
Martin, M.	P06.02
Martin-Martinez, M. D.	AG06.14

Marx, A.	AG08.05
Marx, N.	DGP14.12
Massa, C.	AG11.04, P04.06
Mathiak-Buchhorn, M.	AG06.10
Mathilakathu, A.	P08.04
Mattern, S.	AG05.05, P01.01 , P01.05
Mayer, M.	AG14.12
Mayr, D.	P06.04
Mayr, E.	P03.01
Mayr, T.	AG02.01
McCormack, V.	P06.10
Mechtersheimer, G.	AG03.15
Meerwein, C. M.	DGP07.03
Meier, J.	DGP14.07
Meinardus, A.	AG12.04
Meliss, R. R.	AG03.09
Mellert, K.	AG03.06, AG03.08, DGP05.01, DGP05.07, DGP05.08
Mende, M.	P06.03
Mendelsohn, D.	AG03.07
Menter, T.	AG12.02, P12.01
Mentzer, S.	DGP14.12
Menz, A.	P01.21
Merkel, S.	DGP05.02
Merkelbach-Bruse, S.	AG11.02, AG11.05, AG11.10, P11.03
Merseburger, A. S.	P02.12
Meyer, F.	P01.04, P01.09, P01.10, P01.11, P01.12, P01.13, P01.23, P01.24, P05.01,
P05.02, P12.02, P12.03	
Mihalik, F.	P04.01, P04.05
Mildenberger, P.	P14.15
Miller, S.	AG14.08, P03.04
Minner, S.	P01.21
Moch, H.	P02.09
Moeckel, K.	AG01.05
Mogler, C.	P14.05
Mohenou, D.	P06.10
Mokwa, N. F.	P12.01
Moldenhauer, G.	P04.03
Mölder, F.	AG11.15
Möller, K.	P01.21
Möller, P.	AG03.06, AG03.08, AG04.05, AG11.03, DGP05.01, DGP05.07, DGP05.08,
	DGP14.09, P04.02, P04.03
Monjé, N.	AG06.01, AG06.02
Montavon, G.	P14.16
Morand, G. B.	AG09.03, DGP13.05
Moritz, L.	P11.04
Moser, K. A.	AG04.09
Muckenhuber, A.	AG14.14
Muders, M.	AG02.01, P11.07
Mueller, S.	AG06.14
Mühl, S.	AG06.11
Müller, A. M. ..	P12.01
Müller, B.	AG14.12
Müller, C.	AG01.10
Müller, C.	AG08.01
Müller, D.	AG08.05
Müller, G.	AG04.06, AG14.08
Müller, H.	P14.07
Müller, K.-R.	P14.16
Müller, L.	AG01.11
Muscat, C.	AG03.03
Musial, J.	AG02.02
Naccarati, A.	AG01.06
Nagy, N.	AG02.02

Namba, K.	AG03.12
Nann, D.	P04.01, P04.05
Naumann, M.	P04.04
Navab, N.	P14.09
Nedeva, T.	AG04.12
Neidig, M.	DGP14.08
Nell, J.	DGP05.06
Neubert, L.	AG08.04 , DGP14.12
Neumann, J.	AG01.21
Neumann, O.	AG11.06, AG11.16
Neumann, U. P.	AG01.12, P14.02
Ng, S.	P02.10
Niedermair, M.	AG12.01
Niedermair, T.	AG03.02 , AG03.04 , AG03.05 , AG03.07, AG14.12, P03.02 , P14.12, P14.14, P14.17
Nieß, H.	AG01.21
Niess, C.	AG05.06
Nigussie, M. Y.	P06.10
Nikulu, J. I.	P06.10
Nitz, U.	AG06.07, AG06.14, AG11.09
Niu, Y.	P11.07
Noack, P.	DGP14.07
Novotny, A.	AG01.01, P01.03
Nuding, B.	AG06.07
Nursaitova, A.	AG01.05
Nyiro, G.	AG02.02
Obeck, U.	P06.02, P06.05
Ochsenbein, A.	AG04.11
Oellerich, T.	AG08.07
Offermann, A.	AG09.01, P02.11, P02.12, P11.05, P11.08, P14.03
Ogawa, M.	AG03.12
Ogunbiyi, O. J.	P06.10
Okada, S.	AG08.05
Olah, C.	AG02.02
Opitz, F.	AG01.10
Ormanns, S.	P01.22
Oschlies, I.	P04.01
Otero Baguer, D.	AG14.10
Ott, G.	AG04.03, AG04.04, P04.01
Ourailidis, I.	AG09.04
Paasch, C.	P01.10, P01.11
Pablik, J.	DGP14.08
Pantea, M.-A.	P01.15
Pappesch, R.	P11.03
Pardini, B.	AG01.06
Paul, T.	P05.07 , P05.07 , AG05.07
Paulsen, F.-O.	AG08.06, P02.11
Pavel, M.	P02.07
Pehl, A.	AG06.12
Pelz, E.	AG06.14
Penzel, R.	AG11.06
Perac, K.	AG12.01
Perner, S.	AG02.03, AG08.06, AG09.01, DGP07.04, P02.11, P02.12, P11.05, P11.08, P14.03
Peters, K.	AG01.15
Petersen, M.	P01.24
Pfarr, N.	AG01.03, P11.10
Pickert, J.	AG04.12
Pietsch, C.	AG12.01
Pilny, A.	P06.01, P06.02
Pinter, N.	P02.02, P11.02
Pischimarov, J.	AG04.10

Piwonski, I.	AG06.02
Plass, M.	P14.07
Pohl, J.	AG06.01, AG06.02
Porubsky, S.	P02.05
Pöschel, V.	AG04.02
Pour Farid, P.	DGP05.02
Prade, V.	P02.09
Prechtel, P.	AG01.20
Preisser, F.	AG02.09
Pretzsch, E.	AG01.21
Preuß, E.	AG08.02
Prinz, M.	P11.10
Probst, A.	AG01.01
Prochazka, J.	AG01.06, AG11.14
Proppe, L.	P14.03
Pukrop, T.	AG11.17
Puller, A.-C.	AG03.09
Quaas, A.	AG14.03
Quintanilla-Martinez, L.	DGP05.04, DGP14.11
Quintanilla-Martinez, L.	P04.01, P04.05
R. Heij, L.	P14.02
Raap, M.	AG06.06 , AG06.07, AG06.14, AG11.09, P06.09
Radia, D. H.	AG04.09
Raffler, J.	DGP02.04, DGP02.05
Ralser, D.	P02.06
Ramakrishnan, V.	AG03.02, P14.12 , P14.14 , P14.17
Rao, J.	AG14.14
Rau, A.	P04.01, P04.05
Rau, T.	P02.13
Rauert-Wunderlich, H.	AG04.04, DGP05.03
Ravarino, A.	AG06.14
Rawitzer, J.	AG02.02
Redlich, A.	P12.02
Redlich, U.	P05.02
Reichart, M.	DGP14.12
Reil, L.	AG12.02
Reimer, T.	AG06.07
Reindl, L. M.	AG12.07
Reineke-Plaass, T.	AG06.14
Reis, H.	AG02.02, AG02.09, P02.01, P08.04
Reiser, M.	AG01.03
Reiswich, V.	P01.21
Reiter, A.	AG04.09
Reitsam, N.	P08.01
Rentschler, L.	DGP14.08, P05.06 , P08.02
Rets, A.	AG04.09
Retzlaff, C. O.	P14.07
Reuss, D.	AG03.15
Reuter-Jessen, K.	AG08.05
Reyersbach, N.	AG03.02
Rezaienia, M.	AG02.03
Ribback, S.	AG01.13, AG01.15 , P11.13
Ribbat-Idel, J.	AG09.01 , DGP07.04, P14.03
Richter, A.	AG02.07
Richter, G.	P02.14
Ridder, D. A.	AG01.11
Ried, T.	AG01.04
Riedel, A.	DGP05.03
Rieger, K.	AG03.03
Rieger, L.	AG06.13
Riemenschneider, P.	AG05.05, P01.01, P01.05
Rindt, W.	AG04.10

Ritter, M.	AG02.10, P02.06, P02.10
Robertus, J. L.	DGP14.12
Röcken, C.	AG01.02, AG06.10, AG12.06, P01.02
Rodepeter, F.	AG06.09, AG11.08
Roehrl, M.	AG03.12
Roesch, M. C.	P02.12
Roesch, M. C.	P14.03
Roessner, A.	P03.03
Rogg, M.	AG05.08, P05.03
Rogghmann, F.	AG02.10, P02.06
Rohde, G.	P08.03
Röhrlich, T.	AG11.05
Rókusz, A.	AG03.08
Rolle, U.	AG12.05
Romancik, P.	P05.02
Romanovsky, E.	AG11.04
Romberg, D.	AG14.04
Romey, M.	AG11.08
Röpke, M.	P03.03
Rosch, I.	P02.03
Rose, M.	AG08.05 , AG02.08, AG02.11
Rosenwald, A.	AG04.03, AG04.04, AG04.10, AG04.12, DGP05.03, P04.01
Rosin, M.	P14.02
Rössler, S.	AG11.16
Röst, H.	P11.12
Roth, D.	P02.11
Roth, W.	AG01.11, P01.14, P01.18, P01.19, P02.05, P14.10, P14.15
Rübner, M.	AG06.09
Rückert, F.	AG11.13
Rudelius, M.	AG04.10, P05.07
Rüdiger, T.	AG14.13, P14.01, P14.01
Rueschoff, J.	AG14.03
Rupp, M.	AG03.07
Rupp, N. J.	AG09.03, DGP07.03, DGP13.05
Ruppert, T.	AG01.17
Rüschhoff, J.	AG06.12
Sabidó, E.	P02.02
Sadr, A.	P05.05
Sailer, V.	P11.08
Sailer, V.-W.	P02.12
Saldit, T.	DGP14.12
Saliba, A.-E.	DGP05.03
Salz, A.	P02.04
Salzer, H. J.	DGP14.07
Sammarco, A.	AG05.08, P05.03
Sanchez, M.	AG01.04
Sander, B.	AG06.13
Sander, P.	P04.01, P04.05
Sanders, C.	P02.10
Saraji, A.	P11.08
Särchen, V.	AG12.07
Sarker, R. S. J.	AG14.14 , P14.05
Sarker, S. R.	P14.04
Saur, D.	AG01.03
Saur, F.	AG11.05
Sauter, G.	P01.21
Schade, T.-C.	P04.01, P04.05
Schadendorf, D.	AG14.10
Schäfer, K. W. F.	AG06.10
Schaller, J.	AG14.10
Schaller, T.	AG01.09, DGP02.04, DGP14.08, DGP14.10 , P05.06, P08.01
Schanze, D.	P03.03
Scharf, S.	AG04.02

Schaumann, N.	AG06.14, AG12.04
Scheil-Bertram, S.	AG11.11
Scheiter, A.	AG01.03, AG01.16, AG11.12, AG11.17
Schelbert, S.	P01.14
Schelfhout, A.-M.	AG06.14
Schell, C.	AG05.08, AG14.11, P02.02, P05.03
Schenkirsch, G.	AG01.01, AG01.09
Schick, B.	AG04.02
Schickedanz, O.	AG12.05
Schicktanz, F.	AG01.07
Schiele, S.	AG01.01, AG04.06
Schierholz, S.	AG08.06
Schierle, K.	, AG13.05
Schiffner, C.-J.	P01.23
Schildberg, C.	P01.11
Schildhaus, H. U.	P01.08, AG11.15
Schilling, O.	AG11.13, AG14.11, P01.15, P02.02, P11.02, P11.04, P11.06, P11.12
Schimmöller, L.	P02.13
Schindeldecker, M.	AG01.11, P01.14
Schirmacher, P.	AG01.17, AG09.04, AG11.04, AG11.06, AG11.16, DGP14.09, P01.14
Schlenzog, M.	AG01.10
Schlitter, A. M.	P01.20
Schlitter, A. M.	AG01.18
Schlößer, R.	P02.04
Schlue, J.	AG06.14
Schmelmer, J.	AG02.04
Schmid, K. W.	AG06.03, AG11.15, P01.08, P08.04
Schmidt, C.	AG06.09
Schmidt, M.	AG14.10
Schmidt, T.	P01.03
Schmitt, C.	P11.11
Schmitt, J.	AG01.17
Schmitt, M.	AG01.03, AG01.07
Schmitt, R.	P11.11
Schmitt, W. D.	AG06.01, AG06.02
Schmoeckel, E.	P06.04
Schneider, U.	P02.04
Schneider-Stock, R.	AG01.05, AG01.06, AG01.19, AG01.20, AG02.01, AG11.14, DGP05.02
Schnitzbauer, A. A.	P14.06
Schnitzler, T.	P02.04
Schoenmehl, R.	P14.14
Scholl, C.	AG03.10, AG03.11
Schömig-Markiefka, B.	AG11.10
Schraml, P.	P02.09
Schreder, M.	AG04.10
Schreiber, L.	DGP05.06
Schreier, J.	P03.03
Schreiner, W.	P08.03
Schüffler, P.	AG14.05 , AG14.12, AG14.14, P14.04, P14.09
Schuler, M.	P08.04
Schulte, M.	AG01.10
Schultheiss, M.	AG03.08
Schulz, G. B.	P02.04
Schulz, S.	P14.15
Schulze, F.	P14.06
Schumacher, C.	AG11.09
Schütze, L. M.	AG01.07
Schwab, K.	DGP14.09
Schwamborn, K.	AG01.07, AG02.10, P01.20, P02.06
Schwarz, A.	P02.01
Schwarzfischer, M.	AG04.12
Schweiger, E.	DGP05.07
Schweizer, L.	DGP14.10
Scott, D. W.	AG04.04

Sehouli, J.	AG06.01, AG06.02
Seidel, A. D.	AG08.04
Seidl, M.	DGP14.08
Seidler, D.	P14.13
Seker-Cin, H.	AG11.06, AG11.16
Seliger, B.	AG11.04, P04.06, P06.10
Sendrói, M.	AG03.08
Shanmugalingam, S.	AG12.07
Shehabeldin, M.	P01.10
Shen, J.	P02.09
Shibata, T.	AG03.03
Sholl, L.	DGP14.10
Siebolts, U.	AG11.05, AG11.10
Siemanwoski, J.	AG11.10
Sigel, C.	P11.02
Sigler, M.	AG05.07
Sikic, D.	AG02.04, AG02.10, AG14.02, P02.03, P02.06
Silva, M.	AG01.03
Simister, G.	AG11.08
Simon, R.	P01.21
Singer, S.	AG05.05, P01.01, P01.05
Sini, M.	AG01.13
Sinn, B.	AG06.02
Sinn, B. V.	AG06.12
Sinn, P.	AG03.15
Sipos, E.	DGP14.08, DGP14.10
Siskova, A.	AG01.06
Sjödahl, G.	AG02.02
Slotta-Huspenina, J.	P01.03, P01.07, P04.05
Snítílá, M.	P14.13
Solimeno, C.	AG11.08
Sommer, F.	AG14.08
Sommer, S.	AG04.08
Sommer, U.	AG09.02
Soteriou, D.	AG01.05
Soyka, M. B.	DGP07.03
Spada, F.	AG04.05
Spring, O.	DGP14.08
Stahl, R.	AG01.04
Staiger, A. M.	AG04.03
Stange, R.	AG03.05
Stark, H.	AG06.13, AG08.04, DGP14.12
Starz, H.	AG04.12
Stefek, A.	AG06.07
Stegmann-Frehse, J.	P11.08
Stehle, A.	P08.03
Steib, F.	AG06.11
Steiger, K.	AG01.03, AG01.07, AG14.05, AG14.12, AG14.14, P01.03, P14.04, P14.05
Stein, H.	AG04.03, P04.01
Steinbrunn, T.	AG04.10
Steinbuss, G.	P14.08
Steinemann, D.	AG06.13
Steiner, Y.	AG04.02
Steinestel, K.	AG08.03 , P11.01
Steinmann, S.	AG01.13
Steller, D.	P14.03
Stenzel, P.	P14.15
Stenzinger, A.	AG03.15, AG09.04, AG11.04, AG11.06, AG11.16
Stephan, C.	P02.10
Stephan-Falkenau, S.	P05.01, P08.04
Stern, M.	P05.07
Steurer, S.	P01.21
Stilgenbauer, S.	AG04.02
Stiller, M.	P06.05

Stiller, M.	P06.02
Stillger, M.	P11.04
Stillger, M. N.	P11.06
Stöckl, S.	AG03.04
Stoehr, R.	AG02.04, AG14.02, P02.03
Stögbauer, F.	AG06.04 , AG09.04, P14.04
Stöhr, R.	AG02.07, AG06.09, P02.14
Strahler, L.	AG12.03 , AG12.03
Straub, B. K.	AG01.11, P01.14
Straub, R. H.	P03.02
Streck, E.	AG04.06
Strick, R.	AG02.04, AG02.10, AG14.02, P02.03, P02.06
Strissel, P.	AG02.10, P02.06
Strissel, P. L.	AG02.04, AG14.02, P02.03
Ströbel, P.	AG02.07, AG08.05, AG08.07
Strobl, S.	P14.15
Strohmenger, K.	AG14.04
Stühmer, T.	AG04.10, AG04.12
Su, Q.	AG01.15
Suhren, J.-T.	AG12.04
Sulyok, M.	AG05.05
Sun, N.	P02.09
Surov, A.	P12.03
Swedlund, B.	AG11.08
Sylvester, M.	AG02.01, AG02.03
Szabolcs, M.	DGP14.03
Szarvas, T.	AG02.02
Tan, X.	AG01.12, P14.02
Tanaka, A.	AG03.12
Tang, L.	P11.02
Taube, C.	P08.04
Taube, E.	AG06.01, AG06.02
Taubert, H.	AG02.04, AG14.02, P02.03
Tautenhahn, J.	P05.02
Tekeli-Camci, N.	P08.03
Teply-Szymanski, J.	AG11.08
ter Hoeve, N.	AG06.14
Tessmer, C.	P04.03
Teufel, A.	P14.12
Theilen, T. M.	AG12.07
Thierauf, J. C.	AG07.05
Thomas, M.	P02.13
Thomas, M.	AG11.06
Thomas, T.	AG14.14
Thun, S.	AG14.13
Thurner, L.	AG04.02
Timme, S.	P01.15
Timms, K. M.	AG11.08
Ting, S.	AG02.02
Tittmann, P.	AG08.01
Todorova, R.	AG01.21
Tögel, L.	P02.14
Toma, M.	P02.10
Topolčan, O.	P14.13
Tornóczky, T.	P03.04
Traore, C. B.	P06.10
Trautmann, M.	AG03.10, AG03.11, AG03.13
Trautwein, I.	P01.24
Trepel, M.	AG04.08
Tschäbunin, A.	AG02.09, P14.06
Tschurtschenthaler, M.	AG01.03
Tulessin, M.	P14.05
Tureckova, J.	AG01.06

Turial, S.	P12.02, P12.03
Turko, P.	AG09.03
Turzynski, A.	AG14.06
Tutina, L.	P14.01
Tzankov, A.	DGP14.12
Ueffing, M.	AG05.05
Uhlig, R.	P01.21
Uhrig, S.	AG11.16
Ullmann, S.	P03.03
Ullrich, E.	AG12.07
Urlaub, H.	AG08.07
Utpatel, K.	AG01.13, AG01.16, AG11.12, AG11.17
Uzun, G.	DGP14.09
Vafadarnejad, E.	DGP05.03
van Bockstal, M. R.	AG06.14
Van de Vijver, K.	AG06.14
van den Berg, E.	P06.10
van Deurzen, C. H. M.	AG06.14
van Diest, P. J.	AG06.14
van Luttikhuizen, J. L.	AG06.13
van Mackelenbergh, M. T.	AG06.10
Van Wymersch, C.	AG05.08
Varadi, M.	AG02.02
Vaxevanis, C.	P04.06
Verhoff, M. A.	AG05.06
Verleden, S.	DGP14.12
Vermeulen, D.	AG14.12
Vesce, R.	P01.17
Villwock, S.	AG06.11
Vincent-Salomon, A.	AG06.14
Vitek, O.	P11.04
Vlasenko, D.	AG01.01, AG01.09, P05.06
Vodicka, P.	AG01.06
Vodickova, L.	AG01.06
Vogel, A.	AG11.16
Vogel, U.	DGP05.04, DGP14.11
Vogler, M.	AG12.07
Vöhringer, M. C.	AG04.03
Volckmar, A.-L.	AG11.06, AG11.16
Volkman, V.	P11.04
Volland, P.	AG14.02, P02.03
von Baer, A.	AG03.08
von Brünneck, A.-C.	AG06.02
von Bubnoff, F.	AG01.17
von Hammerstein-Equord, A.	AG08.07
von Stillfried, S.	AG06.11, P05.05
von Werder, A.	AG01.07
Vrugt, B.	P08.03
Vymetalkova, V.	AG01.06
Wach, S.	AG02.04, AG14.02, P02.03
Waelput, W.	AG06.14
Wagner, A. H.	AG11.16
Wagner, D.-C.	P02.05 , P14.15
Waidhauser, J.	AG04.08
Walch, A.	P02.09, P05.07
Walker, M.	P11.10
Waller, C. F.	P11.09
Walter, N.	AG03.07
Walz, G.	AG05.08
Wank, I.	AG03.05
Wardelmann, E.	AG03.09, AG03.10, AG03.11, AG03.13, AG06.11

Warm, V.	DGP05.04, DGP14.09 , DGP14.11
Watermann, C.	P11.08
Weber, F.	P01.04, P01.09
Wehner, S.	AG12.07
Weichert, W.	AG01.01, AG01.03, AG01.07, AG01.18, AG02.10, AG06.04, AG09.04, AG14.05, AG14.12, AG14.14, P01.03, P01.07, P01.20, P02.06, P02.09, P06.08, P11.10, P14.04, P14.05
Weidemann, S.	P01.21
Weiler, S.	AG01.17
Weingart, A.	P02.12 , P11.05
Weinmann, A.	P01.14
Weißinger, S. E.	AG07.05
Weiskirchen, R.	AG02.08
Weiss, N.	P14.11
Weissinger, S. E.	P04.03
Weller, J.	P04.01
Wellmann, A.	AG06.14
Welte, T.	AG08.04, DGP14.12
Welter, V.	AG11.10
Wendler, O.	P02.14
Wenzel, M.	AG02.09
Werlein, C.	AG08.01, DGP14.12 , P06.09
Werner, J.	AG11.13 , AG01.21, AG03.14, P01.22
Werner, M.	AG05.08, AG12.02, AG14.11, P01.15, P02.02, P05.03, P11.02, P11.04, P11.06, P11.09, P11.12
Werner, T.	P02.02, P11.02
Wernig, G.	AG03.03
Wesener, M.	AG01.17
Wessolly, M.	AG06.03, AG11.15, P08.04 , P01.08
Westhoff, C. C.	AG06.12
Wickenhauser, C.	P04.06, P06.10
Wiedemann, S.	AG12.07
Wiesweg, M.	P08.04
Wilczak, W.	P01.21
Wild, P.	AG02.09, AG14.03, P01.16, P02.01, P08.03, P11.11, P14.06, P01.06
Wildfeuer, J.	P04.02
Wilhelm, D.	AG01.03, AG01.07
Wilhelm, K.	P11.04
Wilmes, V.	AG05.06
Wiltberger, G.	P14.02
Wirtz, J.	AG02.11
Wirtz, R.	AG02.10, P02.06, P02.07
Wisser, S.	P01.03
Wittenberg, T.	DGP09.04
Wittler, C.	P02.01
Witzel, H.	P01.18, P01.19, P01.14
Woerl, A.-C.	P14.15
Wohlschlaeger, J.	P01.08, P08.04
Woldesonbet, Z. D.	P06.10
Wolf, S.	P05.06
Wolter, S.	P11.09
Wosnig, S.	AG03.10
Wuerstlein, R.	AG06.07
Wullich, B.	AG02.04, AG02.10, AG14.02, P02.03, P02.06, P02.14
Würstlein, R.	AG11.09
Wylezich, C.	DGP14.08
Yalew, T.	P06.10
Yang, H.	AG01.19
Yao, S.	AG08.07
Yasser, M.	P11.13
Yavas, A.	P01.17
Ylaya, K.	AG01.04

Zahn, M.	P04.02, P04.03
Zamboglou, C.	P11.12
Zamo, A.	AG04.04 , P04.01
Zapukhlyak, M.	AG04.03
Zeidler, R.	P06.04
Zenker, M.	P12.02
Zerbe, N.	AG14.04, P14.07
Zeuzem, S.	P14.06, P01.16
Zgorzelski, C.	P14.08
Ziegler, P. K.	P01.06
Zörn, W.	AG06.01
zu Eulenburg, C.	AG11.09